An assessment of archive stereo-aerial photographs for 3-dimensional reconstruction of damaged and destroyed archaeological earthworks

Heather Elizabeth Papworth

Dissertation submitted in partial fulfilment of the requirements for the degree 'Doctor of Philosophy', awarded by Bournemouth University

2014

ABSTRACT

Archaeological earthworks are being damaged and destroyed at a rate and scale never before seen, which has resulted from increased mechanisation of human activity in the landscape since World War II. Along with natural degradation processes, recording earthwork metrics prior to their loss is increasingly difficult, which can subsequently hinder the interpretation of a site or landscape because of this missing evidence. A tool for regaining such data is vital to alleviate this problem and to fulfil the stipulation for metric information as required by national and international conservation charters. This research investigates whether it is possible to regain earthwork metrics from archive stereo-aerial photographs (SAPs) using digital photogrammetry to create digital surface models (DSMs) of archaeological sites within the UK dating from the 1940s to 2010. A literature search confirmed the utility of SAPs for reconstructing geomorphological events, such as landslides, whilst also verifying that such an approach had not been thoroughly investigated for archaeological adaptation.

Via experimentation, a photogrammetric workflow has been designed and a number of variables identified that affect the quality of DSMs obtained from SAPs. The magnitude of these variables has been verified by quantitative assessment using independent survey data, namely Airborne Laser Scanning (ALS) gathered by the Environment Agency, and ground-based collection using Global Navigation Satellite Systems (GNSS) and Terrestrial Laser Scanning (TLS). Empirical differences between these independent data and the SAP DSMs were identified using global statistical measures such as Mean Error (ME), Standard Deviation (SD) and root mean square error (RMSE), and spatial autocorrelation techniques, namely Local Moran's I.

Two study sites were selected on which to ascertain whether variations occur in the empirical quality of SAP DSMs and archaeological content at different locations. Over six decades of photography were collected for Flowers Barrow Hillfort, situated near Lulworth in Dorset, UK, which has remained in good condition throughout this period, due to the protection afforded it by inclusion within Ministry of Defence land. Eggardon Hillfort and earthworks, near Bridport in Dorset, UK, were also selected due to the exceptional preservation state of some earthworks, versus the plough-damaged remains of others. These sites thus offered an opportunity to rigorously test the reconstruction capabilities of the SAPs. The results from both study sites confirmed that the metric quality of SAP DSMs improves as the age of the imagery decreases, although this is dependent on image quality, scanner properties (i.e. whether the scanner is photogrammetric or desktop) and the result of the block bundle adjustment in the photogrammetric software.

This thesis concludes that SAPs can recreate earthwork metrics and provides a list of considerations for archaeologists to consult when planning the use of SAPs for creating DSMs. Recommendations for future work are provided that encourage the investigation of SAPs from other countries and the rigorous assessment of DSMs derived from structure-from-motion (SfM) software that is rapidly gaining popularity.

ACKNOWLEDGEMENTS

As is customary I would first like to thank my supervisory team, Andrew Ford, Kate Welham and David Thackray for their advice and support throughout my research. In particular, Andy deserves a second mention for heading into the field with armfuls of equipment, during some exceptionally cold weather, and always maintaining a chipper outlook (particularly after mine had long deserted me).

Many thanks are due to my external examiner, Professor Stuart Robson, and to my internal examiner from Bournemouth University Iain Hewitt who, together, helped to make my thesis strong and were extremely engaging, helpful and amenable when their advice was sort during the corrections process.

Due to her relentless support, understanding and good humour, when kit was requested with insufficient time for preparation and small crises occurred at inconvenient times, Karen Walmsley always stepped up to help. What a star!

As with such large undertakings, family and especially parents are almost invariably mentioned for their relentless support (including fiscally!) and patience, and mine are no exception. Without their love and sympathetic ears I would not have achieved this feat and nor would I have achieved field work of any description! So thank you Dad for driving me to both sites with the family car (the only one suited to winding across some very hilly terrain and the only car available to me), and for helping me to lug tonnes of kit around some very extensive earthworks! And thank you Mum for letting me borrow him, escape dog walking duties, and for making some of the best lunches *ever* that kept us going, even when it started to snow…

I have also had the privilege to meet many wonderful people throughout my PhD, including those outside this institution, without whose help I would not have succeeded. From UCL, many heartfelt thanks go to Dietmar Backes, who patiently helped me to master SocetGXP over the course of a week in May 2012 and then took me out for a beer to celebrate. After returning to Bournemouth I was able to seek the help and advice of Rick Mort, Steve Forster and Rut Gallmeier from BAe Systems, who all generously provided their time to help me torture the SocetGXP software with my archive SAPs. The same is true of Luke Jarry, Paul Burrows, Mark Francis, Simon Mears and Kate Strange-Walker who, at various stages of my research, answered some very detailed questions and did their utmost to help me try and work with Cyclone, despite never fully succeeding with it at Bournemouth. Last but not least, my grateful thanks go to Defence Estates at Lulworth for granting access to Flowers Barrow and Mrs Lloyd-Harris and the National Trust for their permission to access Eggardon Hillfort and its environs.

Finally, to the PGRs who have been and are going through the PhD journey and who kept me company at various times, whether that was in the office, conferences, on field work or just hanging out: Marie-Christine Dussault, Matt Sumnall, Rebecca Bennett, Katie Hess, Kuro and Emily Norton. I hope life rewards you all for your hard work and excellent friendship.

LIST OF ABBREVIATIONS

3D	Three-dimenional
ALS	Airborne Laser Scanning
APs	Aerial Photographs
ASC	Air Survey Commission
BBA	Block Bundle Adjustment
CAD	Computer Aided Design
CCD	Charge Coupled Device
CCO	Channel Coast Observatory
CIA	Central Intelligence Unit
CMOS	Complementary Metal Oxide Semi-Conductor
CUCAP	Cambridge University Collection of Aerial Photography
DCC	Dorset County Council
DCS	Directorate of Colonial Surveys
DEFRA	Department for Environment, Food and Rural Affairs
DEM	Digital Elevation Model
dGPS	Differential Global Positioning System
DoD	DSM of Difference
dSLR	Digital Single Lens Reflex Camera
DSM	Digital Surface Model
DTM	Digital Terrain Model
DTS	Desktop Scanner
DV	Desserted Village
EA	Environment Agency
EH	English Heritage
GCP	Ground Control Points
GIS	Geographical Information System
GNSS	Global Navigation Satellite System
GPR	Ground Penetrating Radar
HER	Historic Environment Record
ICOMOS	International Council on Monuments and Sites
ICS	Image Coordinate System
IDW	Iverse Distance Weighting
IMU	Image Motion Compensation
INS	Inertial Navigation System
LSA	Least Squares Adjustment
LPS	Leica Photogrammetry Suite
LRM	Local Relief Modelling
ME	Mean or Mean Error
NAPLIB	National Association of Aerial Photographic Libraries
NMP	National Mapping Programme
NMR	National Monuments Record
NMRW	National Monuments Record Wales
NN	Natural Neighbour
NT	National Trust
OS	Ordnance Survey
‘p’ value	Statistical Significance
PC	Personal Computer

PCA	Principle Components Analysis
PDU	Photographic Development Unit
PIs	Photographic Interpreters
PIU	Photographic Interpretation Unit
PR	Photographic Reconnaisance
PRU	Photographic Reconnaissance Unit
'r' value	Correlation Coefficient
RAF	Royal Air Force
RCAHMS	Royal Commission on the Ancient and Historical Monuments of Scotland
RCAHMW	Royal Commission on the Ancient and Historical Monuments of Wales
RCHME	Royal Commission on Historic Monuments England
RCZAS	Rapid Coastal Zone Assessment Survey
RFC	Royal Flying Corps
RGS	Royal Geographical Society
RMSE	Root Mean Square Error
RTK	Real-time Kinematic
SAPs	Stereo Aerial-Photographs
SD	Standard Deviation
SfM	Structure from Motion
SMR	Sites and Monuments Record (commonly referred to now as an HER)
SNR	Signal to Noise Ratio
SOP	School of Photography
Sqn.	Squadron
SVF	Sky-view Factor
TARA	The Aerial Reconnaissance Archive
TIN	Triangulated Irregular Network
TLS	Terrestrial Laser Scanning
TST	Total Station Theodolite
UAV	Unmanned Aerial Vehicle
UNESCO	United Nations Educational, Scientific and Cultural Organisation
USAF	United States Air Force
WWI	World War One
WWII	World War Two
z-score	Statistical Significance of a Moran's I result

LIST OF FIGURES

LIST OF TABLES

1 INTRODUCTION

1.1 Outlining the Problem

The archaeological resource is fragile and finite. Whilst it is subject to on-going damage and decay caused by natural factors (Rowley and Wood 2008), within the last 60 to 70 years historic landscapes have been increasingly threatened. There has been pressure from industry, agriculture, mineral extraction and other economic activities that have sought to exploit the natural resources available within the UK. The efficiency, rate and scale at which many of these activities can take place have risen with advancements in mechanisation. Archaeological assets have subsequently been threatened with damage and destruction at a rate and scale that continues to increase. This is nowhere more apparent than from the tangible loss of earthwork features.

1.1.1 Threats to the Archaeological Resource

As noted by Rowley and Wood (2008) all archaeological sites suffer from natural ongoing decay and damage. Darvill and Fulton (1998) compiled a list of threats for the 'Monuments at Risk Survey' (MARS), which was commissioned by English Heritage in 1995 to quantify the archaeological resource within England, identify and assess the factors causing detrimental change to monument survival and condition, and to investigate the future implications this has on their survival (Oxford Archaeology 2002). Darvill and Fulton (*ibid.*) identified an extensive list of factors that threaten the archaeological resource, both anthropogenic and natural. Many of these factors are illustrated in Figure 1.1. Not only have the physical effects of human activity had the greatest impact upon archaeology, through the construction of buildings and roads, agricultural requirements, industry and a general lack of maintenance, but it has also had an unanticipated side-effect that, until recently, has been hitherto unacknowledged. Climate change is a consequence of mass-consumption and intensification of the processes employed to extract and synthesise natural resources. The effects of this phenomenon are now recognised as a threat to the archaeological resource, particularly at the coast. It is anticipated that within the next 50 to 100 years, there will be a palpable increase in storm-events, erosion rates and sea-level globally (Murphy et al. 2009).

(a.) Housing development
(© Wessex Archaeology

(b.) Agricultural attrition (© NMR 4228-450)

(c.) Infrastructure i.e. road and rail
(© Steve Patterson)

(d.) Mineral Extraction i.e. coal mining
(© West Yorkshire Archaeology Service

(e.) Coastal erosion and weathering
(© RCHME)

(f.) Floral damage
(Peter Crow © Crown Copyright)

(g.) Faunal Damage
(© Northumbria National Park Authority)

(h.) Footpath Erosion (© National Trust)

Figure 1.1: Photographic examples of the threats faced by archaeological features.

1.1.2 Recording Requirements for Threatened Archaeology

The requirement for recording archaeological features is evidenced in the large number and variety of conservation charters available through organisations such as the International Council of Monuments and Sites (ICOMOS), International Scientific Committee for the Documentation of Cultural Heritage (CIPA) and the Institute of Field Archaeology (IFA), as well as the conservation policies utilised by large heritage organisations, namely the National Trust (NT) and English Heritage (EH). ICOMOS state that documentation plays a vital role in advancing knowledge, promoting interest, facilitating management and appropriate conservation of the archaeological resource (ICOMOS General Assembly 1996). The Venice Charter, also published by ICOMOS (Bassegoda-Nonell et al. 1964) states that "there should always be precise documentation in the form of analytical and critical reports, illustrated with drawings and photographs" before, during and after any intervention. This is particularly important if the site is threatened with destruction. Ensuring that a full record, from which a variety of analyses and other investigations can be undertaken post-disaster, is essential to mitigate the loss of knowledge.

Survey data is also an imperative tool for understanding a site, such that it enables the monument to be understood and thus more suitable decisions to be made relating to the allocation of resources for conservation and managing the process of change (Clark 2003). Ainsworth et al. (2007) echo this sentiment by adding that it also provides a "broader context to more narrowly focused investigations and for public enjoyment". The reasons why earthwork and landscape surveys are undertaken relates to the representation of the features that are visible within a study site that can help to describe the form and condition of these monuments (Ainsworth et al. *ibid.*). Further, they may also provide clues as to the antiquity of a feature, particularly if the size and shape are similar to other such features situated within the same region or landscape, as they may all belong to the same period (Clark et al. 2003 p.86). This approach helps archaeologists to form a typology, or classification, of earthworks from which further inferences can be made about their antiquity and usage.

The Valetta Convention (Council of Europe 1992) stipulates that archaeological surveys should be updated and subsequently published to promote public awareness of the value provided by archaeological heritage, stating that this approach educates people about the factors threatening the survival of their historic environment. The Burra Charter (Australia ICOMOS 1999), was the first to remark upon 'significance' in its guidelines, illustrating that a variety of elements relating to a feature can make it significant: its appearance, history, scientific merit or social value (Brooks 1992). Brooks (*ibid.*) states that these values are likely to change over time and are influenced by our understanding of a feature. Survey documentation can assist in the process of understanding a feature, particularly in advance of works relating to the documentation of changes that are anticipated to the historic fabric (Clark 2003). The Burra Charter lists change that reduces cultural significance as undesirable, and where change has reduced this significance it should be reversible. To facilitate the management of change, Article

27.2 states that “existing fabric, use, associations and meanings should be adequately recorded before any changes are made (to the place)” (Australia ICOMOS *ibid.*). Thus recording and survey form an important part of the analytical process to facilitate the understanding of a monument and the mapping of any change that is anticipated to occur, which is summarised in Figure 1.2. However, the number of English monuments has been estimated to be 2.25 per kilometre square (Darvill and Fulton, 1998), which indicates the magnitude of the resource required to fulfil the ideal of updating the survey data of a monument.

Within the UK there have been a number of Government policies that have sought to ensure archaeology is considered by a number of industries prior to the commencement of development. Since 1947, the Town and Country Planning Act has required that developers gain planning permission before proceeding with development, with the introduction of Planning Policy Guidance note 16 (PPG16) in 1990 specifically requiring the consideration of archaeology during the planning process (Dormor 1999, p.44). PPG 16 effectively demands that the protection, enhancement and conservation of archaeological sites are considered during the planning process to mitigate for any potential losses during construction. This includes a number of different approaches to ensure mitigation is achieved, which includes excavation and survey (Association of Local Government Archaeology Officers No Date). Whilst Darvill and Fulton (1998) state that initial studies of the efficacy of PPG 16 suggested it was working well,

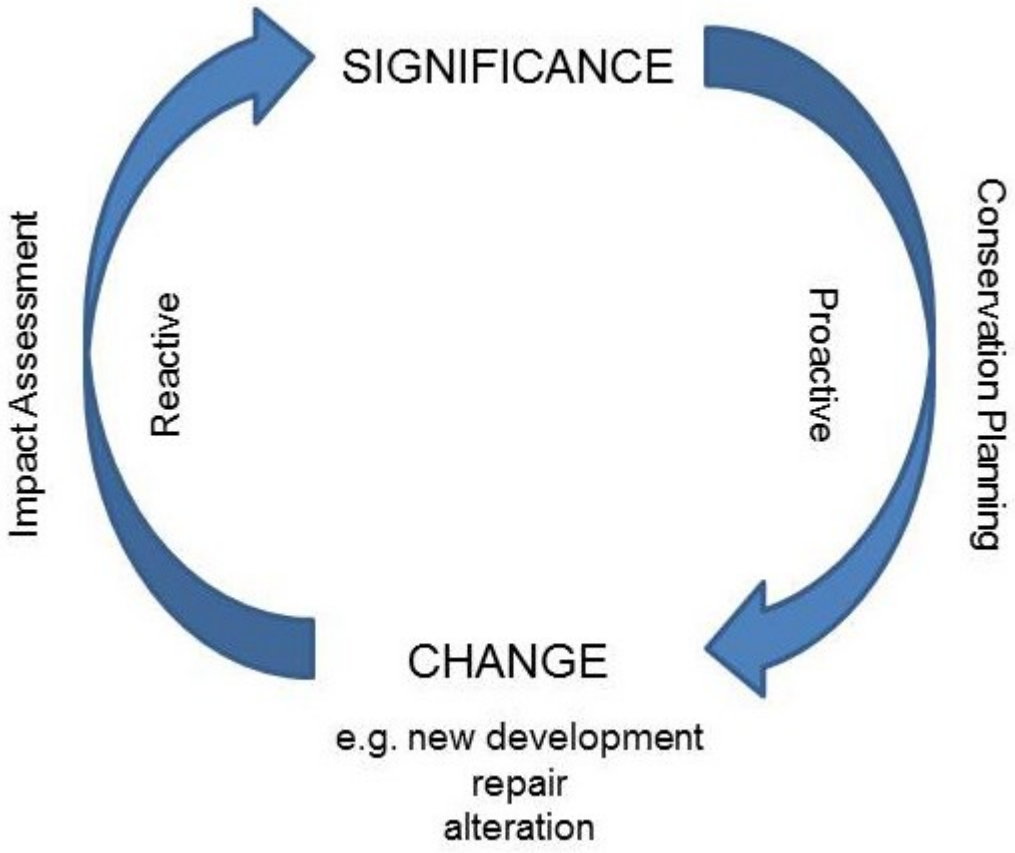

Figure 1.2: The Conservation Cycle (Clark 2003, p.23).

Dormor (*ibid.)* argues that it is not applicable to 75% of the land surface within England, as PPG16 cannot be applied to regions utilised for farming and forestry practices. PPG16 was replaced by Planning Policy Statement 5 (PPS5) in 2010, although this was quickly superseded by the National Planning Policy Framework (NPPF) in March 2012 (Association of Local Government Archaeology Officers *ibid.*). No legislation exists to protect archaeology at risk from natural threats however, although archaeologists are aware that this is a huge issue, particularly along the coast (Fulford, Champion and Long 1997). Subsequently, a great deal of time and planning has been allocated to developing Rapid Coastal Zone Assessment Surveys (RCZAS), a form of desk-based assessment and rapid baseline survey of coastal archaeology, since the late 1990s.

The idea of creating documents of archaeological features is often referred to as 'preservation by record', which is a term that has been used to describe attempts to mitigate the loss of historic assets by providing a way in which to reconstruct a site or feature for further research or to ensure its meaning lives in perpetuity. Whilst the recording process is evidently encouraged by a series of conservation charters, selecting the most appropriate technique to record a threatened feature is difficult, and the needs of a project must be identified to ensure the correct choice of tools for the job (Eppich and Chabbi 2006). One might be tempted to employ survey methods that generate a vast amount of detailed data to ensure that the minutiae of a feature is also recorded, whether in fact such detail exists of not. However, this approach would be exceedingly expensive, particularly for large features, such as earthworks, due to the time required to both survey and process the data, not to mention the expertise that would be required to achieve an output.

A broad knowledge of the survey methods available and their associated strengths and weaknesses is therefore fundamental to making an informed decision and an appropriate selection for documentation purposes. Whilst the quality of a record is dependent upon the current state of a technology or skill of the practitioner creating the dataset, guidelines are increasingly available to assist those unfamiliar with using or commissioning surveys (Letellier 2007; Bedford and Papworth 2009; Bryan et al. 2009; National Parks Service 2010). However, to complement government guidance notes, heritage bodies, such as NT and EH, have also outlined their own approaches to heritage conservation (National Trust No Date; English Heritage 2008; Cowell 2009). EH have also produced a survey specification for cultural heritage practitioners to ensure that, when commissioning a survey for archaeological purposes, a well-defined brief can help to ensure that appropriate records are obtained (Bryan et al. 2009).

1.1.3 Archaeological Survey Techniques

Whilst the terms 'recording' and 'documentation' have many connotations, one of the fundamental components of these processes is the production of a metric survey describing the dimensions of an earthwork feature. Metric Survey is defined as "the use of precise and

repeatable measurement methods to capture spatial information for reproduction at scale" (Bedford and Papworth 2009). The use these techniques has been long established in the archaeological profession and can be divided into two groups to help distinguish the way in which information is captured using the technologies that fall within each definition, namely Direct and Indirect, each of which are described in Section 1.1.3.1 and Section 1.1.3.2 respectively.

The choice of which survey tool to use is influenced by a series of factors, defined by Ainsworth et al. (*ibid.*) as:

- The purpose of the survey and subsequently the data scale;
- The size of the area of interest (AOI);
- The available equipment and their suitability for the task;
- Expertise of the field team;
- The timescale allocated to the project;
- The budget allocated to the task (Jones, *ibid.*p.5).

These factors will influence at what scale an earthwork is depicted, which will also dictate whether smaller details are recorded. For ground-based surveys that focus on small areas, scales of 1:500 are commonly used, although 1:1,000 is often sufficient (Ainsworth et al. *ibid.*). The instruments used for this work are called direct techniques, which are explained in Section 1.1.3.1. The survey scale becomes smaller if a broader area is to be mapped, i.e. 1:1,250 or 1:2,500, which will allow for the basic identification of an earthwork type, whilst 1:10,000 is useful for examining landscape-scale regions (Ainsworth et al. *ibid.*). The latter approaches often require remote sensing data in the form of aerial photography (APs) or airborne laser scanning (ALS), which are referred to as indirect techniques (see Section 1.1.3.2).

Metric survey is useful for its repeatability, which introduces scientific rigor into the archaeological discipline, as acknowledged by Jones (1985), facilitating a number of activities, including change monitoring and management. This is particularly important as the values associated with the accuracy and precision of a dataset are an indicator as to how much change will have to occur before there can be confidence that the measurement technique has actually detected any. Whilst there are a wide variety of survey tools that allow archaeologists to create such a record, in general the higher the density of the data they can record, the higher the parity of the feature's archival record. If the intention is to preserve a site by record Taylor (1974) recommends undertaking as detailed a survey as possible. This requires the scale of the survey to be chosen so that the smallest detail contained within a site is recorded, which is an approach generally best suited to mass-capture techniques due to the amount of data required.

1.1.3.1 Direct (Terrestrial) Techniques

Direct survey techniques are characterised by the careful selection of feature details at the point of capture by a surveyor. The survey tools defined as direct techniques range from the more traditional tools, such as an alidade and tape, and measured and sketch drawings, to the modern electronic instruments, namely the Total Station Theodolite (TST) and Real-time Kinematic Global Navigation Satellite Systems (RTK GNSS). Traditional survey techniques, such as the alidade and tape and measured sketches and drawings, are all capable of providing useful data relating to the shape and form of archaeological earthworks and other features. As stated by Howard (2007) the low levels of funding within the archaeological discipline often require that lower cost methods of surveying are applied. However, as the cost of electronic equipment is reduced as technological advancements are made and the option to hire equipment facilitates its use, TSTs and GNSS do provide a rapid method for generating digital data that can be manipulated in a variety of different ways. These technologies are described in Appendices One and Two.

All of these tools are ground-based in their application. The process of using any of this equipment in the field allows archaeologists to exercise their judgement and knowledge when selecting the features of interest to record (Ainsworth et al. 2007). However, due to their highly-selective nature, the size of the object and its complexity will dictate whether a direct technique is appropriate for the task. In general, the smaller and less complex a feature is, it becomes more suited to recording by a direct technique. For example, the production of a plan outlining break-lines of earthworks contained within a small site would be quicker to produce using measured drawing, TST or GNSS than it would be to set-up a terrestrial laser scanner (TLS) numerous times and subsequently post-process the data. In many cases, the data collected using direct techniques requires very little post-processing in comparison with that created using indirect or mass-capture methods. Subsequently, the majority of archaeological earthwork survey has been undertaken using direct techniques, although mass-capture methods are gaining popularity for earthwork documentation.

Howard (2007) notes that Bowden (1999, 2002) and English Heritage are exponents of the plane table method for earthwork recording. Bowden (1999, p.60) lists a number of reasons as to why plane table surveying is superior to electronic techniques, which Howard (*ibid.*) has subsequently countered. In his first point, Bowden (*ibid.*) states that “an experienced team can produce a survey at least as fast” with an alidade and tape as they can with a TST, which Howard (*ibid.*) does not refute. Bowden (*ibid.*) also asserts that the end product from an alidade survey is of higher quality because it forces the surveyor to “treat features as complete entities rather than a series of lines”, unlike the survey from a TST or GNSS. Howard (*ibid.*) disagrees with this statement, arguing that a bad survey is produced by a bad surveyor, and not by the equipment applied to the survey itself, which is unequivocally true. The appropriate selection of information is made by the surveyor themselves, who utilises the instrument to collect the data, not to make the decision on his or her behalf. Lock (2003) believes that the use of electronic

survey methods might encourage the site to be surveyed too quickly, and thus the risk of a surveyor ignoring more subtle features is increased.

Bowden (*ibid.*) continues by stating that drawing in the field facilitates the checking of data and "instantly identifies any errors". This is indeed the case although, whilst traditional techniques were once the sole means of generating a survey drawing in the field, this is now possible with modern, electronic equipment. Howard (*ibid.*) also states that the use of a plane table in good weather is ideal for creating a field drawing, although the opposite is true in adverse conditions. Finally, Bowden (*ibid.*) refutes the reliability of electronic systems, indicating that breakdown and battery failure is not an issue with traditional methods. Whilst this may be the case, Howard (*ibid.*) states that electronic equipment is not prone to failure if it is maintained properly and if sufficient diligence is applied when organising the equipment so as to obtain a sufficient number of well-charged batteries. Although Bettess (1998) is a proponent of electronic survey equipment, stating that it can result in savings in work and time, Bowden (*ibid.*) pleads for caution, stating that the ability to press buttons does not produce a surveyor. Subsequently, the choice of a particular survey technique can be built upon previous experience with the equipment and personal preference.

1.1.3.2 Indirect (Airborne and Mass-Capture) Survey Techniques

Indirect or mass-capture survey techniques, such as airborne laser scanning (ALS), terrestrial laser scanning (TLS) and photogrammetry, are non-selective at the point of capture and record everything in the field-of-view of the sensor. Decisions about the form or function of the subject are made after data processing has taken place, allowing the extraction of feature data to be made in an office environment (Shaw and Devlin 2010). These techniques are often operated remotely, which is of benefit if the area to be recorded is extensive, or where access is limited or dangerous. In contrast to direct techniques, mass-capture technologies are well suited to documenting large and complex objects, as illustrated in Figure 1.3. For example, if a DSM of a large site was required that contained a series of earthworks, RTK GNSS could be applied to produce such a survey. However, the regularity of the point spacing and the time required to generate a large number of points using this method would be limited in comparison to airborne mass-capture techniques that can generate much higher densities of data in a fraction of the time (Barber et al. 2007). The operational considerations and technical information relating to photogrammetry, ALS and TLS, is provided in Sections 2.2 and 2.3 respectively, including a discussion of the archaeological projects to which these mass-capture techniques have been applied.

Direct techniques allow surveyors to ignore or choose not to record features and select the requisite data at the point of capture. As stated by Bowden (1999) "data collection for its own sake is not valid…" and whilst mass-capture can be beneficial because nothing is 'left out' of the survey, the process does not allow the surveyor to truly engage with the features they are

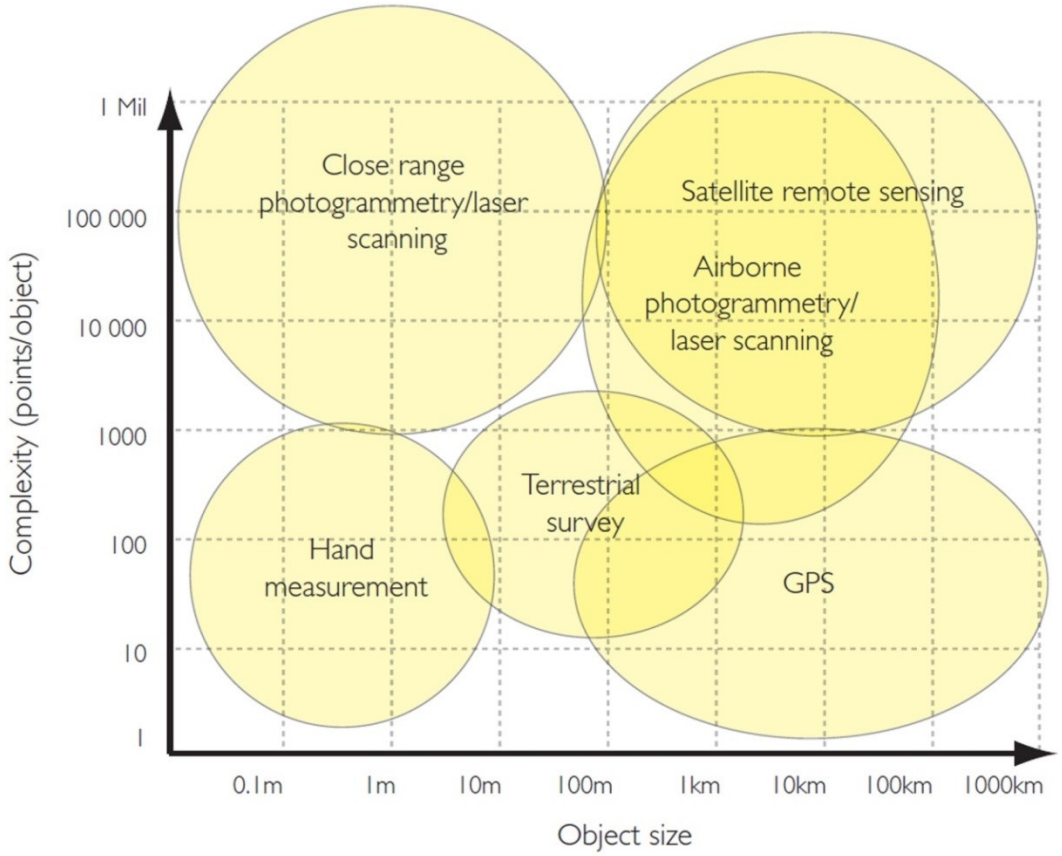

Figure 1.3: Diagram illustrating how size and complexity of an object influence the choice of survey technique (Böhler and Marbs 2002).

recording or develop their understanding of the features through prolonged contact and careful consideration and selection. It is generally agreed by most authors (Doneus et al. 2008; Corns and Shaw 2009) that a field assessment of processed mass-capture data is necessary to confirm that the features discovered after data processing are truly of an archaeological nature; if such features are large enough or contrast significantly with their surrounding environment, the pictorial record generated using photogrammetry may negate this task, except in woodland. Should mass-capture data be incomplete, however, a further site visit may be necessary to fill-in any data gaps. If this is not possible, any data not collected at the time of the survey could be lost in much the same way as the unnoticed feature during the application of a direct technique. This is especially detrimental if the purpose for survey is the preservation by record of an object or site that is in danger of damage or destruction.

Unlike ground-based methods, the datasets produced by TLS, ALS and photogrammetry are computationally challenging. These survey methods are referred to as ‘mass-capture’ techniques, due to the large volumes of data they generate, which have been labelled as ‘big data’, causing a data “deluge”. This is an issue currently being debated by the archaeological community, as well as in other disciplines, due to the problems associated with their manipulation, analysis and storage. Whilst a discussion of this particular issue is beyond the scope of this research, the interested reader is referred to the English Heritage project document on the topic of ‘big data’ (Austin and Mitcham 2007). Therefore the application of

mass-capture techniques to preserving an archaeological site by record has to be carefully planned.

1.1.4 Interpretive versus Metric Survey Records

As discussed in Section 1.1.3, there are often two approaches to archaeological earthwork survey: the first relies predominantly on direct techniques, whereby the surveyor is able to exercise their own subjective interpretation when deciding what, or what not, to record, which will vary from person to person, depending on experience. The second approach relies on a more clinical methodology that aims to produce a metric survey of the earthworks and a record of their form in both planimetric and vertical dimensions.

Irrespective of the survey techniques used to gather data, as discussed in Section 1.1.3, archaeologists have used a variety of methods to represent their outputs as surface data that have predominantly resulted in 2-dimensional drawings. Hachure plans, contour maps and line drawings have all been used to symbolise archaeological features, albeit the process of creating these products is based on interpretation. Bowden and McOmish (2012) state that the production of a hachure plan is "openly subjective and interpretive", requiring the archaeological surveyor to exercise skill, judgement and experience throughout the survey. The end product is a plan that utilises hachures to represent slopes as well as the chronological relationships between earthworks across a site (Bowden and McOmish *ibid.*). This type of survey tends to be produced using direct techniques (see Section 1.1.3.1).

It is important to understand the benefits and drawbacks of hachure representation. Many archaeological earthworks in the UK have been recorded using this approach, particularly for the RCHME surveys conducted during the mid-20th Century. Payne (2006, p7) states that these surveys were conducted on a county-by-county basis from the 1920s to the 1970s to create archaeological inventories of those still observable in the landscape. Subsequently, as archaeological earthworks within the UK are damaged and destroyed, these surveys may constitute the only records we have of their existence and form. However, their subjective and interpretive nature impedes the reconstruction process due to a lack of empirical data in the form of elevation values associated with them. Subsequently, archaeological hachure plans have been criticised by a number of authors who prefer a more empirical approach to earthwork survey (Wheatley and Gillings 2002; Blake 2014). Although Blake (*ibid.*) is complementary about the graphical representation of earthworks using hachures, the author is critical of their ability to "depict precise slope metrics", slope angles and height information. The lack of empirical information in the modern era appears to exasperate Blake (*ibid.*), who bemoans its deficit in anything other than the planimetric dimension. Most importantly, the author states that a hachure plan presents us with "an interpretation of the terrain rather than a record".

Whilst an interpretive survey can be part of a 'preservation-by-record' strategy, to ensure the ability to reconstruct earthworks after damage or destruction an objective survey is required. These are not infallible, however. The presence of subtle earthworks may go unnoticed during an interpretive metric survey, particularly one that employs purely direct techniques, and thus their existence is not recorded. Subsequently, the accuracy of any philosophical interpretations made using such a dataset could therefore be affected, which will consequently influence how well the site is understood. If the survey is designed to record an archaeological site that contains a series of earthworks that are threatened with destruction, for example, any unobserved features may be lost forever.

Taylor (1998) argues that data capture often comes at the expense of analysis, which may be of concern to those working with mass-capture datasets. As pressure upon the archaeological resource has increased during the 20th Century, Taylor (*ibid.*) states that limited study of a site under threat has prompted data to be collected in volume to preserve what is to be lost, such that this information can be archived and analysed in the future. Taylor (*ibid.*) believes that the lack of analysis in favour of data gathering has prevented the true understanding of the record as it is being created, which subsequently invalidates the information collected: "without understanding, information is useless". This is indeed a difficult situation, as the numbers of archaeological sites that require recording before they are damaged or lost far surpass the capacity of the industry to fully analyse each individual case. There are also too many features that are at risk to even consider providing field teams to survey each and every monument. Where a site is discovered that has not previously been recorded, but is in imminent danger of destruction, the pragmatic solution would be to produce a record as soon as possible, as advocated by Bowden (1999). This would be preferable to losing something that may be of hitherto unknown importance. Whilst the preservation of archaeological monuments is of ongoing debate with those involved in policy-making, the issue still remains as to how best we can obtain metrics of such features that may have once been in good condition post-WWII, and how we might best record those that are still in existence.

Irrespective of the advice from international conservation organisations, who recommend an almost continual cycle of monitoring and recording threatened archaeological resources (see Section 1.1.2), the practicalities of doing so pose a logistical challenge for the heritage community. A large number of upstanding features will continue to be damaged and destroyed at a rate too fast for each and every one to be recorded using a planned regime of data capture. To add further complications, a great variety of archaeological features exist, ranging from small, site-based earthworks to landscape-scale regions that contextualise sites. Flexibility is therefore required from survey techniques to ensure that these features are suitably recorded. They should also facilitate investigations regarding the evolution of a landscape to fully understand which areas are most at risk from deterioration and to anticipate what the future may hold for these regions.

If limited survey data exists with which to examine landscape change or if features have been lost that would further facilitate the interpretation of the landscape, achieving these goal will be

problematic for landowners and those with management responsibilities and limited resources to both monitor and map these features. To recover features that have already been destroyed requires the use of historic stereo-aerial photography. Photogrammetry offers a potential solution, based upon its established record as a tried-and-tested method for ante-disaster recording (Dallas et al. 1995). If enough control data is captured at the time of the photography, or can be obtained at a later date, this technique facilitates the reconstruction of an object post-destruction (see Section 2.2.9). Despite the reticence of archaeologists such as Taylor (*ibid.*) and Bowden (*ibid.*) towards techniques that generate large amounts of data, which are often archived before full analysis, others have found that this approach can help to mitigate disaster, namely by utilising photogrammetric restitution (Dallas et al. 1995).

However, over the last forty years (Wheatley and Gillings 2002) the availability of mass-capture techniques has further enhanced the detail in which archaeological topography can be represented, including the production of digital surface models (DSMs). A full discussion of DSMs and the procedures involved in their generation is provided in Chapter 3. In contrast to hachure plans, DSMs are empirical in nature and can be manipulated in a number of ways using GIS and CAD systems. Prior to DSM analysis taking place the survey data is often converted into a gridded dataset, or raster. This requires point data to be interpolated, the processes for which are described in Section 3.2. By converting survey data into a raster, something of an analogue to an aerial photograph is created as archaeological features can be identified within in. However, a DSM has the added benefit of containing elevation values for 3D examination. One of the simplest methods of archaeological analysis that can be conducted on a DSM is the extraction of point, polyline and polygon shapefiles to represent archaeological features that are observable in the data. This is the approach taken by the National Mapping Programme (NMP) (see Section 2.1.1.1).

1.1.5 Archaeological Information Content of Aerial Photography

1.1.5.1 Calculating Information Content

The success of recording archaeological data from aerial photography is dependent on two factors: the scale of the earthwork or feature and the spatial resolution of the photograph. The former factor is difficult to define because of the large variations in feature dimensions. Examples of such metrics are provided in Table 1.1, with more detailed information on a large number of period-specific earthworks and features available from English Heritage on the '*Monument Class Descriptions*' website (English Heritage, no date). The spatial resolution of a photograph, sometimes referred to as ground sample distance (GSD), can be determined from the information provided with it using the following formula:

$$GSD = f/H$$

Class	Type	Width/diameter (m)	Length (m)	Height/Depth (m)
Prehistoric	Linear	-	10+ to 80,000	-
	Ringworks	40 to 120	-	~3
	Pit Circles	0.75 to 2	~1 to 7	0.2 to 2
	Cursus	20 to ~150	~10mm to 10,000	-
Barrows	Long	25 max.	50 max.	-
	Round	5 to 50	-	6 max.
	Bell	30 max.	-	4
	Disc	40 min.	-	-
Henges	-	110 max.	-	-
Banjo Enclosures	Ramparts	-	-	0.7
	Trackways	5 to 10	25 to ~90	-
Hillforts	Ramparts	-	150m	10
Trackways	Medieval	9 to 27	-	-
	Roman Roads	5 to 10	-	0.75
Burnt Mounds	-	3.5 to 15.5	-	c. 1.1
Water Meadows	Ridges	3 to 15	-	0.5 to 0.6
Earthwork Castles	Ringworks	20 to 50	-	-
Cultivation Ridges	Prehistoric/Roman	1 to 1.5	-	-
Medieval Ridge and Furrow	Furlongs	-	up to 700	-
	Ridges	~5, rarely 20	-	-
Pre-Industrial Lime Kilns	Clamp hearth	~2.5	-	~2
Pre-Industrial Mines and Quarries	Pits	-	-	0.6 to 12

Table 1.1: A selection of earthwork dimensions extracted from the English Heritage Monument Class Descriptions (English Heritage, no date).

Whereby '*f*' is the focal length of the camera lens and 'H' is the flying height, or altitude, of the aircraft. This formula works for both analogue and digital systems, although the following formula can be utilised for digital images:

$$GSD = (\text{pixel size} \times H)/f$$

There is, however, a further complicating factor when analogue photography is converted to digital using a scanner. To preserve as much information in the photograph as possible, the archaeologist should adopt a large scanning resolution, which is often given in dots-per-inch (dpi), which subsequently increases the pixel size (or information content) of the digitised image. As an example, to calculate the pixel size of an image based upon dpi, the following formula can be used (Linder 2009):

$$\text{Pixel size (µm)} = 25400/\text{dpi}$$

Therefore an image scanned using 2400 dpi would provide a pixel size of 10.583µm, whilst a 600dpi setting would create an image with a pixel size of 42.333µm, which is poorer and contains less information.

By examining the dimensions of earthworks in combination with the GSD of aerial photography, it is possible to establish whether or not the imagery will provide suitable metrics for recording archaeology. This can be established with the help of sampling theorem, which states that an object can be reconstructed as long as the sampling interval, known as 'δx', is correct (Axford, 2000 p.409). To establish what 'δx' should be in terms of an earthwork, the smallest dimension to be reconstructed is selected and then halved i.e. if a 5m wide ridge from ridge and furrow were to be recorded, its width should be sampled in intervals of at least 2.5m or smaller to ensure capture. Another way of calculating the quality of a pre-specified sampling routine is to use the following formula from Bedford and Papworth (2009):

$$Q = l - (m/l)$$

Whereby 'Q' is the quality ratio, 'l' is the smallest object size to be recorded and 'm' is the post spacing. A good outcome would result in a positive value for 'Q'. Subsequently, if the 5m ridge referred to earlier was recorded on an aerial photograph whose GSD was 0.15m, theoretically we would obtain the following result:

$$Q = 5 - (0.15/5)$$

$$Q = 4.97$$

This would be an acceptable result. However, if the object was a prehistoric pit circle with a width of 0.75m, and the GSD of the aerial photograph containing this feature was 1m, the result would be as follows:

$$Q = 0.75 - (1/0.75)$$

$$Q = -0.583$$

Subsequently the aerial photography would not be suitable for recording this feature.

1.1.5.2 Aerial and Spaceborne Systems

There are many remote sensing systems that are utilised by archaeologists beyond aerial photography, which include satellite data as listed in (Table 1.2). Each sensor provides data that is captured in raster format or, in the case of the Shuttle Radar Topography Mission (SRTM) and the Spaceborne Imaging Radar (SIR), post-processed to provide a raster product. Whilst many of the sensors listed in

Table 1.2 provide imagery that is akin to aerial photography in the visible and panchromatic formats, data is also available in differing spectral bands i.e. near infrared (Near-IR), short-wave infrared (SWIR), long-wave infrared (LWIR), and thermal infrared (TIR). Wavelengths in the non-visible spectra have been utilised by a number of archaeologists for prospection, whereby ephemeral features, such as crop and soil marks, or evidence of damage to archaeological sites may be identifiable based upon their reflectance characteristics.

Whilst satellite imagery in the visible, panchromatic, multi- and hyper-spectral wavelengths is invariably useful for monitoring archaeological sites, these data do not have the temporal resolution of aerial photography, although CORONA was launched and began data collection in

	Sensing Platform	Format	Spatial resolution (m)	Spectral Resolution (µm unless otherwise stated)	Temporal Resolution
Aerial Platforms	Frame Camera	Imagery	~0.1 min*	Panchromatic (B&W)/Infrared/Colour	On demand and weather dependant
	Digital Camera	Imagery	~0.05 min*	Panchromatic (B&W)/Infrared/Colour	
	Multi-/Hyper-spectral Sensors	Imagery	0.52 - 0.68m @ 1000m altitude	Visible to Near-IR (400 - 970) i.e. AISA Eagle 3.3nm	
				SWIR (970 - 2450) i.e. AISA Hawk 8nm	
			1m @ 660m altitude	Visible to SWIR (380 - 2500) i.e. AISA FENIX in 620 bands (3.5nm in VNIR, 12nm in SWIR)	
			1.1 - 1.5m @ 1000m altitude	LWIR/Thermal (760 - 1250) i.e. AISA OWL in 100 channels (~100nm)	
	InSAR	DSM	5	X-band (3cm) i.e. Star-3i	On demand and weather independant
Satellite Platforms	Corona/KH7&8/KH9	Imagery	1 - 120	Panchromatic (B&W)/Infrared/Colour	Variable (Corona from 1959 - 1972; KH7 from 1963 - 1967 and KH8 from 1966 - 1984; KH-9 from 1971 - early 1980s)
	KVR-1000 (on COSMOS)	Imagery	2 - 3	0.49 - 0.59	Variable (from 1985 - 1992)
	Landsat	Imagery	15 - 60	Visible (0.45 - 0.69)	Launched in 1972 Revisit time c.18 days
				IR (0.76 - 0.9)	
				Middle (1.55 - 1.75)	
				TIR (10.4 - 12.5)	
				Mid-IR (2.08 - 2.35)	
	SPOT	Imagery	1.5 - 20	Visible (0.43 - 0.47; 0.5 - 0.59; 0.61 - 0.68)	Launched in 1986 Revisit time 16 days
				Near-IR (0.79 - 0.89)	
				Mid-IR (1.58 - 1.75)	
	ASTER	Imagery	15 - 90	VNIR (0.52 - 0.6; 0.63 - 0.69; 0.76 0.86; 1.6 - 1.7)	Launched in 1999 Revisit time 16 days
				SWIR (2.14 - 2.225; 2.36 - 2.43;)	
				TIR (8.125 - 8.825; 8.925 - 9.275; 10.12 - 11.65)	
	SRTM	DSM	30 (1 arc second) or 90 (3 arc seconds)	C-band (6 cm)	Single 11-day mission in February 2001
				X-band (6cm)	
	Quickbird	Imagery	0.65 - 0.73 (panchromatic) - 2.62 - 2.9 (multispectral)	Panchromatic (0.526 - 0.929)	Launched in 2001 Revisit time (depending on altitude and latitude) 2.4 - 8.7 days
				Blue (0.445 - 0.516)	
				Green (0.506 - 0.595)	
				Red (0.632 - 0.698)	
				Near-IR (0.757 - 0.853)	
	IKONOS	Imagery	0.82 (panchromatic) - 3.2 (multispectral)	Panchromatic (0.526 - 0.929)	Launched in 1999 Revisit time ~3 days
				Blue (0.445 - 0.516)	
				Green (0.506 - 0.595)	
				Red (0.632 - 0.698)	
				Near-IR (0.757 - 0.853)	
	SIR-A	Imagery	40	L-band (24cm)	Launched in 1981 (duration 3 days)
	SIR-B	Imagery	16 - 58 (range) and 20 - 30 (azimuth)	L-band (24 cm)	Launched in 1984 (duration 1 week)
	SIR-C/X-SAR	Imagery	30 (azimuth); L-band and C-band 13 and 26, and X-band 10 and 20 (slant range)	X-band (3 cm)	Two missions only in April and October 1994
				C-band (6 cm)	
				L-band (24 cm)	

Table 1.2: Image sources from airborne and spaceborne systems detailing their spatial, spectral and temporal resolutions.

1960 (Altmaier and Kany 2002; Beck et al. 2007). However, CORONA coverage tended to focus on data collection over the Soviet Union, Middle-East, China and South-east Asia (Ruffner 1995) and thus is of limited utility to archaeologists working beyond these regions.

A further obstacle to the adoption of satellite imagery by archaeologists is the often coarse spatial resolution of the data, as noted by (Philip et al. 2002; Galiatsatos et al. 2005; Beck et al. 2007; Challis et al. 2009; Beck 2011). Subsequently, smaller features are not recorded in the requisite detail and thus only general, site and landscape-scale studies are possible. Whilst the spatial resolution of satellite imagery will continue to improve as technology advances, the deficit of temporal resolution remains and thus it cannot be used to obtain information about archaeological earthworks that have been lost in all but the most recent years.

1.2 Discussion

It is apparent that both landscape-scale and local-scale, or site-based, survey data are desirable when assessing risk to and providing high-parity records of archaeological earthworks. Whilst direct techniques were once thought to be more suited to interpretive and site-based survey, they cannot provide the density of data required to readily conduct condition monitoring or detect small features that should be recorded if the site is to be destroyed. Nor can they be practically applied to landscape surveys. Whilst datasets produced using mass-capture techniques provide landscape coverage because the data is captured remotely, with the exception of TLS (see Section 2.3.2), their ability to detect smaller features is dependent on a number of factors, not least data resolution. This latter point is not often in the control of archaeologists, who work with mass-capture data that has been produced for the purposes of another industry or discipline. An example of this would be the purchase of ALS data from the Environment Agency's Geomatics Group, who regularly produce ALS surveys across the UK for monitoring coastlines and regions that are particularly prone to flooding (Environment Agency 2014). Subsequently, the level of detail for extracting earthwork metrics may not be ideal, but it is all that may be available for a particular area. This is especially so if a feature has been destroyed prior to being recorded in any great detail. Although laser scanning has received a lot of attention from the archaeological community over recent years, particularly focusing on the identification of subtle earthworks, the commercial product has only been available in the UK since 1998 via the Environment Agency (2014). Therefore ALS does not have the time-depth available to facilitate the assessment of archaeological site evolution.

However, there is a large archive of stereo-aerial photographs within the UK that dates back to the 1940s, if not earlier, from which archaeologists could derive information similar to that of ALS using photogrammetry. Photogrammetry is the means by which 3D data can be extracted from SAPs, whilst the photogrammetric process facilitates the production of a digital surface model (DSM) from the photographs. Archaeologists have been reluctant to apply this technique to derive 3D data from stereo-photographs (see Section 2.2.3), despite their familiarity with

utility of SAPs. For example, Darvill and Fulton (1998) suggest that the identification and charting of change begins with an assessment of historic aerial photographs, which were produced in many regions of the UK from the early 1940s. By transcribing the horizontal extent of a monument from aerial photography over a period of five decades, from the 1940s to the 1990s, a crude, subjective but simple measure of change can be produced. To fully appreciate how the resource has diminished, however, a volumetric measure of change would be required, and the only way in which this can be achieved is with a dataset that facilitates the production of 3D data. The utility of SAPs for assessing landscape change has been identified by geomorphologists and surveyors (Adams and Chandler 2002; Walstra et al. 2004; Walstra 2006; Miller et al. 2008b), although their 3D properties have not been acknowledged by the archaeological community (Verhoeven et al. 2012a).

1.3 Summary

The rate of change to archaeological monuments and the sporadic nature with which some of these changes occur, make the monitoring of such factors problematic. Dramatic changes, such as those related to development and industry activity will destroy the archaeological resource at a much faster rate, although the planning stipulations placed upon wholesale destruction should ensure a record is made of a feature prior to its destruction. Natural processes of erosion and the anthropogenic activities that require elongated periods over which to damage and destroy archaeological remains are more subtle, thus providing the greatest challenge for recording techniques to detect these changes. Whilst unacknowledged deterioration of an upstanding feature degrades the resource and prevents its careful management, the situation degenerates should the archaeology remain unrecorded and subsequently destroyed.

To fully comprehend the agents of change acting upon the archaeological resource and anticipate their future evolution, a historic dataset is required with which to assess the development of change over time. It is impossible to create a high-fidelity record of every threatened feature prior to its destruction, the likelihood is that many have and will be lost before recording can take place. The effective management of a threatened resource or obtaining data about information that no longer exists is challenging. It requires the identification of a technique or techniques that both facilitates the detection and monitoring of change as well as providing suitable metrics for archaeological documentation

Whilst direct techniques have been and still are utilised by archaeologists for data collection, they generally provide sparse, 3D data densities for producing two-dimensional products. In recent years, however, the utility of dense, 3D datasets has been more readily acknowledged by archaeologists, and have been identified by Chapman, Adcock and Gater (2009) as enabling a more proactive approach to change management of the archaeological resource. As earthworks are not planar objects, 3D data is more capable of providing the metrics required to fully describe their form. Mass-capture technologies inherently produce 3D datasets and are

known for their ability to rapidly produce dense quantities of data over much larger areas, particularly when operated aerially. These techniques are described in Section 2.2 and 2.3. Historic SAPs are, in many cases, the only dataset that provides the temporal resolution required for reconstructing lost archaeological features and changes to them over the last 60 or 70 years. It is therefore imperative to assess whether DSMs extracted from SAPs using digital photogrammetric techniques can provide this information.

1.4 Contribution to Knowledge

Whilst archaeologists have long recognised the utility of SAPs for identifying earthworks and, in some cases, their decline, the application of photogrammetry to capitalise on the 3D data offered by this process has largely been ignored. Although historic aerial imagery in both vertical and oblique formats has been rectified by archaeologists to provide basic, 2D transcriptions of earthworks simply to identify them and place them into a Historic Environment Record (HER), far more can be achieved through photogrammetric restitution of archive SAPs. This research aims to clarify the extra benefits that digital photogrammetric techniques can bring to the archaeological community for the first time by comparing the datasets obtained through this process to existing archaeological surveys, which are used as the baseline datasets required by archaeologists. The outputs from the restitution of archive SAPs will also be compared to more modern topographic data from airborne and terrestrial laser scanning and SAPs to establish the quality of data obtained from archival imagery and the factors that affect them. It will therefore be possible to provide advice and guidance to archaeologists wishing to adopt this approach on the considerations for archive SAP use, the areas in which they can be successfully applied, and the type of archaeological data they can generate.

1.5 Aims and Objectives

1.5.1 Aim

The aim of this research is to assess the ability of archive stereo aerial photographs (SAPs) to reconstruct extant, damaged or lost archaeology and subsequently determine their utility to provide data that assists in the management and mitigation of loss.

1.5.2 Objectives

1. To review and critically evaluate survey methodologies currently in use by archaeology and other disciplines;
2. To review and identify how mass-capture techniques have been applied to the recording and documentation of archaeological earthworks;
3. Identify the errors inherent in mass-capture data which may influence the accuracy of archaeological data derived from these sources;
4. Design a workflow for processing archive SAPs using digital photogrammetry software;
5. Assess the 3D metric quality of DSMs produced using digital photogrammetry from which archaeological data will be extracted;
6. Evaluate the capability of archive SAPs to provide data for reconstructing extant, damaged or lost landscape archaeology;
7. Compare profiles and breaklines as derived from SAPs and other mass-capture techniques to traditional survey methods to determine benefits and drawbacks of applying mass-capture techniques for recording landscape archaeology;
8. Investigate the repeatability of SAPs and other mass-capture techniques to assess their wider applicability to other archaeological sites;
9. Evaluate the extent to which 3D mapping of heritage structures mitigates the associated effects of loss by providing a metric record of archaeological features;
10. Assess the results of objectives 3 through 8 and construct a list of considerations for archaeologists wishing to employ archive SAPs for earthwork reconstruction.

1.6 Structure of the Thesis

This thesis begins with a literature review (Chapter 1) that introduces the requirement for recording and documenting earthwork remains and other archaeological and heritage assets. Chapter 2 discusses mass-capture techniques, beginning with the role of aerial photography in the documentation process (Section 2.1), followed by the history of the technique's development that specifically examines military and Ordnance Survey assistance in providing APs for archaeological use. The role of key archaeologists who pioneered the use of APs for archaeological reconnaissance and mapping will be considered concurrently. Section 2.2 describes photogrammetry, beginning with the historical development of the technique followed by an explanation of the main photogrammetric principles and how the technique has been

applied by archaeologists and the heritage sector. This Section finishes by looking at issues relating to data quality and outputs from the photogrammetric process (Section 2.2.9). Section 2.3 outlines the technical principles behind airborne and terrestrial laser scanning before examining the archaeological and heritage applications of these instruments. Section 2.4 provides a summary to the chapter that further identifies gaps in the application of mass-capture techniques to archaeological recording.

Chapter 3 focuses on Digital Surface Models as it is the process of obtaining and processing datasets that will dictate how accurately archaeological analysis can be performed by using them. It is therefore necessary to have some understanding of where uncertainly and error can enter the data. The uses of DSMs for archaeological and cross-disciplinary purposes will be examined prior to highlighting the way in which errors can enter and accrue in a dataset as a result of creating them. The outcomes of each of these chapters will provide a basis for the choice of methods employed in this research, discussed below.

Chapter 4 outlines the methodology and the approaches taken to answer the aims and objectives of this research as listed in Section 1.4. Data collection and processing workflows will be discussed and are based upon the findings from the literature review, as are the methods and statistical tests that will be applied to assess the data produced by processing the SAPs. This Chapter will also describe the extant survey data for each of the chosen field sites that have been selected as representing the baseline requirement for archaeological survey content. The methods by which these will be compared to the data obtained from the SAPs, ALS, TLS and GNSS datasets will be explained, as it is the comparison of the more traditional requirements from archaeological surveys with the outputs from modern mass-capture techniques that will illustrate the benefits that photogrammetry and laser scanning can provide.

Chapter 5 is a technical appraisal of the photogrammetric process that begins by developing workflows for the photogrammetry software and the analytical procedure for DSMs created by it (see Section 5.1). A number of factors known to influence the quality of photogrammetric DSMs are analysed to assess their potential influence on the results that will be extracted from the archive SAPs, prior to conducting the pilot and transferability studies in Chapters 6 and 7.

Chapter 6 presents the Pilot Study field site, Flowers Barrow, as the initial region over which SAPs and other techniques have been tested. Flowers Barrow hillfort and its terrestrial hinterland provide a stable field site that has not been significantly altered over the period for which SAPs are available to facilitate this assessment. This allows for the DSMs extracted from the SAPs to be tested against other, more modern methods, such as ALS, TLS and other ground-based technologies for their ability to produce metrically accurate results. Breaklines and profiles have been extracted from each epoch and compared to those depicted by a hachure survey, inclusive of profiles, conducted at Flowers Barrow by the Royal Commission on the Historical Monuments of England (RCHME) in 1970. As this is the only survey to exist of the Hillfort prior to the data created for this research, the 1970 hachure plan is representative of the baseline dataset required for recording such a monument. The comparison of data extracted

from SAPs with that from the 1970 survey indicates the suitability of each epoch of archive SAPs for reconstructing archaeological earthworks.

Chapter 7 describes the Transferability Study field site, Eggardon Hillfort and environs, which was chosen to increase the variety of earthworks on which SAPs could be assessed as well as validate the findings from the Pilot Study results. Eggardon Hillfort also presents the opportunity to examine the differential erosion caused by ploughing, as the northern half of the interior has lost the surface expression of its earthworks due to post-World War II agricultural activity, whilst the southern section has remained protected by the ownership and stewardship of the National Trust. As before, the DSMs extracted from the SAPs to be tested against other, more modern methods, such as ALS, TLS and other ground-based technologies for their ability to produce metrically accurate results. To establish their suitability for reconstructing archaeological earthworks, breaklines and profiles are extracted from the DSMs of each SAP epoch, the TLS and as collected with the GNSS and compared with the 1952 RCHME data of the Hillfort interior (as well as data from the NMP), which represents the baseline requirement for archaeological survey at this site.

The Discussions in Chapter 8 will summarise the results from each case study to examine what role archive SAPs can play in the reconstruction of archaeological earthworks and in providing a historical perspective on how archaeological landscapes have altered over the last six or seven decades. The factors that affect the quality of data obtained from SAPs will be discussed and the impacts upon the applicability of photogrammetric restitution to the future of archaeological survey will be discussed. The conclusions and further work identified by this research are then given in Chapter 9.

2 MASS CAPTURE TECHNIQUES

Chapter 1 introduced the threats facing archaeological earthworks, the conservation principles and charters that advocated pre-damage and loss documentation, and the survey tools used to achieve this, including aerial photography. This Chapter introduces mass-capture techniques, namely aerial photography, digital photogrammetry and laser scanning and their application by archaeologists.

Section 2.1 focuses on aerial photography, it application by archaeologists, the historical development of the technique, and the archives in which this resource is held. Section 2.2 outlines the history of photogrammetry prior to discussing its archaeological applications. Important concepts and the generic workflow stages of photogrammetry are described before providing a discussion of its limitations. The final Section (2.3) introduces airborne and terrestrial laser scanning as alternative mass-capture technologies and describes the theory behind their operation, before discussing their applications by archaeologists and heritage professionals. The Chapter ends with a discussion (Section 2.4) of the issues surrounding the application of mass-capture methods in archaeology.

2.1 Aerial Photography

This Section examines the current applications of archive SAPs to recording archaeological earthworks (see Section 2.1.1) and the methods that are used to interpret the information that is extracted from them (see Section 2.1.2). The history and development of aerial photography will be examined, including advancements made with aeroplane and camera technology, without which archaeologists would not benefit from the unique viewpoint of SAPs (Section 2.1.3). An overview of the archives that hold SAPs will be provided to illustrate the wide distribution of these datasets (Section 2.1.4) before closing this Section with a Conclusion (Section 2.1.5).

The application of aerial photography for archaeological prospection and mapping has been in use for over a century. It is a well-established technique that is actively practiced, developed and researched today, both nationally and internationally. Vertical aerial photography is particularly useful for mapping purposes and the collection of overlapping imagery within the UK to create stereo-aerial photography, or SAPs, for this purpose dates back to World War II. Although the development of aerial photography pre-dates WWI to some degree, the realisation and advancement of the technique for archaeological use would not have survived were it not for the keen RAF officers who were curious about the earthworks they could see from their aircraft (Wilson 2000). Archive SAPs thus provide nearly 70 years of historic photography that, in many instances, is the only record of archaeological earthworks that have subsequently been damaged and destroyed.

2.1.1 Archaeological Applications of Aerial Photography

The most familiar applications for aerial photography in archaeology are arguably prospection and mapping. O.G.S. Crawford is universally credited with developing the methods for using aerial photography to identify and record archaeological features from the air, whether they are upstanding earthworks or what can be described as proxy indicators i.e. crop and soil marks. Crawford's career is described in detail in Section ?, but it was his position as an aerial observer during WWI that developed his appreciation for the different perspective aerial photography offered, particularly as it was used to map enemy trenches and earthworks. This experience subsequently laid the groundwork for a future career with the Ordnance Survey, where Crawford utilised aerial photography and survey in the field, undertaken by him and others, to transcribe details of archaeological earthworks onto OS mapping products.

Due to the temporal richness of the historic aerial archive, archaeologists have been able to visually assess the effects of change upon the archaeological resource. Keevill and Linford (1998) note that within the three decades prior to their publication, ploughing has degraded the gardens and house at Hamstead Marshall in Berkshire, now visible as parchmarks and soil marks in APs. The authors state that it is essential to know and understand how plough damage has affected the site if it is to be considered as a part of future site management initiatives that would consider the long term preservation of archaeological features threatened by plough damage. Subsequently, they consider whether enough of the remains are still extant to facilitate a reconstruction of the original features.

There is evidently a requirement to investigate the potential of historic SAPs to assist in the reconstruction process, particularly as this may be the only opportunity with which to extract any metric information from upstanding features that are now damaged or destroyed. In an article published by English Heritage (Anderton and Went 2002), the loss of ridge and furrow systems in Northamptonshire was examined. By consulting historic maps to determine the original extent of these field systems and subsequently comparing this value to the number identified from aerial photography of the same region, the rate of destruction was revealed. Unsurprisingly, during the 20th century, the decline of these features had been rapid, and attributed to the effects of reverting ridge and furrow, that were often managed as grasslands, for use as arable lands once more, but subjected to modern farming methods. The majority of destruction had been found to occur in the most recent decades. Rowley and Wood (2008) note the effects of intensified agricultural practices on deserted villages (DVs), of which 75% of identified DVs in APs taken during the 1960s in Herefordshire had either been damaged or destroyed by the 1980s.

2.1.1.1 The National Mapping Programme

In many respects, the work of the National Mapping Programme (NMP) echoes the work that Crawford began in the 1920s as regards the mapping of archaeological features from aerial photographs. The NMP was initiated in the 1980s after a series of successful pilot projects were undertaken in counties across England, during which workflows and methodologies for extracting mapping information from aerial photographs was developed (Horne 2009). The NMP began in earnest in the early 1990s, employing both English Heritage staff as well as those from county councils across the country to undertake the huge task of mapping England's historic landscape. The imagery that is used for this purpose dates back to 1945, when the RAF first started to produce aerial photography for mapping purposes, beyond what was required for the military.

Photography from a number of other sources, such as local and county councils and the Ordnance Survey are also examined, from which baseline data is created by documenting the earthworks visible in the imagery as well as any obvious soil and crop marks. Air photograph interpreters also utilise other sources of information, such as historic mapping, to identify what the earthwork may represent and its function within the landscape. This information is also recorded and appended to the identified archaeological feature. To extract mapping information from the APs, the photographs are rectified using software known as 'AERIAL' and then imported into AutoCAD from which the archaeological information can then be transcribed. Another method of transcription utilises permatrace, the results from which are then digitised in AutoCAD and entered into a database. The scale of the mapping produced from APs is usually 1:10,000 and the accuracy of the measurements is stated to be ± 5-15m (Small 2002, p.11). The data from a particular NMP project is subsequently provided to the local or county council in the mapped region for inclusion in their Historic Environment Records (HERs).

The data obtained by the NMP from APs is utilised for making informed planning decisions as well as managing and preserving archaeology within the defined project area (Royall 2011). The process of completing an NMP always results in bolstering the local or county HER, which are usually bereft of up-to-date information regarding the archaeology within their care, and do not represent a full picture of this resource. As an example, the NMP had mapped 40% of England by 2009, which resulted in a 50% increase in the number of identified sites (Horne 2009). Evidently there is still a long way to go before the remainder of England is completed, as shown in Figure 2.1, but the work undertaken by the NMP is vital for establishing the extent of the archaeological resource so that it can be more effectively managed and preserved. Inevitably, if a feature has not been identified, it cannot be protected or measures formulated to mitigate for its loss.

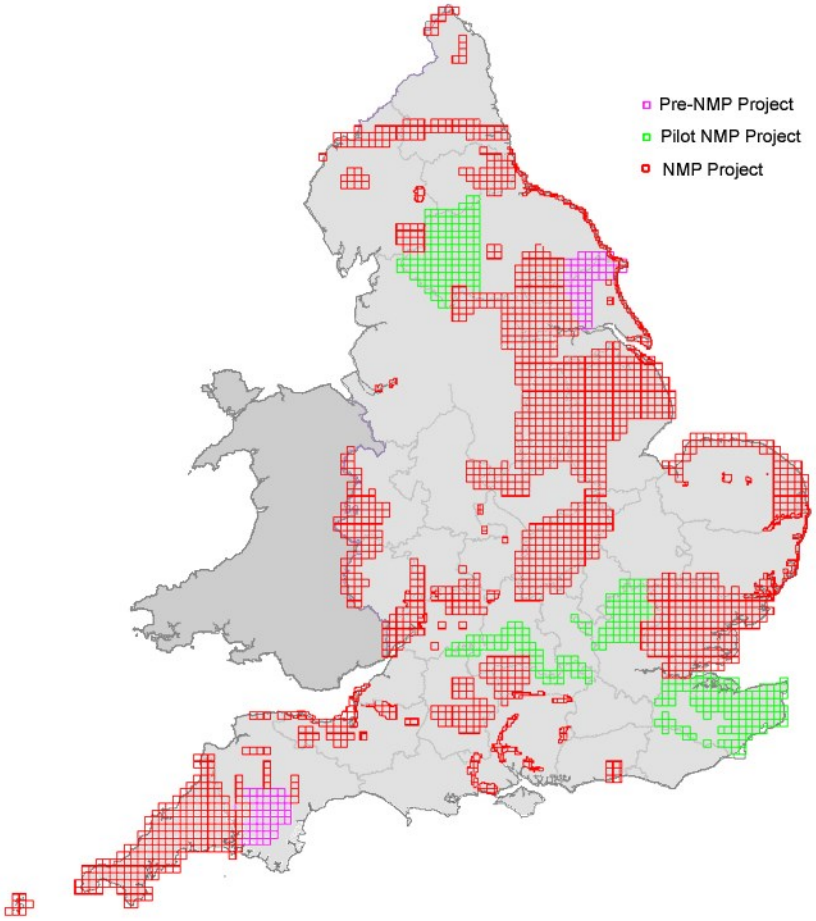

Figure 2.1: NMP Progress Map from January 2008 from Horne (2009).

2.1.1.2 Prospection

It should be noted that ongoing aerial reconnaissance for detecting archaeological features in the landscape has been and still is practiced. Historic imagery can only go so far in identifying archaeological remains, particularly when the identification of ephemeral features such soil marks is often dependent on a number of conditions being met at the same time. Weather conditions, geology and the time of day all affect the appearance of an earthwork that was once an upstanding feature but has since been ploughed or levelled only to appear infrequently. This is why regular reconnaissance flights are still required and why some archaeologists have turned to exploiting spectral data for prospection purposes. By employing multi- and hyper-spectral imagery for prospection purposes, archaeological features with spectral signatures that exhibit themselves in the non-visible wavelengths are more likely to be detected. This type of imagery is often obtained from satellite sensors or, more infrequently, airborne sensors, the latter of which produces higher resolution datasets. Satellite data is cheaper to acquire, which explains its popularity with the archaeological community, and the resolution of the imagery continues to improve. However, in comparison with its airborne counterpart, satellite datasets produce lower resolution data and are only suited for prospection purposes rather than

obtaining detailed transcription data. As the resolution of imagery deteriorates, the chances to detect smaller features disappear and thus prospection tends to occur at a landscape-scale. The factors influencing the formation of soil and cropmarks are shown in Figure 2.2.

Cropmarks, on the other hand, do appear in panchromatic images, such as the historic and modern APs. Cropmarks appear when crops grow differentially over buried archaeological features. Crops that are planted where a buried negative feature exists tend to grow taller as they are healthier, due to the higher moisture and nutrient content in the soil (Beck 2011). Such features tend to represent back-filled earthworks i.e. ditches and post-holes, which also allow crop roots to extend deeper into the soil. Crops that are planted over buried positive features, such as a wall or foundations, tend to be shorter and look unhealthy (Beck *ibid.*). However, the appearance of cropmarks are also affected by the geology of a region and appear more readily in free-draining soils, such as those in chalk environments, where a lack of water i.e. during summer drought conditions, causes stress in crops. Clay environments retain moisture more readily and thus do not exhibit crop-stress unless drought conditions are extreme. To try and capture as much information about these ephemeral features as possible, English Heritage, the Royal Commission on the Ancient and Historical Monuments of Scotland (RCAHMS) and the

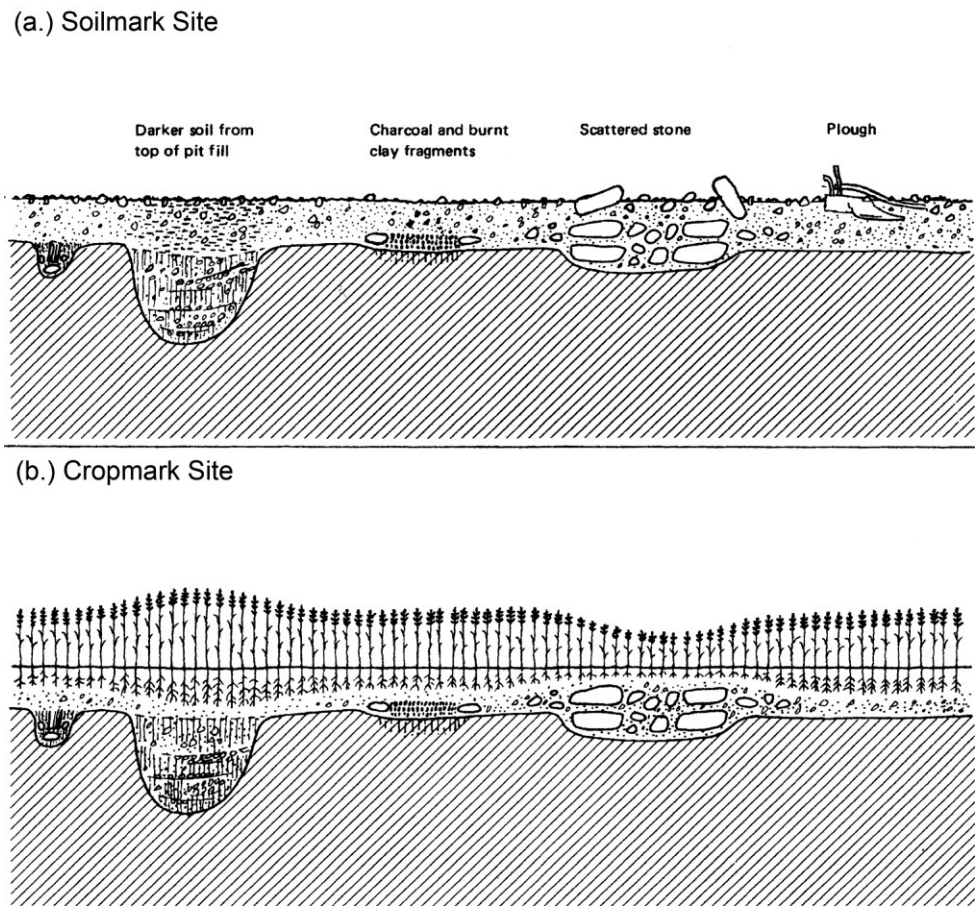

Figure 2.2: Factors leading to a.) soilmark and b.) cropmark formation taken from Green (2002 p.63).

Royal Commission on the Ancient and Historical Monuments of Wales (RCAHMW), all undertake aerial reconnaissance surveys every year.

2.1.2 Interpretation

Whilst aerial and satellite imagery can reveal upstanding and ephemeral earthworks and features in the landscape, archaeologists do have to interpret what they see in the data. When archaeologists are responsible for planning a flight and taking photographs of a landscape, they are already beginning the process of interpretation. They are limiting the area of their survey, which introduces bias to the collection process, and also an element of subjectivity too, as each archaeologist may approach this task in a subtly different way. Finally, they have to interpret the information contained within the imagery they gather, the results of which will depend upon their perception of the archaeology and their experience. Examples of the mapping conventions and data transcriptions from SAPs are shown in Figure 2.3. However, this facet of aerial reconnaissance does not go unnoticed in the archaeological community, particularly amongst aerial archaeology practitioners. Cowley and Gilmore (2005) draw attention to the narrative style Crawford used in his publications, in which he describes the decision-making processes he used to collect and interpret the archaeological information contained within the imagery. Subsequently, this approach allows other to identify where any of Crawford's biases may have crept into his work. Other forms of bias are discussed by Wilson (2005), who notes that archaeologists can focus their aerial surveys on 'honeypot' areas, where archaeology is plentiful and in particular where cropmarks, soil marks and parchmarks are most likely to be found. Familiar routes are also noted by Wilson (*ibid.*) as preferred due to the difficulties caused by requesting airspace access in particular areas: for permission to enter, the archaeologist must be specific about the route they wish to take through this airspace. For the purposes of transparency, each aerial survey must have a pre-defined objective that explains the reasoning behind conducting the survey in the chosen area.

Cowley and Gilmore (*ibid.*) state that when survey processes are described, the focus tends to be on the technical aspects of the techniques being used, rather than the "perception, experience and cognition" of the surveyor or interpreter extracting information from the dataset. The authors argue that extracting the required information from a survey dataset is a subjective process, whether consciously acknowledged or not, and naturally different people will create slightly different end products from the survey, despite being asked to achieve the same goals.

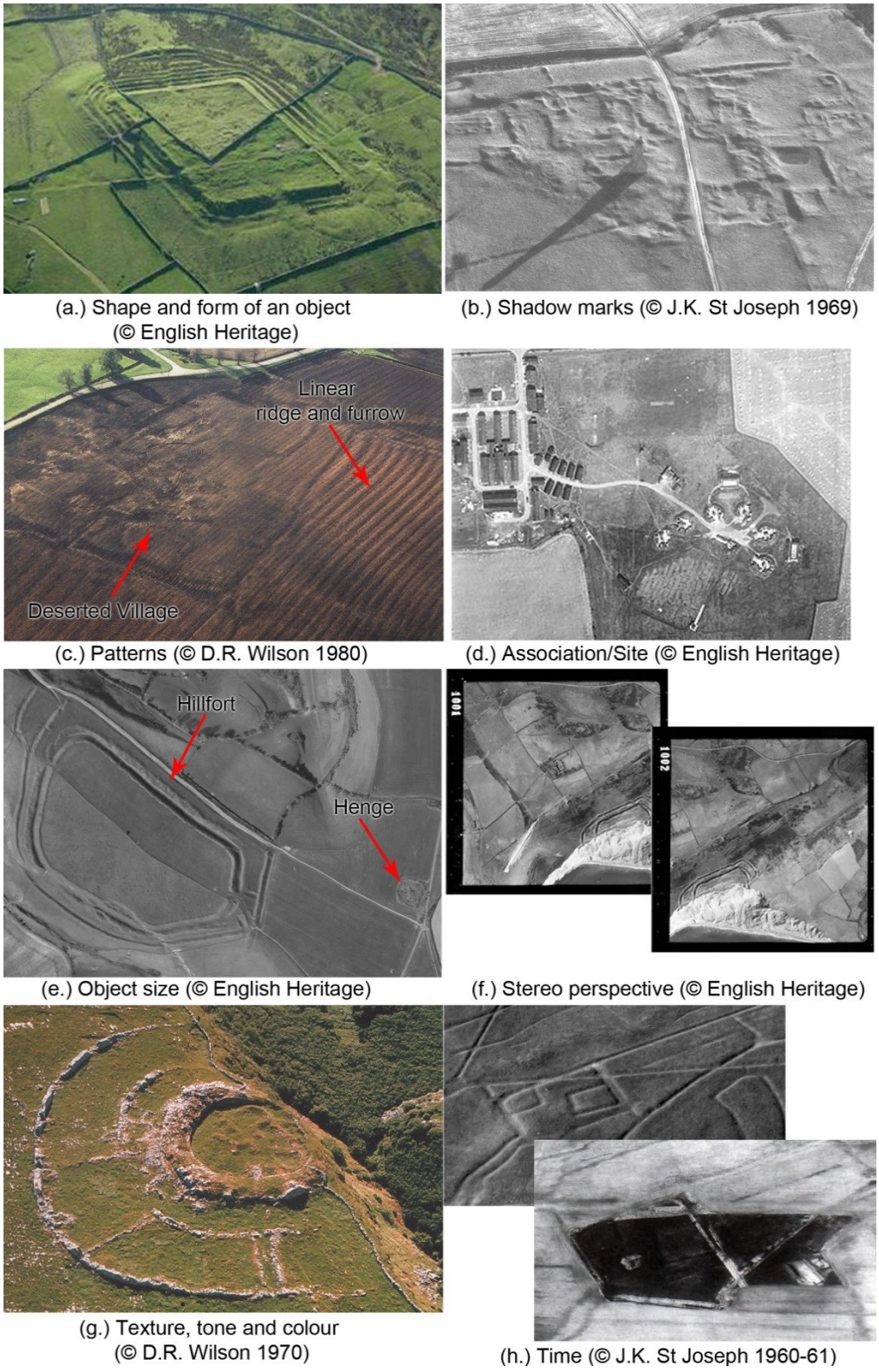

Figure 2.3: Elements of air photo interpretation for archaeologists, based upon those listed by Lillesand et al. (2008 p.191-195).

This is an in-escapable fact and cannot be separated from the objective processes that occur when employing hardware and software to facilitate the production of a survey at any stage of the process. There will always be an element of subjectivity about survey, and not just aerial survey at that.

However, what can be said for the work of aerial archaeologists is that they are working with a technique that is approximately a century old, and thus the processes involved in collecting and examining APs are understood. It is also recognised that there are two types of aerial photography that each bring slightly different benefits to the process of archaeological interpretation: vertical and oblique imagery (see Figure 2.4). Oblique photography is favoured by archaeologists, who usually prefer to collect their imagery in this way when undertaking their own surveys. It can be easier to see topographic variations in the landscape, including those of subtle features, particularly when the imagery is captured at the beginning or the end of the day, when light from the sun rakes across the terrain. However, these images are not well suited to the production of survey data because of the perspective distortion introduced due to the angle of photography to the subject, and thus it is difficult to georectify. It is the archaeologists themselves who usually capture the imagery during a flight and thus it is certain they contain sites of archaeological significance.

Vertical aerial photography, however, has been and still is generated by survey and commercial companies with objectives other than archaeology in mind. Many historic and modern vertical photographs are held by a number of repositories across the UK, which are outlined in Section 2.1.4. Archaeologists are therefore faced with the challenge of identifying the regions in which they are interested in and requesting the corresponding imagery from a particular archive or archives for examination. It is often harder to identify archaeological features in the landscape by using a single vertical image due to the perspective, although this situation changes when a stereo-pair of images are viewed using a stereoscope. The 3D effect enhances the appearance of the topography and any upstanding archaeology within the imagery, from which

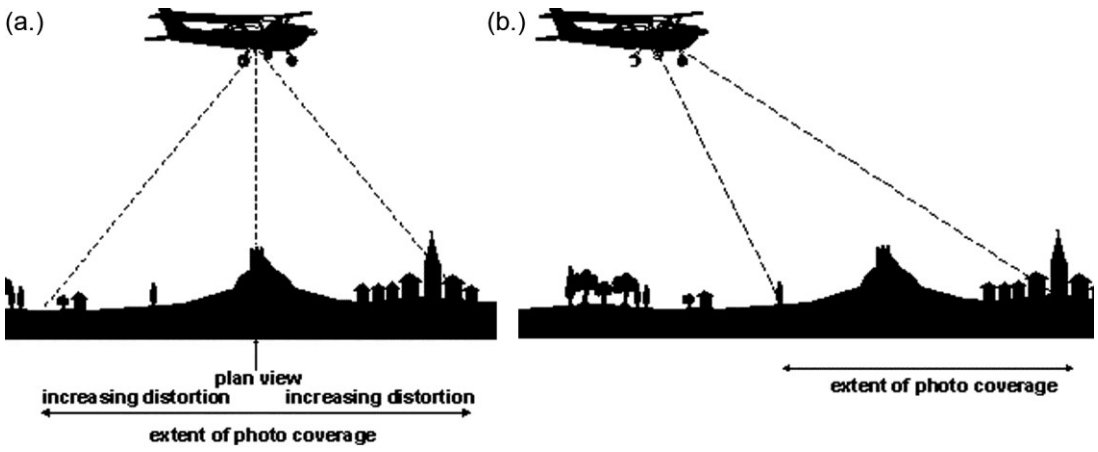

Figure 2.4: Diagram illustrating (a.) Vertical and (b.) Oblique aerial photography (Deegan 1999).

archaeologists can make interpretations as well as transcribe data. What archaeologists have not readily adopted is the process of photogrammetry from which to obtain orthorectified imagery and DSMs, which can be utilised for creating maps and plans.

In 1985, Jones (1985) stated that archaeological recording mechanisms were inefficient and expensive, after which he stressed the need for a low-cost alternative, namely photogrammetry, from which to plot upland sites. At this time, the photogrammetric techniques that were available, as discussed in Section 2.2.2, would have required the expertise of a skilled operator as well as large investment in complicated machinery which would have discouraged many archaeologists. However, since the advent of digital photogrammetric solutions in the form of software that runs on a personal computer (PC), it is surprising that this has not encouraged the uptake of photogrammetry for producing data products that are of great utility to archaeologist, namely orthophotographs and DSMs. Whilst they rely on simply rectifying the photography they use, as is the case for the NMP, the metric data they extract cannot be used for anything more complicated than simply indicating the basic shape and extent of a feature. It is acknowledged that this is the remit of the NMP, to identify archaeology to ensure that it is cared for appropriately and thus rapid methods are necessary for achieving this gigantic task. However, once their current remit has been achieved, it would be of utility to identify whether photogrammetric techniques can be applied to historic SAPs for generating a number of other archaeological datasets.

2.1.3 History and Development

The history and development of aerial photography, including its uptake and exploitation by archaeologists, has been covered in detail by Barber (2011). For descriptions of the RAF's role in gathering aerial photography for reconnaissance and mapping, see Nesbit (2003) and Brookes (1975), or Owen and Pilbeam (1992) who describe the role of the Ordnance Survey in developing these methods. MacDonald (1996) focuses on the collection of aerial photography for the Department of Overseas Survey, which indicates the potential to expand archaeological air-photo interpretation activities to other countries.

2.1.4 Archives

Due to the huge number of aerial photographs that have been collected, both in the past and during the present day, there are a number of repositories across the UK that store various AP collections. As stated by Walstra (2006 p.65) identifying and acquiring APs is a time consuming procedure because they are distributed across a number of these repositories. For those who wish to examine the holdings of each archive, some provide online catalogues whilst others require that an online form is submitted identifying the area of interest. Most archives provide

information relating to whether they hold the original plates or film, or in some instances only the prints. The cost of scanning these materials is sometimes advertised, if indeed this service is offered, but for more specialist requests, such as photogrammetric scanning, it is worth making a specific query. The major archives that hold APs are described below.

2.1.4.1 The National Monuments Record (NMR)

The NMR is stated by English Heritage (English Heritage No Date-b) to be the largest public archive of vertical and oblique aerial photography in England, consisting of historic imagery captured by military and commercial organisations alike. The NMR collection contains APs created by the RAF and Ordnance Survey from 1945 onwards (English Heritage *ibid.*), the National Rivers Authority and others, as well as the photography currently produced by the Aerial Survey Team at EH. Hall et al. (2003) provided an overview of the AP collections in the NMR, stating that around 2.5 million photographs were held here as of 2003, but the collections will have grown since then.

A selection of one of the most important collections housed at the NMR is from Aerofilms Ltd, which is stated by the 'Britain From Above' website (Britain From Above No Date) to "include the largest and most significant number of air photographs of Britain taken before 1939". During its operational lifetime, Aerofilms Ltd acquired two further AP collections, namely AeroPictorial (1934-1960) and Airviews (1947-1991), before being amalgamated with Simmons Mapping (UK) in 2001. The company subsequently became known as Simmons Aerofilms, who themselves were acquired by Blom ASA, a Norwegian survey company, in 2005. Blom sold the entire Aerofilms collection in 2007 to English Heritage, the Royal Commission on the Ancient and Historical Monuments of Wales (RCAHMW – see Section 2.1.4.3) and the Royal Commission on the Ancient and Historical Monuments of Scotland (RCAHMS – see Section 2.1.4.2). EH is responsible for archiving the entire collection of negatives, as well as photograph albums and their associated documents (English Heritage No Date-a), whilst the albums containing regional coverage of Wales and Scotland are held by their respective heritage bodies.

The Aerofilms collection contains imagery from across the UK and consists of 1.2 million negatives taken between 1919 and 2006, comprising of glass plates and film negatives, and more than 2000 photo albums (Britain From Above No Date). These images depict a wide range of natural and anthropogenic landscape types, detailing the changes that occurred country-wide since 1919, making this resource invaluable for management can change studies. However, a number of images from the collection could not be easily identified, prompting EH, RCAHMW and RCAHMS to create the 'Britain From Above' project to help address this issue. By securing funds from the Heritage Lottery Fund, The Foyle Foundation and other donors, a website was launched in July, aiming to engage the public to both identify some of the locations that are hitherto unidentified as well as share their memories of the areas covered by the APs

(English Heritage No Date-a). In total, 95,000 APs are being scanned to produce digital copies of the oldest and most valuable negatives in the Aerofilms collection, which are then made available online for the public to download and interrogate on their own computers. The 'Britain From Above' project is due to complete in 2014.

The NMR provides an online enquiry form for requesting information relating to their AP holdings, for which an OS grid reference and placename are required. The results will include information relating to the date the image was taken, its scale, focal length of the lens, format, and whether the negatives are held. Arrangements can be made to view the imagery, although this does not include the original film: only the prints can be examined and, if they do not hold prints of a particular negative, then the image cannot be seen at all prior to making a purchase.

2.1.4.2 Royal Commission on the Ancient and Historical Monuments of Scotland (RCAHMS)

The RCAHMS is home to the National Collection of Aerial Photography (NCAP) and is one of the largest historic aerial photography archives in the world, with holdings estimated to be in the tens of millions (NCAP No Date-a). The NCAP holds imagery from across the globe, consisting of declassified military images to those created for non-military uses, dating back to WWII (NCAP *ibid.*), although APs from England, Wales and Ireland are held by archives maintained by each country. In 2008, NCAP subsumed the photography held by the Aerial Reconnaissance Archive (TARA) that was held at Keele University for 45 years (NCAP 2008). The major role of NCAP is to care for the images held in the archive that all require preservation and this is undertaken when a particular collection of prints or negatives are to be digitised. Prior to scanning, dust is removed from the surface of the material and any tears or scratches are repaired. Once scanned, the materials are replaced, either in their original containers or provided with new ones if these have deteriorated (NCAP No Date-b). It is interesting to note that the photography from WWII was often washed and/or fixed inadequately, and thus the preservation state of these images is fragile (NCAP *ibid.*).

The methods used to digitise imagery and produce master copies of each image are dependent on the material, with the NCAP staff identifying the most appropriate procedures to use. These procedures are based on "national and international standards and practices for digital capture, metadata, storage, preservation and access" of aerial photographs (NCAP 2012). In-house photogrammetric scanners or high-resolution flatbed scanners are available, or materials can be photographed using medium or large format digital cameras if a more rapid copy of an image is required. The NCAP also holds aerial microfilm. Many of these images are geo-located so that potential customers and researchers can download NCAP holdings, in the form of a Google Earth KMZ file, for a particular location or country to enable the identification of appropriate materials for their work. However, where this information is not available online because the imagery for the area in question has yet to be scanned, then a search request has to be

submitted, although these searches are not free. However, if the researcher can visit the public search rooms, which are based in Edinburgh, then they can perform their own search for no fee. Clear guidelines are given by the NCAP as to what information they require to perform a search and they also provide an example report, which contains a selection of the imagery that has been requested for the customer to view, presumably before placing a full order for the photographs.

2.1.4.3 Royal Commission on the Ancient and Historical Monuments of Wales (RCAHMW)

The aerial photographic collections of Wales are held by the Central Registry of Air Photography Wales, situated at the Aerial Photographs Unit in the government offices in Cardiff and The National Monuments Record of Wales (NMRW), located in Aberystwyth. In total, the AP collection is stated to hold over 500,000 vertical and oblique photographs taken by the RAF, Ordnance Survey, Aerofilms and others, as well as those created by the Aerial Reconnaissance Team of the RCAHMW (RCAHMW 2007-a). The RAF and Ordnance survey collections consist of mainly black and white vertical images, with those from the RAF dating from the late 1940s to the 1960s, and those from the OS produced between the 1970s and 1980s (RCAHMW 2007-b). There are over 14,000 images in the RAF collection and approximately 84,000 from the OS, providing extensive coverage of Wales (RCAHMW *ibid.*). As covered in Section 2.1.4.1, the Aerofilms collection is shared across three of the UK's main heritage bodies, namely EH, the RCAHMW and the RCAHMS (RCAHMW 2010), according to location.

The imagery produced by the RCAHMW's own Aerial Reconnaissance Team dates back to 1986 (RCAHMW 2013), when the RCAHMW began to produce its own imagery, right up until the present day, and consists of oblique photographs, taken with either black and white or colour materials (RCAHMW 2007-b). There are some 35,000 images within this particular collection, which continues to grow as new imagery is created. However, this particular collection is archaeological in nature and has been undertaken since 1986 to identify new archaeological sites as well as monitor and record known sites and landscapes. As a part of their present day practice, the RCAHMW undertakes aerial monitoring of 600 scheduled ancient monuments for the Welsh Government's heritage body, Cadw, each year for documentation purposes as well as the monitoring of their condition for effective management (RCAHMW 2013). Flights are undertaken to photograph sites and landscapes in a variety of lights, i.e. dawn to dusk, and seasons, ensuring that both subtle and ephemeral features are more likely to be detected.

2.1.4.4 Local Government

In 1945 the RAF began the National Air Survey to photograph the majority of the UK to assist in map revision, planning and development schemes. The photography was generally taken at a scale of 1:10,000 and took just under two years to complete (Le Pard 2011), with organisations such as Norfolk County Council (NCC) and Dorset County Council (DCC) now holding copies of this imagery. As it stands, NCC has 8,300 photographs from this period, although they do not cover the entire county, due to the effects of cloud obscuring the landscape or camera failure (Norfolk County Council 2012), and because the initiative was terminated prior to its completion (Hall et al. *ibid.*).

Le Pard (2011) states that many local government bodies and councils commissioned their own aerial photography subsequent to the RAF survey because of their utility for mapping and planning purposes. NCC commissioned a commercial company to produce an aerial survey of the entire county in 1988 to coincide with large-scale development in the region and thus provide an up-to-date series of vertical images at a scale of 1:10,000 (Norfolk County Council 2012). Although the OS was collecting vertical aerial photography across the county on a repeated basis, back in the 1980s it was not refreshed as quickly as it is today, requiring some County Councils to commission their own surveys. However, NCC advertised the imagery for sale to the public and organisations such as the District Councils, University of East Anglia and Anglian Water (Norfolk County Council 2012).

2.1.4.5 Cambridge University Collection of Aerial Photography (CUCAP)

The CUCAP is a large collection of aerial photography, consisting of nearly 500,000 images in both oblique and vertical format, taken with black and white, colour and infra-red film (University of Cambridge 2014). The basis for the CUCAP began in 1947 when J.K. St Joseph undertook aerial reconnaissance work for Cambridge University, which produced photography all over the UK (Wilson 2000). The archive also holds imagery from France, Denmark and The Netherland, all of which can be searched for online.

2.1.4.6 Commercial Companies

There are a number of commercial companies throughout the UK who can be commissioned to fly a sortie for bespoke aerial photography or who generate photography for generic mapping on a regular basis. Ordnance Survey is arguably the most well-known UK-based agency, who currently refreshes approximately 25% of UK mapping each year, equating to 60,000 to 70,000 km (Ordnance Survey 2010). To achieve this objective, ground-based survey techniques are

used in conjunction with digital aerial photography, which is captured by the OS as well as external contractors. Both the ground and aerial survey products are processed using photogrammetric software to create a number of OS mapping products, including the OS MasterMap topography and imagery layers (Ordnance Survey 2010).

Other companies that have offices within the UK are Fugro, Blom ASA and Getmapping Plc. Fugro-BKS Ltd. and Fugro Geospatial generate digital mapping data from aerial photography as well as a number of other information sources. The company creates orthophotographs, 3D models and vector maps from aerial imagery to meet the requirements of a number of industries, using photogrammetric techniques. Fugro-BKS currently provide older aerial photography to Bluesky International Ltd. for inclusion in their online historic imagery database, oldaerialphotos.com (OldAerialPhotos 2010). Bluesky International Ltd. is a dataset repository for a number of remote sensing products whilst also creating their own data, including aerial photography. Blom ASA is a Norwegian company that dates back to 1919 and continues to specialise in creating aerial photography for a number of applications (BLOMASA 2012). The current camera system used to create their imagery is the digital Vexcel UltraCam, which has also been adopted by other companies, such as Getmapping plc. Whilst Getmapping provide the facility to search for older imagery on their company web pages, Blom ASA do not.

2.1.4.7 The National Association of Aerial Photographic Libraries (NAPLIB)

Although NAPLIB no longer exists as an organisation, having ceased in 2008, the main activity of the organisation was to produce a directory of aerial photograph collections and companies within the UK (Aslib 1993). This publication was known as the 'NAPLIB Directory of Aerial Photograph Collections in the United Kingdom'.

2.1.5 Conclusion

The collection of aerial photography that was taken by the RAF, USAAF and Luftwaffe provide archaeologists with an excellent and unparalleled record, not only of the UK landscape but in numerous other countries, that spans more than a century. How our landscapes have been utilised and changed has been captured, detailing how military operations have altered the towns, cities and countryside in times of need. They have also served as a record to the changing face of the UK as post-war expansion saw urban areas grow rapidly and increased mechanisation and intensive farming alter the landscape (Barber *ibid.*).

As a tool for both archaeological prospection and mapping this body of images is unparalleled, but within the UK there are a large number of archives that store this vast body of historical imagery, which can make the research and identification of such datasets a daunting task.

However, many of these archives have an internet presence and have developed methods by which potential users can establish what coverage is available in a particular region. It is unfortunate that any document charting the history of care is not provided with such imagery that details the life of the negative or print from 'field to finish'. It is also unfortunate that many SAPs have not been held with their camera calibration certificates, and thus no specific information relating to the quality of the imagery can be determined. As will be explained in Section 2.2.6, this lack of information can complicate the process of extracting metric data from SAPs, although it does not preclude it.

2.2 Photogrammetry

2.2.1 Introduction

This section examines the development of Photogrammetry and introduces the main principles of operation. The process of undertaking photogrammetric restitution will then be described before looking at some of the applications of the technique. A summary of the photogrammetric software currently available will be provided before concluding with a discussion on the limitations of the technique.

Photogrammetry can be defined as "the art, science and technology of obtaining reliable quantitative information about physical objects and the environment through the processes of recording, measuring and interpreting photographic images" (Thompson and Gruner 1980). A variety of techniques exist to extract measurement information from photographs that are taken with a degree of overlap, which are known as stereo-pairs. As with laser scanning, applications of this technique can be split into aerial and terrestrial categories, which are also known as topographic and non-topographic respectively. Terrestrial photogrammetry may also be referred to as close-range photogrammetry.

The process of extracting metric data from a stereo-pair or a series of overlapping imagery, known as a strip (if the imagery is collected in a line) or block (if the imagery consists of a series of strips) (Figure 2.5), has until recently been a rather convoluted process requiring specialist technology with which to process the imagery. However, in recent years, the invention of digital workflows has reduced this complexity and made the technique more accessible to non-specialists, particularly as consumer-grade digital cameras are capable of providing high-quality photographs for photogrammetric analysis. An example workflow for extracting data from a digital photogrammetric workflow is given in Section 4.4.1 (Figure 4.7).

The datasets that can be extracted from a photogrammetric survey range from point data and DSMs to linework and orthophotography, and thus the technique is extremely versatile. However, the drawbacks associated with data extraction from photogrammetry stem from its passive nature: sufficient light is necessary to produce a high-quality exposure, and thus

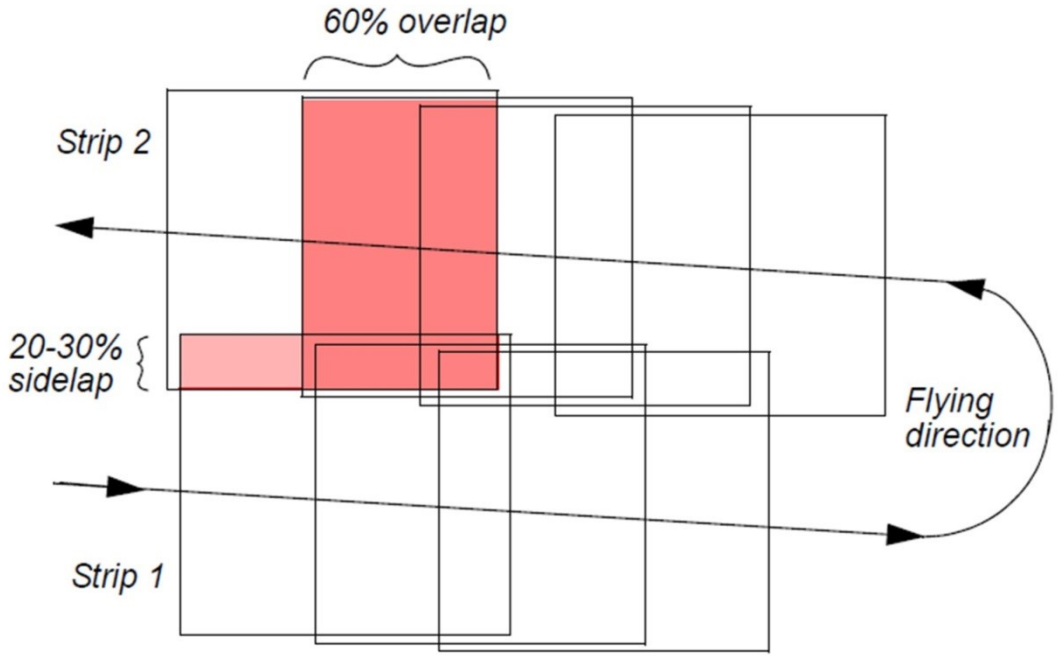

Figure 2.5: Diagram showing the required overlap between images along a strip (60%) and with a subsequent strip (20-30%). More than one strip of images forms what is known as a 'Block' (ERDAS Inc. 2010).

photogrammetric survey cannot be undertaken at night, nor can it be conducted aerially if there is dense cloud cover, which will obscure the object to be photographed. Unlike ALS, the presence of vegetation will prevent the survey of obscured topography. Where photogrammetry is superior over ALS and TLS is the rich textural detail the imagery captures of a subject or an area. Although TLS systems generally contain cameras, they are seldom of the quality necessary for anything other than general orientation around the dataset.

2.2.2 History and Development

There are four main stages in the development of photogrammetry, cited by Konecny (1985) to be Plane Table Photogrammetry, Analogue Photogrammetry, Analytical Photogrammetry and Digital Photogrammetry.

2.2.2.1 Plane Table Photogrammetry

Developed and applied between 1850 and 1900, the principle of this technique is stated by Albertz (2001) as being able to record "any object point which has been identified in two (or more) convergent images could be plotted in the ground plan". This method was used by

Prussian architect Albrecht Meydenbauer to produce condition surveys of historic buildings. It was also utilised to produce topographic mapping of the border between Canada and Alaska by Canadian surveyor Eduard Deville. Whilst instrumentation during this period did not advance rapidly until WWI, the geometric principles of relative orientation were identified by a Bavarian scientist, Professor Sebastian Finsterwalder (Walker and Alspaugh 2013). The first stereoscope that allow measurements to be extracted from a stereo-pair appeared in 1896 and was created by the Canadian surveyor, Edouard Deville, who named it the Stereo-Planigraph (Walker and Alspaugh, *ibid.*).

2.2.2.2 Analogue Photogrammetry

Konecny (*ibid.*) states that the analogue period for photogrammetry occurred between 1900 and 1960. It was during this period that the aeroplane was invented and aerial photogrammetry developed rapidly. In 1921, the first universal analogue plotter was invented in Germany by Reinhard Hugershoff, and was called the Autocartograph (Walker and Alspaugh, *ibid.*), capable of working with both terrestrial and aerial stereophotography. Despite various advances in mechanical-optical instruments within this period that facilitated the production of more accurate surveys from aerial photography (Walstra 2006), instruments for close-range photogrammetry were slow to develop.

2.2.2.3 Analytical Photogrammetry

From 1960 to 1985, analytical photogrammetry developed (Konecny, *ibid.*), predominantly due to the invention of computers that replaced some of the optical and mechanical components of the analogue systems. By 1957, a scientist based at the National Research Council, Canada, called U.V. Helava introduced the first analytical system at the International Conference on Aerial Triangulation in Ottawa (Blachut 1995). Computer hardware and software facilitated the use of complex mathematics to extract terrain coordinates from stereo-pairs of images, utilising mathematical concepts that had long since been developed (Wolf and Dewitt 2000). As computers became more advanced, the mapping processes were quicker to solve, as were the calculations involved in analytical applications, but still required human input to guide the floating mark within the stereo model. Eventually, further information could be introduced into the analytical procedure through developments such as the *reseau* plate (see Section 2.2.2.5 below) for creating reference marks on an image (for performing interior orientation), and auxiliary orientation sensors for providing information relating to the position of the imaging device and accompanying data relating to object space measurements (Walker and Alspaugh,

ibid.). This information allowed the mathematical calculations undertaken by analytical photogrammetry to account for the systematic and stochastic factors affecting each stage of the process (Walker and Alspaugh, *ibid.*). Analytical systems are still in use today and, as stated by (Wolf and Dewitt, *ibid.*), generally require information about the camera system used to produce the photographs, measured photo-coordinates and ground control.

2.2.2.4 Digital Photogrammetry

Digital photogrammetry software began to appear in 1985 (Konecny, *ibid.*) and continual advancements in computing hardware and software have continued to this very day with the aim of creating a fully digital, largely automated, workflow. Walker and Alspaugh (*ibid.*) infer that developments in remote sensing platforms forced the advancement of photogrammetric techniques to adapt to the demands of digital imagery, which was computationally intense to process and analyse. Scanners that could convert analogue imagery into a digital facsimile further allowed the automation of photogrammetric processes and in many ways simplified the technique and made it more accessible.

Due to the adoption of digital imagery, image processing routines could be employed to automate some of the manual and laborious tasks undertaken by photogrammetric operators, such as the identification of tie points (see Section 2.2.7.3) with which to identify identical features across a large number of images. Subsequently, image matching algorithms were created to complete such tasks in a matter of seconds, facilitating a more efficient workflow and removing the tedium that once faced an operator who had to manually identify and mark many of these features. As limited input is required from the user, they are no longer required to have extensive experience with the technique in order to extract useful results, unlike analogue and analytical methods (Chandler 1999). There was also an expectation of cost saving because of the ease with which digital products could be transferred between different systems (Hassani and Carswell 1992). This has facilitated the uptake of photogrammetry by non-expert users, of which archaeology is one discipline that has made use of the digital toolkit (see Section 2.2.3).

2.2.2.5 Development of Metric (mapping) Cameras

The sophistication of aerial camera design has advanced significantly from their first use a century ago. Aerial cameras are now equipped with numerous elements that reduce or negate distortion of the imagery and photographic lenses have developed to provide high resolving power such that details in the imagery are clearer, and produce minimal distortion (Wolf and Dewitt 2000).

In the late 19th Century astute practitioners, such as Edouard Deville, noticed geometric errors in photographs taken during their surveys, with Deville establishing a laboratory in 1910 to calibrate his terrestrial camera (Clarke and Fryer 1998). During WWI, the photographic pioneer, Sherman Mills Fairchild, developed the between-the-lens shutter system to reduce image distortion in aerial photography (Centre for Photogrammetric Training no date). Aerial camera calibration did not occur until after WW1, however, with Canada implementing calibration in 1920 (Clarke and Fryer *ibid.*). The United States also began calibration at around the same time, with the National Bureau of Standards (NBS) undertaking this activity on the behalf of other government agencies (Clarke and Fryer *ibid.*).

Critical to the development of photogrammetry was the concept of defining the image plane, which is the interior orientation of the film in relation to the camera and lens. One means of achieving this is the use of a *reseau* plate; a glass plate with a regular grid of precise index marks etched upon it (Figure 2.6a). The coordinates of these index marks, which appear as cross-hairs when the film is exposed (see Figure 2.6b), must be established precisely via calibration. These coordinates not only allow the orientation of the film to be calculated in relation to the camera and lens, but also to correct any subsequent distortion in the film or print. These benefits aside, *reseau* are a hindrance to both the production of orthophotographs, as they either obscure objects in the photo map or have to be removed, and automatic image matching for the generation of DSM (see Section 2.2.7.3).

In contrast, fiducial marks, namely index marks whose locations are also calibrated but are only placed around the edge or corners of the frame (Figure 2.7a and b), permit interior orientation without creating additional distortions or hindrance to orthophotography and automatic image matching. One of the first mentions of a camera system that employed fiducial marks was a terrestrial system designed by Meydenbauer in 1867, which utilised glass plates (Alberz 2001).

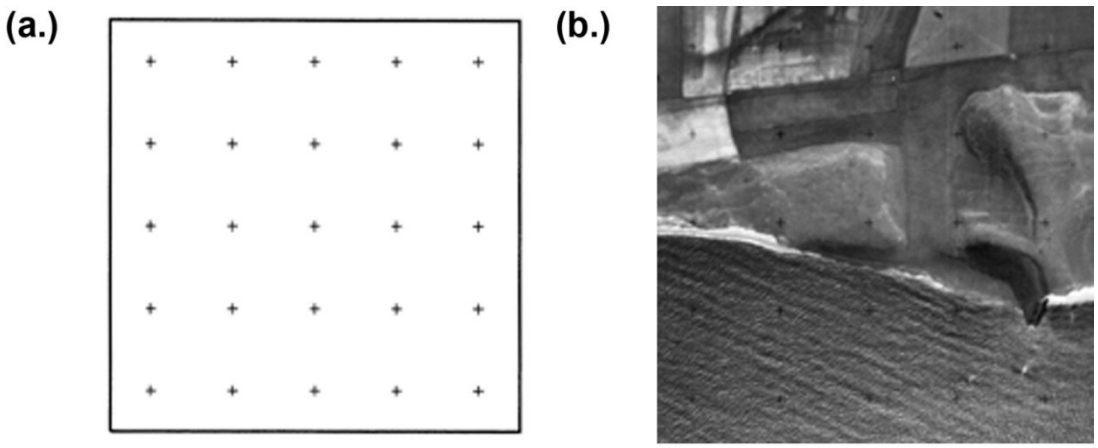

Figure 2.6: (a.) Sketch illustrating the layout of index marks in a grid pattern on a reseau glass plate, (b.) Example of index marks on exposed film (in this case a scan of a negative) resulting from a reseau.

An example of an early, relatively crude fiducial mark from an F24 camera is shown in Figure 2.7c. Fiducial marks on F52 and later cameras, such as the F95, are very similar. Such fiducial marks were not created with rigour and were poorly calibrated, if at all.

Film formats and lens combinations advanced during WWII to create larger scale images. At the beginning of the war, F24 cameras were producing 1:48,000 scale photographs, which were not sufficient to provide the amount of detail required by the PIs for analysis. By 1942 the F52 camera had been developed and, when fitted with a 36in lens, produced a photo-scale of 1:8,000 with the aircraft flying at 24,000ft above ground level (AGL) (Brookes 1975). The F52 had a 500-exposure magazine and thus it was possible to complete an entire mission without running out of film and having to repeat the sortie to capture more photography (Brookes *ibid.*). By mid-1944 the F52 had been modified to prevent image blur during low-level, large-scale photography (Brookes *ibid.*). This modified camera was known as the F63 and was fitted with an 'Image Motion Compensation' (IMC) system that kept the film moving (Brookes *ibid.*). Further

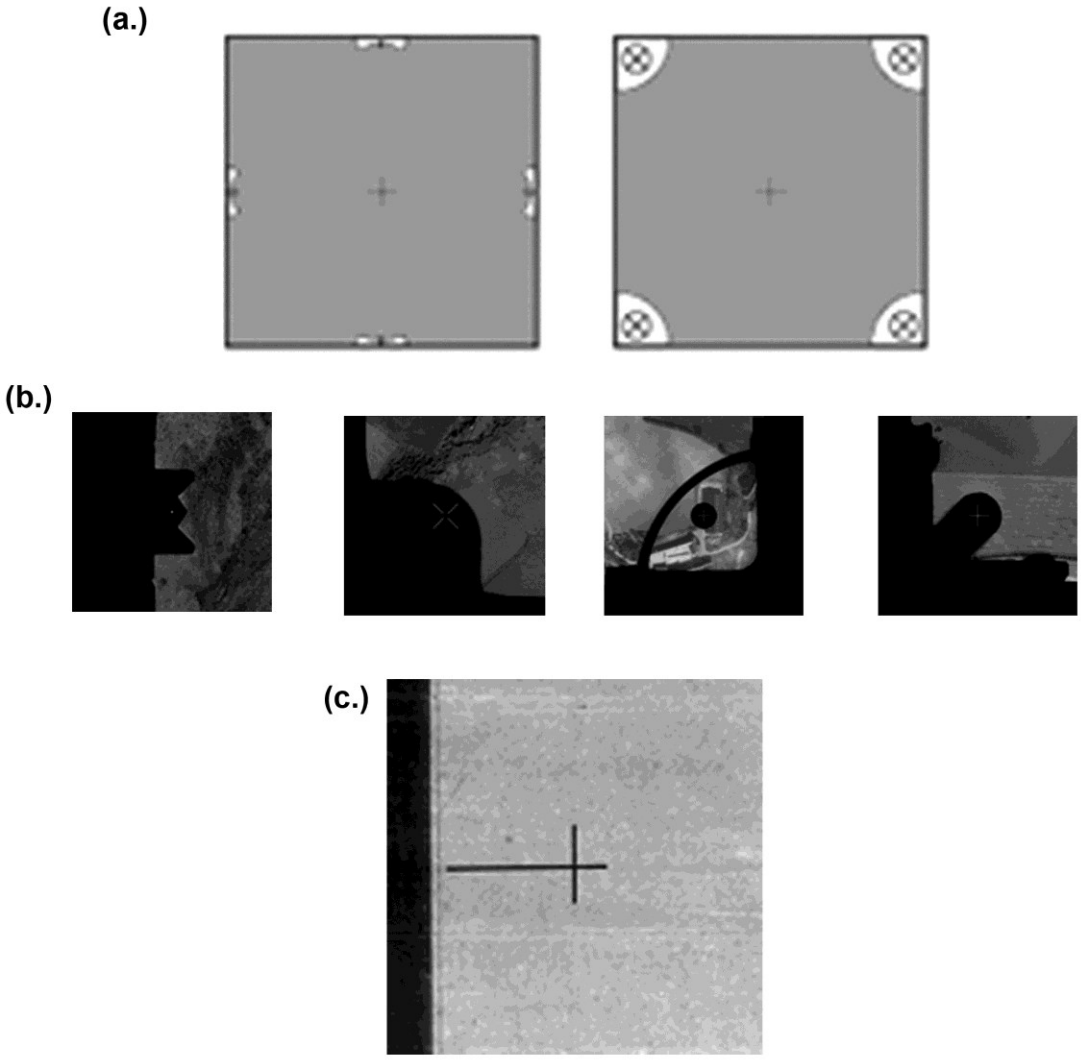

Figure 2.7: (a.) Sketch illustrating typical fiducial mark locations around the image frame. At left are edge-fiducuials and at right are corner fiducials, (b.) Examples of fiducial marks from metric cameras. At the extreme left is an example of an edge-fiducial, the remainder being corner-fiducials, (c.) Crude edge-fiducial, typical of F24 and F52 non-metric cameras.

developments in IMC resulted in cameras designed for low level, oblique photography, such as the F95.

The calibration of a metric film camera also accounts for any distortion in the film plane, although in a frame aerial camera the film is effectively flattened by adopting one of four techniques, as listed by Wolf and Dewitt (*ibid.*):

1. Applying tension to the film during exposure;
2. Flattening the film against a focal plane sheet of glass;
3. By forcing the film against the platen by applying air pressure into the airtight camera cone;
4. By using a vacuum plattern against which to flatten the film (see Section 2.2.6.1 Figure 2.12).

Digital camera calibration differs slightly from its film-based counterpart. The silicone CCD chip in a digital system stays flat and is effectively distortion free (see Section 2.2.6.1 Figure 2.25). Each pixel is, in effect, a fiducial mark as it is assumed to be part of a perfect grid pattern in the rectangular CCD array, although in reality Wolf and Dewitt (*ibid*.) state that the positions may depart slightly from this assumed arrangement.

Lens distortion is a further consideration and occurs when the path of light rays deviate when travelling from object to image points, subsequently shifting the theoretical location of the image point to a different location (Ray 1999). This deviation from the true position of the image point is caused by imperfections in the manufacture and alignment of the lens system and must be quantified in order to subsequently be corrected (see Section 2.2.7.1 Figure 2.16). Such distortions are usually calibrated against a two-dimensional array of illuminated collimator targets, the angles between which are well known (Figure 2.8). The differences between these angles and those projected in the focal plane result in an array of vectors (Figure 2.9), which describe symmetric radial and decentring lens distortions, which combine to describe the lens distortions listed in a *camera calibration report,* together with the calibrated focal length and calibrated coordinates of the fiducial marks/*reseau* grid. Such reports are usually printed on a few sides of paper, making them easy to mislay or accidentally dispose of, resulting in few surviving that relate to archive aerial photography. In these instances digital photogrammetry offers a solution in the form of self-calibration using multiple photographs of the same target taken from the same camera, as is the case with SAPs.

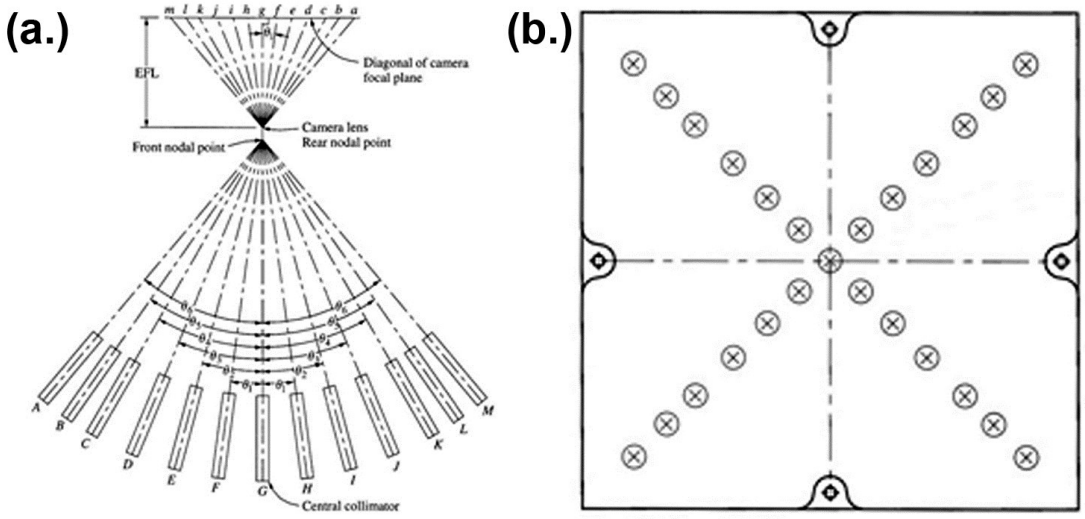

Figure 2.8: Plan (a) and frame view (b) of illuminated collimator targets (in this case in the form of an X), between which the difference in angles are used to measure lens distortions (modified from Wolf & Dewitt, 2000).

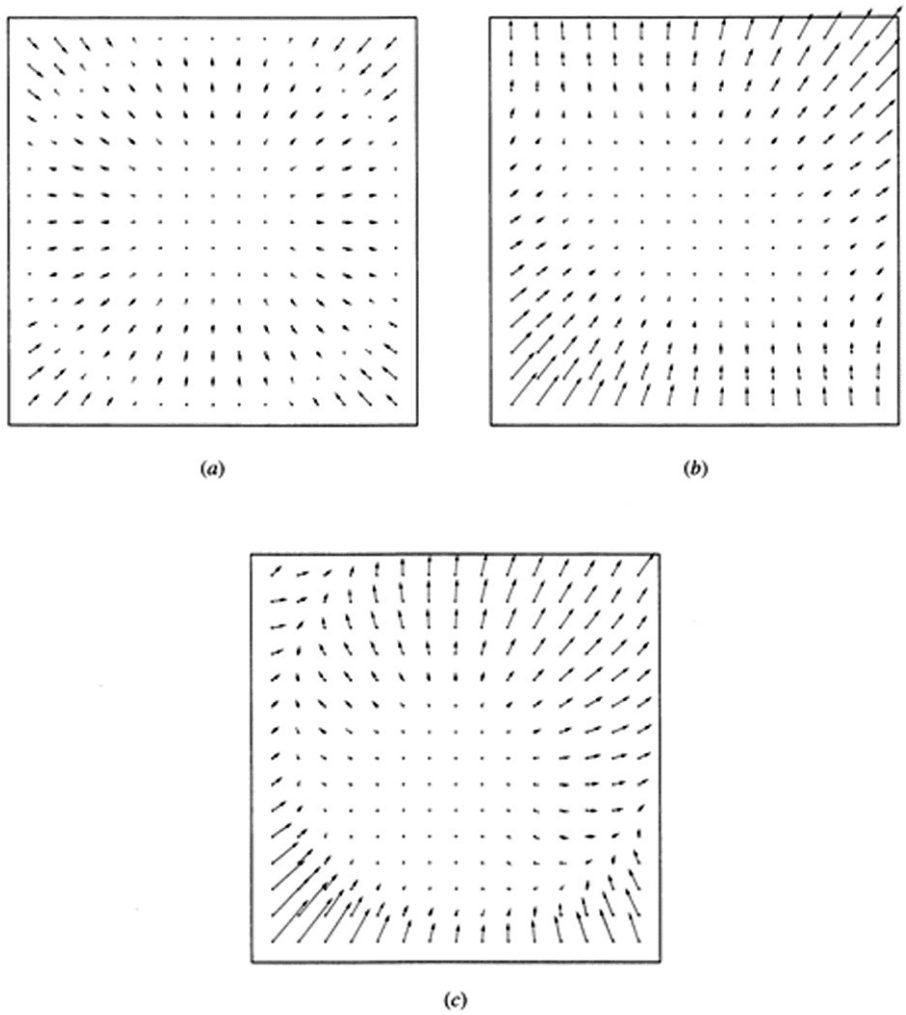

Figure 2.9: Lens distortions described as vectors, where a) is symmetric radial; b) is descentering; and c) are the combined distortions (Wolf & Dewitt, 2000).

2.2.3 Archaeological Applications of Photogrammetry

Photogrammetry can be split into airborne and terrestrial applications, much like laser scanning (see Section 2.3), and there are many examples of the application in the archaeological and cultural heritage disciplines. Terrestrial photogrammetry tends to be utilised for the survey of historic buildings and smaller artefacts, whilst aerial photogrammetry is useful for providing DSMs and orthophotography for GIS applications. Overall, photogrammetry is a well-established technique, useful for the extraction of metric data (Bedford and Papworth 2009; Núñez Andrés and Buill Pozuelo 2009) and for providing a high-resolution texture map of its subject. Thus it is also useful for image analysis purposes, proving its importance as a flexible, multi-product technique.

Terrestrial archaeological applications range from documenting excavations (Doneus and Neubauer 2003; Orengo 2013), documenting underwater shipwrecks and their associated cargo (Canciani et al. 2003; Seinturier et al. 2004; Drap et al. 2007), recording historic landscapes and buildings (Lambers et al. 2007; Yastikli 2007; Remondino and Menna 2008; Al-kheder et al. 2009; Bedford and Papworth 2009; Salonia et al. 2009), assessing structural damage to buildings (Fujii et al. 2009) and deformation of artifacts (Robson et al. 2004), and the documentation of engravings and rock art (Chandler et al. 2007; Garcia-Lázaro et al. 2012). In many cases, photogrammetry of the built environment is generally undertaken by architects, surveyors and academics who have better access to the requisite technologies and their associated skill-set. This technique has been, and still is, extremely popular in the cultural heritage documentation arena, based on its tried and tested ability to provide flexible outputs, which are often the foundation for analysis subsequent to capture, such as degradation detection and monitoring, survey drawings prior to conservation or restoration projects, anti-disaster mapping (Dallas et al. 1995) and the provision of textured 3D models for museum exhibition or reverse-engineering initiatives (Cooper et al. 2006; Remondino and Menna 2008; Salonia et al. 2009).

Aerial photography is a well-established, well understood tool in the archaeological discipline, with archaeological transcription from rectified aerial photography forming one of the largest uses of this data (see Section 2.1.1). Archaeological features are commonly mapped from 1:10000 scale imagery, recording the shape, size, form, location, date and monument type of any sites identified in the photographs (Bewley 2003). This activity is the basis for the National Mapping Programme (NMP), which was instigated by English Heritage in the early 1990s (see Section 2.1.1.1). The examination of archival aerial photography is said by Wilson (2000) to be the only way to combine information from a number of photographs to facilitate the interpretation of the landscape as a whole. However, photo-rectification does not remove distortions in the imagery, particularly in hilly or mountainous areas, as the process does not account for errors in the photographic materials, such as film flatness, lens distortion, camera tilt, varying ground height and, if using contact prints, paper stretching (Wilson *ibid.*).

Beyond photo-rectification, archaeologists have employed photogrammetry for a variety of uses, such as the generation of DSMs for landscape and GIS applications (Neubauer 2004; Lambers et al. 2007; Colosi et al. 2009; Corns and Shaw 2009), and the creation of earthwork hachure plans (Stone and Clowes 2004). Aerial photography that is specifically captured for archaeological use is often limited to oblique photographs of a landscape taken from a light aircraft using a small or medium format digital camera (Wilson 2000, p.33; Brophy and Cowley 2005). Very rarely is an aircraft commissioned to capture stereo-photography for archaeological purposes, as in the example from Stone and Clowes (*ibid.*). The stereo-aerial photography used by many archaeologists have come from the RAF, Ordnance Survey or other private companies, as discussed in Section 2.1.4, which have not been captured specifically for archaeological mapping purposes. In recent years, however, the release of low-cost photogrammetry software in combination with the increased popularity of unnmaned aerial vehicles (UAVs) and low-cost, consumer-grade digital cameras has seen an uptake by the archaeological community to produce their own aerial imagery (Chiabrando and Spanò 2009; Eisenbeiss and Sauerbier 2011; Mozas-Calvache et al. 2012).

Low-cost Photogrammetry and Structure from Motion (SfM)

As previously discussed there is often a requirement to obtain an aerial perspective of a site or feature for optimising the perspective of an archaeological site or excavation, which is only achievable through using a variety of low-cost techniques. Archaeological researchers have utilised balloons (Celikoyan et al. 2003; Colosi et al. 2009; Verhoeven et al. 2009; Chiabrando et al. 2010; Verhoeven 2011), unmanned aerial vehicles (UAVs) and blimps (Lambers et al. 2007; Gomez-Lahoz and Gonzalez-Aguilera 2009), kites (Blake 2010; Bogacki et al. 2010) or a form of elevated frame (Poulter and Kerslake 1997; Chiabrando et al. 2010) to obtain aerial perspectives. In many cases, low-cost photogrammetric software and consumer-grade digital cameras have been used to generate products from these projects, which has been a pleasing development over recent years, making the technology financially more accessible to archaeologists and non-experts (Canciani et al. 2003; Bryan and Chandler 2008; Gomez-Lahoz and Gonzalez-Aguilera 2009; Sanz et al. 2010; Barazzetti et al. 2011).

The conception of low-cost photogrammetric software is nearly 20 years old and was identified by Pollefeys et al. (2000) as a useful tool for obtaining 3D textured data of archaeological buildings and sites. Since then, the technique has burgeoned rapidly, and has been applied to the recording of inscriptions and rock art (Hullo et al. 2009; Plets et al. 2012), building recording (Hullo et al. 2009; Koutsoudis et al. 2013), aerial photography (Verhoeven 2011; Verhoeven et al. 2012a), excavation documentation (Ducke et al. 2011; De Reu et al. 2013; Dellepiane et al. 2013; Olson et al. 2013; De Reu et al. 2014; Stal et al. 2014), orthophotograph production (Verhoeven et al. 2012b), archaeological artefacts (Koutsoudis et al. 2013; Olson et al. 2013), and for public presentation (Ducke et al. *ibid.*). In a small number of papers, the use of low-cost

photogrammetry and SfM by volunteers has been described (Bryan and Chandler 2008; McCarthy 2014), which has been facilitated by the automation of complicated photogrammetric processes. Bryan and Chandler (*ibid.*) state that their approach to recording archaeological features, which in this instance was rock art, reduced labour-costs although, more importantly, it empowered local people and helped to encouraged them to care for and monitor their local history. This approach is also a requirement by ICOMOS (ICOMOS General Assembly 1996), who encourage community engagement.

It is heartening to note that many archaeologists who have employed the SfM technique for archaeological documentation purposes have also compared their results with other survey technologies to establish the metric performance of SfM (Plets et al. 2012; Verhoeven et al. 2012b; De Reu et al. 2013; Koutsoudis et al. 2013; Green et al. 2014; McCarthy 2014). Only Verhoeven (2011) has attempted to assess the ability of SfM to process archive SAPs using SfM software with a stereo-pair of photographs taken over Adriatic Italy in the 1960s. However, the results the author presents are not accompanied by empirical comparisons with other datasets and thus it can only be inferred that the visual results of the DSM from the SfM software package were convincing. Subsequently there is a need to further assess the ability of SfM for processing archival SAPs against other techniques, including the higher-cost photogrammetric packages, to determine their utility. This is particularly so as James and Robson (2014) discovered that SfM software can generate 'erroneous radial distortion estimates' and error statistics for a DEM, based upon the methods used by the software to perform camera calibration. Although the authors state that their results are tested upon imagery taken from a UAV, they highlight the relevance that their work also has upon terrestrial applications.

McCarthy (*ibid.*) states that the original, high-cost photogrammetry software was still highly specialised and expensive to use when it was first released in the 1990s. Subsequently, the author is hopeful that SfM will now be widely adopted by the archaeological and volunteer communities due to the minimal training required to generate an output and the reduction in time required on-site because of the rapidity of the image-capture process for the technique. On the one hand this approach is laudable as SfM can be an efficient means of data capture and the cost of SfM can be massively reduced if open-source software are utilised. However, whilst low-cost, rapid surveys may be desirable for commercial archaeological units, this approach cannot override the requirements of a survey, and the most appropriate tool for the job should be selected irrespective of cost, within reason. McCarthy (*ibid.*) states that the SfM "technique is essentially scale-independent", which provides a false impression that a large number of photographs can capture every requisite detail of a subject. This is compounded by a further statement from McCarthy (*ibid.*) that there is "minimal preparation required" for "ad-hoc recording". These sweeping generalisations give the impression that archaeological surveyors are desirous of a quick and easy method of survey that does not require the careful planning associated with other techniques, which could be construed as unprofessional and haphazard. It also contradicts the desire of many archaeologists to undertake a more considered approach to their surveys that facilitates interpretation of the archaeology as a survey progresses.

2.2.4 Influence of the Geographical Disciplines in Photogrammetric Adoption

Yet again, it is the geographic disciplines that provide interesting ideas for consideration by archaeologists interested in examining change to the archaeological resource. Airborne and terrestrial photogrammetry have been applied to the mapping of landscape change, in particular coastal erosion (Adams and Chandler 2002; Gulyaev and Buckeridge 2004; Lim et al. 2005; Miller et al. 2008a; Lim et al. 2010), and landslide modelling (Walstra et al. 2004; Walstra 2006; Walstra et al. 2007). The challenges of using older aerial imagery to reconstruct changing landscapes have also been recognised (Walstra et al. 2011).

Miller et al. (2008b) have developed a surface matching routine for disparate sets of current and historic photography and scan data, based on the difficulties of working with the rapidly changing nature of some coastlines, highlighting the challenges of conducting regression studies in such environments. Matching older imagery to more recent data may be difficult or impossible if a surface has very few distinguishing features or surface texture (Fryer et al. 2005) or there is insufficient overlap between subsequent datasets, stated by Miller et al. (2008b) to be due to geohazard activity and vegetation change. Despite this apparent obstacle, it is possible to process a block of aerial stereo-photographs that cover a wider area and propagate control points that can be collected in the terrestrial hinterland, in unchanged areas, to provide enough information to generate a DTM.

Where distinctive features in the terrestrial hinterland do exist, archive stereo-aerial photographs may be of utility in constructing a time-series of events relating to the evolution of a site. Walstra (Walstra et al. 2004; Walstra 2006; Walstra et al. 2007) successfully processed a series of SAPs at two field sites to examine past landslide dynamics. Ground control was collected using a GNSS system and used to process the historic imagery and, subsequently, their accuracy was assessed using information provided by the processing software and by visual inspection. In his thesis, Walstra (2006) states that DEMs from another source should be used for comparative purposes to assess the quality of the DEMs output from the SAPs, although the author did not achieve this during his research. Despite Walstra (*ibid.*) demonstrating the ability of archive SAPs as a means of generating DEMs and orthophotography, they have not been examined for their ability to provide a method for recording and reconstructing archaeology that has been and is at risk, damaged or that has been destroyed, and not necessarily by coastal processes. These datasets therefore need to be tested to examine the suitability of the resolution provided by SAPs to discern whether it is good enough to extract archaeological metrics. Subsequently, the question as to whether the data quality of SAPs is comparable or better than other survey methods must also be addressed.

Kennie and McKay (1987), with reference to Thompson (1962), state that photogrammetry is an appropriate technique to use when there is uncertainty relating to the desired end-product. This may be the case when producing a record for the purposes of preservation (see Section 1.1.2). As with laser scanning, it is also a non-contact method of recording, removing the need to come into contact with fragile structures, or features in hazardous environments. The imagery and

associated survey files can also be archived for processing at a later date, although this does assume that the imagery is in an archive-stable format and that data migration will also take place as technologies develop, particularly if the imagery is digital. The archival advice for laser scanning data is still in its infancy (Austin and Mitcham 2007), unlike photogrammetry (ICOMOS General Assembly 1996; Eppich and Chabbi 2007; Bryan et al. 2009). If the survey framework for photogrammetric data capture is created for optimal resolution of a subject, re-processing of the imagery can be undertaken to provide varying level of detail when required. This cannot be achieved with laser scan data as the point density at capture cannot be increased post-survey, except by interpolation methods, which can introduce inaccuracies into the data. Photogrammetric processing methods are also becoming faster and, as a result, extracting the requisite data from them is becoming easier, which is highlighted by the uptake of such methods by the volunteer community.

2.2.5 Summary

Whilst photogrammetry has been regularly applied to recording architectural heritage, it has not been widely adopted for landscape archaeology and producing earthwork measurements, with few notable exceptions. As the disappearance of these features has been accelerating since WWII, it is surprising that no concerted effort has been made to try and quantify this loss, with the exception of a very rudimentary attempt by Darvill and Fulton (1998). The authors produced a census and condition survey of the archaeological resource in the UK to assess survival rates. This could only be achieved by employing a sampling strategy to estimate the magnitude of the problem and aerial photography was utilised to identify causes of change and its extent, albeit by assessing changes in monument area. This helps to provide some idea of the damage that has been wrought but change does not happen in 2-dimensions, and the only way to extract 3D data is by employing photogrammetry.

2.2.6 Photogrammetric Concepts

There are a number of important and detailed concepts that explain the various aspects of the photogrammetric process, which are outlined in this Section. These concepts can be separated into a number of steps, beginning with the formation of an image within a camera system. The next stage is processing this imagery in photogrammetric software, within which there are a number of mathematical concepts that describe it performs restitution i.e. establishes a relationship between the camera parameters, the photo and ground coordinates (Walstra 2006). Section 2.2.7 subsequently provides a description of the practical workflows and various stages of data input that employ these principles to generate a solution.

2.2.6.1 Image Formation

The photogrammetric process starts with the basics of image formation in a camera system, whether it is a film or CCD-based sensor. For photogrammetric purposes, light travels in a straight line from an object, through the camera lens to be finally recorded by the sensor in the camera, which forms the image plane. In this way a detailed image is built up of an object or area, consisting of image points from a great number of light rays that each enters the lens at a different angle. However, the basics of photogrammetry are more simply explained by Mitchell (2007) using an example of just a single light ray, which has been referred to by the author as the 'chief ray', as shown in Figure 2.10. Mitchell (*ibid.*) states that if this ray is thought of as travelling in the opposite direction i.e. from the image plane and towards the object, this can be useful, as the ray will travel for an unknown distance but at a fixed angle that is relative to the camera. Subsequently, if positional and orientation information relating to the camera is available, a 3D location for the chief ray can be established (Mitchell, *ibid.*). If two images of a single object point have been produced from two different camera positions, then the path of two chief rays to the single point can be reconstructed, as the point will be located at the intersection of these rays (see Section 2.2.6.4) (Mitchell, *ibid.*). If this procedure is repeated for

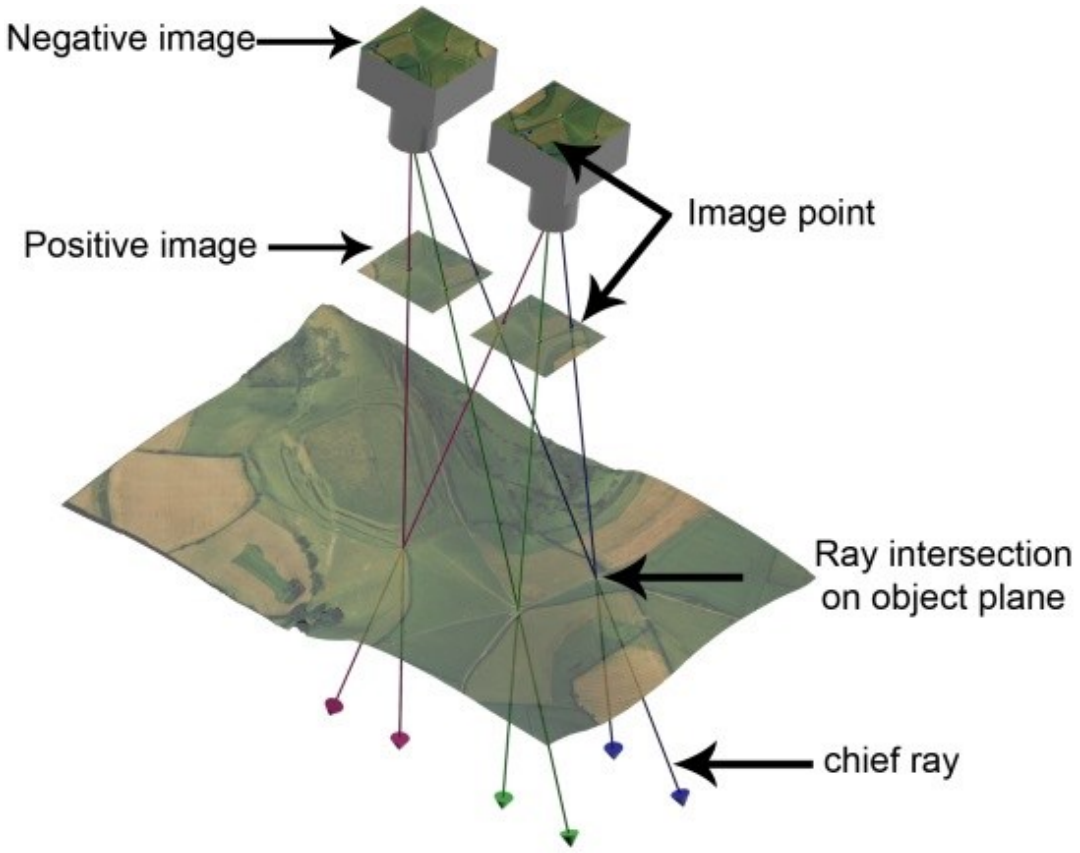

Figure 2.10: Diagram illustrating the concept of the 'chief ray' and the relationship between the terrain (object) and image plane.

enough points on the object, then a number of 3D points can be generated across the surface of the object that will describe its topography (Mitchell, *ibid.*). The number of images that are used to achieve this can be, and often is, greater than two.

Image Materials

Whilst modern stereo-photography is increasingly captured with digital cameras, a vast body of modern and historic aerial photography are archived as negatives, diapositives or contact prints. For use in a digital photogrammetric system these images must be scanned, and there are a series of factors that will affect the quality of the scanning procedure, beginning with the original quality of the analogue imagery. Photographic film consists of silver halide crystals, which may be as tiny as 0.03μm in size (Jacobson et al. 2000), and respond to light when exposed to form silver metal. These are embedded in a binder such as gelatin, which together are known as the film *emulsion*, that lies atop of a *celluloid* plastic base with an opaque (*anti-halation*) backing, as shown in Figure 2.11, which also serves to make the film hard wearing. It is the size of the silver halide crystals that determine the resolution of the image formed i.e. the smaller the crystals and the greater the quantity of these crystals, the smaller the amount of the light scattering effect. Once developed, the invisible latent image formed upon the crystals will become visible, and hence the image is produced. This method of image capture supplies images with a high resolution and very little distortion, although the digitisation process, as discussed later, must try to maintain this image quality.

During an aerial survey, photographic film is kept flat through the use of a reseau plate or vacuum back, as shown in Figure 2.12, thus reducing or ameliorating distortions at this stage of the process. Photographic film used for photogrammetric work can shrink or expand depending on how it is processed and subsequently stored, although the amount by which it alters ranges from insignificant to 0.2% (Wolf and Dewitt 2000). The distortion of photographic negatives and prints, however, is dependent upon the material. Glass negatives are virtually distortion-free, whilst paper prints have low dimensional stability (Wolf and Dewitt *ibid.*). Many distortions in paper prints occur at the drying stage, especially if they are hung to dry, which will stretch the paper. However, once the prints are dry, the temperature and humidity of the site in which they are stored will further influence their distortion. Depending on paper type and thickness, expansion or shrinkage can be as much as 3% depending on how the print has been handled, with distortion occurring differentially across the print (Wolf and Dewitt *ibid.*).

(a.)

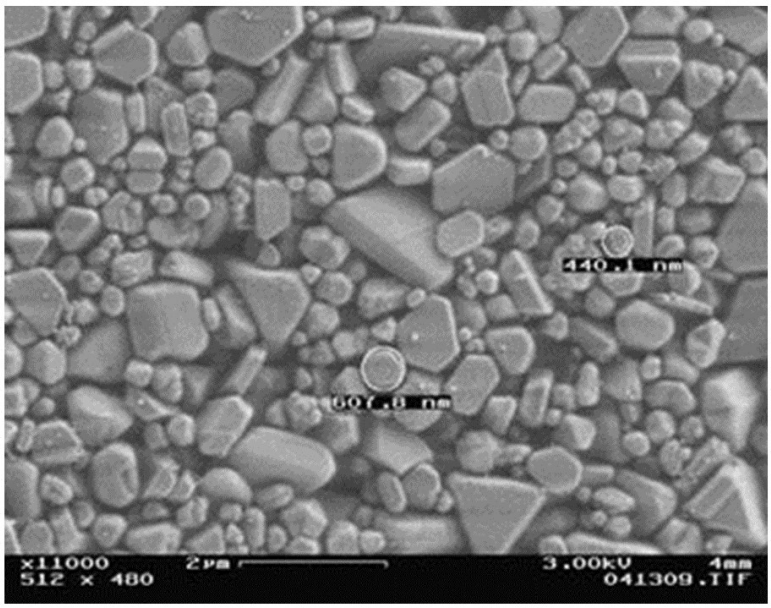

(b.)

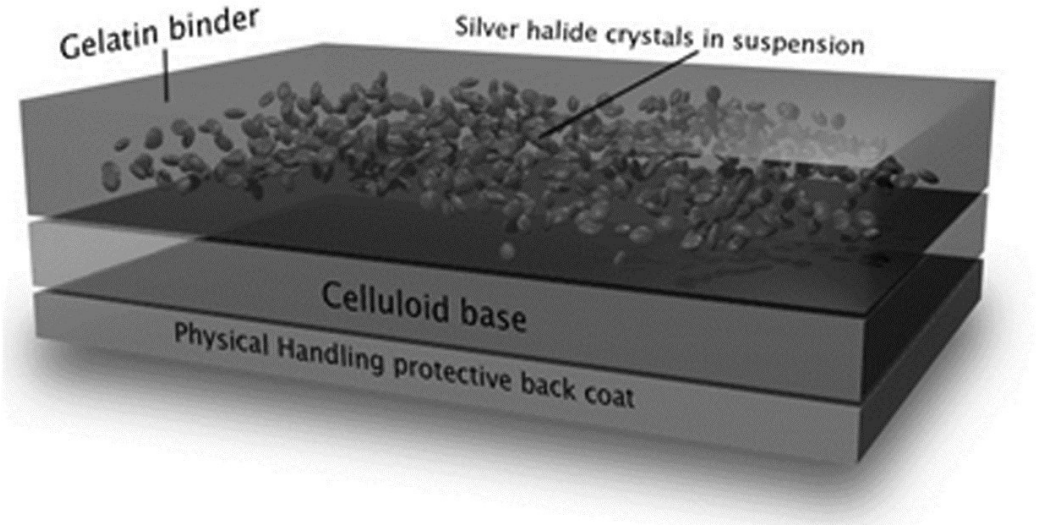

Figure 2.11: (a.) Silver halide crystals seen under a microscope (note scale). It is the size of these cystals which determine the resolving capability of the film (b.) The basic structure of film (adapted from http://photography.tutsplus.com/articles/what-is-iso-a-technical-exploration--photo-11963).

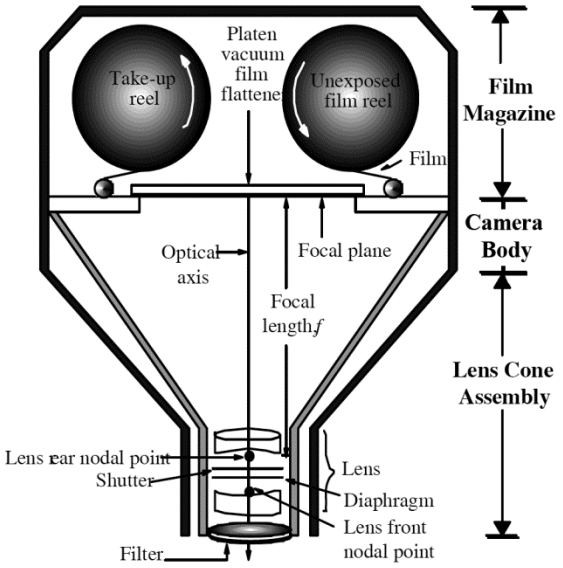

Figure 2.12: (Left) Diagram of aerial camera components (after Jensen 2007).

Digital photography is based upon Charge Coupled Device (CCD) or Complementary Metal Oxide Semi-Conductor (CMOS) technology, and is also relevant when considering the digitisation of film-based photographs using a scanner. The light sensitive picture elements or pixels will generate an electrical charge proportional to the amount of light that falls upon each individual pixel, as shown in Figure 2.13. This charge will be measured in terms of its voltage, which is amplified and digitised to create an array of spatial positions with an intensity value. Pixels in a camera are usually contained within a rectangular or square CCD chip, whilst the pixels in a scanner are often in a linear array. The information being recorded by the CCD undergoes a process known as sampling, in which the intensity of light that represents the objects in an image is sampled at regular intervals, defined by the size of the pixels that comprise the CCD chip. The coordinates of an intensity value are defined by the position of the pixel on the CCD chip. In order for all the detail present in the scene to be resolved, the sampling interval, or pixel size, will need to be small and present in great quantities. If the sampling interval is not fine enough, the sampling frequency will decrease and cause aliasing, or the incorrect reconstruction of the more detailed objects being photographed.

The intensity, or amplitude, of the frequencies within an image are quantized in order to represent the grey levels within a scene, which usually involves an error. The number of levels will depend on the number of bits that will be allocated to them. The amplitude of each analogue grey level will be compared to a set of decision levels and, if a particular amplitude falls between two decision levels, it will be quantized to a fixed reconstruction level in order to create an integer proportional to the original amplitude. Grey levels usually range between 0 to 255, creating 256 levels represented by 8 bits for a single channel. If the digital image is in colour, then 8 bits will be required to represent each of the three channels (red, green and blue),

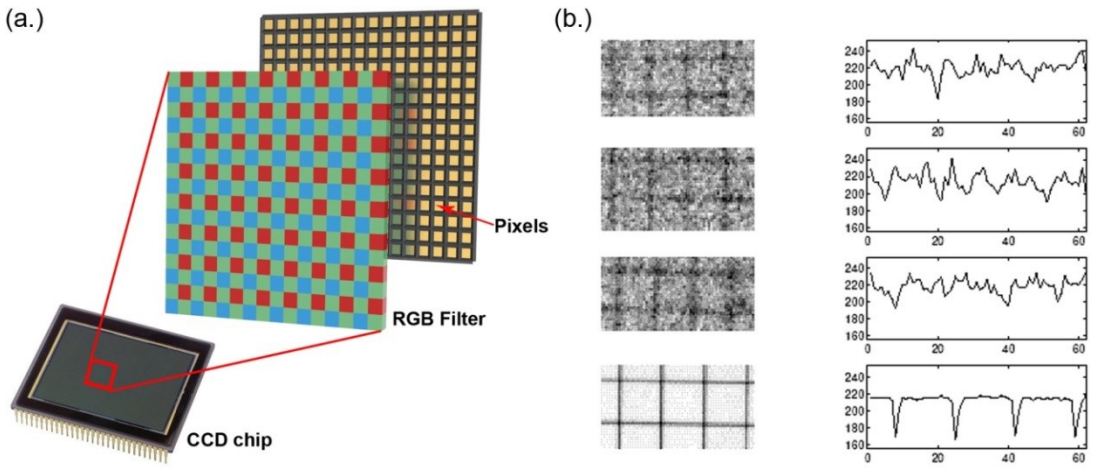

Figure 2.13: Image showing (a.) the composition of a CCD and (b.) results of comparing the image of a test grid taken with analogue film and a digital camera (Perko and Gruber 2002). The top three photographs show three types of analogue film and their accompanying profiles of the image intensity. The bottom image is taken using a CCD camera.

therefore 24 bits represent the colour information. The minimum number of bits required to represent grey levels in an image destined for photogrammetric use is usually 8 bits.

2.2.6.2 Image Noise

Image noise is the unwanted fluctuations in a signal that describes the intensity value of a particular point in an image, as illustrated in Figure 2.25. Analogue systems produce noise, which is caused by light scattering amongst the silver halide crystals, and thus the smaller the grain size and greater the number of grains, the higher the signal to noise ratio (SNR) i.e. the effect of unwanted noise in an image is reduced. However, both digitised analogue imagery and digital images suffer from other forms of noise that are specific to the digitisation process. One problem associated with digitized images is noise, a fluctuation in image intensity over the area of an image. The addition of noise can occur at various stages due to non-image generated electrons. Dark current noise is induced by thermal means, while saturation equivalent exposure occurs when the charge well is full. Noise may also be generated during quantization. An analogue image undergoing digitization in a scanner, for example, will generate photoelectric noise. The maximum contrast available from an image sensor can be defined by the Signal to Noise ratio (SNR):

$$SNR = 10\log\left(\frac{InputSignal}{NoiseSignal}\right)$$

The noise in a signal should not be overpowering, and should be smaller than the quantization level of an image to prevent the reduction of image information (Dowman 1996).

2.2.6.3 Film Scanners

Whilst photography produced with digital cameras is in the requisite format for processing in photogrammetric software, photographic film and prints must be scanned first to convert them into a digital raster file. It is recommended that the original film material should be used from which to scan the photographs, if possible, as the grain size of the crystals in the film emulsion have a superior resolving power than that of print materials (Walstra 2006). However, access to the original negatives may not always be possible in the case of SAPs. As mentioned in Section 2.2.6.1, the process of creating photographic prints can introduce further noise, which will be detected during, or caused by, digitisation.

The basic requirements of a scanner that is to be used for digitising film and paper-based photographic materials is that it should be capable of scanning the entirety of the largest format to be used, which will be the contact print. Photographic prints can be as large as 23cm x 23cm, and thus an A3 format scanner is vital. Photogrammetric scanners have been designed to ensure maximum geometric and radiometric resolution, and geometric accuracy during the scanning process. Geometric accuracy relates to the positional accuracy of the pixels in the resultant digital image, which needs to equate to the same spatial accuracy of the original imagery (Wolf and Dewitt 2000). The spatial accuracy of a scanner is influenced by the quality of the CCD. The pixels should each be the same size, separated by the same distance and be in alignment, as well as move with a constant step width (Linder 2009). Photogrammetric scanners should have a geometric accuracy of 2-3 micrometres (µm) (Wolf and Dewitt *ibid.*), although Baltsavias and Waegli (1996) provide a figure in the region of 2-5µm, whilst low-cost flatbed scanners often have values in the region of 50µm (Linder *ibid.*).

Geometric resolution describes the size of the pixels in the scanner, and is also referred to as spatial resolution. The smaller the pixel size, the higher the geometric resolution. When scanning an image, this value is usually stated as ‘dots per inch’ (dpi) or in micrometres (µm) (Linder, 2009), and the greater the dpi, the more accurate the spatial resolution. Baltsavias and Waegli (*ibid.*) state that a scanner should be capable of scanning at a resolution of at least 600 dots per inch (dpi). The maximum resolution attainable by a scanner is given by the uninterpolated resolution value, with photogrammetric scanners consisting of pixel sizes between 5-15µm (Wolf and Dewitt *ibid.*), whilst most flatbed scanners are restricted to 50µm (Linder, 2009). The relationship between resolution (dpi), pixel size (µm) and image size can be seen in Table 2.1.

Resolution [dpi]	150	300	600	1200	2400	4800
Pixel size [µm]	169.3	84.7	42.3	21.2	10.6	5.29
Image size ca. [MB]	2	8	32	128	512	2018
Photo scale						
1: 5000	0.847	0.423	0.212	0.106	0.053	0.026
1: 7500	1.270	0.635	0.318	0.159	0.079	0.040
1:10000	1.693	0.847	0.423	0.212	0.106	0.053
1:12500	2.117	1.058	0.529	0.265	0.133	0.066
1:15000	2.540	1.270	0.635	0.317	0.159	0.079
1:17500	2.963	1.482	0.741	0.370	0.175	0.093
1:20000	3.386	1.693	0.846	0.424	0.212	0.106
1:25000	4.233	2.117	1.058	0.529	0.265	0.132
1:30000	5.080	2.540	1.270	0.634	0.318	0.159
1:40000	6.772	3.386	1.693	0.846	0.424	0.212
1:50000	8.466	4.234	2.116	1.059	0.530	0.265
	Pixel size in terrain units ca. [m]					

Table 2.1: The relationship between scan resolution, image size, photo scale and GSD for a greyscale image (Linder 2009).

Radiometric resolution refers to the ability of a scanner to convert the amplitude (analogue signal) from analogue imagery to a discrete level (digital signal) in sufficiently high detail to capture the variation in intensity, or brightness, across an image. This process is known as quantization, and the larger the number of levels a scanner is able to obtain, the more accurately it will represent the original image (Wolf and Dewitt *ibid.*). Quantization was discussed in more detail in Section 2.2.6.1. Baltsavias and Waegli (*ibid.*) recommend that the radiometric resolution of a scanner should be at least 10-12 bits and have a density range of 3.5D (density is the ability of a device to capture shadow and highlight detail) if colour imagery is to be scanned.

2.2.6.4 Mathematical Procedures

The Collinearity Condition

The description of image formation is a useful introduction to one of the most important mathematical concepts in photogrammetry: the collinearity condition. This principle states that the exposure station (the optical centre of the camera lens), an object point and its corresponding photo image lie on a straight line in 3D Space, which is illustrated in Figure 2.14. This condition is still valid regardless of whether a photograph is tilted. The collinearity

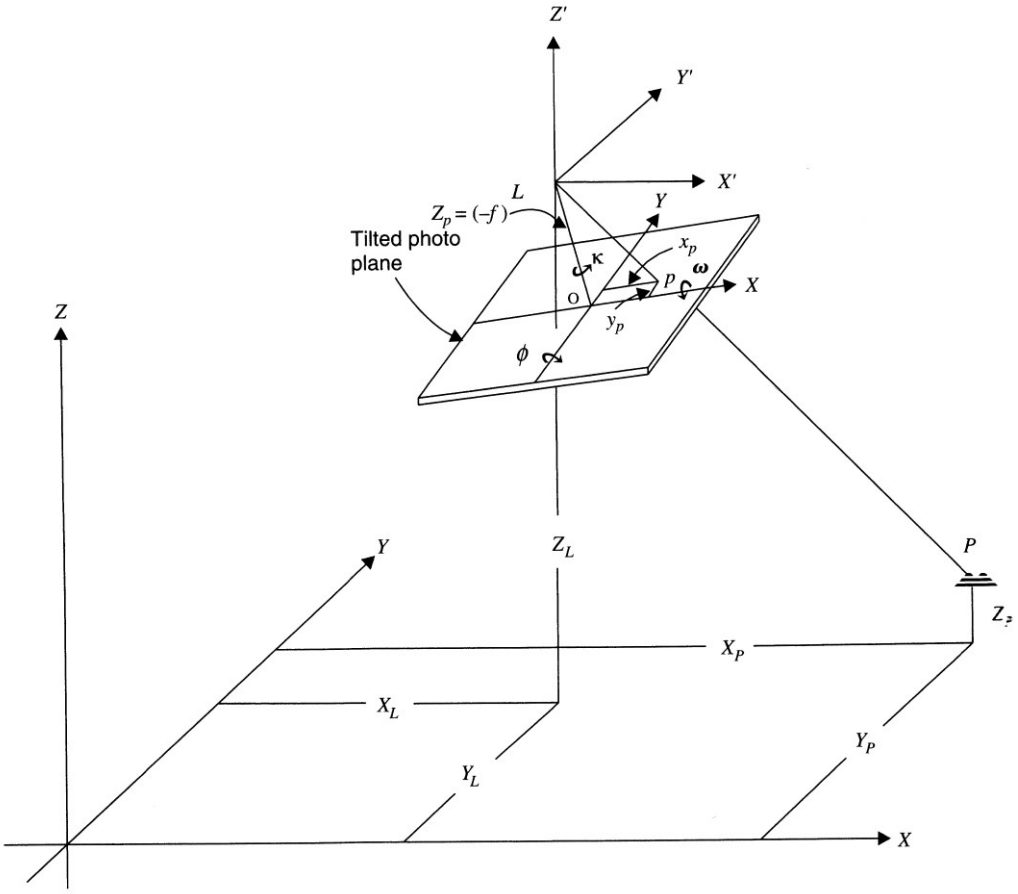

Figure 2.14: The collinearity condition where P (object point), p (image point) and L (position of the exposure station) are all situated on the same line (Lillesand et al. 2008).

equations thus describe the relationship between the ground coordinates, image coordinates, exposure station position and angular orientation of a photograph (Lillesand et al. 2008). The equations themselves can be found in Wolf and Dewitt (2000, p.235) and Lillesand et al. (*ibid.*, p.176).

If the interior and exterior orientation of the camera is known at the time the exposure is made then it is possible to calculate the 3D coordinates of an object within a stereo-pair of photographs (Walstra 2006). However, it is likely that the interior and exterior orientation parameters may not be known, particularly when working with archival imagery. These values subsequently have to be deduced, often by utilising control points (the collection of which is covered in Section 2.2.7.3), that have known X,Y,Z coordinates and measured image coordinates (Mitchell 2007). The process of deducing unknown quantities is described in 'Space Resection and Intersection'.

It is important to note that light rays will never reach the image sensor from the object in an absolutely straight line. The effects of lens distortion, atmospheric refraction and, over large areas, earth curvature will influence the deviation of light (Wolf and Dewitt 2000), for which corrections should be made. If a camera calibration certificate is associated with a set of stereophotographs, lens distortion will have been accounted for and these values can be

entered into the photogrammetric software for inclusion in the calculations. If not, some software packages, such as Leica Photogrammetry Suite (LPS) can estimate lens distortion parameters during the process of bundle adjustment.

Space Resection and Intersection

Space resection is used to establish the six parameters of exterior orientation, namely the positional and angular orientations of the camera at the time of exposure (i.e. XYZ, ωφκ), if they are not available. To obtain a solution requires at least 3 control points with known object space coordinates, an image of which must appear in the photo. This provides a solution that is accompanied by a residual quantity for each element. This residual amount, as defined by Wolf and Dewitt (*ibid*.), provides a measure of the difference between a measured quantity and a probable value for that quantity. A least squares solution to the calculation can be generated if more than four control points are provided. The least squares method is addressed in Section 2.2.6.4.

Space intersection is, in effect, the reverse of resection and is utilised to calculate all object point coordinates that lie in the stereo overlap area (Wolf and Dewitt *ibid.*), and can be calculated if the exterior orientation parameters are known. This concept is illustrated in Figure 2.15, and shows the corresponding rays from overlapping photographs intersecting at the same object point (Lillesand et al. *ibid.*). The collinearity equations are used to calculate the unknown object point coordinates by employing the known photo-coordinate quantities, from which a least squares calculation can be performed to obtain ground coordinates for each point (Lillesand et al. *ibid.*).

2.2.7 Photogrammetric Workflow

When undertaking photogrammetry using specialist software, there are a series of options the operator can select, albeit this usually follows a general workflow with specific stages designed to obtain the most accurate results from the imagery. These stages are outlined below with example workflows illustrated in Section 4.4 (Figure 4.7).

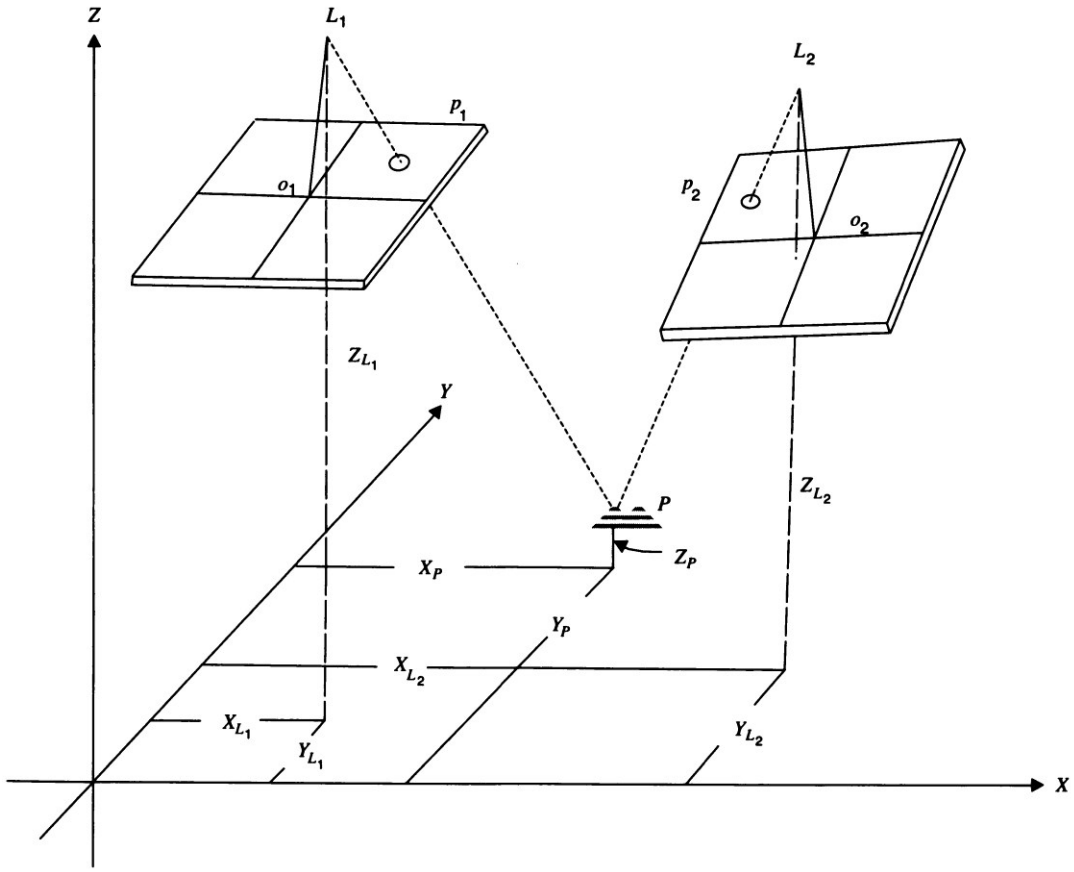

Figure 2.15: Diagram illustrating the concept of Space Intersection. Corresponding rays travel from L (exposure station), form an image point 'p' and both intersect at object point 'P' (Lillesand et al. 2008).

2.2.7.1 Interior Orientation

An important and often first stage in the photogrammetric process is 'interior orientation', which is required for accurate spatial information to be derived from the camera. This process is used to correct for any inherent distortions within the camera system that was utilised for generating the photographs prior to further photogrammetric operations taking place. This is achieved using camera calibration information. The parameters that are used to determine the interior orientation for a metric camera are the calibrated focal length (or more correctly the calibrated principle distance, which is measured between the perspective centre and principle point), principle point location, fiducial mark coordinates (if it is a film-based system) and the lens distortion characteristics, which are illustrated in Figure 2.16. There are a number of techniques in use with which to calibrate camera systems and model their imperfections, although their description is beyond the scope of this work. Interested readers are referred to Wolf and Dewitt (*ibid.*) and Ray (1999) for detailed information regarding this process. Many of the interior orientation parameters form what is known as the image coordinate system (ICS). By providing

a 3D coordinate for the lens, this allows the image object coordinate systems to be related to one another (Mitchell 2007).

Once the various characteristics of the camera have been calibrated, the interior orientation process utilises these parameters to correct for distortions and recreate the geometry of the camera that existed at the time of image exposure (Wolf and Dewitt *ibid.*). The process of interior orientation usually involves the operator identifying the location of the fiducial marks on the imagery (which in some software packages can be automatically detected) and also providing the software with their calibrated x,y positions along with the calibrated location of the principle point (see Figure 2.16). This allows the software to convert the image coordinates, as measured by the operator, to the coordinate system based upon the calibrated values of the fiducial marks and principle point, the latter of which subsequently becoming the centre of the ICS. This is achieved by utilising a 2D affine transformation, with the lens distortion corrections

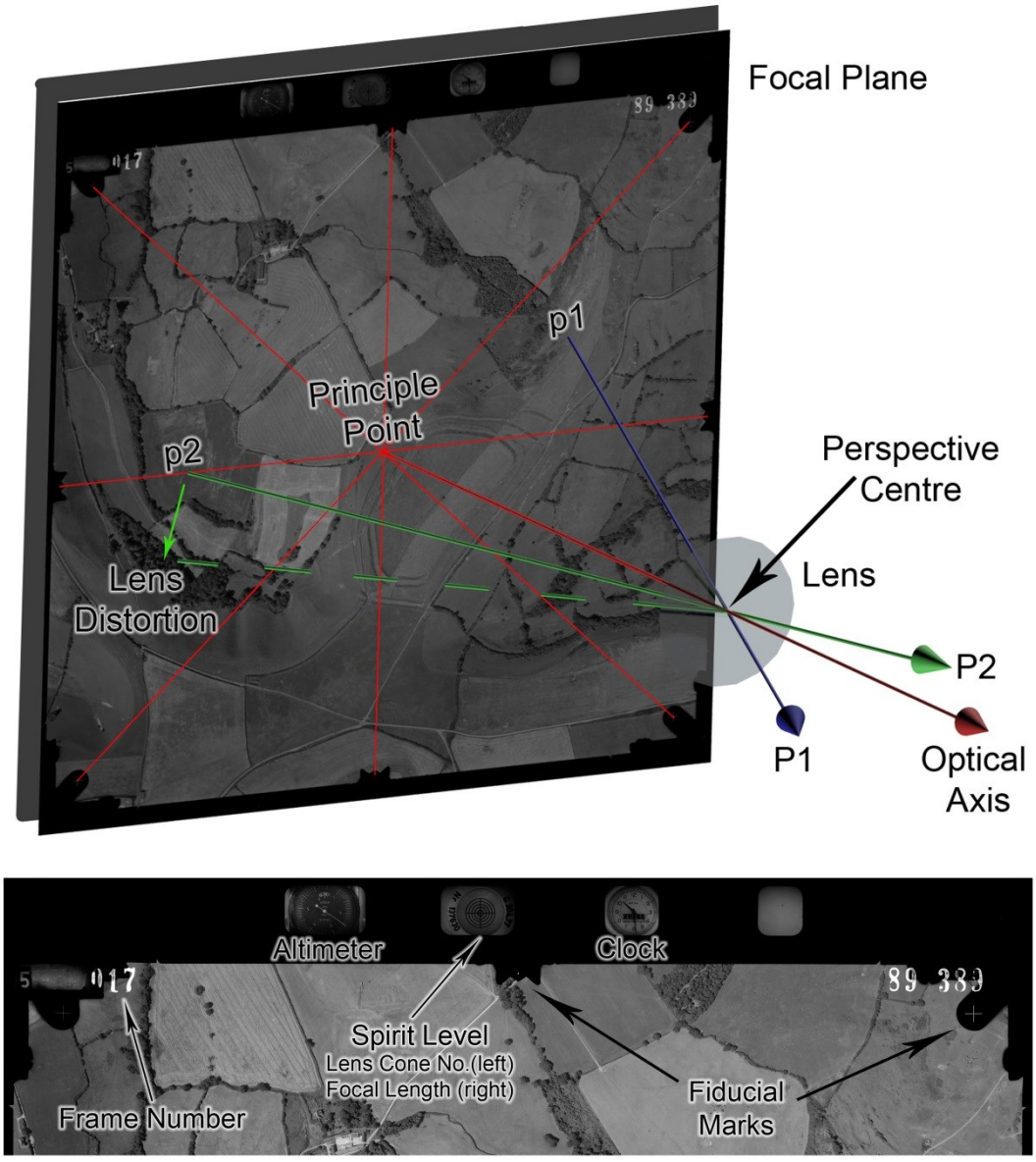

Figure 2.16: Diagram illustrating the components of interior orientation (top), and the data contained within an aerial photograph (below).

applied simultaneously. As stated by Mitchell (*ibid.*), the image coordinates will now comply with the assumptions made using the collinearity equations (see Section 2.2.6.4).

2.2.7.2 Exterior Orientation

The exterior orientation of a photograph requires knowledge of the 3D camera position and angular orientation of the camera during exposure, provided in a 3D Cartesian system. Measurements are often depicted in X,Y,Z format, with the X and Y coordinates representing horizontal locations and the Z value representing elevation as illustrated in Figure 2.17 (Walstra 2006). These measurements relate to the location of the exposure station, or perspective centre, and are often provided in the same coordinate system as that for the ground control points (see Section 2.2.7.3). In many cases, the coordinates for the perspective centre of the camera, the ground control points and the object points in the imagery are provided in state, national or global coordinate systems, which helps to explain why the object coordinate system may also be referred to as the ground coordinate system (Mitchell *ibid.*). Cartesian measurements for the camera location are often gathered using an on-board GPS to provide locational data and an IMU to measure the angles of rotation (see Figure 2.17). These

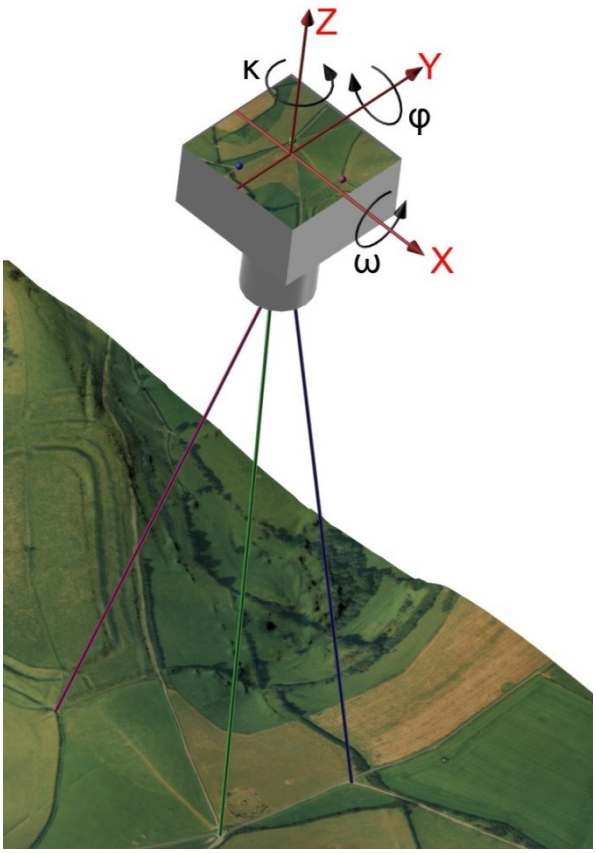

Figure 2.17: Exterior Orientation parameters showing the location of the camera (X,Y,Z) and the rotation angles, ω omega (roll), φ phi (pitch) and κ kappa (yaw).

instruments are mounted in the aircraft for the duration of the aerial survey. However, if locational and rotational information has not been gathered at the time of the survey flight (as is commonplace with archive SAP acquired before the advent of GNSS and IMU), the camera position and angular orientation data can be calculated by the photogrammetry software by utilising ground control points and the process of space resection, as described in Section 2.2.6.4.

The angles of rotation ω, φ, κ are influenced by the attitude of the platform (i.e. aircraft) at the instant the camera shutter is released, assuming no camera stabilisation device is in use, such as a gyro-stabilised camera mount i.e. Leica's PAV30, which is rare with older archive SAPs. Figure 2.18 illustrates how ω, φ, κ relate to the roll, pitch and yaw of the platform, respectively. According to the principles of flight, any change in one of these influences the others. A change in pitch or roll between successive frames will effectively result in the capture of low-oblique photography (Figure 2.19) and in turn one-dimensional changes in scale (known as tip or tilt) across the photograph, or commonly a two-dimensional combination of both (Figure 2.19).

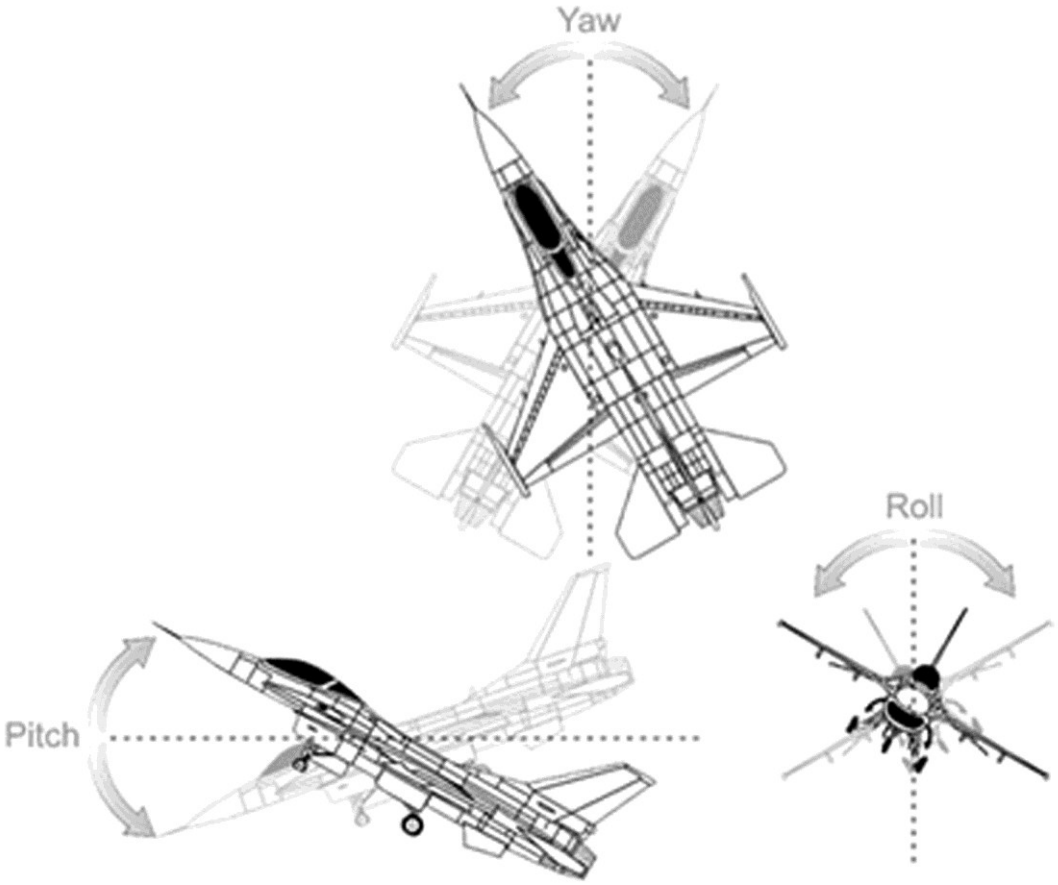

Figure 2.18: Sketch illustrating yaw, pitch and roll of a platform (aircraft).

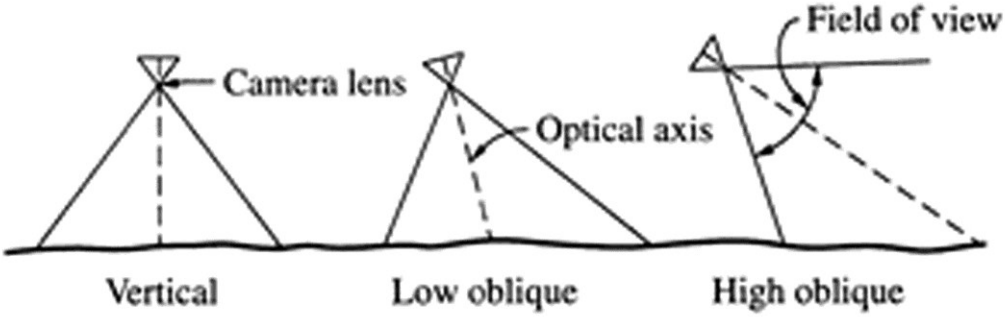

Camera orientation for various types of aerial photographs

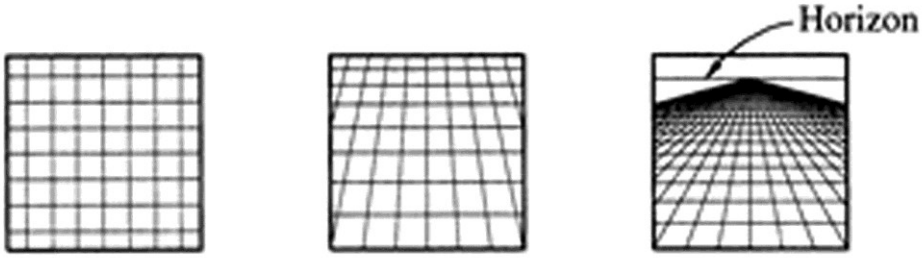

How a grid of section lines appears on various types of photos

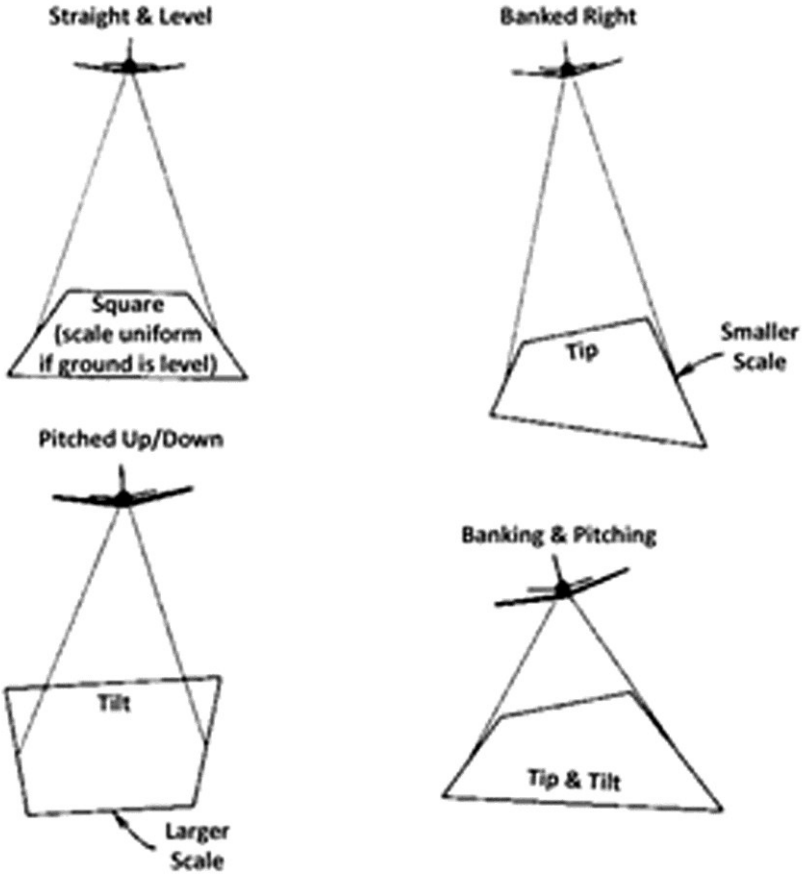

Figure 2.19: Image orientations, as definined by Wolf & Dewitt (2000).

Changes in pitch and roll also result in excessive or diminished stereo overlap. Such changes are generally the result of turbulent air that is caused by the presence of thermals on warm sunny days. However, a pitch angle (φ) can consistently be greater or lesser than zero if the aircraft is *trimmed*, which means that the *angle-of-attack* to the oncoming airstream by the aircraft and its wings may be deliberately set nose-high by the pilot in order to generate sufficient lift to keep the mass of the aircraft aloft for a given airspeed. For most survey flights a key objective is to have the platform flying at sufficient airspeed into or out of any head-wind or tail-wind that it can be *trimmed* to be level (i.e. approximating zero φ), have sufficient ground speed and an appropriate photo interval to achieve photo stations which result in sufficient stereo overlap (i.e. 60% in the direction of flight).

Yaw (k) is commonly the result of the desired flight line not being parallel with the prevailing wind direction. In such cases the platform (aircraft) is said to be subject to a cross-wind and is obliged to fly heading into wind, known as crabbing, in order to maintain the desired direction of travel for the survey flight line (Figure 2.20).

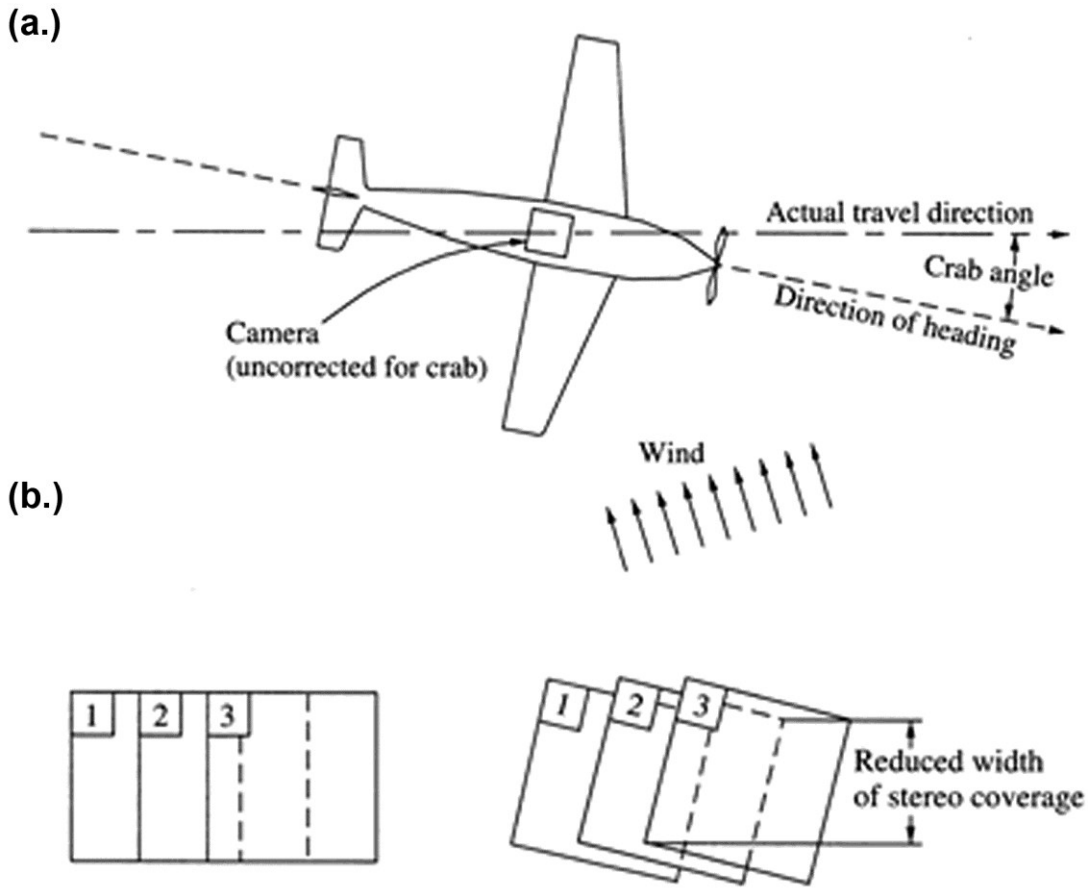

Figure 2.20: (a.) Sketch illustrating the crab angle of a platform (aircraft) as a result of a cross-wind. In such instances if the camera is not mounted on a swivelling mount to correct for this then the photography will be subject to an excessive k angle (b.) Sketch illustrating how an excessive k angle can result in a reduced stereo overlap (right) compared to k approximating to zero (left) (Wolf and Dewitt 2000).

2.2.7.3 Tie Points and Ground Control Points (GCPs)

Tie points are useful for identifying matching image points across a number of overlapping images and thus creating a relationship between them. The selection of tie points can be performed manually, automatically, or a combination of both, with the former potentially a time-consuming process. Image matching algorithms can be used to identify matching pixels between overlapping images whereby a tie point can be automatically placed. The basic process of image matching is illustrated in Figure 2.21. A stereo-pair of photographs is shown, with the left-hand image containing the reference window whilst the right-hand image contains a larger search window. These windows are also known as kernels. The search window is always the larger of the two to ensure that it surrounds the region containing the pixel to be matched. As a number of parameters should have been entered into the photogrammetry software at this stage, such as the focal length of the camera and the degree of overlap between images for example, the search window can be placed approximately in the correct location on the right-hand image. A sub-search kernel moves within the search window from pixel to pixel, comparing the pixel numbers with those in the reference window to identify the region in which there is peak correlation between the two images. The success of this process is, however, dependent upon the strength of the image signal and contrast, as well as minimal geometric and radiometric distortions (Walstra, *ibid.*). If image quality is good then the kernels can be

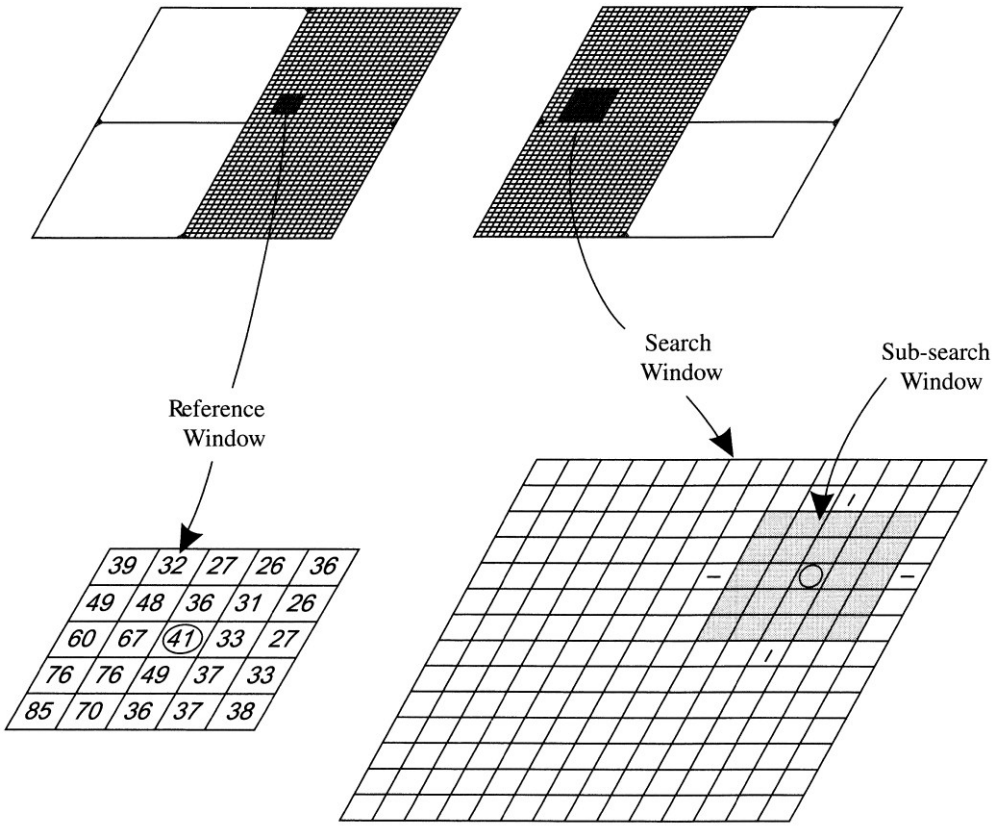

Figure 2.21: The image matching process (Lillesand et al. 2008).

smaller because the likelihood of peak correlation (matching) is much greater than if the image was of poor quality. Kernel size should be increased in this instance to enhance the probability of identifying matching areas within the stereo-pair.

Ground control points (GCPs) are necessary for a number of reasons during the photogrammetric process. They provide ground reference data that is often inclusive of a horizontal coordinate system, such as the UK's OSGB36, and/or vertical datum, such as the Ordnance Datum Newlyn (ODN) in the UK (Lillesand et al. *ibid.*). GCPs are also required to determine the exterior orientation parameters if these are not provided with the imagery. GCPs are selected based upon their visibility in the imagery and are stated by Lillesand et al. (*ibid.*) to be representative of physical points on the ground. Ideally ground control is positioned proactively, that is high-visibility markers (usually fabric) are placed within the landscape which is to be photographed (Figure 2.22) beforehand and their locations surveyed by conventional (terrestrial) means. However, ground control for photogrammetry is more commonly collected retrospectively, that is after the photography has been acquired. In the case of archive SAPs, this is the only option.

A suitable distribution of retrospective GCPs must be present within the imagery (Wolf and Dewitt ibid.), as illustrated in Figure 2.35. Examples of suitable features for locating GCPs are road and watercourse intersections, the corners of buildings and fences, small, lone features such as bushes and patches of grass etc. (Wolf and Dewitt *ibid.*). However, where historic stereo-imagery is to be used, particularly over decades rather than years, some features may have been removed or altered. It is therefore important to identify suitable locations for GCPs prior to collecting them in the field by comparison with modern imagery to ascertain if they still exist.

Figure 2.22: Examples of high-visibility markers placed in the landscape as pro-active ground control points.

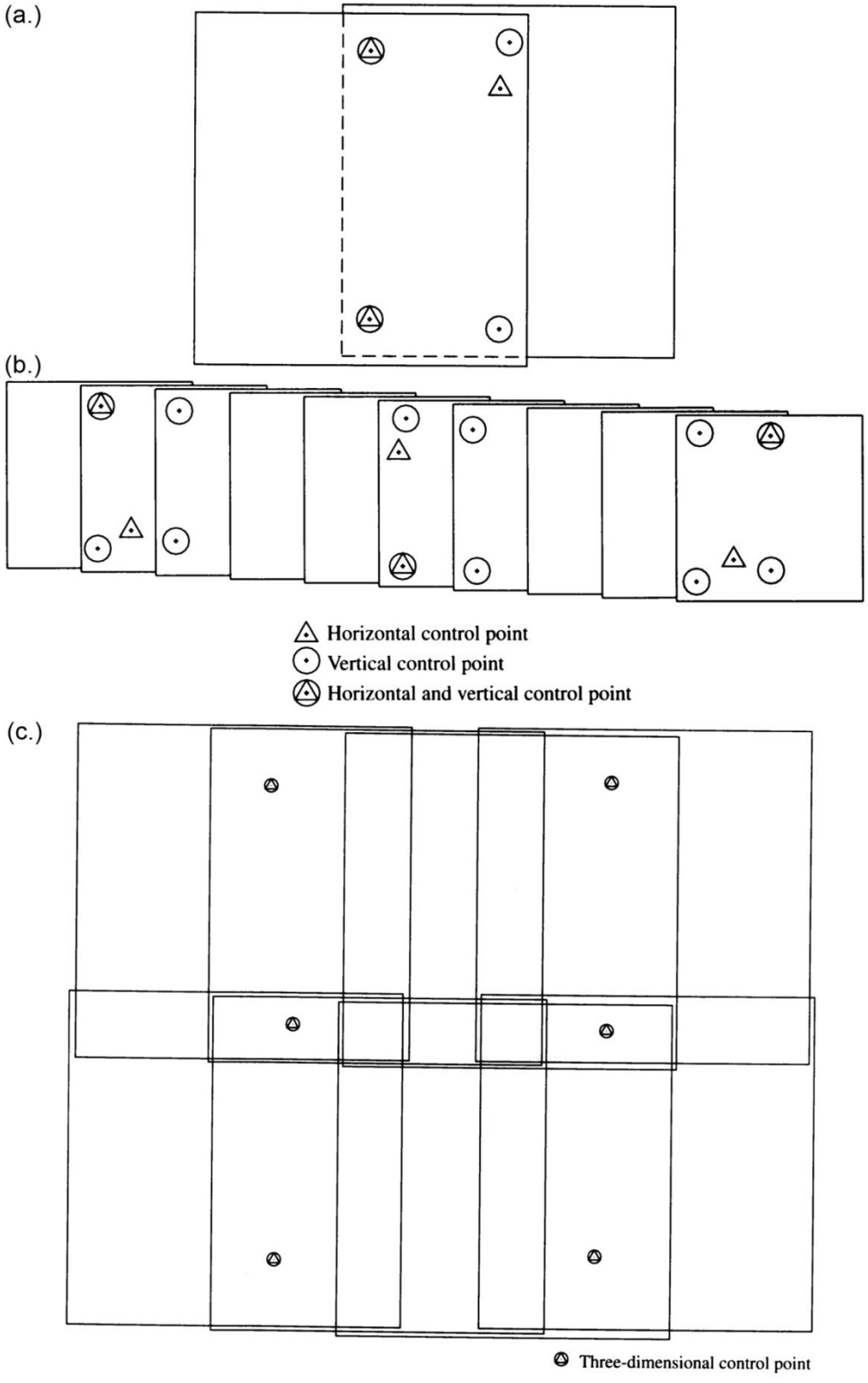

Figure 2.23: Recommended layout of GCPs from Wolf and Dewitt (2000): (a.) single stereo-pair, (b.) image strip and (c.) image block.

The number of control points required for topographic plotting using a single stereo-model, comprising of two overlapping images, is a minimum of three vertical and two horizontal GCPs, although more points are required for redundancy and blunder detection, and thus three horizontal and four vertical GCPs are recommended (Wolf and Dewitt *ibid.* p.349). GCPs should be well distributed throughout the overlapping area, with the vertical GCPs situated towards each corner of the overlap, with potentially a fifth point close to the centre (see Figure 2.35). Finally, the GCPs must be identifiable in the imagery and not situated close to the edge of the image as the lens distortion and image resolution are degraded here.

For triangulation to proceed (see Section 2.2.7.4), fewer GCPs may be sufficient, although the number depends upon the nature of the area being recorded i.e. whether the terrain is flat or mountainous, and the desired accuracy of the project. As a general rule, the accuracy of the additional control calculated by the triangulation process increases as the number of GCPs increases. For a strip of stereo-photographs, the optimal control suggested by Wolf and Dewitt (*ibid*.p.350) is illustrated in Figure 2.35. Thus when triangulation is subsequently performed, it increases the amount of ground control throughout strips or blocks of stereo-imagery in a process sometimes referred to as 'bridging', thereby creating large numbers of control points from just a limited number of collected GCPs and the stereo-imagery.

Whilst exterior orientation data can theoretically negate the need to collect GCPs, the collection of a nominal number of GCPs is still recommended, and especially so when working with historic SAPs. GNSS is often used to gather GCPs as it makes the process relatively rapid, although care must be taken to understand the performance of the technique that is used to collect them. Lillesand et al. (*ibid.*) state that accurate ground control is essential to predominantly all photogrammetric processes, as photogrammetric measurements can only be as reliable as the ground control on which they are based.

2.2.7.4 Triangulation and Bundle Adjustment

Wolf and Dewitt (*ibid.*) state that Triangulation, alternatively known as Aerotriangulation, is the process of establishing the 3D ground coordinates of individual points based on photo-coordinate measurements. The triangulation process generally requires the input of control points and tie points prior to execution. If only tie points are entered, then relative orientation can be achieved, which describes the way in which each of the images, whether it be a stereo-pair, strip or block, relate to one another in a relative sense. The collinearity condition (see Section 2.2.6.4) can be utilised to establish the relative positional offset and angular attitude between the images at the time of their exposure (Wolf and Dewitt *ibid.*). However, for absolute orientation to be achieved, GCPs are required. Absolute orientation is defined by Heipke (1997) as the relation of the image coordinate system to the object coordinate system. Wolf and Dewitt (*ibid.*) state that a minimum of two horizontal and three vertical control points are required in the

area of overlap, although more will provide redundancy and the opportunity to derive a least squares solution, as explained below.

Block Bundle Adjustment (BBA) is a part of the triangulation process and simultaneously applies the processes of space resection and intersection, effectively the collinearity equations, to all of the images, known as a 'block', within a photogrammetric project. BBA is so called because it handles all of the bundles of light rays, defined by the identification of object points and their representative image points, at once (Linder 2009). It is during this process that the ground coordinates for tie points are created.

Least squares adjustment (LSA) is the method applied to address errors in data caused by random error sources and is stated by Wolf and Dewitt (*ibid.*) to be the theoretically correct way of dealing with random errors. Errors are those remaining once the gross and systematic errors have been accounted for and are further described in Chapter 3, Section 3.3.1. For the LSA to be successful there have to be more known values than there are unknowns. Thus, without camera calibration information and the potential lack of exterior orientation measures, GCPs are an important requirement when working with SAPs as they are the sole means of providing location data for object points in the photographs. Subsequent to the performance of the LSA, residual values are usually returned, which represent the difference between a measured value and the most probable value for that measurement. It is the residual value for each measurement that is adjusted during the iterative process of LSA (Wold and Dewitt, *ibid.*), which reduces the sum of the squares of the errors until it cannot get any smaller and thus represents the best fit between the observed values and those of the values estimated by the software.

Within the SocetGXP software, the least squares bundle adjustment, described above, is used to solve a number of unknowns, such as the camera angles, camera locations and the adjusted ground locations for tie points (BAE Systems 2009). Whilst tie-points can be used for this purpose, they are only a means of identifying matching image points across photographs as they do not have known locational values, unlike GCPs. By only using tie-points, a relative solution can be created but not an absolute, or georeferenced, solution, for which control points are required.

2.2.7.5 Automatic Terrain Extraction

After the stereo-photography has been registered and the triangulation process has been completed, terrain generation can be undertaken. Photogrammetric software packages utilise image matching techniques, as described in Section 2.2.7.5, to generate terrain data, although they are often referred to as 'area-based' matching. However, there are other processes that can be employed during terrain extraction to increase the accuracy of the end product. Back-matching is one such method whereby the reference window remains static in the left image whilst the search window moves across the right image to produce a correlation result. The

process is then reversed and the reference window remains static on the right image whilst the search window moves across the left. Back-matching therefore allows the software to identify any discrepancies between these results, and thus reject any erroneous points by comparing them to a threshold correlation value.

An alternative to the area-based method is 'feature-based' matching. This approach involves looking for distinct features in the imagery, such as edges, which are often distinct and indicative of a number of objects in a landscape, such as buildings, roads, cliffs etc. When identifying edges, the matching process is looking for dramatic differences in image intensity values (i.e. large changes in the greyscale or pixel number), which the correlation threshold might reject when performing area matching (Zhang et al. 2007).

The software user is often able to select the post-spacing required from terrain extraction on which image-matching takes place, which suggests that the end-product is a regular grid of 3D coordinates. Wolf and Dewitt (*ibid.*) state that this is rarely the case due to the influence of tilt and relief displacements contained within the imagery. The choice of point-spacing is related to the GSD of the imagery, with users either selecting a multiple of this value or inputting this exact number to obtain pixel-for-pixel matching.

2.2.8 Software

There are a number of dedicated digital photogrammetry software packages available, ranging from low-cost, as discussed in Section 2.2.3, to high-end products such as BAE Systems Socet Set and SocetGXP. More recently, GIS packages have also been providing the facility to extract terrain data from stereo-photography, either as dedicated features within the software or through the use of plugins from other manufacturers. ENVI utilises its own integrated tool called 'DEM Extraction Wizard' that works with a single stereo-pair of images, taking the user through a series of steps that follow a specific workflow. GCPs are added to the process prior to the addition of tie points, which can be generated either manually or automatically. Once the terrain extraction step is reached, the user is prompted to set a number of parameters, which require the user to be familiar with the photogrammetric process and the way in which image-matching works. The minimum correlation value, moving window sizes and terrain type can all be altered, each of which are explained within the software help file.

Parameter input for photogrammetry software products such as Leica Photogrammetry Suite (LPS) was more extensive than for ENVI, requiring users to be familiar with the way in which image matching worked. The terrain extraction module, known as e-ATE, presented consumers with a large number of parameters to alter, which required even the more advanced users to conclude that experimentation was often the only way to obtain optimal results (Gooch 1999). However, photogrammetry has long been a part of the ERDAS IMAGINE product, with Stereo Analyst, OrthoMAX and OrthoBASE forming previous incarnations of LPS. The last version of

LPS was released in 2013 as a part of the IMAGINE GIS software created by ERDAS, who are now part of the Intergraph Corporation owned by Hexagon. LPS is now known as IMAGINE Photogrammetry and is an add-on module for IMAGINE, along with 'Auto-DTM' and 'Stereo Analyst', which facilitate the extraction of terrain and vector data respectively. Many of these tools are also available as extension modules for ArcGIS. However, the updated photogrammetry suite to tools still requires considerable user input for a large number of parameters, which is likely to deter all but the more advanced practitioners from working with it.

Socet Set and Socet GXP are high-end packages produced by BAE Systems that are utilised by the military as well as universities, researchers, mapping agencies and others (BAE Systems 2014). Socet Set was the initial photogrammetric and geospatial software developed by BAE Systems that required consumers to be familiar with the concepts and workflows for photogrammetry. SocetGXP was conceived in 2001 to encourage consumers to migrate from Socet Set as it employed a more user-friendly graphical user interface (GUI) and streamlined the workflows. Subsequently, stages of the processing chain, such as interior orientation, do not require consumers to search through menus to find the individual tools to import photographs, input calibration data and fiducial measurements, add GCPs etc., as they did in Socet Set. Each of these tools is combined into a unified workflow in SocetGXP that is similar to a 'wizard' approach, which takes the user through a number of steps and prompts them to input certain information. Processes such as terrain extraction also require limited input from the consumer, unlike LPS and IMAGINE Photogrammetry. Whilst advances users can elect to alter the pre-defined parameters for generating terrain, Socet Set and SocetGXP provide strategies that are designed for generating terrain across particular topographies that are predominantly flat, steep and urban or a combination. Modules are also available to provide Socet functionality to the popular GIS software package ArcGIS.

Dedicated photogrammetry software for expert users, such as SocetGXP, can be prohibitively expensive. Whilst the modular approach offered by a number of vendors allows consumers to select the software tools that are most appropriate for their purpose and budget, the cost of these additions and the learning-curve associated with them has to be considered. As alluded to in Section 2.2.3, archaeologists have adopted low-cost packages such as Topcon's ImageMaster or SfM alternatives, ranging from commercial options such as AgiSoft's PhotoScan and Acute3D's Smart3DCapture, to open-source alternatives like Bundler and SFMToolkit. In many cases these packages require minimal input data and employ a 'black-box' approach to obtain results from images. This means that users are not privy to the algorithms used to derive triangulation solutions or extract DSM data from the imagery. However, they do not require consumers to be photogrammetric experts, and thus the learning curve for generating DSMs from imagery is minimal. What must be considered by those utilising SfM is whether it is fit-for-purpose, which includes the metric performance of the data extracted from it, as discussed in Section 2.2.3.

2.2.9 Photogrammetry Limitations

As photogrammetry uses cameras that are referred to as passive systems, the technique relies on sufficient ambient lighting or an artificial light source to illuminate a surface sufficiently to capture textural detail. Subsequently its efficacy is reduced in poor lighting conditions. Laser scanning, on the other hand, is an active sensor that provides its own light source, which is reflected from a target to provide measurements and can therefore operate in both light and dark conditions. However, a successful photogrammetric campaign provides textural detail of an object, which is often an important requirement for heritage documentation as it inherently delivers information about the state of preservation (Al-kheder et al. 2009). Although most scanners have built-in digital cameras, they rarely produce high-resolution, high-quality imagery, and thus for texture mapping and the production of photorealistic models the photography has to be captured with a digital camera (Bruno et al. 2009).

Data occlusions are not a problem purely encountered by TLS systems. Many authors have grappled with this issue when using photogrammetry (Dawson et al. 2008; Hetherington et al. 2007; Lambers et al. 2007), despite the application of an apparently rigorous method of field survey. This emphasises the complexity of trying to provide a complete 3D record of a site or object. This is particularly prudent when adopting the 'preservation by record' approach, as an incomplete record may nullify or prevent the reconstruction of the subject. Photogrammetry is a tried-and-tested method for ante-disaster recording (Dallas et al. 1995), with the chances of a successful outcome assisted by the development of digital photography: imagery can now be assessed almost immediately after the photography has been taken, reducing the probability of collecting unsuitable images.
Many TLS systems contain an inbuilt camera, or provide the facility to attach a camera system to the scanner. The latter method often provides the opportunity to generate high-resolution imagery during a scan, combining the benefits of photogrammetry and scanning into one system. However, this often increases the time required to conduct a survey from one particular survey station as the scanner has to gather the imagery as well as the point cloud. The result can be a large dataset that requires computer hardware and software that is capable of handling huge data volumes.

Further limitations of the technique relate to issues that are specific to the use of archive SAPs. The initial development of SAPs, from exposed film to developed negative or diapositive, and subsequently to photographic print and storage is frequently unknown and untraceable. If these photographs have not been carefully managed and stored, in conditions that are both dry and cool, the materials could have been subjected to a number of degradations that will subsequently affect the quality photogrammetric result. If a photograph has been taken with an aerial camera that uses a reseau plate, which can be ascertained if a large number of cross hairs are marked upon the image, then the effects of geometric warping may potentially be reduced. However, this would rely on the availability of the camera calibration certificate. Geometric distortion can be caused by storage in a warm, damp environment, which can cause

images to stick together and even develop mould (U.S. National Archives and Records Administration No Date). Dust and scratches may be noticeable on negatives and prints, which can also be a sign that these materials have not been stored carefully. Subsequently, the life-cycle of archival materials will dictate the quality of the data that can be extracted from them.

2.3 Airborne and Terrestrial Laser Scanning Techniques

Böehler and Marbs (2002) define a laser scanner as "…any device that collects 3D coordinates of a given region of an object's surface automatically and in a systematic pattern, at a high rate (hundreds or thousands of points per second), achieving the results (i.e. 3D coordinates) in (near) real time." This statement summarises the common properties of all laser scanners, regardless of their principle of operation. These systems are known as 'active' sensors because they provide their own energy source with which to generate the laser and conduct a survey. For this reason, laser scanning can be undertaken during the day or at night.

The following Sections describing airborne and terrestrial scanning techniques are indicative of the relative ease with which point data can be generated when compared with the concepts and workflows associated with Photogrammetry (see Sections 2.2.6 and 2.2.7). However, data collection and processing for airborne systems is often undertaken by a commercial company, which significantly reduces the workload for a user. Terrestrial scan data does require a significant time investment and this is further discussed in Section 2.3.2 below.

2.3.1 Airborne Laser Scanning (ALS) Techniques

ALS instruments are mounted in an aircraft, whether it be fixed wing or a helicopter, and obtain measurements by deflecting the laser beam in a direction perpendicular to the flight path, whilst the forward motion of the aircraft provides subsequent measurements in the forward direction (Petrie and Toth 2009). The location of the ALS is provided by a GNSS whilst an Inertial Measurement Unit (IMU) collects information about the attitude of the plane (i.e. the way in which the pitch, roll and yaw alter during the flight). These concepts are illustrated in Figure 2.24a. The data can therefore be georeferenced and is expected to provide vertical and horizontal accuracies of between 5-15cm (Crutchley 2010), although the latter is affected by the altitude of the aircraft, which influences the degree to which the beam spreads, and the instrument settings (see Figure 2.24b).

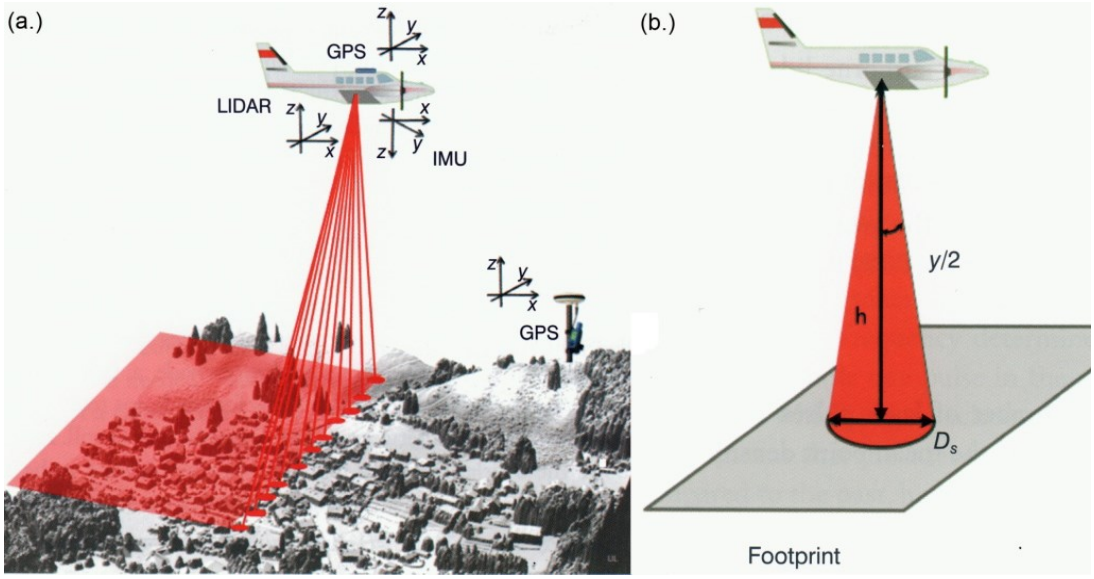

Figure 2.24: Diagram showing (a.) an aircraft-mounted laser scanner and the geo-location components GPS and IMU, (b.) the influence of aircraft altitude, h, and the diameter of the footprint, D, which is affected by altitude (Beraldin, Blais and Lohr 2010).

Data collection with ALS is based on the time-of-flight (ToF) principle, whereby distance is based upon the time it takes for the laser beam to travel to and from the terrain. Each laser pulse generates a measurement, of which millions can be produced in a single sortie over a wide area, thus explaining why ALS is suited to recording landscape-scale areas. However, the reflected laser pulse may not have been returned from the ground surface but from the first surface it hits after leaving the aircraft, whether it be a building, tree, or other vegetation type. If the laser has managed to penetrate the vegetation canopy or clipped the edge of a building, with a fraction of the laser energy reaching the ground, it may be possible to obtain a ground measurement from the energy that returns to the aircraft. The systems that are able to distinguish between return pulses are called discreet or full-waveform systems, the concepts for which are illustrated in Figure 2.25.

The first echo returned to the aircraft is generated by the first obstacle it hits, whilst the last echo, or return, is reflected from the ground surface. If the data is being collected over areas with dense vegetation, however, this may not be the case. Discreet return systems are only able to digitise a small number of returning echoes, whilst full-waveform systems can digitise a large number of them. Once each of the returns are separated the measurements can then be assigned 3D coordinates (X,Y,Z) from which a digital surface model (DSM) can be derived. The process of creating DSMs using ALS data is explained in Chapter 3. If a digital terrain model (DTM) is required, which provides a bare-earth representation of the survey area, only the last return data is required. The process of digitising and separating the returns requires specialist software to filter the data, although commercial companies offering ALS data often provide pre-filtered products as text files or interpolated raster grids (see Chapter 3 for details).

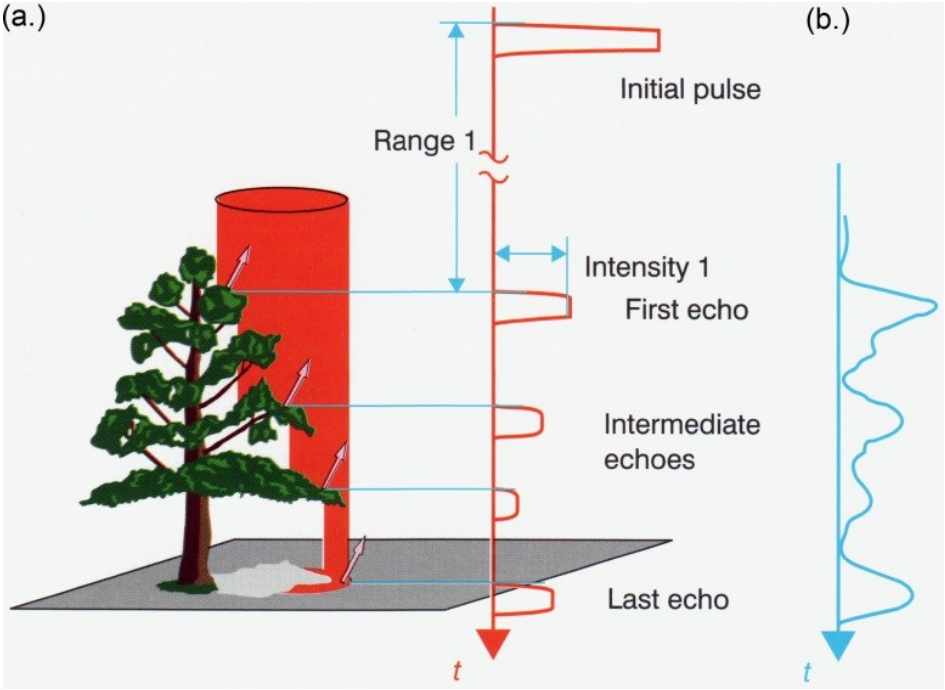

Figure 2.25: Diagram showing laser pulse return data from (a.) a discreet and (b.) full waveform system.

2.3.2 Terrestrial Laser Scanning (TLS) Techniques

TLS systems that are regularly applied by field surveyors work on ToF principles, which are provided in Section 2.3.1. These scanners are useful for the increased distances at which their lasers are able to travel, with most operating to at least 100m (Barber et al. 2007, p.7). During a survey conducted with a TLS instrument, the scanner position remains static whilst a scan is conducted and the instrument is mounted upon a tripod for stabilisation. To obtain measurements the scanner rotates about a vertical axis to generate data in the horizontal (or azimuth) direction whilst the rotating mirror deflects the laser beam across the subject in the vertical direction (Petrie and Toth 2009). For georeferencing purposes, the TLS usually requires specially designed targets to be placed within the area to be scanned, which are themselves surveyed using a GNSS. These can be seen in Figure 2.26.

The operating range of a TLS designed for use on larger objects, such as building facades and landslides for example, is 2-300m, although typical accuracies usually quoted, namely 3-6mm, are based on a range of up to 50m (Barber et al. 2007). As the TLS is a close-range system it is capable of generating much more dense point clouds than an ALS and thus it records objects with greater detail. The drawback of a TLS system is that it is designed for covering much smaller areas than ALS, although some TLS systems have been adapted for mounting on vehicles, such as boats, vans and helicopters, to exploit the benefits of generating both a dense point cloud of a large area in a shorter amount of time. Ultimately the TLS generates a similar

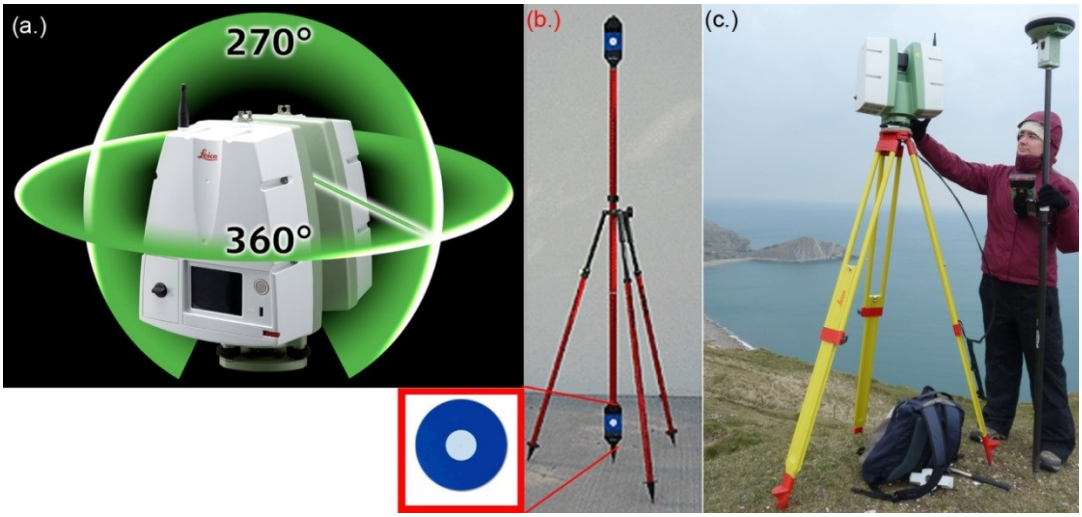

Figure 2.26: Components of a TLS (a.) vertical and horizontal rotation (Leica Geosystems AG 2011) (b.) twin pole and circular target (Leica Geosystems AG 2014), and (c.) TLS and Leica Viva GNSS at Worbarrow Bay.

product to that of the TLS, namely a large point cloud consisting of millions of measurements, which requires processing to create the desired end-product. This can be a DSM, although there are few TLS systems that gather information about waveform echoes, unlike the TLS. Therefore any data filtering to remove unwanted or spurious points can either be undertaken with software that automates this process or by manual editing of the point cloud. Automation usually involves setting a maximum height offset such that any points within an area that exceed this value are removed, which can be a more efficient process than manual editing. However, due to the file sizes that are often generated by TLS systems, it is vital to have access to a PC that has sufficient processors and memory to be able to handle large data volumes.

2.3.3 Archaeological Applications of Laser Scanning

As with photogrammetry, laser scanning can be separated into airborne and terrestrial applications for archaeology, which are discussed under separate headings in this Section. The decision to differentiate between ALS and TLS applications is due to the former's application for landscape-scale recording, whilst TLS is useful for covering smaller areas. This is not the case with photogrammetry, whereby the terrestrial applications do not lend themselves as easily to recording earthworks and sites.

2.3.3.1 Airborne Laser Scanning (ALS) for Archaeology

The applicability of airborne laser scanning (ALS) for documenting the archaeological resource has been principally applied to terrestrial sites, using ALS for a multitude of applications:

prospection, predominantly assessing the capabilities of airborne scanners to detect features obscured by vegetation (Bewley et al. 2005; Devereux et al. 2005; Ullrich et al. 2007; Doneus et al. 2008; Gallagher and Josephs 2008; Millard et al. 2009), enhancing the existing historic environment records (Bewley et al. 2005; Challis et al. 2008b; Challis et al. 2008c), documenting alluviated landscapes and river valleys (Carey et al. 2006; Challis et al. 2008a; Challis et al. 2008b; Howard et al. 2008), and in some cases highlighting the under-researched area of intensity data (Wehr and Lohr 1999; Shell and Roughley 2004; Challis 2006; Challis and Howard 2006). In such projects, data generated through the use of ALS equipment has been interpolated to provide digital elevation models (DEMs), in the form of either digital surface or digital terrain models (DSMs and DTMs respectively), to form layers in a GIS over which a range data from other sources can be draped. These include results from soil sampling (Entwistle et al. 2009), data from inventories and aerial photography (Challis et al. 2008c) or the results derived from geo-prospection techniques, like ground penetrating radar (GPR) and multi-spectral imaging (Bewley et al. 2005; Carey et al. 2006; Howard et al. 2008).

Full-waveform ALS for archaeological prospection in forested areas has proved fruitful in identifying previously unknown archaeological earthworks (Devereux et al. 2008; Doneus et al. 2008; Bollandsås et al. 2012; Johnson and Ouimet 2014), although the full-waveform product is not readily available as an off-the-shelf dataset. Instead the waveforms are often digitised to create discreet return data, much like the first and last return products that can be requested from the EA. Whilst a number of open-source softwares are appearing that allow archaeologists to work with this data, such as LAStools and GRASS, proprietary software such as ArcGIS and ENVI are also providing tools for ALS manipulation.

Beyond the capture and processing of ALS data, geo-spatial analysis (in GIS) for archaeological purposes using ALS has focused upon enhancing the appearance and likelihood of detecting subtle archaeological remains. Examples of such analysis are height-ratio exaggeration (Crutchley 2006; Kvamme et al. 2006; Millard et al. 2009), contour generation (Bewley et al. 2005; Harmon et al. 2006; Challis et al. 2008c; Lerones et al. 2009) and hill-shading (Bewley et al. 2005; Harmon et al. 2006; Kvamme et al. 2006; Devereux et al. 2008; Corns and Shaw 2009; Millard et al. 2009; Bernardini et al. 2013), and local-relief modelling (LRM) (Hesse 2010). Viewsheds are another technique that have been utilised for identifying the intervisibility of archaeological sites (Shell and Roughley 2004; Bewley et al. 2005; Rowlands and Sarris 2007), which is useful tool for interpreting historic landscape use.

The boundaries of analysis using ALS data are ever widening within archaeology as familiarity with the technology grows and experimentation with GIS-based processing tools increases, as illustrated in Figure 2.27. A number of authors have experimented with principle components analysis (PCA) using multiple hillshaded models to extract the maximum information from DSMs (Devereux et al. 2008; Challis et al. 2011; Bennett et al. 2012). Bennett et al. (*ibid.*), Challis, Forlin and Kincey (*ibid.*) and Stular et al. (2012) have all conduced comparisons between a number of image processing methods designed to visually enhance ALS data, such as PCA,

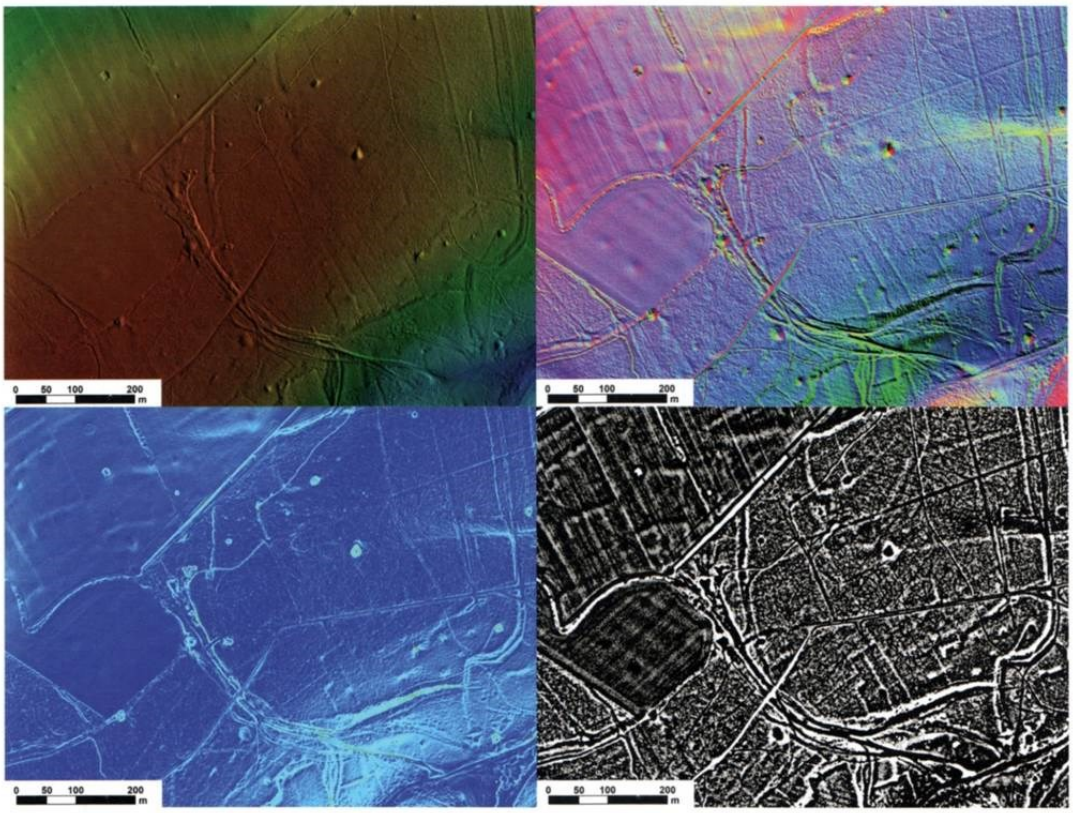

Figure 2.27: Examples of GIS analysis performed on ALS data, from top left to bottom right: colour height shading, principle components analysis, local relief modelling and slope (Crutchley 2013).

slope, aspect, LRM and sky-view factor (SVF), to inform ALS users of how best to produce data with which to interpret archaeological landscapes.

Bennett et al. (*ibid.*) have conducted an empirical analysis on ALS data, comparing the number of archaeolligcal features that can be identified across a number of visualisation techniques within the same region, and further copmared the resultant values with the number of features identified by the NMP. Whilst this is a useful exercise in establishing the archaeological detail contained within ALS, the authors have subjectively recorded the archaeological features from each of the ALS visualisation techniques. It is therefore impossible to establish whether prior knowledge of the archaeological content of the area has influenced the feature count conducted by the authors. However, it is heartening to note that Bennett et al. (*ibid.*) discovered that land-use between ploughed versus non-ploughed areas did not influence feature detecting in the ALS data, and that microtopographic features of the order 0.05m to 0.15m could be identified.

More recently, Doneus (2013) has compared SVF and LRM to a technique known as ‘Openess’. Whilst LRM enhances the appearance of micro-topography and SVF utilises the effects of diffuse light to alter the contrast across an area based on the visibility of the sky at that point in a hemisphere, openness takes SVF one step further and considers each pixel to be surrounded by a sphere rather than a hemisphere. Doneus (*ibid.*) reports that LRM performs more favourable in regions characterised by shallow relief, whilst openness is more appropriate for

steeper regions. As regards SVF, openness apears to be a superior technique for enhancing micro-topographic features. Despite the large number of visualisation tools available to archaeologists for enhancing the appearance of features in ALS DSMs, many authors advocate using a number of these techniques rather than just one (Bennett et al. *ibid.*; Challis et al. *ibid.*; Doneus *ibid.*; Stular et al. *ibid.*). As further proof of the maturing applications of data visualisation for ALS, a data processing guide has been released by the RCAHMW (2012) for archaeologists to consult.

ALS has been identified by archaeologists such as Barnes (2003) and Kincey and Challis (2010) as having potential for change detection and monitoring. Whilst Barnes (*ibid.*) merely highlights this potential use, Kincey and Challis (*ibid.*) examine the uses of ALS for monitoring upland landscapes, particularly for assessing path erosion caused by visitors, land-use and climate variations. However, their approach in detecting change is predominantly visual, and requires the supplementation of an ALS DTM with orthorectified aerial photography to assist identification of erosion. Profiles were extracted from the ALS data to examine the depth of erosion, with Kincey and Challis (*ibid.*) stating that the ALS data, with a spatial resolution of 0.5m, could detect elevation changes as small as 1-2cm. These observations are not confirmed by using another survey technique, the inclusion of which would be prudent given the generally accepted ~±15cm absolute vertical uncertainty (equating to a maximum observed vertical change of ~30cm) of an ALS DSM. Interestingly, the authors note that change mapping using ALS has tended to focus on detecting large-scale changes, such as landslides and coastal erosion, as discussed by Miller, Mills and Bryan (2008a), rather than smaller-scale issues that afflict archaeology. This subsequently highlights the potential to further investigate the change detection properties of ALS in comparison with another technique, such as photogrammetry.

The threat of coastal to archaeological features has been identified by a few authors. Miller, Mills and Bryan (2008a) purport to have investigated the use of ALS for examining natural processes such as erosion and accretion in coastal areas by applying the technique to recording cliffs at Whitby headland. Again, this project focuses on large-scale change in a single epoch, rather than assessing the utility of regular monitoring to detect smaller-scale phenomena, such as spalling, or the recording of the archaeological features affected by such change. In light of the anticipated increase in erosion rates and sea-level rise around the UK, regular recording of the UK coastline is undertaken by the EA using their ALS system, an Optech ALTM Gemini (Geomatics Group 2010). Although the majority of data is collected to generate approximate densities of 1 point per $1m^2$ or 1 point per $2m^2$, thereby corresponding to interpolated grids of 1m or 2m respectively, there are some sections of coast that have 0.5m and 0.25m gridded data. The EA have been generating ALS surveys since the 1990s, although the ALS data that is commercially available dates from 2000. This provides eleven years of data with which to establish coastal change using a data format already in digital structure. However, establishing coastal change over a number of decades would require photogrammetric processing of older aerial stereo-photography as ALS does not have the time depth to facilitate an in-depth study of prolonged coastal change. Should archaeological earthworks have been damaged or destroyed by such change prior to 2000, the only means by which to recreate these

data would also reside with historic SAPs. These data require testing to discern their ability to detect the effects of erosion, and not just coastally, on archaeological condition.

The spatial resolution of commercially produced ALS data, which is flown without archaeological purposes in mind, is the limitation this has upon the detection of upstanding features. It is important that fine spatial-resolution data is available for archaeological evaluation. A project undertaken by the Royal Commission on the Ancient and Historical Monuments of Wales (RCAHMW) examined cliff retreat at promontory forts in Wales (Page et al. 2009). ALS data with a 2m resolution was, unsurprisingly, found to be inaccurate in comparison with differential Global Positioning System (dGPS) data, leading the authors to conclude that subtleties in survival and interpretation information were missing when the ALS data was examined onsite (see Figure 2.28). Higher resolution detail was felt to be necessary where an important monument was threatened. Corns and Shaw (2009) advocate the use a helicopter-mounted ALS system capable of providing higher-density data. Two differing resolution datasets were collected, namely 50pts/m^2 and 15-30pts/m^2, to assess the resolution required to successfully document upstanding archaeology. However, the extensive size of the datasets prohibited the archaeologists from processing the data, thus requiring the survey company to generate DSMs and DTMs on their behalf. The authors felt that the data produced more accurate models and would be useful for identifying damage to archaeological sites because of the higher data density, although the costs of utilising helicopter-mounted ALS systems are likely to be vastly prohibitive. It is noteworthy that the authors conclude by echoing similar sentiments to Bowden (1999) and Taylor (1998), namely that there is little point in applying high-resolution data

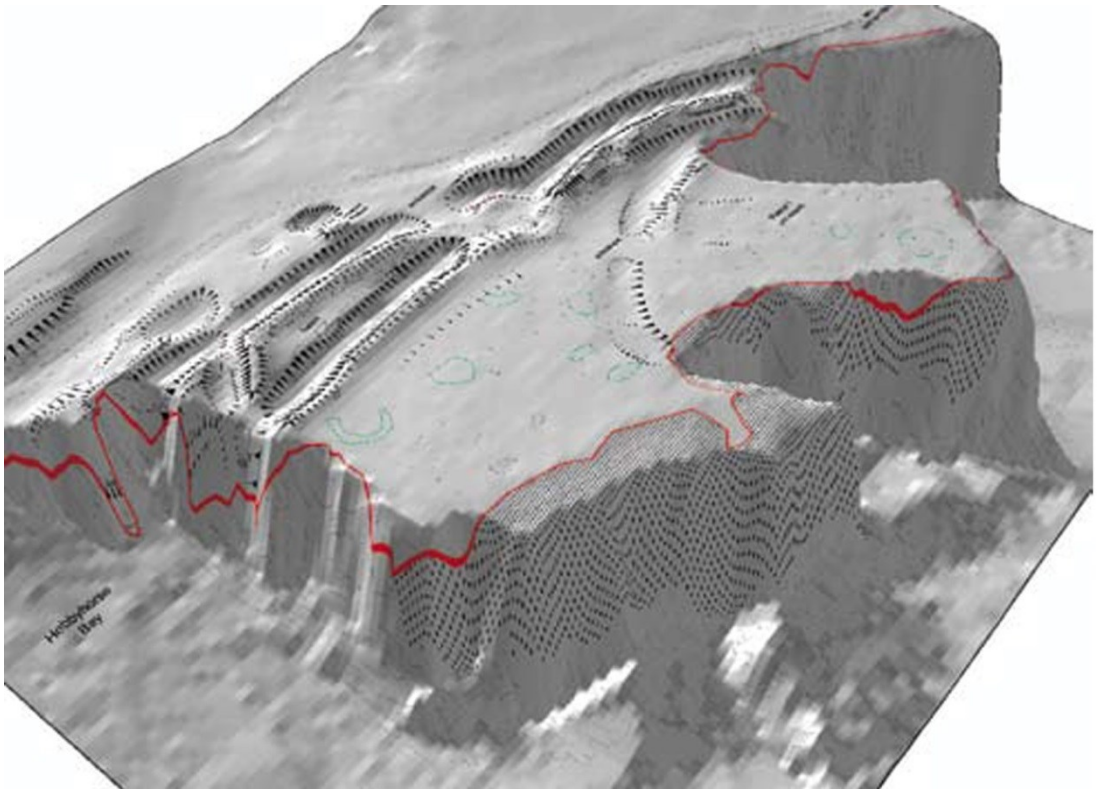

Figure 2.28: RCAHMW GCP survey (shown in red) draped over EA ALS data (NPRN 94226, © Environment Agency copyright, D0055624. All rights reserved.).

capture methods to archaeological landscapes of which little is known.

Page et al. (*ibid.*) concluded that ground survey techniques were the only reliable methods for generating baseline data with which to compare ALS, particularly where the assessment of cliff edge erosion was a primary aim. The team also felt it unlikely that an ALS survey could be mobilised quickly enough at short notice, for example after a storm event, to record any damage sustained by a coastal site. Aerial photography was the suggested alternative because the pictorial information provided a way of assessing vegetation condition and soil erosion. Overall, they concluded that traditional field survey methods could not be replaced for site recording. This opinion is shared by Corns and Shaw (*ibid.*) despite their access to a much higher resolution dataset, albeit generated for different purposes. It must be acknowledged, however, that airborne techniques, such as ALS, are useful for placing archaeological features and sites within their landscape context, although further investigation is required to assess their suitability for mapping archaeological earthworks and other features.

Fortutiously, this need is gradually being addressed. Gallay et al. (2013) have assessed an ALS DTM, generated for terrain modelling on sloped and flat ground, against data created by other ground-based methods, namely TLS and GNSS. The authors discovered that GNSS delivered the most acurate elevaion data, with an RMSE of 0.16m on slopes and 0.02m on flat ground. Whilst TLS was more efficient for covering larger areas, elevation accuracy decreased in areas where there were slopes and dense braken coverage to 0.52m and performed less favourably than ALS data, whose RMSE was 0.23m. This is due to the vegetation coverage, through which the TLS could not penetrate. However, on flat terrain, the TLS out-performed the ALS, with RMSE values of 0.07m and 0.29m respectively. Overall, the type of terrain was found to influence the accuracy of the elevation measures, with the flat surface producing more favourable RMSE scores, although the ALS was found to have overestimated the terrain. Gallay et al. (*ibid.*) had expected DTM accuracies to be worse in the slope region, although the removal of outliers and non-terrain points improved any measures of error. Subsequently, their findings have imprtant implications for archaeologists employing these instruments for data collection in areas with steeper slopes, although it is unlikley that TLS will be eomployed for data collection across regions that are covered with dense vegetation.

At this stage it is worth noting the more extensive treatment of ALS data by archaeologists is in contrast to the shorter discussion on the photogrammetric applications by this discipline. There are a number of reasons as to why this could be. Firstly, the native format of ALS is digital, which facilitates the immediate processing and rasterisation of the data once it has been supplied to the archaeologist. During the early 2000s the technique was enthusiastically adopted by archaeologists after EA ALS data was show to reveal subtle earthworks that were once thought to be extinct (Bewley and Raczkowski 2002). Digital photogrammetry, however, has predominantly remained in the sphere of technical specialists since its development during the 1980s. As the software at this time was both expensive and required knowledge of the photogrammetric process to output digital data for archaeological use, this precluded its enthusiastic uptake by the archaeological community. However, this situation is changing with

the advent of SfM, for which empirical comparisons are now being made with ALS and TLS data for a number of archaeological features (Green et al. 2014; McCarthy 2014; Risbøl et al. 2014).

Whilst ALS has been adopted enthusiastically by the archaeological community, a few authors have expressed their concern regarding its ability to carefully describe earthwork features (Page et al. 2009). As a relatively new technology, ALS does not have the tempoal range to facilitate the assessment of change to archaeological earthworks over a prolonged period. This is also problematic if upstanding features have been destroyed prior to the late 1990s, when the technology started to produce commercially available data. Subsequently, the only way to retrieve such information is through the processing of SAPs using photogrammetric techniques.

2.3.3.2 Terrestrial Laser Scanning (TLS) for Archaeology

Earlier literature describing the application of TLS for recording cultural heritage and archaeology has predominantly focused on the recording of architecture (Dawson and Levy 2005; Lambers et al. 2007; Yastikli 2007; Dawson et al. 2008; Lerones et al. 2009; Camarda et al. 2010). There are notable exceptions, however. Entwistle et al. (2009) utilised TLS for collecting high-resolution data for modelling microtopography, which they argue is significant when considering the destruction of archaeological remains due to development or environmental processes. For manageability reasons, the authors had to reduce the size of their point-cloud from 36-million to 2.5-million points. Doneus and Neubauer (2003) used TLS to rectify photography of a trench section for the extraction of stratigraphic information, which they cite to be 80% faster than photo-rectification using other techniques, such as photogrammetry. Lobb et al. (2010) used TLS data to re-scan wood samples over the course of a month to reveal regions of change on the samples. The authors found that this high-resolution, objective, 3D recording method was highly applicable to their investigations, particularly when compared with more traditional techniques, and could form the basis of an on-going method for monitoring the degradation of such fragile artefacts.

TLS has also been utilised for recording coastal archaeology, namely along the Keiss foreshore in Scotland (Cavers 2007) and the Fregus Estuary in Country Clare, Ireland (Sands 2010). The Keiss project produced a high-resolution topographic record of the foreshore to digitally preserve it and complement a series of archaeological surveys and excavations, some of which were also recorded using the TLS. This data was coupled with a dGPS survey that interpreted the archaeological features along the foreshore. The Fergus Estuary project utilised TLS to scan a fishweir, whose structure was felt to be too complicated to record using other survey techniques. Intertidal mud hindered survey progress, which could only take place during low tide when the fishweir was exposed for 3 hours (Shaw and Devlin 2010). A significant amount of noise was present in the TLS data, as shown in Figure 2.29, caused by the laser reflecting from the wet mud and standing water. Shaw and Devlin (*ibid.*) state that photogrammetry would have augmented the scan dataset, especially for more complex structures, such as wattle and daub

baskets. Due to the hostile environment in which the survey took place, the authors felt that there was some utility in being able to perform data analysis back in the office, irrespective of the preference to perform archaeological interpretation on-site.

As mentioned in relation to ALS data, TLS generates fine spatial resolution for the production of DEMs/DSMs, which is also of interest to geographers who wish to record microtopography, much like archaeologists. Hetherington et al. (2007) and Guarnieri et al. (2009) state that topographic variation occurs at a variety of different scales, and finding a method to document both macro- and microtopographic features is challenging, and no less so for archaeology. TLS provides a way in which to capture such diverse scales. However, using a TLS to record a large area is problematic, given its reduced operating range, which is in contrast to ALS. Although Hetherington et al. (*ibid.*) was observing changes to the micro-topography of a creek over a short period using a TLS, the authors found it challenging to select scan positions that ensured there was enough overlap between scans as well as minimise data occlusions. This would be an important consideration for any archaeologist wishing to use TLS for documenting archaeological feature, especially earthworks. The TLS would need to be moved frequently to record areas that are occluded or under-represented in the data from other survey positions, which elongates the survey process. This problem can be countered with some TLS systems by scanning small sections at a time and adjusting the point spacing for each, to ensure it remains constant.

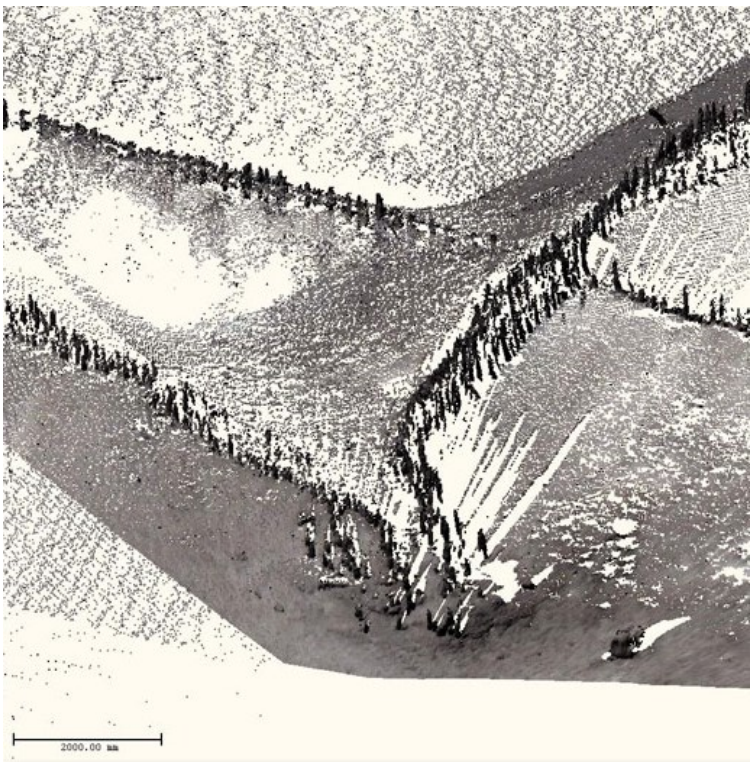

Figure 2.29: TLS point cloud of the fishweir on the Fergus Estuary (Shaw and Devlin 2010/Copyright © 2014 The Discovery Programme. All Rights Reserved.).

The issue of data occlusion and scan overlap is exasperated by the scanner position, as problems arise with point-spacing if the TLS is not perpendicular to the object it is recording. Figure 2.30 illustrates the concept of data occlusions in TLS point clouds. Solutions to such a problem have been make-shift in nature, requiring the TLS to be elevated in some way. Doneus and Neubauer (2003) addressed the issue by their TLS on top of a stationary vehicle, while Guarnieri et al. (2009) chose to perch a TLS on a 3-metre custom-built aluminium tripod. Hetherington et al. (2007) opted to choose suitable vantage points along the Dartford Creek, which is perhaps the most viable option. However, the solution adopted by Doneus and Neubauer (*ibid.*) is similar to vehicle-mounted TLS systems that are in operation within the UK. These offer another means by which to rapidly collect high-resolution datasets of a large area (Mills and Barber 2007), which may produce a dataset that rivals airborne capture methods. An example of a commercial system is StreetMapper (Hunter et al. 2006), which combines two TLS systems with an inertial navigation system (INS) and a GPS. From an archaeological perspective, however, vehicle damage could be a potential risk to upstanding archaeological features in certain circumstances, particularly if the ground is wet. Whilst vehicle-mounted systems are an alternative to helicopter-mounted scanners, as utilised by Corns and Shaw (2009), the cost of commissioning such surveys and processing a large dataset would preclude their use in many instances.

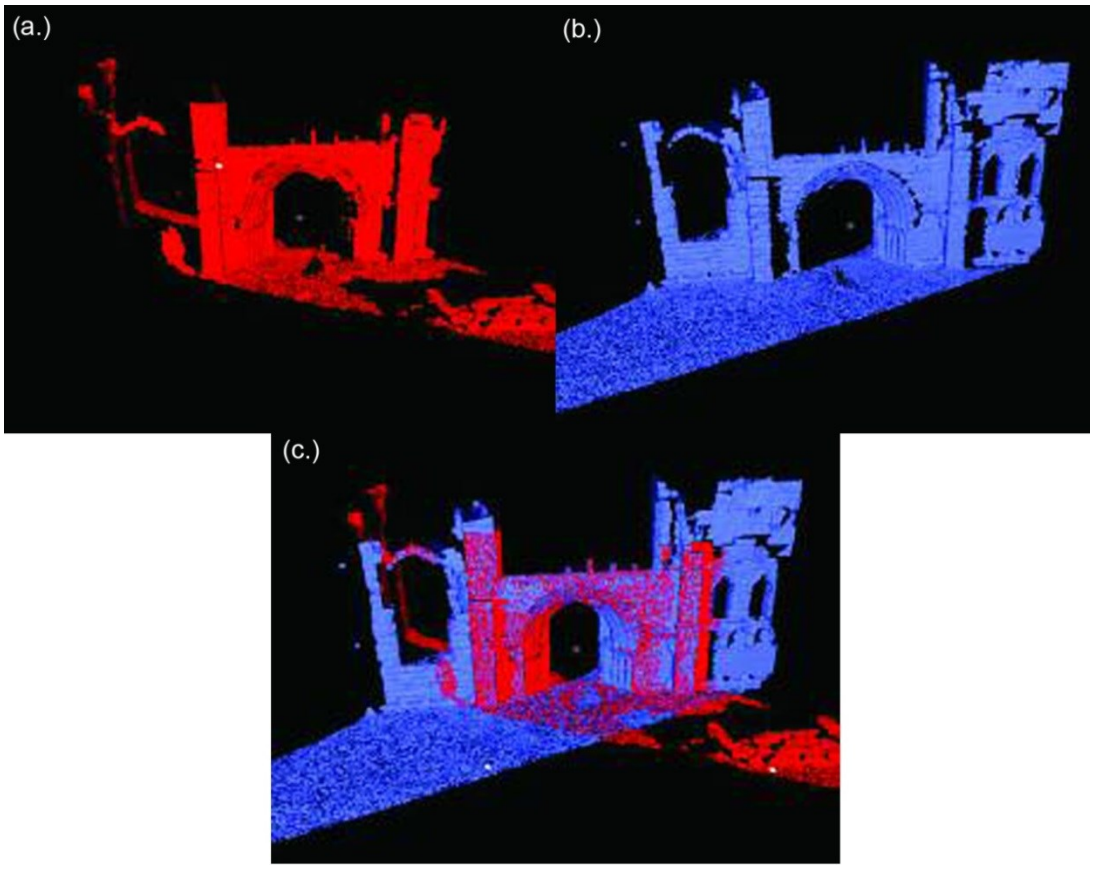

Figure 2.30: TLS scan of a building façade from two different viewpoints. Occlusions are especially visible in (a.) to the left and right of the building. By combining the scans from (a.) and (b.), the resultant point cloud (c.) addresses the occlusions (Crutchley 2010).

The literature discussing the application of TLS to archaeological and cultural heritage topics often advocates combining TLS with photogrammetry in the same survey campaign. By utilising the strengths of each technique, it is often possible to overcome the separate weaknesses of both systems and obtain a multi-resolution product (Vozikis et al. 2004; Lerma et al. 2010). There are some TLS systems that combine a laser with a calibrated digital SLR camera and thus high-resolution imagery and scan data can be captured together. This approach was adopted by Neubauer, Doneus, Studnicka and Riegl (2005), who utilised this instrument to demonstrate its ability to document and monitor the Giza Pyramids. It is disappointing that the only product to be presented is a 3D model of the pyramid and Sphinx, without any associated data relating to the metric performance of the technique.

There does not appear to be a similar approach for earthwork features, despite the range of factors that have been identified as a threat to this resource (see Section 1.1.1). Whilst the importance of recording micro-topography has been alluded to (Hetherington et al. *ibid.*), it appears that this can only be effectively achieved over small areas and with considerable effort by a field team. Subsequently, there is scope for investigating the utility of TLS for recording such features and its role in generating survey data that records subtle earthworks that might be missed by both ALS, photogrammetry and direct techniques (see Section 1.1.3).

2.4 Discussion

Throughout this Chapter a number of archaeological applications for mass-capture data have been discussed, although some authors (Bowden 1999, Corns and Shaw 2009, Page et al. 2009) appear to have placed greater importance on the capture of data relating to upstanding features using ground-based, direct methods as opposed to airborne mass-capture systems. However, direct methods do not provide the landscape context for upstanding features, and nor do they provide the data density of their airborne counterparts, which assist in identifying hiterto unnoticed, often subtle features. Whilst the ability of an airborne system to achieve higher data resolutions and detect subtle features is dependant upon its mode of operation (flying height, pulse rate, beam divergence etc.), their ability to provide data coverage for a much wider area and at a faster rate than ground-base methods, is more cost effective. Mass-capture techniques, and in particular photogrammetry (Dallas et al. 1995), have been utilised for creating anti-disaster records, albeit of buildings. Whilst any survey dataset must be subject to interpretation, including those produced using mass-capture techniques, it is mass-capture technology that facilitates the extraction of lost spatial information, as direct techniques can offer nothing beyond the discrete data that has already been collected.

Bowden and McOmish (*ibid.*) eloquently summarise the problem between the technical advocates versus the interpretive approaches employed by archaeologists to earthwork survey: “this is a classic scientific paradigm – we are starting from such divergent viewpoints that common ground is hard to find”. However, as the trend in feature loss continues and other

mass-capture techniques are developed, such as laser scanning, questions arise as to whether newer technologies provide metrics that are more suited for describing archaeological feature metrics post-destruction. Mass-capture techniques have rarely been applied for monitoring archaeological landscapes and the extraction of metrics relating to upstanding features have relied upon rectifying historic SAPs to provided limited, 2D datasets that simply identify where a feature either exists or did exist. This situation is only just changing, as evidenced by the work of Doneus (2014) and Verhoeven et al. (Verhoeven et al. 2012a), who have examined the role that SfM techniques can play in creating DSMs from archive SAPs (see Section 2.2.3), with Doneus (*ibid.*) utilizing ALS data against which to compare the results. However, neither Doneus (*ibid.*) or Verhoeven et al. (*ibid.*) have fully investigated the variables that influence the production of DSMs using archive SAPs, including the use of SAPs that are no longer accompanied by camera calibration and exterior orientation data. As SfM is not specifically designed for utilising high-resolution, traditional stereo-photography, but for lower-resolution, multiple overlapping photographs, it would be beneficial to conduct a comparison between SfM and high-end photogrammetric software outputs. This is the situation facing archaeologists in the UK who also wish to capitalise on the 3D information inherent within archive SAPs. Whilst archive SAPs have been utlised by other disciplines for detecting and quantifying changes in the landscape (Chandler 1989; Walstra et al. 2004, 2007), no investigation exists as to whether photogrammetric methods can recover archaeological metrics from these data.

Photogrammetry is a mature, well-established technique that has a proven ability to be cost-effective. Stereo-photography can be processed and analysed post-destruction of a feature (ante-disaster records) and is suitable for use by non-experts (Bryan and Chandler 2008). Aerial photogrammetry is also becoming more accessible to non-expert users since the advent of digital photogrammetric software that can run on personal computers. In comparison with the raw data from ALS and TLS systems that is difficult to collect and process, digital photogrammetry does not present any greater challenge to the data manipulation and extraction procedure. It must be noted, however, that ALS data supplied in gridded format by commercial companies has the potential to remove data processing issues and thus provide a product ready for use in a GIS by archaeologists. However, the ambiguity surrounding the preparation of this data presents some issues as it is unknown how much archaeologically important data may have been lost during the processing stages (Challis et al. 2008b).

The practicality of applying ALS and TLS technologies, particularly to coastal recording, appears to be problematic when they have been utilised, especially where small-scale features are present. Whilst TLS can provide high-resolution datasets of these features, the bulk of the equipment and difficulty of operation in coastal areas, which are often hard to access, make it an impractical choice in many cases (Shaw and Devlin 2010). The purchase of such datasets and the requisite software and skills to process them may also preclude their consideration for frequent application to regular recording assignments for landowners with a large estate. Although ALS data appear to have enhanced the ability to prospect for archaeological features, in some instances the data is felt to be too coarse for producing suitable metrics for archaeological survey. However, a balance has to be struck between the purpose of the survey

and the scale at which the data is required, which will also be dictated by the resources available. If a survey has not been undertaken by a field team in a timely manner to collect data relating to an earthwork monument prior to its deterioration, the only way in which this can be achieved is via photogrammetric restitution using archive SAPs.

It is surprising that, given the frequency with which archaeological data is transcribed from archive aerial photography, this resource is not fully utilised for its ability to produce photogrammetric DSMs. As proven by Walstra (2006) these images are capable providing DSMs and, as the only dataset to allow for the reconstruction of historic landscapes, offer the only opportunity to provide metrics about archaeological features that have since been damaged or destroyed. As this is the fate awaiting or being suffered by many earthworks, the accuracy and quality with which SAPs provide metric data needs to be addressed.

Concurrent with the ability to reconstruct lost archaeology is the assessment of change as a threat to the archaeological resource. Archaeologists have referred to the use of ALS for detecting changes due to visitor numbers, agricultural practices or natural agents, such as animal burrowing or from climate-driven processes (Barnes 2003; Kincey and Challis 2010). It is important to establish the rate at which the resource is being damaged to enable the effective management of the archaeology and subsequently allocate suitable resources with which to mitigate the effects of change. Whilst ALS does not have the time-depth with which to supply historic rates of change, SAPs do and it is important to establish the accuracy and quality of the data with which change can be detected.

Whereas it was once believed that laser scanning, as the newer technology, may eventually replace photogrammetry, many authors have discussed the utility of combining the two techniques (Riegl et al. 2003; Harmon et al. 2006; Lambers et al. 2007; Díez et al. 2008; Núñez Andrés and Buill Pozuelo 2009; Costantino et al. 2010; Lerma et al. 2010; Nex and Rinaudo 2010). This combination attempts to extract the best facets of each technology and, in some cases, assists the production of a dataset with varying levels of detail (Al-kheder et al. 2009; Remondino et al. 2009; Lerma et al. 2010). Lambers et al. (2007) required a detailed 3D model of their study site to examine the architectural, functional and contextual components. This was generated using TLS data, which was placed into its landscape context by producing a large scale photogrammetric survey of the surrounding 89km^2 from which to generate a DSM. Photographic information was an integral part of the data gathering process as the authors allude to the importance of textural information when considering the condition of features on site. They also highlight the difficulties of using TLS to record an area with complicated topography: despite an apparently rigorous method of field survey, data occlusion was still an issue, which emphasises the complexity of trying to provide a complete 3D document of a site regardless of the technique applied.

2.5 Summary

This chapter has outlined the technical aspects of operation behind mass-capture survey techniques, namely photogrammetry and laser scanning, their limitations and application to archaeological practice. By ending with a discussion on the benefits and drawbacks to archaeological surveyors, the technicalities and issues of creating DSMs with these data are discussed in the next chapter.

3 DIGITAL ELEVATION MODELS (DEM)

Whilst Chapter 2 explained the technicalities of mass-capture techniques and identified their archaeological applications, this chapter examines the methods by which data from Photogrammetry, ALS and TLS is processed to form raster datasets. The introduction and propagation of errors during DEM production will be discussed and the type and sources of error will be defined. Subsequently the way in which the quality of a DEM might be ascertained will be examined before the Chapter ends with a conclusion, outlining the decision-making process for analysing the datasets to be collected for this research, which are described in Chapter 4.

3.1 Introduction to DEMs

One of the most useful products derived from photogrammetry, ALS, and TLS for archaeological use are Digital Elevation Models (DEMs). DEM quantify the elevation of observations with reference to a vertical datum (conventionally a national or global Mean Sea Level, MSL) stored in a raster format. DEM is an umbrella term for Digital Terrain Models (DTM) and Digital Surface Models (DSM). A DSM quantifies the elevation of any object present, be it bare earth, vegetation, buildings, infrastructure etc. (Maune et al. 2007). A DTM represents elevations of the bare-earth, produced from data that has been filtered or manipulated in some way to remove vegetation, buildings, infrastructure etc. (Maune et al. 2007). Maune et al. (*ibid.*) state that whilst a DEM is often assumed to be a raster file, the term can be used to denote a model that also includes breaklines and mass points that are used to more precisely describe the terrain. Examples of these differing surface models are illustrated in Figure 3.1. DSMs and DTMs are often created from interpolated point data, the processes for which are described in Section 3.2.

As discussed in Section 2.3.3, ALS has received much attention from the archaeological community for its ability to provide high-resolution DSMs and DTMs. However, long before ALS was available, Photogrammetry provided a means by which to extract terrain data across a landscape-scale area. What prohibited its wide-spread adoption by the archaeological community was the cost involved in procuring the time of specialists to obtain terrain data from highly-complicated analogue and analytical machinery (Pollefeys et al. 2000; Pollefeys et al. 2003; Ducke et al. 2011; Verhoeven et al. 2012b; Koutsoudis et al. 2013; McCarthy 2014) (see Section ? about photogrammetric history). Unlike today, there was no low-cost alternative available for archaeologists to use that would allow them to extract data from stereo-photography in an intuitive manner, which is a sentiment echoed by Jones (1985), who stated that "…we must develop low-cost, low-level recording techniques that will enable us through photogrammetry to move direct plotting of upland sites…". With the invention of digital

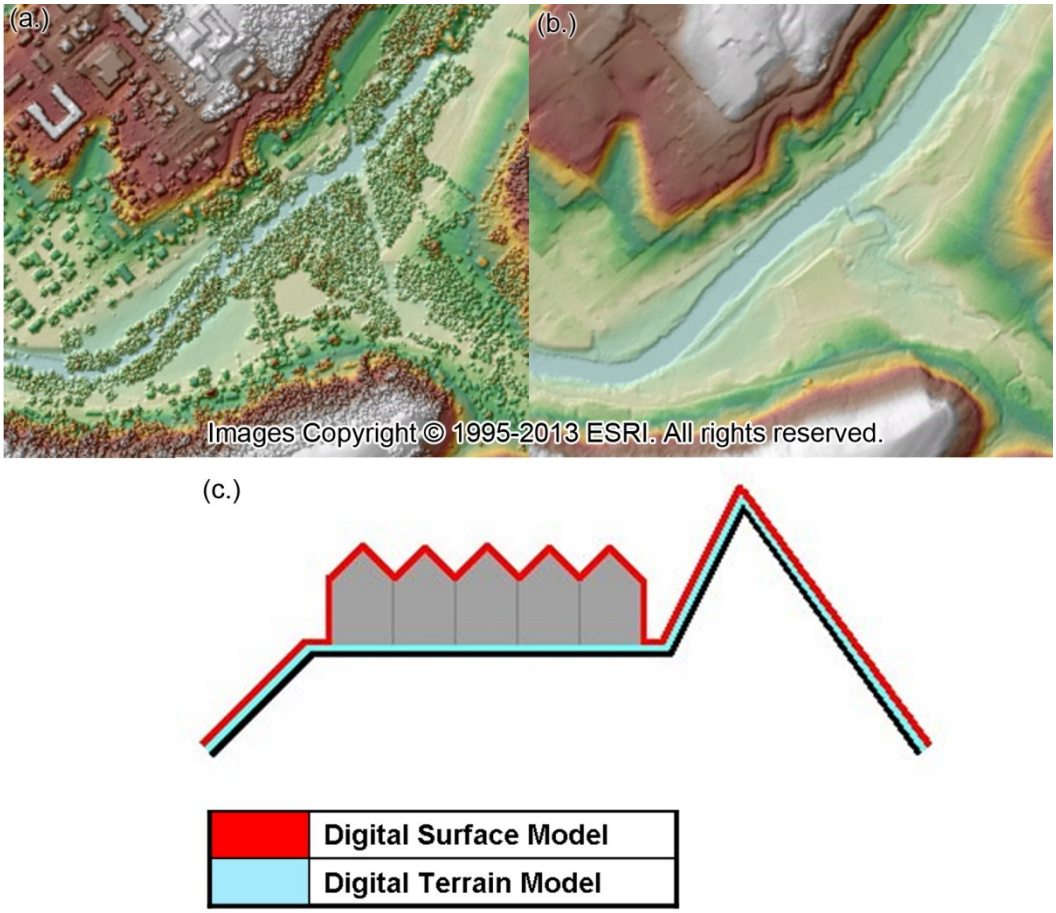

Figure 3.1: Diagram illustrating the difference between (a.) a digital surface model (DSM), (b.) a digital terrain model (DTM) and (c.) a schematic representation of their differences.

photogrammetry software dating to 1985 (see Section 2.2.2.4), the processing of stereo-pairs has gradually become less problematic and more automated, thus providing another dataset from which to extract DSMs.

As stated in Section 1.3, archive SAPs are the only means available with which to produce DSMs that facilitate the reconstruction of damage and destroyed earthworks and assess their rate of change because of the 3D nature of the data and the time span for which they are available. To fully understand the accuracy with which these data can provide metrics to achieve such ends, archaeologists must acknowledge where errors and inaccuracies can creep into the data and the data processing routines prior to undertaking their analysis.

3.2 Interpolation Methods

Gridded datasets are often interpolated from irregularly distributed elevation data (Ravibabu and Jain 2008) as shown in Figure 3.2, the collection of which is discussed in Section 1.1.3, and there are a number of methods that can be used to interpolate this data. Interpolation, with

respect to creating gridded data, describes the processes used to create a regular array of cells from random point data, each of which is assigned a value that represents elevation (Maune et al. 2007). Maune et al. (*ibid.*) state that these cells are usually square, and represent a particular unit of area, such as a square metre or square kilometre for example. Cells can be used to represent either surfaces or areas, which will affect how the data is interpreted. Cells representing a surface store the elevation value at the geometric centre of the cell, with the area in between each of these centres resembling a value that is somewhere between the adjacent cells (Maune et al. *ibid.*). If cells resemble areas, then the entire cell represents the same value, and thus the boundaries of the cell are called 'discrete', as they represent the regions at which cell values change (Maune et al. *ibid.*). Cell representation of other variables, in the form of first order derivatives is discussed in Section 3.4.3.

Although different types of interpolation algorithms exist, they predominantly work on a principle known as spatial autocorrelation, or spatial dependence, which is based on the belief that closer features are more similar than those farther apart (Lloyd 2007). When utilising interpolation to establish values at predicted locations, the existing values that are closer to those to be predicted are more likely to be representative and should thus be given larger weights, or more influence (Lloyd *ibid.*). Thus a weighting system is often used to reduce the influence more distant points will have on a result: if a value is used that is too far away, it may be dramatically different from the predicted value, and thus produce a spurious result (ESRI 2012). This concept is illustrated in Figure 3.3. An example of such a method is Inverse Distance Weighting (IDW), as explained below. Weighting functions thus try to account for spatial dependence which, as stated by Lloyd (*ibid.*), may vary in degree from place to place, and will be affected by the spatial scale of a dataset and by spatial location. Geostatistical interpolators, such as Kriging (discussed below), apply weighting functions as well as considering the influence that distance and direction may have on a predicted result, and subsequently evaluates the uncertainty associated with it.

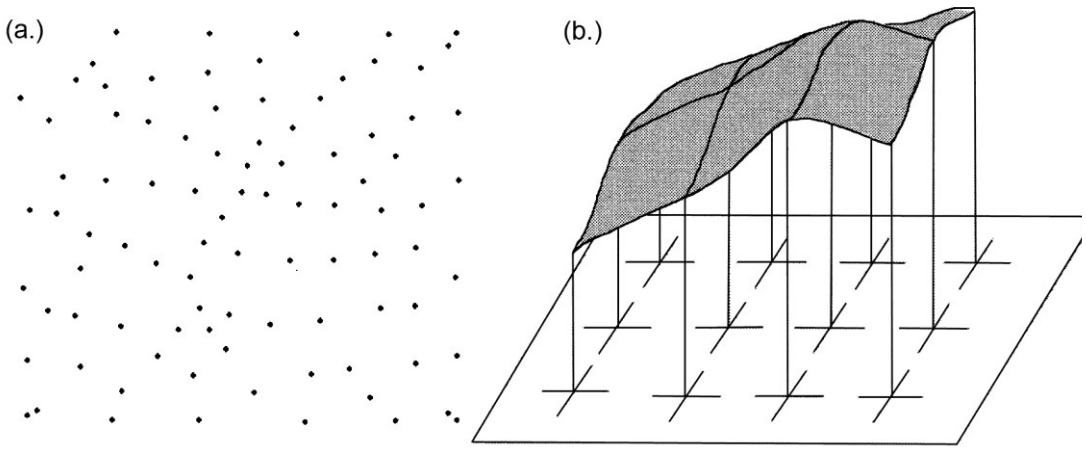

Figure 3.2: Diagram illustrating (a.) a set of irregularly spaced mass points and (b.) the way in which a surface is represented by a grid (after Maune et al. 2007).

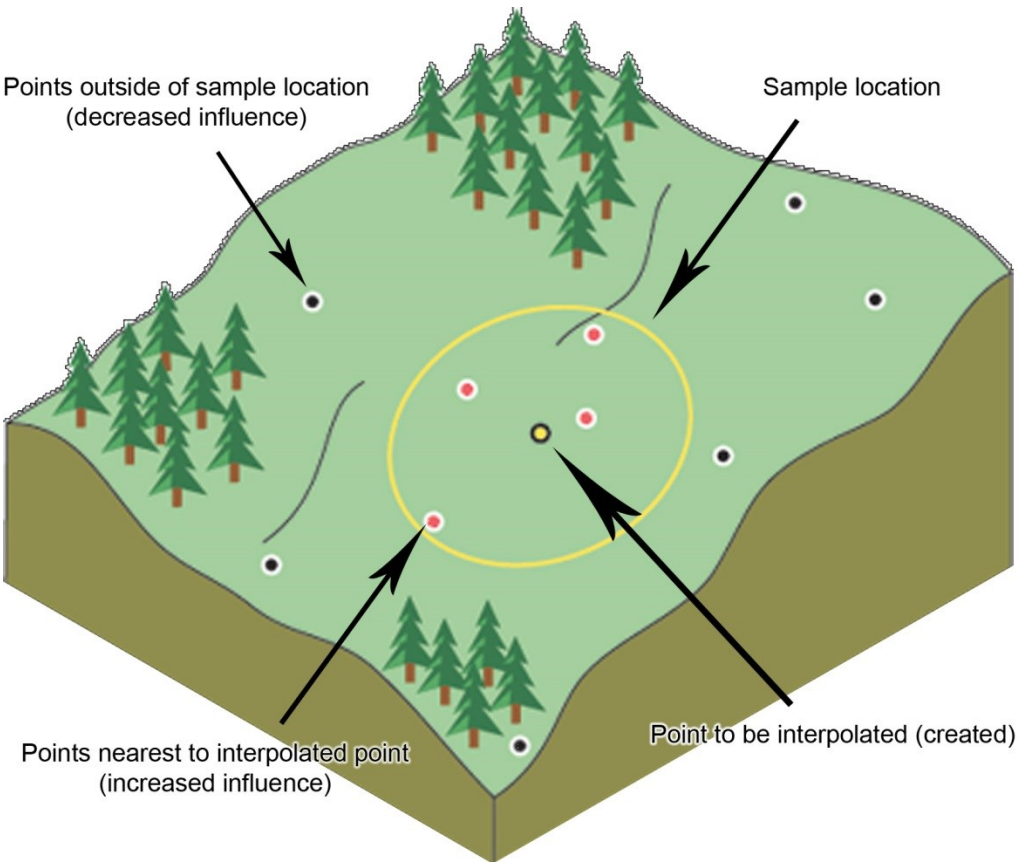

(after ESRI 2012 © ESRI)

Figure 3.3: Distance weighting is dependent upon how near or far points are to the sample to be created. The closer the point, the more influence it has on the result.

IDW belongs to a group of interpolators known as “Deterministic interpolators”, which utilise the surrounding point values to predict values for unmeasured locations. IDW applies a weighting function to reduce the influence that existing values have on a predicted result the further they are away from the location to be predicted. Thus the weight assigned to the furthest distances is much lower. An example DEM is shown in Figure 3.4. Maune et al. (*ibid*) state that this interpolator should not be used on terrain data. The authors state that IDW is useful when “the variable being interpolated decreases in influence with distance from the sample location, such as consumer purchasing power”, and they argue that this is not the case for terrain data. Kienzle (2004) states that IDW creates “unrealistically shaped terrain features” known as “bull’s eyes”, recommending algorithms such as regular spline with tension or ANUDEM instead. Bater and Coops (2009) state that ANUDEM created smooth, visually appealing surfaces that were free from artifacts in their study, whilst IDW produced surfaces that were dimpled and contained stepping artifacts where data was sparse and elevation changed abruptly. The authors also found that the parameters ascribed to the IDW interpolator heavily influenced the accuracy of the output surface. However, it is likely that this would be the case for every interpolator that provided a number of variable parameters and not just for IDW.

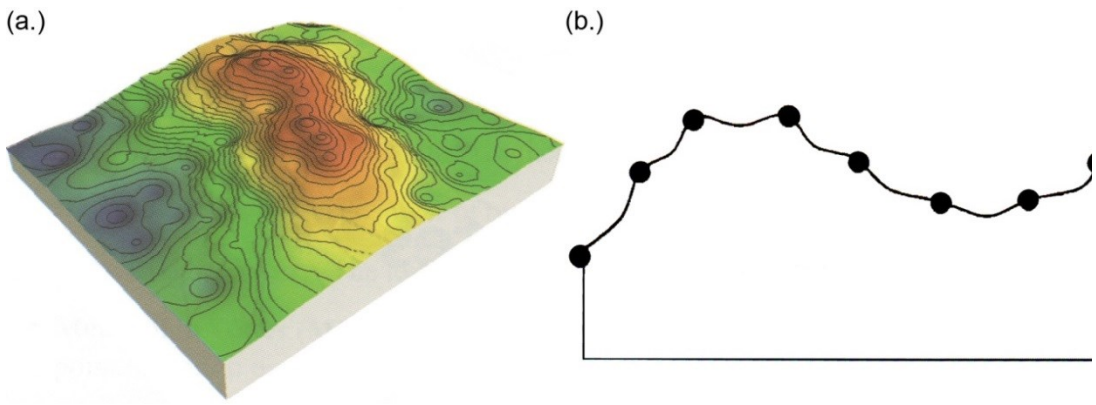

Figure 3.4: Diagram showing (a.) an IDW surface and (b.) a profile across an IDW surface (after Maune et al. 2007).

The natural neighbour (NN) interpolator initially converts point data into a TIN to identify which points are adjacent to one another. Voronoi tessellation, or Thiessen Polygons as they are also known, are then calculated that enclose each individual point within a polygon that Wheatley and Gillings (2002) state "enclose all of the space that is closer to that point than any others". When interpolating a particular point, the TIN is used to locate the closest of the existing nodes to which it would form edges if it existed in the original data (Maune et al *ibid.*). To determine the weight of influence the elevation values of the surrounding nodes have on the new point, the voronoi polygons are used to assess the area that the new point would generate as a voronoi polygon itself, and thus the area it would remove from the existing polygons. Maune et al (*ibid.*) state that this interpolator works well with both regular and irregularly distributed data, providing a surface that is a true representation of the input data, although peaks and valleys must appear in the input data in order to be depicted in the surface. Again, this would also apply to other interpolators and not just NN. An illustration of the NN interpolator workflow is shown in Figure 3.5. Both Abramov and McEwen (2004) and Bater and Coops (*ibid.*) found that NN interpolation was the most accurate interpolator for higher resolution data, and also created fewer visual artifacts. However, the visual artifacts that natural neighbour did produce were in areas where input data was sparse, exhibiting faceted surfaces that are representative of the TIN from which they were obtained (Bater and Coops *ibid.*).

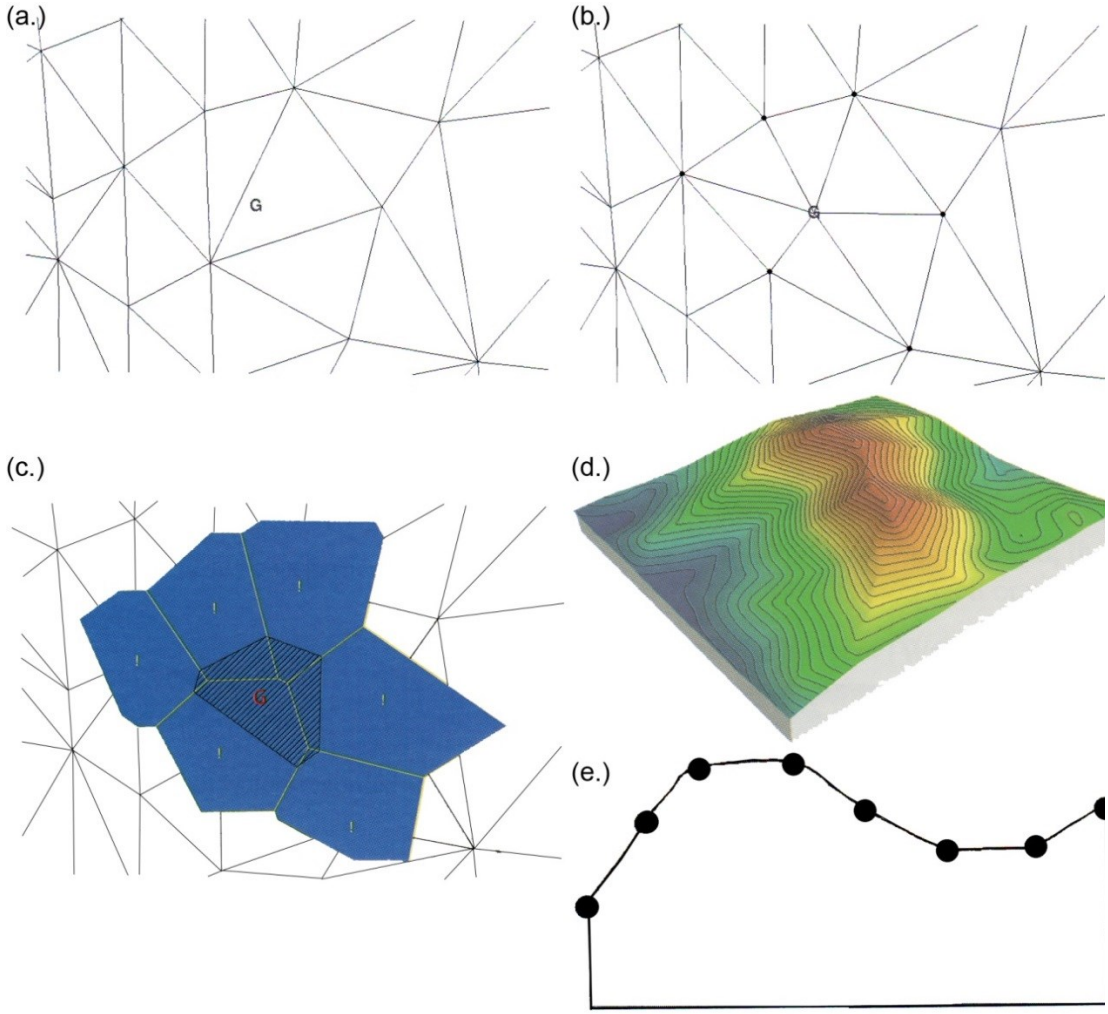

Figure 3.5: Diagram after Maune et al. (2007) illustrating the NN processing steps: (a.) 'G' is the sample location within a TIN (b.) the closest surrounding nodes to 'G' are identified (c.) the hachured area represents the voronoi region surrounding 'G' whilst the blue areas are the voronoi areas for the surrounding nodes (d.) DSM from NN interpolation and (e.) a profile across a NN surface.

Geostatistical, or probabilistic, interpolators are also used to establish values for locations that have not been measured and are thus unknown, albeit using statistical methods. Lloyd (2007) states that little is often known about how properties, such as elevation, vary in space, and thus by applying geostatistical methods that determine the probability of a value occurring at a specific location, the uncertainty of this prediction is also accounted for. One of the most popular geostatistical interpolators is a process called Kriging, which has some similarities to its deterministic counterparts due to the weighting process it employs over distances. However, Kriging also looks at the spatial correlation between neighbouring points to establish how elevations change over both distance and in a particular direction (see Figure 3.6a), which is achieved by producing a semivariogram (Maune et al. *ibid.*). A semivariogram is a graph that illustrates this concept by producing a series of points, where each single point is representative of a pair of points, whose position is stated by Maune et al. (*ibid.*) to be "based upon their difference in variance and map distance and direction away from each other". As illustrated in

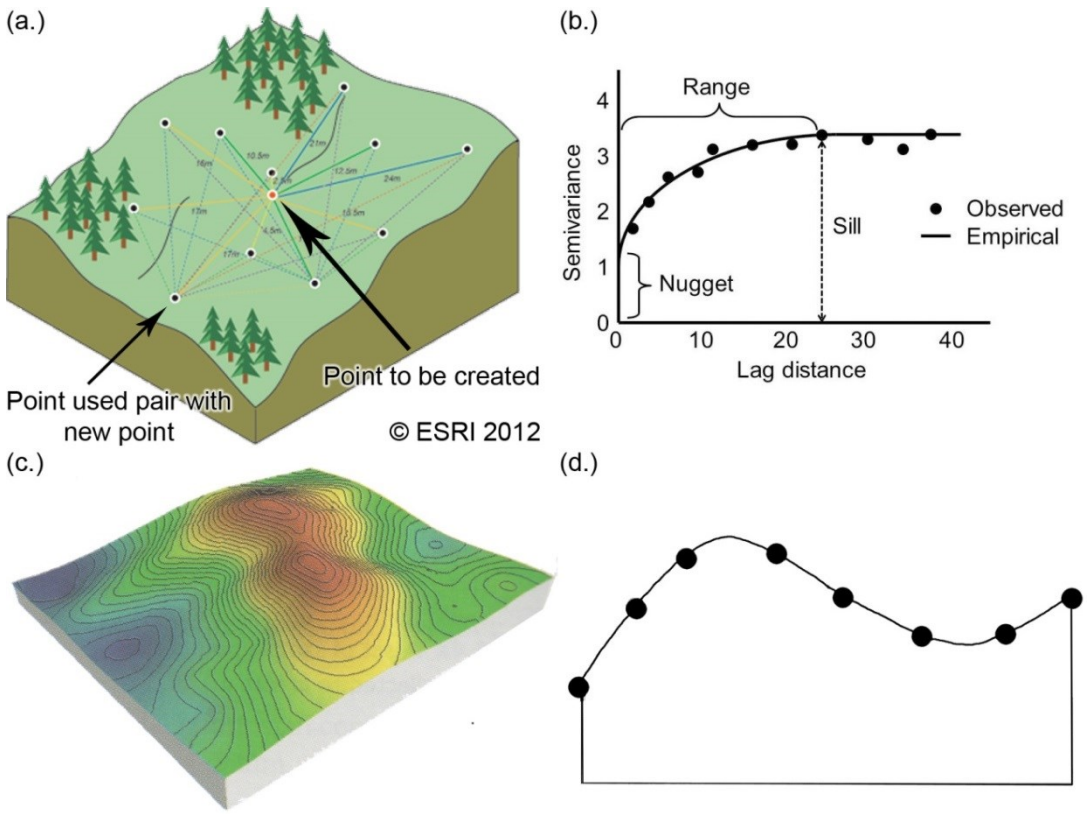

Figure 3.6: Diagram illustrating the concepts of Kriging: (a.) Paired locations between the red point and each of the black points after ESRI 2012 (b.) semivariogram illustrating how variance changes over distance after Biswas and Si 2013 (c.) DEM created by kriging and (d.) profile taken across a DEM produced using kriging (both after Maune et al. 2007).

Figure 3.6b, the points that are closer to 0 on the distance axis, or lag, are also those that have similar values, as illustrated by the y-axis that represents variance. Maune et al. (*ibid.*) cite 'Ordinary Kriging' to be the most appropriate interpolator for terrain data. However, in software such as ArcMAP, the number of variables that must be considered before the Kriging process is run are more numerous than those for IDW or NN. Subsequently there are more sources of variability to consider when comparing the DEM outputs of Kriging than for more simple interpolators.

Many researchers have studied the effect of various interpolation methods on terrain data (Abramov and McEwen 2004; Kienzle 2004; Chaplot et al. 2006; Fisher and Tate 2006; Bater and Coops 2009; Wise 2011; Wilson 2012), with the majority of authors stating that the choice of technique is rarely straightforward, mainly due to the fact that terrain can have many characteristics (Fisher and Tate 2006; Maune et al. 2007; Bater and Coops 2009). Whilst each method has its strengths and weaknesses, each interpolator is likely to introduce and propagate the errors in a DEM, which will already be present in the data due to the errors introduced during the data collection process. Fisher and Tate (*ibid.*) state that the nature of the terrain, i.e. rough or smooth, and the distribution of measurements across it, namely regular or irregular, will also determine the quality of output from a particular interpolator. Kienzle (2004) states that local errors within DEMs can be very large due to the interpolation process, with input

parameters requiring careful selection (Wise 2000). Wilson (2012) states that the choice of interpolator may also be determined by the quality of the input data: if a dataset is of high precision, an exact interpolator would be of utility, whereas a noisy dataset would require an approximate interpolator. Lloyd and Atkinson (2002) discovered that Kriging was more accurate for datasets with low point densities but provided little benefit for use with large datasets.

As noted by Fisher and Tate (*ibid.*), no general conclusions can be drawn from the existing literature about the choice of interpolation method and thus it appears that the choice of algorithm is based on the preference of the researcher. Based upon the research presented in this section, the NN interpolator has been selected for interpolating the point data from the SAPs, ALS and TLS datasets, which are expected to produce dense datasets. Subsequently, NN should produce sufficiently accurate results. Kriging is unnecessarily complex and is suggested by Wheatley and Gillings (2002 p.198) to be "computationally expensive", and thus it will not be employed here. However, it is important to recognise that, whilst interpolation algorithms can introduce their own errors into a dataset, other sources of error may be introduced into DEM data. These errors will also affect the validity and accuracy of any inferences made when a DEM is used for analysis purposes along with those introduced through interpolation. The causes and effects of error, both from interpolation and data collection are explained in Section 3.3.2.

3.3 Error in DEMs

Before utilising data for analysis, it is important to recognise where in the data collection and processing chain errors can occur that may subsequently affect any results obtained from a dataset. By establishing sources of error, attempts can be made to either address them or to at least understand how they may affect the dataset and any subsequent analysis conducted with it. Wilson (2012) lists a number of questions as stated by Reuter et al. (2009 p.90) that must be addressed prior to subjecting any type of DEM to geomorphological analysis, which will also be pertinent to and influence the accuracy with which archaeological information can be extracted:

1. "How accurately is the surface roughness represented?"

    - In some instances, small depressions in the ground are useful for archaeologists as they indicate the presence of pits, house platforms or other evidence of land use. However, any researcher must be able to distinguish whether these features are actually of importance or if they represent noise in a DEM.

2. "How accurately is the shape of the land surface represented?"

    - The form of the surrounding land places archaeological earthworks in their context and thus it is important that hills, valleys, spurs and other

geomorphological features are accurately portrayed, particularly for landscape-scale archaeological analysis.

3. "How accurately are the "real" world ridgelines and streamlines detected?"

    - For archaeological purposes, breaklines are important for defining the extent of features with topographic expression, and therefore this question as raised by Reuter et al. (*ibid.*) is pertinent to the representation of these features.

4. "How consistently are elevations measured over the whole area of interest?"

    - Elevation measurements are likely to alter in regions with steep slopes, for example, as compared to flatter ground. Subsequently, a more varied or mountainous terrain may be considered to contain elevation measurements that are less accurate in areas with steeper slopes, resulting in inconsistent measurements. This factor is particularly important where larger earthworks, such as hillforts, are measured as the ramparts can consist of very steep slopes.

The factors that affect the number of errors present in a dataset as well as their magnitude are dictated by the complexity of the terrain, the technology used to collect the data, and any pre- and post-processing algorithms applied, which include interpolation and data filtering (Wilson *ibid.*). Thus it is evident that errors can creep into a dataset at every stage from data capture to data analysis. During the data collection and processing stages, errors can generally be separated into three groups or types: Systematic Errors, Gross Errors and Random (Stochastic) Errors.

3.3.1 Types of Error

Systematic errors are those defined as following some mathematical or physical law (Wolf and Dewitt 2000) and are generally predictable, caused by an imperfection in the equipment being used. This may be due to a variety of reasons, such as a lack of careful equipment maintenance and calibration, imperfections in the manufacturing process etc. Photogrammetric examples of systematic errors as stated by Mitchell (*ibid.*) are errors in the pixel geometry of a digital sensor (camera or scanner), a non-flat image plane (either digital or film-based), lens distortion and errors in the assumed position of the principle point. Systematic errors remain consistent if the cause of the error does not alter and, if such errors are modelled, a correction can be applied that eliminates the issues they cause (Wolf and Dewitt *ibid.*). A schematic representation of systematic error can be found in Figure 3.7.

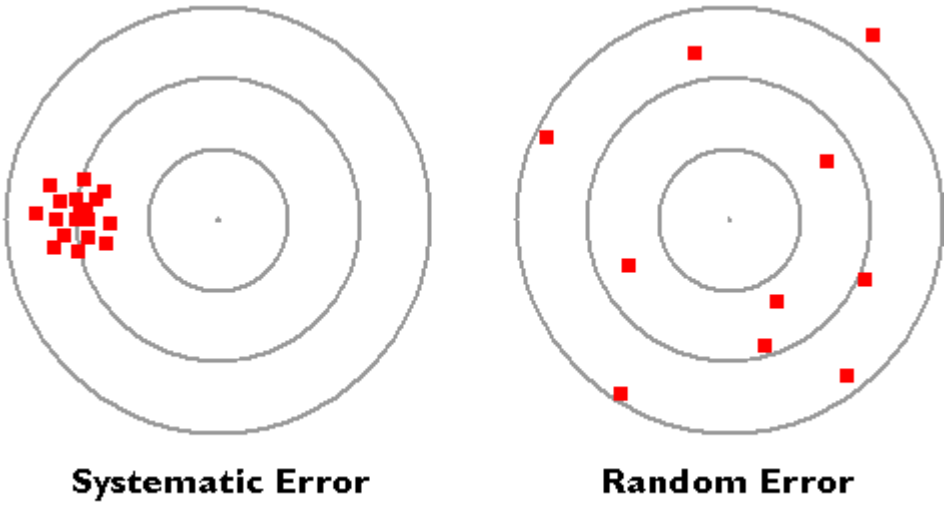

Figure 3.7: Diagram illustrating error distribution based upon Error Type (DiBiase and Dutton 2014).

Systematic errors in ALS systems come from the sensor itself and the flight parameters it must fulfil (i.e. swath width, sample distance etc.), position and orientation errors introduced by the GPS and IMU systems and the data filtering parameters (Rusk 2007). Differential GPS is often used to provide positional information which can introduce inaccuracies of between 1-2cm. When this is coupled with the slight measurement inaccuracies of the IMU, the coordinates produced by this system have an accuracy value of 10cm (Lichti and Skaloud 2010). The accuracy of the distance measurement is dependent on the timing mechanism used by the sensor, although range errors are usually limited to a couple of centimetres (Lichti and Skaloud *ibid.*). Beam divergence of the laser, which is related to angular uncertainty, increases with distance to the terrain and with terrain slope, further contributing to measurement uncertainty. A widening of the beam footprint on the ground increases the area within which a location can be recorded, adding ambiguity about the actual point at which a measurement is made (Lichti and Skaloud *ibid.*). Subsequently, laser returns closer to the nadir angle will be more accurate than those closer to the edge of the field of view of the scanner, which will be more oblique. Petrie (2009) provides values for the effect of flying height on range and elevation accuracy, stating error to be 5cm at 500m, 10cm at 1km, 15cm at 2km etc. Petri (*ibid.*) also states that it is the GPS/IMU combination that contributes the greatest error to ALS measurements.

Gross errors are also known as mistakes or blunders. They are caused by a lack of care and attention during the observation, measurement and processing stages of data collection and manipulation. Examples of gross errors during photogrammetric processing are the misidentification of points i.e. when identifying control points in imagery, or the entry of a wrong value during data input, such as the focal length of a camera, whereby the decimal place may be incorrect or the wrong units are entered (i.e. centimetres rather than metres) (Mitchell *ibid.,* Wolf and Dewitt *ibid.*). Generally, if a large blunder is made it is easier to identify and correct. These errors are usually possible to eliminate through exercising great care when making observations or entering numerical values.

Random errors, otherwise known as stochastic or non-deterministic errors, are those that introduce inconsistencies into a dataset that do not follow a physical law (Wolf and Dewitt *ibid*.) and thus they are modelled using measures of probability as they cannot be predicted. Such errors tend to be small and consist of both positive and negative values, which tend to counteract each other (Wolf and Dewitt *ibid*.). Walstra (2006) states that precision is closely related to the presence random errors in a dataset, which are inherent in any measurement procedure. Fisher and Tate (2006) suggest that during the photogrammetric workflow the lack of precision in identifying target points on the photographs will affect the aerial triangulation result, for example. This may be pertinent whereby GCPs and tie points have to be manually placed in a stereo-pair, strip or block, but this should not be an issue with automatically generated tie-points. Subsequently, if redundant observations can be made i.e. repeated measurements, then it is possible to reduce their impact by using least squares adjustment (see Section 2.2.6.4). If random errors are plotted so as to provide a histogram and associated curve, Blak (2007) states that they should follow a normal distribution (see Section 3.4.2).

Random errors can also be considered as the cause of noise in a dataset, the presence of which should exhibit a normal distribution, but in practice rarely does. Random errors are stated by Li, Zhu and Gold (2005) to be referred to as random noise in image processing and white noise in statistics. The authors state that noise distorts the appearance of regional and local terrain, especially the latter, and is considered to be a high-frequency, or small-scale, component of the data (Li, Zhu and Gold *ibid.*). High-frequency noise occurs more often within a specified area than low frequency noise, causing variations in elevation values across the dataset. As an example, ALS data often contains an absolute vertical uncertainty in each measurement of ~±15cm. The discrepancies this produces can be addressed by applying low-pass or median filters to the data to remove high frequencies, which are further explained in Section 3.3.2.4.

3.3.2 Sources of Error

Beyond errors introduced by the technologies and systems used to collect data (systematic errors), operator blunders (gross errors) or random factors (random or stochastic errors), the influence of errors can be further compounded by terrain type and data resolution, interpolation methods, as previously discussed in Section 3.2, and the methods used to remove noise or other unwanted artifacts from the data, namely data filtering.

3.3.2.1 Data Resolution

Spatial resolution, namely the vertical and horizontal resolution of a dataset, is one of the factors that dictate whether a particular terrain feature, both natural and man-made, can be

resolved in a DEM (see Figure 3.8). In the geomorphological discipline, the scale-dependency of terrain features is acknowledged (Gao 1997; Kienzle 2004, Reuter et al. 2009; Wilson 2012), as is the effect that grid cell size in a raster has on first order derivatives, which are discussed in Section 3.4.3. Archaeologists have also commented upon the requirement for finer spatial resolution data, particularly in reference to off-the-shelf ALS products, that will define earthwork features with suitable detail (Page et al. 2009). Spatial resolution is limited by the system design of the technology capturing terrain data and, in the case of commercially available, off-the-shelf products, the original survey specification.

3.3.2.2 Terrain Relief

Micro-relief is an issue for both geomorphologists and archaeologists alike. If the measurement

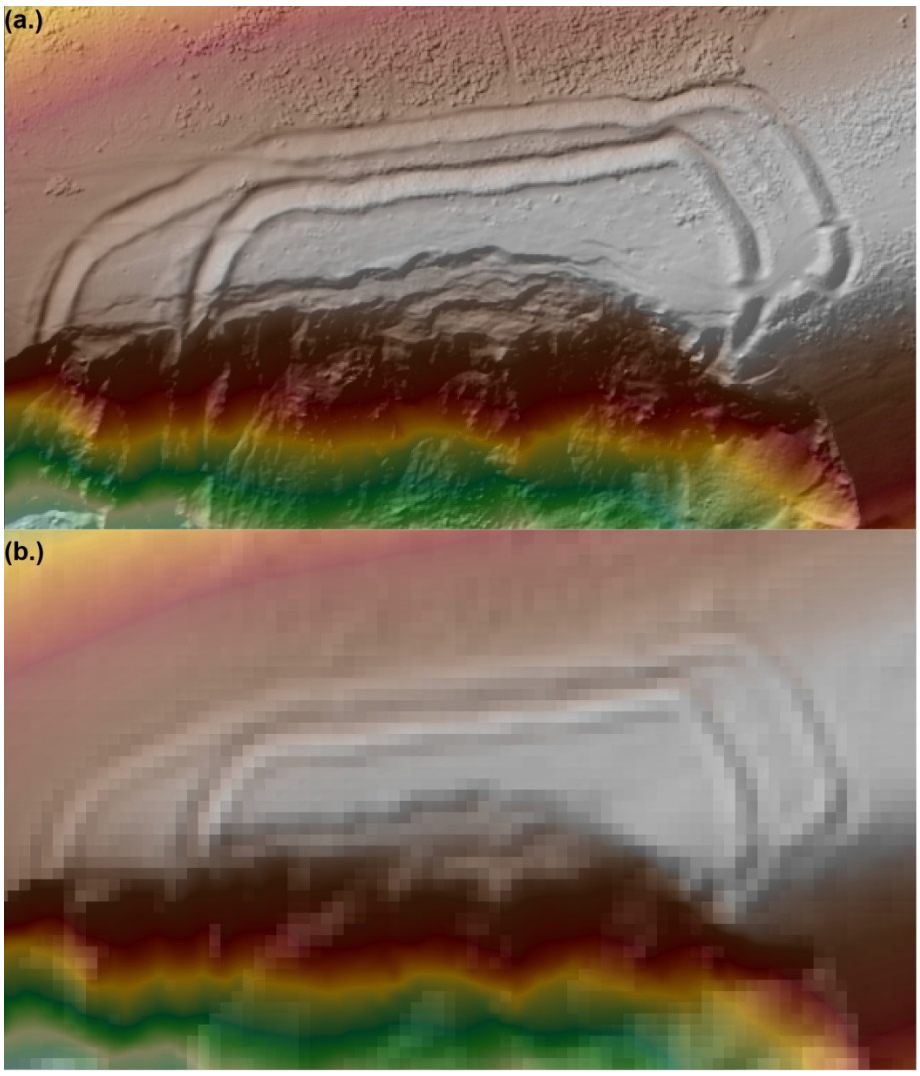

Figure 3.8: Figure showing (a.) a fine spatial resolution (1m) grid and (b.) a coarse spatial resolution (7m) DEM.

density of a technique is not fine enough, there is a risk that smaller features might go unrecorded and thus the measurements are not representative of spatial variation in a landscape. In archaeological terms, features that are important to the interpretation of a site may be missed, which could impact negatively on its meaning and significance. This issue is highlighted in Figure 3.9 whereby the appearance of subtle earthworks, namely occupation platforms, are not as well-defined in the 1m DEM as they are in the 10cm DEM. However, Figure 3.9 illustrates the complicated relationship between data resolution and the presence of vegetation. In Figure 3.9b the original TLS dataset has been reduced from 10cm to 1cm and interpolated using the maximum elevation values to form a DSM. The presence of vegetation in the data has produced a 'blocky' appearance across the regions in which it appears. In contrast, Figure 3.9c is the result of interpolating the data using the minimum elevation values, which has removed the vegetation and the occupation platforms can be seen, although the data resolution is the same as before i.e. 1m.

Lemmens (1999) has applied the term 'blind sampling' to the mass-capture techniques utilised for terrain survey, such as photogrammetry and laser scanning, as they do not discriminate in the measurements they take, unlike the ground-based survey methods undertaken by surveyors in the field (see Section 1.1.3.2 for further discussion). However, for large areas, mass-capture techniques are indispensable. Fisher and Tate (2006) state that the density and distribution of measurements in point data can influence error, citing Östman (1987) as having identified a reduction in the RMSE of DEMs created from an increased number of points derived using photogrammetric data. This would intimate that higher resolution datasets are more desirable if trying to avoid the introduction of errors caused by poor data resolution, although the selection of an appropriate resolution is dependent on the requirements of the survey. Fisher and Tate (*ibid.*) do also state that resolution issues are related more to uncertainty rather than simply 'error'.

Many authors have noted a link between terrain characteristics, land cover type and the accuracy of DEM data (Adams and Chandler 2002; Fisher and Tate 2006; Bater and Coops 2009; Wise 2011; Wilson 2012), with the accuracy of terrain representation noticeably decreasing as complexity increases (Gao 1997). The shape of the terrain can influence how representative elevation values are for a particular type of feature. Adams and Chandler (*ibid.*) found that as the slope of terrain increased, ALS underestimated the elevation value. This could be due to beam spreading, which subsequently returns a mean elevation value for steep terrain. Higher errors in ALS data have also been noted in areas that are covered by vegetation, particularly of the scrub and shrub variety (Hodgson et al. 2005), which are perticularly dense and unlikley to facilitate laser penetration through their stands. The effect of vegetation upon terrain data can be seen in Figure 3.9b.

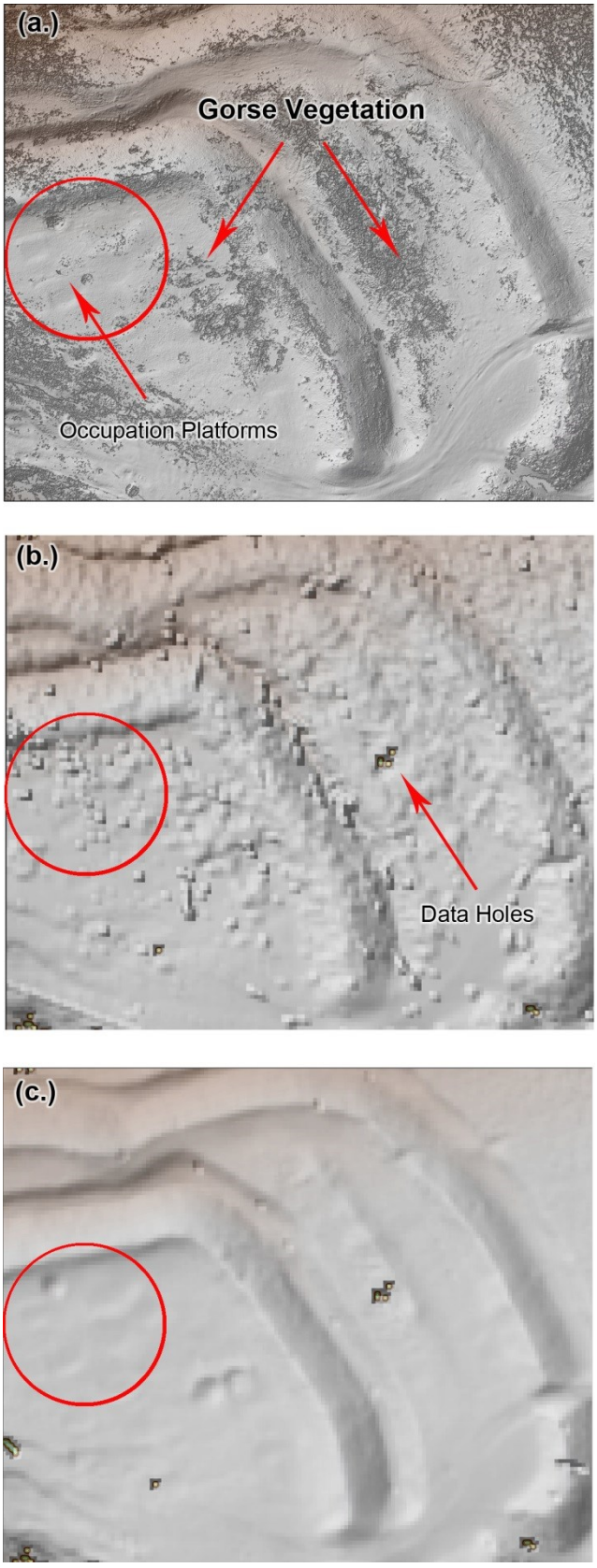

Figure 3.9: TLS data highlighting the effects of data density and vegetation cover on the representation of archaeological features (a.) 10cm DSM (b.) 1m DSM (c.) 1m DTM.

3.3.2.3 Interpolation and Artifacts

As discussed in Section 3.2, interpolation also introduces error, the extent of which depends on the interpolator and, as stated by Fisher and Tate (*ibid.*), the way in which it estimates height values at the same point. Artifacts can appear during the process of converting point data to a gridded DEM. It was noted that Kienzle (2004) identified "bull's eyes" in terrain models produced using the IDW interpolator. Wise (2011) has observed that the spatial pattern of errors across the interpolation methods he trialled were similar. His research illustrated the underestimation of elevation values where slope was upwardly convex, especially where there is a marked change in elevation, with the largest errors occurring along narrow crest lines and tops of ridges. Wise (*ibid.*) also noted that overestimation of elevation values occurred in areas that are upwardly concave i.e. hillside hollows and valley sides and bottoms. However, whether these effects are also due to the character of the survey technology, such as ALS, these over- and under-estimations may not be due simply to the interpolator. Interpolation also affects the resolution of source data when converting it to a grid because it is during this process that sampling of the original values occurs (Fisher and Tate *ibid.*). Bater and Coops (2009) discovered that increased resolutions for input data helped to improve the accuracy of interpolation results.

In recent years, archaeologists have become more familiar with the appearance of data artifacts in DEMs, particularly in ALS datasets. Crutchley and Crow (2009) discuss the methods used to distinguish between what may at first appear to be archaeological features but are in fact data artifacts. These involve using contemporary aerial photography with which to compare the ALS data, or by establishing whether any suspect 'features' cross modern roads or hedgerows – if they do, then the feature is actually a data artifact. These unwanted effects are caused by interference between overlapping swaths (see Figure 3.10), which exhibit as wavy lines in the data, or as steps in the data where processing has rounded the elevation values to become either integers or removes a number of decimal places, producing what might be referred to as quantization noise or round-off errors (Crutchley and Crow *ibid.,* Li, Zhu and Gold 2005). The effects of rounding-off errors and random noise are shown in Figure 3.11.

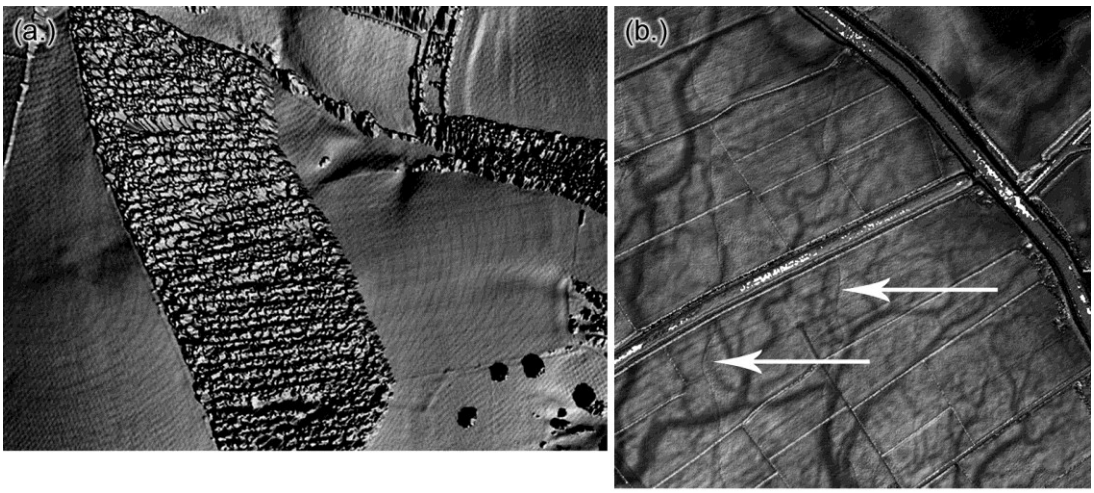

Figure 3.10: ALS artifacts (a.) wave patterns caused by rounding errors and (b.) processing artifacts from overlapping ALS swaths, indicated by arrows (Crutchley and Crow 2010).

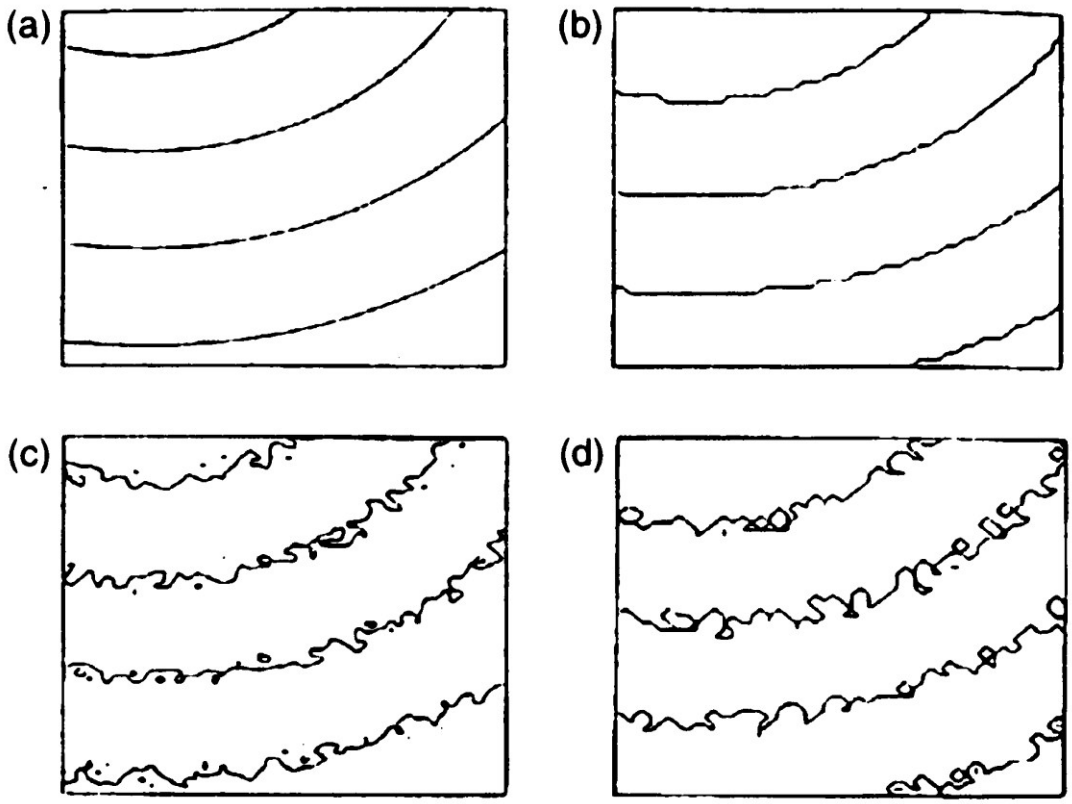

Figure 3.11: Effects of errors and random noise on contours (a.) original data (b.) round-off noise created by rounding-off the decimal fraction of the original data (c.) random noise of ± 0.165m added to original contours (d.) contours with round-off and random noise (Li, Zhu and Gold, p.138).

3.3.2.4 Data Filtering

One way of removing errors and artifacts in terrain data is to use filtering techniques. Filtering algorithms also influence DEM quality by altering elevation values across the terrain dataset in a number of ways. The application of spatial filtering techniques to rasterised terrain data is common, whereas filtering raw point data is less so. The software available to filter point data, as produced by ALS, TLS and points output by photogrammetric software is nowhere near as widespread as the ability to perform spatial filtering on rasterised DSMs, which can be undertaken in many GIS and image processing packages. Filtering, in general, is applied to remove unwanted features from a raster or point-based dataset, such as vegetation and buildings, especially if a DTM is required. It can also be used to remove or reduce the effects of noise in a terrain model.

The quality of filtration algorithms will affect how well erroneous data is removed as well as the accuracy of the terrain data once it has been filtered. Although the spatial filtering of a raster DSM, which often applies a low-pass kernel across the terrain model, is frequently used to address systematic and random errors in the data, Fisher and Tate (2006) state that few methods appear to exist for detecting and removing other types of error from a DSM. However, this appears to be at odds with the stance taken by Li, Zhu and Gold (*ibid.*) who advocate the use of low-pass filters for removing random errors. Burrough and McDonnell (1998 p.193) also recommend using a low-pass filter to smooth the terrain data to reduce the effects of noise on a DSM prior to plotting the dataset as a map. Whilst the authors state that a low-pass filter can be applied to an elevation DSM to reduce the effects of noise prior to creating derivative DSMs from it, this approach also removes extreme values from the data which will affect the calculation of slope, aspect and curvature and, hopefully, reduce the errors in these datasets too.

A low-pass filter is used to remove high-frequency noise and has a smoothing effect on the image. This is achieved by a process known as convolution, whereby a small, square array of pixels is convoluted with the pixels of an image (Jacobson et al. 2000). The dimensions of the array are commonly 3x3, 5x5 or 7x7. Using the example shown in Figure 3.12, the value to be altered by the filter is number ‘7’, which has been highlighted in orange, with the other pixels included in the process highlighted in grey. The new value is calculated by multiplying the values within the filter with the corresponding pixel value, adding the nine results together and dividing this value by the number of cells within the kernel.

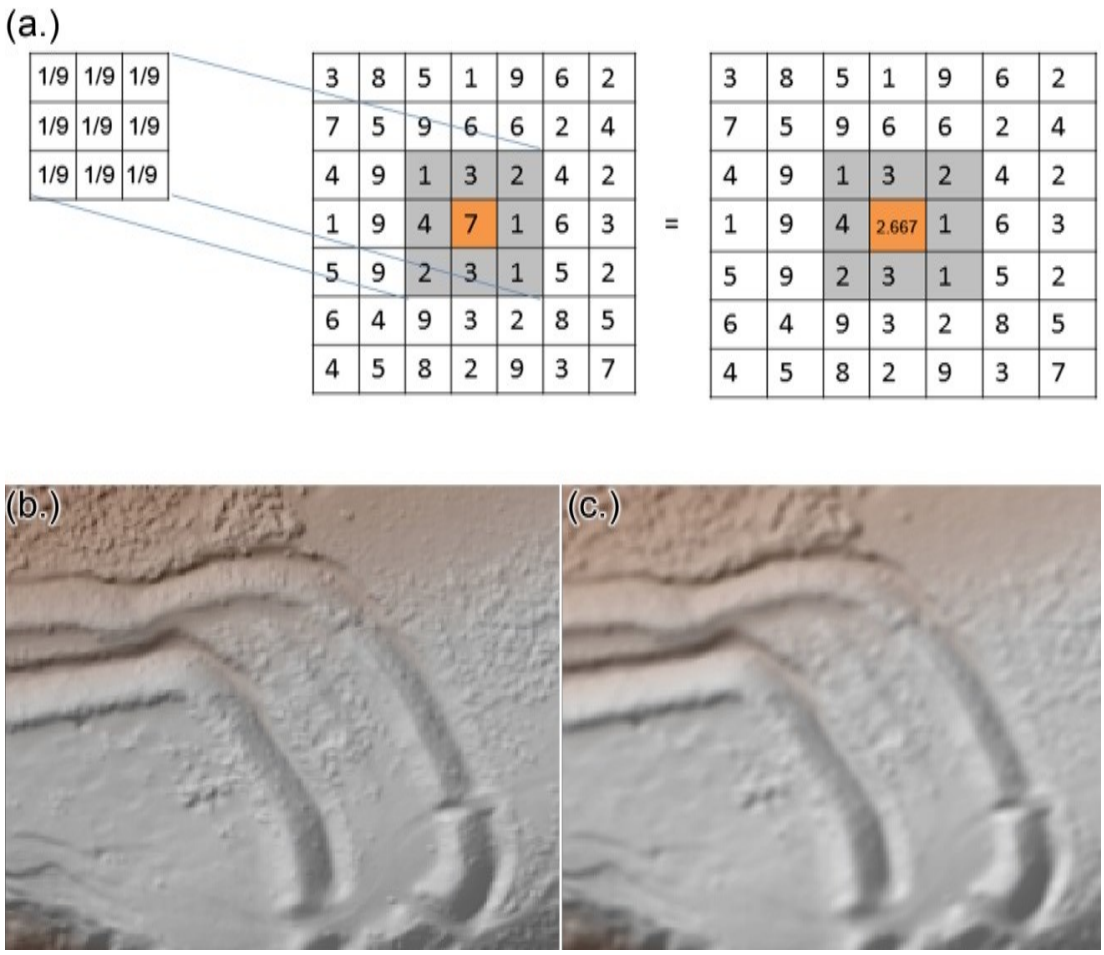

Figure 3.12: Raster Filtering: (a.) The filter kernel (top left) and the region of the image to which it is being applied is highlighted in grey. The value of the orange pixel (left) will be altered. The resultant change is also shown in orange (right). Examples: (b.) no low-pass filter (c.) low pass filter applied, indicated by the softening of the detail.

The values within this kernel are all '1', ensuring that equal weighting is allocated to all of the pixel values:

Value = ((1x1)+(1x3)+(1x2)+(1x4)+(1x7)+(1x1)+(1x2)+(1x3)+(1x1)) /9

= 2.667

The result is an average (mean) value of the 3x3 neighbourhood on which the kernel operates (ESRI 2008).

A median filter also uses kernels with similar sizes and dimensions to that of the low-pass filter but it differs by using a decision-making step (called the 'operator') to decide on the value of the output pixel (Jacobson et al. 2000). Depending upon the kernel size, the median value of the image pixels over which the kernel is positioned is chosen to replace the value of the image pixel that is situated beneath the central kernel cell. This filter is stated to be effective at removing strong, spikelike noise (Gonzalez and Woods 1992), replacing such values with those similar to the neighbouring pixels, preserving the sharper edges in the image.

3.3.3 Summary

Overall it is important to acknowledge that errors creep into a dataset from many different sources that will subsequently affect any further analysis performed with such data. Some of these errors can be avoided by careful data collection and processing, whilst others cannot be accounted for, such as random errors. Wilson (2012) notes that change detection studies will be one of the areas particularly affected, complicating the subtraction of DEMs from disparate sources from one another to assess change, erosion and deposition, for example. However, it is impossible to identify and remove every error in source data, regardless of whether an attempt has been made to model the error in a DSM through methods such as Monte Carlo analysis (Wilson *ibid.*). This situation becomes more complicated when a dataset has been obtained from a supplier who does not publish their data processing workflows. Subsequently, those who are reusing commercial data must recognise the limitations this creates by acknowledging the unknown effects these processing methods may have on error distribution, particularly as users are not often provided with information relating to these parameters (Aguilar et al. 2007). There are, however, some methods available to assess the accuracy of a dataset, which are discussed below.

3.4 Quality Assessment

As discussed above, it is important to be aware of the quality of a DEM and any other factors that may affect the results derived from this data prior to utilising a DEM and its derivatives for analysis. Subsequently, a number of methods have been employed to assess DEM quality that includes studies of the effects that different interpolators have on terrain models. To be able to assess a DEM for its quality it is important to consider what is meant by the terms accuracy and precision, often used to describe data quality, which are outlined below, before addressing the methods that have been utilised to assess data quality.

3.4.1 Accuracy and Precision

The assessment of data quality is often achieved by evaluating the accuracy of the data and by considering the precision of the system that produced it. Accuracy describes how close a measured value is to the true value, the latter of which is often defined by utilising a measurement produced by a superior, or more accurate, measurement technique. It is important to note, however, that the true value can never be known, as every measurement, regardless of how it is captured, will contain a source of error, no matter how small. Precision, on the other hand, refers to the ability of a technique to produce consistent measurements, such

that the repeated observation of a particular point will deliver duplicate or similar values. Precision also differs from accuracy in that it does not take account of whether a value is close to the correct value (Mitchell 2007 p.25). Figure 3.13 illustrates the differences between these two terms.

Poor accuracy is caused by systematic error, which is the result of a poorly calibrated instrument, or a lack of calibration data, although the influence of this effect can be removed if calibration information is available. These errors tend to exhibit clustering when examined. Poor precision, however, is caused by random errors that cannot be accounted for and are thus beyond the control of the surveyor. Small mistakes are one such example and comprise one of three of the factors that Mitchell (*ibid.*) has identified as contributing to how well the overall precision is estimated: the precision with which the measurement of the (x,y) image coordinates are made (which is dependent the on the skill and diligence of the operator), the geometry of and angles between the intersecting rays, and the precision of the control points (both as located on the ground with a particular technique and as identified in the imagery by an operator). During photogrammetric processing, Mitchell (*ibid*.) states that precision is often determined by the least squares estimation of the parameters in the collinearity equations (see Section 2.2.6.4). Other factors that may introduce random errors are changes in temperature or wind during a survey. Wind can destabilise the equipment, causing it to vibrate or move during measurements, whilst temperature can cause equipment to expand and contract, which adds to the instability of the technologies being employed. The influence of these errors can be reduced by taking repeat readings to find the average value.

3.4.2 Statistical Measures

To assess the accuracy of the elevation values in a DEM, the collection of another dataset using a method with greater accuracy is often employed (Baily et al. 2003; Oksanen and Sarjakoski 2006; Dowman and Muller 2011; Gonga-Saholiariliva et al. 2011), requiring that a selection of sample or check points is gathered across the region of interest. Höhle and Höhle (2009) state that this can be very labour intensive, as enough samples are required so as to ensure the accuracy assessment is reliable and statistically significant. Whilst using check-points to assess the calculated triangulation solution in photogrammetric software is advocated, the USGS (1996) suggest utilising at least 28 to validate the quality of the result. However, this is impractical when processing archive SAPs as finding a sufficient number of GCPs can be challenging. Therefore conserving some of these measurements for use as check-points can be unrealistic.

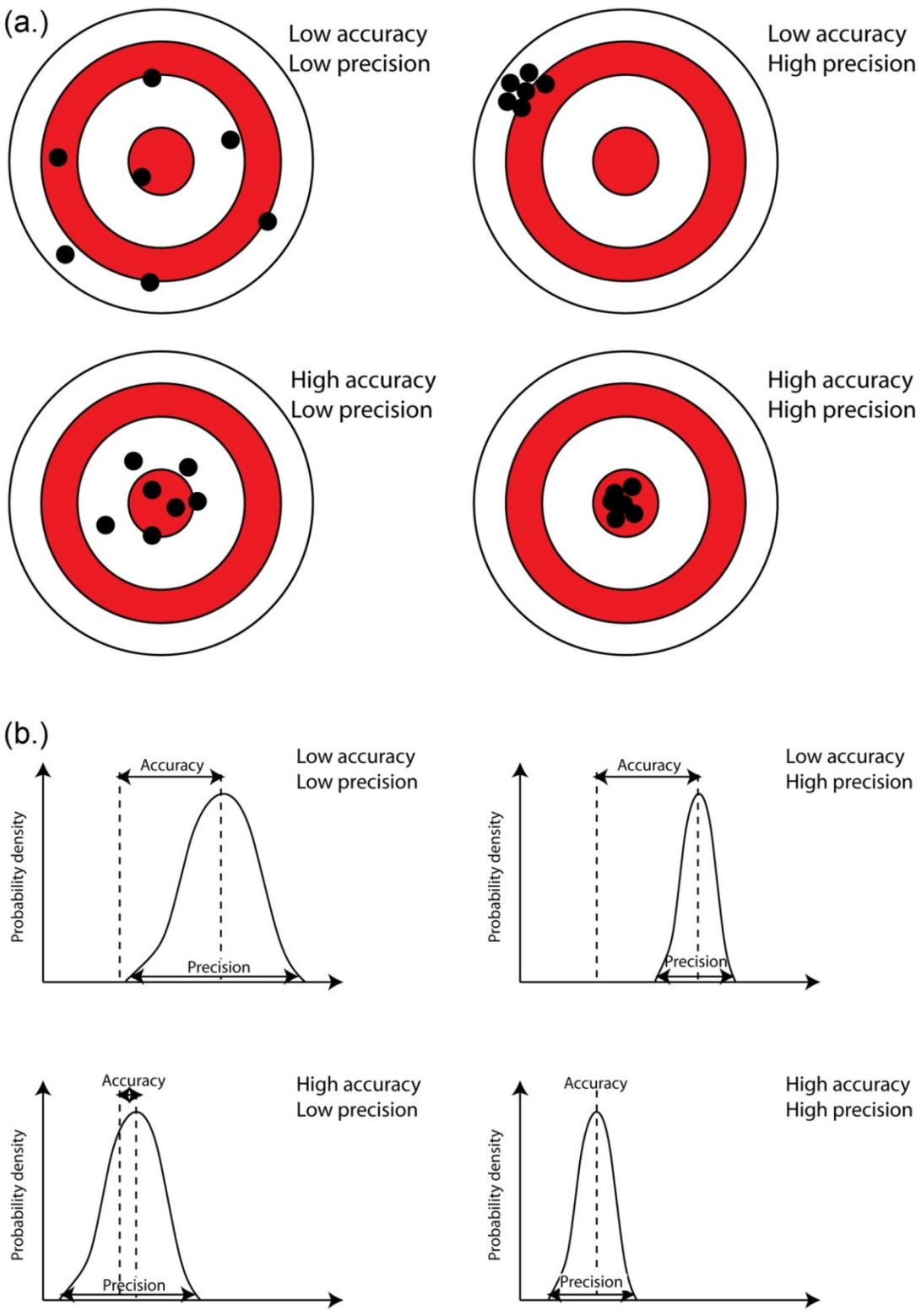

Figure 3.13: Schematic illustrating the concepts of accuracy and precision: (a.) relationship of accuracy and precision based on location (b.) relationship based upon a probability density curve (Davies 2013).

Höhle and Höhle (*ibid.*) advocate the use of a sufficiently large number of random sample points to assess accuracy, ensuring that samples are not just taken along breaks of slope or close to buildings, for example, as large errors are often present at these locations. GNSS is a popular method of gathering independent elevation data against which to test the elevation measures produced by digital photogrammetric software (Baily et al. 2003; Walstra 2006), although ALS data has also been employed (Barrand et al. 2009). However, Papasaika, Poli and Baltsavias (2008) state that "absolute measures of elevation do not provide a complete assessment of (DEM) quality", and intimate that interpolation errors can also influence quality and should therefore be considered. The authors note that slope and aspect, as derived from an elevation dataset (see Section 3.4.3), can help to identify systematic and random errors in the data.

It is from the comparison between the sample points gathered by GNSS and those in the same locations in the DSM produced by ALS, TLS or photogrammetry, that are used to generate statistical measures. The most popular descriptors of error are the root mean square error (RMSE), mean error (ME) and the standard deviation (SD) (Baily et al. 2003; Walstra et al. 2004; Papasaika et al. 2008; Aguilar et al. 2009; Walstra et al. 2011; Pérez Álvarez et al. 2013). Dowman and Muller (*ibid.*) identify the RMSE as a measure of accuracy, whilst the SD and variance (σ^2) are indicators of precision. Slight variations on these measures have also been applied, particularly for the RMSE, where this value can be calculated for X and Y coordinates, rather than purely for the differences in Z (Aguilar et al. 2009; Aguilar et al. 2013). The minimum and maximum ranges are another measure of disparity between datasets, as employed my Miller (2007).

Maune et al. (2007) state that the RMSE is calculated by finding the "square root of the average set of squared differences between the dataset coordinate values and coordinate values from an independent source with higher accuracy for identical points". Each of the error values are squared, which means that larger errors will have more weight than smaller errors according to Januchowski et al. (2010). The RMSE is a common, if global (or absolute), measure for establishing vertical accuracy for a set of elevation points, which is useful if the errors contained within the data follow a normal distribution, although this is rarely the case (Maune et al. *ibid.*, p.65). To establish whether an elevation dataset, such as a DSM, has a normal distribution of errors, the elevation difference between the DSM and a more accurate sample of elevation points is calculated and then plotted using a frequency histogram (see Figure 3.13b and Figure 3.14c). The frequency value indicates the number of errors of similar magnitude per 'bin' or band. If the errors were normally distributed, the mean error would be zero and the remaining bins would form a 'bell-shaped' curve that is symmetrical about the mean. If, however, the data do not follow a normal distribution, there may be a number of outliers causing the histogram to appear 'skewed' (see Figure 3.14a and Figure 3.14b) or the distribution may be peaked, the degree of which is called 'kurtosis' (see Figure 3.14c). Outliers may occur in the DSM to be tested, as previously suggested, in areas covered by scrub vegetation, particularly when a technology such as ALS has not been able to penetrate thick scrub and thus leaves large gaps in the point data for an interpolator to fill. Undulating terrain with varying slope may produce outliers, particularly when the data has been subjected to interpolation (Blak 2007).

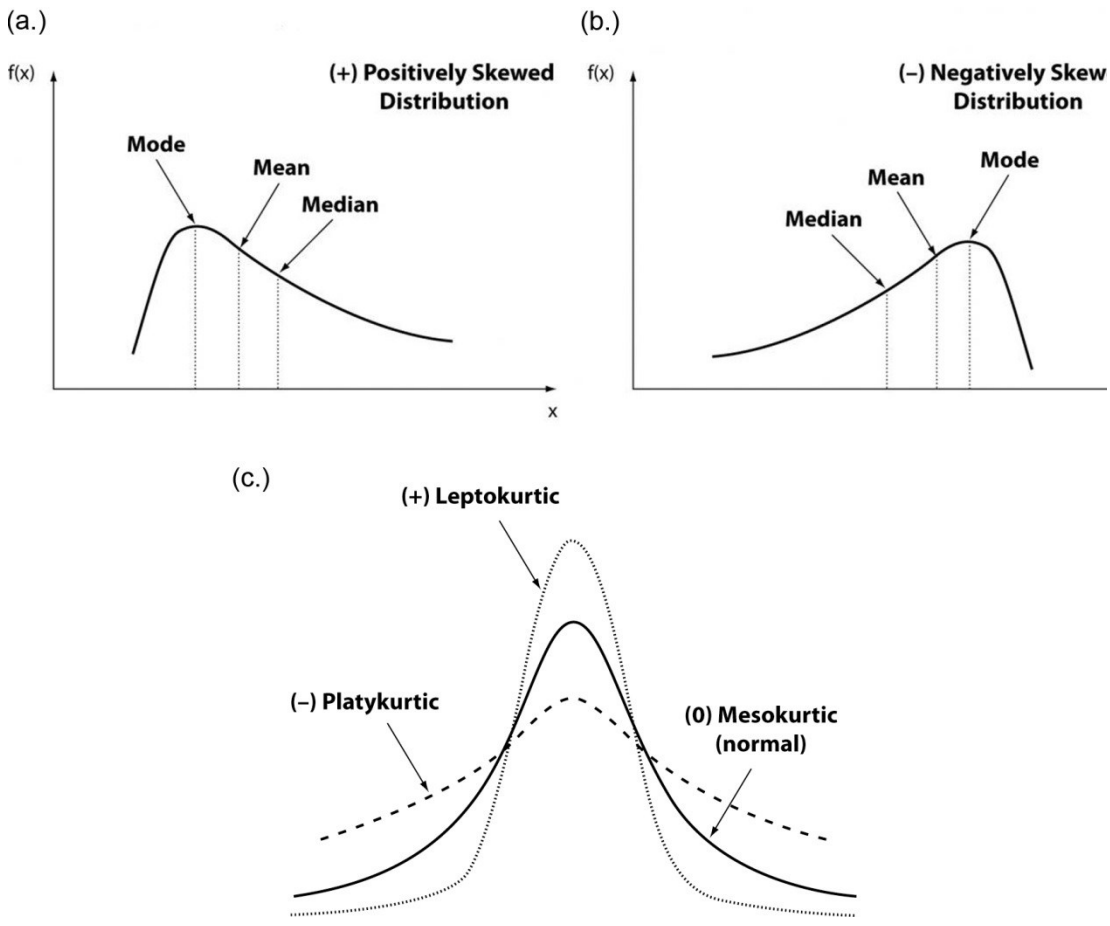

Figure 3.14: Distributions curves showing (a.) Positive skewness, (b.) Negative skewness, and (c.) Kurtosis (Guidi and Salvagno 2010).

Precision is measured by calculating the standard deviation or the standard error within a dataset (Maune et al. *ibid.*), albeit for normally distributed errors (Mitchell *ibid*). Fisher and Tate (2006) state that the RMSE is equal to the standard deviation of the error if the mean error is, or assumed to be, zero, which it often is not. The authors note that other researchers have advocated the use of ME and SD values to accompany the RMSE as they provide a more complete picture of the errors that may be present in a DEM (Höhle and Höhle 2009, Januchowski et al 2010). Miller (2007) utilised SD to evaluate normal distribution errors and states that 68.3% of all measurement errors should fall between ±σ whilst 99.7% should lie within ±3σ, and it is this latter measure that indicates the precision of the data. The remaining 0.3% of values could thus be classified as outliers. Fisher and Tate (*ibid.*) state that the ME is an indication of systematic under- or over-estimation of elevation values in a DEM and thus will provide a measure of bias. The position of these measures on a normal distribution curve will change depending on the frequency distribution of residuals, as illustrated in Figure 3.14a and b. As Fisher and Tate (*ibid.*) point out, ME and SD are also global statistics and do not describe the spatial pattern of errors in a DEM. However, Januchowski et al (*ibid.*) use the difference

between the RMSE and ME to indicate the spatial variation in individual cell error within the DEM: the larger the difference, the greater the variation.

Blak (*ibid.*) also utilises the measure of error 'skew' to further establish whether the elevation data has a normal distribution, as shown in Figure 3.14a and b. Blak (*ibid.*) states that if the value of skew is greater than 0.5, it indicates a departure from a normal error distribution, as would a deviation in the mean and median values. As an accuracy assessment, Blak (*ibid.*) advocates the use of the 95th percentile method to establish the accuracy of a dataset. The author states that this method can be used regardless of whether error is normally distributed or not and regardless of whether errors are or are not outliers. The percentile calculation uses all of the error values and returns an interpolated absolute value for which 95% of the error values should be below, the remaining 5% will be higher. This absolute value can then be compared to an error threshold that might have been set, for example, by a company commissioning an ALS, or other mass-capture, survey, and will determine whether the dataset is fit for the purpose it was originally sought for.

However, a number of authors have utilised other statistical tests to assess the impact of particular stages in the processing chain on the presence of errors in a DEM. The analysis of variance statistical test (ANOVA) has been applied for identifying the effects different self-calibration bundle adjustment routines (SCBA) and varying numbers of GCPs have on triangulation results for archive SAPs (Aguilar et al. 2013). ANOVA was used to assess the influence of a number of different factors concurrently and ascertain how these variables interact with one another, which is achieved by comparing the mean values, or RMSE values, obtained from processing two epochs of SAPs. In this case, three variations of the RMSE were used: $RMSE_{3d}$, $RMSE_p$ or the planimetric mean, and $RMSE_z$ representing the vertical mean. The Kolmogorov-Smirnov test was also utilised for examining the normality of distributions produced by the X, Y and Z residuals i.e. the difference between the check point data and the DSM data from the two SAP epochs. An alternative method is the t-test that calculates the significance of the results, or difference, between two means. It does not provide multiple comparisons as ANOVA does. However, there is no indication of the t-test being applied to DEM data in the literature.

3.4.3 First Order Derivatives

Subsequent to the creation of gridded DSMs, the production of 1st order derivatives can be undertaken and have also been used to indicate the quality of an elevation dataset (see Section 3.4.3.1). These derivatives represent important attributes of a terrain, namely slope and aspect, each of which are explained below. Slope and aspect are described as 1st order derivatives as they are extracted directly from a DSM in one processing step, for which examples are given in Figure 3.15. To calculate each of these derivatives from a gridded elevation dataset, a 3x3 filter kernel is passed over the DSM and applies an equation to the values within the kernel window

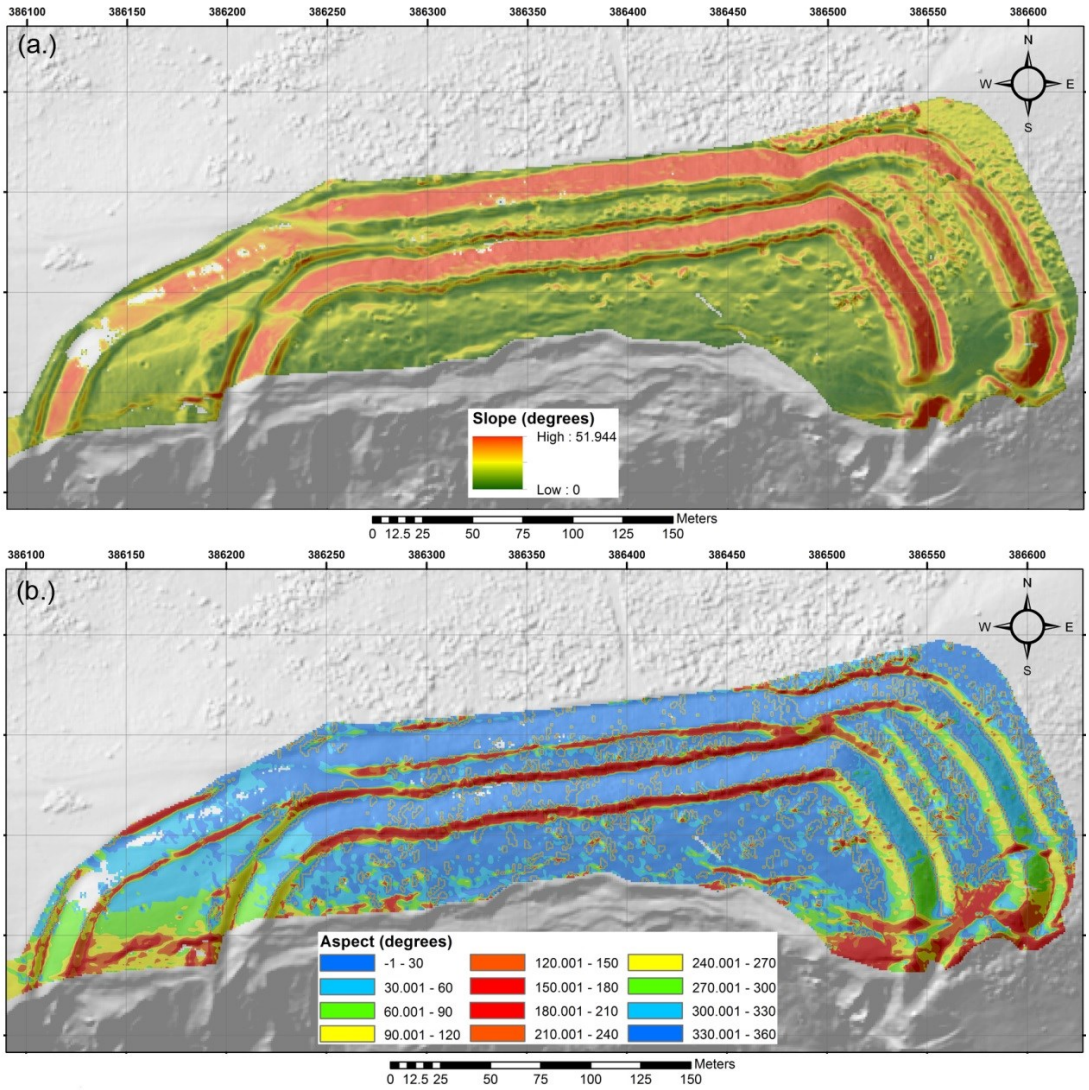

Figure 3.15: Diagram illustrating first order derivatives of (a.) Slope and (b.) Aspect.

to generate a derivative value for the target cell (Burrough and McDonnell 1998; Wilson 2012). The concept of filter kernels was introduced in Section 3.3.2.4.

Slope, also known as gradient, examines the rate of change of elevation (Gallant and Wilson 2000), and can be measured in units of degrees or percentage (see Figure 3.15a). It is an important determinant in water velocity and runoff rate, soil water content, and vegetation composition (Gallant and Wilson *ibid.*), which will determine a particular region's suitability of use for anthropogenic purposes. Thus slope has been examined by archaeologists for a number of purposes. Bevan and Conolly (2011) found slope to be influential in the placement of cultivation terraces and evolution of track-ways. Kuna and Adelsbergerova (1995) utilised slope for examining the distribution of prehistoric settlements in the Czech Republic. Chapman (2006) has also highlighted its use for predictive modelling and cost-surface analysis. The slope algorithm in ArcGIS is said by Kienzle (2004) to be that of Horn's (1981) which, although widely used, was found to be ranked behind the Zevenbergen and Thorne method by Jones (1998).

Aspect is a measure that is used to indicate the direction of maximum slope and thus the direction of flow of material over a surface (see Figure 3.15b). This attribute is also indicative of how much solar radiation a surface might receive. This in turn will influence the amount of water contained within a region and thus the flora and fauna it can support (certain 'aspects' are more prone to erosion processes because of lack of vegetation/water/animals/people). Thus its use by the archaeological profession has focused on whether slopes facing a particular direction, depending on whether they are in the northern or southern hemisphere, contain more evidence of occupation. Again, this factor has been utilised for predictive modelling (Chapman *ibid.*) and examining the distribution of anthropogenic features in relation to aspect (Llobera 1996). As above, ArcGIS uses the Horn (*ibid.*) method to calculate aspect, which was also found by Jones (*ibid.*) to be ranked behind the Zevenbergen and Thorne method.

3.4.3.1 DEM Assessment with First Order Derivatives

The errors that are present in an elevation model will, naturally, propagate into the products derived from them. Thus the errors associated with interpolation and the uncertainty introduced by the resolution of a DEM will impact upon derivatives (Fisher and Tate 2006). Chang and Tsai (1991) discovered that there is a positive relationship between DSM resolution and the accuracy of slope, aspect and gradient derivatives, although (Florinsky 1998) found that errors may even creep into the derivatives due to the methods by which they are calculated. Florinsky (*ibid.*) also demonstrated that the relationship between derivative error and the RMSE of elevation is directly proportional, whilst being inversely proportional to DEM resolution (Fisher and Tate *ibid.*). This indicates that a higher-resolution DEM will contain fewer errors in first order derivatives than a coarser resolution DEM.

Visual analysis of data is also important, as advocated by Fisher and Tate (2006). The authors state that DEM derivatives, such as slope and relief, are useful for identifying systematic errors. Burrough and McDonnell (1998, p.193) state that gridded derivative datasets obtained from gridded elevation data contain more noise than the original surface, with the degree of noise increasing with derivative order. Subsequently, errors in second order derivatives will be more exaggerated than in the first order products. The use of derivatives as a method for assessing the quality of DEMs is also recommended by Gallant and Wilson (2000 p.55) who state that the histograms of the aspect derivative are useful tools for detecting the results of poor quality interpolation, as shown in Figure 3.16. This may prove to be beneficial when investigating the difference between the gridded commercial ALS produce from the EA versus the interpolation methods used to derive gridded information from their raw data sets. Kienzle (2004) also advocates the use of terrain derivatives for revealing the statistically significant differences between DSMs of the same area but with differing grid resolutions. The author notes that the sensitivity of terrain derivatives to grid cell size is independent of the DSM interpolation method used.

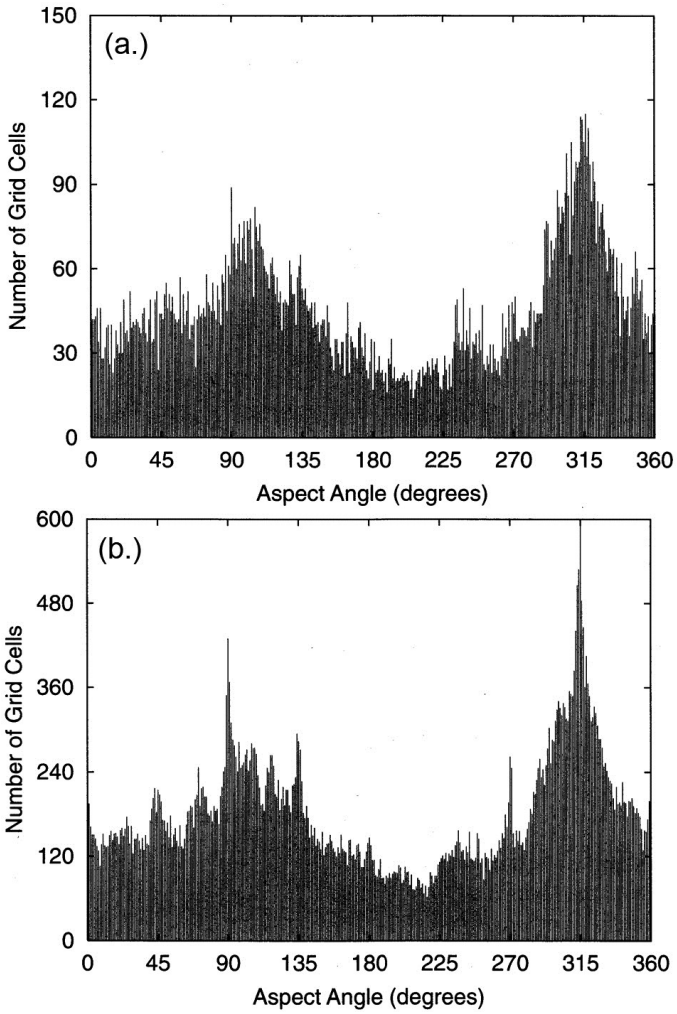

Figure 3.16: Aspect histograms from (a.) 15m DEM and (b.) 7.5m DEM, with the latter showing bias to values that are multiples of 45º, indicating the presence of errors (Gallant and Wilson 2000).

As opposed to the discussion in Section 3.4.2, the RMSE cannot be used to compare the first order derivatives to elevation or to derivative types other than their own i.e. slope must be compared to slope. This is due to the values of each derivative being an abstract of the elevation (Florinsky 1998) and thus they do not have the same units. However, the slope values of one DSM can be compared to slope values from other DSMs and thus RMSE can be used to look at differences between each different derivative in this way.

As indicated in Section 3.4.2, the same statistical measures can be used to assess derivative datasets, i.e. mean, median, SD and RMSE. Frequency distribution histograms and normal distribution curves provide information describing how frequently a particular value occurs within a DSM i.e. slope values are plotted against the number of times they occur, either within a whole DSM or for a selected area within a DSM. The similarity of this measure across one particular derivative type for all of the mass-capture datasets can be used to indicate whether the information content between each varies and the amount by which it varies. Despite the potential for any two histograms with differing resolutions to appear visually similar, summary statistics can help to reveal any underlying discrepancies, if there are any. Thus, based upon

the evidence from the literature, associated summary statistics can be used to indicate a level of confidence in the information provided by the frequency distribution by examining the location (mean and median), spread (SD) and shape (skewness and kurtosis) of the distribution of values represented in the histogram. The measure of location describes the centre of the distribution in a dataset using two different types of average: the arithmetic mean and the median the latter of which is more sensitive to outliers in the data. As previously stated SD is a measure of spread and describes the distribution of values based around the mean with the added advantage of representing the same values as the dataset it represents. Whilst two samples i.e. two DSMs illustrating slope, may have the same mean value, their standard deviation may be different, which will highlight variations between datasets. The shape of a distribution is described using skewness and kurtosis. Skewness indicates how symmetrical a distribution is while kurtosis examines how 'peaked' it is and can indicate whether outliers are likely.

3.4.4 Spatial Distribution of Errors

Whilst global statistics, such as RMSE, ME, SD and frequency distribution graphs are useful, they do not illustrate the spatial distribution of errors across a DSM. As Carlisle (2005) explains, errors are spatially variable and, whilst convenient to obtain one value that indicates the quality of a dataset, it is unlikely that errors across the DSM are uniform. If it were possible to identify areas of a DSM that contained a greater number of errors than elsewhere, efforts could be focused upon these areas in order to correct them. A number of authors (Gooch and Chandler 2001; Walstra 2006; Höhle and Höhle 2009) have utilised DEMs of difference (DoDs) to identify regions of difference between two DEMs, one of which acts as the reference. This provides a series of residual values between the two datasets, which can be utilised by a spatial autocorrelation algorithm to identify clusters of errors across the DoD. One such measure is Moran's I, which Gonga-Saholiariliva et al (2011) state is a standard tool for assessing spatial autocorrelation. The output from performing Moran's I analysis on a DEM is a value that ranges between -1, indicating a dispersed pattern or values that are less similar than expected, and +1 that indicates a clustered pattern or values that are more similar than expected. If a value of 0 is returned, then the pattern is random (see Figure 3.17).

Further to the assessment of error patterns using Moran's I some GIS tools, such as ArcGIS, calculate z-scores and p-values with which to identify the statistical significance of the residual values. The p-score represents the probability of the spatial autocorrelation pattern being caused by random errors. If this value is small then it is unlikely that random errors produced the observed result. The z-score is representative of standard deviation and indicates spatial correlation in Moran's I analysis. Together with the p-value, the z-score indicates whether the distribution of errors follows a normal distribution. ArcGIS utilises Moran's I to generate a map of cluster and outlier types, for which the p- and z-scores are utilised for deciding upon five outcomes: "statistically significant cluster of high values, statistically significant cluster of low

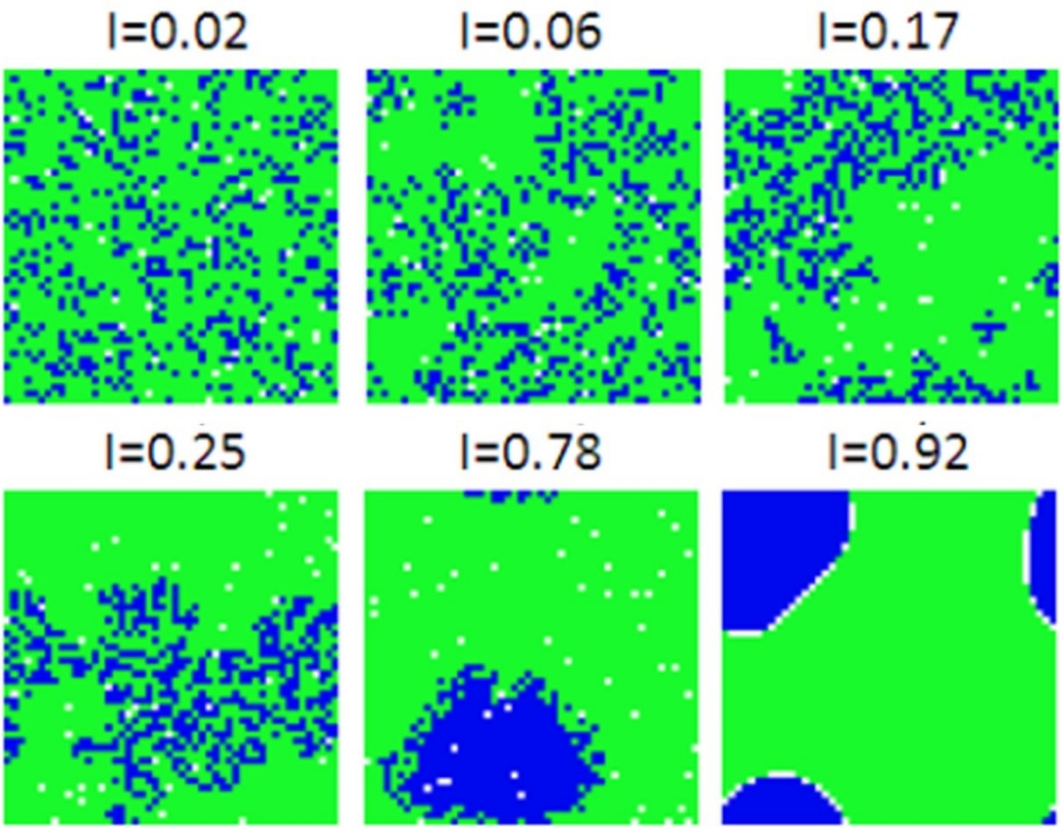

Figure 3.17: Schematic illustrating distribution patterns created using Moran's I, ranging from Random (top left) to clustered (bottom right)(after Hatna and Benenson 2012).

values, outlier in which a high value is surrounded by low values, outlier in which a low value is surrounded by high values" (ESRI 2013), and the final class is reserved for non-significant residuals. In this way, visual identification of the error-prone areas within a DEM can take place, which may help to identify the cause of the disparity between the reference DEM and the DEM being examined.

3.4.5 Archaeological Assessment

It is important to establish the quality of archaeological data that can be extracted from SAP DSMs and other datasets. In this way the DSM can be assessed as regards its fitness for purpose in tandem with the sole integrity of the DSM. As has been noted in Section 3.1, breaklines and profiles are recorded to define the form of earthworks across a landscape. Thus the appearance of this data upon extraction from a DSM is an important factor in determining its conformity with the shape of the feature, which can be compared by two methods. Firstly, breaklines and profiles can be compared to a more accurate dataset, such as that produced by a TLS or GNSS. Secondly, they can be compared with extant survey data. Profile comparison between extant datasets and those extracted from DSMs is straightforward and can be

achieved by plotting elevation against distance along the profile, which is further explained in Section 4.5.4 of Chapter 4.

Breakline comparison is more problematic as the process of digitising breaklines from a number of DSM is laborious and subjective. Morphological classification was identified as a potential method for identifying breaklines in DSMs, based upon the automated tools utilised for landform classification in the geographic disciplines (Prima et al. 2006; Iwahashi and Pike 2007; Minár and Evans 2008; Saadat et al. 2008; Anders et al. 2011). These tools are designed to detect features akin to breaklines, such as shoulders and footslopes, for which one of the most recent tools is the web-based '*Geomorphons*' algorithm (Jasiewicz and Stepinski 2013). The application of classification to delineating the breaklines of archaeological earthworks, however, is limited, as archaeologists tend of focus on applying other image enhancement options, such as hillshading, skymapping and local-relief modelling for example, to terrain data prior to digitising the earthworks that are visible (Crutchley 2009; Hesse 2010; Bennett et al. 2012; Doneus 2013). Automatic delineation of breaklines for archaeology has focused on using edge detection methods on aerial photographs and satellite imagery (Trier et al. 2009), which has been mooted by some archaeologists as a poor substitute for human interpretation (Palmer and Cowley 2010). It is acknowledged by the archaeological community that collecting aerial photography and delineating features from it introduces bias into the archaeological record as interpretation is based upon individual perception and subjectivity, and is not infallible (Cowley and Gilmore 2005; Wilson 2005). However, by utilising DSMs rather than 2-dimensional aerial and satellite photographs it may be possible to detect breaklines across archaeological earthworks. The process adopted for this comparison is outlined in Section 4.5.4 of Chapter 4.

3.5 Discussion

Kienzle (2004) states that realistic terrain analysis is limited by the DSM in terms of:

- The accuracy and distribution of elevation points used for interpolation
- The interpolation algorithm used
- Chosen grid cell size

The first of Kienzle's (*ibid.*) observations is dependent upon how the researcher gathers their data. If they have access to their own equipment that is well maintained, then the influence of systematic errors should be minimal or accounted for. However, problems may arise if the data is procured from another source, particularly if it is a legacy dataset as metadata relating to the instrumentation with which it was created may be absent, in which case systematic errors may not be mitigated. Data also has to be created or selected based upon it fitness for purpose. Fisher and Tate (2006) address the latter point by stating that the determination of fitness for use of a DSM for a particular application is difficult if an 'off-the-shelf' product is obtained. In

previous years this may once have been dictated by the limited availability of DSM data, particularly from sources that only produced low-resolution datasets. However, fitness for purpose may have been considered a moot issue if very little, or any, alternative data sources were available for use (Fisher and Tate *ibid.*). With an increasing number of data suppliers appearing and an increase in methods by which to produce DSM data, this is less likely to be the case as technology continues to improve.

Researchers using legacy datasets, such as archive SAPs and other imagery, may still be limited in terms of the data resolution they can extract, based upon the GSD of the imagery, which will subsequently influence the choice of grid cell size when undertaking interpolation. Selecting an interpolation algorithm is less problematic, as there are many GIS packages available, including open-source options, which allow users the choice of many algorithms. However, this does not negate the responsibility of the researcher to be aware of the issues inherent in each interpolator and how it will affect their data. Whilst the choice of interpolator has been identified as an error-inducing process, this research does not seek to examine the numerous outputs that can be created by a number of different interpolators. Subsequently only one interpolator will be applied to the rasterisation of point-cloud data, which assists in limiting the variables to be accounted for. Based upon the information presented in Section 3.2, the NN interpolator appears to be both simple and effective, particularly with high-density datasets as applied by this research, and thus NN will be utilised for this project.

Data quality testing does not appear to be conducted by archaeologists, although many are aware of the limitations from airborne data (Challis 2006; Page et al. 2009). The NMP, as discussed in Section 2.1.1.1 of Chapter 2, are aware of the limitations of the transcription data from rectified aerial photography, but no systematic investigation has been conducted that examines the metric quality of the archaeological data that ALS provides to aerial archaeologists for this purpose. There are subsequently two approaches taken by this research as regards the assessment and suitability of DSMs extracted from archive SAPs for archaeological use. The first addresses the importance of comparing the results of SAP-derived DSMs to other sources of metric data, such as ALS, TLS and GNSS, to establish the ability of SAP DSMs to produce useable results. This is particularly important for archive SAPs as they are often devoid of camera calibration information, the level of care they have received during their lifetime is uncertain, and the number of check points that can be utilised during the photogrammetric process is low, if indeed any can be utilised at all. If any metric information is to be obtained from these datasets for identifying any changes occurring to archaeological sites or to extract measurements describing the shape and form of earthworks, then the quality of data from SAP DSMs is fundamental to the accuracy with which they do this.

The objective assessment of the archive SAP, ALS and TLS DSMs will be initially conducted by utilising random points collected with a GNSS to serve as the baseline dataset against which to test the variations in each DSM. This population assessment will facilitate the identification of any large errors in the data which may require addressing prior to undertaking further analysis. The differences between the GNSS and each specific DSM dataset will be established using

the measures described throughout this Section i.e. RSME, ME and SD. A census analysis of the SAP and ALS datasets will be conducted using the TLS data as a baseline dataset, from which a DoD will be constructed to identify the magnitude of the residuals. A paired t-test will be conducted to assess the significance of these differences, whilst the spatial autocorrelation of the residuals will be visualised using the local Moran's I tool in ArcMap. This process will be replicated with the 1st order derivatives to examine, in greater detail, whether any errors in the original data are significant enough to show in the derivatives.

The second approach is based upon an observation by Fisher and Tate (*ibid.*), who note that fitness for purpose can only be assessed relative to a DSMs intended use. Therefore, it is important to establish how well SAP DSMs produce archaeological data in the form of breaklines and profiles of particular features. This will be achieved by comparing the data extracted from SAP, ALS and TLS DSMs to that obtained from RCHME hachure plans of each chosen case study site.

3.6 Summary

This chapter has identified the optimal interpolation strategy for high-density terrain data and described methods of subsequently quantifying DSM quality using global statistical measures and spatial autocorrelation techniques. A method for assessing the archaeological content of this data has also been described.

4 METHODOLOGY

The previous chapter discussed and identified methods for quantifying SAP DSM quality and assessing the archaeological content of these datasets. This Chapter discusses the methodology employed by this research for selecting field sites and processing the SAP and other datasets associated with them.

It begins by outlining the rationale for the selection of the field sites utilised by this research in Section 4.1. Further details relating to the archaeological earthworks, geomorphology and anthropogenic activities affecting these sites are given in Chapters 6 and 7. Acquisition strategies for collecting both archive data sources and ground-based survey data for testing the research objectives are described in Sections 4.2 and 4.3 respectively. The methods applied to processing each of these datasets is described in Section 4.4, whilst the procedures for assessing data accuracy and quality are explained in Section 4.5.

4.1 Selection of Field Sites

The first stage of the research required a pilot study to be chosen that focused on developing and testing a methodology designed to assess the accuracy and quality of DSM data as derived from SAPs and subsequently their applicability for documenting and reconstructing archaeological earthworks. To assess the transferability of this methodology, a second site was selected to validate the results from the pilot study and to provide a larger variety of earthworks on which to test the technique.

Flowers Barrow, near Lulworth in Dorset, was chosen as the pilot site due to a.) the threat of erosion to the archaeology at the cliff edge, thus representing a site at risk, and b.) the stability of the topography and earthworks in the terrestrial hinterland. This factor was imperative for testing the DSMs from each SAP epoch, ALS and TLS dataset. The full criteria for selecting the pilot study site are outlined in Section 4.1.1, below, and the criteria for selection the transferability study site is described in Section 4.1.2.

4.1.1 Pilot Site Criteria

In order to begin an investigation to test the potential for producing 3D data and reconstructing archaeological earthworks from archive SAPs, a site had to be selected that contained a suitable number of earthwork features as well as a dataset of appropriate type, spatial and temporal coverage. To test the quality and accuracy of the SAPs and survey datasets, a stable hinterland was required that had not been subjected to sustained changes over the period for

which archive and modern data is available. Finally, as this research also considers the effects of deterioration to the archaeological resource the pilot site also had to be undergoing either natural or anthropogenic deterioration.

The criteria for selecting a suitable study site were thus:

- Active erosion caused by natural factors;
- Section of the monument threatened by change;
- Restricted public access to site;
- No mechanised agricultural activity, and limited use for pasture, to have occurred during the epoch for which SAPs and other data are available;
- Archaeological data available:
    - Sites and Monuments record (SMRs) of the area
    - Historic Environment Records (HERs)
    - National Monuments Record (NMR)
    - Published work
    - Unpublished work
- Survey Data available:
    - SAPs (from the NMR, CCO and any other identifiable sources)
    - ALS (from the EA and CCO)
    - Archaeological Surveys (i.e. RCHME Historical Monuments Inventory)

Flowers Barrow Iron Age hillfort was selected because it has lost a section of its multivallate defences along the southern edge of the feature to eroding cliffs since its construction. Conversely, the landward side has been preserved due to a lack of mechanised agriculture or significant public access, thus providing a stable hinterland on which to assess the SAP DSMs.

The juxtaposition of both a stable hinterland, unaltered by visitation or agriculture, and an eroding coastline allow SAPs and other mass-capture techniques applied to Flowers Barrow to be examined for their conformity with each other, in a quantitative sense, and for their ability to detect change at the boundary between land and sea. Flowers Barrow hillfort is thus a suitable pilot study site. Testing each survey technique on a stable feature ensures that any variability between techniques that is detected is predominantly a function of the technology rather than any other variable. This is important for establishing the limitations of the survey method. Further, a historic and presently eroding coastline permits the examination of the ability of mass-capture techniques to detect change over time as a threat to the resource. Subsequently, other datasets must be available with which to compare the data from SAPs, which is provided by modern ALS and TLS data.

4.1.2 Transferability Site Criteria

Eggardon Hillfort, situated in West Dorset, has been chosen as the transferability site because (a.) the hillfort is of similar character to Flowers Barrow and thus limits the variables to consider during the analysis stages, (b.) there is a greater variety of earthworks within the landscape, in terms of form and subtlety, on which to test the SAPs, and (c.) the threat to earthworks here has been anthropogenic, in the form of plough damage. It is on this latter point that Eggardon offers a unique opportunity to test SAP reconstruction abilities. The hillfort itself is split in half by a parish boundary, with the northern half in the ownership of a farmer who has subjected it to irregular ploughing cycles since the 1940s, thus destroying the surface expression of the earthworks here. However, the southern half of the interior has been in the ownership of the National Trust, and thus retains all of its earthworks. Subsequently, it will be possible to test whether the older SAPs can detect any remaining surface remnants of earthworks in the northern hillfort interior as well as smaller-scale changes that are linked with agricultural attrition. The rate and extent of change to the ploughed half of the monument can be measured against the preserved half, which can be used as a control for the detection of any change that is identified to have taken place.

4.2 Archive Data Acquisition

Archive data acquisition was the first of two data gathering stages, the second of which is the ground-based collection that is described in Section 4.3. A number of archives were identified for interrogation regarding the extant datasets for the two Dorset-based study sites. Fortuitously, many archives, whether for archaeological data or modern survey data, have online search tools that make the identification of appropriate datasets a little less time-consuming. This section lists the archives that were investigated for particular data types.

4.2.1 Photographic Archives

Whilst both Flowers Barrow and Eggardon Hillfort and environs were identified as suitable study sites, it was necessary to establish what SAP resources were available for each area. It was imperative that each site was fully covered by vertical SAPs and that an SAP dataset was available in each decade ranging from the 1940s to the 2000s. The SAP data obtained for each study site is outlined in Table 4.1. Each of these datasets were viewed to ensure suitable coverage prior to purchasing or borrowing them from their source.

Flowers Barrow Archive Stereo-Aerial Photographs								
Date Flown	**Archive/Creator**	**Scale**	**Focal Length mm (inches)**	**Flying Height (m)**	**Scan Resolution (dpi)**	**Ground Sample Distance (m)**	**Image Type**	**Format (cm)**	**Original Media**
27/03/1945	NMR/RAF	1:10500	203.2 (8)	2133.6	2400	0.110	B&W Vertical	12.7x12.7	Negative
26/08/1968	NMR/RAF	1:10000	152.4 (6)	1524	2400	0.118	B&W Vertical	23x23	Negative
29/06/1972	BU/J.A.Storey	1:12000	151.85 (6)	1822.2	2400	0.132	B&W Vertical	23x23	Print
16/04/1982	NMR/OS	1:8000	304.8 (12)	2438.4	2400	0.081	B&W Vertical	23x23	Negative
14/06/1986	DCC/C.E.G.B.Winfrith	1:12000	153.05 (6)	1836.6	2400	0.135	B&W Vertical	23x23	Print
1997	DCC/C.E.G.B.Winfrith	1:10000	153.15 (6)	1531.5	2400	0.114	Colour Vertical	23x23	Print
27/09/2009	GetMapping Ltd.		100.5 (4)		7.2(µm)	0.150	Colour Vertical	10.3896x6.7824	Digital
Eggardon Hillfort Archive Stereo-Aerial Photographs									
Date Flown	**Archive/Creator**	**Scale**	**Focal Length mm (inches)**	**Flying Height (m)**	**Scan Resolution**	**Ground Sample Distance (m)**	**Image Type**	**Format (cm)**	**Original Media**
22/01/1948	NMR/RAF	1:10000	508 (20)	5029.2	2400dpi	0.104	B&W Vertical	20.955x19.05	Negative
09/03/1948	NMR/RAF	1:10000	508 (20)	5029.2	2400dpi	0.114	B&W Vertical	20.955x19.05	Negative
02/04/1969	NMR/OS	1:7500	304.8 (12)	2286	2400dpi	0.072	B&W Vertical	23x23	Negative
18/04/1969	NMR/OS	1:7500	304.8 (12)	2286	2400dpi	0.072	B&W Vertical	23x23	Negative
19/10/1972	DCC/J.A.Story	1:12000	151.85 (6)	1822.200	2400dpi	0.122	B&W Vertical	23x23	Print
13/04/1984	NMR/OS	1:8000	304.8 (12)	2438.400	2400dpi	0.078	B&W Vertical	23x23	Negative
20/07/1989	NMR/OS	1:8200	304.8 (12)	2499.360	2400dpi	0.084	B&W Vertical	23x23	Negative
21/9/1997	DCC/NRSC Airphoto Group	1:10000	153.15 (6)	1531.500	2400dpi	0.104	Colour Vertical	23x23	Print
2010	GetMapping Ltd.		100.5 (4)		7.2	0.150	Colour Vertical	10.3896x6.7824	Digital

Table 4.1: SAP datasets obtained for both the Pilot and Transferability study sites.

4.2.2 Archaeological and Historical Archives

Archaeological datasets are often held by a number of archives. One of the main repositories of archaeological survey datasets in the UK is the National Monuments Record (NMR) in Swindon, as maintained by English Heritage. There are also many local, county and national councils that maintain an archaeological database of their own, currently known as Historic Environment Records (HER), that often include records that overlap with those held in the NMR. Subsequently, the NMR, Dorset County Council (DCC) and the National Trust were consulted for the records they held relating to the Flowers Barrow and Eggardon Hillfort environs. The results of this search are summarised in Table 4.1.

4.2.3 Airborne Laser Scanning

The largest repository for ALS data in the UK is held by the Geomatics Group of the Environment Agency (EA). ALS data was available from the EA as both gridded (pre-processed) and raw (point cloud) data for the Flowers Barrow field site. As the processing routines applied to the raw ALS data to generate a raster file are not disclosed by the EA, it was felt that the raw ALS should be processed as a part of this research. This ensured that the methods used to manipulate the data would be transparent and repeatable, the process for which is described in Section 4.4.3. Only one epoch of ALS data was utilised for this research, which was the latest datasets available and was collected by the EA on the 7th November 2009.

No ALS data was available for the Eggardon Hillfort area, thus reflecting the remit of the EA to focus on data capture over areas of the UK that are prone to flooding and to monitor coastal change. As an alternative source of terrain data against which to compare the SAP DSMs, a 2m gridded DSM was downloaded from the Landmap Kaia portal. This product has been derived from modern aerial photography, produced by Bluesky, and the DTM created with Intermap DTM. However, no further information is given in relation to the dataset.

4.3 Ground-Based Data Collection

Two survey methods have been used to generate ground-based data for this research: GNSS and TLS. Ground-based techniques are not intended for covering large areas (for example, greater than 10,000m^2, as intimated in Section 1.1.3.2 Figure 1.3), unlike aerial survey methods. Thus their use has been constrained to a select area in and around Flowers Barrow and Eggardon Hillfort due to the time-consuming nature of their application, as described below. The exception is data collection using the GNSS that has been employed for collecting GCPs and reference points over the coverage of the SAP datasets.

4.3.1 Ground Control Points for SAPs

The selection of suitable ground control points (GCPs) for processing the SAPs was undertaken after the imagery from the NMR, DCC and BU archives had been viewed and selected for use, and prior to GCP collection in the field. This ensured that any features identified on the older photography as potential GCP points were still extant and accessible by comparing them with modern OS mapping and aerial photography. These GCPs were then marked on a map to enable fieldwork collection to be as quick and efficient as possible. The process of GCP collection at Flowers Barrow (Chapter 6) and in the surrounding area was more challenging than at Eggardon Hillfort (Chapter 7). Some of the GCP locations required for the Flowers Barrow SAPs were based on the Lulworth Range and thus permission to collect these points had to be obtained from the Range Officer and Wardens, based at DIO Lulworth Camp. Limited access to the site was granted and field work to be conducted on and around Flowers Barrow had to wait until the Ranges were opened to the public i.e. at weekends and during school holidays. Access to GCPs in the Eggardon environs was not an issue as the area is accessible via many minor roads, public footpaths and bridleways.

The Leica Viva GNSS was used to collect GCPs in the field because it provides real-time, geo-referenced point data that does not require post-processing in the office prior to use and was considered to be an efficient, rapid way of creating this data. GCPs collected using the Viva have an expected planimetric accuracy of ±0.8cm and a vertical accuracy of ±1.5cm (Leica Geosystems AG 2012), which will be taken into account by SocetGXP when redistributing error throughout the image block to minimise its effect on the overall solution (ERDAS Inc. 2010). However, the Viva GNSS relies on a good signal for the mobile phone to be able to communicate with the Leica server to obtain real-time corrections for its location and, fortuitously, the reception was good across the Flowers Barrow field site.

If this signal is not available, the reference station provided with the equipment has to be utilised. This was the situation at Eggardon Hillfort and thus the reference station was set-up at a high point close to the Hillfort from which to broadcast a correction signal to the rover via a radio connection. As the Eggardon landscape is characterised by a number of steep-sided valleys, the reference station had to be positioned twice to ensure that the correction signal broadcast by it could be received by the rover. Each separate set-up of the reference station was conducted on a different day and thus it was important to download the appropriate RINEX data from the OS website within a month after each survey was completed with which to post-process the data using Leica GeoOffice. For each different reference station position, the data was downloaded from the reference and the rover and copied into the same folder as the RINEX data for that particular day's survey. Prior to completing GCP collection across Eggardon, a number of permanent control points were established by placing a small number of nails into some old, metal fence posts, as shown in Figure 4.1. This ensured that a known-point had been established, which could be reoccupied after post-processing had occurred, which negated the requirement to repeat this process for future surveys. Leica GeoOffice was used to

Figure 4.1: Control point used to position the reference (base) station at Eggardon Hillfort.

correct the position of the reference station using the RINEX data, before altering the positions of the GCPs that had been collected using the rover, the process for which is described in Section 4.4.2.1. The GCPs were then converted into the local coordinate system, OSGB36, with their uncertainties provided and the offset between the elevation data and the geoid calculated.

To ensure that each epoch of SAPs would contain enough GCPs to obtain a suitable photogrammetric solution, a large number were collected over the area surrounding Flowers Barrow and Eggardon Hillfort, the distribution of which is shown in Figure 4.2a and b. As photogrammetry is a well-established technique, advice on the optimum number and distribution of GCPs is prevalent (ERDAS Inc. 2010; Linder 2009 p.76; Wolf and Dewitt 2000 p.349-350). Despite these well-established guidelines, a degree of pragmatism has to be adopted when applying these rules to historic imagery, as noted by Walstra (2011) and Aguilar et al. (2009, 2013). Established convention cannot always be achieved with archive SAPs, particularly if features identifiable in older imagery (for example foliage and built structures) are no longer extant due to change over time in a landscape, whether coastal or inland (Walstra 2006; Linder 2009). Within the Flowers Barrow study site, there were a number of GCPs that could not be measured in the field, due to access difficulties. Whilst this type of issue may have been overcome by obtaining a larger number of images to form a strip or block of photos, this solution was not financially viable and it would require a powerful computer to handle the increased amount of image data. Subsequently, where there appeared to be a lack of control in some areas of the Flowers Barrow field site, GCP values were obtained from OS 1:1000 MasterMap

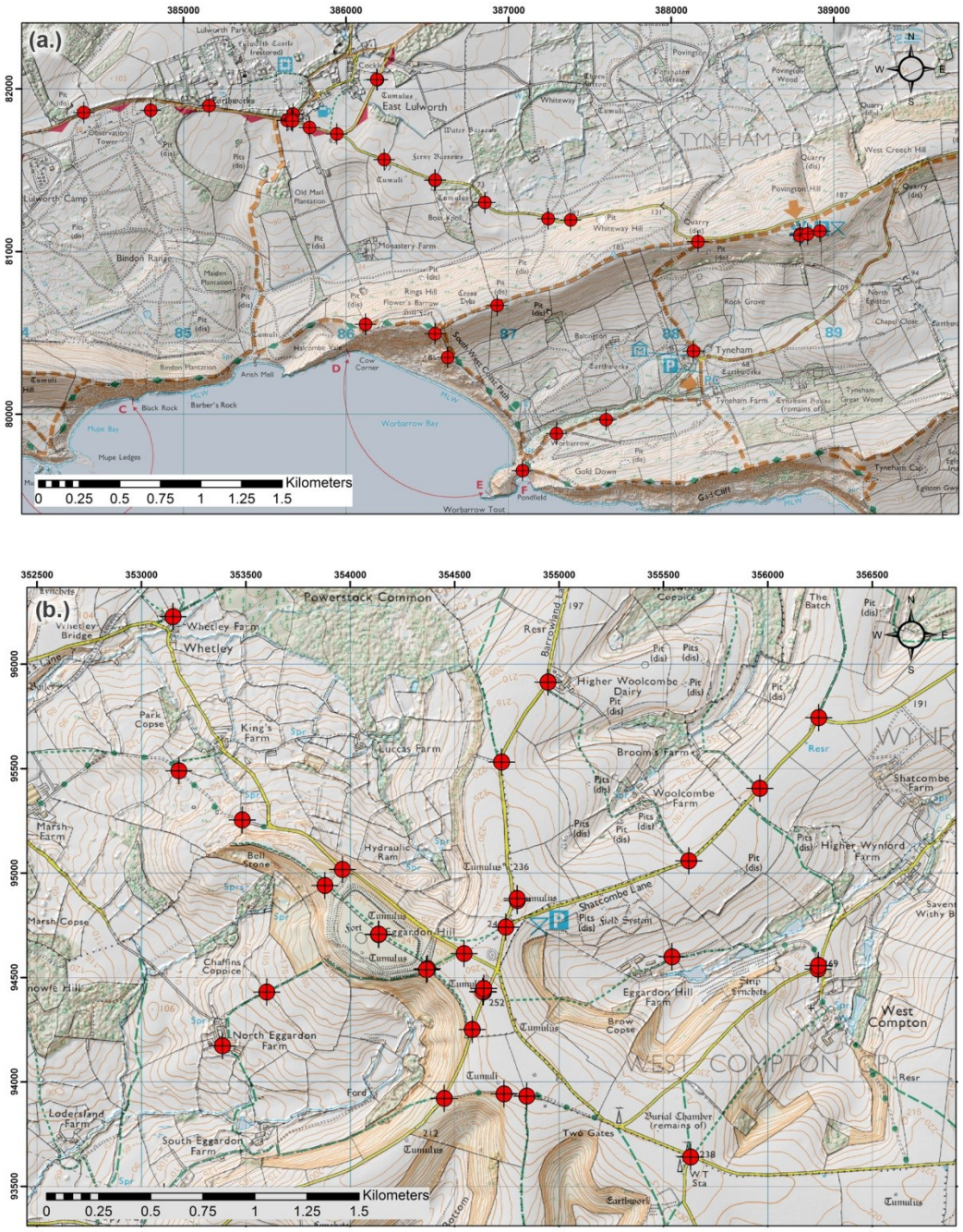

Figure 4.2: Maps showing the distribution of GCPs collected using GNSS at (a.) Flowers Barrow and (b.) Eggardon Hillfort (© Crown Copyright/database right 2014. An Ordnance Survey/EDINA supplied service).

data and a photogrammetric DSM provided by Landmap with a resolution of 2m. This ensured that GCPs were well distributed across the SAPs and surrounding the hillfort. Details relating to photogrammetric data processing using GCPs are given in Section 4.4.2.1.

4.3.2 Terrestrial Laser Scanning

The Leica C10 terrestrial laser scanner was used to capture topographic data across both Flowers Barrow hillfort (Chapter 6), Eggardon Hillfort and the henge monument situated close by (see Chapter 7 for details). TLS data was used to provide a high-density terrain model against which to test the SAP DSMs and to establish whether the more subtle features, such as the occupation platforms at Flowers Barrow and the linear features within Eggardon Hillfort, could be identified using this equipment. As TLS data has rarely been applied to examine archaeological earthworks, particularly those as big as a Hillfort, this element of the research will examine the utility of applying high-resolution data collection to archaeological earthworks. Permission to collect TLS data on Flowers barrow had to be sought from the DIO Lulworth Ranges Warden and vehicular access arranged to transport the heavy equipment onto the hillfort every day of the survey. Permission to survey the southern half of the Hillfort was sought from the National Trust, whilst the private owner of the northern half and the henge, Mrs Lloyd-Harris, was also approached for permission to survey on her land. In both cases, permission was granted and the periods for which the survey could be conducted was flexible for each. However, the decision was taken to undertake the TLS survey during the late winter and early spring to ensure that the grass within the region was not too high as this could obscure some of the more subtle features.

The C10 is capable of generating dense point clouds with a maximum density cited to be <1mm through the entire distance range. This value was seen as impractical for this research as not only would the scanner take an inordinate amount of time to complete one scan, the amount of data this would produce could not be handled by the computing facilities available at BU. A value of 10cm was adopted for all of the scans conducted, which is an order of magnitude smaller than the 1m resolution generally provided by ALS. The data was therefore manageable in size, which is often a problem where dense point clouds are created in terms of the processing requirements from PCs.

To identify the most appropriate areas to collect overlapping scans across Flowers Barrow, Eggardon Hillfort and the henge monument, a DSM had to be obtained for each area. For Flowers Barrow and for Eggardon this was a 2m DSM downloaded from Landmap (see Section 4.2.3). After importing one of the DSMs into ArcMAP, a polygon was created that enclosed the area to be surveyed with the TLS. A plugin called ‘Repeating Shapes’ from Jenness Enterprises (Jenness 2012) was used to create a number of circles within the polygon, with each circle having a radius that was set to equal the range of the TLS, which in this instance was 80m (Figure 4.3). The circles that were largely peripheral to the polygon were removed before the remaining circles were shifted to ensure that their centres were not in inconvenient locations, i.e. the middle of a road. Points were then generated to be positioned at the centre of each circle as these would be used to define the station at which the TLS would be positioned to collect data. To ensure that the scanner would cover the defined area, viewshed analysis was employed to identify any occluded areas. The maximum range parameter was set to equal that

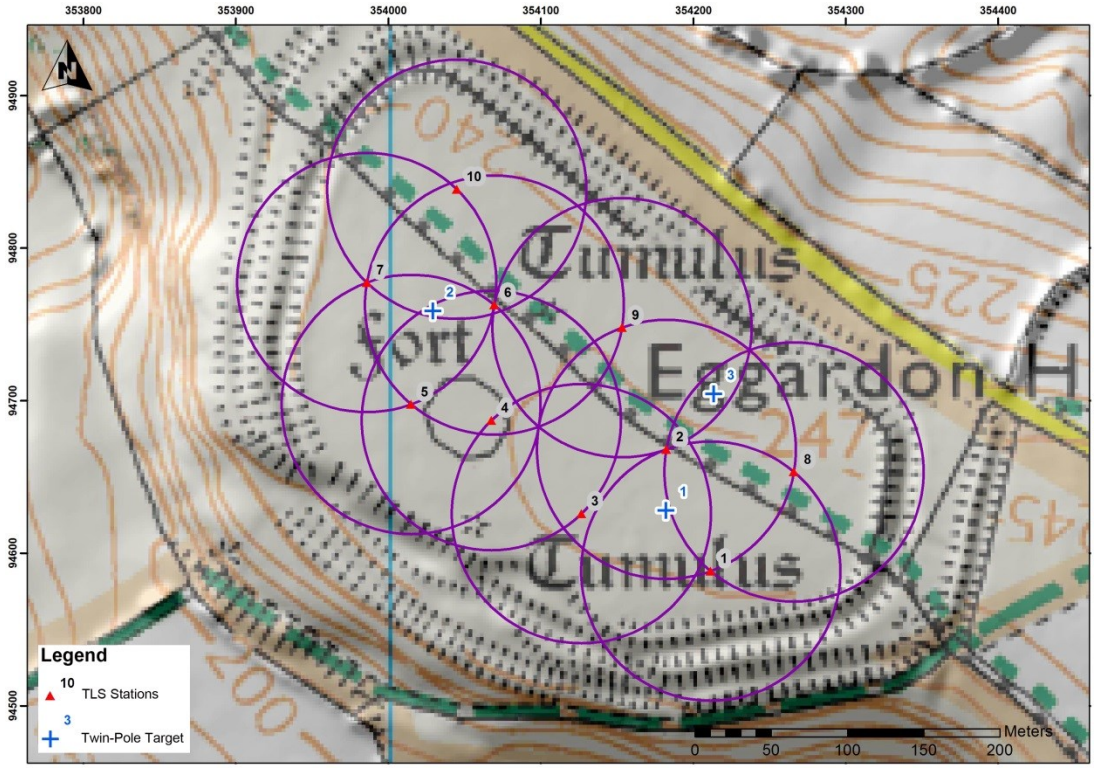

Figure 4.3: Planned locations for the TLS and Twin-Pole targets across Eggardon Hillfort (© Crown Copyright/database right 2014. An Ordnance Survey/EDINA supplied service).

of the scanner i.e. 80m, and the scanner height above the ground was set to 1.7m, which would be the minimum height limit for each set-up. The angle of the range the scanner used was -45° to +90° were also input into the viewshed process that, once it had been run, could be used to identify areas within the polygon boundary that might benefit from the addition of another survey station. The viewshed process was then repeated to ensure that the coverage for each field site was optimal.

The points created from this process were output for use with the GNSS and stations were named so that they could be occupied sequentially. Using this technique, it was also possible to select locations on which to position the twin-pole target so that it could be seen from multiple TLS survey stations. By identifying areas of maximum overlap between the circles denoting the TLS range, the number of positions the twin-pole would have to occupy could be optimised. This reduced the number of times the twin-pole had to be moved and set-up, which also saved time in the field. The pre-defined locations of the TLS stations and the twin-pole target were uploaded to the Leica Viva prior to heading out to the field sites so that the 'stakeout' function could be utilised for positioning both pieces of equipment. By utilising this method to position the control for the survey, the random errors generated by the GNSS were expected to combine and nullify each other.

4.3.3 Global Navigation Satellite Systems (GNSS)

Beyond the collection of GCPs, the Viva GNSS was also used for collecting two extra products at both field sites: profile information and a series of stratified-random samples across Flowers Barrow hillfort and associated cross-ridge dyke, and Eggardon hillfort, including the henge and barrow monuments. The RCHME 1970 hachure plan of Flowers Barrow and the RCHME 1952 hachure plan of Eggardon Hillfort contain measured profile information of the earthworks that were reproduced using the GNSS, as shown in Figure 4.4. The hachure plans were scanned, scaled and geo-referenced using AutoCAD Civil3D 2011 before entry into ArcGIS, which was used for extracting the coordinates relating to the start and end points of the profile lines for each site. These locations were uploaded to the GNSS so that they could be relocated in the field and the same profile line replicated by the GNSS. This enabled the direct comparison of profile data taken from a traditional archaeological survey to be compared with the same

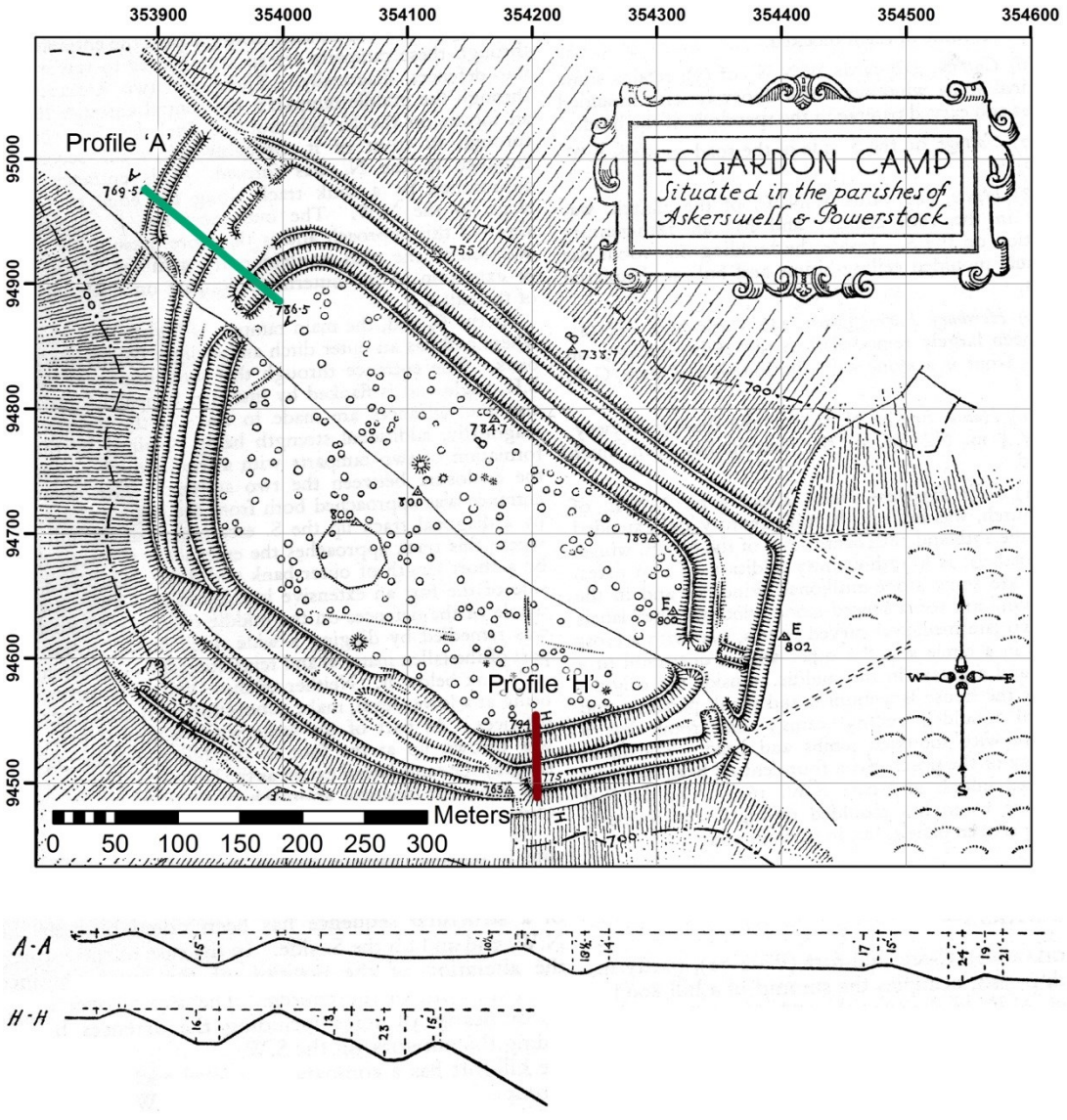

Figure 4.4: Rampart profile positions across Eggardon Hillfort (above) and the profiels as drawn by the RCHME (below) (RCHME 1952).

product as extracted from the mass-capture techniques and the GNSS. The results of this analysis are given in Chapters 6 and 7 (Sections 6.7.1 and 7.7.1).

Profile collection at Flowers Barrow utilised tent pegs as markers against which to run a 100m tape that denoted the path of the profile, which could only be pushed into the soil to a very shallow depth because of the risk of hitting buried ordnance. The GNSS was used to manually record a point at every 50cm interval, as marked upon the tape. It was decided not to use any automatic measurements as the profile involved carefully moving up and down steep-sided ramparts, which would not be conducive to keeping the GNSS pole vertical whilst measuring a point. Manual measurements take longer to perform and thus only one profile was completed at Flowers Barrow. The comparison of the 1970 profiles to those taken from the ALS, TLS and SAPs, as well as the GNSS, can be found in Section 6.7.1. Profile collection across Eggardon Hillfort employed a slightly different method in comparison with Flowers Barrow. Whilst the locations of each profile was determined in the same way, uploaded to the GNSS, and the stakeout function used to locate the beginning and end points, survey cord was used to delineate the direction of the survey. It was felt that this approach would be quicker and thus the point spacing of GNSS measurements was determined by pacing out two foot-length in between each point. The results of profile comparison between the GNSS and SAP DSMs can be found in Section 7.7.1.

Stratified-random samples were deemed necessary to provide a dataset for generating comparative statistics for testing the similarity of SAP DSM datasets to elevation data provided by ALS and TLS techniques as well as the GNSS. This sampling method has been chosen to ensure that the sample points are not so random as to cluster in certain areas and avoid others, as addressed by stratification, whilst also reducing bias in the sampling procedure, as dealt with by the random component. Subsequently, there should be no sampling biases with the random points. To calculate the stratified-random points across both Flowers Barrow and Eggardon Hillfort and environs, ArcMAP was used along with a plugin called ‘Repeating Shapes’ from Jenness Enterprises (Jenness *ibid.*). This plugin generates a number of hexagons across an area that is predefined by a polygon in ArcGIS, with each hexagon having a set radius (Figure 4.5). The polygon itself was drawn around the area of interest at both field sites over the 1:1000 OS MasterMap dataset. The ‘Create Random Points’ tool can then be run on the hexagonal area, with one random point inserted into each hexagon. This process was repeated a number of times to make sure that the area of interest was covered with sufficient random points, albeit without creating so many that collecting them in the field would be prohibitively time consuming.

The coordinate values of the random points were extracted from ArcGIS and uploaded to the GNSS for location in the field using the Leica Viva’s Stakeout routine. To ensure the collection of random points using the ‘stakeout’ function on the GNSS was as efficient as possible, the points were ordered so that the first set of points were collected along the top of a rampart, and then the next set of points were collected along the sides or the bottom of a rampart. In this way, the surveyor did not have to continuously walk up and down the steep-sided ramparts, but instead moved along each level of these features before advancing to the next.

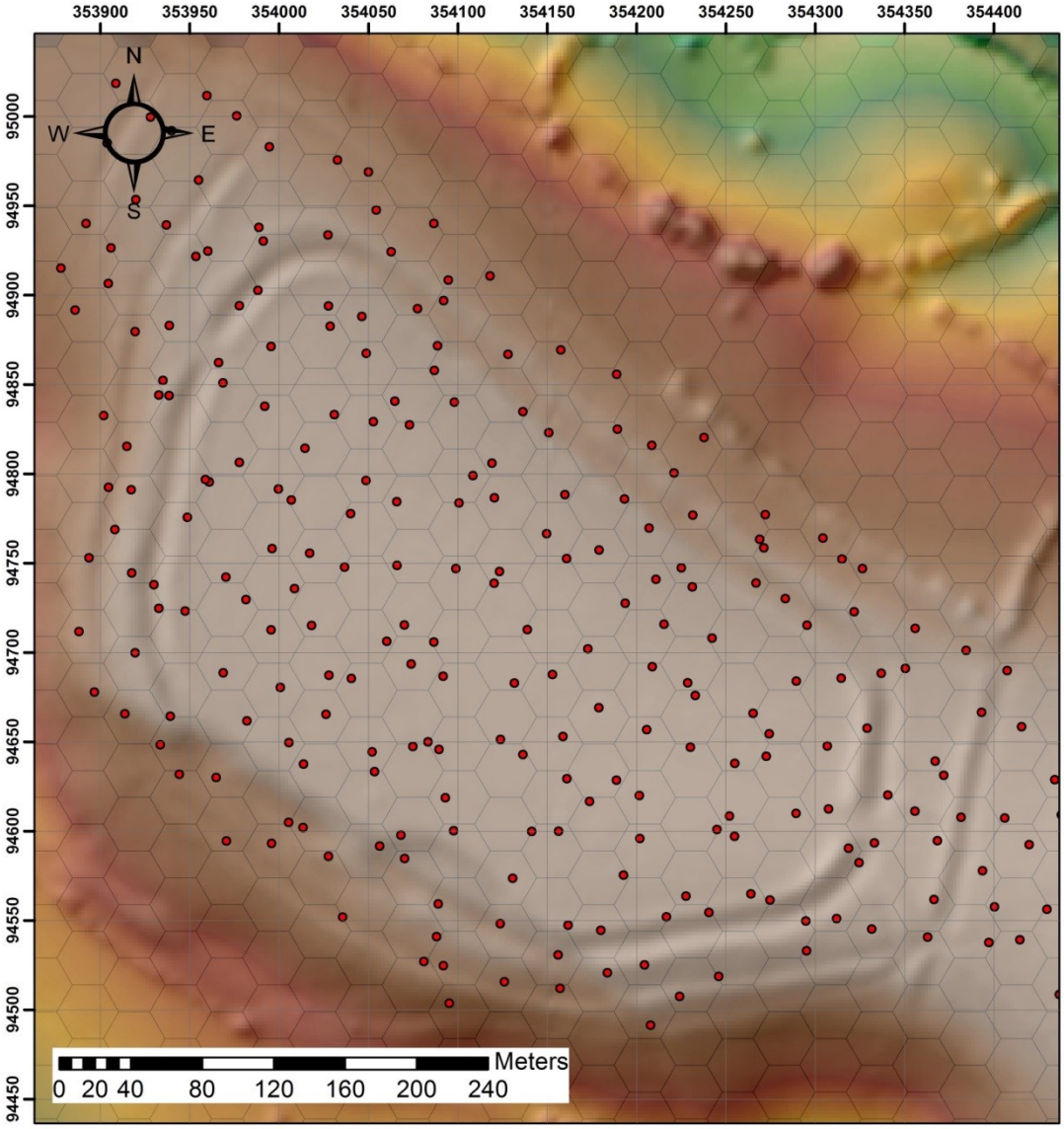

Figure 4.5: Hexagons with a 30m diameter, each containing a point positioned randomly in ArcMap.

4.4 Data Processing

As each survey technique, namely the SAPs, ALS, TLS and GNSS have different processing requirements, their processing workflows differ from one another. The processing stage aims to convert often large, segregated (i.e. many APs covering one area, or a series of concurrent ALS strips) datasets into a single dataset from which the appropriate data products can be extracted. The various workflows employed by the research are outlined below whilst the results are discussed in Chapters 6 and 7.

4.4.1 Archive Stereo-Aerial Photographs (SAPs)

The digital photogrammetric software package used by this research is SocetGXP 4.1.0., which is produced by BAE Systems. Whilst it is designed for working with “industry-standard imagery” (BAE Systems 2013), it has not been used for processing historical SAPs, unlike other photogrammetric software packages such as Leica Photogrammetry Suite (LPS) (Lambers et al. 2007; Wackrow et al. 2007; Walstra 2006). The outputs from SocetGXP are generated semi-automatically by the software, based on the parameters the operator enters. The quality of the outputs depends on the successful processing of the SAPs, which in turn will be affected by the quality of the imagery used, availability of camera calibration information (interior orientation information), good image contrast (i.e. not large areas of desert or water), range of variation in topographic relief and the successful identification of the GCPs within the imagery (each operator that identifies the location of a GCP in the image to match it with the value recorded in the field may select a slightly different pixel, introducing a stochastic – random – error into the process).

SocetGXP does not provide specific processing solutions for imagery that is not accompanied by much (if any) control data, such as camera calibration files or GCPs, and thus it was initially unknown as to how the end result would suffer in its accuracy and quality. The accuracy and quality of the SocetGXP output is discussed further in Chapters 5, 6 and7. However, a bespoke workflow was created by the technical manager at BAE Systems UK for this research to address this problem and is presented in Figure 4.7. Entering interior and exterior orientation information is straightforward, if the imagery is accompanied by camera calibration information as well as IMU data, as is the situation for the 2009 and 2010 GetMapping photographs provided for both field sites. However, a rudimentary set of calibration data must be created for archive SAPs, much of which can be found on the information strip on the photography and the coordinates of the fiducial marks have to be determined by different means. These have been established based upon a technique developed by Niwa (No Date). Niwa (*ibid.*) suggests setting the principle point value to 0,0, which it would be in the ideal case with no distortion, and obtaining the fiducial coordinates by measuring the distance between them both horizontally and vertically (see Figure 4.6). The fiducial measurements were performed using AutoCAD Civil3D 2011, as shown in Figure 4.6. Once these values were obtained, they could be used in SocetGXP to provide the software with initial values to use in its calculations, although because of distortions in the imagery, the fiducial marks could not be automatically located by the software and required manual identification by an operator.

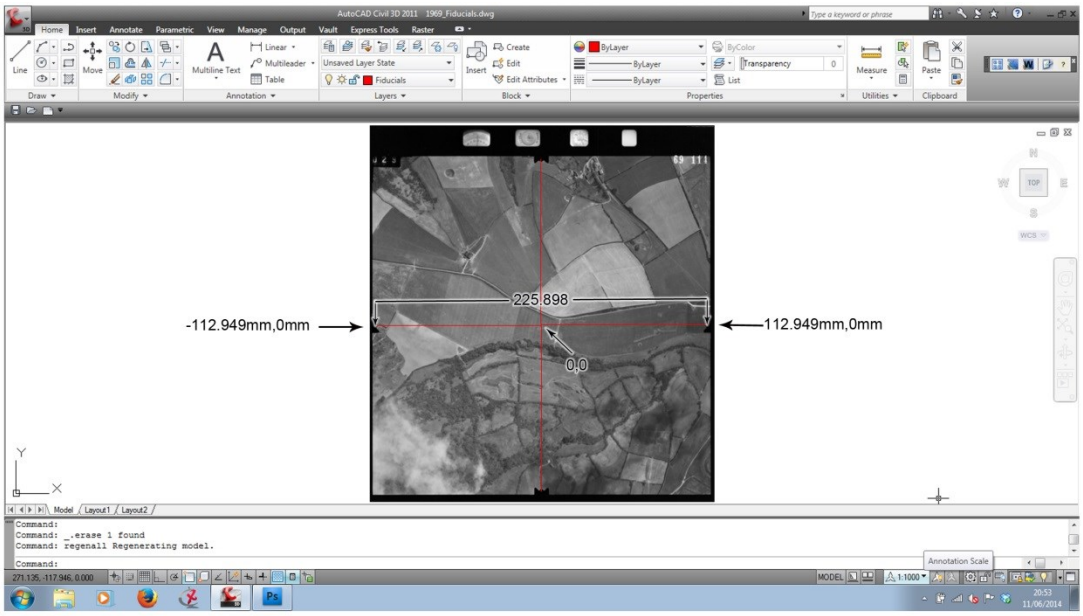

Figure 4.6: Example of the fiducial measuring process as performed in AutoCAD.

Much of the exterior orientation information for the archive SAPs was estimated by the software during the image import process using both the GCP file that was uploaded, which was utilised by the 'Set Up Block' dialogue that allowed the SAP strips to be positioned manually with respect to the GCPs. Subsequently, the camera elevation value needed to be manually entered, and the kappa value altered to reflect the orientation of the photographs. Once all of these steps had been achieved the imagery was ready for the triangulation process to begin, which is outlined in the flow chart shown in Figure 4.7. As is evident from the flow chart the accuracy of the camera position and attitude could be altered to allow the bundle adjustment greater degrees of freedom to find a least-squares solution to the exterior orientation values for the SAPs. When the imagery looked to be positioned well and the RMSE value returned during the 'Solve' process was acceptable, which was considered to be between 2 to 5 pixels, GCPs were added to further refine the exterior orientation information and constrain the relationship between the SAPs and the terrain. The process of adding tie points and GCPs is necessarily iterative and requires extensive input by the operator to refine the results after each 'Solve' process is run, which subsequently provides measures of error in the form of RMS values. GCPs were added three or four at a time, followed by another 'Solve' process, until all of the GCPs for a particular field site were added to the imagery.

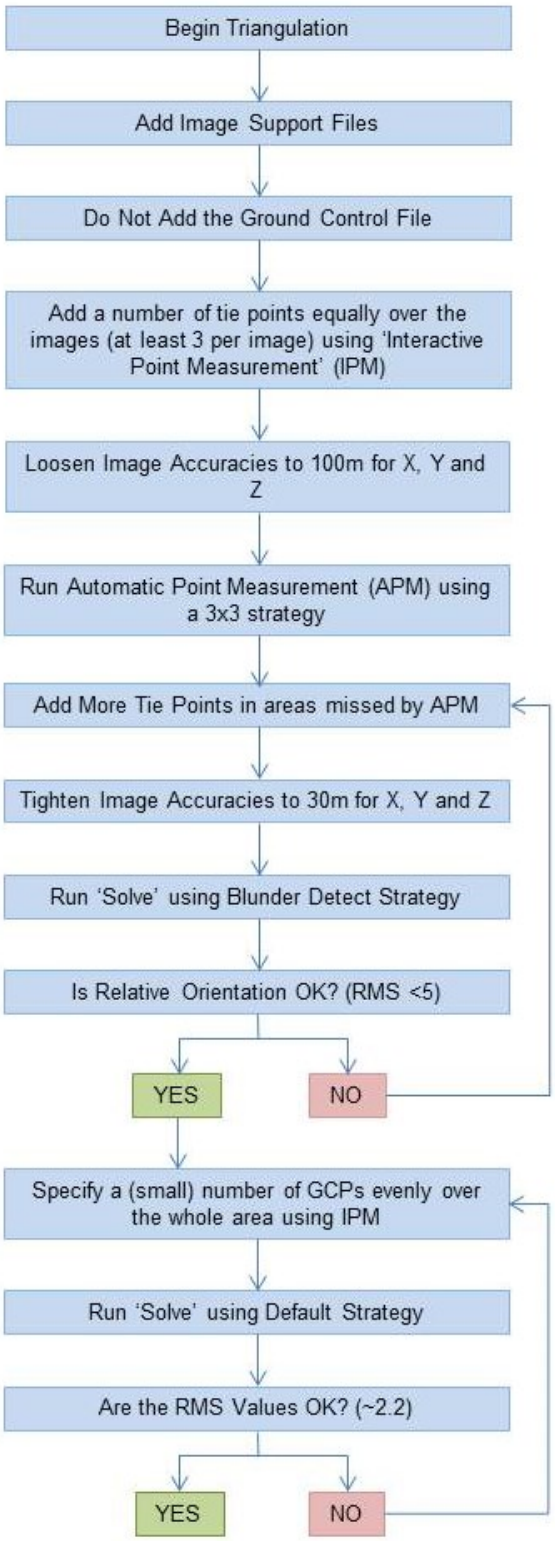

Figure 4.7: Workflow for processing SAPs in SocetGXP.

It was recommended by BAE Systems (personal communication, 29th November 2012, see Appendix Three) that the absolute fit of the data was checked prior to exporting the data for further use. This was an issue with the Flowers Barrow dataset, which exhibited an obvious tilt in the data. The steps taken to resolve this issue are outlined in Section 5.1 of Chapter 5. After each 'Solve' solution was returned it was possible to check the overall RMS error for each of the control and tie points. This provided the option to remove any points that have significantly large errors, which can be deactivated before another Solve process is undertaken. Whilst this may appear to be a laborious process, devoid of automation, it provides the operator with the flexibility to refine the result and observe how making minor alterations may improve or degrade a solution.

Although RMSE values were provided by the software relating to the residual errors in the ground X, Y and Z values, it was decided that no check points would be used to further indicate the quality of the triangulation result. This was for two reasons: firstly, the lack of access to a site over which to collect high-quality GNSS points and secondly, the potential lack of identifiable features in older imagery, such as buildings and roads, that are likely to have altered or disappeared from the landscape over time. Therefore any GCPs collected with the GNSS were used to provide control in both the Flowers Barrow and Eggardon Hillfort study sites (see Chapters 6 and 7 respectively). Instead, the assessment of DSM output quality from SocetGXP was obtained by comparing elevation values within each DSM to the stratified random points as measured by the dGPS in the field (see Section 5.2). Whilst this may appear to be laborious, by adopting this approach the focus of DSM quality was placed firmly on analysing the region surrounding the area of interest i.e. the hillfort, rather than on a purely global RMSE value.

After completing aerial triangulation, a DSM as created. Socet GXP uses two different terrain extraction applications to generate DSM data from triangulated stereo-aerial photography: Automatic Terrain Extraction (ATE) and Next Generation Automatic Terrain Extraction (NGATE). To establish which of these strategies would provide the most accurate DSM from archive SAPs, an investigation was conducted that is described in Section 5.2 of Chapter 5. DSM resolution was set to be 1m in both the X and Y direction to match the estimated $1m^2$ point density of the ALS data. The DSM values from SocetGXP were output as points in a '*.asc file' for interpolation within ArcMAP using the natural neighbour algorithm. The reasons for selecting this algorithm were given in Section 3.2. However, by applying this interpolator to all of the datasets, including ALS and TLS, this particular variable remains consistent across the research project. The analysis of this data will be covered in Chapter 6 Sections 6.4 to 6.7 and Chapter 7 Sections 7.4 to 7.7.

4.4.2 Ground-Based Data

GNSS and TLS data were both collected at Flowers Barrow to provide further datasets against which to test the SAP DSMs. The TLS was used to create a high density DSM of the Hillfort itself, whilst the GNSS was employed to collect GCPs, random points, a profile across the ramparts and a selection of breaklines. The collection and processing of these datasets is described below.

4.4.2.1 GNSS

The data gathered by the Leica Viva GNSS, namely the GCPs, random points and profiles were directly imported into ArcGIS and required no processing, except in situations where the mobile internet could not be used to obtain corrections in the field. As previously mentioned, there was very little mobile phone reception in the Eggardon landscape. There was enough of a signal to obtain corrections from the Leica server from within the Hillfort, along the fence line, and thus a small number of survey nails were inserted into extant iron posts close to the fence over which the reference station could be positioned (see Figure 4.1). This allowed the unhindered collection of data to occur within the Hillfort itself, in terms of random points, profiles and breaklines, as the reference could be set up over a known point and simply broadcast corrections to the rover.

However, the collection of GCPs in the Eggardon landscape was more onerous and required the reference station to be set up over a number of unknown points for two reasons. Firstly, the lack of mobile phone reception (and 3G mobile internet) with which to establish control beyond the hillfort interior and, secondly, to ensure that the radio reception between the reference station and the rover was unhindered in the steep-sided valleys of Askerswell and Powerstock. The reference station was set up to collect satellite observations for 20 minutes prior to undertaking the collection of GCPs. This approach allowed the equipment to calculate an accurate 3D location by using the observations to calculate a mean positional value based upon these readings. Thereafter the reference station is able to calculate the instantaneous positional error (caused by the GNSS radio waves ricocheting through a randomly, rapidly varying layer of charged particles in the upper atmosphere, known as the ionosphere, which results in a random delay of travel time), which is transmitted to the rover by radio.

To further improve upon the locational accuracy the reference station's position was further improved post-processed using permanently fixed "active" GNSS stations (of which a network exists around the country (see Figure 4.8a), many of which are maintained by the OS or the Natural Environment Research Council - NERC), whose positions are accurately known. These stations record raw GNSS signals at regular intervals (typically 30 seconds), which are

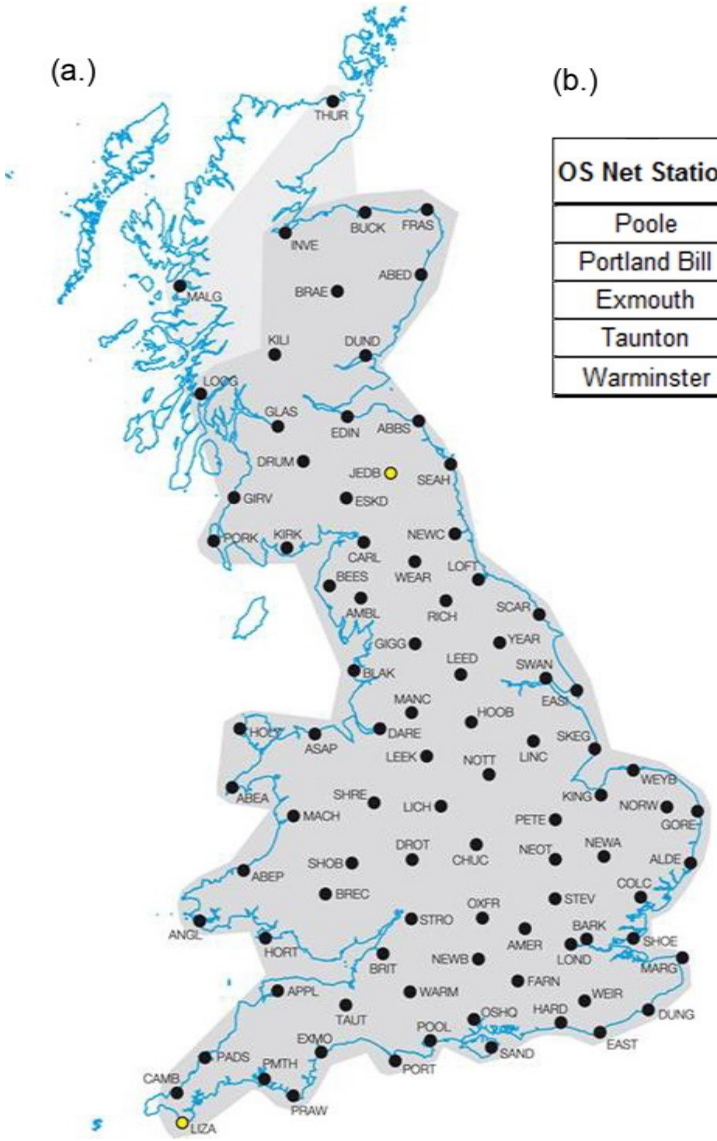

OS Net Station	Abbreviation	Distance (km)
Poole	POOL	52.45
Portland Bill	PBIL	29.04
Exmouth	EXMO	55.63
Taunton	TAUT	42.56
Warminster	WARS	60.33

Figure 4.8: Diagram illustrating (a.) OS Net reference station locations (Ordnance Survey 2006) and (b.) OS reference stations used for Eggardon Hillfort.

distributed (usually via File Transfer Protocol, FTP, or web server) in a format conforming to the standard Receiver Independent Exchange Format (RINEX) standard.

By using this data, the distance dependant errors between the OS/NERC active stations and the temporary reference station set-up for this research were reduced. The raw GNSS signals from the Viva reference station (which can also be stored and downloaded as RINEX) were imported into Leica GeoOffice to re-position the reference station based upon the positions of the five nearest active stations (see Figure 4.8b). This increases the redundancy of the triangulation result between them and the temporary reference. The data from the rover could then be imported and transformed to their correct locations based upon the repositioning of the reference station. This data could then be exported as XYZ data, ready for import into ArcGIS or SocetGXP for use as GCPs.

4.4.2.2 Terrestrial Laser Scanning

The way in which the TLS data was captured in the field meant that registering the data using Leica Cyclone was a straightforward process. Both the survey stations over which the TLS was positioned and the HDS targets it was aimed at were georeferenced using the Leica Viva GNSS, and thus the TLS was orientated in the field using the 'orientation to reference' procedure programmed into the on-board software. Thus the data could be imported into Leica Cyclone already registered (i.e. the point clouds were both orientated in a relative and absolute sense).

To try and remove any vegetation within the TLS data, small sections of each dataset were selected with a 'Fence' and isolated. The points to be deleted within the selection were subsequently selected and removed. Whilst CycloneTOPO offers the ability to remove unwanted artefacts in the data, such as vegetation and other spurious points, access to suitable computing power and prolonged access to the software was not available. Subsequently, the most efficient means of dealing with outliers and vegetation was adopting a manual approach to data cleaning.

Each dataset was unified before being exported from Cyclone as an unreduced '*.txt' file that could be read by text editing software prior to import into ENVI 5.0 where it was converted into '*.las' file format using a plug-in called BCAL LiDAR Tools. This file was subsequently rasterised to create a 1m grid containing the minimum elevation values. Again, the value of 1m was chosen to match the raster files created for each of the SAP and ALS datasets. The interpolation method employed by the 'Create Raster Layer' tool in the BCAL LiDAR Tools is an implementation of the nearest neighbour interpolator. Although ArcMap could have been utilised, as was the case for the ALS and SAP datasets, ENVI was chosen because any outliers identified in the data that were not removed in Cyclone could be allocated a specific value to be designated as 'NULL'. This would ensure that any values from this dataset, which would be utilised to extract corresponding values from the ALS and SAP datasets, would not be considered during the analysis stages, particularly as the data will be examined on a pixel-by-pixel basis.

4.4.3 Airborne Laser Scanning

Raw ALS data required processing prior to use in ArcGIS. The EA provided point data as first and last return ASCII files in x,y,z format, arranged in columns and separated in space-delimited format. The EA state that the last return data produces more accurate DTMs (Geomatics Group 2010). If more than one file for a specified site is provided, then each file will need to be combined to form a single file containing all of the point data, which can be achieved using a text editor, such as gVIM and LTFViewr, which have been designed to handle large files i.e.

those in excess of 5GB. Depending upon the size of the dataset, it may be necessary to reduce the data by cropping it to the area of interest prior to undertaking interpolation in ArcGIS.

Examination of the EA ALS catalogue, available from the Geomatics Group website (Geomatics Group 2011), suggested that data in the Worbarrow Bay region have point spacings cited to be 1 or 2m. As funding did not permit the purchase of a large number of EA datasets, in part due to the extra costs incurred by requesting raw data, only three datasets, all from 2009, were purchased. Raw ALS data was converted into a gridded format so as to be directly comparable with the data extracted from the photogrammetric DSMs. ArcGIS was used to perform this conversion by running the natural neighbour interpolation routine.

Gridded ALS data from the EA has been filtered by the organisation to remove spurious points but not vegetation. The way in which the EA filters their ALS data is not disclosed and is stated to be "held as Commercial in Confidence" (Geomatics Group 2010) because the process adopted has been developed by the EA themselves. As has been noted by other authors (Challis 2006) there can be no certainty that this method does not remove features of archaeological importance. It was therefore necessary to compare the gridded EA data with raw ALS data of the same region to investigate whether there are any differences between the final DEM output from the EA or the same product filtered and process in-house with archaeology specifically in mind. Two tiles of ALS data was provided by the Environment Agency as raw, first and last return, '*.las' files. The 'LAS to Multipoint' tool within ArcMap was used to convert the files into a format to which the natural neighbour interpolator could be applied. By opting for this workflow, it was felt that the interpolation process was kept as similar to that of the SAP datasets as possible.

4.5 Data Testing: Accuracy and Quality

4.5.1 Root Mean Square Error (RMSE)

The root mean square error (RMSE), otherwise referred to as RMS error, is a global measure that provides an indication of the accuracy of a dataset. It is the measure of difference between one dataset and another, one of which is accepted to be more representative of the feature being measured. This approach has been adopted by a number of authors (Adams and Chandler 2002; Barber et al. 2008; Walstra 2006) as well as the Environment Agency, who use real-time kinematic (RTK) GPS as their baseline dataset against which to assess the ALS they collect in a particular area. Subsequently this research will utilise the TLS and GNSS data as baseline datasets against which to test the archive SAPs and ALS DSMs at Flowers Barrow and Eggardon Hillfort. GNSS data will be employed for testing a population sample of data whilst the TLS will be used as the baseline dataset when census analysis is conducted.

Instrument	Horizontal Accuracy	Vertical Accuracy
ALS (Optech ALTM Gemini) @ 900m altitude	16.4cm	5cm – 30cm
TLS (Leica ScanStation 2)	0.6cm	0.4cm
TST (Leica TS06) in reflector (prism) mode	±0.15cm – 0.3cm	0.2cm – 0.4cm
GNSS (Leica Viva)	1cm	2cm

Table 4.2: Expected accuracies from a number of survey techniques.

To extract corresponding elevation data from each of the SAP, ALS and TLS DSMs, the 'extraction by point' tool will be utilised in ArcMap for population analysis with the GNSS data. For census analysis the 'sample' routine will be employed. Subsequently, the coinciding elevation or derivative values from dataset will be exported from ArcMap and combined to form a table in Microsoft Excel, listing all of the values extracted from a particular data type i.e. elevation, slope or aspect values from each of the DSM sources. RMSE is calculated by adding together the squared values of the difference between the predicted values (those from the more accurate dataset) and the actual values (those from the less accurate dataset), dividing this value by the number of samples, and then square root the result. As the value of the RMSE decreases, the survey technique is suggested to be more accurate. Table 4.2 lists the expected accuracies from a number of survey instruments whilst the concept of difference between two datasets, in which the GNSS is the more accurate technique that the photogrammetric DSM from 1984, is shown in Figure 4.9.

4.5.2 First Order Derivatives

Although elevation data is useful, archaeological surveys suggest that other products are required for analysis, which can be derived from a DSM. Hachure plans are traditionally used to represent archaeological earthworks, the process of which involves delineating breaklines to describe their planimetric form, whilst the hachures themselves describe the break in slope and its aspect. Subsequently, it is important to examine how well the archive SAP DSMs represent these terrain derivatives to deduce whether they are fit for purpose when it comes to producing records for archaeology. By conducting both visual and numerical comparisons of archive SAP DSM derivatives with those produced by ALS, TLS and GNSS technologies, it will be possible to ascertain how well each SAP epoch reconstructs archaeological terrain.

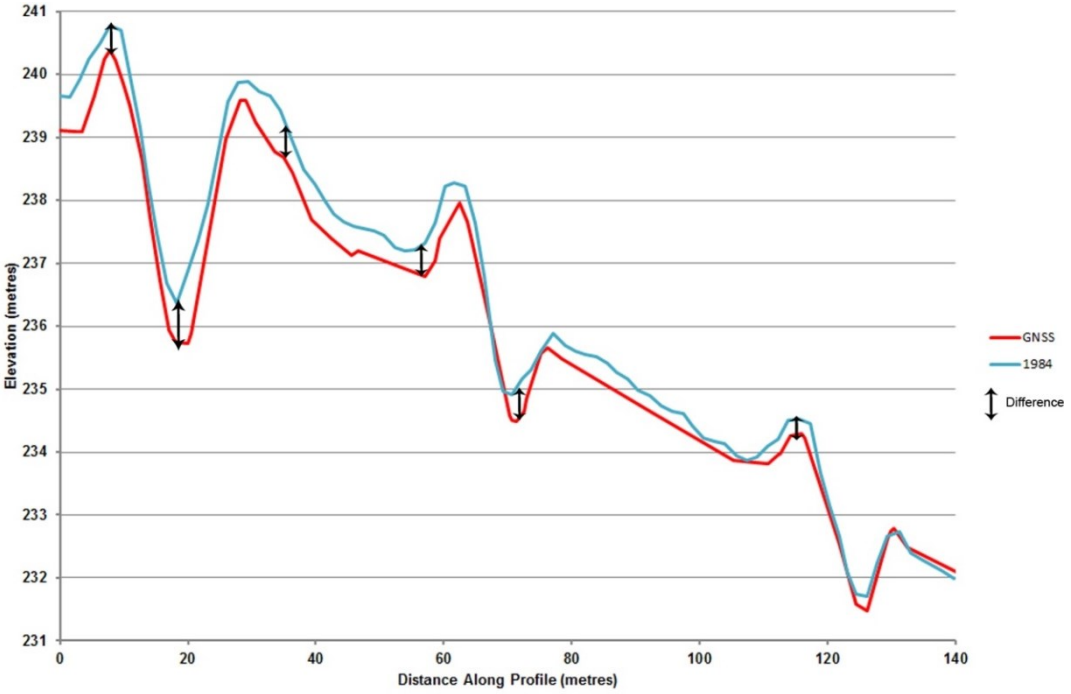

Figure 4.9: Rampart profile showing data collected using a GNSS (red) and a DSM from 1984. Black arrows indicate points where the elevation values differ between datasets.

Further benefits of analysing first order derivatives are their ability to facilitate the assessment of a DSM in terms of its quality as discussed in Section 3.4.3. These products derive from elevation data and are therefore increasingly more sensitive to noise as the order of derivation increases. Subsequently, it is possible to identify the regions within the SAP DSMs that are afflicted by noise, which may be due to the digitisation process and the quality of the equipment used to achieve digitisation, or it may be down to the quality of the photograph negative or print, and the care it has received during its lifetime (or lack thereof) as discussed in Section 2.2.6.

4.5.3 Statistical Analysis

Statistical analysis will be used to compare elevation data and their first order derivatives from each SAP DSM epoch to those generated from TLS data to produce a census comparison of every value in the area covered by the TLS. The residual values between the TLS and the ALS and SAP DSMs will be examined using summary statistics and graphical representations, namely frequency histograms and scatter plots, to provide an indication of residual distributions (see Section 4.5.3.1). Paired t-tests will be employed to identify what correlation exists between the TLS and the SAP DSMs, as discussed in Section 4.5.3.2. Finally, local Moran's I analysis will be undertaken to examine the spatial distribution of residual values, the process for which is given in Section 4.5.3.3.

4.5.3.1 Summary Statistics, Frequency Histograms and Scatter Plots

Summary statistics will be generated to provide global indicators of the quality of elevation and derivative values created using SAP DSMs by calculating the residual values between them and the TLS data. The summary statistics will consist of mean, median and modal values, standard deviation, skewness, kurtosis, variance, range and the minimum and maximum values. The RMSE, as discussed in Section 4.5.1, will also be provided. Graphical representations in the form of histograms and scatter plots will further support the analysis of these statistics by depicting the spread of residual values. Frequency histograms illustrate the quantity of residual values within a defined 'bin' or value, which indicates whether there is a normal distribution or whether these values are skewed. This assists in identifying whether the errors present are systematic or random in character. Scatter plots are useful for identifying whether there is a linear trend between baseline and test datasets and outliers can also be identified.

4.5.3.2 Paired T-Test

This test was chosen as both the SAP and TLS datasets contain the same number of values that will form a pair with one another over terrain of the same area. The paired t-test, as calculated using SPSS, provides the Pearson's correlation, or 'r', value between two datasets, which indicates the correlation between them, as well as a significance value, or 'p'. The significance value identifies whether the null hypothesis, which states that "the variances in the two groups are equal i.e. that the difference between them is zero" (Field 2005), is true. Therefore if the significance value returned for any of the tests has a p value of less than 5% (or 0.05), then the null hypothesis cannot be accepted and highlights the fact that the differences between the two datasets are significant (Field *ibid.*). Subsequently, it is hoped that the significance values returned when examining the TLS and SAP data is greater than 5%, so that the null hypothesis can be accepted and indicates that there is no difference between the two datasets.

A further output is also returned from the paired samples test in the form of a 't' value accompanied by a 2-tailed significance value, which accounts for the extreme positive and negative residual values. As stated by Field (*ibid.*) the 't' value "is calculated by dividing the mean of differences by the standard error of differences", both of which are provided in the table supplied by SPSS, and is subsequently compared to a table of critical t-values. These are listed in columns that are rated by a significance level and ranked by degrees of freedom and used to provide a 'p' value. This research considers that any value lower than a significance level of p=0.05 indicates a statistically meaningful difference between datasets. Field (*ibid.*) states that the 'p' value represents the possibility of the calculated 't' value occurring purely by chance. That author also highlights the importance of the upper and lower limits of the 95% confidence interval of the difference, which are provided by SPSS, the interpretation of which requires

some caution. As an example, the hypothetical mean difference between two paired datasets examining elevation values is -0.347 and has a 95% confidence interval ranging from -0.231 to 0.162. If the null hypothesis states that the difference between the two datasets is 0, this could well be true as the confidence interval crosses 0. Thus the mean of the differences might be 0, as we can be 95% confident that the census mean lies between the aforementioned lower and upper limits. However, if the upper and lower limits were both negative or positive values, this would infer that 95% of the mean values were not 0 and thus it would be possible to say that the differences were due to experimental manipulation (Field *ibid.*). This is not the case in the example used here.

4.5.3.3 Local Moran's I Analysis

The spatial distribution of residual values across a DoD and the change in their magnitude in relation to neighbouring values can be visualised using the 'Cluster and Outlier Analysis' tool in ArcMap. This is particularly useful for identifying where large positive and negative residuals are situated, particularly if change detection is the goal of a project. There are five outlier types to which each residual value can be designated, based upon their statistical significance: "statistically significant cluster of high values at the 0.05 level, cluster of low values, outlier in which a high value is surrounded by low values, outlier in which a low value is surrounded by high values" (ESRI 2013), and residuals that are not significant. These values are output as a colour-coded map, although p-values are not provided to indicate the magnitude of significance. However, these values, along with a Global Moran's I score, can be calculated for the entire dataset using the 'Global Moran's I' tool in ArcMap.

4.5.4 Profiles and Breakline Assessment

Profiles were taken across the ramparts of Flowers Barrow and Eggardon Hillforts in locations that are akin to the profiles marked on the hachure surveys of each field site. Further profiles were also collected across more subtle features in the Eggardon landscape, namely the henge monument and barrow, to assess the ability of archive SAPs to provide metric data for smaller earthworks. This approach facilitates the comparison of data from modern survey techniques and the data extracted from archive SAPs to the only existing records (hachure plans) of each field site that, should the site have already disappeared, would be the only remaining metric record available of these monuments. The process of surveying specific profiles at both Flowers Barrow and Eggardon Hillfort was described in Section 6.3.3 on GNSS. The GNSS points were used to extract elevation values from each of the archive SAP DSMs and, for the Flowers Barrow case study, the ALS and TLS datasets. Elevation values were then imported into Microsoft Excel and were plotted against their distance along the profile. The shape of the

profiles from each DSM were visually compared to the GNSS and the RCHME profiles to assess the similarities and differences. It was subsequently possible to identify which SAP DSMs had succeeded in reconstructing the form of the ramparts and other earthworks. The results of this analysis are presented in Section 6.7.1 of Chapter 6 and Section 7.7.1 of Chapter 7.

Breakline assessment was conducted by comparing the breaklines digitised in ArcMAP from the RCHME hachure plans of Flowers Barrow and Eggardon Hillfort to those detected in the SAP, ALS and TLS DSMs of each field site. The '*Geomorphons*' classification routine was used to identify breaklines in the DSMs (see Section 3.4.5). The breaklines from each hachure plan were separated into top-of-slope and bottom-of-slope features (see Figure 6.27 in Chapter 6 and Figure 7.77 in Chapter 7) to enable the extraction of these values from the *Geomorphons* datasets generated from the best-performing DSM of the field site. The '*Geomorphons*' classification utilises computer vision techniques to define topographic variables that are stated by Jasiewicz and Stepinski (2013) to be akin to the approaches taken by a human observer when conducting visual interpretation. The algorithm searches for differences in texture within the DSM, which will be classified into 10 categories: peak, ridge, shoulder, spur, slope, hollow, footslope, valley, pit and flat, each of which is illustrated in Figure 4.10e and an example of the DSM output provided in Figure 4.10f.

Each of the SAP DSMs, ALS and the Flowers Barrow TLS were processed using the online *Geomorphons* tool (Jasiewicz and Stepinski *ibid.*). The Eggardon Hillfort TLS was not utilised as the DSM extent did not cover the rampart breaklines. The three processing parameters that can be set on the website are search radius (given in cell size), flatness (in degrees), and there is an option to skip cells, although this was not applied to the DSMs in this research. Subsequent to experimenting with the appearance of the *Geomorphons* classification, the search radius was limited to 5 cells and a flatness of 3º. It was also decided to combine some of the single landform classifications into one group, particularly those that could represent a breakline. For example, a top-of-slope breakline could be represented by the peak, ridge and shoulder results, whilst the bottom-of-slope breakline could be represented by pits, valleys and footslopes.

The numerical results of this extraction were entered into an Error (or confusion) matrix, which facilitates the comparison of the results from a reference dataset, namely the hachure breaklines, with that from an automatically derived dataset – the *Geomorphons* DSMs. A detailed description of the procedure for creating an error matrix is given by Lillesand et al. (2008, p.585), and an example matrix is given in Table 4.3 on page 148. The overall accuracy of the classification is calculated by adding all of the correctly classified pixels, represented by the major diagonal values, which are highlighted in red, and dividing this value by the total number of reference pixels. The result is a value that represents the percentage of pixels between the two datasets that agree, thus indicating how similar they are. Subsequently, for each of the study sites the digitised RCHME profiles were compared with the most accurate DSM survey to produce an overall accuracy value. The most accurate DSM was used as a benchmark against which to compare the overall accuracy between in and the other DSMs.

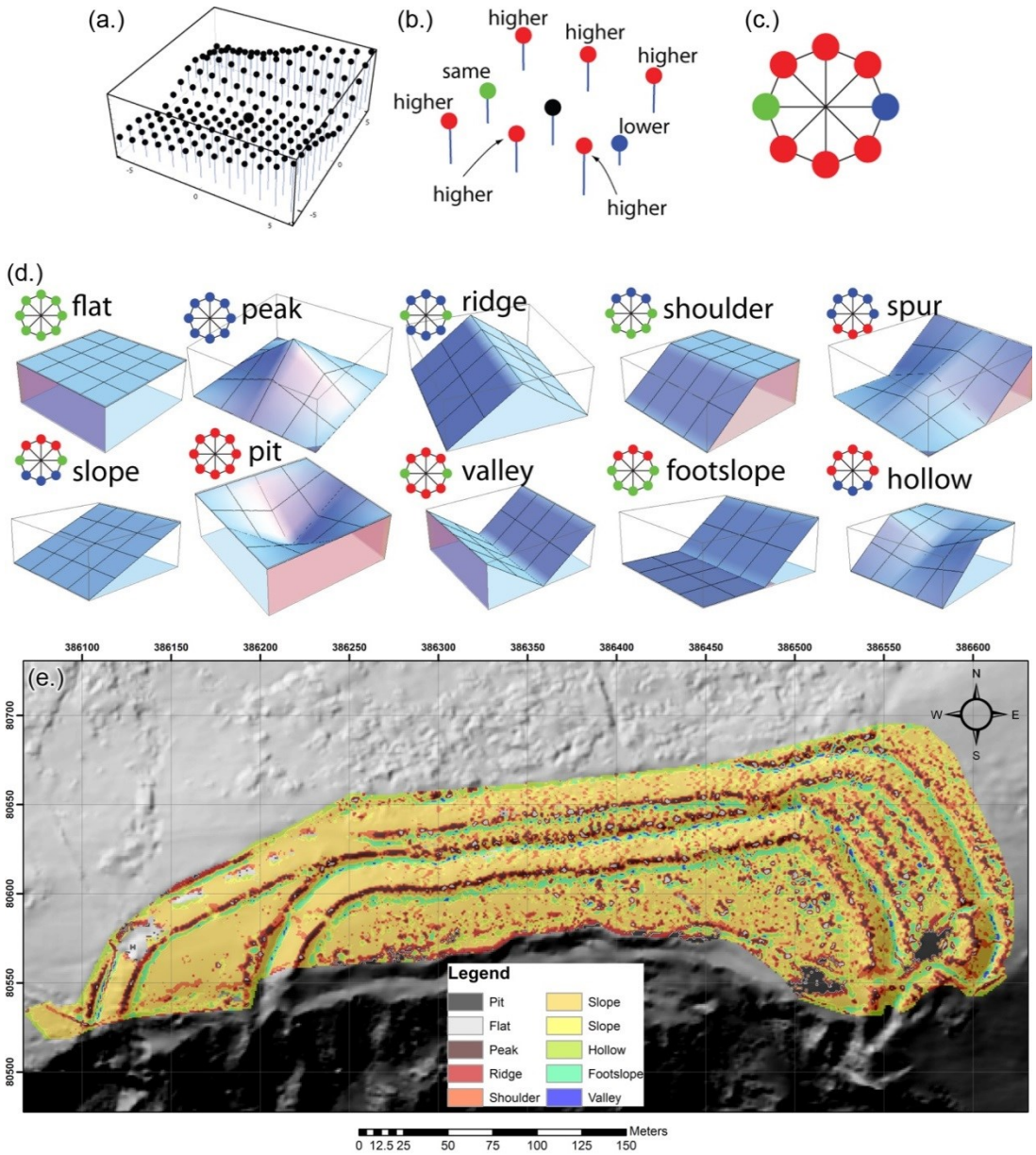

Figure 4.10:Diagram illustrating the components of the 'Geomorphons' tool (a.) DEM and selected cell (b.) Relative elevations of surrounding cells (c.) plan of relative elevations (d.) schematic showing the relationship between relative elevations and landform elements (e.) example of a Geomorphons DSM (Jasiewicz and Stepinski 2013).

Therefore, if they were better than the benchmark value they were considered to be capable of providing archaeological breakline data.

4.6 Discussion

It is important to examine how accurately SAPs and other mass-capture techniques provide archaeological data and whether they can detect changes to earthwork fabric. There has to be confidence that any measure of change or other metric data provided by a particular technique

		TLS						
		Flat	**Top-of-Slope**	**Spur**	**Slope**	**Hollow**	**Bottom-of-Slope**	**Row Total**
2009 SAPs	**Flat**	***17***	58	9	11	2	41	138
	Top-of-Slope	6	***664***	238	237	84	53	1282
	Spur	1	255	***214***	209	69	49	797
	Slope	1	797	690	***2510***	793	693	5484
	Hollow	0	63	42	127	***110***	201	543
	Bottom-of-Slope	15	193	151	315	177	***1171***	2022
	Column Total	40	2030	1344	3409	1235	2208	***10266***

Table 4.3: Error Matrix of pixels showing the Flowers Barrow TLS as the reference, or training, dataset and the 2009 SAPs as the classification results to be compared against it.

is not misleading or inaccurate. In the case of change, under- or over-estimation may prompt action where none is required or, conversely, may fail to identify a site that is suffering from rapid deterioration. Where the reconstruction of extant, damaged or destroyed archaeology is required, the more accurate the data provided, the more suitable it is for analysis purposes. This is particularly the case where comparison of feature size, length, width, height etc. is necessary for establishing typologies, for example. This will also identify the frequency with which SAPs are required to detect subtle change, which may require a large time period to have passed before any change is perceived. As a tool for managing the archaeological resource, mass-capture techniques can potentially identify areas that may require intervention, either to protect and conserve areas that are becoming damaged or to secure resources for other types of archaeological intervention to more fully record threatened archaeology.

4.7 Summary

This chapter has described the methodology behind the selection of field sites, the acquisition of archive data with particular reference to SAPs, collection of ground-based data and the way in which each of these datasets will be processed to obtain the desired outputs. These are predominantly DSMs from the SAPs and thus methods by which to assess their quality, both empirically and archaeologically, have also been explained.

5 DEVELOPING A PHOTOGRAMMETRIC WORKFLOW AND ASSESSING THE INFLUENCE OF VARIABLES

This Chapter identifies the effects that a number of variables have on DSM quality as derived from an SAP dataset: photogrammetric terrain extraction strategy, orientation information, photographic materials and scanners, GCP control, and vegetation. It is important to establish the influence these may have prior to further analysis of the data to ensure that their deleterious effects can be mitigated beforehand, if possible. Although each of the SAP datasets utilised by this research was processed in the same way, it was acknowledged that an in-depth study was required to identify how different variables, as listed in Table 5.1, affected terrain reconstruction.

Prior to identifying the effects different variables had on DSMs from SAPs, a workflow was developed in Socet GXP for processing the SAP images based upon the procedure given in Section 2.2.7. Section 5.1 describes the initial analysis of the DSM results obtained by employing the workflow, which is conducted on the DSM output from the 1982 SAPs. Section 5.2 discusses the DSM results obtained by using different terrain extraction algorithms in SocetGXP as compared to TLS data to identify the optimal algorithm to employ on the remaining SAPs. Subsequent to designing and testing a workflow for processing the SAP datasets, the remainder of this Chapter examines the influence of the variables listed above and whether their effects can be determined by comparing the SAP DSM elevation values to baseline data in the form of GNSS random points or from a TLS survey. The data from the latter two technologies are assumed to be more representative of the terrain surface at Flowers Barrow than the SAP DSMs, thereby explaining the reason for their use as baseline datasets.

Section 5.3 utilises modern digital imagery to examine the influence a combination of exterior orientation and GCPs has on the accuracy of DSMs. Further, the effects of using RGB, greyscale and red channel only photography on DSM production are also assessed. Section 5.4

Variable	Type	Categories	Author
SAP Age	Categorical	Year	Perez Alvarez et al. 2013
Control	Categorical	Exterior Orientation, GCPs	Chandler 1989; Aguilar et al. 2009; Aguilar et al. 2012; Perez Alvarez et al. 2013
Scale	Continuous	N/A	Walstra et al. 2007; Walstra et al. 2011
Photographic Medium	Categorical	Negative, Print, Digital	Walstra et al. 2007; Walstra et al. 2011
Scanner Type	Categorical	Photogrammetric, Desktop	Walstra et al. 2007; Walstra et al. 2011
Terrain Extraction Algorithm	Categorical	ATE, NGATE	Gooch et al. 1999; Walstra et al. 2007; Walstra et al. 2011
Vegetation/ Land Cover Type	Categorical	Grass, Gorse	Gooch et al. 1999; Walstra et al. 2007; Walstra et al. 2011

Table 5.1: Variables identified for testing that will influence the quality of DSMs extracted from archive SAPs.

analyses scanning procedures and their effects on terrain output by comparing two SAP datasets from the 1980s, one of which has been digitised using the original negatives in a photogrammetric scanner and the other using photographic prints in a desktop scanner. Section 5.5 identifies the influence the use of GCPs as the sole control datasets for creating DSMs by examining a number of scenarios using a single SAP epoch. This is particularly important as archive SAPs are rarely provided with other sources of orientation and control data. Section 5.6 establishes whether vegetation can influence the accuracy of elevation values within a DSM, prior to completing the Chapter with a summary of the findings (see Section 5.7).

5.1 Developing the Analysis Workflow

This Section discusses the approach taken to develop an SAP DSM processing workflow, which is represented by a two-stage approach. The first stage, as illustrated in Figure 5.1, was designed to identify and correct the largest errors, such as excess tilt, within an SAP DSM. The second stage, shown in Figure 5.2, removed any horizontal offsets between the SAP DSM and the TLS data. Both the effects of tilt and horizontal offset were either visually identified in the SAP DSM or via empirical investigation using the GNSS stratified random points (see Section 4.3.1) and were removed before undertaking more extensive analysis, the results of which are presented in Chapters 6 and 7.

An initial quality assessment of the SAP DSM was conducted by subtracting it from an ALS DSM, which was considered to be error-free. This produced a residual DSM, or DSM of difference (DoD) that could be used to determine if the SAP DSM contained any significant slope or tilt. If so, there were two approaches that could be taken to rectify this problem. The first and most preferable, from a time-saving perspective, was to remove the tilt within SocetGXP, which involved adding more control points in areas that would help to 'weight down' regions with elevation values that were too high. Despite stating that check points were not used due to the lack of more rigorous control points i.e. GNSS data, it was necessary to extract extra control from other mapping products because of the lack of GNSS data (see Section 4.3.1). This type of control should preferably be kept to a minimum, particularly as the locational accuracy of such values is much worse with GSDs of 0.3125m and 0.625m for 1:1000 and 1:2000 OS MasterMap raster data (Pope 2011). Uncertainty values associated with GCPs, irrespective of their source, can be entered into the software to ensure that they are accounted for. Therefore the GCPs utilised for removing tilts in the data were only 'Z' control points that were given elevation values that were approximate to the modern terrain surface by ±2m as suggested by BAE Systems UK (see Section 4.4.1).

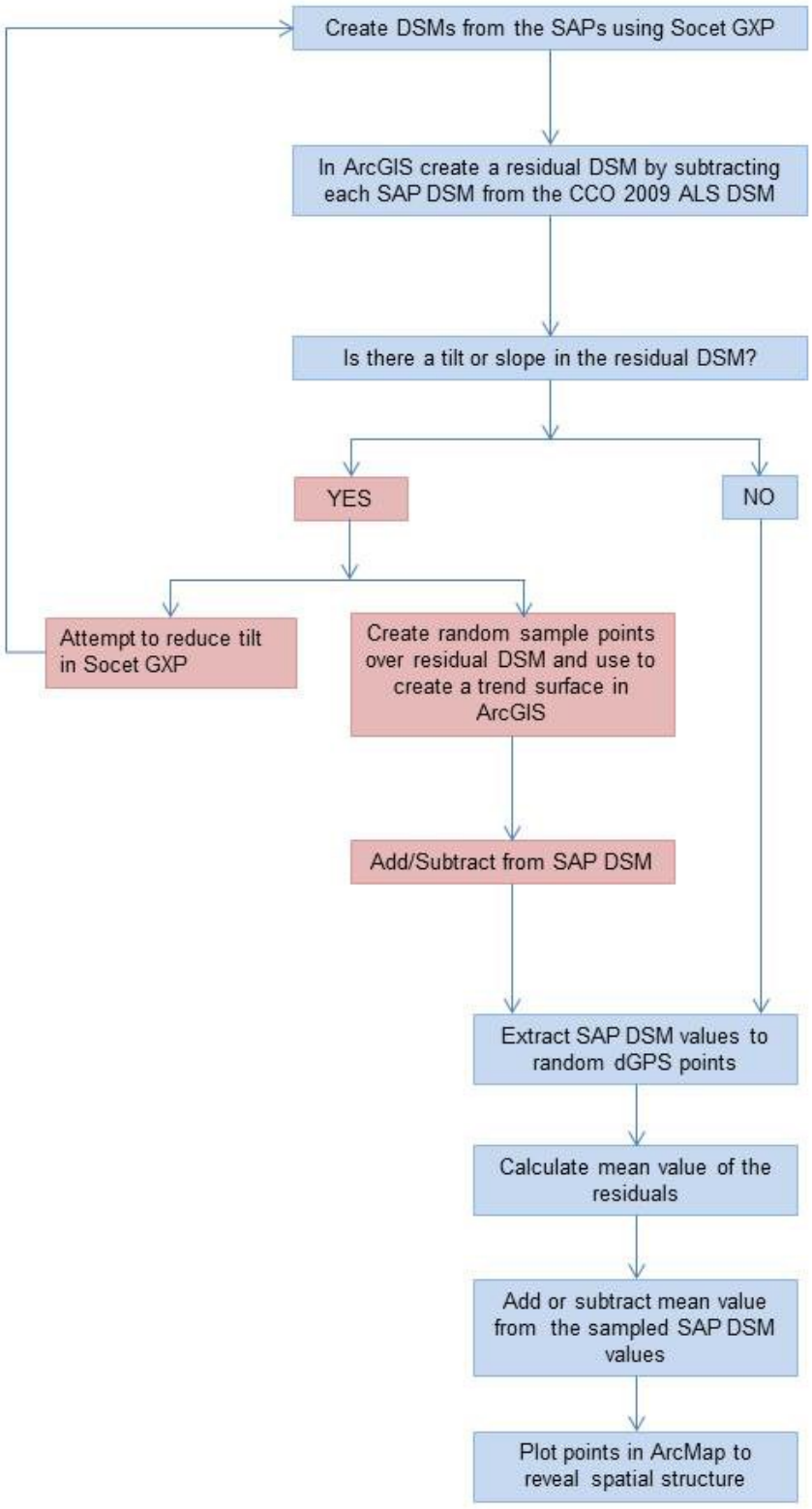

Figure 5.1: SAP DSM Processing steps employed for the analysis workflow.

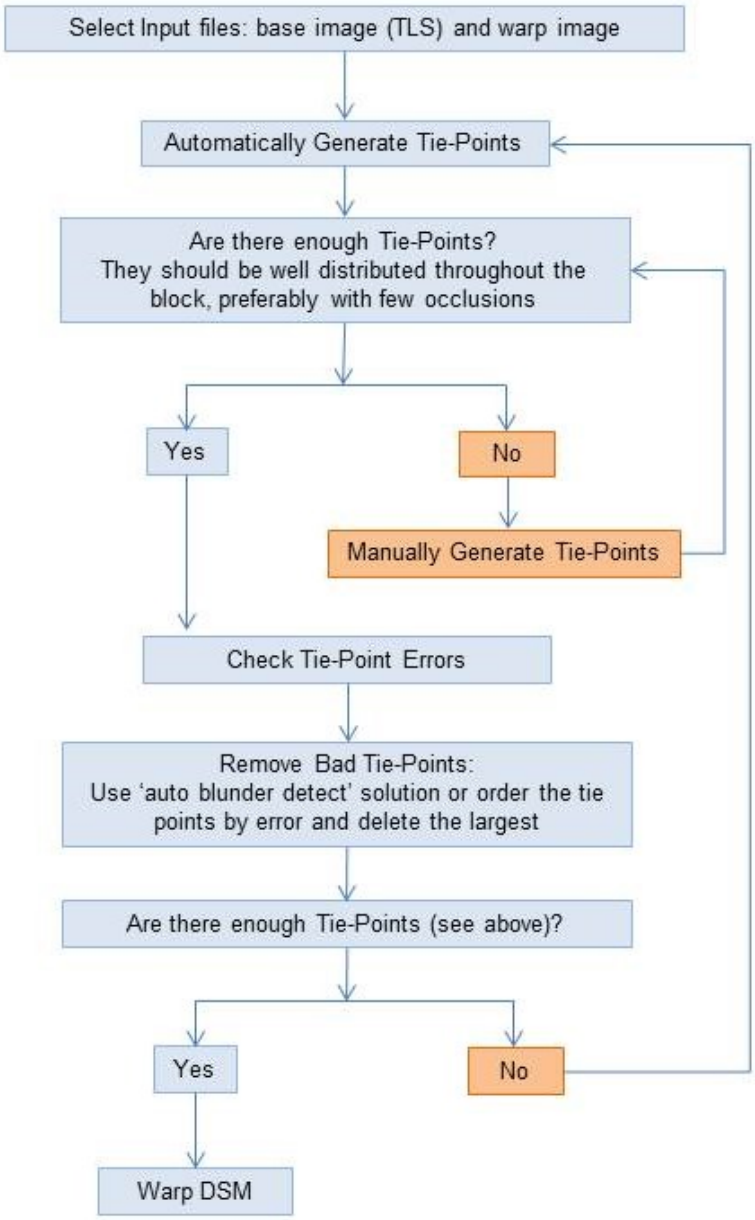

Figure 5.2: DSM Warping workflow in ENVI.

The alternative to adding extra control points in SocetGXP was to construct a trend surface in ArcMap. This approach was adopted if extra control did not solve the tilt issue. The trend surface was created by producing a residual surface by subtracting the SAP DSM from that of the 2009 Environment Agency ALS data. The values from this residual DSM were then extracted using the GNSS stratified random points (see Section 4.3.3), which were converted to a trend surface that could either be added or subtracted from the SAP DSM to remove tilt. The final stage of the DSM analysis identified any remaining elevation offsets between the GNSS data and the SAP DSM. The random points were used to extract the matching values from the

SAP DSM in ArcGIS before exporting them to Excel. The residual difference between each point was calculated and subsequently utilised to provide the mean elevation difference between the two datasets. This value was either added or subtracted from the SAP DSM to remove this difference prior to undertaking further analysis with it.

The 1982 SAPs were deemed the most appropriate dataset on which develop and test an analysis workflow prior to working with the other SAP DSMs as they are the most recent analogue imagery available from the NMR as photogrammetrically scanned negatives. These photographs were also taken by the OS with a metric camera, and would be less likely to exhibit the effects of time on aging photographic materials, such as dust and scratches for example. Further, this dataset was devoid of the issues inherent in the photographic prints that were scanned with a desktop scanner for the purposes of this project (see Section 2.2.6.3). Therefore the more generic issues across the SAP datasets would be addressed by utilising the 1982 imagery prior to undertaking further analysis with other SAP epochs. The resultant statistical quality of the triangulation and terrain extraction stages within SocetGXP for the 1982 SAPs are given in Table 5.2.

Whilst making an initial visual examination of the DSM in ArcMap, there also appeared to be a horizontal and vertical offset between the SAP DSM and TLS datasets. By closely examining the horizontal shift, it was judged that the 1982 DSM had to be moved 1.7m to the north and 1m west. Initially, this offset was corrected in ENVI by altering the information in the image header file of the 1982 DSM. However, this method was later altered to ensure that a comparison of the elevation values in each SAP DSM dataset afflicted by offsetting could assuredly occur on a like-for-like basis with the GNSS and TLS data. The process designed to achieve this utilised the 'Image Registration' and 'Warp and Resample' tools in ENVI, which has a more rigorous approach to the previous method of altering the image header file. The 'Image Registration' process required the selection of a reference or 'base' image which, in this case, was the TLS DSM, and a 'warp' image, such as the 1982 DSM that required correction. ENVI utilises cross-correlation, as explained in Section 2.2.7.3, to match similar greyscale values within the two images to create a tie point file. These tie points can be converted to ground control points for the warp and resample process, which rotates, scales and translates a DSM to fit the same dimensions as the reference DSM. By adopting this approach the horizontal transformation of the DSM pixels matched that of the TLS.

1982 SAP Triangulation Root Mean Square Residuals					1982 SAP ATE DSM Results				
Image Pixels	X (m)	Y (m)	Z (m)	Total RMS (m)	Recommended ATE DSM Post Spacing/GSD (m)	ATE DSM Post Spacing/GSD Used (m)		Circular Error (m)	Linear Error (m)
						X	Y		
1.518	1.588	1.783	2.204	3.142	1.215	1	1	0.857	0.869

Table 5.2: Summary statistics generated in SocetGXP showing the triangulation and ATE quality results for the 1982 Flowers Barrow SAPs.

After correcting the horizontal and vertical offset between the TLS and 1982 DSM data, the first order derivatives were also generated for each dataset. Slope and Aspect were output from the TLS and SAP DSMs using ArcMap to further explore the quality of the data. As these outputs are derived from elevation values in a one stage calculation, they are more sensitive to the effects of noise and are thus a good indicator of image quality (see Section 3.4.3 for further details). The analysis workflow can be found in Figure 5.1.

5.2 SocetGXP Strategy Assessment

5.2.1 Introduction

A number of terrain extraction strategies are available in SocetGXP from which to extract DSM data from the SAPs, which raised the question as to which strategy would produce the most comparable DSM with that of the TLS. The strategies are contained within two applications called 'Automatic Terrain Extraction' (ATE) and 'Next-Generation Automatic Terrain Extraction' (NGATE), the latter of which is the most recently developed algorithm. ATE utilises area-matching (or image correlation) on each post, which is specified by the user, between stereo-pairs (see Section 2.2.7.5), while NGATE performs area-matching and edge-matching on each pixel (BAE Systems 2007). NGATE is stated by BAE Systems (2013) to be the faster, more accurate process of the two, although it has been principally designed for use in urban areas, as indicated by the edge-detection function. There are a small number of strategies within the NGATE application, with the two most appropriate for use on the archive SAPs being the generic 'ngate' strategy and the 'low-contrast' strategy.

There are more strategy options within the ATE application, of which the most flexible is labelled 'adaptive'. This strategy is said to be the most accurate and can be utilised on terrain that varies from flat to mountainous, as detected by the adaptive image correlation parameters defined by BAE Systems. A number of non-adaptive strategies are also available, which can be applied to terrain with particular characteristics, such as steep, flat etc. For the ATE strategy assessment, the settings that were the most appropriate for the Flowers Barrow and Eggardon SAPs were 'adaptive' and 'steep'. Thus, with the two NGATE strategies, a total number of four strategies were assessed.

5.2.2 Method

As outlined in Section 5.1, an initial evaluation of the elevation data was conducted for each of the 1982 DSMs generated using the NGATE and ATE strategies. This approach removed both the elevation and horizontal offsets in the SAP DSMs, with the initial mean elevation offsets

	ATE		NGATE	
	Adaptive	**Steep**	**NGATE**	**Low-Contrast**
Mean Elevation Difference (m)	1.329	1.322	1.478	1.478

Table 5.3: Initial elevation offset, in metres, between SocetGXP terrain extraction strategies and the GNSS stratified random points.

between each DSM strategy and the GNSS random point data given in Table 5.3. These initial offset values were added to their respective DSMs in an attempt to remove their effects. This was achieved using 'Raster Math' in ArcMap. The residual values were then re-calculated and plotted in ArcMAP to examine their distribution (see Figure 5.3). There are many positive residuals, although there is no obvious pattern present in their distribution. There are, however, subtle differences between the three strategies, with the Adaptive ATE strategy showing a residual range between -0.867m and +0.5m, whilst the NGATE strategy had greater positive residual values, namely -0.683m to +0.750m.

Subsequent to assessing the effect of adding the mean elevation offsets, analysis was also conducted on a pixel-by-pixel basis for each of the strategies, with the exception of the NGATE low-contrast strategy. As the results were similar to that of the NGATE DSM there was little to be gained from further analysis using the low-contrast DSM. It was expected that, by adding the mean residual value specific to each of the strategy DSMs, the overall mean would be '0m'. However, this was not the case, as shown in Table 5.4, and there are two causes for this. The first is related to the number of samples from which the residuals were calculated. The number of stratified random samples measured by dGPS is 222, whilst the census analysis conducted with the entire dataset is 63,278 and thus there are likely to be outliers or other spurious values in a larger dataset. Secondly, the census analysis also covers a slightly larger area, unlike the random samples that are confined to the interior of the Hillfort. Within this area there are regions that will affect the mean value, such as the spurious data from the TLS in the lower right-hand corner of the dataset. Therefore it is unlikely that subtracting any further mean values from each datasets would produce a result closer to 0m.

	ATE		
	Adaptive	**Steep**	**NGATE**
Mean Elevation Difference (m)	-0.118	-0.115	-0.15

Table 5.4: Elevation offset between the TLS DSM and SocetGXP terrain extraction strategies.

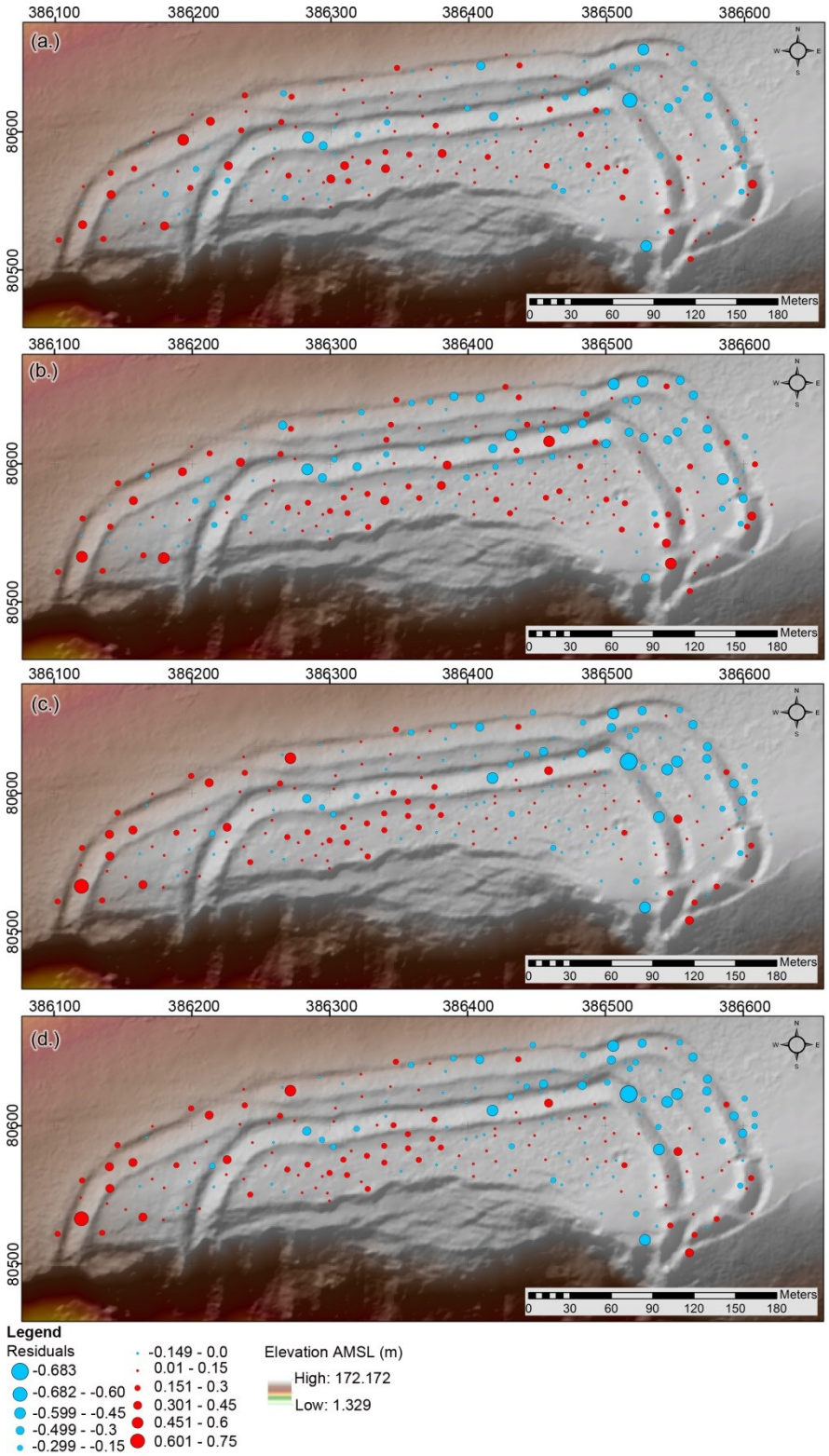

Figure 5.3: Diagram showing the magnitude of residual differences between the GNSS random points and the 1982 DSM (a.) Adaptive (b.) Steep (c.) NGATE and (d.) NGATE low contrast strategies.

5.2.3 Results

Upon visual inspection of the 1982 SAP elevation residual images, shown in Figure 5.4, the pattern of difference between the TLS and each strategy is subtle. However, the most noticeable variations between strategies occur along the north and east banks of the ramparts, many of which were covered with gorse back in 1982 and could thus be causing this offset. The summary statistics related to each dataset, as shown in Table 5.5, help to identify further, albeit subtle, disparities between strategies. The range of residual values for the Steep dataset is larger than both the Adaptive and NGATE DSMs. To visualise the distribution of the residuals, histograms were created for each strategy, as shown in Figure 5.5. The histograms illustrating the residual difference between the TLS data and the Adaptive and NGATE strategies are broadly similar (Figure 5.5a and c), each of which displays a slight skew. The tail on the skew tends to the left and thus there are more negative residuals in both of these strategies, which can be seen as the blue regions in Figure 5.4a and c., with the NGATE DoD containing the most pronounced areas of negative residuals. Based upon the summary statistics (Table 5.5), this observation is misleading as it is the Steep strategy that has bot the greatest range of residual values, including the largest negative minimum of -2.216m. However, the Steep histogram (see Figure 5.5b) contains an almost imperceptible skewness and looks to be the most normally distributed. Thus, irrespective of the summary statistics, the residual distribution makes the DoD in Figure 5.4b appear to contain fewer extreme values.

With respect to the positive residuals, many of these occur in the flatter regions of the Hillfort, irrespective of the terrain extraction strategy employed. The least noisy residual image is produced by the Adaptive and Steep strategies (Figure 5.4a and b), despite the NGATE strategy containing a much lower range value of 3.815m than that of the Steep strategy, namely 3.899m.

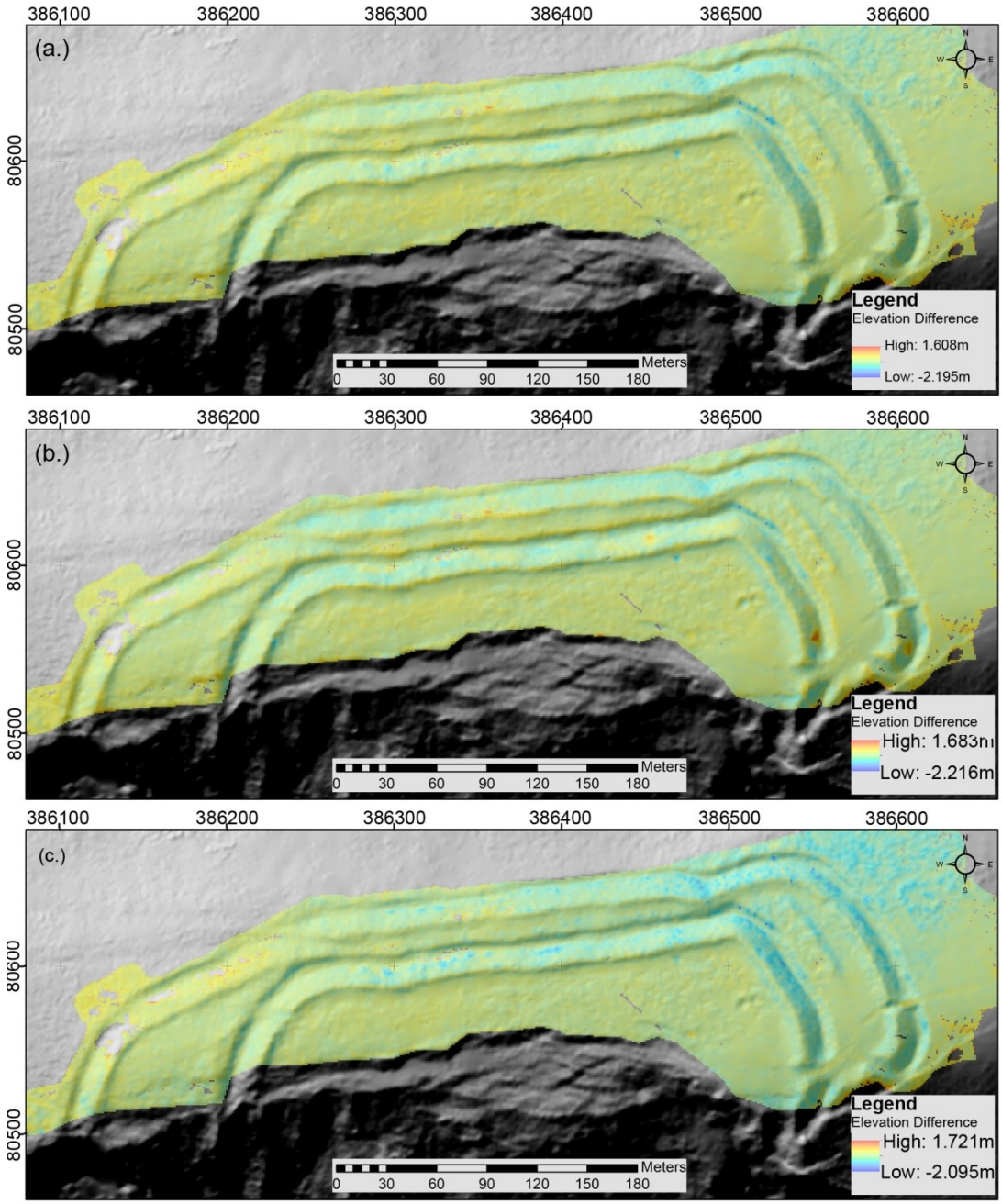

Figure 5.4: DSMs of Difference between the TLS and 1982 (a.) Adaptive, (b.) Steep and (c.) NGATE strategies.

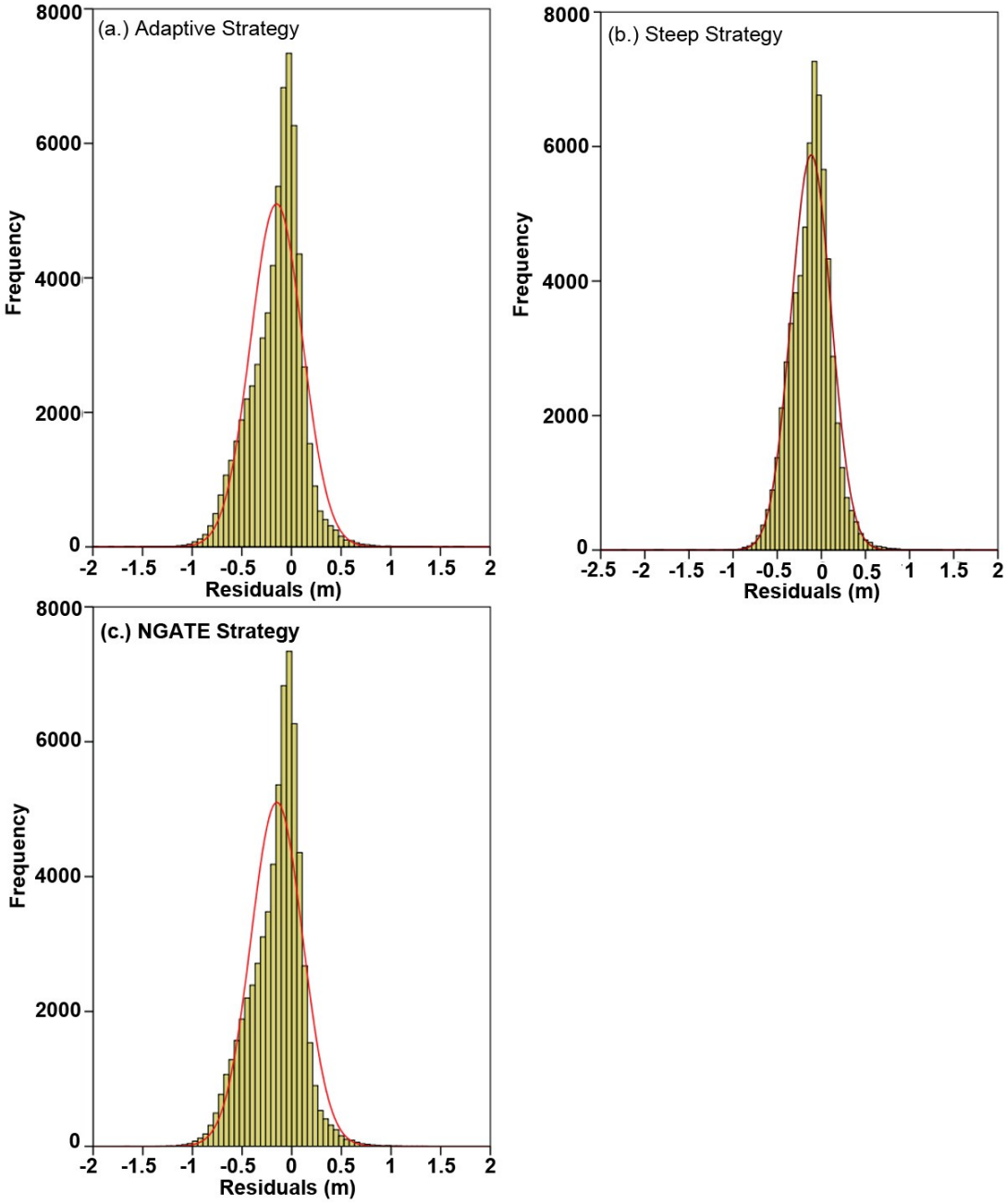

Figure 5.5: Histograms showing the residual distribution between the TLS DSM and the 1982 DSM (a.) Adaptive, (b.) Steep and (c.) NGATE strategies.

		TLS - 1982 Adaptive	TLS - 1982 Steep	TLS - 1982 NGATE
N	Valid	63278	63278	63278
	Missing	0	0	0
Mean (m)		-0.118	-0.115	-0.150
Std. Error of Mean (m)		0.001	0.001	0.001
Median (m)		-0.096	-0.098	-0.103
Mode (m)		-.088[a]	-.116[a]	-0.079
Std. Deviation (m)		0.218	0.226	0.260
Variance (m)		0.048	0.051	0.068
Skewness		-0.174	0.055	-0.351
Std. Error of Skewness		0.010	0.010	0.010
Kurtosis		1.880	1.353	1.129
Std. Error of Kurtosis		0.019	0.019	0.019
Range (m)		3.804	3.899	3.815
Minimum (m)		-2.195	-2.216	-2.095
Maximum (m)		1.608	1.683	1.721

Table 5.5: Summary statistics based upon the residual values between the TLS and 1982 DSM strategies.

5.2.4 Conclusion

Based upon the results of this analysis, the DSM results from each strategy are similar. However, based upon the summary statistics in Table 5.5 and the appearance of the DoD in Figure 5.4a, the Adaptive ATE strategy will be adopted for extracting terrain models from SocetGXP for the remaining DSMs required by this research.

5.3 Examining the Effects of Orientation Data on DSM Production

5.3.1 Introduction

Whilst it has been acknowledged elsewhere within this thesis that many SAP datasets have none of their associated orientation data available (see Section 2.2.6.4), the modern digital imagery captured by commercial companies does. The latest dataset available for Flowers Barrow was collected in 2009 by GetMapping Ltd and the opportunity thus exists to examine the influence of external orientation data, or a lack thereof, on the data quality of a DSM. Three processing scenarios were employed using a combination of the 2009 orientation data, as supplied with the SAPs, and GCPs: exterior orientation information only, exterior orientation data and GCPs, and GCPs only. It was also postulated that elevation values within a DSM may

also be influenced by the image mode i.e. whether it was RGB or Greyscale, and that data in the red channel might also produce superior results. As red wavelengths penetrate atmospheric haze more readily than those in the blue or green (Ray 2000, p.181), it was felt that processing only the red channel would be worthwhile.

5.3.2 Method

Adobe Photoshop was used to convert the original RGB images into both greyscale and red-channel datasets prior to processing in SocetGXP. The same GCPs were used for each scenario that required them, although the position of the tie points varied between datasets as they were generated automatically. The adaptive terrain strategy was used to output each DSM, based upon the results discussed in Section 5.2, and subsequently exported from SocetGXP as a '*.asc' text file. The statistical quality of the triangulation and terrain extraction processes in SocetGXP are provided in Table 5.6. Each dataset was converted to a raster '*.tif' file in ArcMap using the natural neighbour interpolator (see Section 3.2) prior to running the 'sample' routine on each of the DSM datasets to extract elevation values that coincided with those of the TLS DSM. This allowed a census evaluation to be conducted for each of the DSMs derived from the

2009 Oriantation Triangulation Root Mean Square Residuals						**1982 SAP ATE DSM Results**				
Orientation Params.*	**Im. Pix.***	**X (m)**	**Y (m)**	**Z (m)**	**Total RMS (m)**	**RPS.***	**ATE DSM Post Spacing/ GSD Used (m)**		**Abs/Rel Circ. Error***	**Abs/Rel Lin. Error***
							X	**Y**		
RGB EO*	1.953	-	-	-	-	2.250	1	1	27.166/ 0.332	9.500/ 0.638
RGB EO and GCPs	2.135	1.046	7.211	6.95	1.449		1	1	0.960/ 0.331	1.063/ 0.641
RGB GCPs Only	1.587	2.393	1.773	3.122	4.315		1	1	0.432/ 0.330	0.990/ 0.634
Grey* EO	2.8	-	-	-	-		1	1	- / 0.3515	- / 0.633
Grey EO and GCPs	1.136	8.326	9.699	3.157	1.317		1	1	0.875/ 0.331	1.306/ 0.639
Grey GCPs Only	1.048	6.792	4.591	2.195	2.634		1	1	0.549/ 0.331	0.899/ 0.633
Red Channel EO and GCPs	3.768	9.548	7.849	5.905	1.37		1	1	- / 0.33	- / 0.633

* Orientation Params. = Orientation Parameters; Im. Pix. = Image Pixels; RPS = Recommended ATE Post Spacing; Abs/Rel Circ. Error = Absolute/Relative Circular Error; Abs/Rel Lin. Error = Absolute/Relative Linear Error; EO = Exterior Orientation; Grey = Greyscale Image

Table 5.6: Statistical output from SocetGXP indicating the quality of the triangulation and ATE DSM solution.

	RGB EO*	RGB EO and GCPs	RGB GCPs Only	Grey* EO	Grey EO and GCPs	Grey GCPs Only	Red Channel EO and GCPs
Mean (m)	1.674	0.226	0.882	32.300	-0.155	**-0.087**	0.228
Std. Error of Mean (m)	0.002	0.002	0.002	0.038	**0.001**	0.002	0.002
Median (m)	1.727	0.345	0.935	31.677	-0.067	**0.011**	0.360
Mode (m)	1.963	0.486	1.116[a]	24.182[a]	**-.018**[a]	-.112[a]	0.528
Std. Deviation (m)	0.608	0.420	0.388	9.451	**0.342**	0.583	0.468
Variance (m)	0.370	0.176	0.151	89.326	**0.117**	0.340	0.219
Skewness	-0.751	-1.890	-0.920	**-0.090**	-1.365	-1.294	-1.764
Std. Error of Skewness	0.010	0.010	0.010	0.010	0.010	0.010	0.010
Kurtosis	2.014	5.011	1.374	**-0.899**	6.845	2.386	3.752
Std. Error of Kurtosis	0.019	0.019	0.019	0.019	0.019	0.019	0.019
Range (m)	6.370	4.873	**4.167**	45.584	5.700	5.425	4.561
Minimum (m)	-2.697	-2.764	**-1.320**	5.010	-2.803	-3.197	-2.569
Maximum (m)	3.673	2.109	2.848	50.594	2.897	2.227	**1.992**

* EO = Exterior Orientation; Grey = Greyscale Image

Table 5.7: Summary statistics for each of the orientation parameters and image modes applied to the 2009 SAPs. The optimum results for each statistic are highlighted in red.

different orientation scenarios and image modes, with all of the elevation values tested against those created using the TLS. Residual values were produced by subtracting the SAP DSMs from the TLS data (Table 5.7).

5.3.3 Results

The summary statistics for each of the different SAP orientation scenarios, as shown in Table 5.7, do not clearly identify which method produces the DSM most comparable with the TLS data, although the datasets that are processed with exterior orientation information only are the worst performing solutions. This is particularly the case for the greyscale images, which contain a gross error, illustrated by the huge differences between the statistical values for this dataset as compared to the others i.e. an elevation range of 45.584m, and can therefore be discounted. However, the greyscale imagery processed with the exterior orientation data and GCPs contains favourable statistical values when compared to the other datasets, although the greyscale SAPs processed with only the GCPs also performs well. The mean residual value of both the greyscale exterior and GCP solution and the greyscale GCP only solution is -0.155m and -0.08699m respectively, which indicates that these datasets are achieving a level of accuracy akin to ALS data.

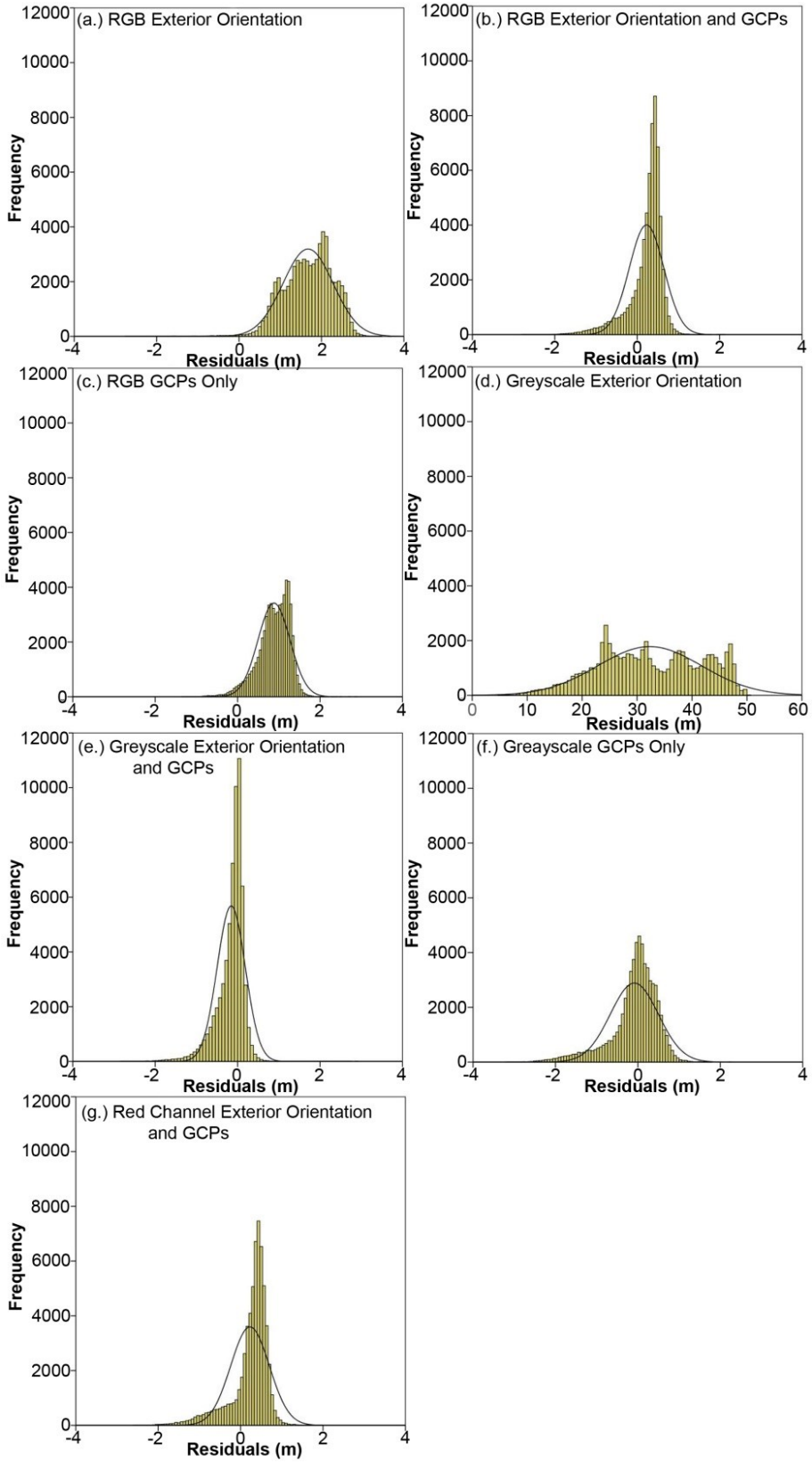

Figure 5.6: Histograms showing the distributions of residuals between the TLS and 2009 DSM orientation parameters.

The differences between each orientation scenario are easier to visualise by looking at the histograms that are produced by the data, as shown in Figure 5.6 (above). The majority of the distributions are broadly normal, although they each exhibit a negative skew. The distribution is therefore not symmetrical and contains a larger number of negative residuals than would be required for a normal distribution. However the majority of the most frequent residuals occur within the positive region of the graph. Whilst the imagery processed using only the GCPs presents a mesokurtic, or normal, kurtosis, the data processed using the exterior orientation data and GCPs is leptokurtic, irrespective of the image mode. Therefore the majority of the residuals are concentrated around the mean, which would also indicate a low variation within the residuals, with the exception of the negative skew.

A final measure of how well each of the orientation scenarios corresponds to the TLS data, which is taken to be the baseline dataset, can be assessed using the paired t-test algorithm in SPSS. By pairing each individual orientation scenario dataset with the TLS, a number of statistical measures are returned that describe how well each data pair match. The results can be seen in Table 5.8 and Table 5.9. In Table 5.8, the correlation values for each pair are close to 1 and indicate a positive relationship. However, the significance value confirms that the null hypothesis, as stated in Section 3.4.2, cannot be accepted and that there are differences between the two datasets.

The results in Table 5.9 corroborate this by also returning a significance value of less than 0.05. Further confirmation of this result can be inferred from the results listed in the 'mean residual' category and the upper and lower boundaries of the 'confidence interval of difference'. The difference between TLS and each of the SAP datasets cannot be 0 as all of the upper and lower values in each pair are either positive or negative. Therefore 95% of the residual values are not 0m and the differences exhibited by each orientation scenario are due to experimental manipulation with the orientation settings.

		No. of Samples	Correlation (r)	Significance (p)
Pair 1	**TLS_Elev & Ext_Ori_MoreTPs**	63278	0.999	0.000
Pair 2	**TLS_Elev & Ext_And_GCPs**	63278	0.999	0.000
Pair 3	**TLS_Elev & GCPs_Only**	63278	0.999	0.000
Pair 4	**TLS_Elev & Grey_Ext_Ori**	63278	0.911	0.000
Pair 5	**TLS_Elev & Grey_Ext_And_GCPs**	63278	0.999	0.000
Pair 6	**TLS_Elev & 2009_GREY_GCP**	63278	0.998	0.000
Pair 7	**TLS_Elev & 2009_Red_ExtAndInt**	63278	0.999	0.000

Table 5.8: Paired Samples Correlation of each orientation scenario as paired with the TLS dataset.

		Mean Residual (m)	Paired Differences		t-value	degrees of freedom	Sig. (2-tailed)
			95% Confidence Interval of the Difference				
			Lower	Upper			
Pair 1	TLS_Elev - Ext_Ori_MoreTPs	1.674	1.669	1.679	692.400	63277	0.000
Pair 2	TLS_Elev - Ext_And_GCPs	0.226	0.223	0.229	135.480	63277	0.000
Pair 3	TLS_Elev - GCPs_Only	0.882	0.879	0.885	571.694	63277	0.000
Pair 4	TLS_Elev - Grey_Ext_Ori	32.300	32.23	32.374	859.694	63277	0.000
Pair 5	TLS_Elev - Grey_Ext_And_GCPs	-0.155	-0.158	-0.152	-114.209	63277	0.000
Pair 6	TLS_Elev - 2009_GREY_GCP	-0.087	-0.092	-0.082	-37.541	63277	0.000
Pair 7	TLS_Elev - 2009_Red_ExtAndInt	0.228	0.224	0.231	122.354	63277	0.000

Table 5.9: Paired Sample Test showing the results of the paired t-test.

5.3.4 Conclusion

In conclusion to this section of the investigation, the orientation scenario to adopt utilised only the GCPs, based upon the summary statistics in Table 5.7, and should be used in combination with greyscale imagery.

5.4 DSMs from Photogrammetrically Scanned Negatives versus Desktop Scanned Prints

5.4.1 Introduction

The quality of a DSM depends on photographic material as well as the scanner used to digitise it. The best case scenario involves scanning the original negatives using a photogrammetric scanner. Whilst the quality of output is still dictated by the density and condition of the negative, i.e. it is devoid of scratches, it has not warped with age etc., the process of creating a photographic print can degrade the information content that is held by the negative. The photographic paper used for creating a print must be capable of reproducing the tones within the negative to ensure that the contrast is neither too low nor too high (Jacobson et al. 2000). However, the paper should be able to produce black (extremely low contrast) and white (extremely high contrast) to meet these requirements. Therefore the exposure range of the paper must recreate the density range within the negative, the latter of which will be dictated by

the amount of light received by the silver halide crystals during exposure and the extent of development (Jacobson et al. *ibid.*). If insufficient exposure or development of the negative has occurred, the contrast will be poor and subsequently the tonal quality of the print will also be poor.

Photogrammetric scanners are designed to preserve the geometric and radiometric accuracy of aerial photography, in negative or print form, and output digital images with a high geometric resolution. Whilst this process does not account for any inaccuracies introduced into the image through the creation of a photographic print, these capabilities ensure that the range of image density is captured such that the image matching processes in photogrammetric software will work optimally because the image texture is preserved (Gruber and Leberl, 2000). Desktop scanners, however, are not precision engineered to the same degree as their photogrammetric counterparts and thus do not produce digital images with the same degree of geometric and radiometric accuracy. Al-Rafidain (2010) states that “errors in point locations are unevenly distributed across the scanning frame” and thus if any errors exist within the photogrammetric scanner, they are precisely calibrated and can be mitigated, whereas this may not be the case with a desktop scanner. Two types of desktop scanner are available, namely flatbed or drum scanners, the latter of which is often more expensive. For this research, an A3 flatbed scanner was used to scan the print materials whilst a Vexcel Photogrammetric Scanner was utilised by the NMR for scanning the negatives (see Section 4.2.1).

As the SAP epochs utilised in this research have been digitised by differing scanner technologies, it is evident that there will be a difference in DSM quality output by the photogrammetrically scanned negatives as opposed to the desktop scanned prints. In effect, the latter is a ‘worst-case scenario’, whilst the ‘former is the ‘best-case scenario’.

5.4.2 Method

The two epochs chosen to test these scenarios are the 1982 and 1986 SAPs. The 1982 negatives were purchased from the NMR and have been photogrammetrically scanned, whilst the 1986 prints were acquired from DCC and were scanned at Bournemouth University (BU) using a desktop scanner. The NMR was approached to request access to the 1982 negatives and prints for scanning with the desktop scanner, as the comparisons made between the DSMs created from the 1982 SAPs would be analogous to one another and more statistically meaningful. However, permission for supervised access was repeatedly refused by the NMR, and thus the dataset closest in date to the 1982 SAPs with which to undertake a comparison were the 1986 SAPs.

The statistical quality of the triangulation and terrain extraction procedures in SocetGXP for each dataset are given in Table 5.10. The GNSS random points were used to extract elevation values from the 1982 and 1986 DSMs. As with the 1982 dataset there was a horizontal offset

	SAP Triangulation Root Mean Square Residuals					SAP ATE DSM Results				
Material/ Scanner Type	**Image Pixels**	**X (m)**	**Y (m)**	**Z (m)**	**Total RMS (m)**	**RPS* (m)**	**ATE DSM Post Spacing/ GSD Used (m)**		**C.E.* (m)**	**L.E.* (m)**
							X	**Y**		
Negative/ Photogram.	1.215	1.518	1.588	1.783	2.204	3.142	1	1	0.857	0.869
Print/ Desktop	2.025	2.882	2.310	3.259	2.526	4.451	1	1	1.007	0.595

*RPS = Recommended Post Spacing; C.E. = Absolute Circular Error; Absolute Linear Error

Table 5.10: Statistical output from SocetGXP for the photogrammetrically scanned negatives and desktop scanned prints, indicating the quality of the triangulation and ATE DSM solution.

observed between the TLS DSM and the 1986 data. This was addressed by using the image registration and warping regime in ENVI, which has previously been applied to the 1982 dataset (see Section 5.1). The elevation values extracted from the 1986 DSM were compared to those of the GNSS and were found to have a mean vertical offset of 0.233m, which was subsequently added to the warped 1986 DSM to correct for this error. The elevation values for the 1982 DSM, 1986 warped DSM and 1986 warped and elevation-corrected DSM were imported into SPSS for analysis. The summary statistics can be found in Table 5.11.

	Residuals for 1982 Warped DSM	**Residuals for 1986 Warped DSM**	**Residuals for 1986 Warped DSM +0.233m**
Number of Samples	222	222	222
Mean (m)	0.000	-0.233	0.0004
Std. Error of Mean (m)	0.0130	0.0714	0.071
Median (m)	0.006	-0.175	0.057
Mode (m)	-0.867[a]	-3.438[a]	-3.205[a]
Std. Deviation (m)	0.194	1.064	1.062
Variance (m)	0.038	1.132	1.127
Skewness	-0.573	0.138	0.138
Std. Error of Skewness	0.163	0.163	0.163
Kurtosis	2.004	0.892	0.910
Std. Error of Kurtosis	0.325	0.325	0.324
Range (m)	1.442	6.798	6.798
Minimum (m)	-0.867	-3.438	-3.205
Maximum (m)	0.575	3.360	3.593

Table 5.11: Summary statistics for the 1982 Photogrammetrically scanned negatives and the 1986 desktop scanned prints.

5.4.3 Results

Based upon the amount of variance and the range of both 1986 datasets in comparison with the GNSS elevations, it is clear that a great deal of noise is present within the DSM, which can be seen in Figure 5.7. The 1982 and 1986 datasets have been warped to fit the horizontal dimensions of the TLS DSM and, with the exception of one of the 1986 DSMs, their elevations have also been altered to remove the offset effects of the EGM96 geoid and Mean Sea Level datum. This process is designed to address the inaccuracies introduced into the DSMs by the datum selection and the uncertainty of GCP locations and their coordinate values. However, these alterations have not greatly reduced the errors in the 1986 DSM, as indicated by the minimal change in the values within Table 5.11, with the exception of the Mean, Median and Mode statistics. The frequency distribution of residual values for each DSM are shown in Figure 5.8, along with the linear relationships between each of the DSM datasets and the GNSS elevation values. The majority of residuals appear to be within ±1σ, or 1.064m, of the mean for both 1986 DSMs. This is in contrast to the 1982 DSM, whereby the majority or residual values lie within ±1σ, which is equivalent to 0.1937m. The 1986 σ is over five times greater than that of the 1982 DSM.

The linear relationship between the GNSS and the 1982 warped DSM illustrates a strong positive correlation, as highlighted in Figure 5.8, which is confirmed by an ‘r’ value of 1.000. Whilst both of the 1986 DSM datasets have ‘r’ correlations of 0.993, which is also suggestive of a strong correlation, the scatterplots shown in Figure 5.8 clarify why correlation is slightly lower, as shown by the distribution of the points. By examining the 1986 DSM (see Figure 5.7), the terrain appears to be noisy and the ramparts, particularly in the north, are not pronounced.

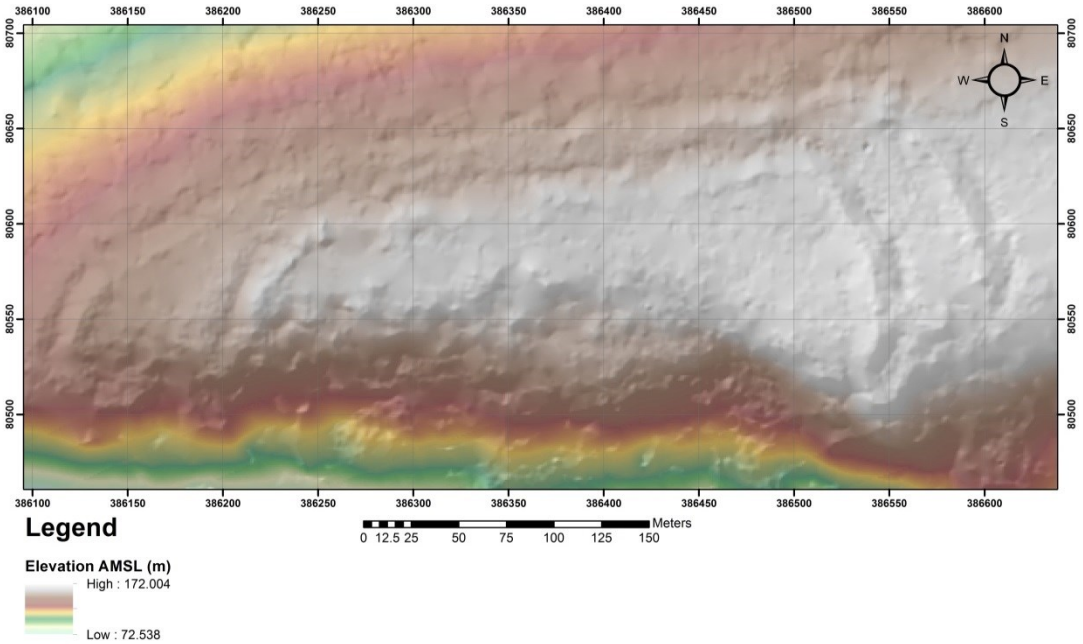

Figure 5.7: 1986 DSM.

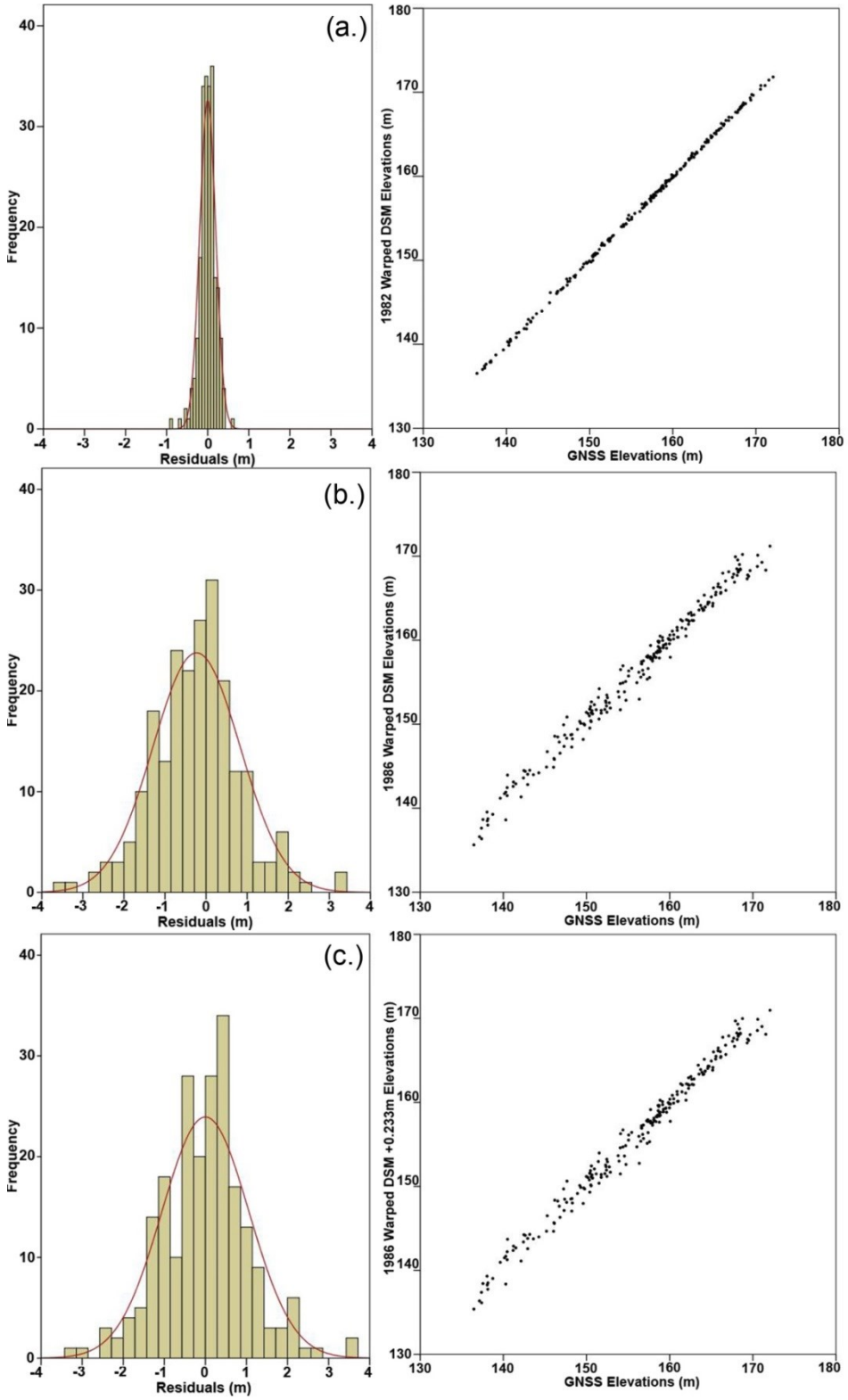

Figure 5.8: Frequency distributions and scatterplots highlighting the relationships between GNSS elevations and the 1982 and 1986 DSMs: (a.) 1982, (b.) 1986 Warped DSM (c.) 1986 Warped DSM +0.233m.

It is in the same region within the 1986 orthophotograph (Figure 5.9b), that there is very little image contrast to delineate the ramparts. Subsequently, the photogrammetric software has struggled during the image matching process and the elevation values within regions of low contrast will not be wholly representative of the terrain in these areas.

Scatter plots of the residual values for each DSM are shown in Figure 5.10. The distribution of residual values maintains a linear appearance in the 1982 DSM (Figure 5.10a), suggesting that their magnitude is consistent across it, with the exception of one or two outliers. However, the magnitude of residual values remains high across the extent of the 1986 DSM (Figure 5.10b and c) and does not adhere to any particular elevation: there is no discernible pattern of distribution. Whilst many of the residual values are within ±1m, the vast majority fall within ±2m, with only four values out of 222 rising above ±3m. The results of performing the paired t-test on these data was to return 2-tailed 'p' values of 1 for the 1982 data and 0.996 for the 1986 Warped DSM with added elevation of 0.233m. Subsequently, these datasets suggest that the

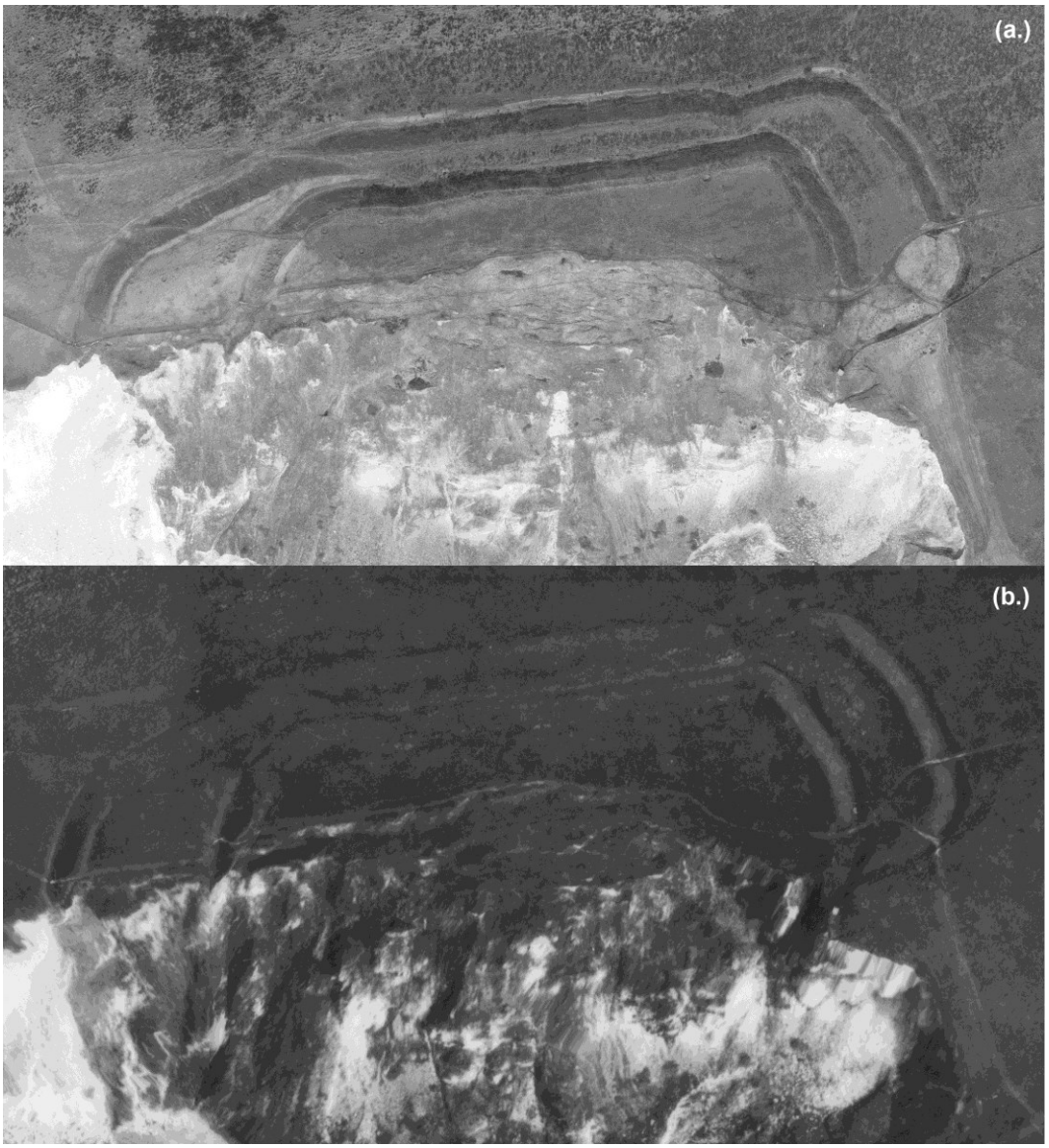

Figure 5.9: Orthophotographs of (a.) 1982 SAPs and (b.) 1986 SAPs.

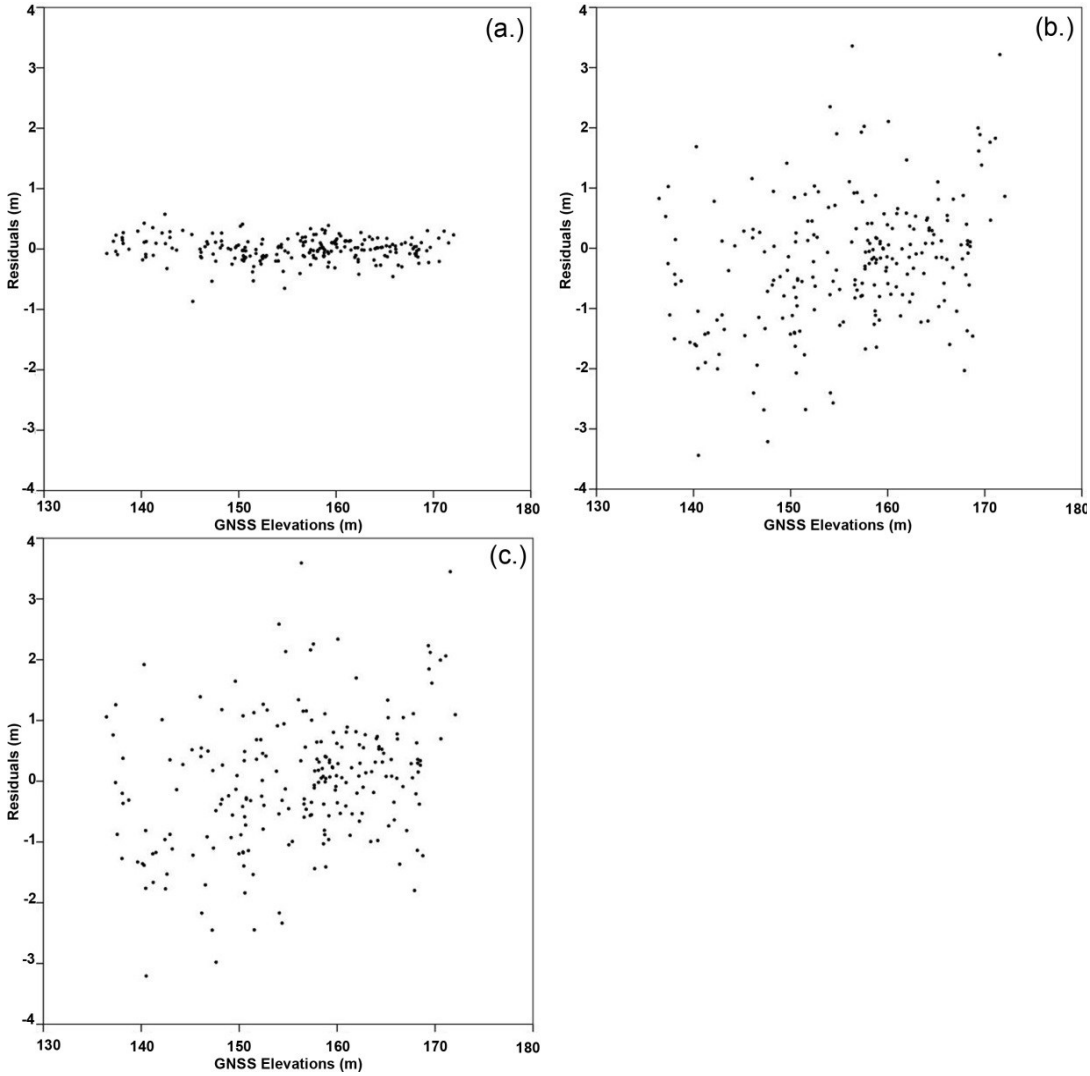

Figure 5.10: Scatter plots illustrating the distribution of residual values between (a.) 1982 DSM, (b.) 1986 Warped DSM and (c.) 1986 Warped DSM +0.233m, and GNSS elevation values.

null hypothesis can be accepted and that there is no difference between the GNSS data and that of the 1982 and 1986 datasets. This conclusion can be confirmed by examining the confidence interval of the difference for the mean difference between the GNSS and the DSM data. Both the 1982 and 1986 DSMs as mentioned above have confidence intervals that straddle zero, suggesting the null hypothesis could be true. However, this is not the case for the 1986 warped DSM that has not been corrected for elevation offset. The 'p' value for this dataset is 0.001, and thus the null hypothesis must be rejected. The confidence interval does not contain both negative and positive values: both the lower and upper values are negative, and thus the null hypothesis can be rejected as there is a 95% confidence that the mean will not be zero.

5.4.4 Conclusion

It is difficult to identify the effects of employing a desktop scanner to create a digital image of the 1986 prints and the influence this has on the DSM quality. In order to separate the effects of scanning practice from other sources of error, the desktop printer would require characterising by scanning a glass plate to examine how the grid pattern etched on the glass warps during this process. It may then be possible to generate a text file that could be imported into photogrammetric software to correct the scanned imagery for any geometric imperfections caused by scanning. However, this will not resolve any issues caused by the lack of radiometric resolution.

As has already been touched upon, the contrast in the 1982 imagery is much greater than in the 1986 SAPs, as shown in Figure 5.9. This is one of the reasons that the 1982 dataset produces an accurate DSM, aside from the quality of the negative and the benefits of using a photogrammetric scanner. The process of image matching during terrain generation is therefore more successful for the 1982 SAPs. Whether the issue with the 1986 photographs is the result of poor printing practices is unknown, as the original 1986 negatives cannot be viewed. On close inspection of the 1986 digital images, no scratches or other imperfections can be identified. However, the scale of the imagery and the ground sample distance (GSD) of the digital SAP images may influence the success of the automatic terrain extraction (ATE) routine in Socet GXP. The values of these metrics are provided in Table 4.1 in Section 4.2.1. ATE was set to return a point every 1m in both the X and Y direction to match the point density of the ALS dataset. This was to ensure that these data could be compared on a like with like basis. This setting does not adhere to the optimal post spacing as recommended by Socet GXP, namely 15 times the GSD, which would equate to a post spacing of 1.215m for the 1982 data and 2.025m for the 1986 SAPs.

5.5 Examining the Effects of GCP Control on DSM Quality

5.5.1 Introduction

As archive SAPs are predominantly unaccompanied by interior or exterior orientation data, the quality of ground control points used in the triangulation process will influence the accuracy of the resultant DSM. It has previously been noted that the 1982 DSM has both a horizontal and vertical offset from the TLS data. Therefore an investigation into how these offsets would affect the analysis and results was required. Three different scenarios were produced from the 1982 data to test the influence of control on DSM quality: unwarped, elevation corrected and warped (horizontal and vertical correction) datasets.

5.5.2 Method

The first dataset consisted of the unaltered DSM as output from Socet GXP and interpolated in ArcMap, with no further alterations made to it. The SocetGXP quality statistics for the triangulation and terrain extraction results for this dataset are provided in Table 5.2. The second dataset had 1.72m added to the elevation values, which was achieved using Raster Math in ArcMap to account for the mean elevation offset between the 1982 DSM and the GNSS random points. The final dataset was a DSM that had an extra 1.72m added to the elevation values and the horizontal values were then warped to fit the TLS DSM by applying the warping tools in ENVI, as described in Section 5.1. The GNSS random points were used to extract elevation values from each of these three datasets in ArcMap for further analysis in SPSS. The GNSS points were subsequently used as the baseline data against which to compare each of the three 1982 DSMs. The summary statistics for this comparison can be found in Table 5.12.

5.5.3 Results

It can be seen that there is little difference between the original 1982 DSM and the surface model with the elevation offset in terms of range, variance, skewness and kurtosis (see Table 5.12). The major differences between the two datasets are highlighted by the measures of mean, median and mode. These differences occur due to the added elevation values although,

	Residuals for original 1982 DSM	Residuals for 1982 DSM +1.72m	Residuals for 1982 Warped DSM
Number of Samples	222	222	222
Mean (m)	1.668	-.052	0.000
Std. Error of Mean (m)	0.036	0.036	0.013
Median (m)	1.626	-0.094	0.006
Mode (m)	0.241	-1.479	-0.867
Std. Deviation (m)	0.534	0.534	0.194
Variance (m)	0.285	0.285	0.038
Skewness	0.149	0.149	-0.573
Std. Error of Skewness	0.163	0.163	0.163
Kurtosis	0.229	0.229	2.004
Std. Error of Kurtosis	0.325	0.325	0.325
Range (m)	2.872	2.872	1.442
Minimum (m)	0.241	-1.479	-.867
Maximum (m)	3.113	1.393	.575

Table 5.12: Summary statistics for the 1982 DSM variations.

as can be seen by the identical variance, skewness and kurtosis values, the distribution of residuals is not affected. This result is thus indicative of a horizontal offset between both the 1982 DSMs in question and the GNSS point locations, as the elevation values from the 1982 datasets are not aligned with those from the GNSS. However, the statistics describing the residual differences between the warped 1982 DSM and the GNSS data shows a much greater conformity as illustrated by the small values. The standard deviation value is 0.194m, as opposed to the 0.534m returned by the non-warped datasets. The residual 'range' was almost half the value of the non-warped datasets, namely 1.442m compared with 2.872m. The histograms for the three 1982 datasets illustrate the distribution of the residual values (see Figure 5.11). Both of the non-warped datasets display a slight multimodal distribution, with peaks of values (outliers) found towards the tail ends of the bell curve. The histogram for the warped dataset exhibits a small number of outlier values just beyond the tails of the bell curve.

By constructing scatter plots to illustrate relationships between the GNSS values and each of the three 1982 DSMs, as shown in Figure 5.11, a linear relationship is identifiable for each datatset. The warped DSM forms the tidiest line, with only one value diviating noticably, situated at appromiately 147m along the 'GNSS' axis. This is indicative of a high degree of positive correlation between the two datasets, which is confirmed by an 'r' value of 1. The correlations are not as strong for the unwarped DSM and the DSM with added elevation, both of which are identical and their 'r' values are both 0.998. The results of performing a paired samples correlation for each of the three DSMs returned significance values for each dataset as 'p'=0.000. The null hypothesis could be rejected for all three comparisons, based upon these values, indicating that the DSM datasets are not identical to the GNSS, despite high correlation. However, rather than rejecting the null hypothesis, it could be said that there is not enough information, or samples, to accept it.

The 'p' values for both the warped DSM and the non-warped DSM with an added elevation constant were greater than 0.05, namely 1.00 and 0.146 respectively (see Table 5.13). For both of these datasets the null hypothesis can thus be accepted and no statistically significant differences exist between both DSMs and the GNSS. The removal of the vertical offset from the non-warped dataset, which produced a result that is statistically insignificant, suggests that this error is the most important one to remove prior to undertaking further analysis and attempting to increase the similarity between a photogrammetric DSM and a more accurate survey technique. However, the 'p' value for the non-warped DSM with added elevation is much smaller than that for the warped DSM, which was also corrected for elevation difference. To ensure data parity, there is an almost seven-fold increase in the similarity between the GNSS and DSM when rotational and translational factors, as applied through a warping algorithm, are applied.

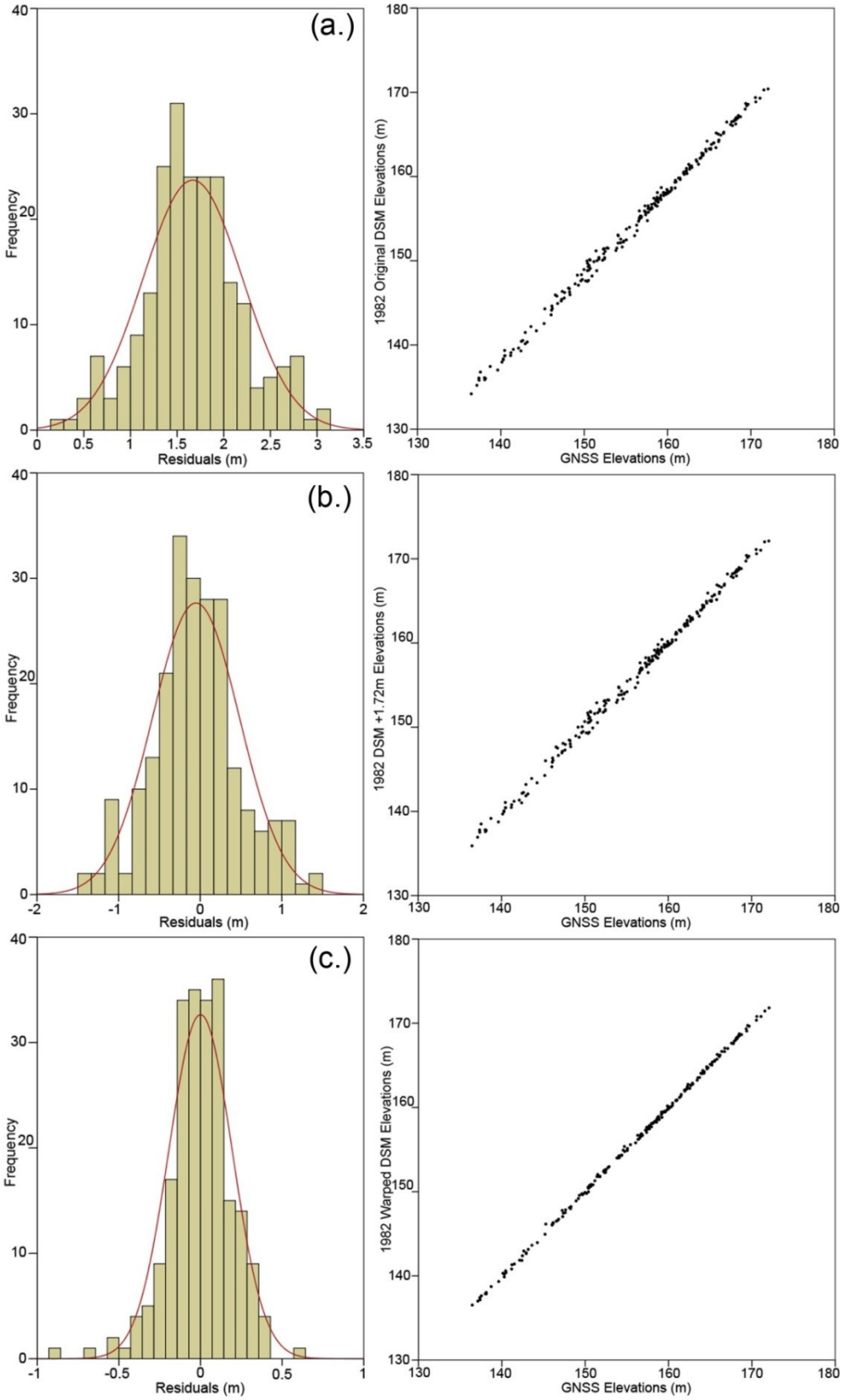

Figure 5.11: Histograms (left) and Scatter Plots (right) illustrating the relationship between the GNSS data and the 1982 (a.) Original DSM, (b.) DSM +1.72m, and (c.) warped DSM.

		No. of Samples	Correlation	Sig.	Paired Differences		t	df	Sig. (2-tailed)
					95% Confidence Interval of the Difference				
					Lower	Upper			
Pair 1	**GNSS - 1982 Original DSM**	222	0.998	0.000	1.597	1.738	46.577	221	0.000
Pair 2	**GNSS - 1982 Original DSM +1.72m**	222	0.998	0.000	-0.123	0.018	-1.459	221	0.146
Pair 3	**GNSS - 1982 Warped DSM**	222	1.000	0.000	-0.026	0.026	0.000	221	1.000

Table 5.13: Paired t-test results comparing GNSS data to the 1982 DSM variations.

5.5.4 Discussion

When considering the results from the paired t-test, the non-warped DSM has a 'p' value of 0.000, which indicates that there is a statistically significant difference between this dataset and that of the GNSS. It is thus likely that the GCPs are not accurate enough to provide a suitable location in the absolute sense for which there are two reasons. Firstly, selecting the location of the GCP in the imagery is a subjective process: one operator may choose to position a point in a slightly different location to another, the GCP location in the imagery is ambiguous due to poor image quality, or because the area in which the GCP resides has changed slightly over the years (Walstra et al. 2011). The second factor is the quality of the GCPs themselves, particularly those extracted from extant OS maps and photogrammetrically derived datasets, as explained in Section 4.3.1. The accuracies appended to these XYZ points in Socet GXP are 3m in X and Y, and 5m in Z, and thus there is a reasonable amount of latitude for the least squares adjustment to address. The reason for selecting large values is based upon the uncertainty associated with the subjective selection of XYZ coordinates from mapping sources, as explained above. It was also difficult to ascertain the uncertainty appended to these sources by the suppliers. Two of the GCPs closest to the hillfort were recorded using the GNSS and thus they have much better accuracies i.e. 0.2m in X and Y, and 1m in Z. As both of these GCPs were positioned next to a fence post or a pill box, it was decided that there could be potential for placing the GCP on a pixel representative of the top of one of these features. It is also likely that in the 30 years since the imagery was produce, the pillbox may have moved slightly because of its proximity to the cliff edge. It was therefore felt necessary to reflect this risk in the Z accuracy for these points.

The addition of Z GCPs along the base of the cliff, on the beach, will also influence the rotation of the DSMs. As was stated in Section 4.4.1, the Socet GXP technical team suggested placing additional GCPs along the beach to mitigate against any severe tilt appearing in the photogrammetric DSMs. Each of the Z GCPs were allocated values of 2m with an accuracy of 2m, to reflect any potential for change along the beach over the 30 years between the production of the photography and this research. An additional factor that will influence the Z accuracies of the dataset is the vertical datum that Socet GXP employs in its calculations. At present, the software only supports geoid heights that are stated to be "measured with respect to the WGS84 ellipsoid" (BAE Systems 2013), but no local ellipsoids are currently supported. The geoid available for this research was the Earth Gravitational Model 1996 (EGM96), and the vertical datum can be set to either 'Ellipsoid (height above the ellipsoid) or 'Mean Sea Level', the latter of which was utilised. The horizontal datum is the Ordnance Survey Great Britain 1936 (Mean Solution), which was suggested for use by the Socet GXP technical support team. As stated in Sections 5.1 and 5.2, there was a noticeable horizontal offset between the 1982 DSM and the TLS. This is due to the horizontal accuracies attributed to the GCPs rather than the horizontal datum.

5.5.5 Conclusion

Whilst removing any vertical offset is important, it appears that removing horizontal error has a greater influence on DSM accuracy, which could further be tested by not adding any vertical corrections to the warped data.

5.6 Vegetation Influence on DSM Quality

5.6.1 Introduction

The final variable that was expected to influence accuracy in the SAP DSMs was the presence of vegetation. The majority of the hillfort is covered in grass, although the density and distribution of gorse across the site has varied over the years for which SAPs and modern data are available.

5.6.2 Method

Whilst quality statistics were not provided with the ALS data ordered from the EA, Table 5.14 contains the triangulation and terrain extraction statistics returned from SocetGXP. To test the influence of vegetation upon SAP elevation data, the GNSS random points were used to extract elevations from the SAP DSMs and the November 2009 ALS DSM. The random points were then separated into those that were measured in regions covered with gorse and those that were not, as illustrated in Figure 5.12, which were determined subjectively using orthophotographs produced from each of the SAP epochs.

Triangulation Root Mean Square Residuals						SAP ATE DSM Results				
SAP Date	Pix.*	X (m)	Y (m)	Z (m)	Total RMS (m)	RPS* (m)	APS* (m)		Absolute/ Relative C.E.* (m)	Absolute/ Relative L.E.* (m)
							X	Y		
1945	8.333	3.592	2.440	4.480	5.915	1.650	1	1	- / 0.305	- / 0.466
1968	1.004	2.776	2.120	6.494	7.374	1.770	1	1	0.618/ 0.606	1.559/ 0.526
1982	1.518	1.588	1.783	2.204	3.142	1.215	1	1	0.857/ 0.218	0.869/ 0.773
2009	1.136	8.326	9.699	3.157	1.317	2.250	1	1	0.875/ 0.331	1.306/ 0.639

*Pix. = Image Pixels; RPS = Recommended Point Spacing; APS = Actual Point Spacing; C.E. = Circular Error; L.E. = Linear Error

Table 5.14: Statistical output from SocetGXP for the photogrammetrically scanned negatives, indicating the quality of the triangulation and ATE DSM solution.

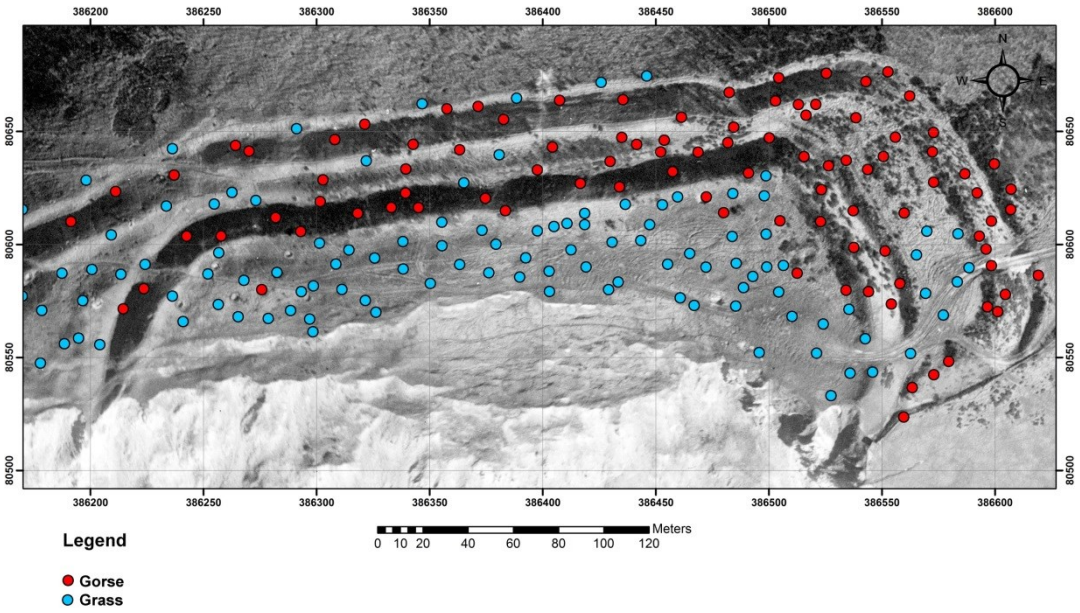

Figure 5.12: Map showing the separation of the GNSS random points into 'grass' and 'gorse' categories

Elevation data for each epoch was exported from ArcMAP and opened in Microsoft Excel, where the categories 'grass' and 'gorse' were allocated to the appropriate random point. The residuals between the GNSS and SAP elevation values were calculated by subtracting the SAP elevations from those of the GNSS. As the GNSS measured the terrain, not the top of the gorse stands, the ALS and SAP datasets should show a clear residual difference in regions of gorse coverage. The spreadsheet containing the residual values was subsequently opened in SPSS where box plots were constructed to examine the outputs. Summary statistics for each of the DSM datasets, which are split into their categories, can be seen in Table 5.15.

5.6.3 Results

The dataset with the smallest residual values for both the grass and gorse categories, based on the mean and median values, was the 1982 data, as shown in Figure 5.13a. However, the SD and variance are more favourable in the ALS, which was created using a last return point cloud that was subsequently rasterised (see Section 4.4.3), although the presence of gorse can still

	1945 Gorse	1945 Grass	1968 Gorse	1968 Grass	1982 Gorse	1982 Grass	2009 Grey Gorse	2009 Grey Grass	2009 Nov ALS Gorse	2009 Nov ALS Grass
Mean (m)	0.548	-0.349	0.386	-0.075	-0.052	0.013	0.068	0.336	-0.096	-0.056
Std. Error of Mean (m)	0.137	0.074	0.167	0.056	0.027	0.015	0.035	0.039	0.015	0.014
Median (m)	0.375	-0.507	0.020	-0.192	-0.007	0.018	0.140	0.373	-0.044	-0.028
Mode (m)	-1.730	-1.912	-1.328	-2.477	-0.527	-0.867	-1.503	-1.095	-0.535	-0.686
Std. Deviation (m)	1.228	0.833	1.004	0.764	0.177	0.196	0.400	0.373	0.170	0.136
Variance (m)	1.508	0.694	1.008	0.584	0.031	0.038	0.160	0.139	0.029	0.018
Skewness	0.867	0.993	0.230	1.981	-0.605	-0.621	-1.128	-1.328	-0.477	-1.583
Std. Error of Skewness	0.269	0.216	0.393	0.178	0.361	0.182	0.213	0.250	0.213	0.250
Kurtosis	1.467	1.416	-1.328	8.947	0.199	2.436	1.777	3.562	-0.165	5.451
Std. Error of Kurtosis	0.532	0.428	0.768	0.355	0.709	0.361	0.423	0.495	0.423	0.495
Range (m)	6.239	4.684	3.467	6.919	0.824	1.442	2.275	2.148	0.887	0.967
Minimum (m)	-1.730	-1.912	-1.328	-2.477	-0.527	-0.867	-1.503	-1.095	-0.535	-0.686
Maximum (m)	4.509	2.772	2.139	4.442	0.297	0.575	0.772	1.053	0.352	0.282

Table 5.15: Summary Statistics showing the residual differences between the 'Grass' and 'Gorse' vegetation categories in each SAP and ALS epoch.

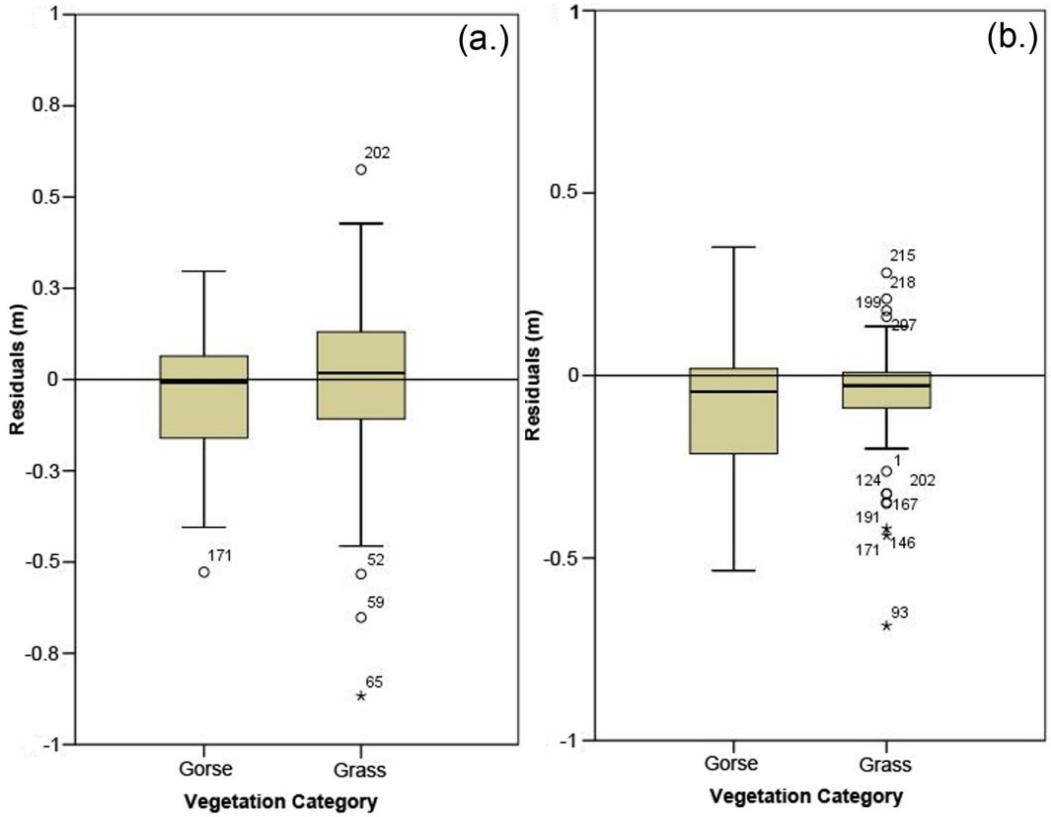

Figure 5.13: Box Plots showing residual elevation values between GNSS data and (a.) 1982 and (b.) November 2009 ALS data in Grass and Gorse regions.

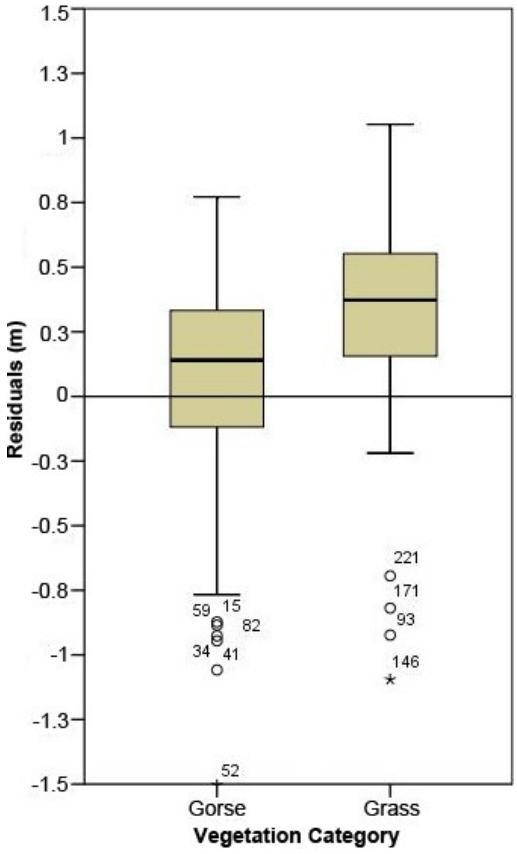

Figure 5.14: Box Plot showing residual elevation values between 2009 Greyscale SAP and dGPS data in Grass and Gorse regions.

be seen.

This is unsurprising given the density of gorse vegetation, which the laser is unlikely to penetrate to reach the ground surface in places. The residual values in the grass regions have a much lower interquartile range than those in the gorse, which is to be expected. The grass on the hillfort is short all year round and thus there should be little elevation difference between the GNSS and the ALS, whereas the height of the gorse varies and the offset between the GNSS and ALS will be greater (see Figure 5.13b). The majority of the values within the grass category are negative, and thus it can be stated that the ALS elevations were higher than the GNSS, especially those values recorded by the ALS in regions of gorse. Vegetation coverage influences ALS DSM elevations as exhibited by the 1m range of the interquartile residual values in the gorse regions that are both positive and negative, whilst the interquartile range for grass regions is 0.25m. However, outlier and extreme values are only present in the grass category, which suggests that noise in the data or misclassification whereby some random points are marked as grass when, in fact, they should have been labelled as gorse. When examining the values in Table 5.15, it is important to remember that the Range and Minimum and Maximum values also include the outlier values, and thus they are misleading when considered on their own.

It is interesting to note that the median value of both vegetation categories in the 2009 Greyscale SAPs is much higher than 0m, as compared to the ALS, namely 0.14m for gorse and 0.373m for grass (see Table 5.15). This is particularly surprising as the two datasets were created approximately 2 months apart. These values indicate that the elevations generated by SocetGXP for the 2009 SAPs are lower than that of the GNSS, regardless of vegetation characteristics. However, the range of residuals in the gorse category is much larger and extends further into negative values than its ALS counterpart, as shown in Figure 5.14 on page 179. Some of the 2009 SAP elevation values are therefore higher than those of the GNSS, which is indicative of the influence gorse has on producing larger residuals in the regions where it is present. This result is expected of the photogrammetry as, unlike ALS, it cannot penetrate the canopy of vegetation. This explains the superior performance of the ALS over SAPs in gorse areas when each is compared to the GNSS elevations. However, given the density of gorse it is unlikely that many laser pulses could have been returned from the terrain itself.

Unlike the ALS, the 2009 SAP DSM exhibits a much wider range of residuals in the grass category, particularly in the interquartile range, which could indicate the presence of noise in the data. Outliers are present in both the grass and gorse categories, all of which are negative in value, although it appears that there are slightly more outliers in the gorse group. There is no great difference between the values for the outliers in both categories, which indicates that misclassification errors have been made as the outliers in the grass category should be much lower. As these values are also situated much further from the whisker with the lowest value than the outliers in the gorse category, misclassification has occurred.

By examining the residual map for the grass region in the 2009 SAP data, as shown in Figure 5.15a, it can be seen that the residuals increase from east to west across the hillfort. This could suggest a tilt in the elevation data although, upon comparison of the 2009 SAP and 2009 ALS DSMs in ArcMap, this does not appear to be the case. The negative residuals remain consistent in size across the hillfort, although they are located upon the steep slopes of the north-facing ramparts. As these values indicate that the SAP elevation data is higher in these locations than the GNSS elevations, these points have been misclassified and belong in the gorse category. On comparison with the gorse residuals map (see Figure 5.15b), this statement appears to be correct. Within Figure 5.15 it can also be seen that there is no tilt in the 2009 SAP DSM. Whilst the majority of positive residuals are found to the west of the hillfort, they are also present, to a lesser degree, in the east. The large negative residuals are located where there are stands of gorse, particularly in the north-east corner of the outer rampart, and thus the results here correspond with the expected results. However, the presence of larger, positive residuals may indicate that some of the random points here have been misclassified.

The performance of the 1982 SAPs was impressive in comparison to the other datasets considering its age. As with the 2009 ALS data there were more outliers in the 1982 grass category. However, as illustrated in Figure 5.16a, the range of residuals in this category was larger (0.575m to -0.867m) than those in the gorse category (0.297m to -0.527m), which is contrary to the findings of the 2009 ALS data. This suggests that there may be more noise present in the grass regions of the 1982 imagery, particularly as the interquartile range of residuals is much larger than it is for the 2009 ALS dataset. As has been the case previously, there are also more outliers within the grass category, with the majority of outliers consisting of negative values and indicating that the SAP DSM has higher elevations at these locations than the GNSS data. The location of these outliers can be identified in Figure 5.16, where they are situated on the north-eastern corner of the inner and outer ramparts. At the time of writing, these same areas are currently afflicted with gorse stands (see Figure 5.17 on page 184), and it is likely that they were in the same condition in 1982. It is therefore probable that these points have been misclassified. It is more challenging to identify the cause of the larger positive residuals within the grass category, however. At these locations, the SAP DSM is lower than the measurements taken by the GNSS. By examining the 1982 orthophotography shown in Figure 5.17, it can be seen that the image contrast is good. Despite this, it remained challenging to separate the points into the two vegetation categories, and thus it must be acknowledged that, as with the other SAP epochs, this subjective approach has given rise to some misclassification errors.

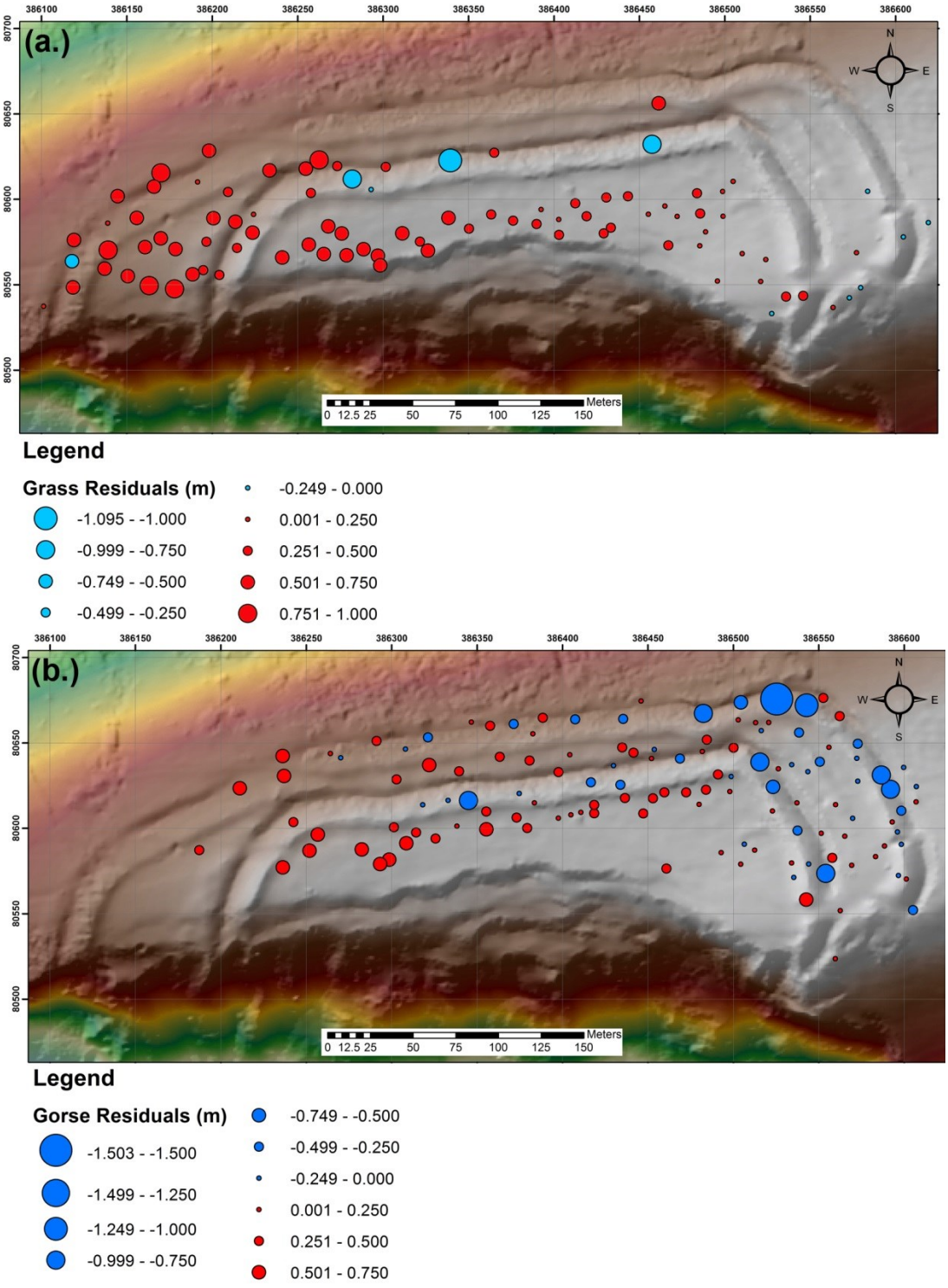

Figure 5.15: Map showing the residual distribution between 2009 Greyscale SAP and dGPS elevations in (a.) grass-dominated and (b.) gorse-dominated regions.

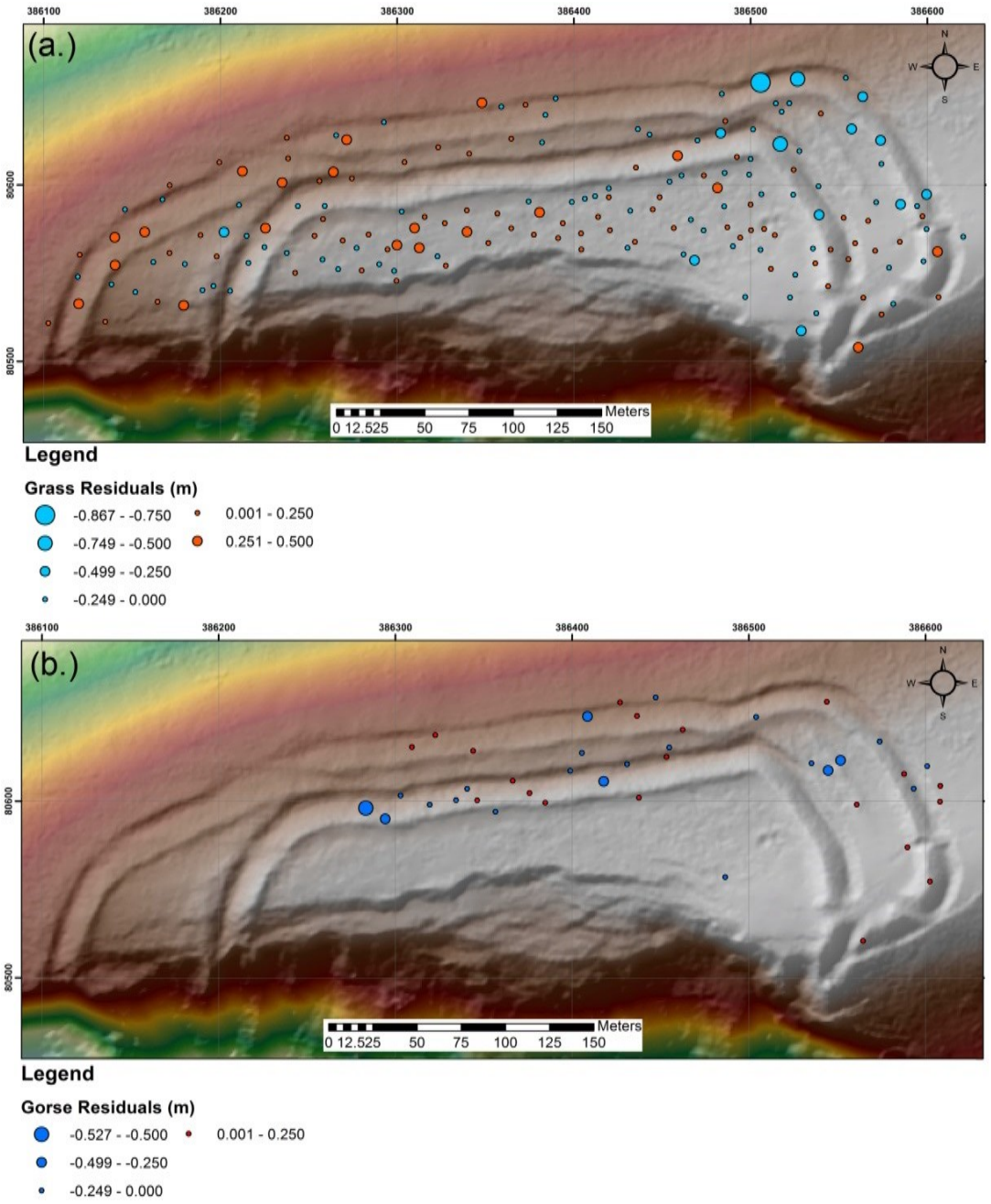

Figure 5.16: Map showing the residual distribution between GNSS elevations and the 1982 DSM in (a.) in grass-dominated and (b.) gorse-dominated regions.

The gorse category, shown in Figure 5.16b, illustrates the position of the largest negative residuals in the areas where they are to be expected. These areas are situated on the northern facing ramparts and within the east inner annex, where gorse tends to grow and the shadows are predominantly located. The smaller positive residuals may indicate misclassified points, or they may indicate regions where the photogrammetric software has underestimated the DSM elevations, particularly where the residuals are found on the rampart slopes. Overall, the 1982 SAP DSM has performed well, although it must be remembered that the DSM was warped to match the TLS dataset by using a rectification routine in ENVI (see Section 5.1).

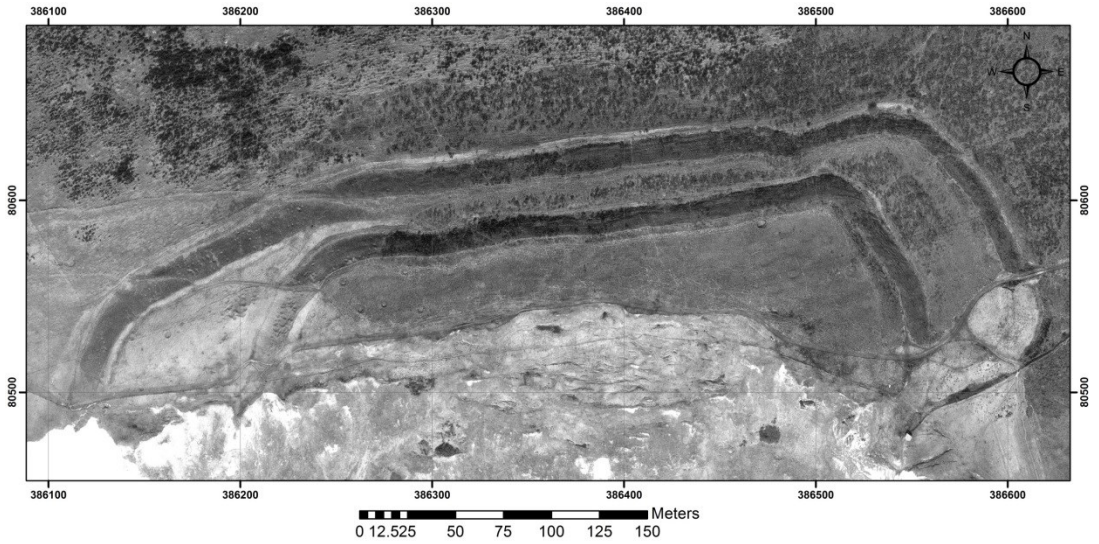

Figure 5.17: 1982 Orthophotograph.

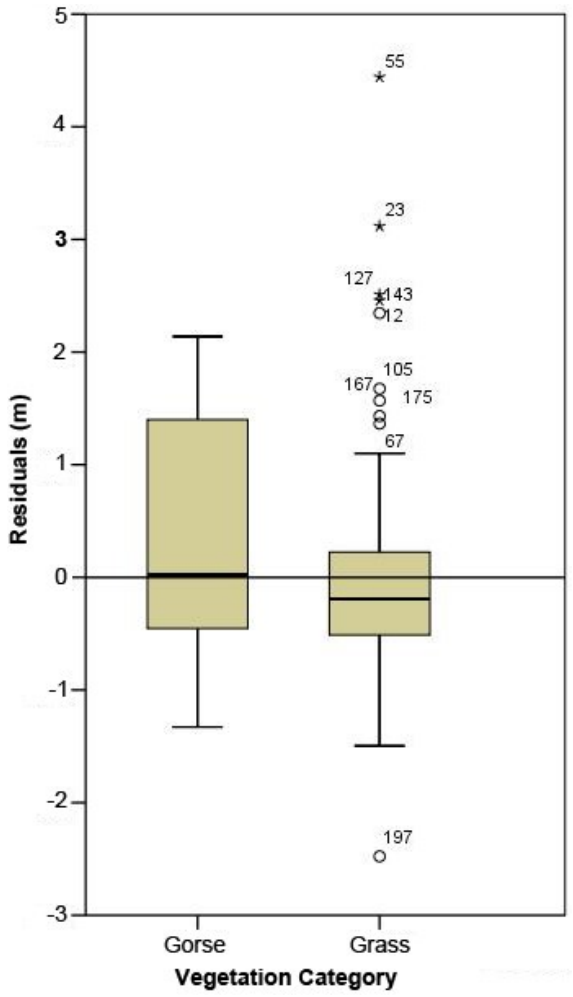

Figure 5.18: Box Plot showing residual elevation values between 1968 SAPs and dGPS data in Grass and Gorse regions.

The correlation of elevation data in the 1982 DSM in comparison to the GNSS random points should therefore be extremely accurate. Whilst the other SAP DSMs could also be manipulated in ENVI, they did not appear to be offset from the TLS data, unlike the 1982 DSM. Subsequently, the 1945, 1968 and 2009 SAP DSMs are purely indicative of the performance of the photogrammetric software and the metadata associated with each dataset.

The 1968 SAP DSMs display a much wider range of residual values than the more recent SAP and ALS datasets in both the gorse and grass categories. Without distinguishing between either category, the range of the residual values is 6.919m, with a minimum value of -2.477m and a maximum of 4.442m. However, based upon the box plot shown in Figure 5.18 (see previous page), the grass category appears to have a slightly larger number of negative residuals, which shows that the elevation value of the 1968 DSM is higher at these locations than that of the GNSS data, and thus it would be expected that these values lay within gorse regions. There is also a particularly large negative outlier within the grass category, which is likely to be a misclassification error. A large number of positive outliers, all of which are greater than 1m, are contained within the grass category. At these points, the 1968 DSM is lower than the GNSS elevations. To explain the differences between the gorse and grass categories, Figure 5.19a and b show the distribution of residual values across the hillfort, and also indicate how many values occur in each category.

It can be seen that the grass category has a much larger number of random points scattered across the hillfort, unlike the gorse category which contains a much smaller number of samples. The majority of the larger residuals in both grass and gorse regions occur along the rampart slopes, in particular those that are north-facing. The largest residuals within the gorse category are greater than 1.5m, indicating that at these points in the DSM the elevation values are lower than those recorded by the GNSS at the same point. This suggests that either gorse is unlikely to be present at these locations, or there is an error in the DSM. The DSM, as shown in Figure 5.19 has a noisy appearance across the entire hillfort, although it is especially noticeable across the eastern ramparts. The noise is less noticeable in the flatter regions and it is here that the smaller residuals are found, both for the grass and gorse categories. The effect of noise also appears to have an influence on the residual values. By examining the 1968 orthophotograph, as shown in Figure 5.20, scratches can be seen that traverse across the hillfort. Although these do not directly coincide with any of the random point locations, they suggest that the image quality for this particular epoch may have been compromised more so than the other archival images. Subsequently, these degradations are likely to be influencing the quality of the 1968 DSM and exhibiting as noise in the data.

There are many positive residuals in the grass category that are large, ranging between 1.5m and 4.5m, although those above 1m are marked as outliers and extreme values by SPSS, as illustrated in Figure 5.18. This result suggests that the photogrammetric process is underestimating these elevations. It is understood that slopes are problematic areas for photogrammetric software to process. Baily et al. (2003) state that low gradients are more likely to be underestimated than higher slope gradients, which is particularly pertinent as their

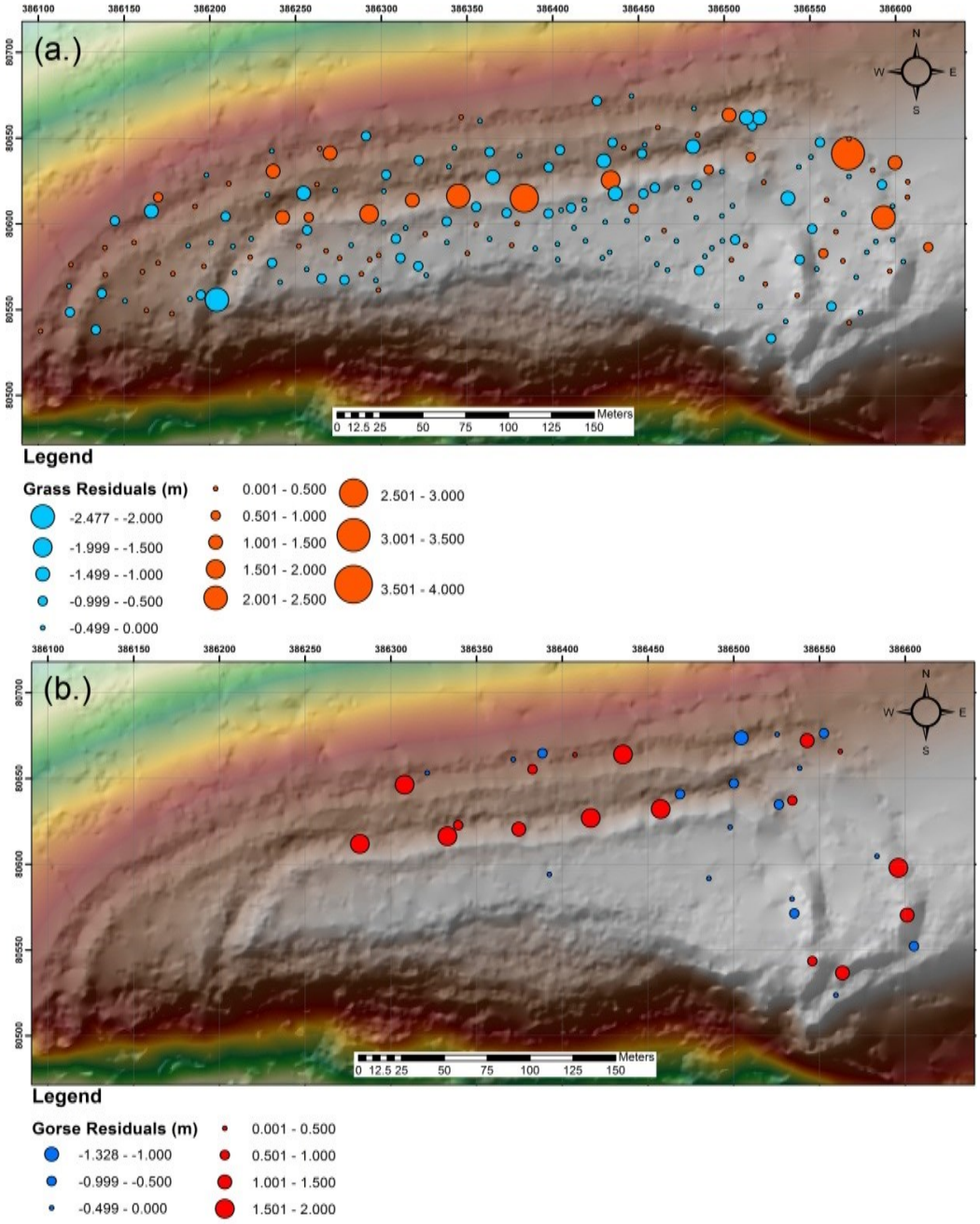

Figure 5.19: Map showing the residual distribution between GNSS and 1968 DSM elevations in (a.) grass-dominated and (b.) gorse-dominated regions.

research was conducted at Maiden Castle hillfort in Dorset. Adams and Chandler (2002) note that slope accuracy decreases as the gradient increases in their study of the Black Ven landslide, also in Dorset. However, many of the north and west facing slopes are also in shadow, as is apparent in the 1968 orthophotograph, shown in Figure 5.20, which will hinder the calculation of elevation values in these areas (Bailey et al. *ibid.*). Due to the limited contrast within the 1968 imagery, delineating the presence of gorse was problematic, and thus it is likely that the random points have been classified in error, which will influence the results.

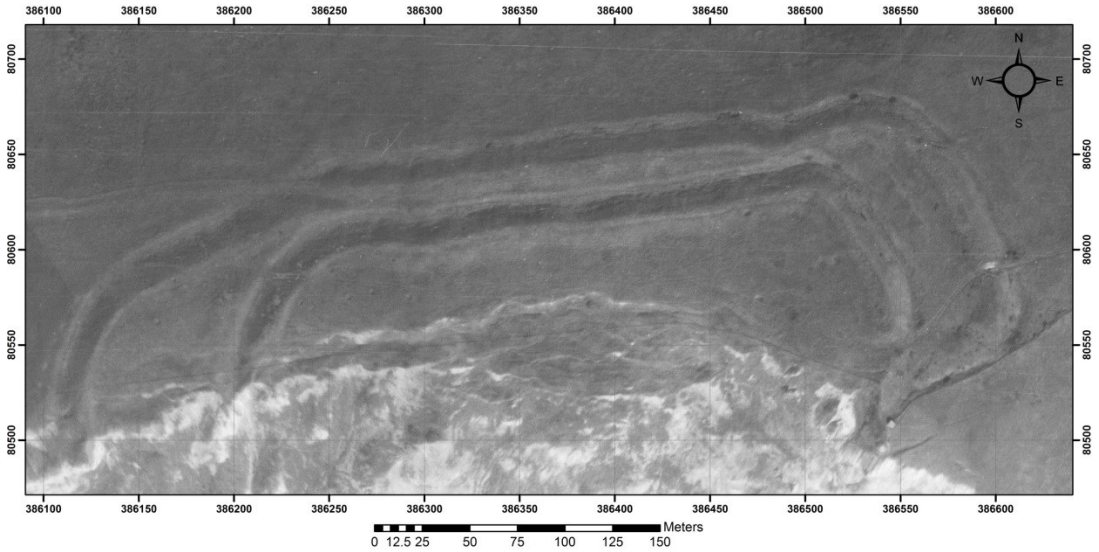

Figure 5.20: 1968 Orthophotograph.

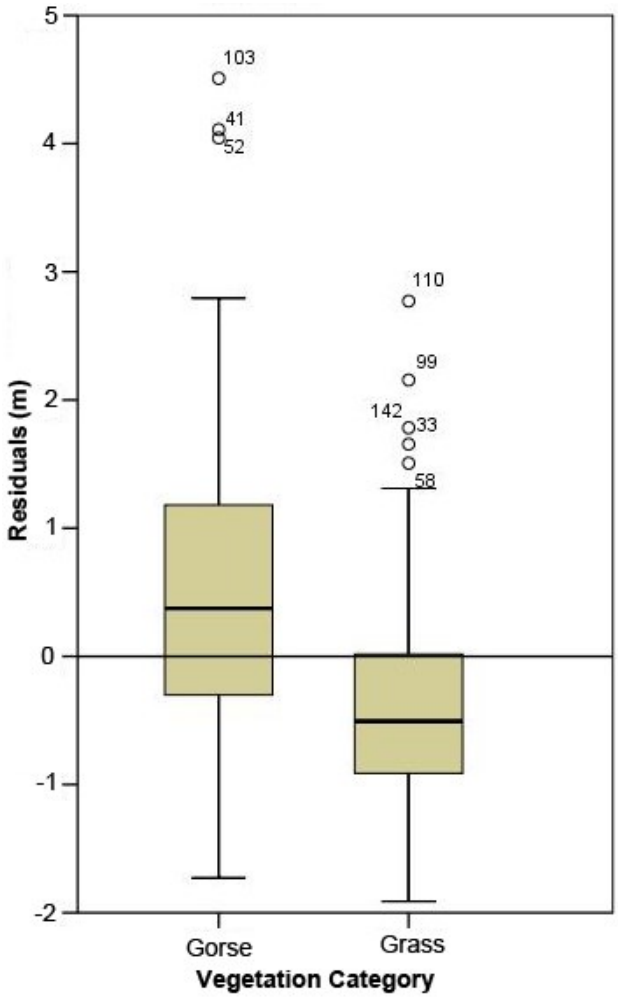

Figure 5.21: Box Plot showing residual elevation values between 1945 SAPs and dGPS data in Grass and Gorse regions.

The final DSM for consideration in this section is generated from the 1945 imagery. There are a slightly smaller number of random points utilised for assessing the influence of vegetation on this DSM than in the other SAP epochs. This is caused by the deficit of stereo-coverage of the 1945 imagery to the west of the hillfort and thus this region cannot be replicated in the DSM. The residual range for the entire population sample has a minimum value of -1.912m and has a maximum of 4.509m, with an overall range totalling 6.421m. Whilst this is much larger than the ranges for the 1982, 2009 SAP and ALS DSMs, it is smaller than the 1968 dataset by 0.5m. The box plot, shown in Figure 5.21 (see previous page), highlights the lack of residuals that are equal to 0m in the grass category. As the majority of the inter-quartile range of grass residuals is negative, this shows that the 1945 DSM in these areas has elevation values that are higher than the GNSS. As with previous datasets, the 1945 DSM has a greater number of outliers in the grass category, all of which are positive in value and indicate regions where the DSM elevations are lower than those from the GNSS. By examining the grass residuals map, shown in Figure 5.22a, there does not appear to be a pattern to the residual distribution. The majority of the positive residuals, including the outliers, are found in areas where gorse stands occur, which could suggest an error in allocating these random points to the grass category. The appearance of the 1945 DSM, as shown in Figure 5.22, suggests that the presence of noise in the data may be influencing these results.

The residuals within the gorse category contain a small number of negative values, but the vast majority are positive, including the outliers, as shown in Figure 5.21. Again, this highlights the fact that the GNSS elevation values are higher than those of the 1945 DSM at these locations, which suggests that the photogrammetric software is underestimating elevations. This result is also counterintuitive as in regions of gorse it would be expected that the residuals would be negative, indicating that the DSM elevations were higher due to the presence of gorse, although this is not the case. By looking at the distribution of the gorse residuals, as shown in Figure 5.22b, the largest positive differences are found along the northern slopes of the ramparts, and in particular the north east corner of the outer rampart. When compared to the 1945 orthophotograph, shown in Figure 5.23 on page 190, the areas of greatest difference occur in regions that are either in shadow or that are characterised by steep slopes. Where the larger negative residuals appear, in particular the top of the rampart slopes which are well lit by sunlight from a south-east direction, the values are akin to what would be expected from this analysis.

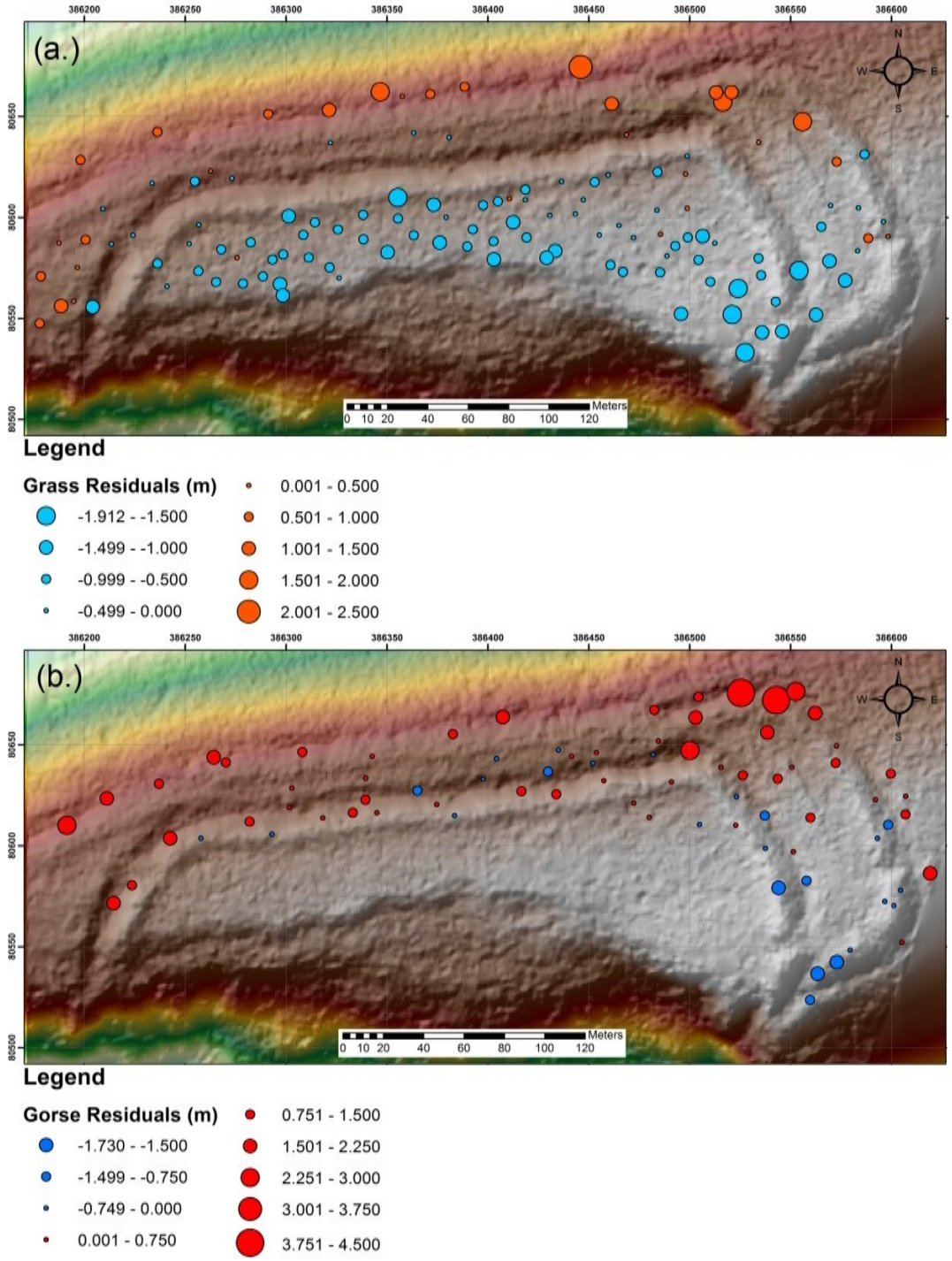

Figure 5.22: Map showing the residual distribution between GNSS and 1945 DSM elevations in (a.) grass-dominated and (b.) gorse-dominated regions.

The variation of residuals in the grass category may be explained by image noise. Upon close inspection of the 1945 imagery, it appears to be slightly blurred and there are what appear to be vehicle tracks running across the interior of the hillfort. It is in this region that the residuals vary between 0m and -1.5m, as shown in Figure 5.22. These image artifacts are likely to be inducing noise into the output from the photogrammetric software, which in turn will influence the differences between the GNSS random points and the 1945 DSM elevations.

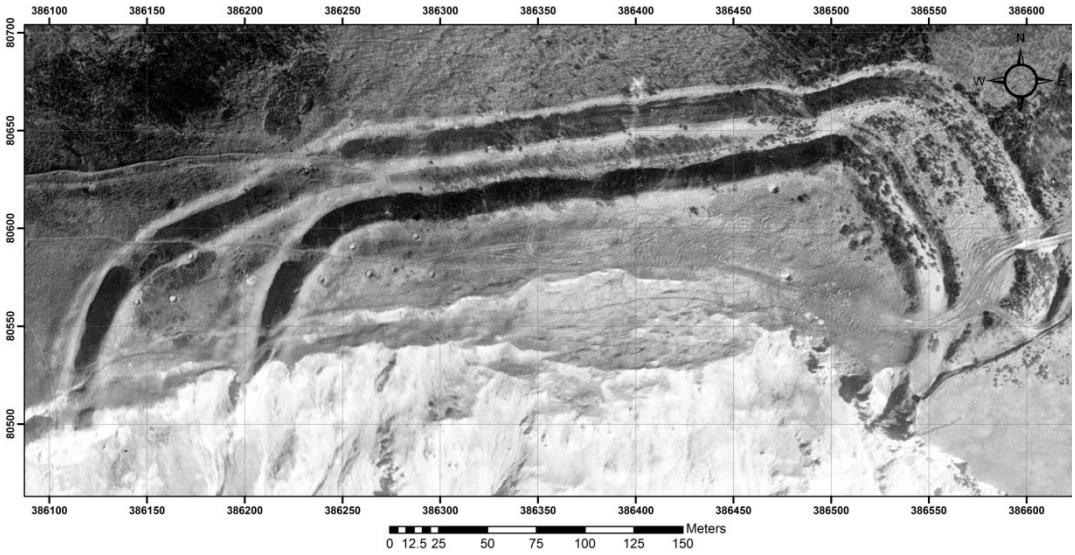

Figure 5.23: 1945 Orthophotograph.

5.6.4 Conclusion

Throughout this section there have been five principle reasons identified as to why there are significant offsets between the GNSS and SAP DSM datasets in grass and gorse-dominated regions:

i. Misclassification
ii. Increased number of outliers in the 'grass' category
iii. Noise in the data (low SNR)
iv. Shadows
v. Gradient of the rampart slopes

Whilst factors i and ii were specifically assessed, the remaining factors have been identified as further sources that require consideration when analysing the SAP DSMs in Chapters 6 and 7.

5.7 Data Analysis Discussion

The various analyses conducted during the course of this Chapter have highlighted a number of issues that may be attributable to a number of different factors, many of which were listed at the beginning of this Chapter. One of the major issues noted was the negative offset which was present within all of the SAP DSMs, the cause of which was identified as the geoid and datum settings available in SocetGXP for exporting the DSM data. The EGM96 geoid and Mean Sea Level datum will contribute a large fraction to the offset values as it has not been possible to correct for these prior to importing the data into ArcMap for interpolation and further analysis. The solution to this offset was to use the mean residual value between the SAP DSM and the

GNSS or TLS for increasing the elevations of the SAP DSM by a uniform value prior to further analysis.

The initial assessment of the 1982 DSM and its derivatives provided positive results in terms of the DSM quality for obtaining archaeological information. Terrain slope was originally thought to influence the accuracy of elevation values in regions with steep values. However, the initial comparisons between the 1982 and TLS slope derivatives indicated that there was not a noticeable difference between the two datasets, as indicated by the linear correlation in the associated scatterplots. The residual values in steeper regions of the hillfort, namely the ramparts, were much lower than those in the flatter regions, suggesting that these archaeological features were well represented in the 1982 DSM. SNR was also mooted as reducing the information content within flatter areas of the hillfort, which was noticeable in the residual image of aspect values between the 1982 and TLS datasets. However, Gooch et al. (1999) have found limited evidence linking low SNR to the accuracy of photogrammetric DSMs.

The results of Section 5.3, examining the various combinations of exterior orientation data, GCPs and image colour modes, concluded that the greyscale imagery performed optimally with only the GCPs providing the control element to the data. By merging the RGB channels of the original digital photography, the contrast from each of these separate channels provides on enhanced greyscale image. As SocetGXP performs its matching on a single colour channel these results suggest that the contrast in one single colour channel, as evidenced by the red-channel DSM result, does not provide a comparable amount of contrast to the greyscale image on which to perform image matching.

Very little could be concluded by examining the photogrammetrically scanned negative SAPs to those of the desktop scanned prints. Whilst it was not possible to conduct this analysis at the NMR due to access restrictions, the approach taken by this research project has attempted to achieve a meaningful comparison with the data in hand. Many reasons were cited for the large difference in DSM quality between the 1982 dataset and the much poorer 1986 DSM data, such as the image contrast, photo-scale, and recommended GSD settings in SocetGXP. It was, however, impossible to separate the effects of using a desktop scanner from the photogrammetric scanner without characterising the former in some way by using a glass plate.

The results of considering the singular effects of GCPs on SAP DSMs indicated that the use of control points taken from other forms of mapping, as described in Section 5.5, contributed to the horizontal offset within the DSMs. This is due to the accuracy values associated with the X and Y coordinates obtained from the OS map, as well as the uncertainly of locating the correct position of the GCP within the imagery. This is likely to be exasperated as the landscape, although afflicted by huge changes over the past 60 years, has seen subtle changes occur, such as the degradation of built structures, increased vegetation growth etc. Although some of the vertical errors can be associated with elevation uncertainties attributed to the Z coordinate, the geoid and datum options in SocetGXP have already been identified as contributing to this offset. The way in which the uncertainty values associated with the GCPs affect the DSM values can be attributed to the latitude they provide to the least squares adjustment routine. As the

degrees of freedom for positioning the SAP prior to extracting a DSM from them are high because of the large uncertainties, the constraints upon this movement is low and therefore likely to introduce errors during processing.

The final variable for consideration was the influence vegetation had on the elevation values of SAP DSMs. In Section 5.6, it was noted that many more outliers and extreme values were present in the grass categories. Although noisy data may influence this result, it is also likely that, given the subjective interpretation of where the random points were situated in relation to areas of grass and gorse, that the wrong inferences were made when looking at each SAP epoch's orthophotograph. Whilst it is likely that vegetation influence s DSM errors, as noted by other authors (Bailey et al. 2003; Green et al. 2014) or questioned by others (Gooch et al. *ibid.*), the results presented here are inconclusive.

5.8 Summary

This chapter has identified a number of variables that empirically affect DSM quality as obtained from SAPs. Whilst using the highest quality GCPs is demonstrated to provide superior results, as is obtaining digital imagery from photogrammetrically scanned negatives, the remaining results have led to the conclusion that an experimental approach is required when generating DSMs using SAPs.

6 PILOT STUDY: FLOWERS BARROW HILLFORT

6.1 Introduction

This Chapter presents the results from processing SAPs obtained of the Flowers Barrow pilot study site. It begins with an overview of the site's geology, geomorphology and archaeology in Section 6.2 before describing the SAP data processing stage in Section 6.3, beyond the generic approach described in Section 4.4 of Chapter 4. Sections 6.4, 6.5, 6.6 and 6.7 contain the results and analysis, whilst the Chapter ends with a discussion in Section 6.7.3.

6.2 Study Site Background

6.2.1 Site Overview

Flowers Barrow is an Iron Age hillfort, situated in Worbarrow Bay (Figure 6.1), Dorset, which forms part of the Jurassic Coast (Dorset and East Devon Coast World Heritage Site, England's first natural World Heritage Site designated UNESCO) and is located within the Defence Estates Bindon and Tyneham Ranges. The geology of Worbarrow Bay is comprised of limestone, mudstone and chalk, which is discussed in Section 6.2.3. It is illustrative of the preferential, or rapid, erosion of the limestone, forming a wide mouth to what was once two separate coves, which have since coalesced (Goudie and Brunsden 1997). The formation of Worbarrow Bay was thought to be assisted by its previous incarnation as a drowned river valley, created by rivers that, as stated by Goudie and Brunsden (*ibid* p.30) would have "flowed out to sea through a valley in the Portland and Purbeck stone". This bay is now a dry chalk valley, with no evident surface flow of water. Flowers Barrow hillfort is situated on a limestone ridgeway that rises from Lulworth Cove to Kimmeridge to a height of 165m Ordnance Datum (Wessex Archaeology 2001).

6.2.2 Land Use

Flowers Barrow and its environs are currently situated within the boundaries of the Lulworth Range, owned by the Ministry of Defence (Defence Estates). Flowers Barrow was deemed to be a Scheduled monument on the 4th October 1932 and was referred to as 'Flowers Barrow Camp' (Hanks 2012). Lulworth and Bovington are home to the Army's Armoured Fighting

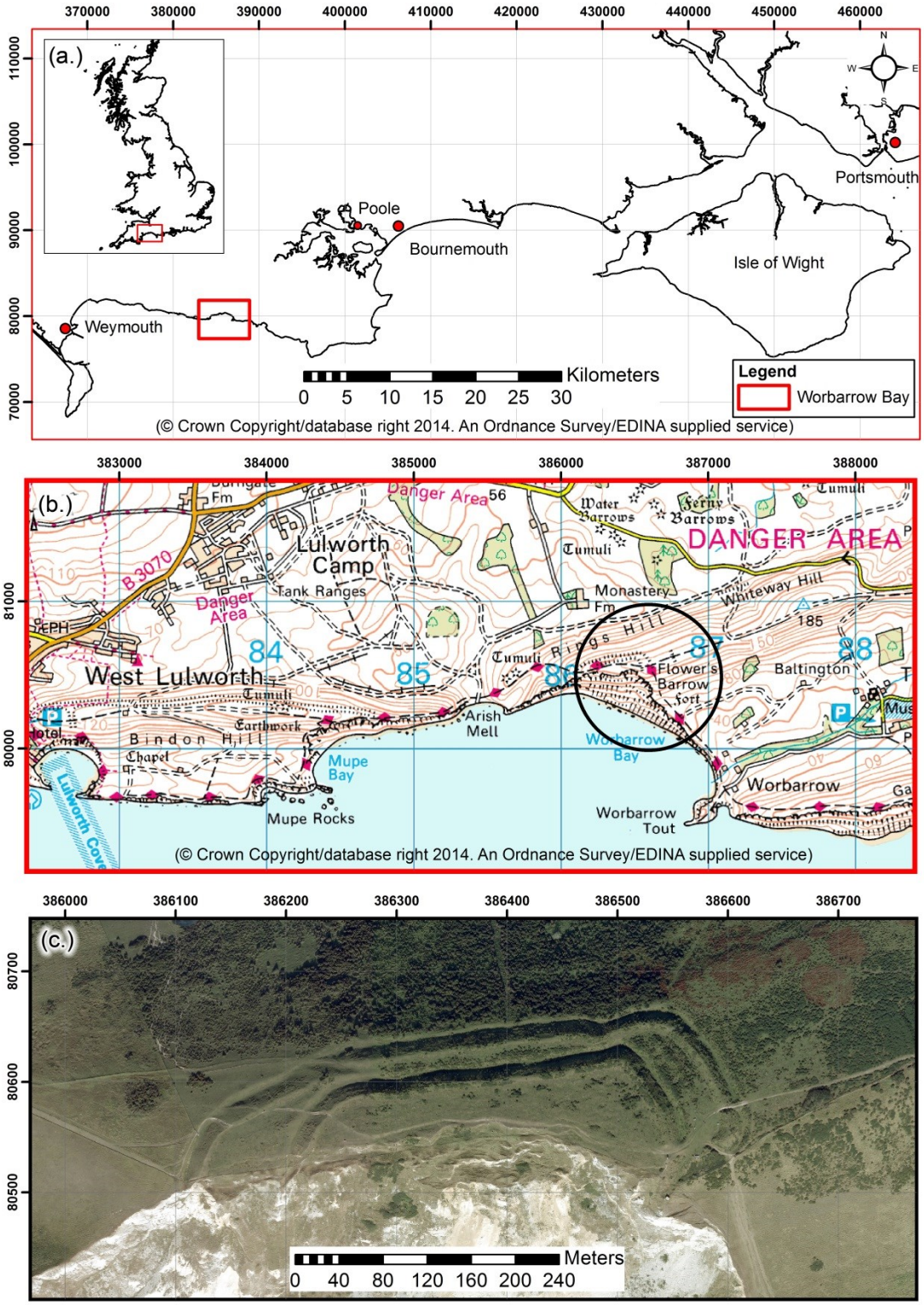

Figure 6.1 Map showing (a.) location of Worbarrow Bay within the UK, (b.) local topography and infrastructure and (c.) orthophotograph of Flowers Barrow hillfort.

Vehicles (AFV) and Gunnery School, with gunnery practice having been conducted in the Lulworth area since 1866, if not earlier (Wessex Archaeology *ibid.*). The Bindon range was first utilised for training in 1916, while the Heath Range and Tyneham village and valley were acquired for army training during WWII (Wessex Archaeology *ibid.*).

In a desk-based assessment and monument condition survey conducted by Wessex Archaeology in 2001 (*ibid.*), the Lulworth range was stated to be little understood because of its use as a firing range since the 1940s. Whilst the range is still used for this purpose to this day, some agricultural practices have been allowed in certain areas of the range. The area surrounding Flowers Barrow is under permanent pasture, with the tenant farmer occasionally using the Hillfort as an area on which to graze cattle (Hanks *ibid.*). The Monument Inspector for this region does not believe that the erosion caused by grazing is bad, although there is noticeable erosion to the monument where a public footpath and vehicle track cut through the ramparts near the south. However, as the range is only open to the general public at limited times, such as weekends and school holidays, although access to the monument is limited to the marked footpath. Further exploration of the Hillfort is not permitted as the army only clear the designated routes through the range of any ordnance prior to allowing public access. Straying beyond these paths is strictly prohibited with exceptions made to contractors and other parties who have sought permission for site access through Range Control.

6.2.3 Geology and Geomorphology

The chalk ridge on which Flowers Barrow sits was formed by geological folding (Brunsden 2003). The rocks forming Worbarrow bay within which Flowers Barrow is situated, is formed from predominantly Cretaceous rock (see Figure 6.2). The Hillfort sits on top of middle and lower chalk geology, the most recent geological layer here, which has been deposited atop an Upper Greensand and Gault layer, formed earlier than the chalk in the Lower Cretaceous period. Beneath this lies the Wealden Group layer, said by Hart (2009) to be comprised of multi-coloured sandstones, grits and clays and well-exposed at the cliffs in between the landslide and Worbarrow Tout. The chalk layer was formed during the Upper Cretaceous period, between 60 to 100 million years ago, and is soft and porous, containing little flint, with the middle chalk layer said by West (2013) to be nodular.

The Greensand and clay Gault layer was formed 100 to 110 million years ago, during the Albian age of the lower Cretaceous period, and is likely to be a cause of landslides at Worbarrow bay as it is a soft layer (West *ibid.*). It has a dark appearance, which looks stark against the chalk layer, with the Gault consisting of silty clay or loam (West *ibid.*). The Wealden Group are older still and were formed during the lower Cretaceous, between 125 to 140 million years ago. At Worbarrow Bay, the Wealden beds are comprised mostly of clay, with quartz grit running through the middle of the group (Hart *ibid.*). Figure 6.3 illustrates the proposed development sequence of Worbarrow Bay.

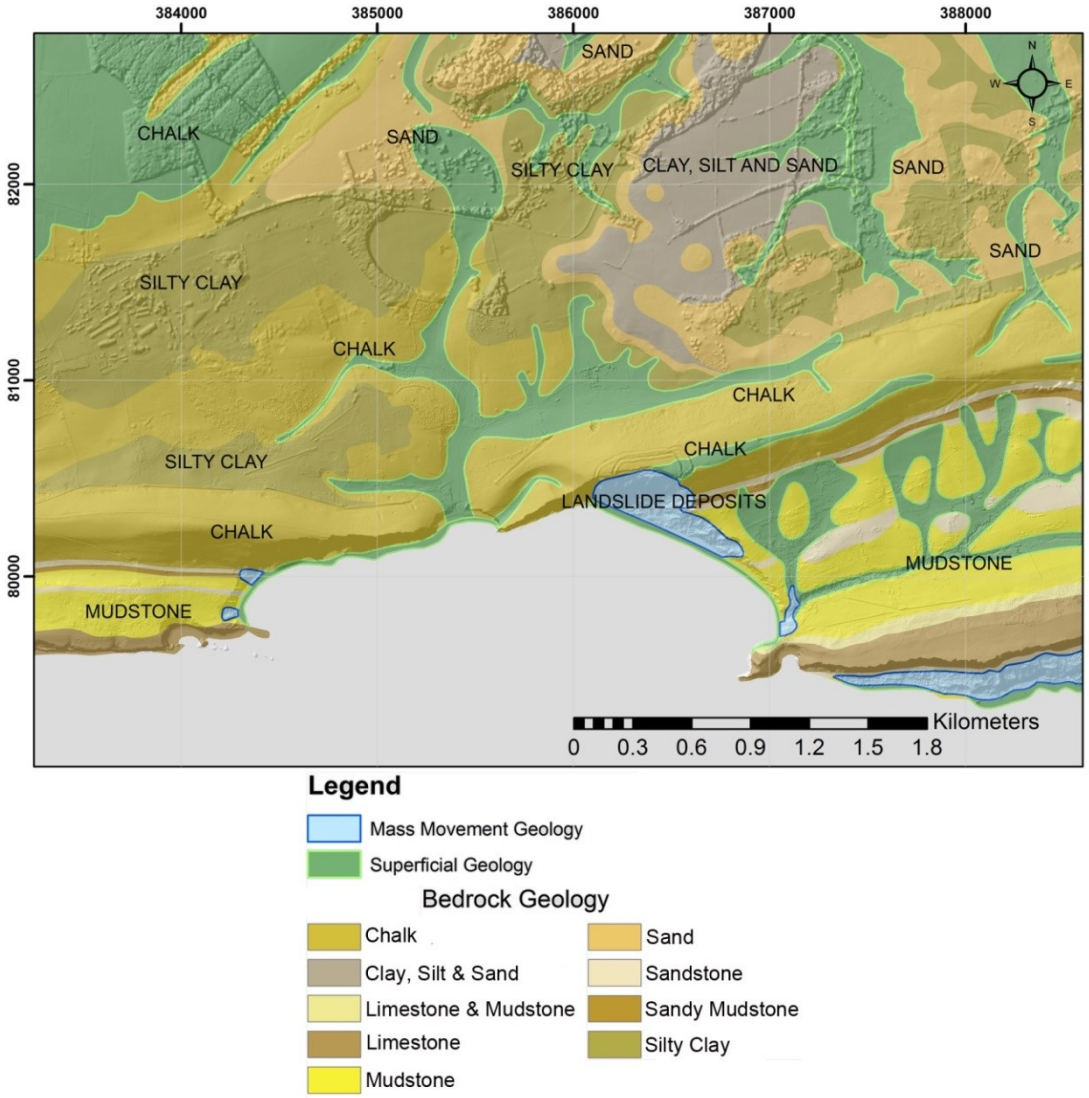

Figure 6.2: Geology Map of Worbarrow Bay (© Crown Copyright/database right 2014). An British Geological Survey/EDINA supplied service).

The topography and geology of the region are said to have influenced land use over time, with the topography of the area ranging from c.25m to 190m OD (Wessex Archaeology *ibid.*). Many of the settlement sites are found on the Upper Chalk outcrop, and it is on this geology that Flowers Barrow resides. West (*ibid.*) believes that Rings Hill, on which Flowers Barrow sits, may have retreated by up to 400 to 500m in the last 2000 years, due to the exposure of the cliffs here to south-westerly storm waves. The author states that this could be a record rate for southern coast chalk cliffs.

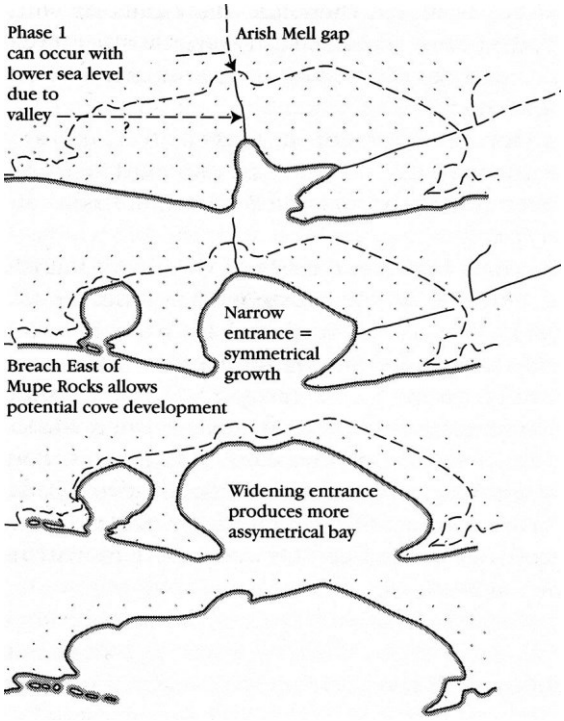

Figure 6.3: Image illustrating the formation of Worbarrow Bay as presented by May (2003).

6.2.4 Archaeology

Flowers Barrow is an Iron Age Hillfort, the likes of which are stated by EH (Hanks 2012) to have been constructed and 'occupied between the sixth century BC and mid-first century AD'. The ramparts at Flowers Barrow are described as multivallate defences and were once to be found inland of their current position. However, in the present day, the hillfort has lost its southern defences due to coastal erosion. The Internal Report for this monument (Hanks *ibid.*) refers to this missing section as the 'southern third' that would have been surrounded by two sets of banks and ditches, including a counter-scarp, although how certain this can be is questionable. However, the removal of the southern defences had occurred by 1744 (Royal Commission on Historic Monuments 1970), which could indicate that there has not been a significant loss of material from Flowers Barrow in c.300 years since. Forde-Johnston (1976) describes the site as being semi-contour in style, explaining that whilst the north and west ramparts adhere to the line of the contours defining the hill itself, the eastern defences cut across them and head across the hill top instead.

Slightly further to the east of the hillfort, an outer bank and ditch can be found, as shown on Figure 6.4, described by the Royal Commission on Historic Monuments England (RCHM) survey of 1970 to be a cross-ridge dyke, which is thought to be related to the defences of the Hillfort (Hanks *ibid.*). The feature is not particularly pronounced; its bank is said to be approximately 0.75m high whilst the ditch has a reported depth of 1m (Hanks *ibid.*). It has been suggested that the cross-ridge dyke could be of Bronze Age origin, meaning that it pre-dates

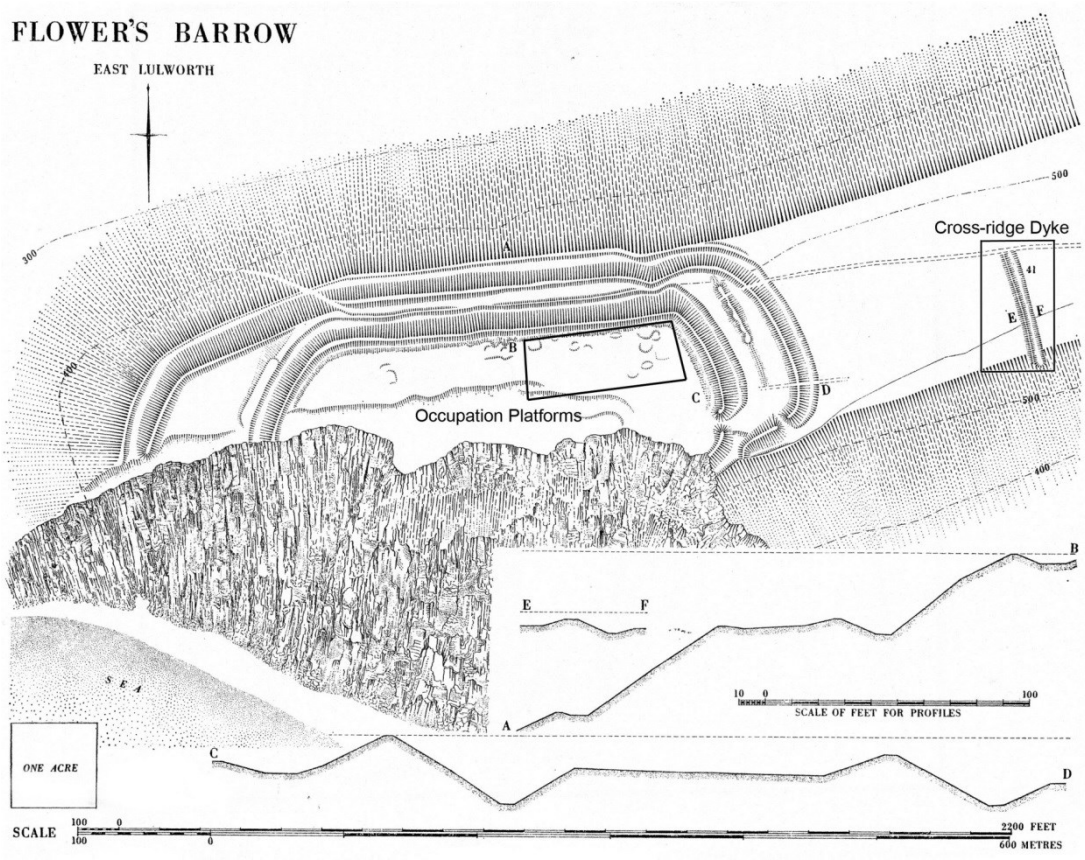

Figure 6.4: Hachure Plan produced by the RCHM (1970) illustrating the multivallate ramparts, with the occupation platforms and cross-ridge dyke indicated.

Occupation of the hillfort is suggested by a number of different features. The first are the annexes of the east and west ends of the hillfort, which are postulated to be areas for stock control (Hanks *ibid.*). The eastern annex contains a linear earthwork that follows the line of the ramparts, although there is no use suggested for this. Within the ramparts remnants of occupation platforms and pit sinkings were apparent in 1970 (Figure 6.4), mostly found in the north-east of the interior, although no investigation has been undertaken to fully discern their broader use. The occupation platforms have been observed along the north-facing slope in the interior, tending towards the eastern end of the monument, and are described as being elliptical in shape (Royal Commission on Historic Monuments *ibid.*). The pit sites are no longer visible, although an excavation of one was conducted in 1939, prior to the threats posed from buried, unexploded ordnance. Finds from the pit excavation consisted of bone and pottery fragments, and a few 'sling-stones', the results of which were published by Calkin (1948). Wessex Archaeology (2001 p8) report that a human skeleton was found buried beneath one of the outer ramparts at the western end of the site, which the RCHM (1970) refer to as being of 'abnormal length' and, as a contradiction, discovered just below the surface of one of the inner ramparts. This is in reference to a document by Pennie (1827), although a copy of this document cannot be sourced to investigate the accuracy of this claim. It is frustrating that no further discussion or documentation appears to exist in relation to this particular discovery as it would lend further insight into the uses and practices conducted at this mysterious site.

Other features are visible in the landscape within the locale of Flowers Barrow. 'Celtic' field systems are noted in the immediate vicinity to the north-west and north-east of the hillfort. They are stated to be small, 'squarish' and irregular fields, denoted by lynchets that follow the contours of the topography (Royal Commission on Historic Monuments *ibid.*). Further south, following the line of Worbarrow Bay, more field systems and strip lynchets are visible. To the south-east of the hillfort, Worbarrow Tout contains an earthwork resembling a rampart that is situated near the isthmus, which is the narrow strip of land that connects the peninsula of the Tout with the mainland (Royal Commission on Historic Monuments *ibid.*), a detail that is also referred to by Hutchins (1861).

In an assessment of its importance, included as a part of the Internal Report (Hanks *ibid.*) for this monument, Flowers Barrow is classified as a small multivallate hillfort, the likes of which are rare in national terms, with only 100 examples thought to exist. They are predominantly found in the Welsh Marches and south-West England, with a small number situated in the North-East (Hanks *ibid.*). Subsequently, Flowers Barrow forms part of a nationally important group of monuments that are of great importance in the understanding of Iron Age settlement and social organisation (Hanks *ibid.*). Many of these smaller hillforts were thought to have been occupied continuously throughout their use, and are thought to be a high-status settlement (Hanks *ibid.*). Due to the lack of excavation that has been conducted here, and is likely to remain so given that military operations in this area have made it dangerous to consider doing so, dense topographic survey, as provided by photogrammetry and laser scanning, are the best hope of further enhancing the evidently subtle features that exists at Flowers Barrow and increasing the understanding of this site.

6.2.5 Site Condition

The southern edge of the hillfort is actively eroding and has been truncated since its construction (see Figure 6.1c), with a third of the monument estimated to have been destroyed due to cliff retreat (Royal Commission on Historic Monuments *ibid*, Wessex Archaeology 2001). Although no figures are available to support this estimate, a document referred to by the RCHM (*ibid.*), held in the Dorset County Records Office and dated pre-1744, refers to the effects coastal erosion has had on the monument by this time. However, the Lulworth Range has been used by the military since 1866 (Wessex Archaeology *ibid.*), thus Flowers Barrow has enjoyed the benefits of its location in an access-restricted area. Coupled with the lack of agricultural activity on the site, save for the occasional use as pasture, and the presence of permanent penning, the remainder of the hillfort structure has been remarkably well preserved and is considered to be stable. Based upon information contained within the Internal Report (Hanks *ibid.*) Flowers Barrow is considered to contain archaeological remains beyond those already discovered through excavation, which include environmental artefacts that will provide evidence relating to the "economy of the site's inhabitants and the landscape in which they lived". However, performing further excavation is almost impossible given the use of the area as a

firing range for the MoD, as the unknown locations of a large amount of unexploded ordnance prohibits any digging. Subsequently, the further investigation of the area surrounding Flowers Barrow is likely to benefit from high-density topographic survey, such as ALS, TLS and photogrammetry, to identify or confirm the presence of smaller earthworks as well as provide a means by which to record them.

Earthworks within the boundaries of the Lulworth Range, which includes Flowers Barrow, have benefited from the lack of arable agricultural practices as well as limited public access and thus their state of preservation is good. Despite the inclusion of Flowers Barrow within an army range used for shelling practice and training tank drivers (see Figure 6.5a), there is negligible evidence for such damage on the monument and ploughing has not been undertaken within or immediately surrounding the site. In 1992 an additional comment was added to the EH Internal Report (Hanks *ibid.*) stating that the monument was under permanent grass and is being utilised by a tenant farmer to graze his cattle, although damage related to this activity is not considered to be detrimental. Gorse coverage of the monument is relatively thick in some areas of the Hillfort, most notably in the north-east corner, although it is not thought to be damaging the monument (see Figure 6.5b). Whilst its presence may cause minor occlusions in ALS and photogrammetry data, the majority of the Hillfort is not afflicted by gorse.

Based on the desk-based assessment and monument condition survey conducted by Wessex Archaeology (*ibid.*), causes of damage to the monument are cited to be footpath erosion (see Figure 6.5c), vehicle movement and rabbit burrowing, the latter of which does not have a large and immediate impact upon the monument, although this is expected to have longer term implications that will be far less severe than those posed by coastal erosion processes. Whilst footpath erosion caused by visitors to the site has been highlighted in the condition report conducted by Wessex Archaeology (*ibid.*), public access to Lulworth Range is restricted to most weekends and the more important school holidays throughout the year, therefore such damage is not as extensive as it otherwise could be. Subsequently, Flowers Barrow has enjoyed a significant level of protection due to its situation within an access-restricted Defence Estates military range. Aside from the gradual erosion of the monument by coastal erosion, for which no measurements or estimates of attrition rates are given, Flowers Barrow is considered to be “in good condition and moderate decline” (Wessex Archaeology *ibid.*, p.30) and thus suitable for this pilot study.

Figure 6.5: Site condition at Flowers Barrow (a.) unexploded ordnance, (b.) gorse vegetation and (c.) footpath erosion.

6.2.6 Potential Change Due to Mass-Movement

The failure mechanisms for Worbarrow Bay are from erosion, rock falls and slides (DEFRA 2002). Wave action at the base of the Wealden clays is thought to be causing cliff overhangs in certain places between Worbarrow Tout and heading west towards Lulworth Cove (DEFRA *ibid.*), and it is in the regions characterised by this geology that the most rapid erosion is expected to take place. The Futurecoast project states the site is sensitive to climate change, with recession potential expected to reach a medium rate (0.5-1m/yr) with a low risk of a single landslide event (up to 10m) (DEFRA *ibid.*). This rate of recession suggests an increase in the estimate provided by West (2013) as stated earlier in Section 6.2.3, who suggested that the site had receded by 400-500m in the last 2000 years; a rate of 0.2-0.25m per year. The frequency of a recession event is expected to be between less than 1 year to between 1 and 10 years, although the uncertainty in this prediction is high (DEFRA *ibid.*). However, as illustrated by the DSM in Figure 6.6, change of up to 8.5m has been detected using the CCO ALS data, particularly in the cliffs beneath Flowers Barrow, which illustrates the change that took place within a year between 2008 and 2009. This DSM was produced by subtracting the 2008 DSM from the 2009 DSM using ArcMap 10.

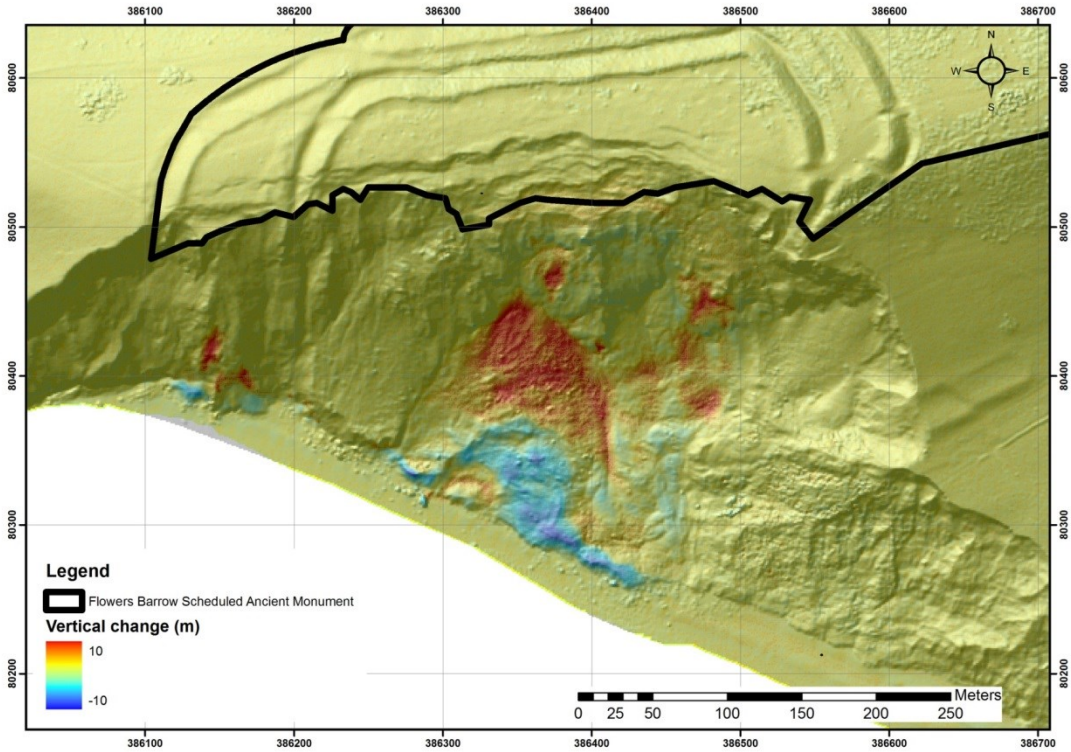

Figure 6.6: Difference model calculated using ALS data from the CCO, identifying and quantifying regions of change during the period 2008 to 2009 beneath Flowers Barrow in Worbarrow Bay (Image courtesy of Channel Coastal Observatory (www.channelcoast.org).

Brunsden (1996) states that knowledge is limited when it comes to the “geomorphological processes and the geotechnical properties of the materials” within landslides. Brunsden (*ibid.*) also states that the spatial coverage and temporal extent of data to monitor the Worbarrow mudslide at the time of writing in 1996 was extremely limited, suggesting that the regular application of mass-capture techniques to document this feature would be of great benefit to it.

The SMP policy for Worbarrow bay is ‘do nothing’, although one of the listed objectives states that minimisation of the “adverse impact upon areas of historical and archaeological interest” should be undertaken (Portland Bill to Durlston Head Coastline Group 1998). Therefore Worbarrow Bay is a great example of the potential application of the same mass-capture techniques for preservation by record.

6.3 Notes on Data Processing

The nature of archive SAPs is such that at each site there may be slight alterations to the workflow as described in Section 4.4.1 of Chapter 4. Based on the results obtained from the absolute orientation of the 1945 SAPs of Flowers Barrow, the terrain contained a slant that ran from east to west, which was exhibited in a ground elevation on the beach being -25m towards the east side of the beach, but -40m to the west. To address situations like this, the solution was to add GCPs to the beach, but with Z-values only, that ranged somewhere between 1m and 5m to more accurately convey the elevations found here. Each time the triangulation solve was run, the various error results were checked: Image RMS (in pixels), and the RMS of the XYZ values (in metres). If these were considered to be too high, the image accuracies were either loosened, some tie points considered to have a high error value were manually deleted and, in exceptional circumstances, a minute number of GCPs were deactivated. Ultimately, the aerial triangulation solution returned by the software was repeatedly run to obtain the best result possible from the data. The triangulation results and the DSM GSD, circular and linear error values returned by the terrain extraction routine, obtained for each of the SAP epochs in SocetGXP, are given in Table 5.14 in Section 5.6.2. The result of performing registration of the TLS dataset for Flowers Barrow returned a mean absolute error of 0.083m.

6.4 Elevation Assessment

Elevation data is used by archaeologists for a number of purposes, including the identification and analysis of sites from aerial photography and ALS data, the production of hachure plans, and the transcription of breaklines, for example. Whilst photogrammetry has rarely been used for extracting such information, except in situations where the photography is produced concurrently with a particular project (see Section 2.2.3), SAPs have hitherto remained

unappraised for their ability to generate such data. It is important to ascertain whether SAPs can be used to produce the earthwork metrics required by archaeologists, particularly if a site has been damaged or destroyed before it has been fully recorded.

In this Section the elevation data from the photogrammetrically scanned negatives, namely 1945, 1968, 1982 and 2009 epochs, will be compared with TLS data to provide a number of summary statistics, graphs and information graphics. These data will allow the comparison of SAP DSMs with a dataset that provides the most accurate means of creating a terrain model of archaeological earthworks, namely the TLS. Prior to undertaking analysis of the four SAP epochs, a mask was produced to ensure that the TLS and SAP DSMs were all of the same shape and size. This would assist in conducting the census analysis of each datasets as the size and extent of each DSM would be identical. Aside from the 1982 DSM in which an elevation and horizontal offset had been identified and addressed, the remaining DSMs did not require any horizontal correction, although the 1945 and 1968 DSMs were corrected for vertical offsets. The extent of the mask and the variation between the DSM epochs and the TLS can be seen in Figure 6.7, which shows each DSM epoch underlayed by its own hillshaded raster.

The 1945 and 1968 datasets contain the greatest level of noise, as evidenced in the 1945 data by a mottled effect occurring over the entirety of the hillfort. The appearance of noise in the 1968 DSM is akin to a TIN surface, with large smooth patches that are bordered by others with a greater or lesser elevation and stippled effects along the ramparts. This can be explained by examining the point density as exported from SocetGXP for each of the SAP epochs, as shown in Figure 6.8. As the point density is sparse for the 1968 SAPs, the natural neighbour interpolator has struggled to populate these gaps. The remaining DSMs produced by the 1982 and 2009 SAP DSMs, the 2009 November ALS and the 2012 TLS data do not exhibit such obvious artifacts, but there are subtle variations between them. The TLS contains the most detail; in particular the occupation platforms can be seen quite clearly in the interior of the hillfort. These features are very subtle in the 2009 ALS but they can still be identified, whilst they cannot be readily distinguished in the 2009 and 1982 SAPs.

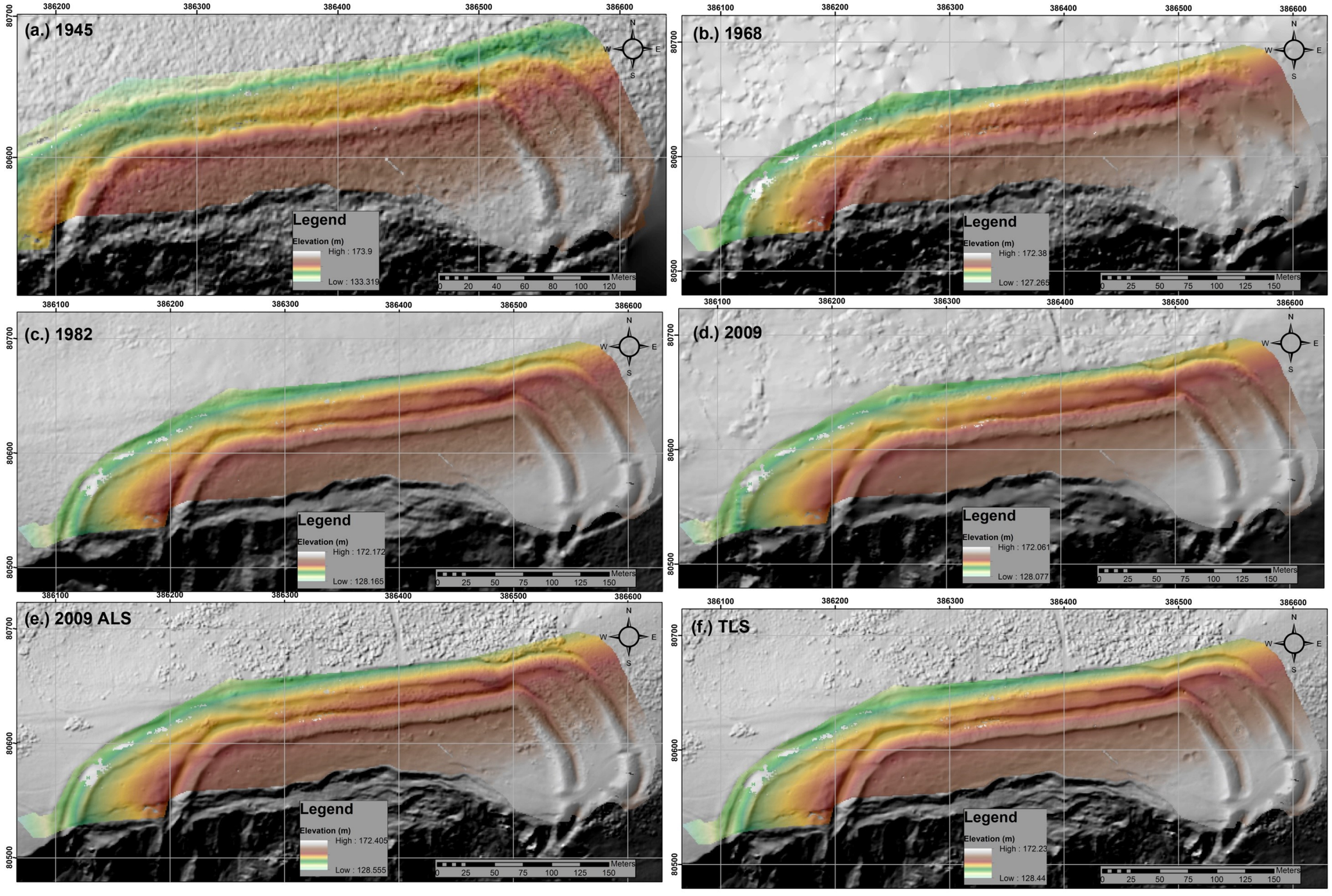

Figure 6.7: DSM elevations for the Flowers Barrow SAP epochs (a.) 1945, (b.) 1968, (c.) 1982 and (d.) 2009, (e.) 2009 ALS and (f.) the TLS.

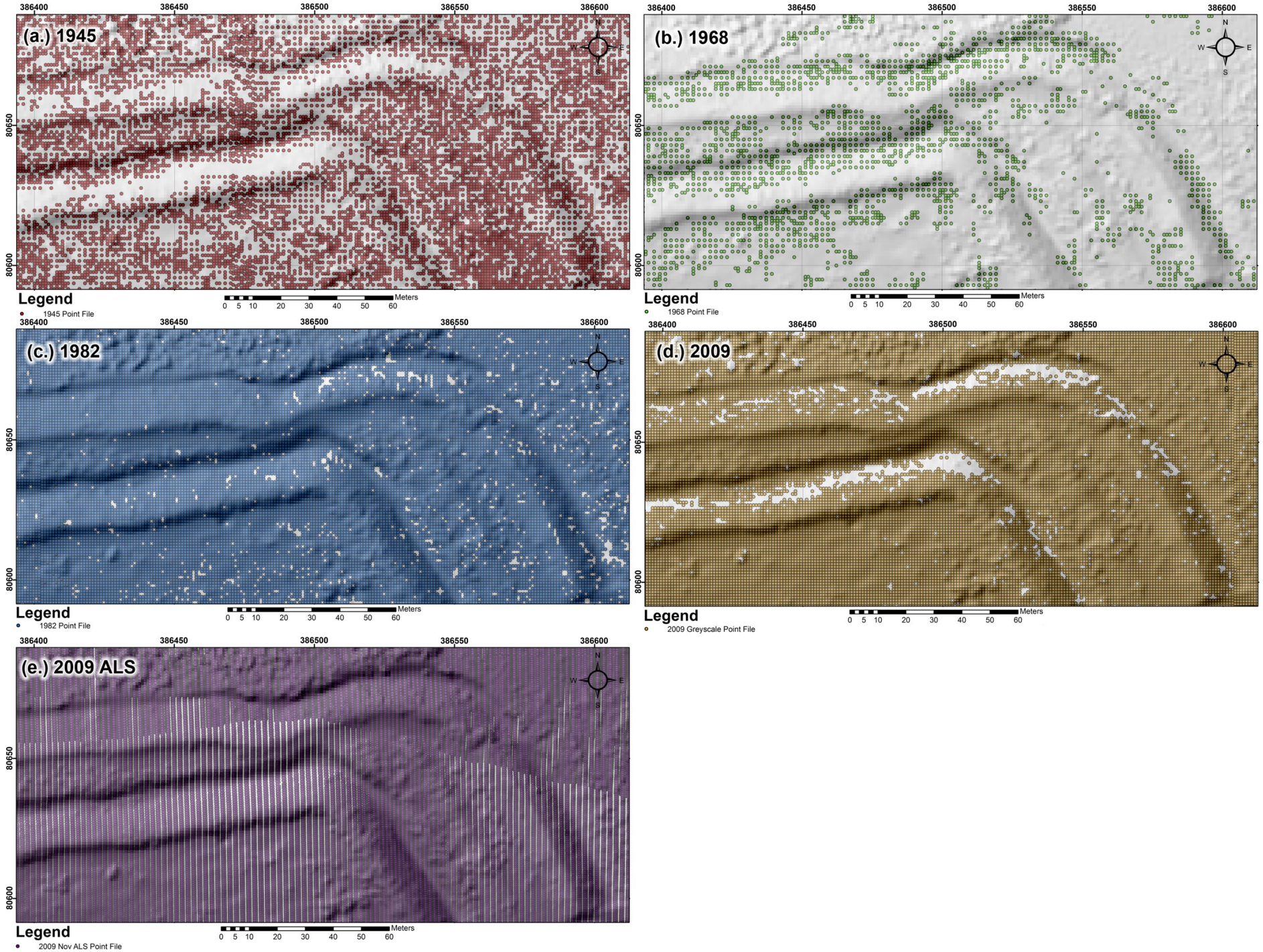

Figure 6.8: SAP point densities from (a.) 1945, (b.) 1968, (c.) 1982, (d.) 2009 as output from SocetGXP in comparison with (e.) the ALS point cloud.

To establish the variation between each dataset, all of the elevation values were extracted using the mask in ArcMap and subsequently exported for viewing in Excel. The residual elevation values for each of the elevation datasets were calculated by subtracting them from that of the TLS. The Excel spreadsheet was opened in SPSS to perform statistical analysis, a summary of which is given in Table 6.1. The 1945 DSM contains slightly fewer values than the others, reflecting a number of missing values which have been caused by gaps in coverage due to the 1945 photographs not completely overlapping in the extreme east and west regions of the hillfort.

As has been previously stated in Section 3.4.2, some of the most frequently examined statistical values for assessing DSMs are the ME, SD and RMSE. However, on comparison of these values for each epoch, as provided in Table 6.1, many of them appear favourable. The mean values for 1945 and the 2009 SAPs are 0.035m and -0.097m respectively, whereas it was expected that the ALS would be the most comparable with the TLS data. Instead, the 2009 ALS has a mean value of 0.399m, which is the highest of the entire group. This could be an indication of a larger number of outliers in this dataset, which would increase the mean value. However, the mean elevation difference between the GNSS and ALS datasets has not been removed from the ALS, unlike for the SAP DSMs, which also explains this result. The standard deviation for the ALS is the second lowest at 0.394m, with the 1982 DSM the best performer at 0.213m. Unsurprisingly, the 1945 and 1968 datasets are the worst performing with values of 1.204m and 0.741m respectively. There is evidently a greater range of variation within these datasets, which is confirmed by their high variance values of 1.450 and 0.550.

		TLS MINUS 1945	TLS MINUS 1968	TLS MINUS 1982	TLS MINUS 2009 GreyGCPs	TLS MINUS 2009 NovALS
N	**Valid**	47361	51759	51759	51759	51759
	Missing	0	0	0	0	0
Mean (m)		0.035	-0.163	-0.126	-0.097	-0.399
Std. Error of Mean (m)		0.006	0.003	0.001	0.003	0.002
Median (m)		-0.134	-0.278	-0.096	0.046	-0.276
Mode (m)		-1.1294	-0.204	-0.122	0.057	-0.135
Std. Deviation σ (m)		1.204	0.741	0.213	0.619	0.394
Variance		1.450	0.550	0.046	0.383	0.155
Skewness		0.578	1.341	-0.484	-1.308	-1.163
Std. Error of Skewness		0.011	0.011	0.011	0.011	0.011
Kurtosis		0.485	3.706	1.436	1.874	1.182
Std. Error of Kurtosis		0.023	0.022	0.022	0.022	0.022
Range (m)		8.780	7.504	3.499	4.771	3.613
Minimum (m)		-4.133	-2.918	-2.195	-3.197	-2.639
Maximum (m)		4.647	4.586	1.304	1.573	0.974
RMSE (m)		1.205	0.759	0.248	0.626	0.561

Table 6.1: Summary statistics for the residual values between the TLS dataset and each of the photogrammetrically scanned SAP epochs.

The RMSE was calculated in Excel by using the following formula:

RMSE = SQRT(SUMSQ(J2:J142)/COUNTA(J2:J142))

The 1945 and 1968 DSMs have the highest RMSE values, which is to be expected given the age of the imagery and the sparse number of points generated by SocetGXP on which to preform interpolation. The 1945 imagery was not produced on a metric camera; this equipment was not in use by the military at this time. Whilst no interior orientation data exists for any of the SAP datasets, bar the 2009 digital photography, the camera systems that took the photographs from 1968 onwards were metric, and thus were manufactured to create minimal distortions. This is not the case for the 1945 imagery, and it is therefore unsurprising that the performance of this dataset is the poorest. However, both of these datasets do contain scratches and other defects, which can be seen in Figure 6.9.

The histograms produced in SPSS illustrate the distribution of residual values and are shown in Figure 6.10. Aside from the 1982 dataset (Figure 6.10c.), the remainder all exhibit skewness, and thus the residuals are not distributed symmetrically throughout the DSMs. The spread of residuals is much greater in the 1945 data (Figure 6.10a.), ranging from -4.133m to 4.647m and is predominantly skewed to the right. There are subsequently fewer residual values in the positive region which indicates that the mean is greater than the median and therefore the mean is not a good predictor of central tendency in the data. The kurtosis value is the lowest of the set, which is likely to be caused by the large residual range. Although this result suggests that the DSM resolution is good, the data clearly exhibits noise. However, there is no information about the spatial distribution of the residuals. The 1968 DSM (Figure 6.10b.), whilst also exhibiting a greater amount of positive skew, has a leptokurtic, or more 'peaked' frequency distribution of the residuals. Based upon this observation, the 1968 DSM might contain less noise but potentially lower resolution.

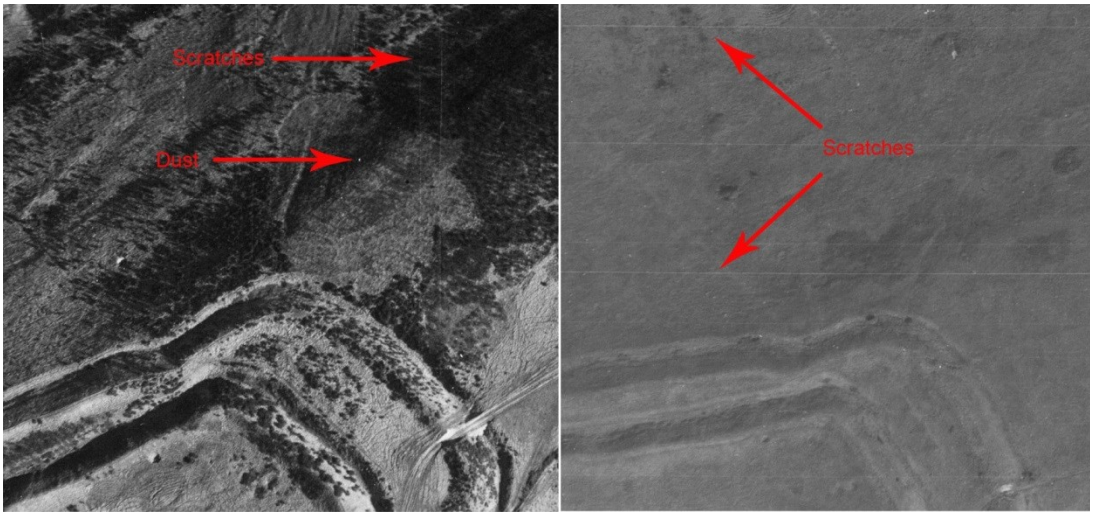

Figure 6.9: Examples of defects that are visible in the 1945 SAPs (left) and the 1968 SAPs (right).

The 1982 dataset has the lowest residual range, exhibits minimal skewness and has a leptokurtic appearance. The peak is higher and sharper than the other datasets and thus there is minimal variation within the 1982 DSM. This is to be expected given the procedures conducted on this data to remove both the elevation and horizontal offsets in the data. The 1982 photographs do not display any form of degradation, unlike the 1945 and 1968 images, and the image scale is also the largest at 1:8000, thus details are more discernible. It is to be expected that the 1982 DSM performs favourably. The 2009 SAP (Figure 6.10d.) and ALS (Figure 6.10e.) datasets both exhibit negative skew, although the SAP DSM has a much larger range of residual values that extends further into both the positive and negative portions of the graph as compared to the ALS. Whilst both the 2009 ALS and SAP DSMs contain the largest number of their residuals within the -1m to 1m range, because the SAP DSM has a larger residual range, it appears to have a less pronounced leptokurtic peak.

To fully establish how residual values from each SAP and ALS DSM are distributed in respect to TLS elevation values, DSMs of Difference (DoD) were created and are shown in Figure 6.11, whilst scatter plots were also produced, as shown in Figure 6.12. The 2009 SAP and ALS datasets appear to be similar in the shape and distribution of their residual values, as shown by both their respective DoDs (Figure 6.11d and e.) and scatter plots (Figure 6.12d and e.). The majority of the negative residuals are found along the north and east facing slopes of the ramparts, to the east, north and west of the hillfort. It is in these areas that the ALS and SAPs have elevation values higher than those of the TLS. The ALS residual image appears to be slightly more noisy, particularly towards the eastern end of the hillfort (see Figure 6.12e), as indicated by the blue speckled effect. This is likely to be caused by the presence of vegetation as the TLS has been filtered to remove as much of the gorse as possible, whilst the ALS has not been filtered. Despite the use of last return data, it is unlikely that the laser pulses have been able to penetrate the thick shrub.

As indicated in the histogram (Figure 6.10d.), the 2009 SAP DSM contains a greater range of negative residual values which, based upon the summary in Section 5.7, is likely to be attributable to the quality of the GCPs, although the influence of vegetation cannot be completely ruled out. This is especially so as the areas in which the negative residuals are found in the 2009 ALS and SAP DSMs are covered by gorse, although the height of the gorse will not be equal to the greatest residual offset value of 3.197m. However, the range of colours depicted in the DoDs is somewhat deceptive. Although they highlight where the elevation differences occur for each DSM, many of the values across the hillfort are more subtle, and thus many of the residual values along the ramparts are between -1m and -2m. If many of the residuals are removed that do not appear to form part of the large body of values, as highlighted in the scatter plots in Figure 6.12, the appearance of the 2009 ALS and SAP DSMs would be extremely similar.

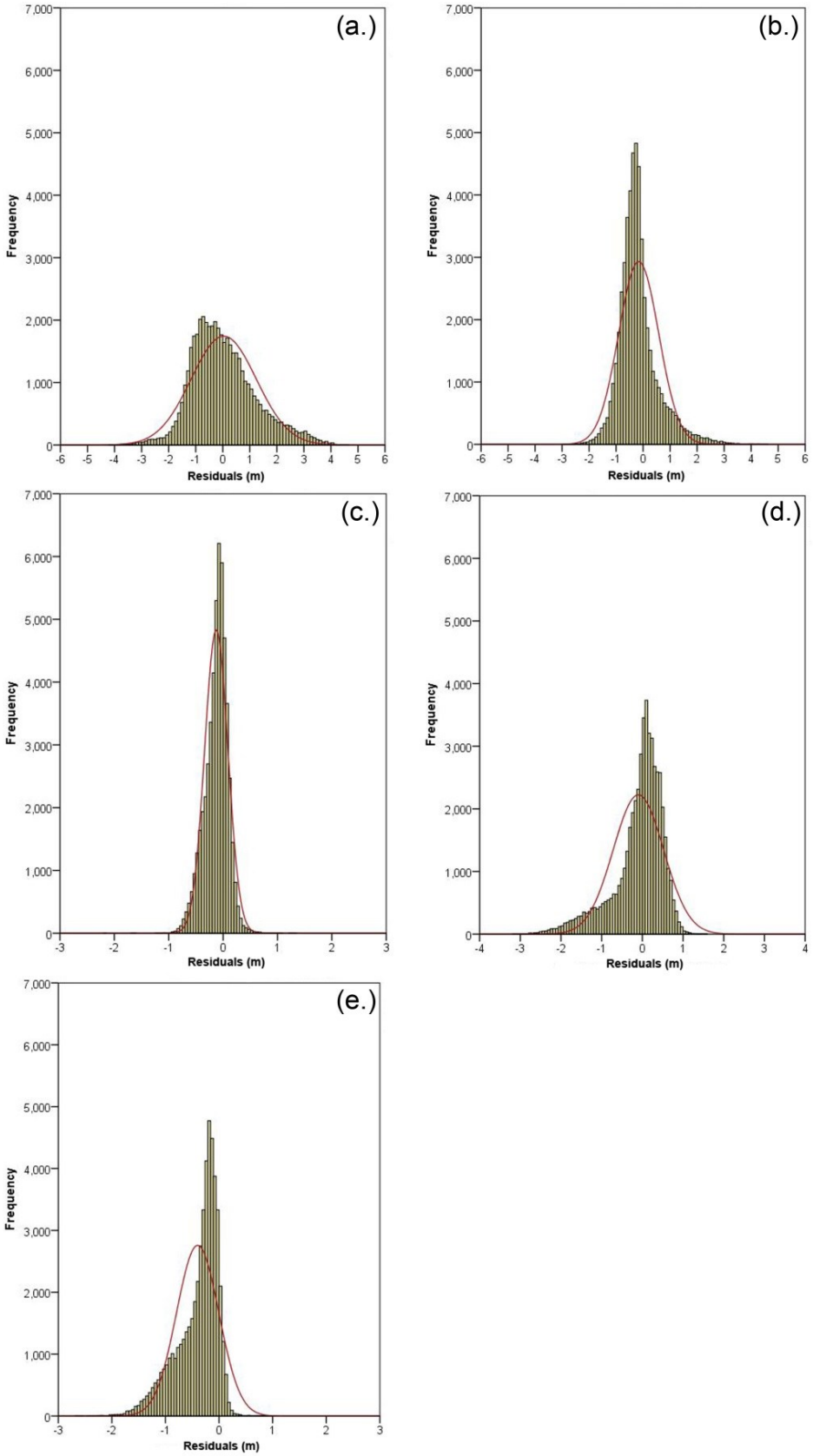

Figure 6.10: Histograms showing the residual distribution between the TLS dataset and the (a.) 1945 SAP DSM, (b.) 1968 SAP DSM, (c.) 1982 SAP DSM, (d.) 2009 SAP DSM and (e.) November 2009 ALS DSM.

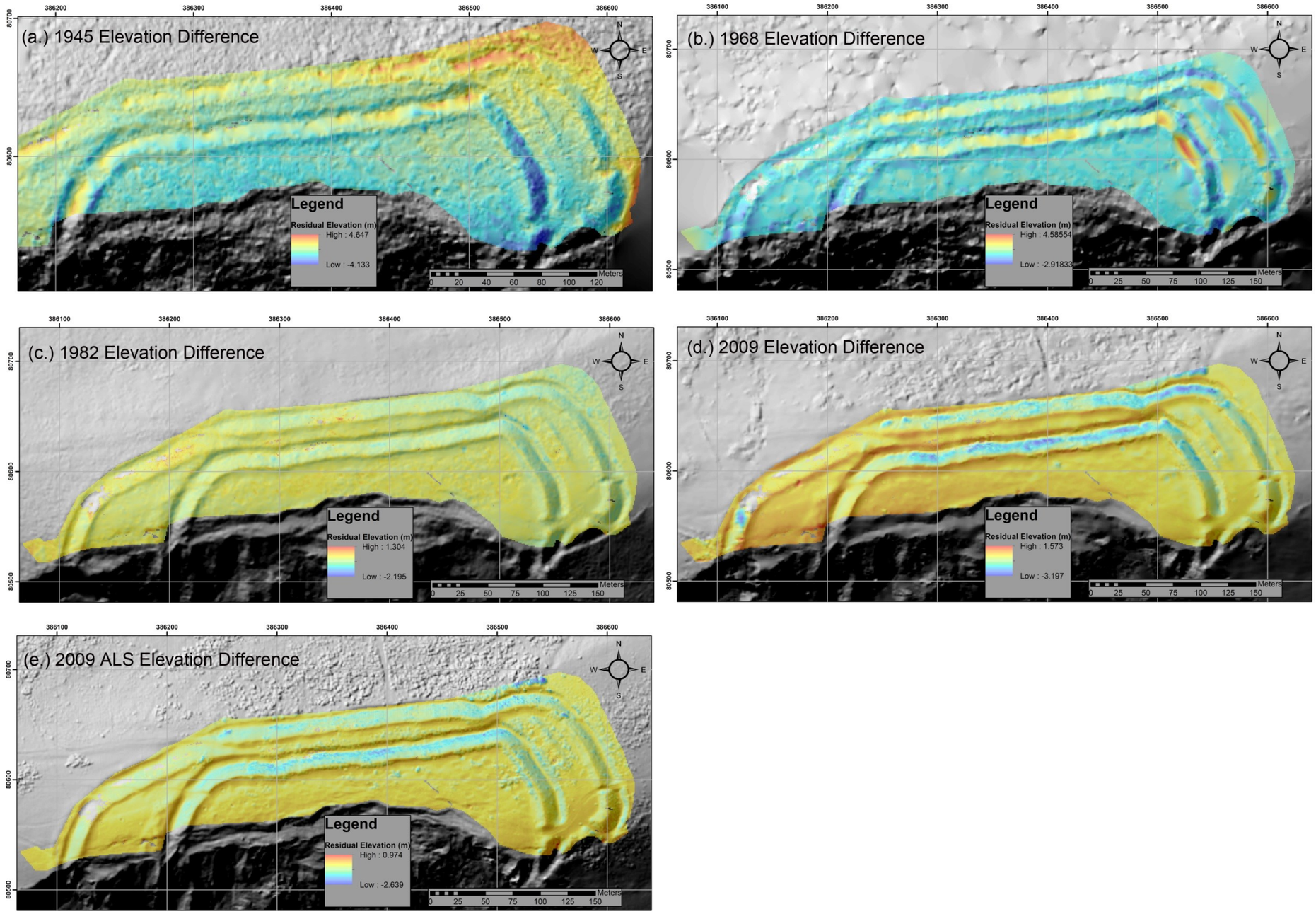

Figure 6.11: DSMs of Difference (DoDs) illustrating the results of subtracting the SAPs and ALS from the TLS data: (a.) 1945 (b.) 1968 (c.) 1982 (d.) 2009 (e.) 2009 ALS.

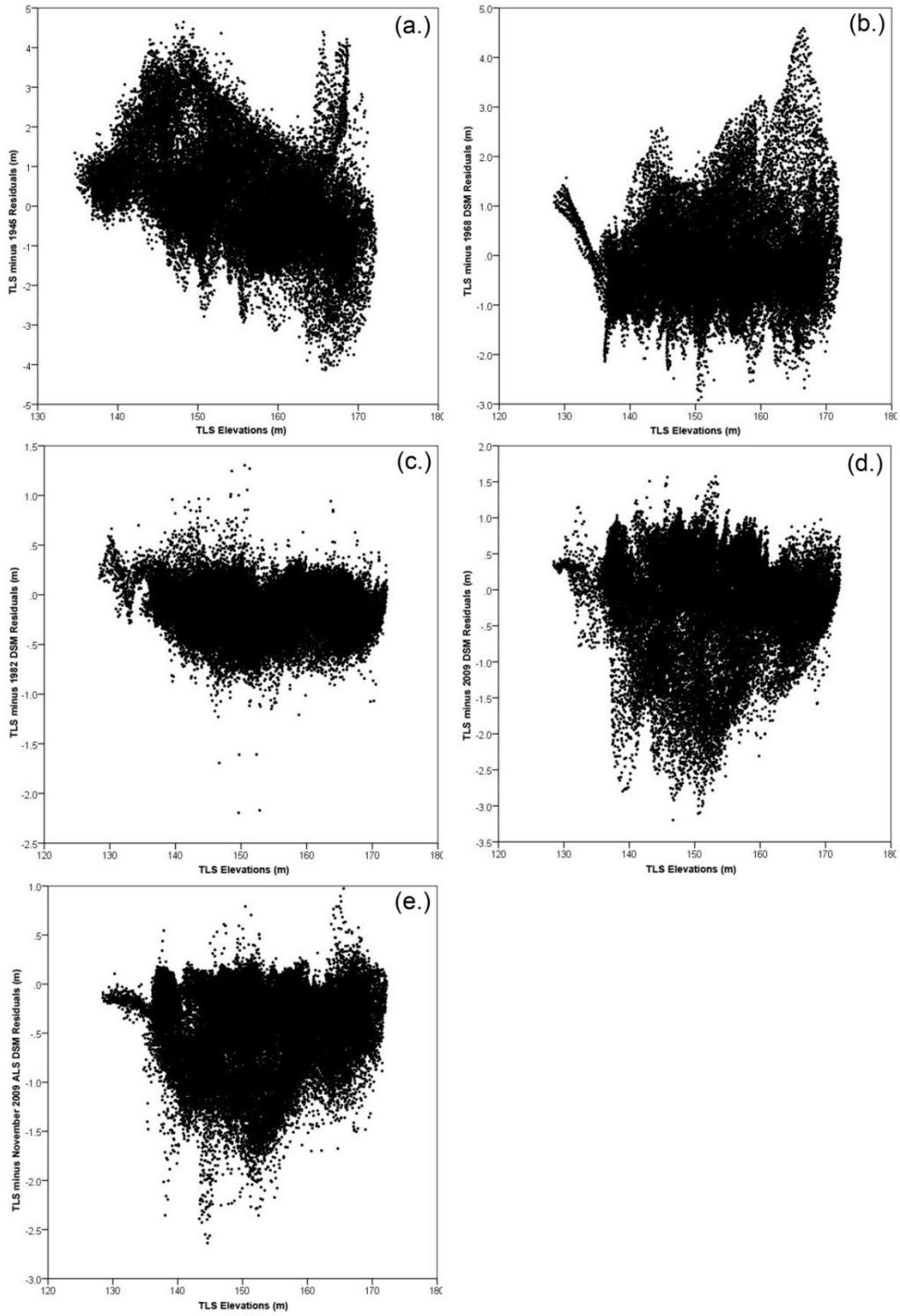

Figure 6.12: Scatter Plots showing the distribution of residuals against TLS elevation values for (a.) 1945 SAP DSM, (b.) 1968 SAP DSM, (c.) 1982 SAP DSM, (d.) 2009 SAP DSM and (e.) November 2009 ALS.

Despite the remarkably good performance of the 1982 SAP DSMs in comparison with the TLS, the DoD has a noisy appearance (Figure 6.11 c). There is a speckled effect across the interior of the hillfort where the SAP DSM elevation values are lower than those of the TLS. In keeping with the distribution of negative residuals as observed in the 2009 SAP and ALS datasets, the majority of these values are to be found along the northern and eastern facing ramparts. However, as illustrated by the scatter plot in Figure 6.12c, the residual range is much smaller, with only five outliers situated between -1.5m and -2.195m. Spurious positive residuals occur across all elevations within the 1982 DSM, but particularly those between elevations of 140m and 160m above mean sea level (AMSL). These areas are shown as deep red on the DoD, but do not appear to be limited to any particular region of the hillfort.

The 1945 and 1968 DoDs (Figure 6.11a. and c. respectively) do not follow the same distribution pattern of residual values. There are many more positive residuals along the rampart slopes in the 1968 data, which coincide with areas that appear to be flat due to the sparse point data generated by Socet GXP and the interpolation process undertaken in ArcMap. It is therefore unsurprising that the TLS in such areas is higher than the SAP DSM. The negative residuals occur along the base of the slopes, which means that the 1968 elevations are higher than those of the TLS. Upon examination of the 1968 orthophotograph (Figure 5.20 in Chapter 5), there is very little contrast in the imagery to define the ramparts, and thus the performance of the slope derivative is also expected to be poor, along with the elevation profile extracted from the 1968 DSM, as shown in Figure 6.9.

The majority of positive residual values within the 1945 DSM occur in the north-east corner of the hillfort and it is here where the TLS elevations are higher than those in the SAP DSM. Much of this area was covered by gorse in 1945 and thus it would be logical to expect the 1945 DSM to contain the higher elevations. However, the contrast in the 1945 photography is high and enhances the texture of the ground, picking up vehicle track marks across the interior of the hillfort and the uneven surface of the ground in and surrounding the areas prone to gorse. Further, there is a lot of shadow detail present, much of which is cast by the gorse but as with other SAPs, also found along the north-facing slopes of the ramparts. These factors are likely to be influencing the calculation of elevation values for the 1945 stereo-photography, thus contributing to the stippled effect in the 1945 DSM. The largest positive residuals can be found in the south-eastern corner of the hillfort, where the extent of the TLS overlaps with an area not included in the stereo-coverage of the 1945 photography, which explains the presence of residual values here. There are also some large negative residual values in this region, the maximum of which is -4.133m, where the hillfort ramparts meet the cliff edge. The 1945 DSM is therefore higher in these areas than the TLS, which might suggest that there has been some subsidence here between 1945 and 2012. However, this dataset has large standard deviation and variance values, particularly in comparison with the other SAP datasets, so change cannot be identified here with any certainty.

		Paired Samples Correlation			Paired Samples Test		
		N	Correlation	Sig.	95% Confidence Interval of the Difference		Sig. (2-tailed)
					Lower	Upper	
Pair 1	**TLS Elevations & 1945 SAP Elevations**	47361	0.993	0.000	0.025	0.046	0.000
Pair 2	**TLS Elevations & 1968 SAP Elevations**	51759	0.997	0.000	-0.169	-0.156	0.000
Pair 3	**TLS Elevations & 1982 SAP Elevations**	51759	1.000	0.000	-0.128	-0.124	0.000
Pair 4	**TLS Elevations & 2009 SAP Elevations**	51759	0.998	0.000	-0.103	-0.092	0.000
Pair 5	**TLS Elevations & Nov 2009 ALS Elevations**	51759	0.999	0.000	-0.403	-0.396	0.000

Table 6.2: Results of the Paired t-test performed between the TLS and each SAP epoch and ALS DSM.

To further establish how similar each of the SAP and ALS datasets are to the TLS, a paired t-test was performed, the results of which are shown in Table 6.2. High correlation exists between all of the datasets and the TLS, with the lowest 'r' value attributed to the 1945 DSM of 0.993. However, all of the 'p' values are zero, and thus the null hypothesis is rejected, meaning that there is a statistical difference between the TLS, SAP and ALS DSMs. This result may be misleading though, as the p-values are more likely to give a meaningful result with a population sample of values rather than a census analysis of all values.

By plotting the TLS elevation values against those of the SAP or ALS elevations, the relationship between these data can be further examined, as shown in Figure 6.13. Whilst the correlation for the 1945 DSM is strong, there is a much greater variation in the elevations values than there are in the 1982 DSM, for example. The appearance of outliers that significantly deviate from the line are found at approximately 165m along each axis, which coincides with the regions in which the TLS is higher than the 1945 DSM. The correlation between the TLS and 1968 DSM is extremely strong in the lower elevations, as shown by the compact section of the line in Figure 6.13b. However, the differences between each dataset increase with elevation, the highest of which tend to be found along the top of the ramparts. Correlation between the TLS and 1982 DSM appears to be perfect, although a number of small outliers can be identified in the mid-range elevations. These are also visible in Figure 6.13c. Finally, the linear correlation for both the 2009 SAP and ALS DSMs are similar, although the differences between the TLS and SAP DSMs are more pronounced, particularly as elevation increases beyond 140m.

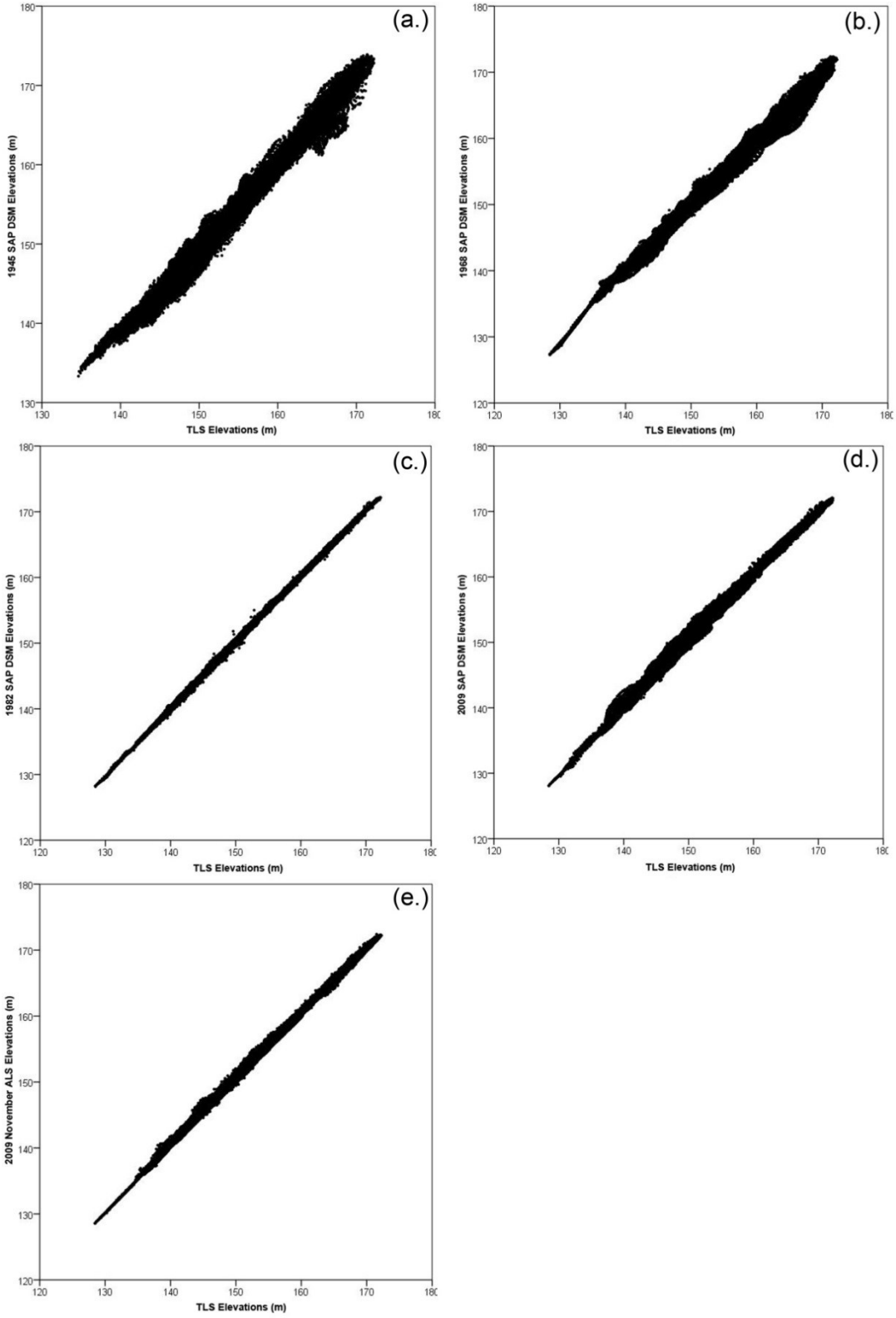

Figure 6.13: Scatter plots showing the linear relationship between TLS and (a.) 1945 SAP DSM, (b.) 1968 SAP DSM, (c.) 1982 SAP DSM, (d.) 2009 SAP DSM, and (e.) November 2009 ALS DSM.

The overall pattern for each of the DSM datasets locates the largest residual values at the higher elevations, and tends to be located on the rampart slopes, or towards the cliff edge in the south-east corner of the hillfort. The 2-tailed significance score for each of the DSM pairs is 0.000 and thus they are significantly different from the TLS data.

6.4.1 Local Moran's I Analysis

The 'Cluster and Outlier Analysis' maps for SAP and ALS elevation values are shown in Figure 6.14, whilst the Global Moran's I statistics for each dataset are provided in Table 6.3. As indicated by Table 6.3, all of the outliers appear to be clustered and, as highlighted in Figure 6.14, the areas of clustering differ from dataset to dataset. Moran's I is used to assess spatial autocorrelation in a dataset that considers both the feature location and its value simultaneously (ESRI 2012). Subsequently, the residuals obtained from the comparison of two datasets, which in this instance are SAP and ALS DSMs with that of the TLS DSM, can be assessed for the degree of clustering, dispersion or random distribution. Whilst this calculation returns a Moran's I value, it must be considered in relation to the null hypothesis, otherwise it is meaningless, and thus the z-score and p-value are required. The null hypothesis being tested with the Moran's I statistic states that the residuals are randomly distributed across the area of interest or, alternatively, that the processes influencing the spatial distribution of these residuals is purely random.

As is apparent from Table 6.3, the null hypothesis can be rejected as none of the results suggest that the residual distribution is random, and the likelihood of these results occurring due to random chance is only 1%. Subsequently, this suggests that the errors here are caused by a systematic factor. The Moran's I value usually ranges between -1 to +1, with -1 representing dispersion of the residual values, whilst +1 denotes that the values are stacked, or clustered. A value of 0 indicates that the residuals are arranged in a random fashion.

Elevation Dataset	Moran's Index	z-score	p-value	Residual Distribution	Likelihood of result due to random chance (%)
1945	0.952	485.381	0.000	Clustered	1.000
1968	0.922	621.596	0.000	Clustered	1.000
1982	0.796	536.246	0.000	Clustered	1.000
2009 Greyscale	0.919	619.325	0.000	Clustered	1.000
2009 Nov ALS	0.842	567.607	0.000	Clustered	1.000

Table 6.3: Table showing the Global Moran's I statistics for the Elevation residuals calculated between the TLS DSM and the SAP and ALS DSMs.

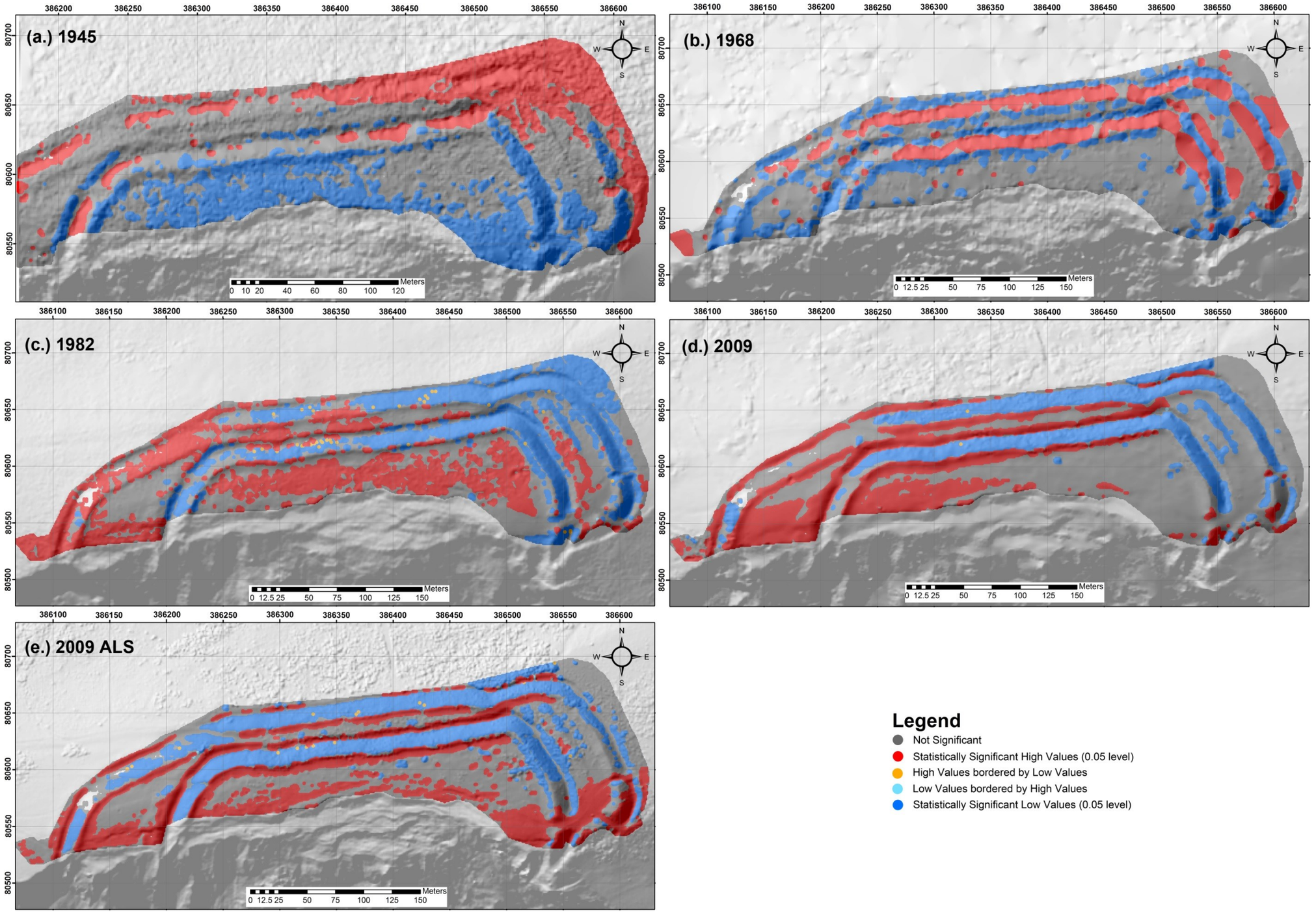

Figure 6.14: Spatial autocorrelation results from the Moran's I cluster analysis of the residuals between the TLS data and the (a.) 1945 (b.) 1968 (c.) 1982 (d.) 2009 and (e.) 2009 ALS elevation DSMs.

Therefore, the further the Moran's I score is from 0, the less likely the errors in the data are due to random factors and are more likely to be systematic.

As stated in Section 3.3.1, the systematic errors that will afflict the SAP DSMs are caused by errors in the digitisation process, a non-flat image plane, and lens distortion. As the archive SAPs have not been kept with their camera calibration certificates, and the 1945 photography was captured with a non-metric camera, lens distortion will be present within all of the SAPs, with the exception of the 2009 digital imagery. Subsequently these errors cannot be eliminated. Further systematic errors that may influence the output, although to a lesser degree, are the inaccuracies of 1-2cm inherent within the GNSS GCPs, although the GCPs extracted from OS mapping will also introduce uncertainties into the triangulation calculations. The ALS data is not without systematic errors, although it is uncertain whether these have been addressed as the data has been created by a third party. The EA has provided raw data whereby each point has an X, Y and height value, suggesting that a projection has been assigned to the data based upon the GNSS and IMU data collected at the time of the ALS survey. It is the GNSS/IMU combination that contributes the most to the error budget and how the EA have addressed any systematic errors in the data is uncertain.

There is a spatial structure appearing in many of the DSM datasets when producing the DoDs between the TLS data and the ALS and SAP DSMs. The partial aim of Chapter 5 was to identify the potential causes of any difference between the TLS DSM and the ALS and SAP DSMs. The TLS was the baseline dataset and the Flowers Barrow hillfort was chosen to represent a well-protected monument over which little change should have occurred, with the exception of the cliff face. Therefore any changes that are identified between the TLS and other DSM datasets should be predominantly due to systematic or random errors. However, the examination of the Moran's I maps, as shown in Figure 6.14, indicates a different spatial structure across all of the DoDs, with the exception of the 2009 Greyscale SAPs and the 2009 November ALS. These DoDs, as shown in Figure 6.11d and e respectively, are created from two datasets that were captured just a couple of months apart: the 2009 digital SAPs were created on the 27th September 2009 whilst the ALS was flown on the 7th November 2009. Subsequently, there should be negligible or no change to the monument over the two-month period between surveys, and thus any change identified in by the ALS and SAP DSMs should be caused by systematic differences.

6.5 Slope Assessment

The benefits of Slope in researching human activity at archaeological sites has been discussed in Section 3.4.3. However, this assessment utilises this derivative as a means of further assessing the differences between the DSMs produced from SAPs, ALS and TLS datasets. First order derivatives have been used to indicate the quality of a DSM, particularly as the process of converting elevation data into a derivative enhances noise within the dataset. From

an archaeological perspective slope is useful for identifying where breaklines occur, and if these regions are unclear, then the SAP dataset from which a DSM has been produced may not be suitable for archaeological use.

Slope maps for the SAP and ALS epochs are shown in Figure 6.15. The 1945 and 1968 maps shown in Figure 6.15 a and b both contain the greatest level of noise, which is not unexpected based upon the results of the Elevation Assessment in Section 6.4. Although the slopes of the ramparts can be identified well in the 1945 map, breaklines could not be digitised from it as they are not sharply defined. This is especially the case for the outer ramparts to the north and east of the hillfort. The 1968 DSM is the worst-performing dataset as the slopes of both the inner and outer ramparts to the east are non-existent, and there is an even greater lack of form exhibited by this dataset than the 1945 SAP DSM. Figure 6.15c shows the 1982 SAP slope map, which performs very well, containing some sharply defined breaks in slope that are visually similar to both the 2009 Greyscale SAP and 2009 November ALS slopes.

To further examine the differences between each of the slope maps, the SAP and ALS datasets were subtracted from the TLS slope map to provide a residual image, shown in Figure 6.16. Although there appears to be random noise in the flat areas of the hillfort for all of the residual images, with the exception of Figure 6.16d, the differences between the TLS dataset and the other slope maps predominantly occur along breaklines. The 1968 slope map (see Figure 6.16b) shows large residual differences on the eastern slopes of the ramparts, indicating the areas where SocetGXP failed to create elevation values representative of the severity of the slope here. The residuals along the breakline regions of the 1945 slope map, shown in Figure 6.16a, are much less coherent than those of the 1982, 2009 SAP and ALS maps (Figure 6.16c, d and e respectively). However, the appearance of residuals along the breaklines, shown at the top and bottom of the ramparts, suggests that photogrammetry tends to soften or ‘round off’ sharp features. As field archaeologists are very interested in delineating breaks of slope, this may suggest that photogrammetry is not so good for identifying breaklines in earthworks.

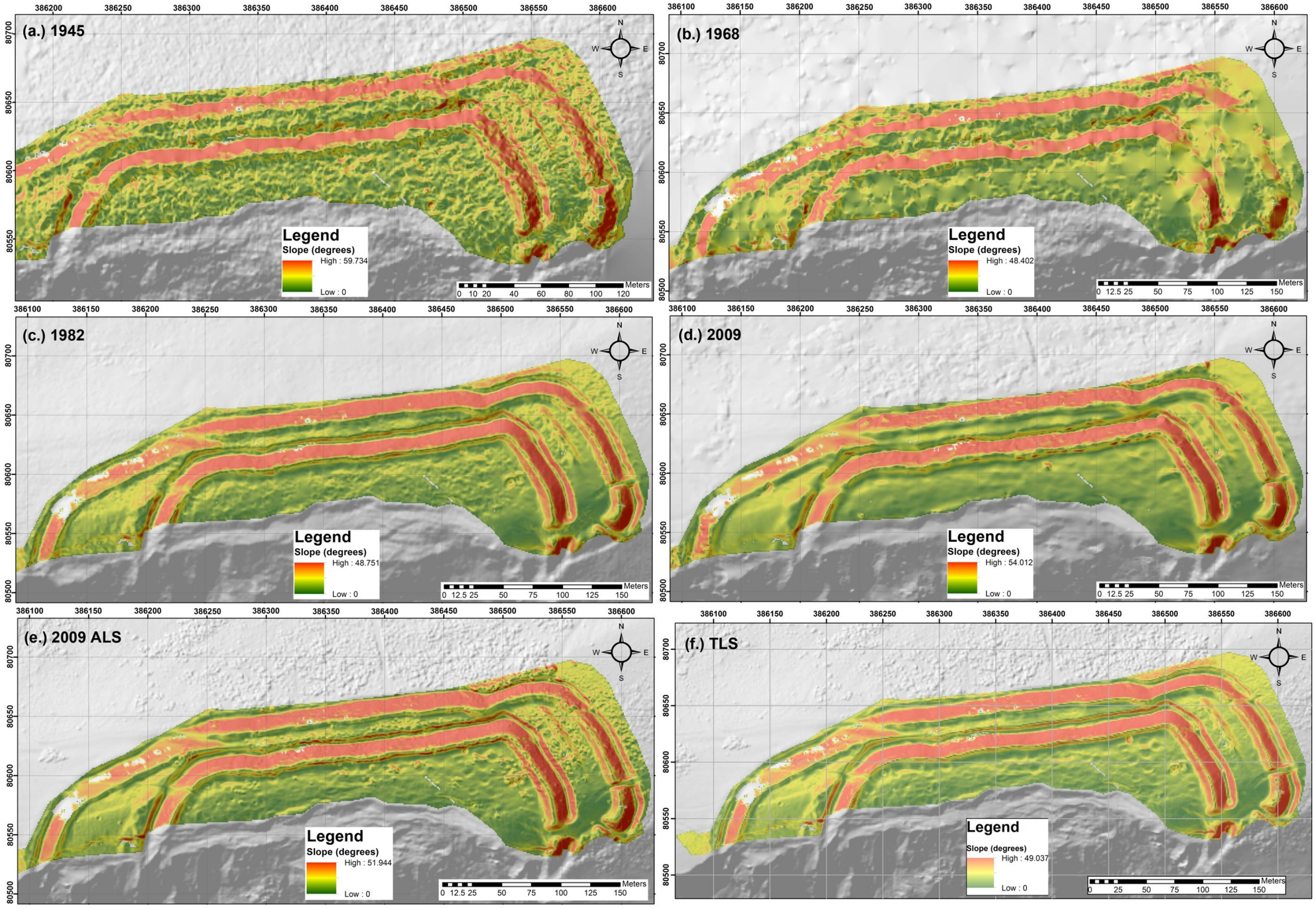

Figure 6.15: Slope derivatives for the Flowers Barrow SAP epochs (a.) 1945, (b.) 1968, (c.) 1982 and (d.) 2009, the ALS (e.) and the TLS data (f.).

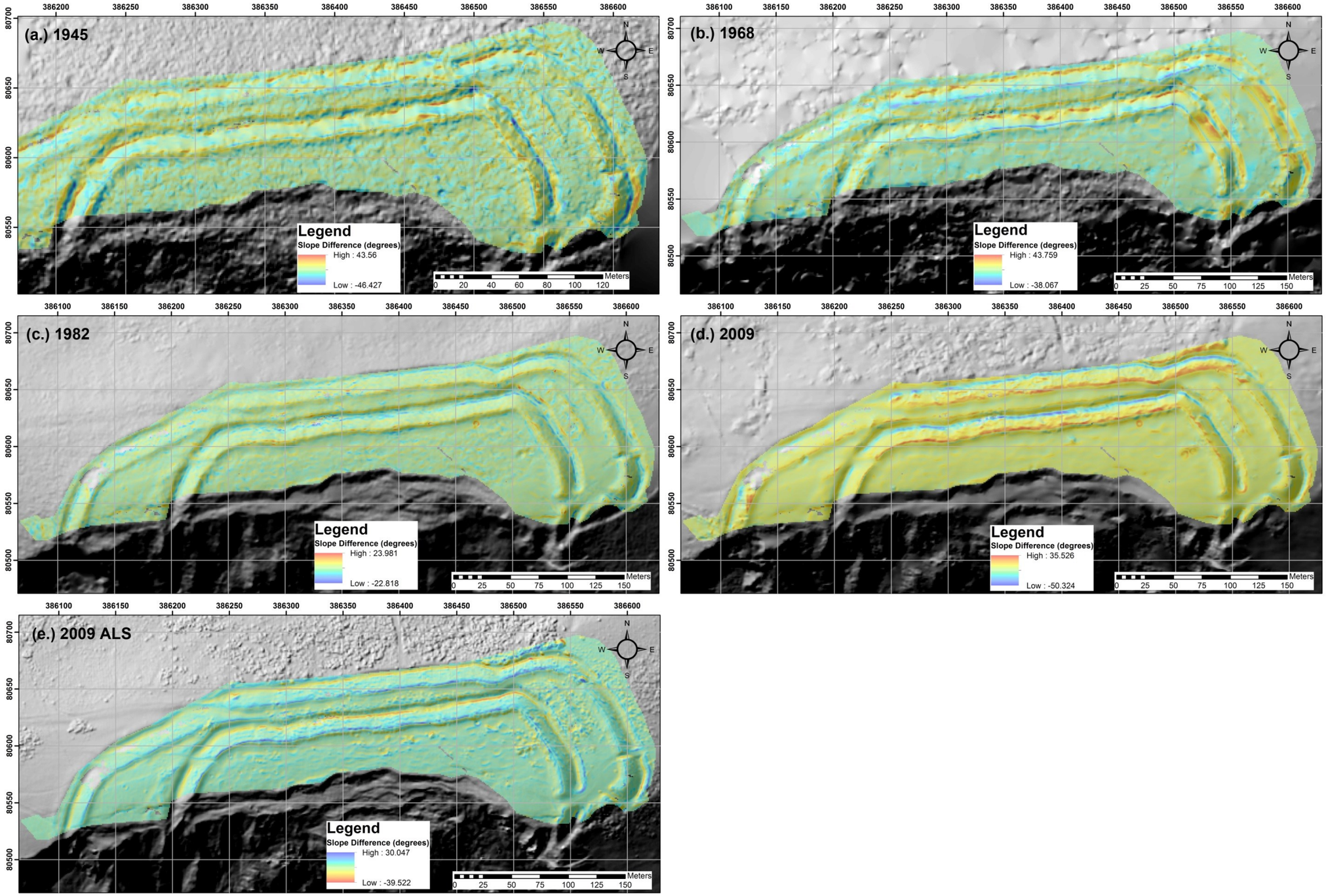

Figure 6.16: DSMs of Difference (DoDs) illustrating the results of subtracting the SAPs and ALS slope derivatives from the TLS data: (a.) 1945 (b.) 1968 (c.) 1982 (d.) 2009 (e.) 2009 ALS.

The appearance of noise in the flatter regions of the hillfort, such as the interior, may have a couple of causes. Firstly, in areas where image contrast is not good, such as areas of homogenous terrain, the photogrammetry software may find it problematic to perform image matching in these regions. This will affect the quality of the elevation values calculated, which will have a knock-on effect for the derived slope values. The SNR may also be much lower in flatter regions, with the expression of any subtle earthwork feature, such as the occupational platforms, hidden within this noise. The larger features, such as the ramparts, consist of a much stronger signal and, whilst there may still be noise contained within the pixels representing the ramparts in the SAPs, the greater majority of the pixel value is the signal itself.

Although the 1968 slope map suggests that it is the worst performing dataset, the statistical analysis contradicts this, as shown in Table 6.4. It is the 1945 dataset with the largest mean and standard deviation values, although the 1968 slope model is a close second. Surprisingly, the 1982 SAP slope data out performs the 2009 ALS, exhibiting the lowest variance and standard deviation value of the set. The frequency histograms of the slope residuals, as shown in Figure 6.17, all display what appears to be a normal distribution, although the range of residual values slightly, with the exception of the 1982 dataset (Figure 6.17c).

		TLS Slope Minus 1945 Slope	TLS Slope Minus 1968 Slope	TLS Slope Minus 1982 Slope	TLS Slope Minus 2009 Greyscale Slope	TLS Slope Minus 2009 NovALS Slope
N	Valid	47361	51759	51759	51759	51759
	Missing	0	0	0	0	0
Mean (degrees)		-2.210	1.630	0.213	0.584	-0.582
Std. Error of Mean (degrees)		0.041	0.0363	0.016	0.034	0.027
Median (degrees)		-2.554	0.614	0.118	0.534	-0.202
Mode (degrees)		-13.0995[a]	-6.722[a]	-5.070[a]	-4.583[a]	-7.344[a]
Std. Deviation (degrees)		8.914	8.250	3.532	7.830	6.059
Variance (degrees)		79.464	68.069	12.474	61.308	36.714
Skewness		0.323	0.526	0.127	-0.779	-0.436
Std. Error of Skewness		0.011	0.011	0.011	0.011	0.011
Kurtosis		1.094	1.505	2.212	4.971	3.204
Std. Error of Kurtosis		0.023	0.022	0.022	0.022	0.022
Range (degrees)		89.986	81.826	46.799	85.851	69.570
Minimum (degrees)		-46.427	-38.067	-22.818	-50.324	-39.522
Maximum (degrees)		43.560	43.759	23.981	35.526	30.047

Table 6.4: Summary statistics for the residual values between the TLS Slope dataset and each of the Slope values from the SAP and ALS datasets.

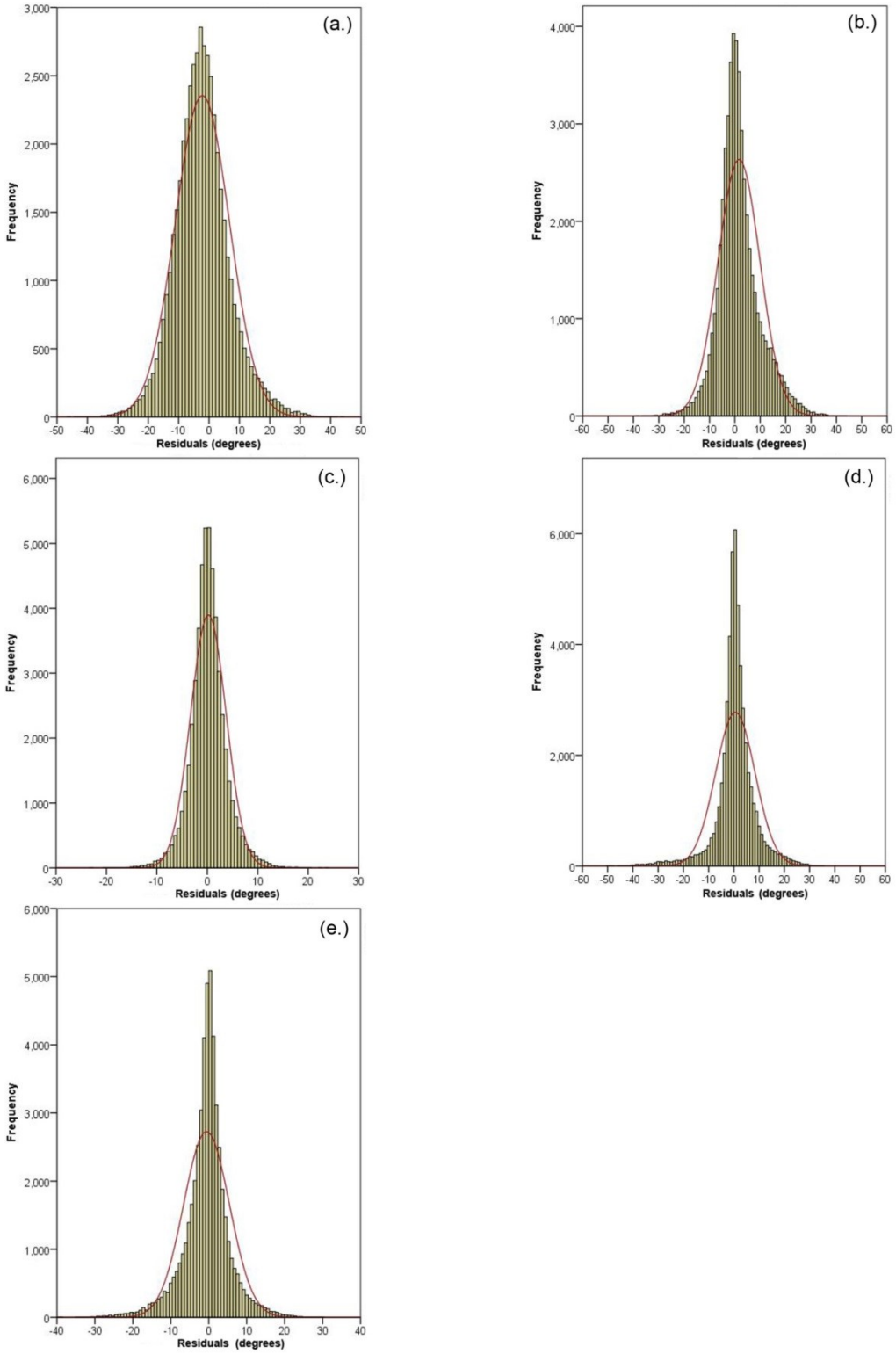

Figure 6.17: Histograms showing the residual distribution between the TLS Slope dataset and the (a.) 1945 SAP Slope, (b.) 1968 SAP Slope, (c.) 1982 SAP Slope, (d.) 2009 SAP Slope and (e.) November 2009 ALS Slope.

Slope		Paired Samples Correlation			Paired Samples Test		
		N	Correlation	Sig.	95% Confidence Interval of the Difference		Sig. (2-tailed)
					Lower	Upper	
Pair 1	**TLS & 1945**	47361	0.710	0.000	-2.290	-2.129	0.000
Pair 2	**TLS & 1968**	51759	0.700	0.000	1.559	1.701	0.000
Pair 3	**TLS & 1982**	51759	0.949	0.000	0.183	0.244	0.000
Pair 4	**TLS & 2009 SAPs**	51759	0.750	0.000	0.516	0.651	0.000
Pair 5	**TLS & 2009 Nov ALS**	51759	0.856	0.000	-0.634	-0.530	0.000

Table 6.5: Results of the Paired t-test performed between the Slope values of the TLS, ALS and each SAP epoch.

The linear scatter plots for each dataset, as illustrated in Figure 6.18, predominantly exhibit a linear distribution of slope values in comparison with the TLS. Again it is the 1945 and 1968 SAPs that deviate slightly from a linear correlation, particularly when the slope values increase beyond 20 to 25º. The variation between the 1982 and TLS slope values tends to remain within ~10º of each other, whilst the remainder of the SAP datasets might vary by upwards of ~60º. Whilst the correlation coefficient for each SAP and ALS slope dataset is strong, as shown in Table 6.5, it is the 1982 SAPs that produce the strongest result.

6.5.1 Local Moran's I Analysis

As with the elevation datasets, the spatial distribution of the slope residual values were analysed using the Moran's I tools in ArcMap (see Section 4.5.3.3 for further details). Yet again the residuals are clustered in specific regions within the hillfort, with the 1982, 2009 Greyscale SAP and 2009 ALS datasets containing similar patterns and locations for these clusters, as shown in Figure 6.19. The 1982 map (Figure 6.19c) is somewhat noisier than both of the 2009 datasets, whilst the 2009 Greyscale SAP slope values (Figure 6.19d) contains the largest number of non-significant residuals. The significant high values are predominantly found on the convex slopes, where the ramparts slopes form their highest peak. The significant low values are mostly restricted to the concave slopes, within the ditches of the hillfort or at the base of the rampart slopes.

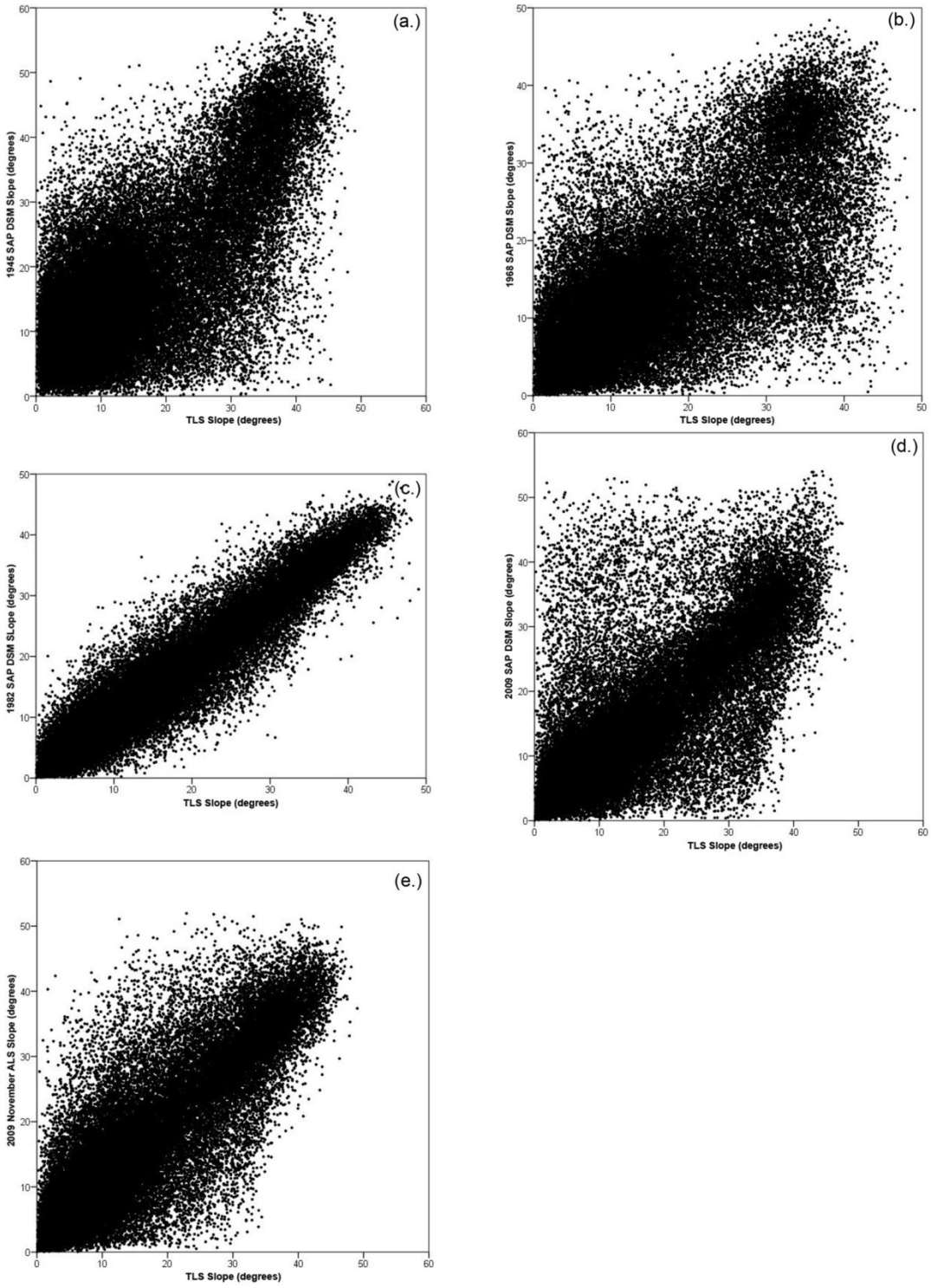

Figure 6.18: Scatter plots showing the linear relationship between TLS Slope and (a.) 1945 SAP Slope, (b.) 1968 SAP Slope, (c.) 1982 SAP Slope, (d.) 2009 SAP Slope, and (e.) November 2009 ALS Slope.

Slope Dataset	Moran's Index	z-score	p-value	Residual Distribution	Likelihood of random chance result (%)
1945	0.600	305.846	0.000	Clustered	1.000
1968	0.684	460.926	0.000	Clustered	1.000
1982	0.441	297.583	0.000	Clustered	1.000
2009 Greyscale	0.675	455.071	0.000	Clustered	1.000
2009 Nov ALS	0.506	340.956	0.000	Clustered	1.000

Table 6.6: Table showing the Global Moran's I statistics for the Slope residuals calculated between the TLS and the SAP and ALS datasets.

There appear to be exceptions to this rule within the 1945 and 1968 maps (Figure 6.19a and b respectively), which is most noticeable in the north and east ramparts of the 1968 illustration. It appears that the locations of the significant high and low values are reversed, as they are in the residuals map in Figure 6.19b. Whilst it is evident that the photogrammetric processing of the 1968 SAPs has failed to recreate the eastern ramparts, the reason for the peak of the ramparts to be overestimated in this dataset, as compared to the TLS, is unclear. However, as the significantly high and low values are positioned along the breaks in slope, the result of the Moran's I analysis agrees with the conclusion drawn by examining the slope maps shown in Figure 6.19: the photogrammetry, as well as the ALS, is producing the majority of spurious values in the regions surrounding breaks in slope, and therefore softening these features. There is also an element of slope overestimation in the ditches and underestimation on the top of the slopes. The Moran's I score, as shown in Table 6.6, confirms that the residuals have a clustered distribution, which is illustrated by their positive nature. Yet again, these results are not due to random chance, and thus this would suggest that there is an unresolved systematic error operating within the archival datasets, including the most modern ALS survey.

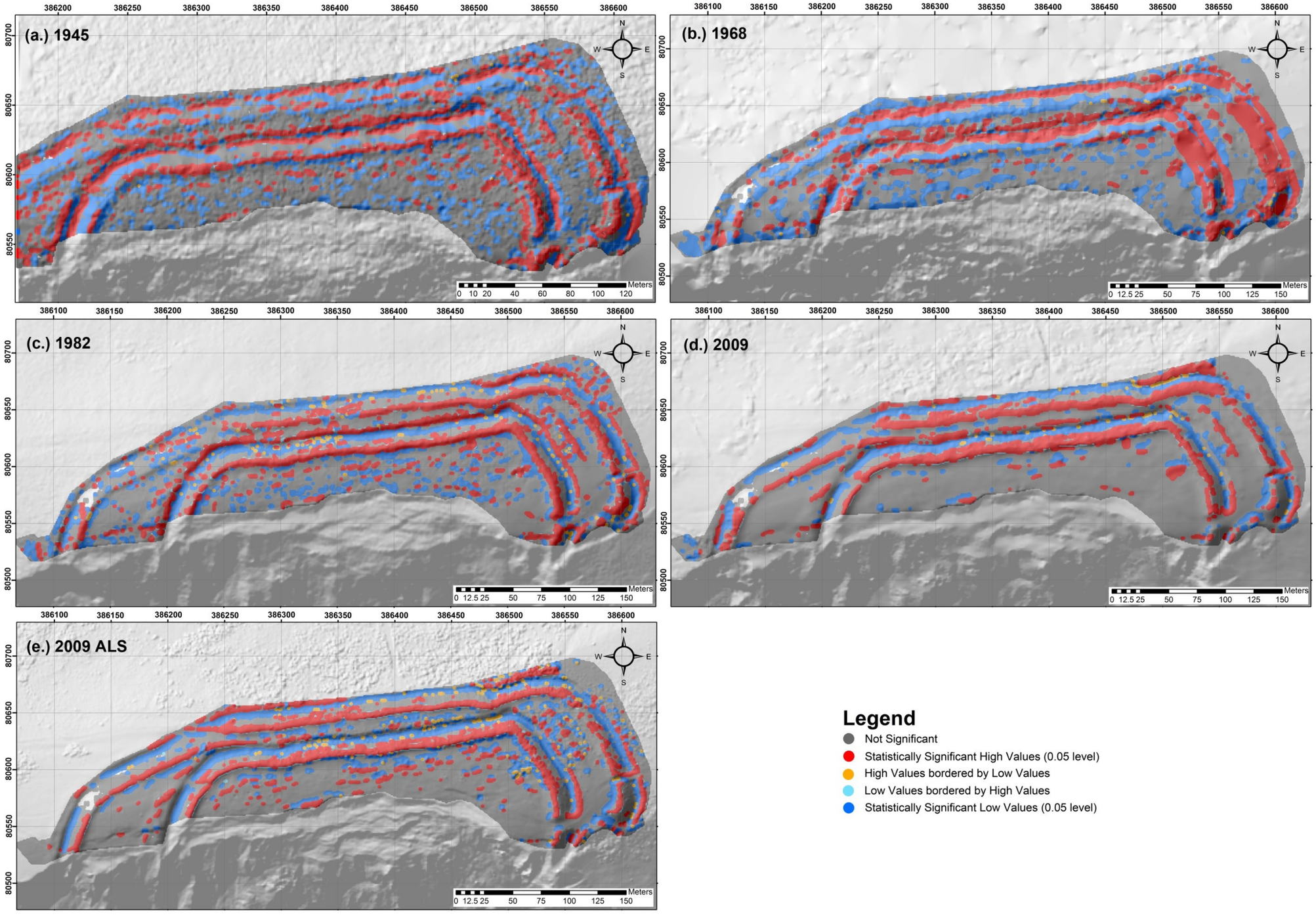

Figure 6.19: Spatial autocorrelation results from the Moran's I cluster analysis of the residuals between the TLS data and the (a.) 1945 (b.) 1968 (c.) 1982 (d.) 2009 and (e.) 2009 ALS slope derivatives.

6.6 Aspect Assessment

Whilst the utility of aspect values to archaeological analysis and the identification of noise in a DSM are discussed in Section 3.4.3, in this Section the results of calculating aspect values for each SAP and ALS are examined for the differences between them and the TLS DSM. Each of the aspect derivatives from the datasets, excluding the TLS, are shown in Figure 6.20. The 1982, 2009 Greyscale and 2009 November ALS results are similar, although the ALS image (Figure 6.20e) appears to contain more subtle detail than the SAP datasets. Visually, the 1982 results (Figure 6.20c) resemble the 2009 ALS data, more so than the 2009 Greyscale SAP results (Figure 6.20d). The interior of the hillfort as depicted by the 2009 SAP dataset is smoother and contains fewer aspect values than the 2009 ALS and 1982 SAPs. This result indicates that the terrain extracted from the 2009 SAP data does not contain the same amount of detail as the 1982 SAPs and the 2009 ALS, hence its smoother appearance.

The 1945 and 1968 aspect values have a much more noisy appearance. In the 1945 data, shown in Figure 6.20a, it is the flat interior that contains the most notable amount of noise in comparison to the other epochs. Whilst the pattern of colours representing aspect values in this dataset adheres to that of the other datasets, there is a distinctly ‘jagged’ appearance across the entire 1945 hillfort structure, which is not present elsewhere. The 1968 aspect illustration, shown in Figure 6.20b, has a more noisy appearance than the 1982 and later epochs, although it is evident that the ramparts, particularly to the east of the hillfort, have not been reconstructed well, as shown by the lack of distinction between the east and west-facing aspect values here. There is also a considerable absence of detail along the northern ramparts, as indicated by the lack of a continuous red strip defining the south-facing aspect of the earthen bank here.

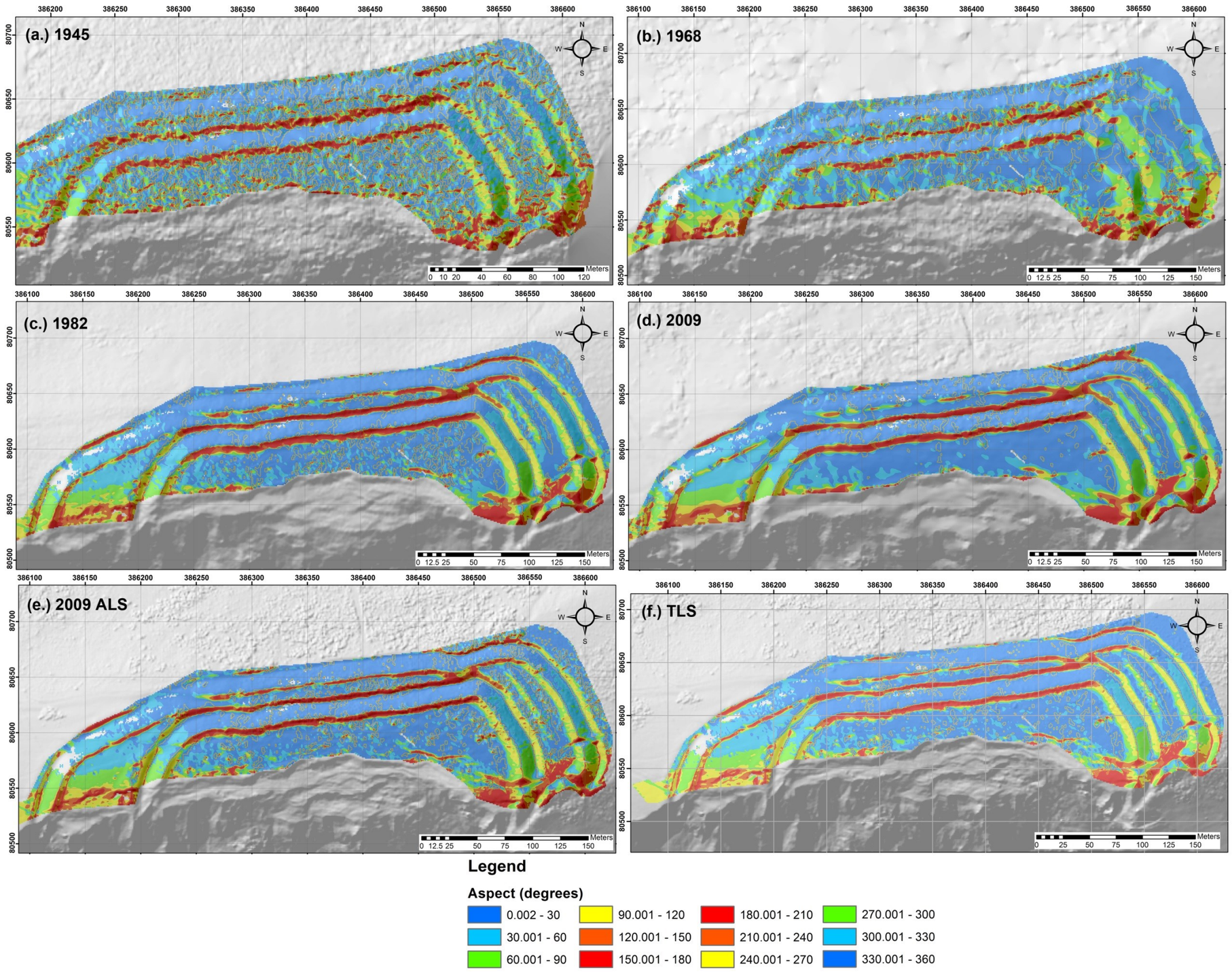

Figure 6.20: Aspect derivatives for the Flowers Barrow SAP epochs (a.) 1945, (b.) 1968, (c.) 1982 and (d.) 2009, 2009 ALS (e.) and the TLS (f.).

Whilst the aspect derivative is used to indicate the direction of maximum slope, as given in units of degrees, from 0º to 360º, the residual aspect values require normalisation before further analysis can take place. When examining the residual values between the TLS and each SAP and ALS epoch, the range of aspect values, as calculated by ArcMap, change from a positive range to encompass negative values too i.e. -360º to 360º. These extreme positive and negative values are produced by subtracting either very small or very large figures in one dataset from another dataset that would contain very large or very small values respectively. However, there are two reasons as to why the residual values cannot have a range of -360º to 360º. Firstly, the value of 0º and 360º are the same and both represent an aspect of 'North'. Whilst it might be said that values of 90º and 270º represent east and west respectively, they both differ from 'North' by 90º. Secondly, and following on from the previous point, the maximum difference between aspect values from two different datasets can thus only be 180º, which suggests that one of the values is facing the opposite direction to the other. The conversion of the residual values from a range of -360º to 360º to that of -180º to 180º was undertaken in Excel by using the following formula:

=IF(C1>=180,360-C1,C1)

The cell 'C1' is arbitrary and chosen to illustrate the value in this cell to which this logical expression is applied, which will subsequently be applied to all of the cells in the spreadsheet. This equation instructs the software how to perform the calculation if a particular condition is met. In this example, if cell 'C1' is greater than or equal to 180, then it should be subtracted from 360 to create a new value. If not, then it should retain its original value, as denoted by the last occurrence of 'C1' in the equation. This process is summarised in Figure 6.21.

By manipulating the data in this way, both positive and negative results are created, which are useful for constructing frequency histograms. If the mean value is 0 or similar, this forms the centre of the bell curve and the extreme values will be either ±180º, hopefully forming a symmetrical distribution of residuals. The frequency histograms for each dataset are shown in Figure 6.22. The 2009 SAP and ALS aspect values are similar, as shown in Figure 6.22 d and e, which is also confirmed by the summary statistics presented in Table 6.7. The 1982 histogram has a more pronounced leptokurtic peak than the 2009 datasets, as indicated by its kurtosis value, shown in Table 6.7, and contains fewer extreme values towards the tails of the bell curve. There is also minimal skewness in all of the datasets, which suggests that the residuals are distributed symmetrically about the mean. The 1968 frequency distribution (Figure 6.22b) looks visually similar to the 1982 and both 2009 aspect histograms, although the kurtosis and mean values in Table 6.7 indicate that this is not the case. By examining Table 6.7 the 1945 and 1968 datasets are more akin to each other, although the appearance of their histograms in Figure 6.22a and b respectively does not suggest this. The residuals within the 1945 dataset appear to be spread much more evenly throughout the data range beneath the bell curve.

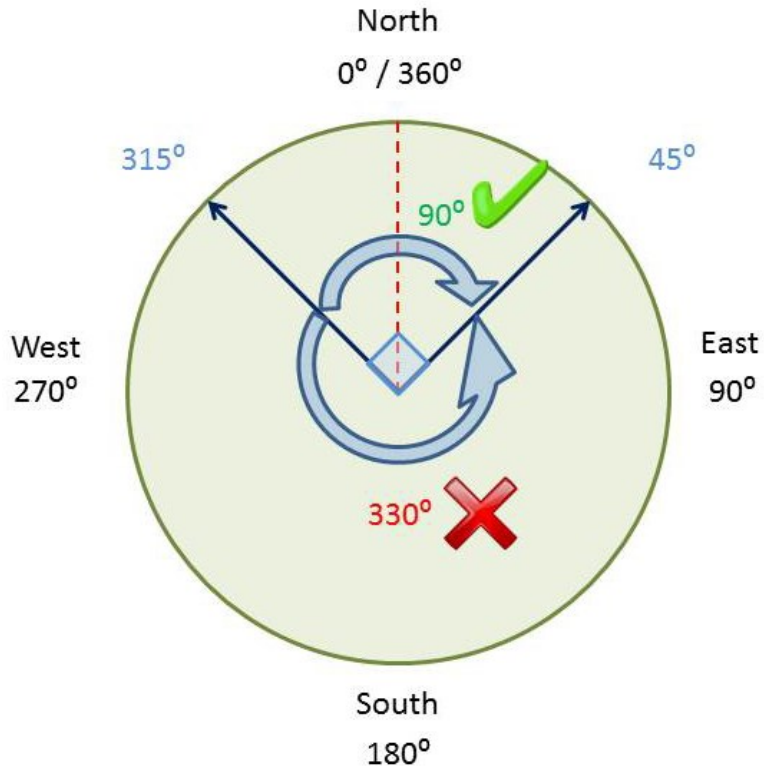

Figure 6.21: Diagram illustrating normalisation of Aspect residual values.

		TLS Minus 1945	TLS Minus 1968	TLS Minus 1982	TLS Minus 2009 Greyscale	TLS Minus 2009 Nov ALS
N	Valid	47361	51759	51759	51759	51759
	Missing	0	0	0	0	0
Mean (degrees)		-5.278	3.949	-0.093	-0.354	-1.920
Std. Error of Mean (degrees)		0.219	0.197	0.090	0.139	0.123
Median (degrees)		-3.078	0.214	-0.181	-0.300	-0.422
Mode (degrees)		-40.791a	0.000	-5.773[a]	0.000	-7.965[a]
Std. Deviation (degrees)		47.767	44.873	20.453	31.628	28.032
Variance		2281.642	2013.620	418.333	1000.307	785.771
Skewness		0.099	0.610	0.220	-0.304	-0.839
Std. Error of Skewness		0.011	0.011	0.011	0.011	0.011
Kurtosis		2.364	2.918	13.421	9.341	10.400
Std. Error of Kurtosis		0.023	0.022	0.022	0.022	0.022
Range (degrees)		356.257	356.468	355.534	356.730	353.687
Minimum (degrees)		-178.981	-177.314	-178.150	-177.296	-178.553
Maximum (degrees)		177.276	179.155	177.384	179.433	175.134

Table 6.7: Summary statistics for the residual values between the TLS Slope dataset and each of the Aspect values from the SAP and ALS datasets.

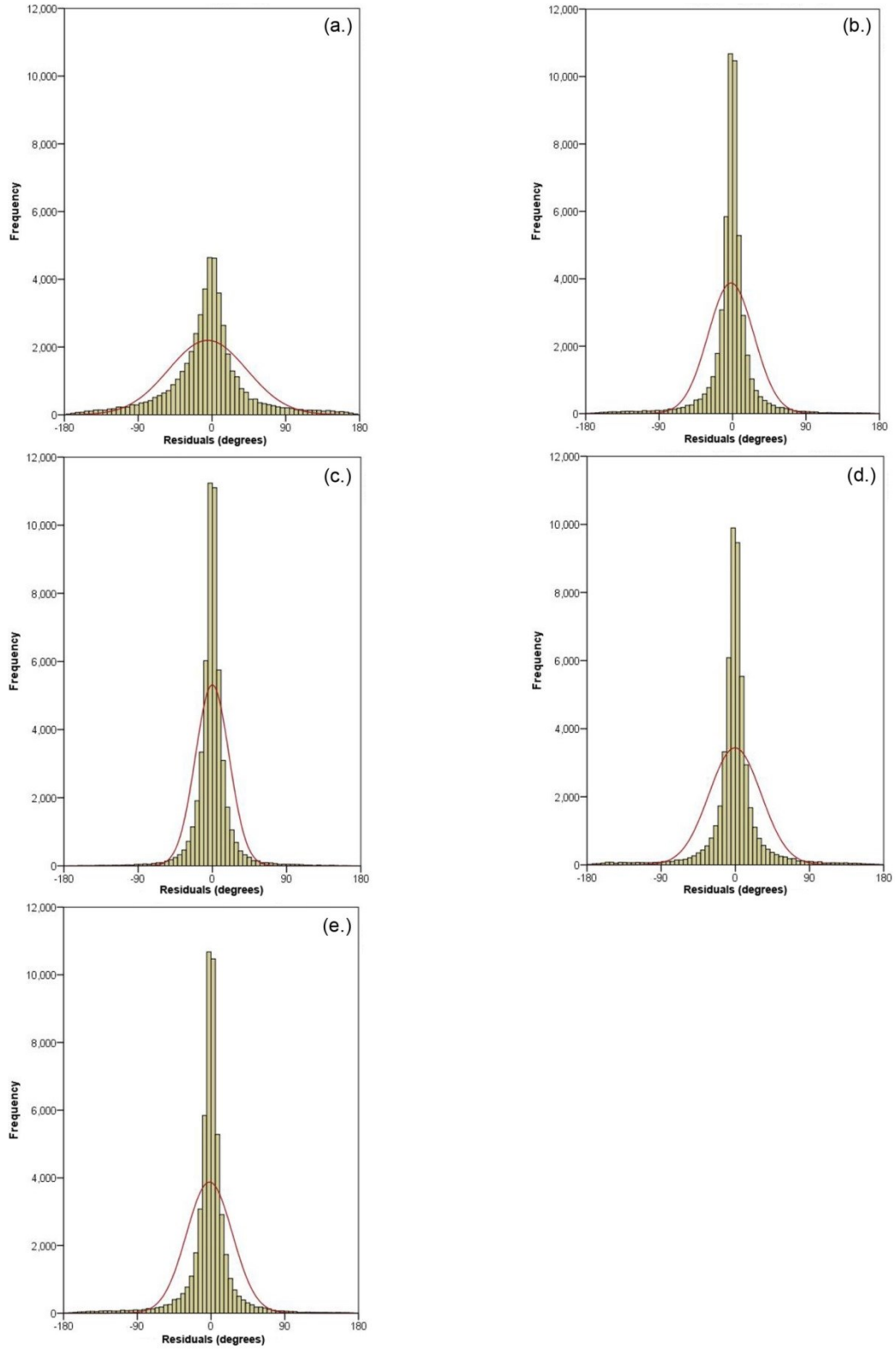

Figure 6.22: Histograms showing the residual distribution between the TLS Aspect dataset and the (a.) 1945 SAP Aspect, (b.) 1968 SAP Aspect, (c.) 1982 SAP Aspect, (d.) 2009 SAP Aspect and (e.) November 2009 ALS Aspect.

The correlation values for each of the datasets, as compared to the TLS, are lower than the results for Slope (see Table 6.5). As might be expected, the correlation increases as the years advance from 1945 through to the 2009 ALS dataset, and all of these data are significantly different to the TLS aspect, as shown in the 'Sig. (2-tailed) column in Table 6.8 (below), therefore the null hypothesis cannot be rejected. However, the 1982 aspect data is the exception, as it has the strongest correlation value of 0.922 and a Sig (2-tailed) value of 0.299. This indicates that the null hypothesis for this dataset can be accepted and that there is no significant difference between the 1982 and TLS aspect values.

Despite correcting the residuals for their extreme range, as explained at the beginning of this Section, the negative values had to be removed before constructing further illustrations and graphs for analysis. The reason for this is that it is the difference between values that is of interest, irrespective of whether the aspect value is clockwise or counter-clockwise from 0º. Subsequently the negative values are meaningless, despite their utility for producing frequency histograms. If the negative values had been removed beforehand, the histograms would have appeared skewed, causing difficulties in trying to describe the residual distributions for all of the datasets. The negative values were removed in Excel by squaring each individual residual value and then subsequently applying the square root.

The residual difference between the TLS aspect dataset and the SAP and ALS aspect values are shown in Figure 6.23. The greatest differences between the TLS, 1982 and 2009 SAP aspects and the 2009 ALS aspect are found along the breaklines at the top of the ramparts and in regions where gorse may be present, such as the flatter section to the east of the hillfort. To some degree the former can be said for the 1945 and 1968 aspect datasets, shown in Figure 6.23a and b, although there are a greater number of higher residual values distributed across their extents, giving them a more pronounced, noisy appearance.

		Paired Samples Correlation			Paired Samples Test		
		N	Correlation	Sig.	95% Confidence Interval of the Difference		Sig. (2-tailed)
					Lower	Upper	
Pair 1	**TLS Aspect & 1945 Aspect**	47361	0.562	0.000	-5.708	-4.848	0.000
Pair 2	**TLS Aspect & 1968 Aspect**	51759	0.595	0.000	3.563	4.336	0.000
Pair 3	**TLS Aspect & 1982 Aspect**	51759	0.922	0.000	-0.270	0.083	0.299
Pair 4	**TLS Aspect & 2009 Greyscale Aspect**	51759	0.814	0.000	-0.627	-0.082	0.011
Pair 5	**TLS Aspect & 2009 Nov ALS Aspect**	51759	0.856	0.000	-2.161	-1.678	0.000

Table 6.8: Results of the Paired t-test performed between the Aspect values of the TLS, ALS and each SAP epoch.

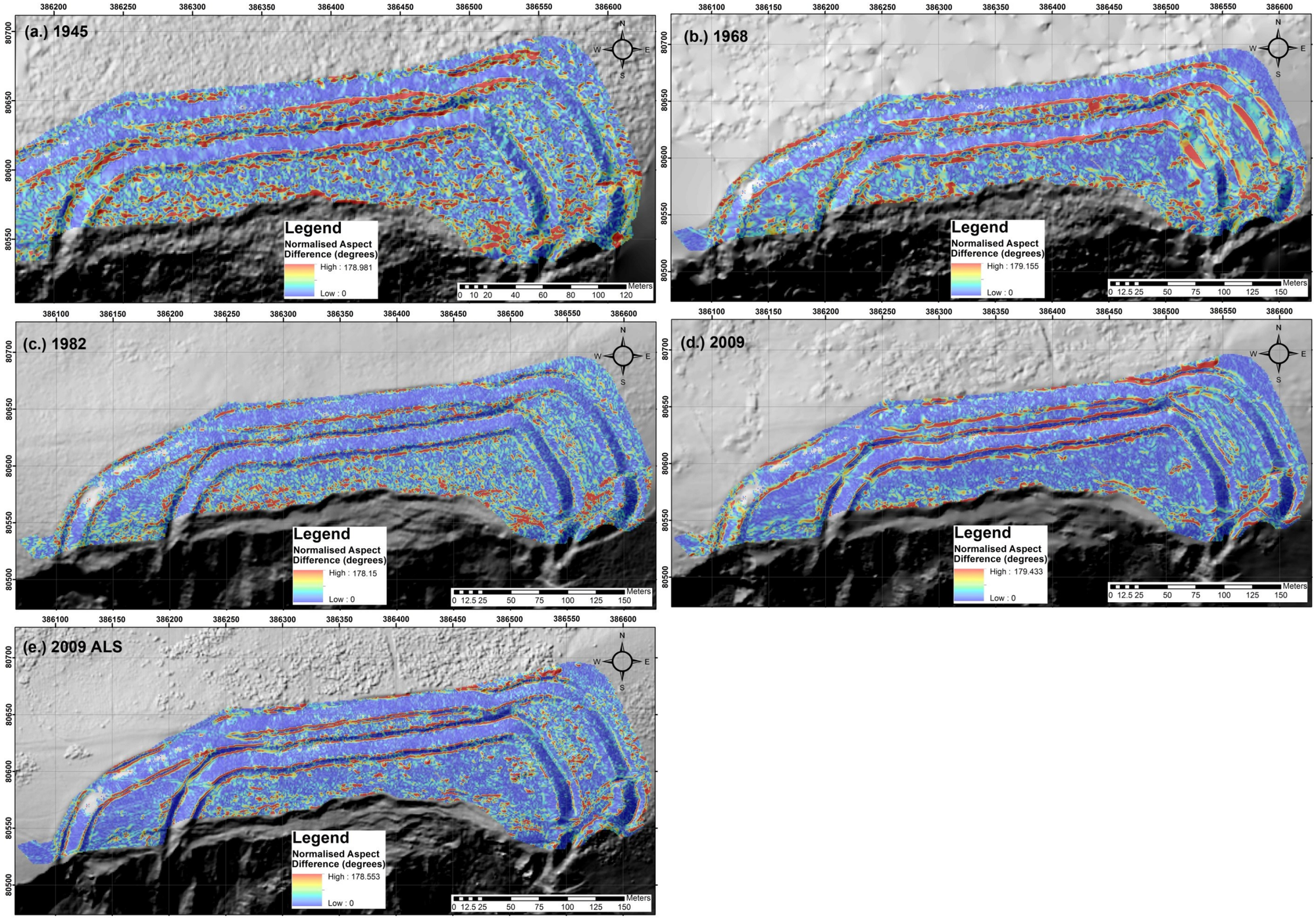

Figure 6.23: DSMs of Difference (DoDs) illustrating the results of subtracting the SAPs and ALS aspect derivatives from the TLS data: (a.) 1945 (b.) 1968 (c.) 1982 (d.) 2009 (e.) 2009 ALS.

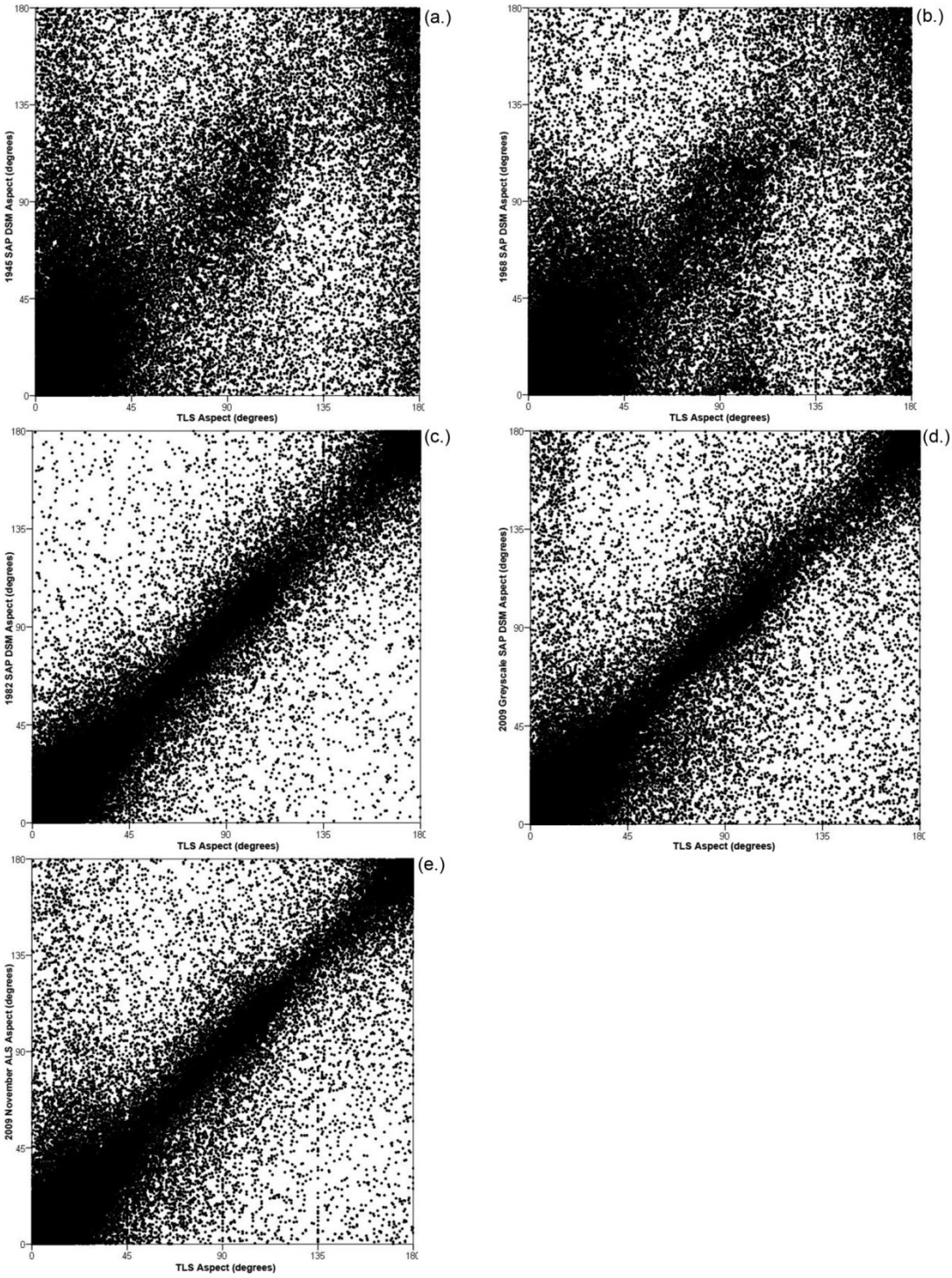

Figure 6.24: Scatter plots showing the linear relationship between TLS Aspect dataset and the (a.) 1945 SAP Aspect, (b.) 1968 SAP Aspect, (c.) 1982 SAP Aspect, (d.) 2009 SAP Aspect and (e.) November 2009 ALS Aspect.

The difference between the aspect values within each dataset can further be examined by plotting them against the TLS aspect values, as shown in Figure 6.24, and can help to explain the noisy appearance of the residual data. There is hardly any linear expression of aspect distribution in the 1945 and 1968 graphs (Figure 6.24 a and b), as inferred by the poor correlation result detailed in Table 6.8. There is a distinct lack of structure to both datasets from 45º onwards. The 1982 aspect dataset appears to contain a smaller number of spurious values as the spaces formed beyond the thick linear collection of values are clearer than those of the 2009 SAP and ALS aspect datasets. All five of the scatter plots illustrate that, across the board, there is no aspect value that is unaffected by noise. In many instances there are aspect values in the TLS data that are coupled with extreme values in an SAP or ALS dataset, and vice versa, which creates the impression of a 'ring' forming around the extremity of each of the scatter plots.

6.6.1 Local Moran's I Analysis

Moran's I analysis of the aspect data reveals an interesting pattern to the location of residual values. As was suggested in Section 6.5.1, many of the largest residuals are clustered along the breaklines of the ramparts, as shown in Figure 6.25. Within the 1982, 2009 SAP and 2009 ALS maps (see Figure 6.25 c, d and e respectively) the vast majority of statistically significant values are high. Therefore, the null hypothesis cannot be rejected in these locations, and subsequently there is a significant difference between the TLS aspect dataset and the ALS or SAP equivalent. Other regions within the hillfort that produce statistically significant differences are found within the central interior, with many of the values occurring close to the cliff edge. However, the vast majority of residual values for these three Moran's I results are not significant, suggesting that noise within the data is contained within particular clusters. This observation is supported by the spatial autocorrelation statistics returned by ArcMap, as shown in Table 6.9.

Normalised Aspect Dataset	Moran's Index	z-score	p-value	Residual Distribution	Likelihood of random chance result (%)
1945	0.506	258.186	0.000	Clustered	1.000
1968	0.554	373.701	0.000	Clustered	1.000
1982	0.332	233.905	0.000	Clustered	1.000
2009 Greyscale	0.430	290.198	0.000	Clustered	1.000
2009 Nov ALS	0.303	204.578	0.000	Clustered	1.000

Table 6.9: Table showing the Global Moran's I statistics for the normalised Aspect residuals calculated between the TLS and the SAP and ALS datasets.

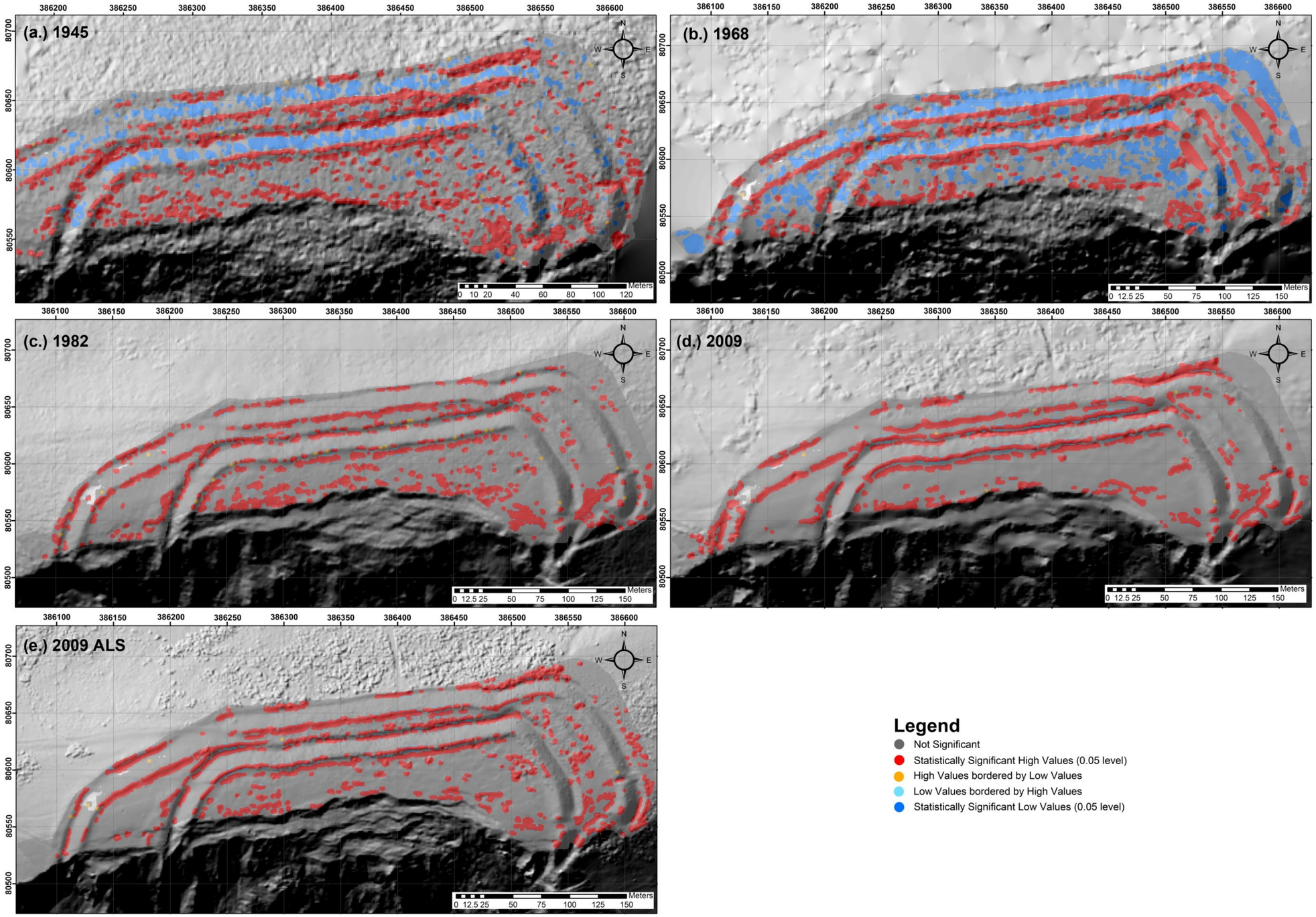

Figure 6.25: Spatial autocorrelation results from the Moran's I cluster analysis of the residuals between the TLS data and the (a.) 1945 (b.) 1968 (c.) 1982 (d.) 2009 and (e.) 2009 ALS aspect derivatives.

The 1945 and 1968 results, as shown in Figure 6.25a and b, contain statistically significant high values in much the same locations as the more current SAP and ALS data. However, they also contain statistically significant low values, with the majority of these occurring along the north-facing slopes of the ramparts. There are a greater number of statistically significant low values in the 1968 map that are located in the interior of the hillfort and predominantly limited to the east. By examining the hillshaded DSM of this dataset it is evident that the eastern half of the hillfort has not been reconstructed well by the photogrammetric process. The attempt of the natural neighbour interpolator to address the 'holes' in the 1968 data has created flat, triangular facets in the DSM, which are causing these large differences in aspect values. The 1945 Moran's I map contains a larger number of non-significant values across the hillfort in comparison to those of the 1968 map, which is surprising given that many of the elevation and slope results that have been discussed previously would tend to identify the 1945 data as containing the most noise. The Moran's Index value for the aspect analysis is lower for the 1945 data than for the 1968, as shown in Table 6.9, which tends to suggest that the residuals in this dataset tend slightly more towards the random. However, the residual values across all of the five datasets discussed in this Section are clustered, which indicates that there is a systematic bias operating on this data.

6.7 Archaeological Assessment

6.7.1 Profile Assessment

Archaeologists measure elevation values of earthworks to establish their shape and form. Whilst DSMs are utilised for extracting the profiles of breaklines, which will be addressed in Section 6.7.2, cross-section profiles are also required for providing a 3D perspective on earthwork form. To further assess the suitability of archive SAPs for producing 3D data suitable for archaeological use, one of the cross-section profiles recorded on the RCHME 1970 hachure diagram was reproduced in the field using the GNSS. This data was imported into ArcMap and used to extract elevation values from each of the SAP DSMs, ALS and TLS DSMs to facilitate the comparison of this profile across all of the datasets. The profile line from the 1970 RCHME survey drawing was digitised in AutoCAD Civil 3D 2011 once the scanned drawing has been scaled and rotated to ensure a best fit between the profile line and that produced by the GNSS. As the RCHME profile was designated as the baseline archaeological requirement for an earthwork monument, such as Flowers Barrow, it was decided that difference in area and perimeter length calculated between this and the GNSS profile would be the standard to obtain from the SAP DSMs in order to pronounce them fit for purpose. If these values were higher, then the DSM from which the profile was extracted could be rejected as unfit for extraction of archaeological data. Figure 6.26 shows the profiles from all of the DSMs.

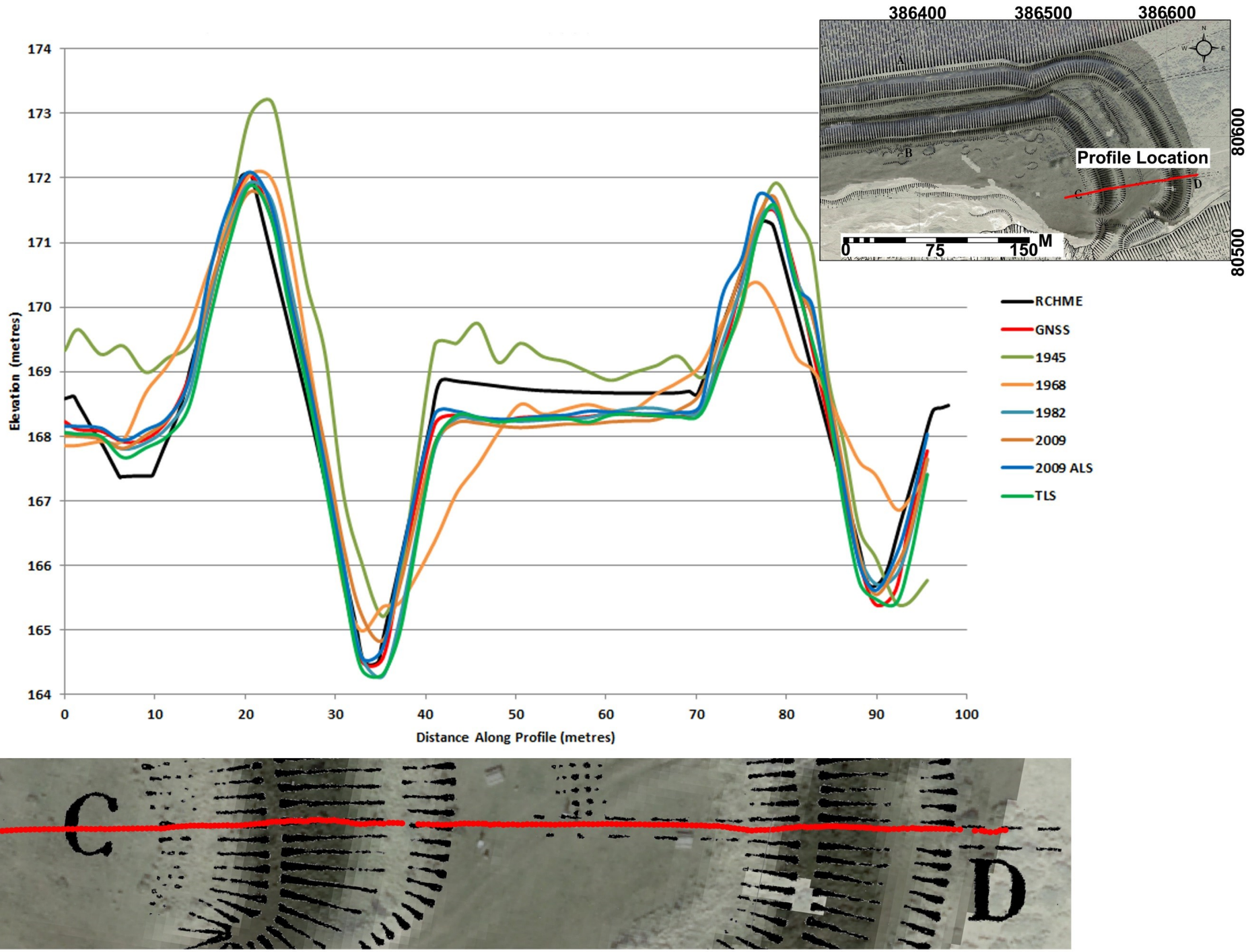

Figure 6.26: Graph showing the profile lines extracted from each SAP DSM epoch, ALS and TLS DSM using the GNSS survey data gathered in the field.

Baseline Dataset	DSM Epoch	Area (m^2)	Perimeter Length (m)	Fit for Purpose
GNSS	RCHME 1970	29.4658	211.249	-
	1945	93.5503	222.6942	No
	1968	57.8521	213.4146	No
	1982	13.9587	217.096	Yes
	2009	13.6579	216.2253	Yes
	2009 November ALS	13.8384	218.4374	Yes
	TLS and GNSS	17.9258	217.586	Yes

Table 6.10: Area and perimeter length calculations for the profiles extracted from SAP and ALS epochs when compared to baseline data.

Whilst examining the shape of each profile is enlightening, a quantitative representation of the differences between each profile and the GNSS was also produced. As mentioned above, the length of the perimeter, formed by the overlapping regions of the profile lines, and the area between the offset of each profile were calculated in AutoCAD after exporting the profiles as polylines from ArcMap. Although the profile graphs were produced using Microsoft Excel, calculating perimeter length and area using this software was complicated, but the process for doing so was relatively straightforward in AutoCAD. The values produced from this process are given in Table 6.10.

Aside from the 1945 and 1968 SAP DSMs, the remaining SAP, TLS and ALS DSMs perform extremely well in comparison with the profiles produced by the GNSS. There are slight offsets between the GNSS and TLS profiles when compared with one another, as illustrated in Figure 6.26. The GNSS profile is smooth, whereas the profile from the TLS contains step artifacts. This is due to the interpolation of the raw TLS point data into a 1m raster to match the spatial resolution of the SAP DSMs (see Section 3.2). If the interpolation had utilised the original point spacing of the TLS data, a 10cm spatial resolution would have produced a smoother profile. Despite the TLS providing the baseline DSM against which to test the SAP DSMs, as discussed in Section 4.3.2, it is evident the interpolation process has reduced the information content in the TLS DSM, although many of the GNSS elevations correspond well with those from the TLS. This is illustrated by the GNSS profile line passing through many of the same points as that of the TLS.

There are a few minor discrepancies in the TLS profile line, however, particularly along the first section of the line, which runs from the interior of the hillfort, shown on the left-hand side of the graph (Figure 6.26), to the top of the first rampart. This is likely to be caused by a combination of factors. Firstly, the effect of elevation uncertainties inherent in the GNSS data, as well as the ability of the surveyor to keep the GNSS rover vertical whilst taking a measurement, will influence the offset between the two profile lines. Secondly, GNSS was used as control for the TLS survey, as described in Section 4.3.2, and this will add further uncertainties into the position of the TLS survey station locations. Finally, the interpolation routine has created a DSM that has attempted to remove the influence of vegetation in the data by returning the minimum elevation values during the interpolation process. The TLS DSM also contains half the resolution of the GNSS measurements i.e. each raster pixel represent 1m, whereas the GNSS measured a point every 50cm. As can be seen in Table 6.10, the area caused by the offset between these datasets is 17.9258m^2, which is not as low as the 1982, 2009 SAP and ALS DSMs, although still within the limits of what is deemed to be the limit i.e. 29.4658m^2.

6.7.2 Breakline Assessment

As outlined in Section 3.4.5 breaklines can be identified using classification techniques, which objectively identify their location. This information is of utility to archaeologists when delineating earthworks from DSMs and thus the *Geomorphons* classification tool (see Sections 3.4.5 and 4.5.4) was applied to the Flowers Barrow SAP, ALS and TLS. As many of the DSMs performed favourably, a number were tested against the digitised breaklines from the hachure plan, as illustrated in Figure 6.27. The TLS DSM was found to be the most similar to the RCHME breaklines, with a 28.823% match, although the 1982 SAP DSM also performed well at 28.336%. Subsequently, the TLS dataset was compared to the other SAP DSMs and the ALS to

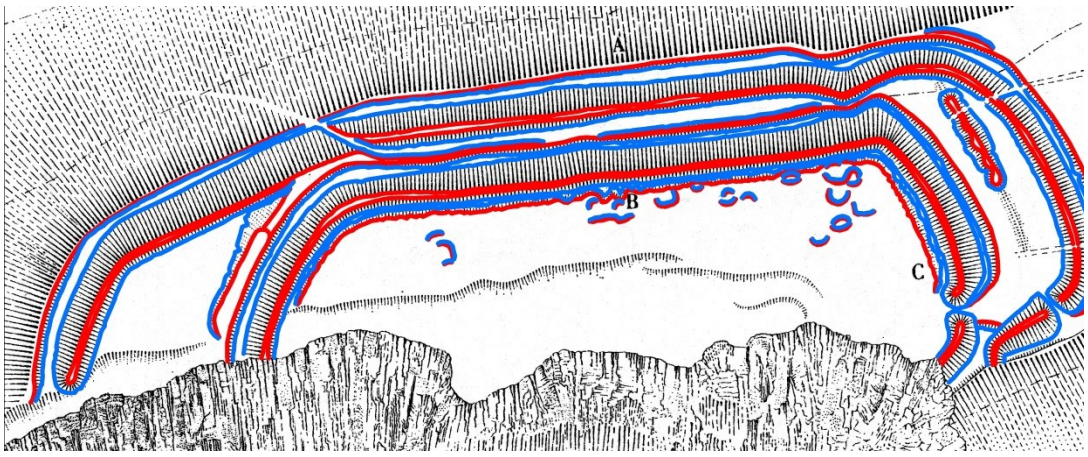

Figure 6.27: Breaklines digitised from the 1970s RCHME hachure plan of Flowers Barrow. Top-of-Slope breaklines are in red, whilst Bottom-of-Slope is shown in blue. Their extents were clipped along the cliff edge to ensure they matched with the DSMs.

Year (vs TLS)	Overall Accuracy (%)
1945	31.987
1968	34.902
1982	**53.234**
2009 SAPs	45.646
2009 ALS	51.149

Table 6.11: Results of comparing the Geomorphons breakline classification of SAP and ALS DSMs with the TLS DSM.

ascertain how similar they were and whether they out-performed the RCHME breaklines. The results are shown in Table 6.11. The 1982 SAPs performed the most favourably, closely followed by the 2009 ALS data. Overall, the breakline data contained within each of the SAP DSMs are more akin to the TLS data than that of the RCHME hachure survey as each of their overall accuracies exceeds 28%.

However, the difference between the TLS and the remaining datasets is still high, even with the ALS dataset. The possible reasons for this can be identified in Figure 6.28. In Figure 6.28a, the 1945 breaklines appear to be patchy and, although the major breaklines can be discerned, there is no trace of the occupation platforms and a very distorted representation of the linear earthwork in the east of the hillfort interior. The 1968 DSM has performed slightly better, with a 34.902% match, although the appearance of the classification result, as shown in Figure 6.28b, suggests that this should be otherwise. The eastern ramparts are not represented well, which is due to the sparse and unrepresentative elevation values within this area that were produced during photogrammetric processing. The remaining SAP and ALS datasets (Figure 6.28c, d and e) appear to be remarkably similar. However, in comparison with the TLS classification shown in Figure 6.28f, these data do not appear as noisy. The TLS classification look very stippled, particularly in the east of the hillfort, which was characterised by the presence of gorse during the survey in 2012. Based upon this result, the vegetation has not been fully removed from the TLS data and may explain why some of the breaklines in the east look patchy. The linear feature is also ill-defined, and thus the variation in the TLS DSM in the east is the area that is most dissimilar to the other DSMs. This explains why the overall accuracy of the classification procedure is not higher.

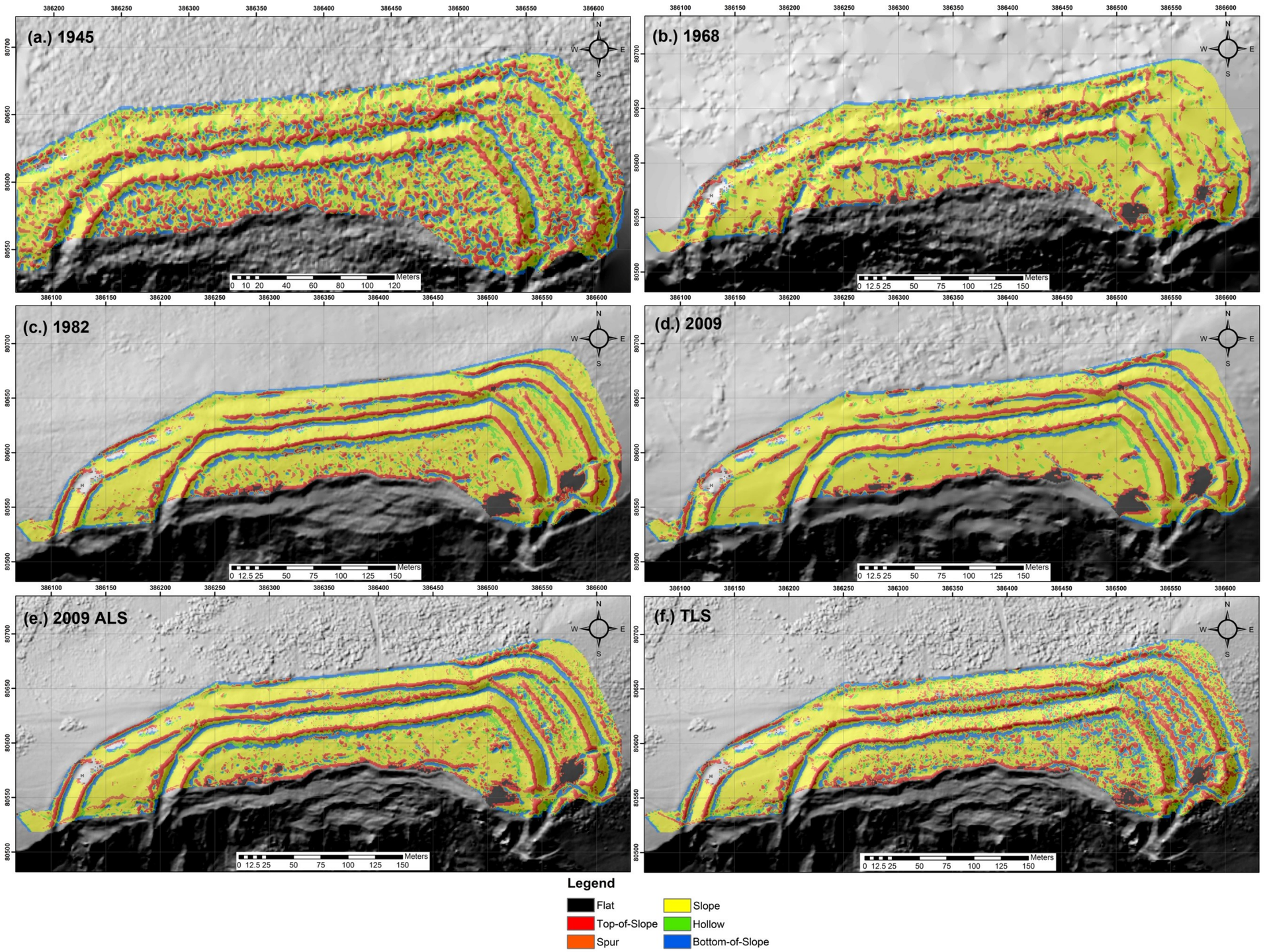

Figure 6.28: Geomorphons classification of the SAP, ALS and TLS elevation DSMs.

6.7.3 Information Content Assessment

As noted in Section 1.1.5 of Chapter 1, the size of a feature can dictate whether earthworks are recorded by a particularly survey method, whether it is conducted aerially or terrestrially. The 1970 hachure plan of Flowers Barrow, shown in Figure 6.4, records many earthworks, ranging from very large (i.e. ramparts) to very subtle (i.e. occupation platforms). If archaeologists wish to ensure subtle earthworks are recorded, this requires the production of a suitably dense, high accuracy survey, with appropriate precision values should one of the aims of the survey be to assess change over time.

Figure 6.29 illustrates the range of earthwork scales and their depiction by the RCHME, TLS, ALS and SAP DSM surveys. The hillfort ramparts are reconstructed by most of the datasets, although the appearance of the 1968 and 1945 SAP DSMs is very noisy. Across all of the datasets the linear feature contained within the eastern ramparts can be identified. However, the 1969 and 1945 DSMs do not provide a clear depiction and, as with the ramparts, the breaklines of this feature are obscured.

The occupation platforms are very subtle earthworks and are not easily observable by eye when visiting the hillfort. A number of these features have been identified in the 1970 hachure plan, and are clearly visible in the TLS, ALS and, to a lesser degree, the 2009 SAP DSM datasets. Whilst this confirms the ability of these data to replicate such small features, the images in

Figure 6.29 highlight occupation platforms that have not been recorded by the 1970 survey. They are extremely clear in the TLS dataset followed by a more subtle representation in the ALS DSM, with a very slight, but still visible, depiction in the 2009 SAP DSM. Based upon these observations, it would appear that the ground-based methods employed in the 1970s to construct the hachure plan have resulted in a number of features going unnoticed. Whilst this may be less of a concern at stable archaeological sites where RCHME plans exist, there is a need to re-survey sites that are under threat, preferably using TLS, to minimise the risk of earthwork features being missed.

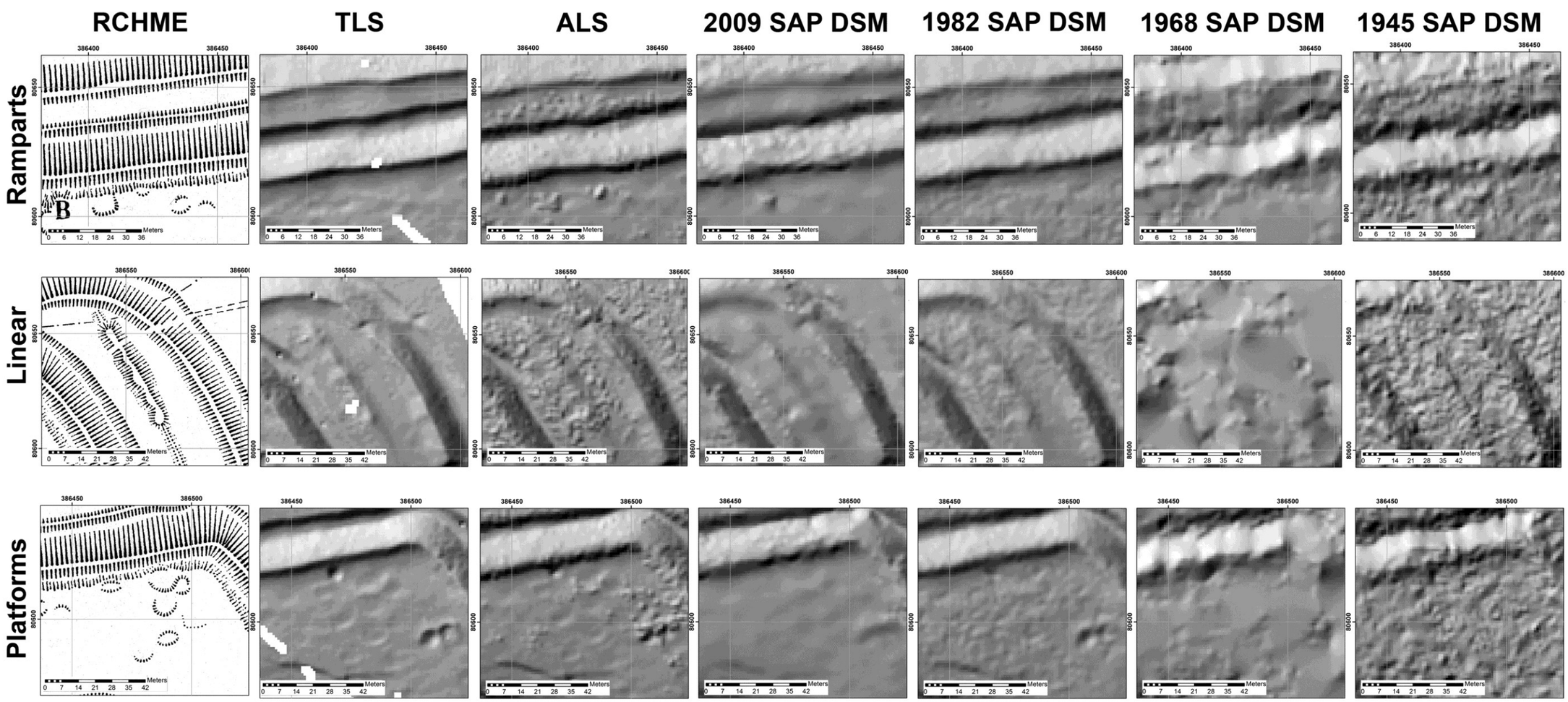

Figure 6.29: Diagram illustrating the information content of the RCHME hachure plan in comparison with data from TLS, ALS and SAP DSMs depicting Flowers Barrow Hillfort. Top: comparison of results across the large earthwork ramparts; Middle: comparison of results depicting a smaller, linear earthwork; Bottom: comparison of results showing the most subtle earthworks at Flowers Barrow, namely the occupation platforms.

6.8 Discussion

The results of this Chapter indicate that, in general, as the age of the photography decreases, the residual differences between the SAPs and TLS datasets also decrease. Point densities as extracted from the older datasets in SocetGXP, namely the 1945 and 1968 SAPs, were poor and thus the NN interpolator was required to fill large gaps. This created some unrepresentative elevation values in the 1945 and 1968 DSMs which was evident in both the elevation analysis and that of the first order derivatives. The poorer point densities are likely to be found in areas where image matching has failed to find corresponding pixels between images. As the older imagery is more likely to contain distortions due to tip and tilt, these will further reduce the likelihood of finding a match between image pairs.

For all of the DSM datasets, some locations across Flowers Barrow were subject to large variations between them and the TLS data. These regions were afflicted by shadows, gorse or poor image contrast within the photography, especially along the north and east ramparts of the hillfort. Many of the significant high residual values in the elevation, slope and aspect datasets were situated along the convex slopes, at the stop of the ramparts. The majority of significant low values were found along the concave slopes within the ramparts ditches. All of the residual values, irrespective of whether they represented differences in elevation, slope or aspect, were clustered, indicating that systematic error is still present within the SAP and ALS DSMs tested.

The archaeological content of the SAP DSMs were found to be similar to that produced by the GNSS and TLS data, with the exception of the 1945 and 1968 DSMs. Profiles of the ramparts were extremely similar in the SAPs from the 1980s onwards, which illustrates that the form of these features can be recreated from archive photography. The classification of breaklines was less conclusive in terms of the empirical results derived from a comparison between the TLS data and the other DSM sources. However, the visual appearance of the classification suggested that a skilled interpreter could extract breakline information from the SAP DSMs, with the exception of the 1945 and 1968 datasets.

6.9 Summary

This Chapter has presented the DSMs obtained by processing SAPs dating back to 1945 over the Flowers Barrow hillfort site. The statistical and archaeological assessment of these data have confirmed that useable terrain information can be obtained from archive SAPs, which tends to increase in quality as the age of the imagery decreases.

7 TRANSFERABILITY STUDY: EGGARDON HILLFORT AND ENVIRONS

7.1 Introduction

This Chapter presents the results from processing SAPs obtained of the Eggardon Hillfort transferability study site. As with the previous chapter, a site overview is provided in Section 7.3 that describes the geology, geomorphology, archaeology and site condition. Any deviations from the data processing methods outlined in Chapter 4 are discussed in Section 7.4, whilst Sections 7.5, 7.6 and 7.7 contain the results and analysis. The chapter ends with a discussion of the findings in Section 7.8.

The reasons relating to the selection of Eggardon as a field site were addressed in Chapter 4 Section 4.1.2. Whilst the transferability study builds upon the techniques and results provided in Chapter 6 and aims to assess whether the method adopted for processing the SAPs and other mass-capture techniques is repeatable at another site, Eggardon Hillfort also provides some further challenges with which to test SAPs. Whilst the Flowers Barrow pilot site (see Chapter 6) tested the techniques on a stable archaeological resource, the transferability study has been conducted on a site that has not been so rigorously protected in places (see Section 4.1.2 for further discussion). This facilitates the assessment of mass-capture techniques to produce useable data of good accuracy and quality where subtle changes in topography over time may be more difficult to detect with confidence.

Eggardon Hillfort has also been chosen based upon the variability of the earthworks present at the site i.e. not solely consisting of a hillfort feature. This ensures that the technologies being tested can be evaluated by their ability to detect a wide variety of features, both large and small, for example a henge monument, round barrows and a later Prehistoric or Romano-British field system, the latter of which is under agricultural cultivation. This approach subsequently ensures that the methodology developed by this research has a wide applicability to the archaeological resource.

7.2 Transferability Study Site Background

7.2.1 Site Overview

Eggardon Hill is an Iron Age hillfort, situated to the east of Bridport, Dorset (see Figure 7.1), on top of a chalk spur which forms a part of the western chalk uplands that in turn belong to a region known as the Dorset Downs (Wells 1978), and is situated at an altitude of 800 feet above sea-level (Colley March and Solly 1901). Within the hillfort are earthworks associated with

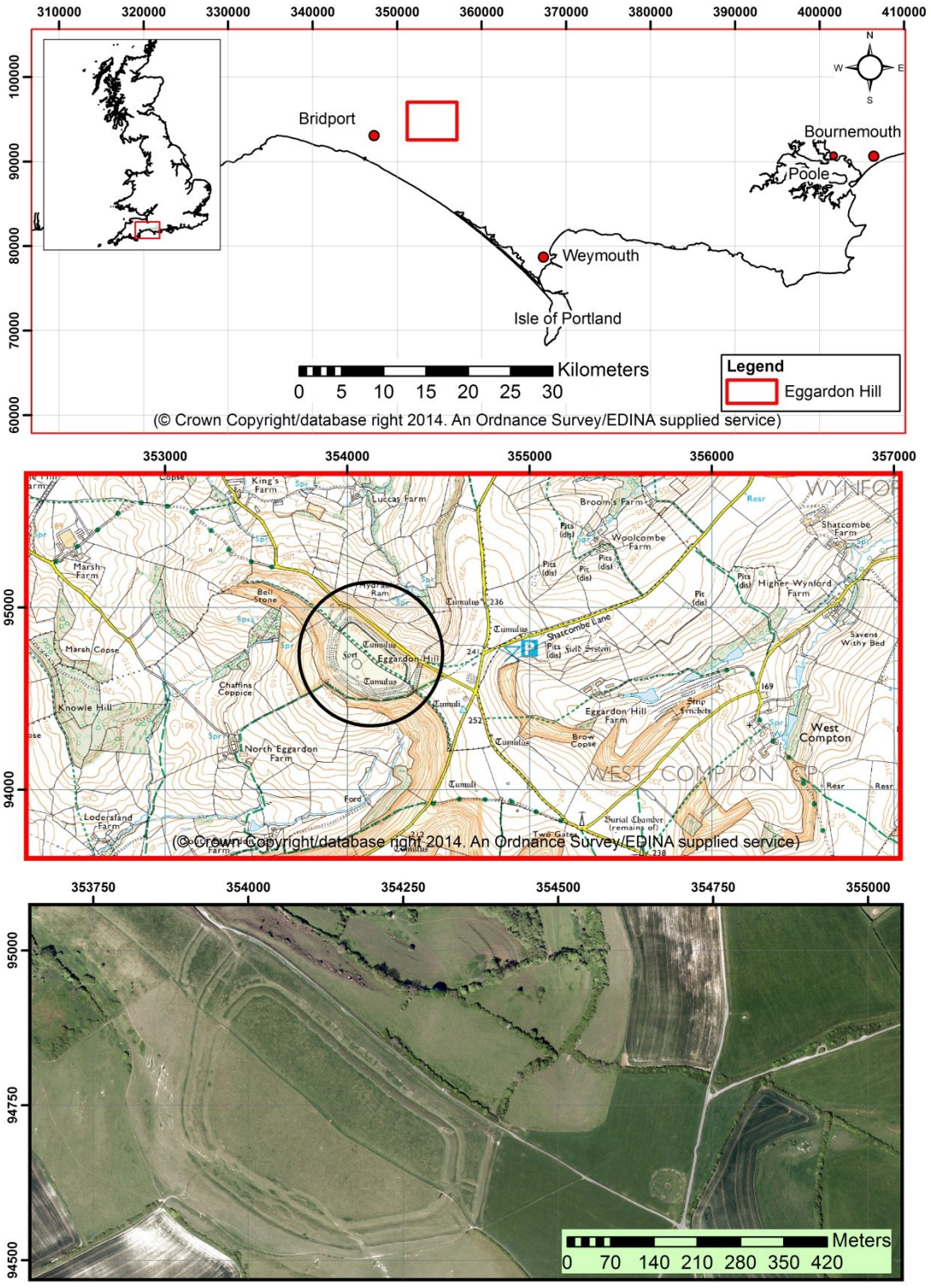

Figure 7.1: Map showing (a.) location of Eggardon Hill within the UK, (b.) local topography and infrastructure and (c.) orthophotograph of Eggardon Hillfort and henge.

earlier occupation of the site that dates back to the Bronze-Age, although finds within the interior also suggest that Neolithic peoples also utilised this site prior to the construction of the defences. The superficial geology deposits overlying the chalk bedrock are comprised of clay, silt, sand and gravel. The north-east and south-west sides of the hillfort are characterised by steep escarpments, providing a natural form of defence with exceptional views across the Bride Valley, western Dorset and towards the south coast and English Channel.

Within close proximity to the hillfort are a number of springs that would have sustained the prehistoric people occupying the hill's promontory, and thus the long period of human activity with the Eggardon environment appears to have been sufficiently supported by the natural resources the region had to offer. The current landscape within which Eggardon Hillfort is situated supports much agricultural activity, although it is also recognised for its special character. The Hillfort has obtained Site of Special Scientific Interest (SSSI) status for the Hillfort, and the inclusion of the parishes of Askerswell and Powerstock as a part of the Area of Outstanding Natural Beauty (AONB).

7.2.2 Land Use

A unique situation exists to test the ability of archive SAPs to discern subtle topographic changes as the northern and southern halves of Eggardon hillfort have each been afforded differing degrees of protection. The northern half has been held in private ownership and subjected to plough damage, resulting in very little, if any, remnants of previous relief in the form of archaeological features extant. The southern half, however, is owned by the NT and, aside from being open to visitors year round, has remained protected from agricultural damage. A wire fence separates the halves and denotes the parish boundary, which once may have been represented by a hedge, and stands upon a small bank on the southern half (Sutherland 1994). To the south of the fence is Askerswell parish and to the north is Powerstock. The National Trust currently lease their half to a tenant farmer who uses the area to graze sheep and, it would appear, that this has been the predominant practice for this section, based upon a note from 1982 the EH Inspectors report (English Heritage 2012a). The northern half of the Hillfort has not been so well preserved, and is not currently being used, although the author has noted cattle grazing the site on previous visits.

Due to the history of ploughing within the northern section of the hillfort over the last century, no earthworks appear visible here today. However, a series of shallow hollows and a barrow are marked on the 1952 RCHM plan of the hillfort (Royal Commission on Historical Monuments 1952) and thus have been destroyed at some point after this date. Within the EH Inspectors report of 1982 (English Heritage *ibid.*), the landowner was consulted on the agricultural activity that had taken place on this site over the last six decades. The site was first ploughed during the 'Dig for Victory' campaign during WWII. Since then the northern section has been ploughed a number of times, albeit not deeply, with the last cultivation period occurring in either 1979 or

1980 (Sutherland *ibid.*). Thus for the past three decades the site has been used for pasture, although the agricultural impact on this site will be discussed in more detail in Section 7.2.6.

7.2.3 Geology and Geomorphology

Eggardon Hillfort is situated within the Dorset Downs, an area characterised by chalk uplands (see Figure 7.2), with the Hillfort itself occupying the widest section of a chalk spur, which projects to the west and overlays greensand rock (Colley-March and Solly *ibid.*). In places, the chalk is covered by a layer of pebbly clay and sand, with Sutherland (*ibid.*) noting that the excavations within the hillfort, as conducted by Rybot in the 1960s (Wells 1978), dug through a layer of clay with varying thickness. The pit excavations, as discussed in Section 7.2.4, required archaeologists to cut through clay that was between 1-3m deep.

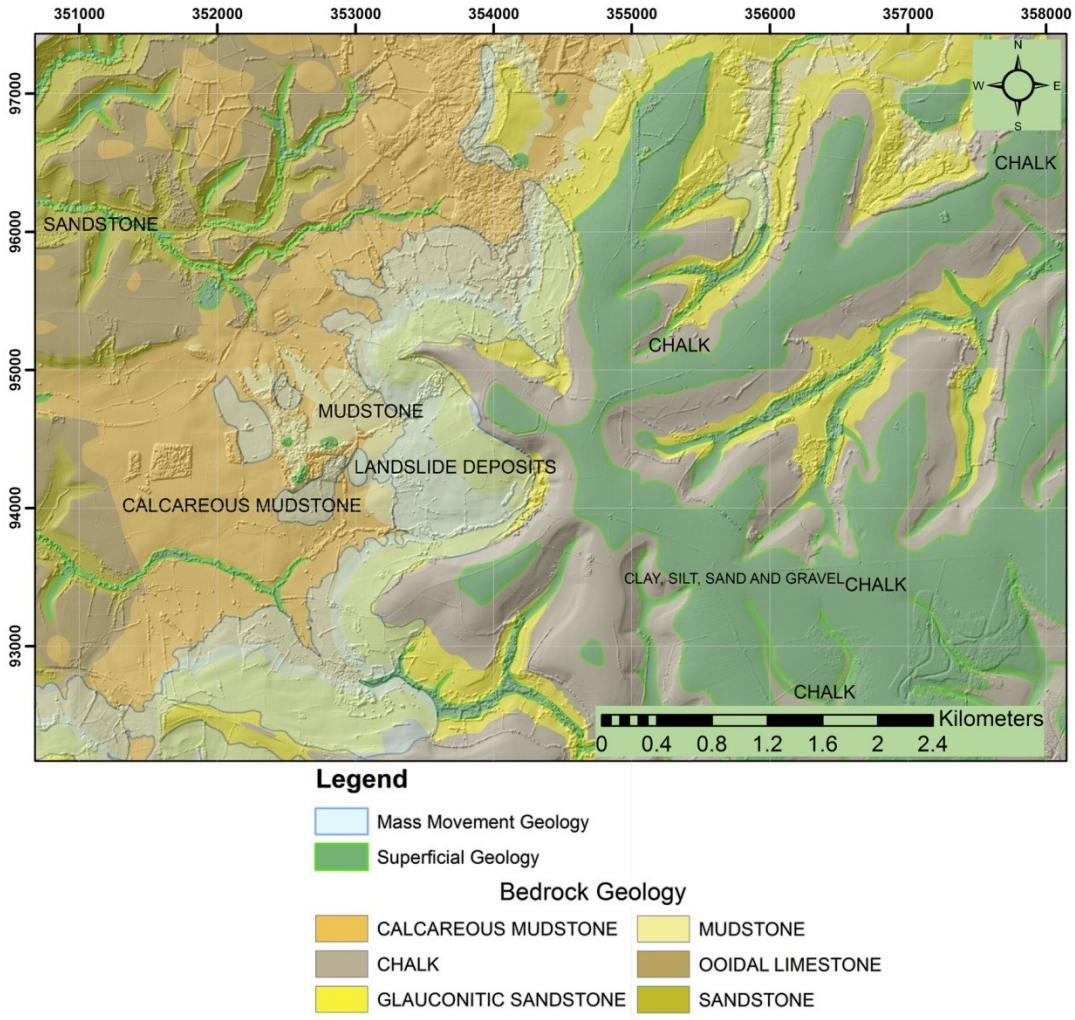

Figure 7.2: Geology Map of Eggardon Hill (© Crown Copyright/database right 2014. An British Geological Survey/EDINA supplied service).

The escarpments on which the Hillfort sits are suited to the natural defence of the site as they have a gradient of approximately 40-45°. These steep slopes bound the Hillfort on three sides: the north-east, north-west and south-west. The ramparts that run along the south-west contours of the spur have been afflicted by a landslide that has obliterated the mid-section, although archaeologists believe that this phenomenon occurred during the Iron Age as there appears to have been an attempt to adapt the defences and absorb them into the structure (see Section 7.2.4 for further discussion). The interior of the Hillfort is reasonably level and, because the site sits at 800 feet above sea level, much of West Dorset and the Askers Valley can be seen from this point (Wells *ibid.*).

7.2.4 Archaeology

Eggardon is a multivallate hillfort with steep escarpments on the north and south sides of the ramparts (Wells *ibid*), the structure of which is extensively described by Forde-Johnston (1976), Colley March and Solly (*ibid.*) and the RCHM (Royal Commission on Historical Monuments 1952). Whilst Wells (*ibid.*) postulates that the hillfort could have been built as a univallate structure initially, the RCHM (*ibid.*) state that there is no visible evidence to support this theory. The monument is scheduled and dates to the Iron Age, for which a reconstruction can be seen in Figure 7.3.

The hillfort contains two entrances: one at the north-west end, the other at the south-east. The arrangement of these openings at each end is such that the gaps in each bank are offset diagonally from each other, as can be seen in Figure 7.3. A series of interesting variations in the

Figure 7.3: Reconstruction of Eggardon hillfort, including the landslip after Skelton (National Trust 2004, p.12).

structure of the ramparts are described by Forde-Johnston (*ibid.*), who notes that the two-ditch system in place for the north-east ramparts reverses the order of the outer bank and ditch to become a ditch then a bank. Where a three-ditch system exists at the western extent of the hillfort, only the middle set does not have a counterscarp bank i.e. there is only a bank followed by a ditch (Forde-Johnston *ibid.*). The main rampart at the East end of the Hillfort is higher than any other within the monument (Royal Commission on Historical Monuments *ibid.*). Forde-Johnson (*ibid.*) also states that there are two dependant enclosures, situated at the south-western and north-eastern ends of the hillfort complex, the former of which could potentially be a cross-ridge dyke, converted from its original form to become part of the ramparts.

The southern section of the ramparts has been largely destroyed by mass-movement, referred to as an extensive landslip by the RCHM (*ibid.*), which appears to be undated in the literature, although Colley March and Solly (*ibid.*) refer to an account written by Hutchins pre-1774, which mentions the 'irregularity' of the ramparts on the southern side. The southern defences were rebuilt after the landslide, although they do not reconnect with the earlier defences (RCHM *ibid.*). A document by Papworth and Keighley (National Trust 2004) focusing on Dorset hillforts suggests that, because of this attempted reconstruction, the landslip occurred during the Iron Age. However, beyond the interpretations produced by studying the form of the reconstructed defences, there is no further evidence to support the theory that the landslip did occur during the Iron Age.

Within the hillfort, two round barrows have been recorded in the 1952 survey as have a large number of pits and a number of irregular mounds. Both barrows are situated in opposing sections of the hillfort and, whilst the barrow in the ploughed half has suffered significant damage to the point at which it can no longer be discerned by the naked eye, the barrow in the southern section has also been significantly damage but not the point of total destruction. The diameter of each barrow was cited to be 42ft (12.8m) by the RCHME (*ibid.*) with heights of 2ft (0.61m) and 4.5ft (1.37m), although it is unclear in the description which height measurement belongs to which barrow. The southern barrow was excavated by George Rybot in 1965, the process of which is described by Wells (*ibid.*). Two trenches were dug to bisect the barrow, thus giving its current appearance that is somewhat best described as a 'hot-cross bun' and, where the trenches were placed, the soil has sunk to form scars in the feature (see Figure 7.4). The artifacts produced by this intervention were in areas previously disturbed by an earlier excavation. The full contents of this barrow are therefore unknown, but the finds discovered by Rybot consisted of pottery sherds, purported to be urns. These can be dated to the Middle Bronze Age, and thus the barrows potentially pre-date the Hillfort.

The 1952 survey also noted a number of irregular mounds distributed across the interior of the site that vary in their dimensions. They are predominantly oval or circular with diameters that vary from 6ft (1.82m) to 23ft (7m), although the largest mound is in fact rectangular and measured 45ft (13.72m) by 9ft (2.74m). The heights of these features also vary between 6ft (1.82m) and 9ft (2.74m), although it should be noted that one of the oval-shaped features has been flagged as a potentially natural element. However, a few of these mounds were excavated

Figure 7.4: Bisected barrow in the southern half of Eggardon hillfort.

in the 1960s to try and establish whether they were the remains of Iron Age round houses, although the results were inconclusive (Wells, *ibid.*). The pits that are strewn cross the interior of the Hillfort, which only remain in the southern half, are approximately 3.66-4.57m in diameter and whose depressions are shallow (RCHME, *ibid.*). Colley-March and Solly (*ibid.*) describe the excavation of five pits situated within the hillfort, each of which had a two-foot wide trench opened across the middle of each feature, with the average depth of a pit reaching 6ft 1in. Contained within them were Neolithic pottery fragments, a flint knife, flint flakes, and a small assortment of other finds, which suggests that a settlement previously existed on Eggardon hill, prior to the construction of the hillfort.

Other features have also been noted within the Hillfort, both by the RCHME (*ibid.*) and Wells (*ibid.*). These consist of a ditch that is situated at the western end of the fort and runs from the southern half into the northern section, although there is no trace of the earthwork beyond the parish boundary that divides the two sections. Further linear banks are also evident within the bounds of the ramparts and are accompanied very shallow ditches, and cited to have a depth of approximately 2 in (5.1cm) (Wells *ibid.*). There are a number of linear features that run from the south-west to the north-east of the southern interior, terminating close to the eastern entrance of the hillfort, that have been identified by Wells (*ibid.*) in an aerial photograph dated 1943,

although these features were said by Wells (*ibid.*) to no longer be distinguishable in the landscape. However, on inspection of the 1989 imagery from the NMR, these features can still be seen. Based upon the trajectory of this long, linear earthwork, Wells (*ibid.*) suggests that it may very well extend beyond the outer ramparts, which would subsequently place its construction prior to that of the hillfort. None of these linear features cut across the pits within the interior, from which Wells (*ibid.*) infers that they do not post-date the pits. Wells (*ibid.*) states that further ditches were once present, although these were only discerned through excavation, and thus the divisions within the Hillfort must have been more numerous. Gale (2010) makes reference to later field boundaries within the ramparts of the hillfort, which could explain the presence of these linear banks. However, dating evidence for the series of banks suggests that some of these features may pre-date the Hillfort, which is a view also stated in the NMR monument report for Eggardon Hillfort. The pottery that was found during excavations conducted on the banks was thought to date from the Middle to Late Bronze age or Early Iron Age.

A more modern feature exists within the hillfort's interior in the form of an octagonal enclosure, which denotes the position of a former coppice as planted by Issac Gulliver, who owned Eggardon Hill and intended the feature to be visible from the sea so that the supposed pirate could steer his ships towards the land (Wells *ibid.*). It was constructed in 1776 and overlays some of the earlier features (National Trust *ibid.*). The earthwork consists of a low bank and outside ditch, although there are no approximate dimensions given by the RCHME (*ibid.*) with which to describe its form.

To the east of Eggardon hillfort are a series of different earthwork features comprising an Iron Age or Romano-British field system, strip lynchets and a series of bowl barrows, including a disc barrow that is also postulated to be a potential henge monument. The survivability of these monuments is variable, which is discussed in Section 7.2.5. The disc barrow situated to the east of the hillfort is Bronze Age and comprises a circular ditch that is complemented by an outer bank, which both flatten out at the point of infringement on a barrow that is situated on the west side (English Heritage 2012a). A second barrow is found within the centre of the feature and thus it is considered by the EH Inspectors Report (English Heritage *ibid.*) as being exceptional and comparable to the barrow at Knowlton. Grinsell (1959 p.18) states that opposing causeways are also present which, in combination with both barrows, might lead to the suggestion that this is a henge monument.

The Iron Age or Romano-British field system is a scheduled monument that covers 63 acres of land close to Eggardon Hill Farm, formed by lynchets up to 3m in height. To the north-east of the Hillfort are a number of strip lynchets, also dating to the Iron Age and Romano-British period, which have not survived well. With an average height of 0.3m, they are still visible on archive SAPs and modern aerial photography. Within the Eggardon Hill environment, a group of three Bronze Age barrows are situated close to the henge monument. One of these barrows resides in the same modern field as the henge, whilst the other two are situated in the field opposite this to the south. The agricultural attrition of these monuments is discussed in Section

7.2.6, although it is important to state here that this group are in relatively poor condition. A further six barrows used to belong to this particular group and all have been lost to the plough. Subsequently the remaining three barrows do not create a particularly stark profile in the current landscape. The northern-most barrow of this group is currently thought to be in fair condition, with 40-59% of it still surviving. When its dimensions were assessed by an EH Inspector in 1958 (*ibid.*) the barrow was thought to be 30ft (9.14m) in diameter and 3ft (0.91m) high. By 1959, Grinsell (*ibid.*) had measured the diameter to be 10 paces, which is unfortunately a subjective measure, and 2.5ft (0.76m) in height. By 1986, the diameter had reduced to 9m although the height had increased to 1m. It is not obvious from any of the EH inspectors reports, or from Grinsell (*ibid.*), how these measurements have been produced, with the exception of paces that do not give a particularly precise indication of diameter. Thus it is difficult to ascertain how any monument measured in this way can be assessed for the changes that have taken place.

7.2.5 Site Condition

The condition of the monuments within Eggardon Hillfort and its environs are variable. As will be explained in further detail in Section 7.2.6, the main cause of earthwork attrition in this landscape is agricultural activity. Whilst some monuments have remained in good condition and have been well protected, others have been significantly damaged or destroyed, predominantly due to ploughing. The majority of information relating to the condition of monuments within this region are the EH Inspectors Reports which do not appear to be available online but were requested from English Heritage for this research.

Within the EH internal reports, details are provided relating to the visit date of the monument inspector as well as the name of the individual who produced the report. Eggardon Hillfort itself has been assessed as being in good condition with an almost complete survival rate of 80-99% (English Heritage 2012). It appears to have been first visited in 1979, whilst the last assessment took place in 2008. Although each site visit does not appear to take place at regular intervals, the site is certainly monitored at least once per decade. During the 1980s the Hillfort was visited three times, which may indicate the concern that was felt as regards the erosion that was occurring in the northern half of the monument. Whilst the earthworks within the north interior have been destroyed due to ploughing, it is the area surrounding the water trough and the entrances at both the east and west ends of the Hillfort that are being eroded by the grazing cattle, which appears to be a problem that has yet to be resolved. The southern section, however, is stable as the National Trust have made several repairs to the ramparts within their jurisdiction (see Figure 7.5) whilst also monitoring any negative effects caused by grazing sheep on this site. However, the movement of sheep is causing erosion on some of the banks, as indicated by the patches that appear on the banks and the pieces of chalk that erode from these holes. Regardless of these issues, the report from 1992 considered the southern half of the Hillfort to be in excellent condition.

The henge monument to the east of the Hillfort is also considered to be in good condition and it almost wholly intact, with a survival rating of 80-99%. Despite having avoided the plough, the monument has been subjected to cattle rubbing against certain sections of the monument. In the statements made by EH inspectors in 1986 and 2008, it appears that the henge has spent some time in an overgrown state, afflicted with brambles, saplings and other weeds. However, comments made in 1989 and 2009 note that efforts have been made to reduce or clear the unwanted flora growing on the monument, which could also be due to the effects of grazing cattle. In any case, the monument is considered to be at Medium risk.

The group of three barrows also situated on Eggardon Hill, close to the henge monument, are in a more perilous state. The barrow closest to the henge is in fair condition and some 40-59% of it survives. In the past it has been ploughed, although the current threat appears to be from cattle rubbing and a few weeds. Within the southern field, the barrow that has a trig-pillar mounted upon it also has a survival rate of 40-59%, but is said to be a poor condition. Whilst plough has clipped the monument, albeit to a lesser extent due to the presence of the pillar, holes have appeared in the earthwork that are further undermined by the grazing cattle. The final barrow in the group is in very bad condition, with only 1-19% of the structure surviving. Again, ploughing has been the primary cause of this destruction, whilst grazing activity will continue to further damage the remains. It is telling that this group is all that remain of what was once a 9 barrow collection, six of which have been lost to the plough. Whilst recommendations were made by the EH inspectors to construct fencing around the remaining barrows to preserve what is left, there are currently no fences around any of these features.

Within the remaining landscape, earthwork survival appears to be mixed. There are some earthworks, such as the Iron Age or Romano-British field system, which have survived well,

Figure 7.5: Repair works conducted on the southern ramparts of Eggardon Hillfort by the National Trust.

despite their situation on cultivated land. They are in good condition and their survival is almost complete. With only a couple of sections of the banks having been clipped by the plough, the only negative observation by the EH field inspectors are the presence of weeds across the site (English Heritage *ibid.*). Earthworks that have not survived well consist of two cross-ridge dykes, both of which lie to the south-east of Eggardon Hill, and an unclassified linear earthwork just to the west of the dyke, of which only 1-19% still remains of each. Both of the dykes were almost invisible by the mid-1980s as this particular region of the Eggardon landscape is said to have been universally ploughed (English Heritage *ibid.*). Based upon this discussion of site condition, it is evident that across the region variable survival rates exist as well as a number of different earthwork types, which vary in their topographic subtlety.

7.2.6 Potential Change Due to Intensification of Agriculture

As has been previously stated, each half of the Hillfort is owned by different parties. The National Trust section has, and still does, enjoy a certain level of maintenance and care. The northern half, however, has been and still is in private ownership, the result of which has been plough damage to the features on this half of the site, which Wells (1978) observes has removed all visible traces of earthworks and depressions. Sutherland (1994) states that the vertical aerial photography of 1947 indicates that the site had already been ploughed at this time, thus giving a "*terminus ante quem*" of 1947. Whilst it would appear from the hachure plan of the site produced by the RCHM (1952) that these features were still extant at this time, this survey is stated by Sutherland (*ibid.*) to have been created prior to the commencement of the war. However, it is possible to identify slight features within the northern section in 1948 vertical photography, which has been obtained for photogrammetric restitution for the purposes of this research.

Records relating to the periods during which ploughing was undertaken and the frequency with which it was employed do not appear to exist, although Sutherland (*ibid.*) has attempted to calculate how many times ploughing took place since WWII. Based upon communications with the owner of the northern section of the Hillfort, Sutherland (*ibid.*) quotes the owner as relating that 'the land has only been ploughed once or twice' between WWII and prior to 1980. Sutherland (*ibid.*) therefore believes that the site may have been ploughed less than 20 times but it could be as high as 80, if this section had been ploughed twice a year, every year, between WWII and 1980. Where earthworks have been recorded by EH, the land class within which it sits is cited on the Internal Reports and, if the land is cultivated, the approximate depth of operations is given. This is usually quoted to be greater or lesser than 0.25m, but whether that refers to the overall ploughing activity that has taken place at each site until the present day, or the depth to which the plough has dug on each and every occasion it was ploughed is unclear.

Grazing is the agricultural activity that takes place on both halves of the Hillfort. As previously mentioned, sheep are allowed to graze the southern part as this land is leased to a tenant farmer by the National Trust. The EH Internal Report from 1982 (English Heritage *ibid.*) states that a small amount of animal damage has been incurred by this time although, in subsequent reports, the condition of the southern monument is said to be excellent, with the NT having introduced a Management Plan for this section by 1989. There were, however, noticeable areas of erosion along the entrances to the Hillfort and access paths, with small pieces of chalk eroding from the banks, presumably where the sheep are inclined to climb in and out of these features (see Figure 7.6). The issues with grazing appear to be more pronounced within the northern section, as it has been utilised for cattle as well as sheep. In 1982, cattle trample as noted, as well as an eroded patch on one of the north-west banks due to the cattle rubbing their heads against this spot. By 1989, this section of the Hillfort had been granted SSSI status, with the management strategy having been altered since 1982. The numbers of cattle had been reduced to no more than 40 during the year, and being reduced to 12 in the wintertime. Thus the inspector responsible for the 1989 report was thus concerned with erosion occurring around the cattle trough, suggesting that stabilising works were conducted to mitigate this problem (see Figure 7.6). However, by 1992, EH had not responded to the Inspector's requests for assistance in this matter.

As much of the Eggardon landscape within the Askerswell and Powerstock parishes is allocated to agriculture, other archaeological earthworks have been, and possibly still are, at risk from this activity. Within the wider landscape, a field system, strip lynchets and disc barrow (see Figure 7.7) are situated in farmland, and many of these monuments have been visited and assessed by EH monument inspectors. Some discussion surrounding these earthworks can be found at the end of Section 7.2.4. The disc barrow, which is sometimes referred to as a henge monument, is stated to be in good condition and almost all of it survives. Whilst the field in which it resides has been ploughed in the past, potentially to a depth of less than 0.25m (English Heritage *ibid.*), a 2009 Inspector's visit notes that the site has not been ploughed for at least 30 years. The disc barrow is therefore not threatened by clipping. However, the field is used for grazing cattle, and in 1986 it was noted that cattle tended to rub against the outer lip of the ditch, although the damage this caused has not been explicitly stated. Tree growth and the presence of bramble and other weeds were also noted, but by 1989 the use of the area for grazing appears to have addressed this issue.

Within the same field as the henge monument and a further field to the immediate south of this, a group of three Bronze Age barrows are listed as scheduled ancient monuments. Whilst ploughing has taken place within these fields, albeit not for at least three decades, this has resulted in some spreading of the monuments around the edges where they have been clipped by the plough. Subsequently, although the faint traces of a ditch were still observable around the northern-most barrow in 1986, the depth of this feature can no longer be discerned by topographic survey. The EH Inspectors Report (English Heritage *ibid.*) suggests that, in 1986, the flattened and misshapen top of this same barrow also inferred that ploughing had been conducted on the barrow itself.

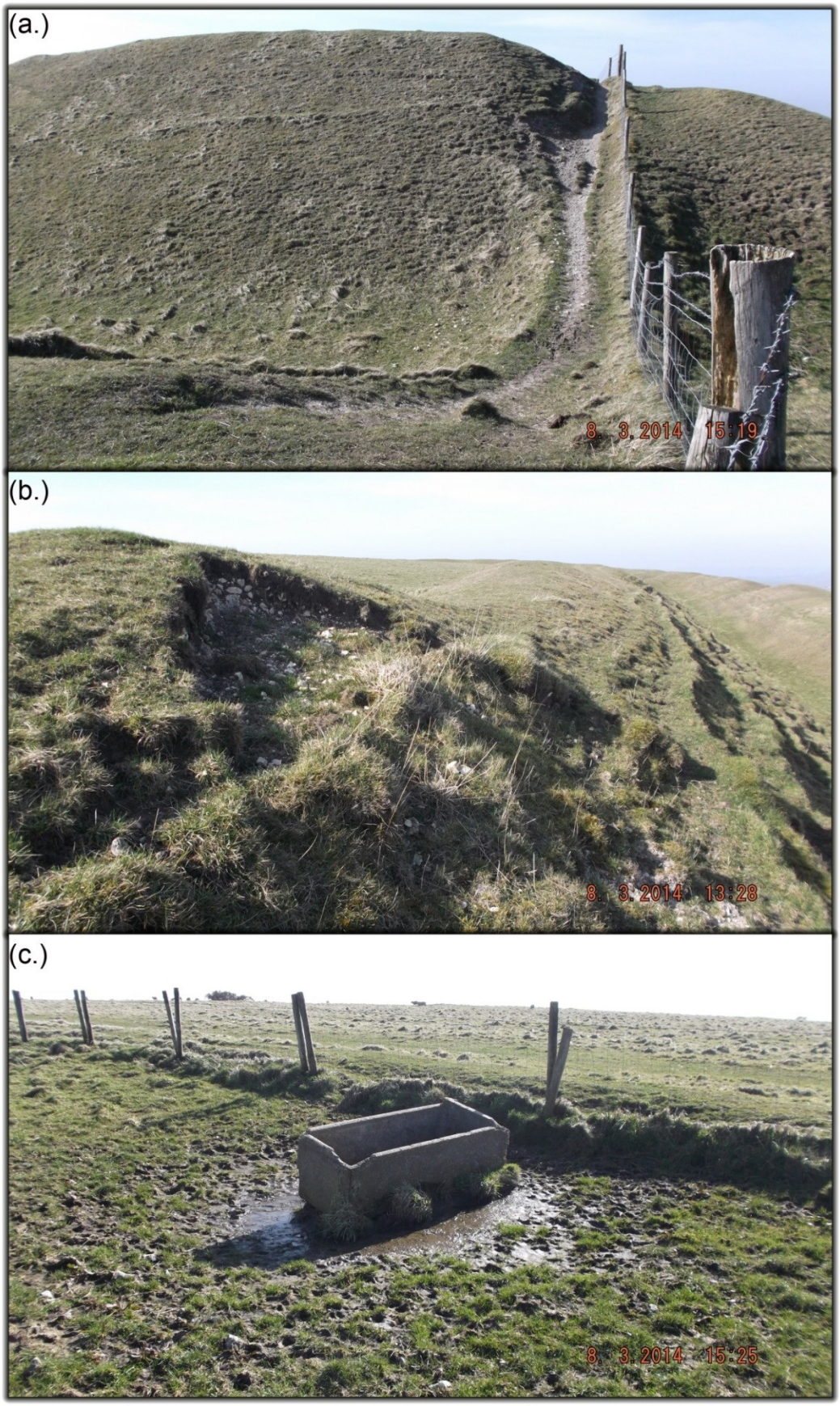

Figure 7.6: Site condition at Eggardon hillfort showing (a.) footpath erosion (b.) example of erosion on the ramparts where sheep and cattle roam and (c.) erosion around the cattle trough.

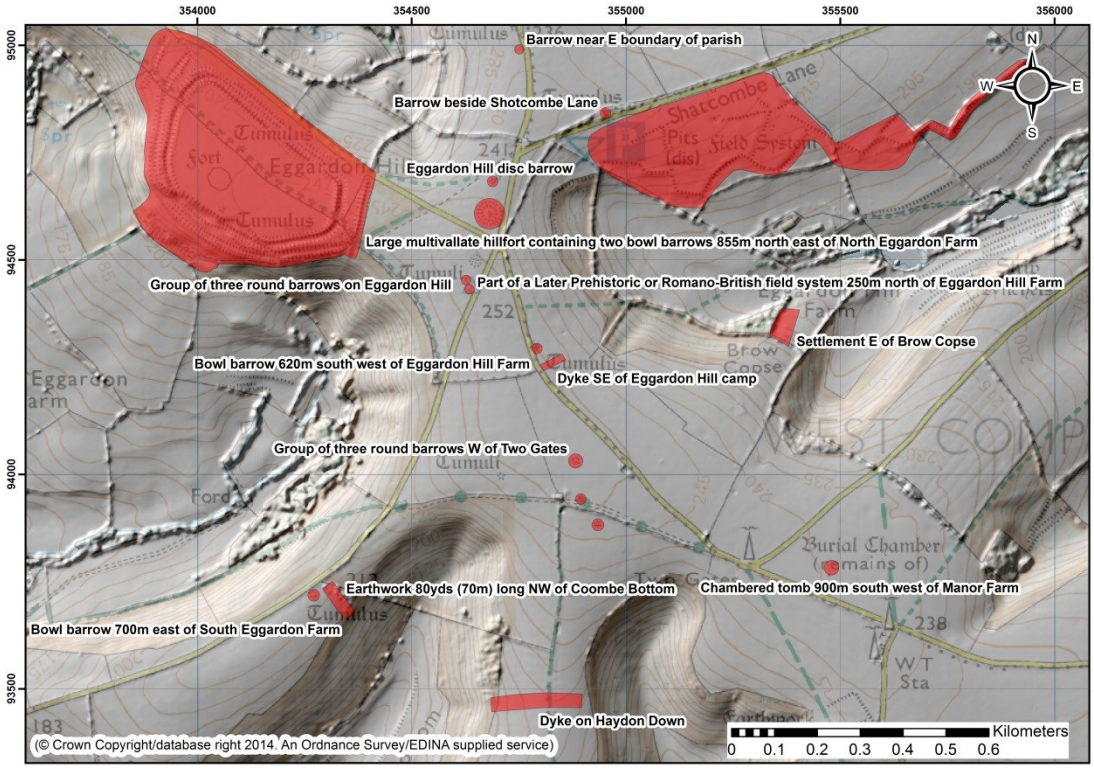

Figure 7.7: Map showing the location of Scheduled Ancient Monuments (© English Heritage) within the region surrounding Eggardon hillfort (© Crown Copyright/database right 2014. An Ordnance Survey/EDINA supplied service).

This seems reasonable as a further six barrows that once formed part of this group have been lost to the plough. Grazing of cattle has occasionally taken place within both fields, causing some damage to the surfaces of the barrows. Within the south field, an OS trig-pillar has been set atop one of the barrows and thus a hole has been dug in which to place this item. Whilst this activity has damaged the monument, it has prevented the plough from encroaching over the top of the barrow, although there is no date given for the erection of the trig-pillar.

The Iron Age or Romano-British field system in the village of West Compton has survived well, despite some of the fields being ploughed in the post-medieval period, although no specific dates are given. This information is provided by Pastscape and based upon an unpublished revision of the RCHME Dorset volumes. However, the strip lynchets to the north-east of Eggardon Hillfort are not very pronounced, with an average height of 0.3m (English Heritage 2012b). It appears that they too have been subjected to the plough, both during the medieval period and later.

Change detection at Eggardon Hillfort will therefore focus on the ability of mass-capture techniques to detect smaller-scale changes that are linked with agricultural attrition. Eggardon is uniquely suited to this purpose as the hillfort has been subjected to two different management regimes as discussed in Section 7.2.2. The rate and extent of change to the ploughed half of the monument can be measured against the preserved half, which can be used as a control for the detection of any change that is identified to have taken place. This will also identify the frequency with which SAPs are required to detect subtle change, which may require a large time

period to have passed before any change is perceived. As a tool for managing the archaeological resource, mass-capture techniques can potentially identify areas that may require intervention, either to protect and conserve areas that are becoming damaged or to secure resources for other types of archaeological intervention to more fully record threatened archaeology.

7.3 Notes on Data Processing

Tilt was a problem with both the 1948 and 1984 SAPs for Eggardon, both of which were addressed in a slightly different manner to the approach developed for the methodology (see Section 4.4.1) and with Flowers Barrow (see Sections 5.1 and 6.3). The 1948 SAP DSM also contained a stripe that ran from the east of the hillfort, indicating where the edge of one of the 1948 photographs occurred (see Figure 7.8). An initial attempt was made to address these issues by adding more tie points and GCPs, extracted from 1:1000 OS MasterMap and a 2m DSM from Landmap. Unlike the success achieved with the Flowers Barrow dataset with this approach (see Section 6.3), it achieved minimal success with the Eggardon SAPs. Subsequently, a different tactic was employed, which involved removing one of the images from the strip when performing terrain extraction in SocetGXP. This mitigated for the 'seam' that had appeared in earlier versions of the DSM. As with the Flowers Barrow SAPs, quality statistics for the triangulation and terrain extraction stages within SocetGXP are provided in Table 7.1.

Once the terrain had been produced, it was opened in ArcMap, where the residual values between the GNSS random points and the DSM elevations were calculated. These residual values were used to construct a trend surface, using the 'Trend' tool in 3D Analyst, to create a

Triangulation Root Mean Square Residuals						SAP ATE DSM Results				
SAP Date	Pix.*	X (m)	Y (m)	Z (m)	Total RMS (m)	RPS* (m)	APS* (m)		Absolute/ Relative C.E.* (m)	Absolute/ Relative L.E.* (m)
							X	Y		
1948	3.198	2.807	1.244	5.220	5.791	1.560	1	1	1.068	1.483
1948						1.710	1	1	1.068	1.483
1969	1.142	3.797	8.092	4.085	8.948	1.080	1	1	0.892	0.597
1969						1.080	1	1	0.892	0.597
1972	6.564	2.115	1.744	1.138	2.969	1.830	1	1	1.370	0.942
1984	6.243	5.900	3.164	1.815	1.934	1.170	1	1	0.557	0.653
1989	6.385	3.758	5.879	2.670	7.471	1.260	1	1	1.114	1.157
1997	2.466	7.829	1.452	5.256	1.731	1.560	1	1	1.198	0.848
2010	6.675	7.325	7.668	2.428	1.088	2.250	1	1	0.565	0.753

*Pix. = Image Pixels; RPS = Recommended Point Spacing; APS = Actual Point Spacing; C.E. = Circular Error; L.E. = Linear Error

Table 7.1: Statistical output from SocetGXP for the photogrammetrically scanned negatives, indicating the quality of the triangulation and ATE DSM solution.

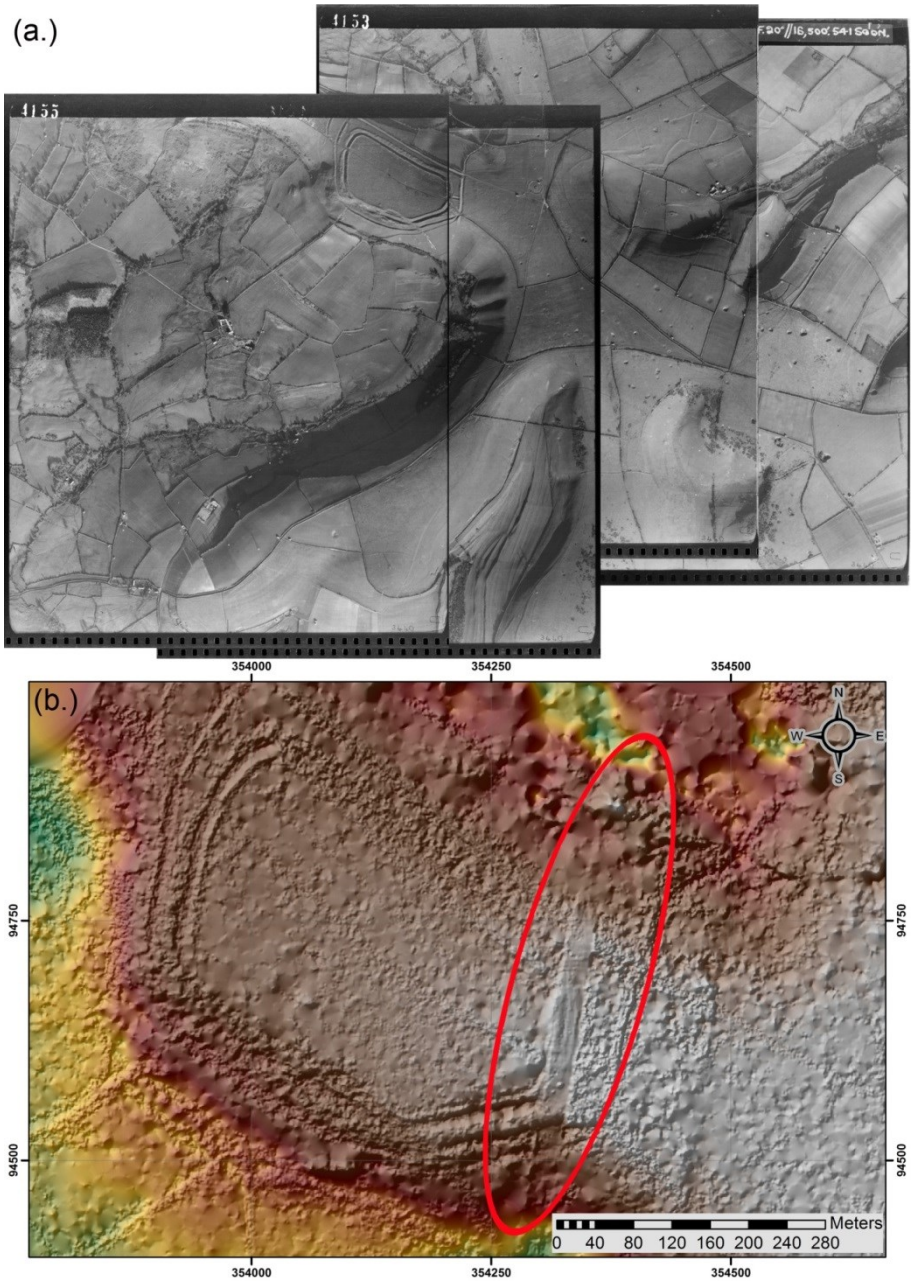

Figure 7.8: Diagram showing (a.) 1948 SAP strip and (b.) the stripe within the 1948 DSM (circled in red).

planar raster surface that modelled the pattern of tilt in the DSM. This procedure was originally mooted as a potential solution to issues of tilt in the Flowers Barrow study (see Section 5.1).The trend surface was subsequently added to the DSM to attempt to remove the disparity in the 1948 dataset.

There were also issues with a horizontal offset in the 1984 SAP DSM, despite utilising the same GCPs as in other SAP epochs. Therefore the 'ShiftXY' utility was utilised in SocetGXP, which allows the user to align a DSM with another by identifying identical features and positioning the DSM over these. The original DSM from the 1984 SAPs was positioned perfectly over the hillfort, but there was a noticeable offset around the henge monument and the barrow, both of which reside in a field further to the east of the hillfort. Therefore 'ShiftXY' was used to create a

1984 DSM that was correctly positioned over the henge monument and another DSM over the barrow. The baseline DSM dataset that was used for this purpose was derived from the TLS scans of these features. The mean absolute error obtained by registering the TLS scans of the hillfort using Leica Cyclone was 0.014m, whilst the registration of the scans across the henge monument returned a mean absolute error of 0.005m.

7.4 Elevation Assessment

In this Section the elevation data from the 1948, 1969, 1972, 1984, 1989, 1997 and 2010 epochs are compared with TLS data to provide a number of summary statistics, graphs and information graphics. These data allow the comparison of SAP DSMs with a dataset that provides the most accurate means of creating a terrain model of archaeological earthworks, namely the TLS. These comparisons will identify which of the archive SAPs are most similar to the TLS dataset, except in the regions whereby changes may have taken place due to agricultural activity or other factors.

7.4.1 Eggardon Hillfort

As with the Flowers Barrow study (see Chapter 6) it is the oldest SAP epoch, namely the 1948 imagery, which produces the poorest DSM. This is evident in the elevation DOD in Figure 7.9a, which also highlights the lack of detail along the ramparts running north-west to south-east at the top of the diagram. As the hillfort is situated at the top of the original photographs, where lens distortions are at their greatest, particularly in non-metric cameras, the poor result from the 1948 SAPs is not unexpected. It is also in this region that the strip of aerial photographs indicates a change in the apparent position of the aircraft (see Figure 7.10). However, rather than being a change in the aircraft's position, it is likely that the aircraft has rolled, creating a slightly more oblique set of image pairs. This alteration in image geometry will further hinder the production of an accurate DSM.

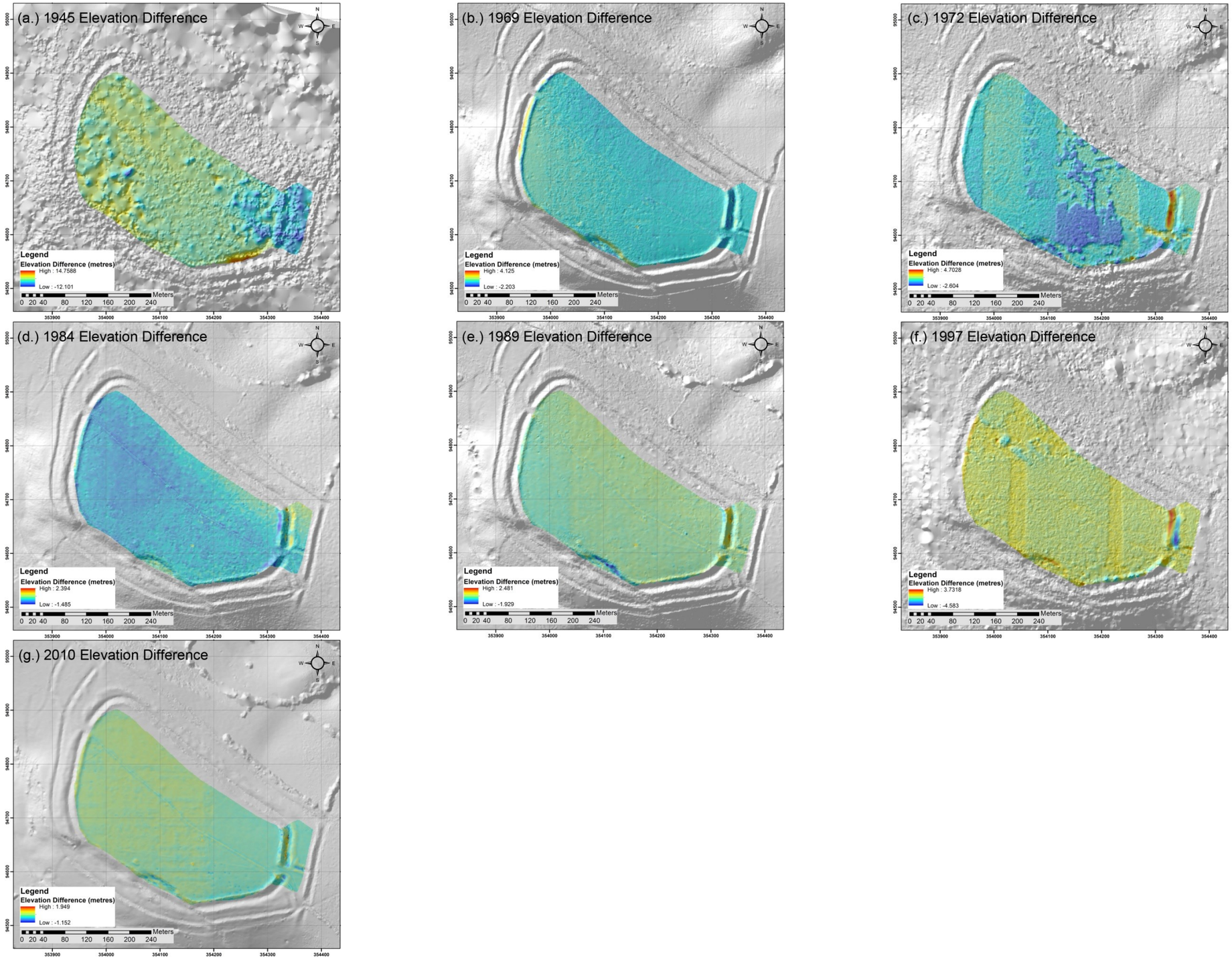

Figure 7.9: DSMs of Difference between the TLS and the SAP datasets.

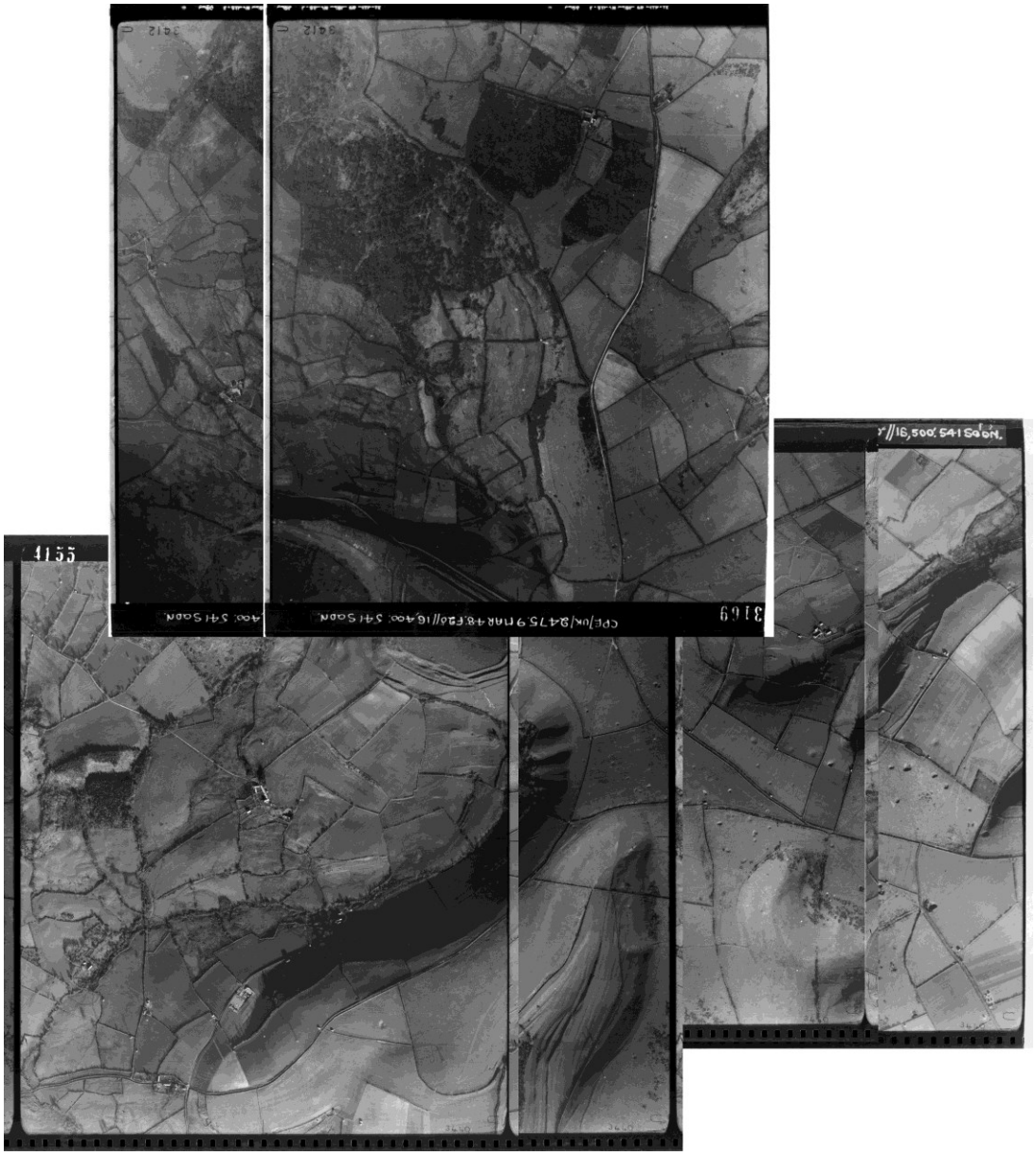

Figure 7.10: the 1948 SAP photographic block.

The appearance of the remaining DoDs generally become increasingly less noisy as the age of the SAPs decreases, which is indicated by the range of elevation differences shown in the legends provided in Figure 7.9. However, the DSMs produced from desktop scanned prints, namely the 1972 and 1997 SAP datasets, show a significant 'striping' effect in the DoDs (Figure 7.9c and f). Whilst this is also evident in the 1989 and 2010 diagrams (Figure 7.9e and g), it is more subtle and does not appear to contain the visible effects of noise, as indicated by the more 'lumpy' appearance of the 1972 and 1997 DoDs.

The summary statistics shown in Table 7.2 broadly support the observation that the accuracy of the SAP DSMs tend to improve as the age of the imagery decreases. Despite being utilised as one of the main indicators of data quality of a DSM, as discussed in Section 3.4.2, the ME statistic is the most misleading value for the Eggardon DSMs. As a measure of central

		TLS Minus 1948	TLS Minus 1969	TLS Minus 1972	TLS Minus 1984	TLS Minus 1989	TLS Minus 1997	TLS Minus 2010
N	Valid	89021	89021	89021	89021	89021	89021	89021
	Missing	0	0	0	0	0	0	0
Mean (m)		0.172	-0.044	-0.145	-0.386	0.076	0.171	0.282
Std. Error of Mean (m)		0.009	0.001	0.002	0.001	0.001	0.002	0.001
Median (m)		0.519	-0.117	-0.080	-0.424	0.088	0.141	0.304
Mode (m)		0.246	-0.153	-0.292	-0.525	0.092	-0.004	0.393
Std. Deviation (m)		2.572	0.390	0.664	0.248	0.150	0.505	0.155
Variance		6.613	0.152	0.441	0.061	0.023	0.255	0.024
Skewness		-0.779	2.835	0.492	1.411	-0.023	-0.769	-0.329
Std. Error of Skewness		0.008	0.008	0.008	0.008	0.008	0.008	0.008
Kurtosis		1.862	21.501	4.622	4.684	7.256	12.159	2.194
Std. Error of Kurtosis		0.016	0.016	0.016	0.016	0.016	0.016	0.016
Range (m)		26.860	7.879	6.793	3.431	3.524	8.254	3.100
Minimum (m)		-12.101	-2.819	-2.495	-1.606	-1.640	-4.676	-1.152
Maximum (m)		14.759	5.060	4.297	1.826	1.883	3.578	1.949
RMSE (m)		2.577	0.392	0.68	0.459	0.168	0.533	0.321

Table 7.2: Table containing summary statistics for each of the SAP epochs.

tendency, ME suggests that the residual values between the 1948 and TLS DSMs are not as deficient as those in the 1984 or 2010 data. However, the median value for the 1948 dataset, 0.519m, is the largest and, as such, suggests that elevation data produced from this dataset is the least similar to the TLS. In this instance, the median value is a more appropriate measure of central tendency as the influence of outliers and skewness is much lower. As the appearance of noise in the 1948 DoD is the most extreme, this indicates that the median is the more appropriate statistic to use in this particular case as a measure of central tendency.

Both the standard deviation and range measures (see Table 7.2) further support the observation that the 1948 data is the least similar to the TLS. These measures are at their most extreme for the 1948 residuals, which have returned a standard deviation value of 2.572m and a range value of 26.860m. The DSMs derived from the desktop scanned prints, namely the 1972 and 1997 SAPs, are the second and third most error-prone datasets, with standard deviations of 0.664m and 0.505m respectively, but with ranges that are both lower than that of the 1948, namely 6.793m and 8.254m. However, the 1969 residual values produce a range of 7.879m, but a standard deviation of 0.390. Range is another measure that can be influenced by the presence of outliers, much like ME, and thus may give an unfair representation of the errors in a dataset, particularly if there is only one extreme value which will create an unfavourable result. This highlights the need to use more than one statistical measure to examine the quality of a dataset. Conversely, the newest set of SAPs, the 2010 imagery from GetMapping Ltd, and the 1989 photogrammetrically scanned negatives, have similar standard deviation and range

values, indicating that the DSMs derived from these images are the most similar to the TLS data. Both have standard deviation values of ~0.15m, which is akin to the uncertainty often associated with ALS data (see 1.1.3.2 and Table 4.2).

The histograms illustrating the residual difference between the SAP DSMs and the TLS data are shown in Figure 7.11. The 1969, 1984, 1989 and 1997 datasets display a normal distribution of residuals and a higher degree of kurtosis as compared to the remaining SAP datasets. Unlike the elevation histograms presented in the Flowers Barrow case study (see Section 6.4 Figure 6.10), the 1948, 1972 and 2010 histograms exhibit a bimodal distribution. This indicates that there are two values in the data that occur most frequently, which in statistical studies indicates the potential presence of two differing groups of data. In both the 1948 and 1972 datasets, the second, smaller distribution of residuals consists of the lowest negative values, which appear in different regions within the hillfort for each of these epochs (see Figure 7.11a and c). In the 1948 imagery, the lowest negative values reside on the eastern ramparts, as highlighted by the darkest blue colour listed in the diagram's legend. In the 1972 data the negative residuals are contained within a strip that appears to resemble an area of overlap between the SAP images. This strip is situated to the south-east of the hillfort, predominantly within the southern half.

There are two suspected cause of this bimodal distribution. Firstly, the spread of tie points and GCPs across the image strip and their proximity, or otherwise, to the edge of the images and their information strips. If insufficient control is present in these areas the triangulation process may perform sub-optimally and image matching in these regions may fail. The second potential cause of failure is the image matching algorithm in the terrain extraction process used by SocetGXP to create representative elevation values in the areas where the SAPs overlap.

The smaller bimodal region in the 2010 data is not immediately obvious by examining the DoD, shown in Figure 7.9g. This is unsurprising as the peak of the negative residuals in the 2010 histogram (see Figure 7.11g) is much larger than those of the 1948 and 1972 datasets, but not as wide. Therefore the effect of this double peak is much more subtle. In general, the majority of the residuals are positive, whilst the smaller peak is centred close to 0m. These values are contained within the hillfort to the centre and the west of this area. There appears to be a slight difference between this region and the east of the hillfort, where the overlapping images in the 2010 dataset have not been matched properly during the terrain extraction process.

The reasons as to why stripes have occurred in the DSMs are not clear. With both the 1948 and 1972 SAPs there could be an excessive amount of distortion in the imagery that impedes the accurate matching of identical regions in the overlapping images during the terrain extraction process. The source of this distortion in both images is based upon the lack of camera calibration data, which will not exist for the 1948 dataset as the RAF cameras at this time were non-metric. However, the 1972 SAPs would have been created with a metric camera, although the accompanying certificate was not available. A further source of error with this dataset is that the digital version has been produced by scanning photographic prints. This introduces additional errors due to the unknown distortion characteristics of the desktop scanner used to create a digital copy, which can only be mitigated if the scanner itself has been characterised.

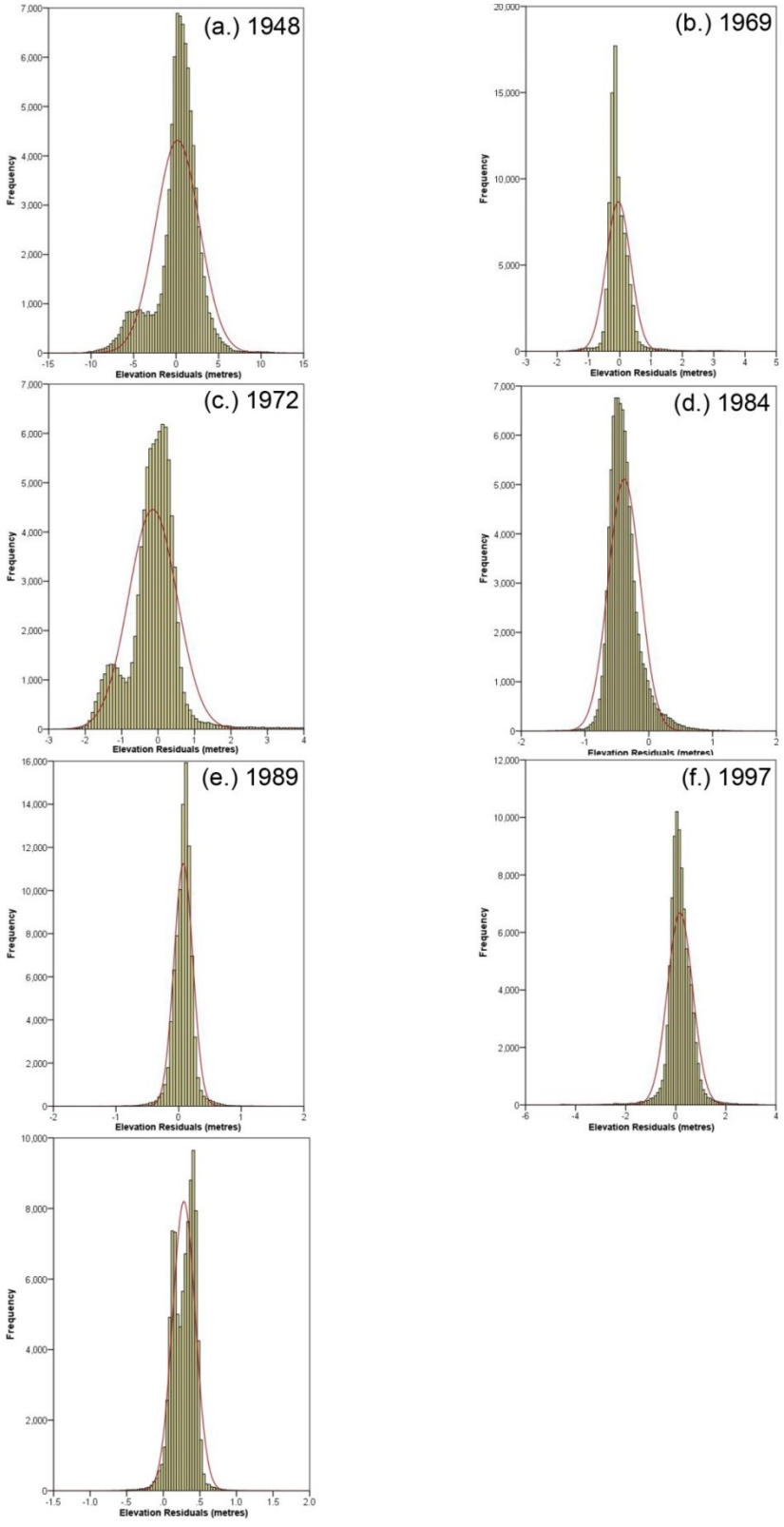

Figure 7.11: Histograms for the hillfort region showing the frequency distribution of residual differences between each SAP epoch and the TLS data.

As there is also a subtle stripe effect in the 2010 DSM, which was processed with the full camera calibration details available as well as a large number of tie points distributed across overlapping regions of photography, it is logical that the process causing this issue is the terrain extraction stage.

After consultation with BAE Systems (personal communication, 11th April 2014, see Appendix Three), the tentative suggestions as to why these stripes appeared were limited. As the stripes coincided with some of the information strips or the edge of an image it was suggested that these could be the cause and that removing these images may solve the problem. Another solution was to use the minimum number of images that covered only the area of interest or, alternatively, set the maximum number of image pairs used by the software to "1" and turn off back-matching. As all of the SAP DSMs had been created by this stage and the majority of analysis had been completed, any experimentation with these settings are consigned to further work (see Section 9.1).

The linear correlations for each of the SAP elevation datasets, when compared to the TLS, indicate that the 1984, 1989 and 2010 data, shown in Figure 7.12d, e and g, are comparable with the TLS. Each of these datasets were scanned from negatives by the NMR using a photogrammetric scanner, and the majority of elevation values conform to the positive correlation, with a few notable exceptions that form the outliers. Outliers from the 1984, 1989 and 2010 DSMs appear across the range of elevation values, although those in the 1984 dataset very to a much greater degree. By examining the photography from each of these epochs, some of the factors that may cause outliers are the presence of cattle in the SAPs as well as the presence of the fence that divides the north and south sections of the hillfort (see Figure 7.13). There also appear to be instances of dust and scratches on the 1984 imagery, which may also influence the presence of outliers in the resultant DSM. The remaining epochs, namely 1948, 1969, 1972 and 1997, all exhibit outliers that deviate significantly from the linear distribution. In the case of the 1948 DSM, there is minimal linear structure, whilst the range of elevation values in this dataset is much greater than those of the remaining epochs. As mentioned previously in this section, it is the outliers that can make the range statistic appear large and may not be representative of the quality of the DSM.

The distribution of outliers at particular elevations in the data is enhanced by plotting the residual values between each SAP epoch and the TLS against the TLS elevations themselves, as shown in Figure 7.14. Although the 1984 DSM appears to conform to a positive, linear correlation, much like the 1989 and 2010 scatterplots, the spread of outliers is more exaggerated in the 1984 diagram (Figure 7.14d) than in the 1989 and 2010 graphs (Figure 7.14 e and g respectively). In the 1984 and 1989 datasets, there is a noticeable 'hook' shape that appears at an elevation of c.238m. The regions of the hillfort that coincide with this elevation value are the landslip to the south and the flat interior to the north-west. However, it is difficult to identify the regions in which these outliers occur by simply examining the residual and linear scatter plots.

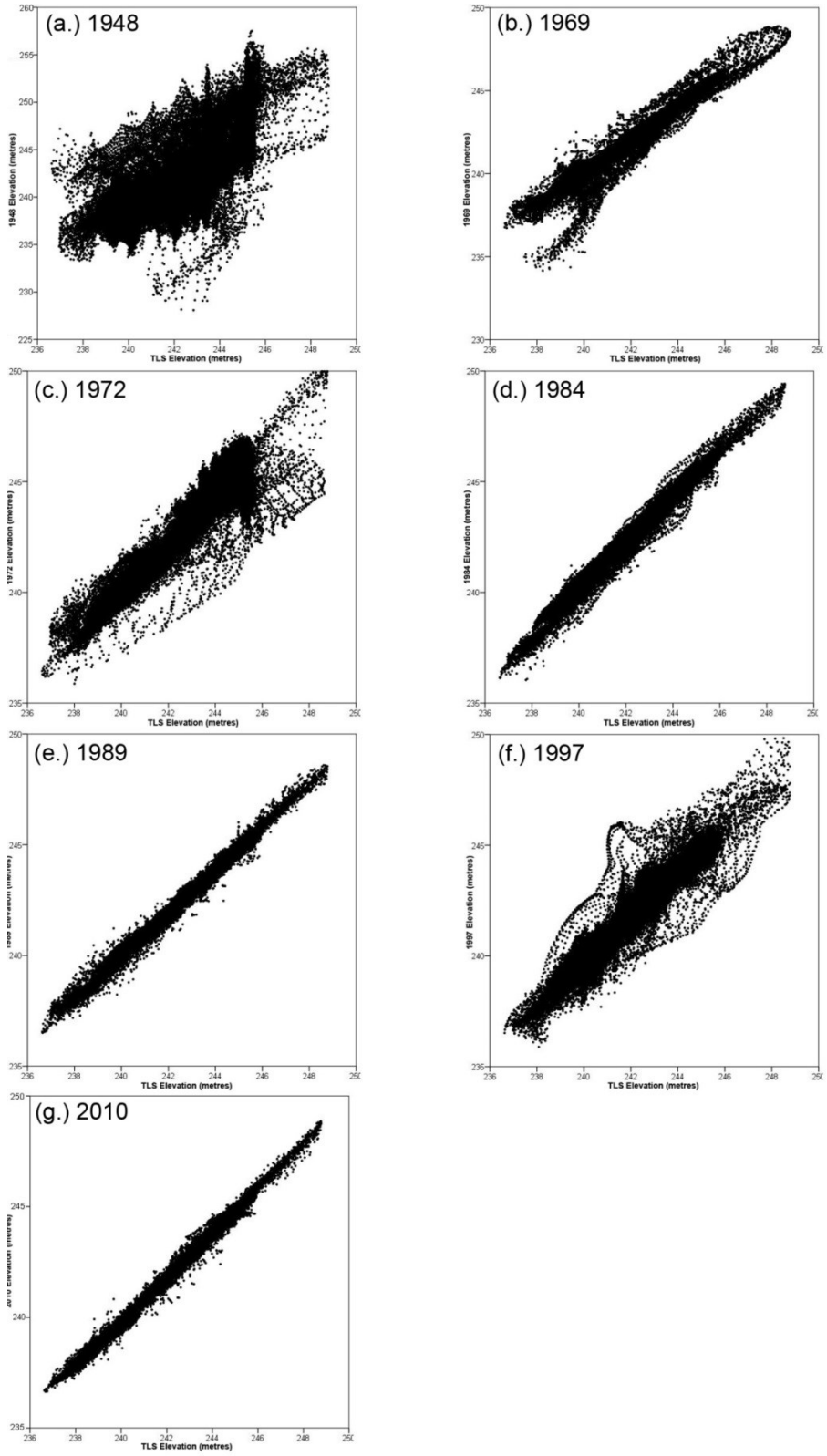

Figure 7.12: Scatterplots illustrating the linear correlations between each of the SAP epoch elevation values and those of the TLS.

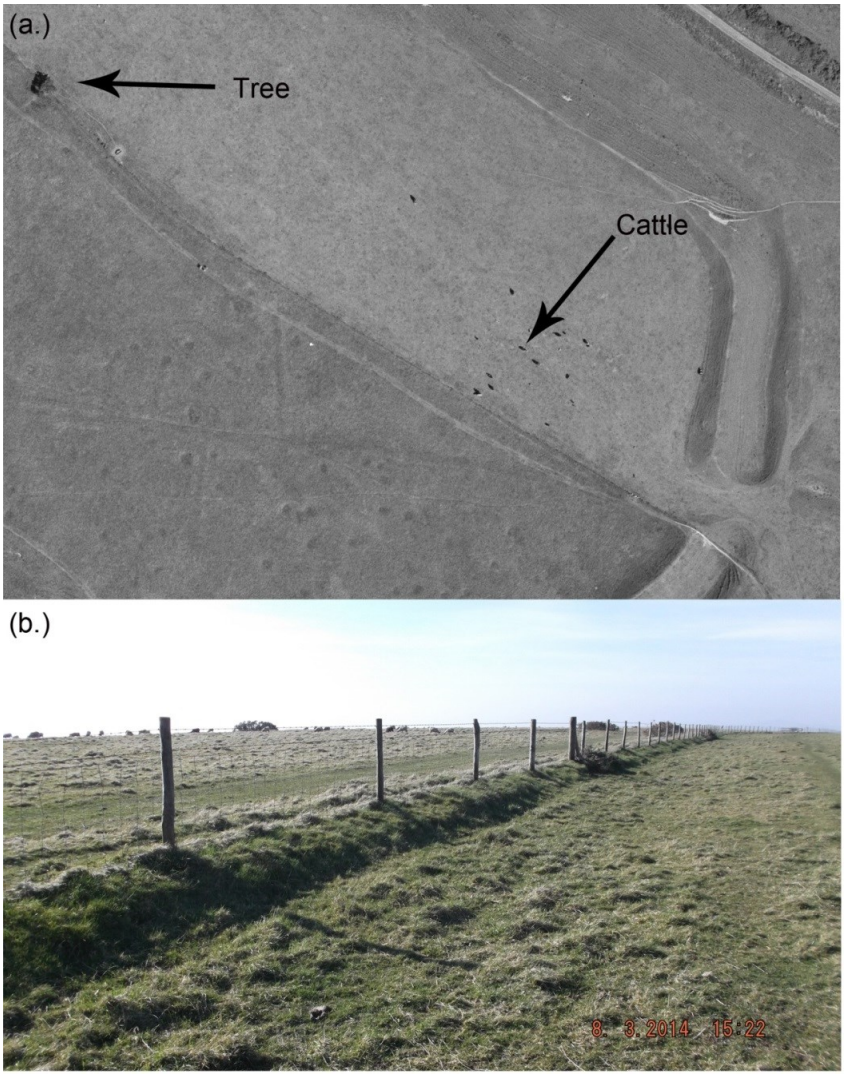

Figure 7.13: Potential causes of outliers in the Eggardon SAP DSMs (a.) vegetation and cattle (b.) fence line.

	Paired Samples		Paired Differences			
	Correlation	Sig.	95% Confidence Interval of the Difference		t-value	Sig. (2-tailed)
			Lower (m)	Upper (m)		
TLS minus 1948	0.717	0.000	0.155	0.189	19.963	0.000
TLS minus 1969	0.981	0.000	-0.047	-0.041	-33.680	0.000
TLS minus 1972	0.949	0.000	-0.150	-0.141	-65.309	0.000
TLS minus 1984	0.992	0.000	-0.388	-0.384	-464.402	0.000
TLS minus 1989	0.997	0.000	0.075	0.077	151.509	0.000
TLS minus 1997	0.967	0.000	0.168	0.174	100.993	0.000
TLS minus 2010	0.997	0.000	0.281	0.283	543.853	0.000

Table 7.3: Results from a paired t-test, performed in SPSS, comparing the TLS and SAP DSM elevations.

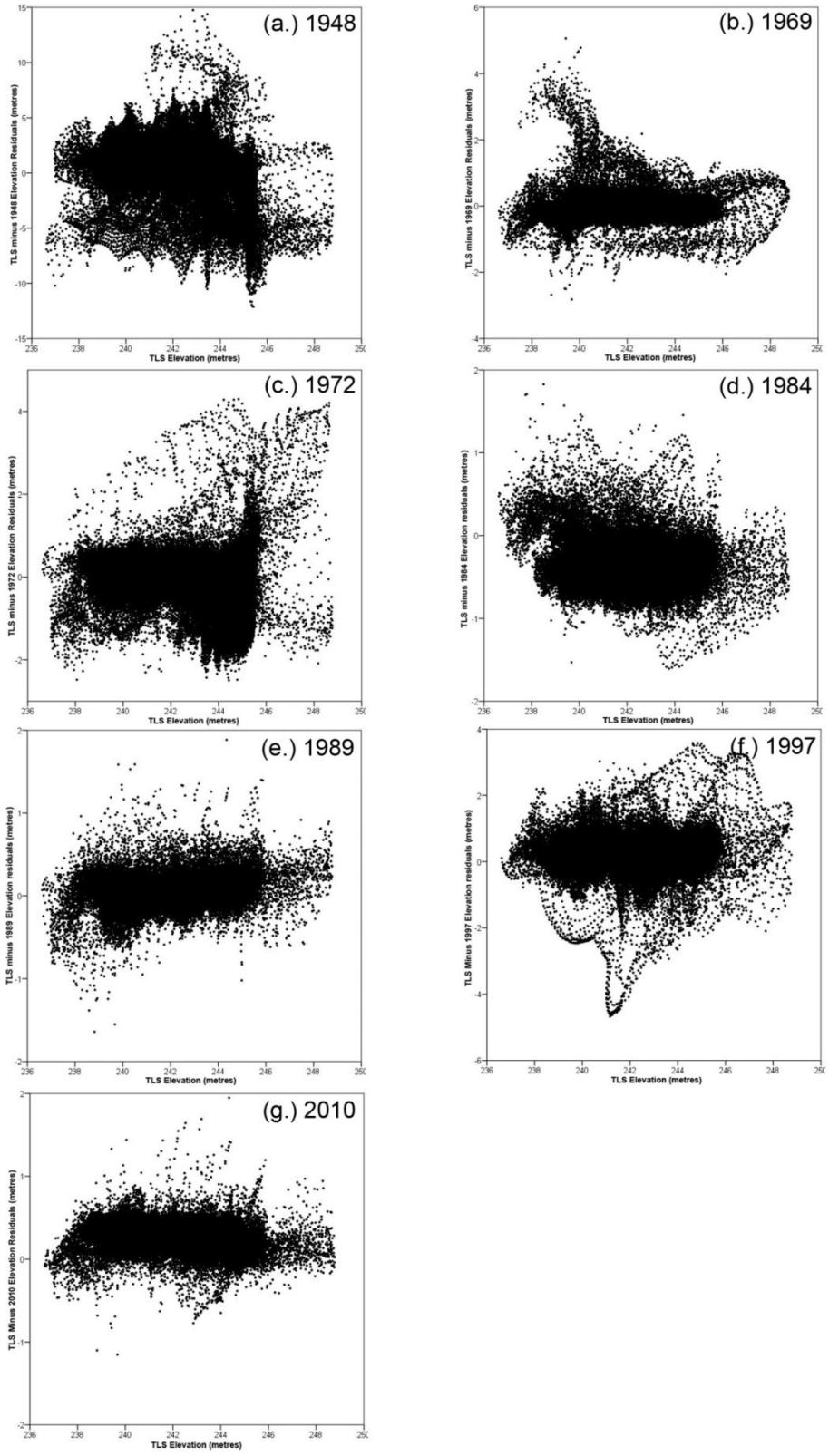

Figure 7.14: Scatterplots showing the relationship between TLS elevation values and the residual values between the TLS and SAP epochs.

To ascertain the spatial distribution of these error values and potentially any further inferences about their cause, a Moran's I analysis has been conducted on this data and is discussed in 7.4.3.

The results of the paired t-test indicate a high correlation between the TLS elevation values and the majority of the SAP DSMs, with the exception of the 1948 dataset, which has an r-value of 0.717 as shown in Table 7.3 on page 272. However, the p-value denoting significance of each of the SAP DSMs in relation to the TLS is 0.000 for all of the datasets, which suggests that the null hypothesis must be rejected i.e. it cannot be stated that there is no difference between the TLS data and the SAP DSMs. As the p-values are based upon a census analysis that compares datasets with almost 90,000 elevation values, the significance measure may not be as meaningful as it would be on a much smaller dataset. As discussed in Chapter 3 Section 3.4.2, if the lower and upper boundaries of the 95% confidence interval crossed 0, then there would be a case for arguing that it is likely that the null hypothesis can be accepted i.e. there is a chance that there is no difference between the TLS and SAP datasets. By looking at the upper and lower boundaries given in Table 7.3, this is not the case for any of the SAP and TLS pairs as none of the intervals cross 0.

Due to the inconclusive result provided by the census analysis, the paired t-test was run on the stratified random points that were collected across the extent of the hillfort, the surrounding fields and the henge monument. There are 348 random points and by examining the results from this population sample, comparing the GNSS values to those of the SAP DSM elevation values, a set of more meaningful p-values has been produced (see Table 7.4). The p-values for all of the SAP DSMs, with the exception of the 2010 data, are not statistically significant as they are all greater than 0.05 and thus the null hypothesis cannot be rejected. The upper and lower boundaries of the 95% confidence interval also cross 0m, and thus it is likely that many of the residual values could be 0m. It is surprising that the 2010 DSM, which should be the most error-free dataset, is thought to be statistically different to the GNSS values. The mean residual value is much higher than the other DSM epochs, although this can be accounted for as there has been no attempt to reduce elevation disparities in the 2010 elevations by adding or subtracting the mean difference from the elevation raster. This process has been performed on the majority of the other SAP epochs and thus their mean errors appear to be favourable.

7.4.2 Eggardon Henge Monument

The henge monument and associated barrows to the east of Eggardon Hillfort are more subtle earthworks as compared to the ramparts of the hillfort. They thus provide a greater challenge for the photogrammetric software to extract elevation values representative of these features from the SAPs. Visually, the worst performing DSMs have been produced by the 1948, 1972 and 1997 epochs (see Figure 7.15 a, c and f respectively), as indicated by their noisy appearance,

		Paired Differences					t	df	Sig. (2-tailed)
		Mean (m)	Std. Deviation (m)	Std. Error Mean	95% Confidence Interval of the Difference				
					Lower (m)	Upper (m)			
Pair 1	**GNSS - SAP1948**	0.001	3.496	0.187	-0.368	0.369	0.004	347	0.997
Pair 2	**GNSS - SAP1969**	0.000	0.834	0.045	-0.088	0.088	0.000	347	1.000
Pair 3	**GNSS - SAP1972**	0.000	0.694	0.037	-0.073	0.073	0.000	347	1.000
Pair 4	**GNSS - SAP1984**	0.000	0.622	0.033	-0.066	0.066	0.001	347	0.999
Pair 5	**GNSS - SAP1989**	0.000	0.293	0.016	-0.031	0.031	0.000	347	1.000
Pair 6	**GNSS - SAP1997**	0.000	0.956	0.051	-0.101	0.101	0.000	347	1.000
Pair 7	**GNSS - SAP2010**	-0.077	0.286	0.015	-0.108	-0.047	-5.056	347	0.000

Table 7.4: Results from a paired t-test, performed in SPSS, comparing the GNSS and SAP DSM elevations across the hillfort.

especially in the case of the 1948 data. The 1969, 1984, 1989 and 2010 SAPs have all performed well and the presence of both the barrow and the henge can clearly be identified.

The histograms produced by the census analysis of the TLS data with the SAP DSM datasets in this area also exhibit some bimodal distributions, particularly in the case of the 1972, 1984 and 1989 data (see Figure 7.16c, d and e respectively). There is a visible seem running down the right-hand side of the 1972 DoD (see Figure 7.17), which would explain the plateau of the negative residuals displayed by the histogram. In the 1984 data there appears to be a subtle tilt running from positive residuals in the north-east to smaller positive residuals in the south-west. The DSM was manipulated in ENVI to remove the horizontal distortion in the DSM, as output by SocetGXP, whilst the tilt in the elevation values was addressed by constructing a trend surface and subtracting this from the 1984 DSM. However, it appears that some error remains. By examining the aerial photographs for the 1984 epoch it can be seen that there was a large amount of gorse growing on the henge monument, as shown in Figure 7.18, which had been identified in the Monument Inspector's report in 1986 (see Section 7.2.5) as something that needed to be removed. As there was no gorse present during the TLS survey in 2013, there is likely to be an elevation offset across the henge monument in any case.

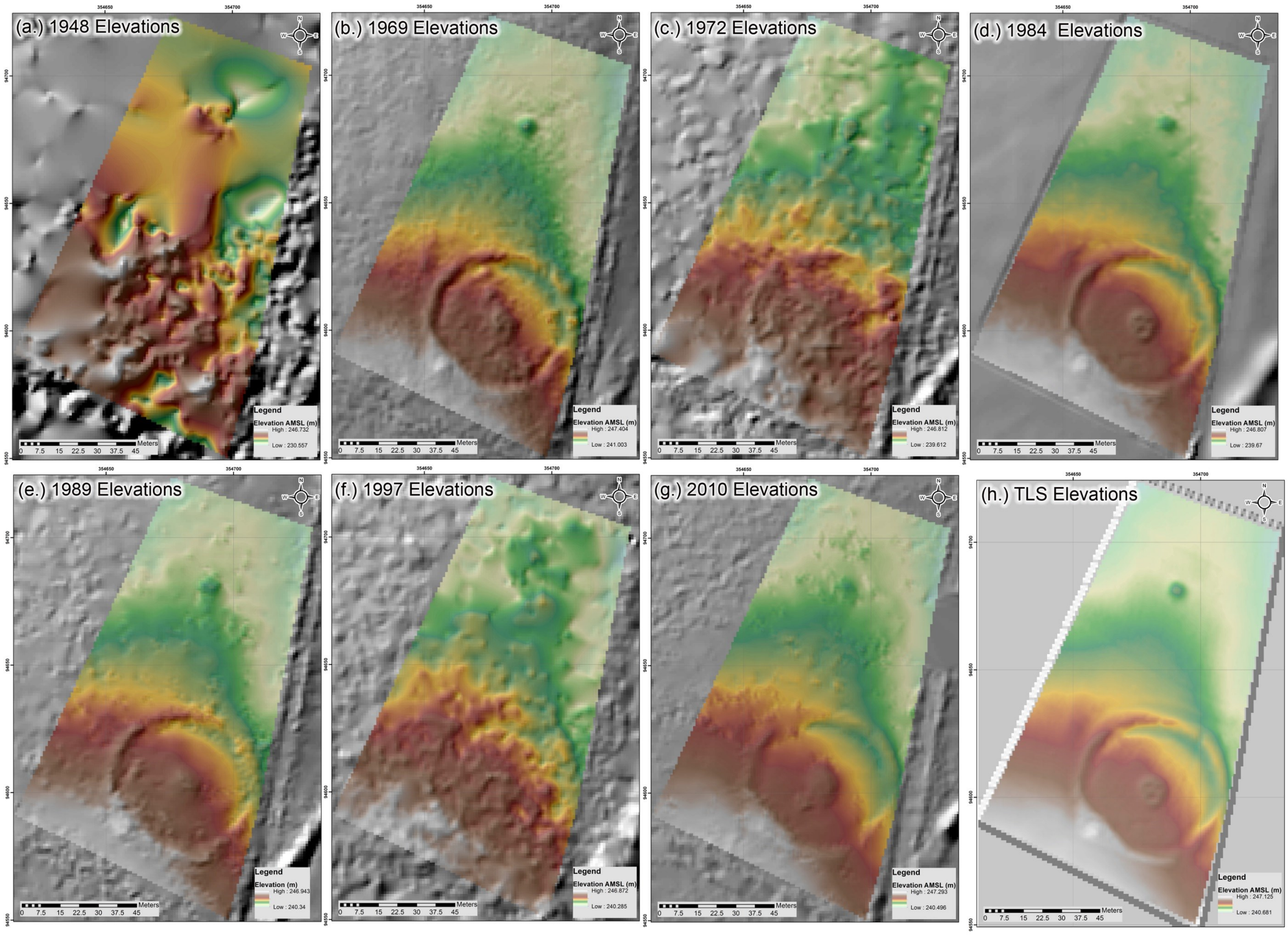

Figure 7.15: Diagram showing the DSM elevations across the Eggardon Henge monument.

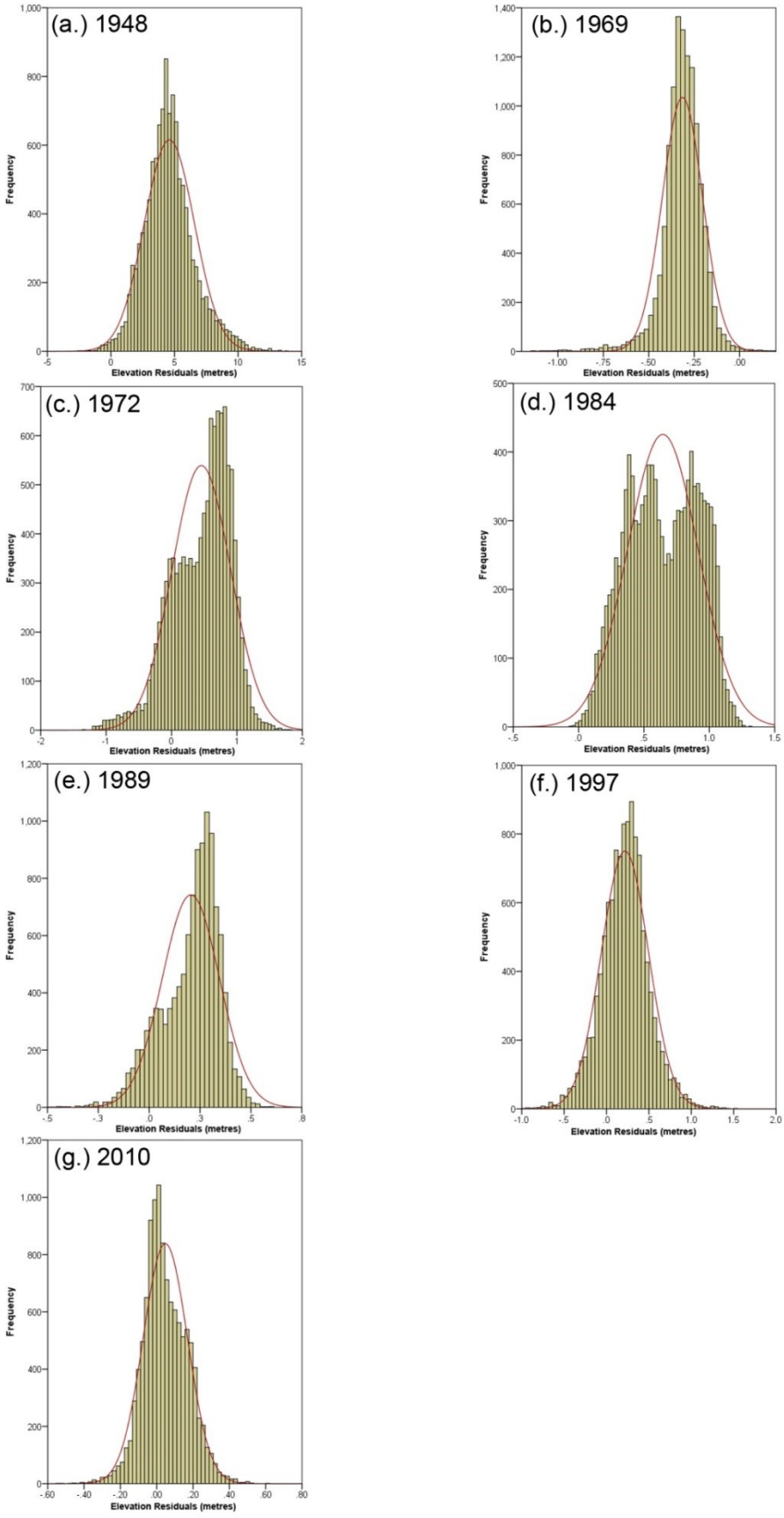

Figure 7.16: Frequency histograms showing the residual difference in elevation values between the TLS and SAP DSMs across the henge region.

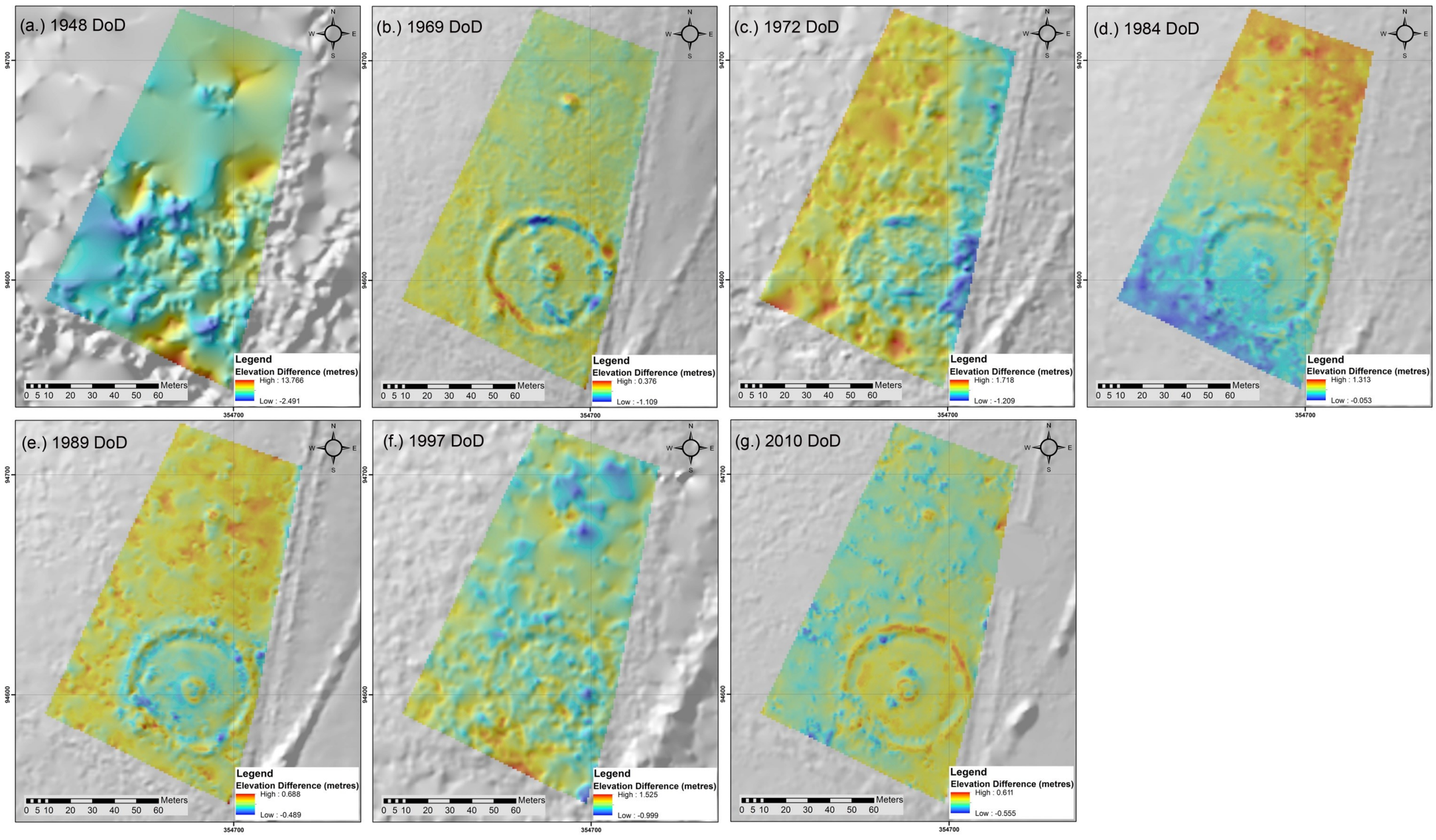

Figure 7.17: DSMs of Difference for the Eggardon Henge Monument.

Figure 7.18: Condition of the henge monument as shown in the 1984 SAPs.

Scatter plots showing the linear correlation between the TLS and SAP elevation values for this area, as shown in Figure 7.19, do not appear to exhibit as many outliers as were apparent in the hillfort diagrams (see Figure 7.12). However, there are 11,500 values to compare in the henge area, as opposed to 89,000 for the hillfort, and thus it is expected that the hillfort statistics will exhibit fewer large residuals. The 1948 dataset still contains the largest range of residual values compared to the other SAP epochs. The statistic for range, as shown in Table 7.5, is high for the henge area, as it was for the hillfort, namely 16.257m and 26.86m respectively. The second highest range value for the henge area is from the 1972 data, with a range of 3.152m, which highlights just how error-riddled the 1948 DSM is. The 1969, 1984, 1989 and 2010 scatterplots (Figure 7.19b, e and g) all appear to be linear, whilst the 1972 and 1997 graphs indicate that there are regions of the henge which do not agree with the TLS survey across the range of elevation values.

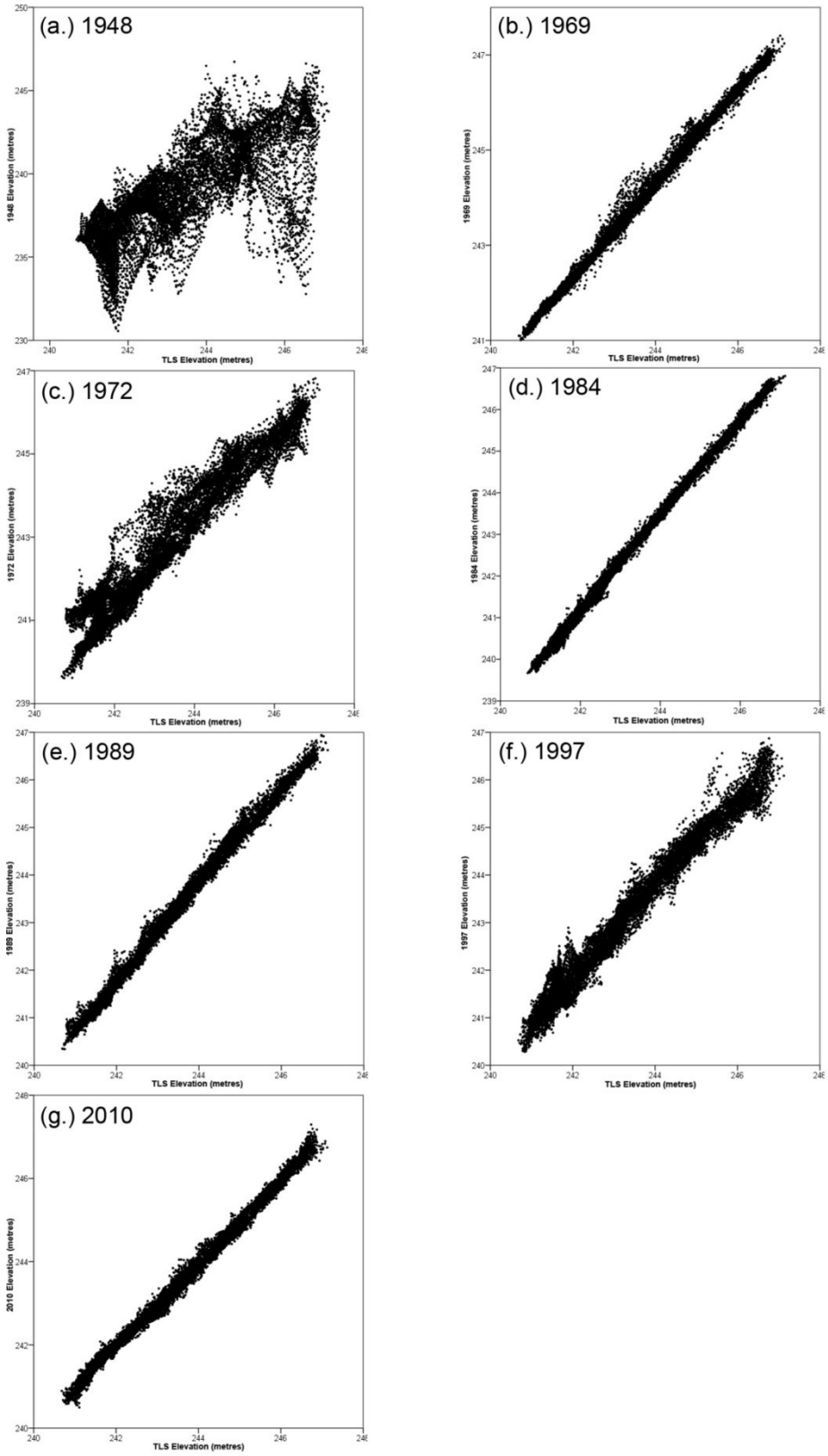

Figure 7.19: Scatterplots showing the linear correlation between the TLS and SAP elevation data.

		TLS Minus 1948	TLS Minus 1969	TLS Minus 1972	TLS Minus 1984	TLS Minus 1989	TLS Minus 1997	TLS Minus 2010
N	Valid	11544	11544	11544	11544	11544	11544	11544
	Missing	1	1	1	1	1	1	1
Mean (m)		4.597	-0.315	0.456	0.644	0.205	0.217	0.047
Std. Error of Mean (m)		0.018	0.001	0.004	0.003	0.001	0.003	0.001
Median (m)		4.457	-0.310	0.549	0.636	0.238	0.225	0.033
Mode (m)		4.422	-0.343[a]	0.701	0.856	0.242	0.214[a]	-0.005
Std. Deviation (m)		1.970	0.111	0.450	0.271	0.141	0.279	0.122
Variance		3.881	0.012	0.202	0.073	0.020	0.078	0.015
Skewness		0.510	-1.212	-0.636	-0.076	-0.747	0.004	0.152
Std. Error of Skewness		0.023	0.023	0.023	0.023	0.023	0.023	0.023
Kurtosis		0.924	6.128	0.218	-1.014	0.420	0.942	0.516
Std. Error of Kurtosis		0.046	0.046	0.046	0.046	0.046	0.046	0.046
Range (m)		16.257	1.326	3.152	1.366	1.177	2.524	1.166
Minimum (m)		-2.491	-1.140	-1.359	-0.053	-0.489	-0.999	-0.555
Maximum (m)		13.766	0.186	1.793	1.313	0.688	1.525	0.611
RMSE (m)		5.002	0.334	0.640	0.698	0.249	0.353	0.131

Table 7.5:Table containing the summary statistics for elevation residuals within the henge monument region.

By plotting the residual values against TLS elevations, as shown in Figure 7.20, the results are subtle for the 1989 and 2010 DSMs. The 1969 scatterplot shows a cluster of extreme residual values at an elevation of ~243m, which appears as a dark blue patch on the north-west interior of the henge in the DSM (Figure 7.15). This suggests that the 1969 DSM here is higher than the TLS, which can be explained by looking at the 1969 SAP photography (see Figure 7.21). There is patchy gorse coverage across the henge monument, which is not present in the TLS survey, and thus a negative difference is expected. The 1984 scatterplot indicates that there is a tilt within the DSM based upon the negative correlation between the TLS elevation values and the residuals. Aside from the tilt, however, there appear to be few extreme residual values that deviate from the main body of points.

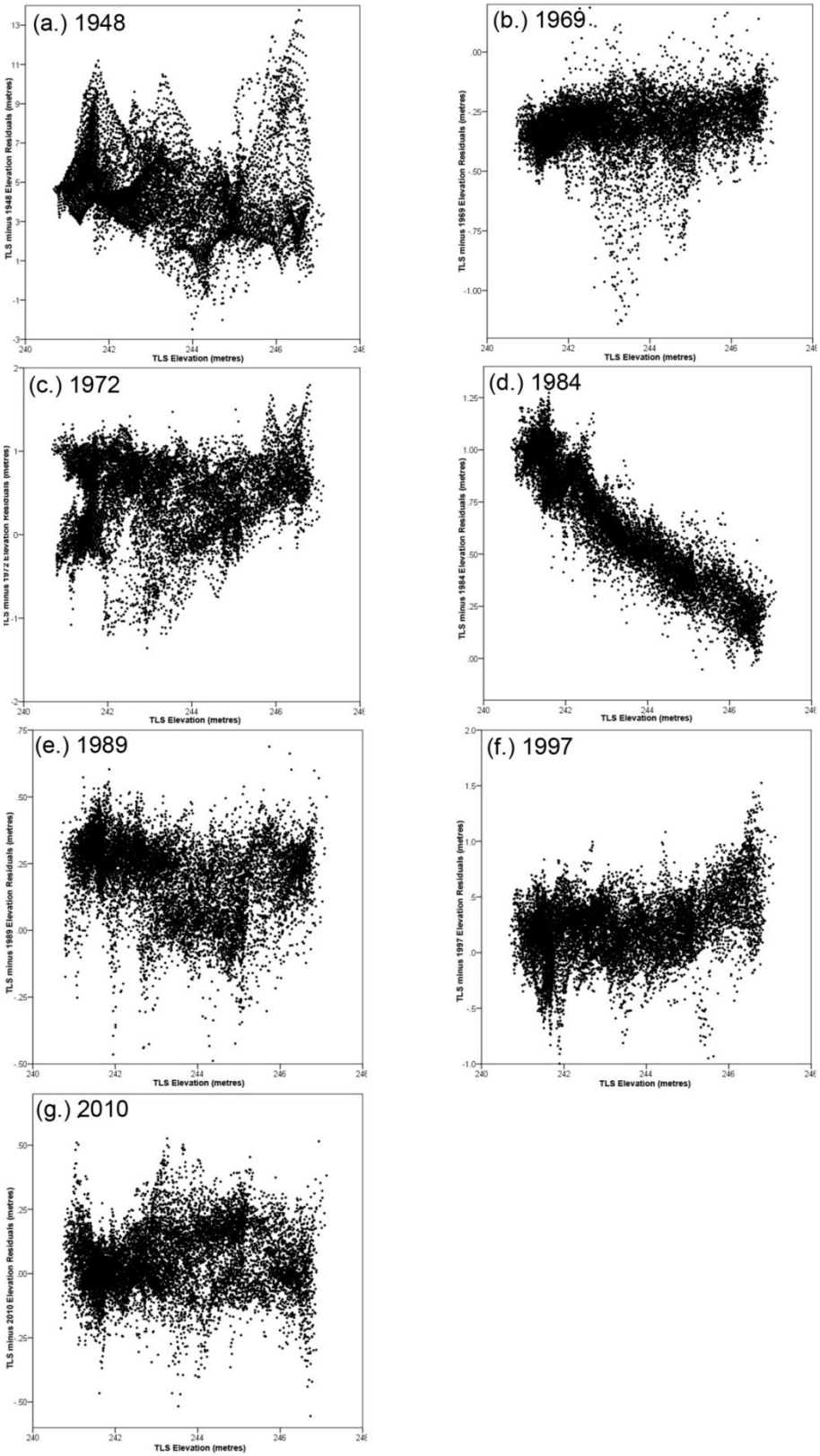

Figure 7.20: Scatterplots showing TLS elevations plotted against elevation residuals for each SAP epoch for the henge region.

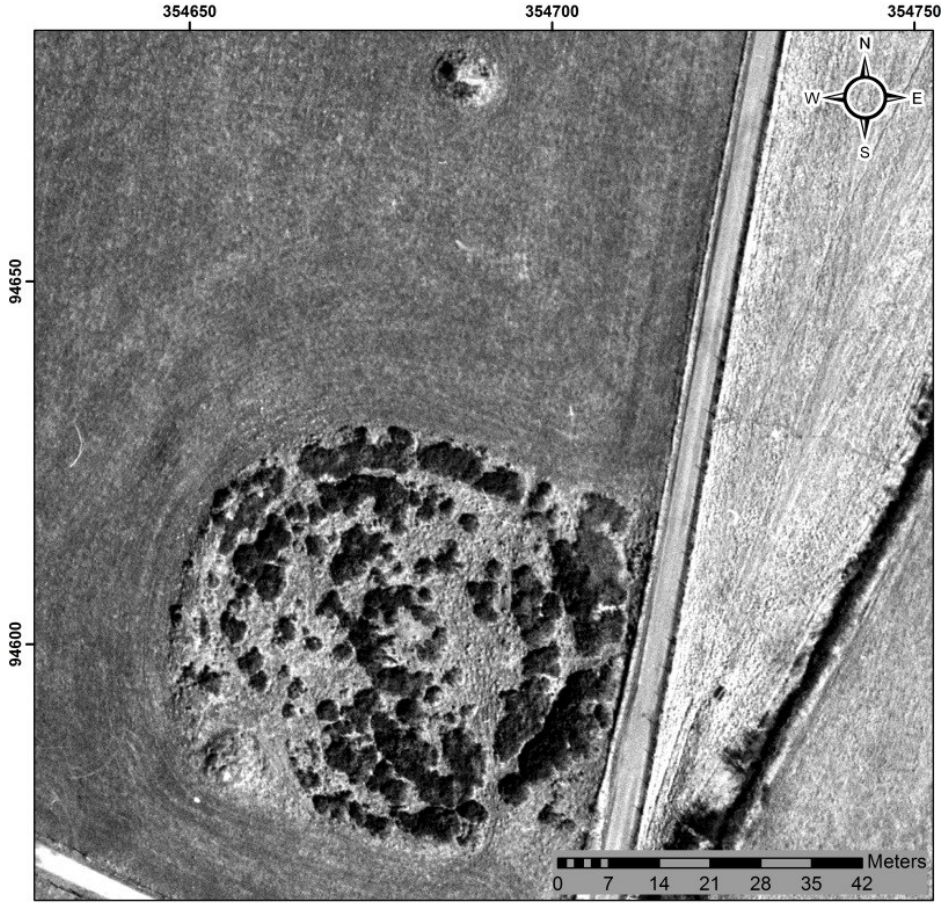

Figure 7.21: Condition of the henge monument as shown in the 1969 SAPs.

Upon performing a paired t-test for each SAP epoch and the TLS data, the p-values suggest that there are significant differences between the TLS and each SAP DSM as each p-value is 0.000. The upper and lower 95% confidence intervals do not cross 0m either, and therefore the null hypothesis must be rejected. However, as explained in the previous section, it is unlikely that these results are meaningful because of the number of values being tested i.e. 11,544. Therefore, the reader is referred to the last paragraph of the previous section, which discusses the alternative result by utilising the stratified random points across the Eggardon landscape.

7.4.3 Local Moran's I Analysis

As the spatial distribution of the residuals and their magnitude cannot be easily appreciated by examining scatter plots and statistics, the Local Moran's I maps help to overcome this problem. Whilst the distribution of residual values is similar to the graduated differences shown in the DoDs for the hillfort (Figure 7.9) and the henge (Figure 7.17), the Moran's I provides solid boundaries delineating variance. If each of the SAP epochs produced DSMs that were not significantly different to the TLS DSM, then the entire map of the hillfort and henge monument would appear grey, as shown in Figure 7.22 and Figure 7.23 respectively. In one respect this

outcome is desirable as it would show that the photogrammetry was comparable to TLS in areas where change to the landscape is not occurring. Within the Eggardon landscape, the southern half of the hillfort should be showing signs of minimal or no change as it has been in the care of the National Trust since the 1940s. Whilst there is a large percentage of each map that does show results that are not statistically significant in terms of the elevation difference between each SAP DSM and that of the TLS, there are also areas where there are red and blue regions, highlighting statistically significant high or low residual values.

In each of the Moran's I diagrams, the areas outlined in red, showing statistically significant high values, indicate regions where the TLS data is higher than the 1948 elevations. Blue regions highlight areas where the TLS data is much lower than that of the SAP DSM. If error in a DSM was not a consideration, this result would suggest that in blue regions there had been a destructive process at work, such as ploughing. As an example, it would be expected that the northern half of the hillfort would be labelled blue as this region has been ploughed previously, and thus there should be a negative difference between the TLS and the SAP DSMs, as the TLS elevations should be lower here.

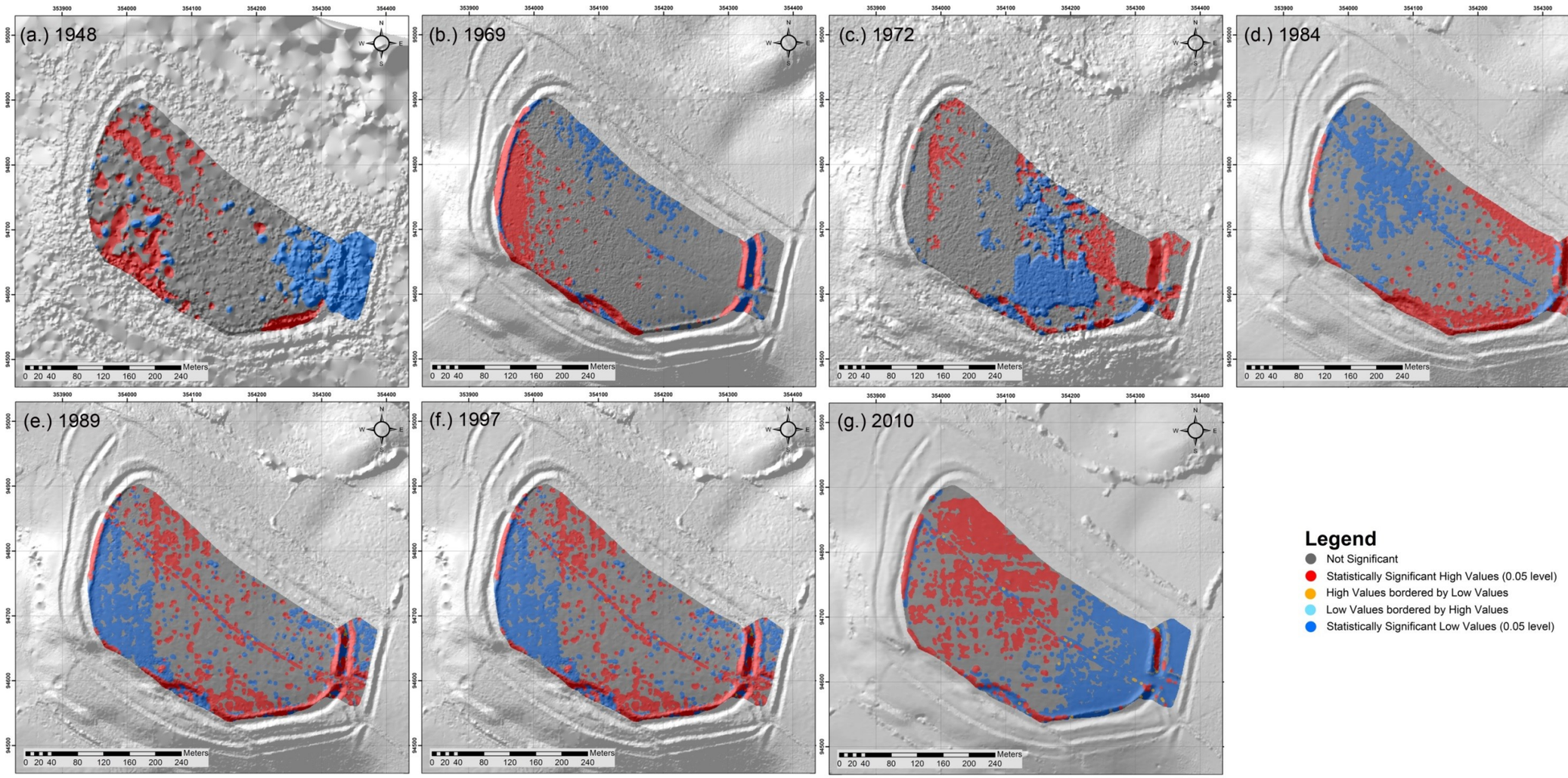

Figure 7.22: Moran's I diagrams of Eggardon Hillfort showing the distribution of residual values of difference between the TLS and SAP DSMs.

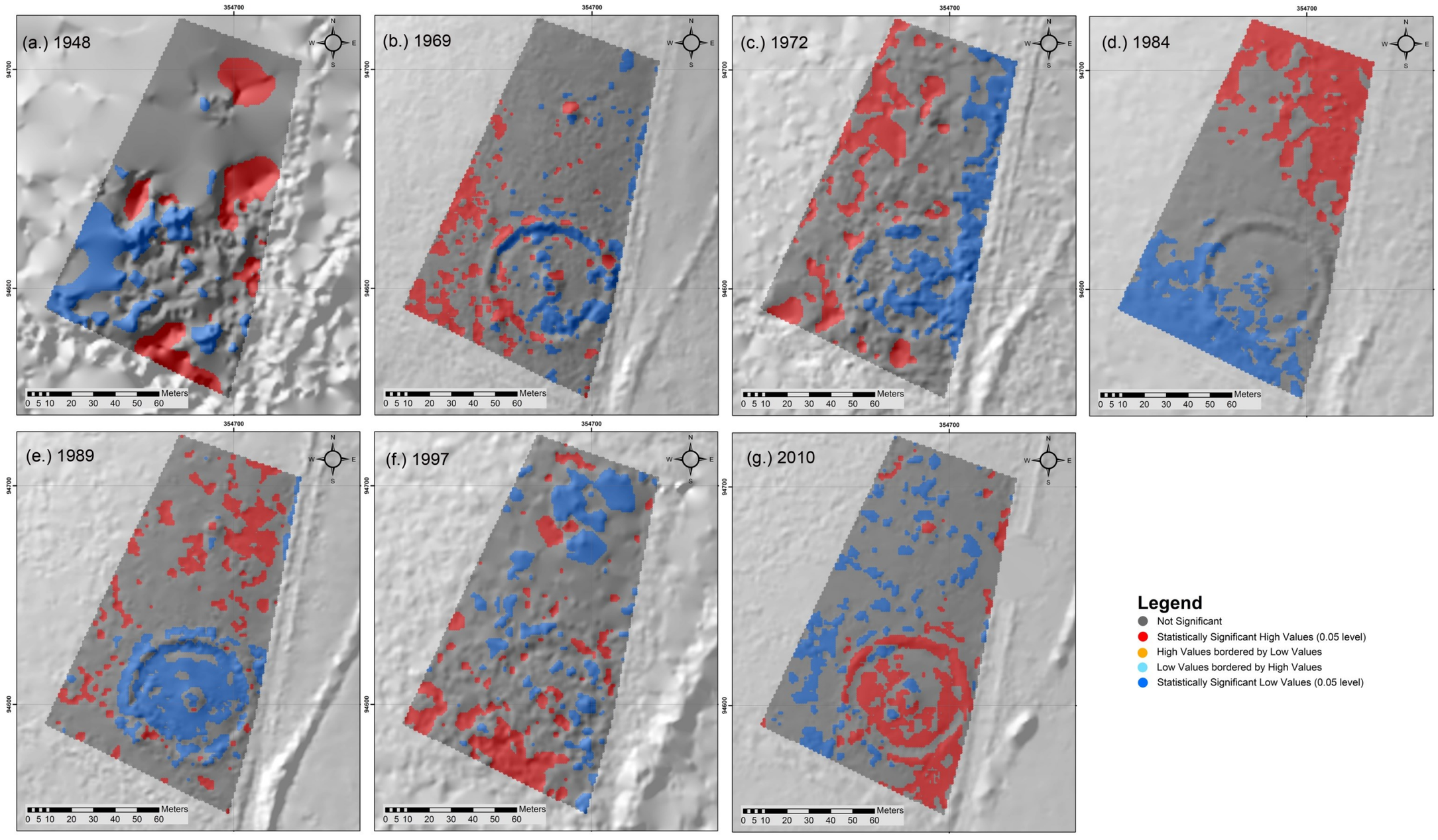

Figure 7.23: Moran's I diagrams of Eggardon henge monument showing the distribution of residual values of difference between the TLS and SAP DSMs.

7.4.3.1 Hillfort

By examining the 1948 SAPs (see Figure 7.24) there is no feature in the landscape that can explain the presence of this large blue region of low values. It is unlikely that there would have been changes of up to 12m over the last 65 years between the 1948 imagery and the 2013 TLS survey. There also appears to be a spatially distinct area of change to the south-east of the hillfort, as indicated by a strip of yellow and red residual values. Within the 1969 imagery, as shown in Figure 7.25, this region is illuminated well and appears to be reasonably well defined in the hillshaded DSM. This area contains statistically significant high values, which indicates that the land here has either risen over the past 65 years, or material has accrued on the slope of the ramparts in this region. Whilst the latter observation is not unreasonable, the material is unlikely to have increased in depth by nearly 15m at the bottom of the slope, as indicated in the DoD (Figure 7.9a). However, it has been noted that photogrammetry struggles to create accurate elevation data on steep slopes (Adams and Chandler 2002; Hodgson et al. 2005), which could also be a factor in the presence of residuals in this location.

As has been previously noted (see Section 7.4.1) in two out of the four SAPs in the 1948 strip, the hillfort and henge are situated close to the edge of the photography, which traditionally contains the largest amount of lens distortion. This is likely to be especially so in this case as the camera used to gather these photographs is not a metric one. Lens distortions will influence the location of each individual pixel in the image, which GCPs cannot completely account for, and thus it is to be expected that the points created from these miss-registered pixels will be offset from their correct locations by a certain amount. There is also no record relating to the storage conditions of the film after it was processed by the RAF until the time it was handed to the NMR. If the film was not archived carefully then it may have been subject to further distortions, such as warping, which will hinder the image matching process in any photogrammetric software and subsequently the results of performing terrain extraction.

The large range of residuals between the 1948 and TLS DSMs cannot be easily accounted for. If the camera calibration certificate was available it would be possible to examine the role of lens distortion upon the DSM as the imagery could be processed with and without this information to produce two different surface models and subsequently compare the results. As well as unquantifiable lens distortion, the other causes of elevation difference in the 1948 images can be attributed to noise in the data, caused by random dust and scratches, as visible on the imagery itself, as well as minor errors in the positioning of GCPs, which is attributable to the subjective interpretation of their positions in the imagery.

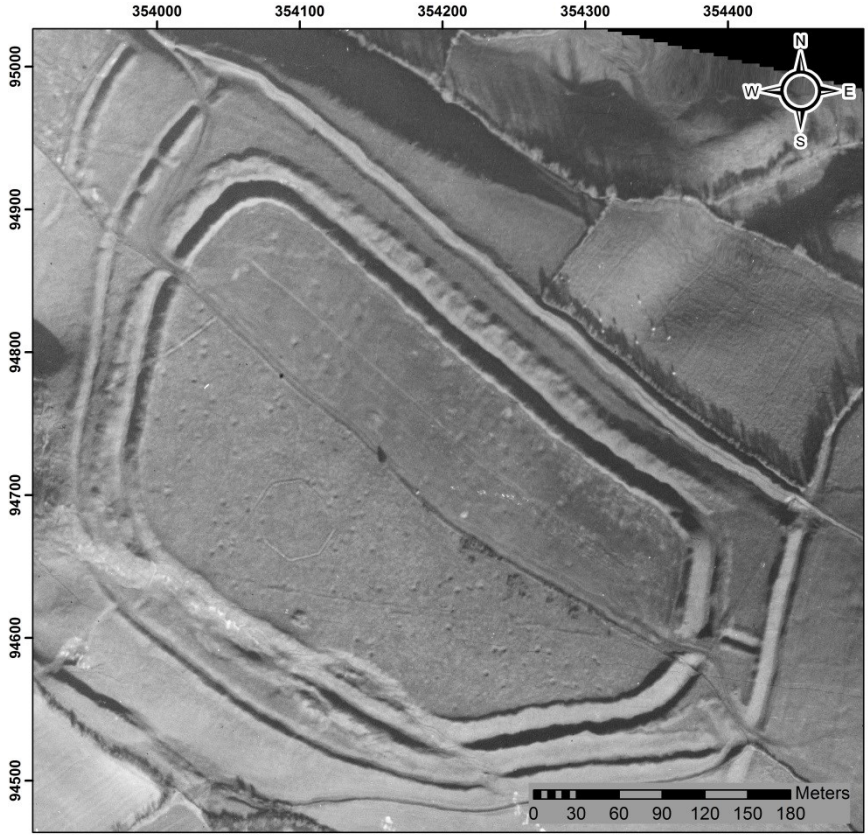

Figure 7.24: Eggardon Hillfort in 1945.

Figure 7.25: Eggardon Hillfort in 1969.

Point density also influences the Moran's I results across the hillfort, diagrams for which are shown in Figure 7.26. Many of the significant high and low values in the Moran's I analysis (see Figure 7.22) occur in areas where there are gaps between points, but these do not have to be large. To the east of the hillfort there is a large blue region suggesting statistically significant low values, although much of this area contains a dense number of points. This suggests that the input data also contain errors that are influencing the interpolation, as the natural neighbour algorithm does not produce artifacts, such as ridges and pits, which are not present in the original point data. Therefore the irregular hillfort surface results from noisy elevation data as created from the 1948 SAPs.

The Moran's I result for the 1969 DSM of the hillfort also shows spatial structure. The south-west facing slopes of the ramparts appear to have accrued material, whilst the north-east facing slopes appear to have lost it. By examining the 1969 orthophotograph (see Figure 7.25), the areas that have amassed material are covered by shadow, whilst the areas that have lost material are illuminated. This could suggest that the results have been influenced by the effect of contrast in the imagery, which would not be unexpected. However, this explanation is doubtful as the landslip, situated on the southern ramparts, has also seen an increase in material, much like the western facing slopes of the hillfort, yet it is well-illuminated in the 1969 photographs. Whilst the Moran's I identifies regions with statistically significant high and low residual values, it does not allude to the magnitude of the residual, unlike the DODs. The statistically significant high and low values defined by the Moran's I, shown in Figure 7.22b, which also appear to indicate regions of change that are spatially distinct in the DoD are shown in Figure 7.17b. These regions are situated along the western rampart slope, along the inner western rampart slope, the south-facing landslip, and the east-facing rampart slope. Areas of positive change, highlighting material accumulation, are found along the west and south-facing slopes of the hillfort. The largest region of accrual is at the bottom of the west rampart as indicated by the hint of red, which has a maximum elevation difference of 4.125m. The standard deviation of residual values between the TLS and 1969 DSM is 0.39m, and thus the change identified here is likely to be slightly more subtle, but indicative of actual change. Whether accrual of material is due to soil creep, or material being removed from the top of the ramparts due to footfall, sheep grazing and weathering, cannot be easily established.

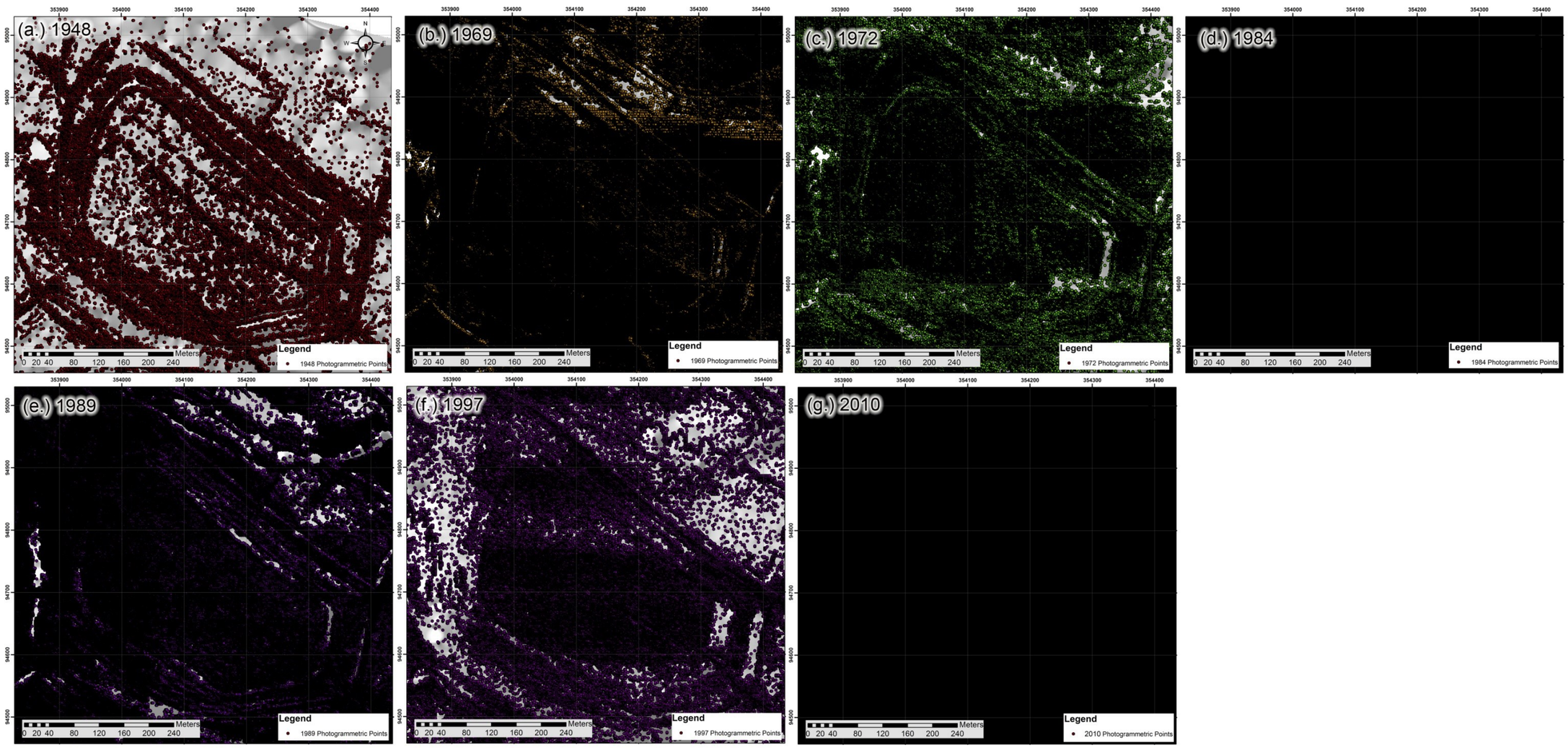

Figure 7.26: SAP DSM point densities, prior to interpolation, for Eggardon Hillfort.

Areas across the hillfort where material has been lost are limited to subtle variations across the northern half of the hillfort and more obvious changes to the east-facing rampart slopes. The maximum amount of loss is 2.203m, and is most apparent to the east of the hillfort, towards the bottom of the rampart slope. The cause of this is uncertain, although this half of the hillfort is grazed by cattle, and it is feasible that trampling by them has damaged the slopes. However, this area is also accessible to hikers who may take the opportunity to wander across this area of the hillfort, particularly as it is situated close to the eastern entrance to the monument. The views afforded across the landscape from the top of the ramparts are likely to encourage walkers to climb them, and thus footfall is a further source of degradation (see Figure 7.6). It is also likely that footfall may be eroding the top of the western ramparts, which show a darker blue appearance in the DoD. Weathering may be a further factor due to the exposed position of the ramparts, which may encourage eroded material to travel down the slope and accrue either to the west, or to the east and into the flatter interior of the hillfort. As it would appear from the Moran's I diagram that the interior of the hillfort to the west has gained material, this may be where the transported material is deposited.

The results from the 1972 Moran's I analysis are difficult to interpret, due to the presence of stripes in the DSM that have introduced errors into the 1972 elevations. Whilst meaningful interpretation cannot be conducted on the hillfort interior, there does appear to be some spatial structure along the eastern-facing rampart slope to the east of the image and across the landslip feature in the south. There still appears to be accrual of material along the steep face of the landslip, as there was in the 1969 dataset, and a loss of material at the base of this feature. Whether this loss is as great as the 1972 DoD suggests (see Figure 7.9c), 2.604m, is uncertain, particularly as this feature is situated close to the stripe artifact in the DSM. As the SD of this dataset is 0.664m it is feasible that the loss of material here between 1974 and 2013 is more likely to be ~2m. What is unlikely is the accrual of material across the eastern rampart to a value of 4.703m, as highlighted by the red values in both the Moran's I diagram (Figure 7.22c) and the DoD (Figure 7.9c). This is especially so as ~6m of material is unlikely to have accrued over a period of 3 years between 1969 and 1972. Whilst change in this area is expected, based upon the results of the 1969 dataset, the results from the 1972 DSM is dubious. It can be seen in the underlying hillshade in both the Moran's I and DoD diagrams for 1972 that there is a line in the elevation data to the north of the rampart in question, and it appears to run into the rampart slope here. Therefore any interpretation based upon this data cannot be stated with any confidence.

Along the western-most, west-facing rampart in the 1984 Moran's I diagram, shown in Figure 7.22d, the process of material accumulation is still occurring. This is also true for the vertical face of the southern landslip, although material is accruing on the flatter slope at the bottom of this feature, whereas this appears to be losing material in the 1969 and 1972 Moran's I diagrams. However, the changes located in the landslide are more subtle than in previous years, as indicated by the 1984 DoD (Figure 7.9d). The bright yellow colour indicates that up to ~0.8m is accumulating at the base of the landslide, whilst the darker blue areas indicate that ~0.65m has been lost from the slope between 1984 and 2013.

Figure 7.27: Vegetation difference between the (a.) northern half and (b.) southern half of Eggardon Hillfort.

The eastern ramparts are still showing signs of material loss, although the location has changed from the east-facing slope to the west-facing slope. Over 29 years between the 1984 SAP capture and the 2013 TLS survey, ~1.4m has been eroded from this area. On the east-facing slope material has been lost, although to a lesser degree as denoted by the light blue colour. In the rampart ditch, it appears that material has accrued, most likely comprised of the materials that are eroding from the slope, by ~2.39m in red regions, although the yellow areas show more subtle accumulation of between ~0.17m to ~1.45m.

As the northern half of the hillfort has been subjected to plough damage since the 1940s, albeit not on a regular basis, it is surprising that there is not a larger collection and more extensive distribution of negative residuals across this area. The Moran's I map again exhibits a large number of non-significant values, particularly in the southern half of the hillfort, which indicates that little or no change has occurred here since 1984. Both halves of the hillfort are covered in long grass, which forms 'clumps' as shown in Figure 7.27, explaining the lumpy appearance of both sides, but this does not appear to have unduly influences the location of statistically significant differences between the 1984 DSM and the TLS.

There is a line of material loss that follows the fence dividing the two sections of the hillfort, which indicates a region of erosion along the northern side of this line. There is an elevation offset of approximately 0.6m between the two halves (see Figure 7.28), which has exposed a section of soil and is more prone to erosion and it is the fence line that hikers are likely to follow. This could explain the cause of erosion closer to the fence, although cattle may also congregate along it too, as they have been noted to spend quantities of time close to fence posts to assist scratching (see Section 7.2.5). The water trough is another feature that is likely to draw the cattle closer to this line and encourage further soil erosion. The areas of material accumulation, located towards the north-east and south-east ends of the hillfort, may highlight where the material lost from the region along the fence line is going. It may also indicate where soil from

the rampart slopes accrues. Despite what may first appear to be a severe build-up of material, based upon the Moran's I map, in most cases the maximum accrual is ~0.3m in the northern half of the hillfort and less than ~0.15m in the south.

The Moran's I diagram for the 1989 DSM, as shown in Figure 7.22e, continues to indicate that accretion is occurring on the western facing slopes of the ramparts and in sections across the vertical face of the landslip by virtue of the clustering of statistically significant high values in these regions. The statistically significant low values also indicate that material loss is still occurring on the eastern-facing slopes of the ramparts but, unlike the 1984 results, material is also eroding from the base of the landslip. The DoD (see Figure 7.9e) helps to clarify whether these observations coincide with the differences identified between the TLS and 1989 DSM. Broadly speaking, the two datasets agree with one another, although using the Moran's I data as a proxy for the DoDs can be misleading, as the results tend to look more severe than in the DoD. This is particularly so for the rampart slopes, where the Moran's I indicates a significant difference between the TLS and 1989 DSMs, whilst the DoD illustrates that these differences can be subtle. However, the landslip does appear to be losing material from the base of the landslip and, to some degree, across the vertical face too. In the 24 years between 1989 and the 2013 TLS survey the DoD suggests that 1.929m of material has eroded from the base of the landslip, which is a significant. There also appears to be significant accrual of material at the base of the rampart slopes to the east of the hillfort, which had started to occur in 1984. The

Figure 7.28: Elevation offset between the northern and southern sections of Eggardon Hillfort.

DoD suggests that nearly 2.5m of accretion has taken place between 1989 and 2013, whilst there has been a small amount of erosion in other areas of the slope.

There are two other features of the 1989 SAP DSM that appear in the Moran's I analysis. The first occurs along the fence line that runs across the hillfort and shows material accretion, rather than loss, as was identified in the 1984 dataset. To establish the difference between the 1984 and 1989 DoDs along this feature, a number of points were measured in ArcMap using the 'Identify' tool on the DoDs themselves. Differences between the two datasets were ~0.4m and ~0.9m, although establishing why there was material loss from 1984 to 1989, and then accretion between 1989 and 2013 is difficult. The SD of the 1989 residuals is 0.15m, which is akin to the values quoted for ALS data (see Table 4.2), and thus an uncertainty of ±0.15m can be appended to the 1989 residuals, whilst ±0.248m can be appended to the 1984 residuals. Subsequently the changes occurring along the fence line may be smaller than suggested by the DoDs, and the change could be due to vegetation growth or die-back rather than soil accretion or loss. The second feature is a large cluster of statistically significant low values situated in the south-western corner of the hillfort. By examining the 1989 photographic strip (see Figure 7.29) it can be seen that this feature coincides with an information strip of one of the 1989 SAPs. Based upon the DSM results from other epochs, namely the 1972 and 1997 datasets, it appears that SocetGXP is including the data strips when calculating terrain.

The results of running the Moran's I test on the hillfort dataset has not generated meaningful results either. Two stripes of statistically significant high values run through the east and west portions of the hillfort, from north to south, although the 1997 SAP strip, shown in Figure 7.30, suggests that the information strip from the image furthest to the left may run beneath the eastern half of the hillfort. This may explain the presence of the eastern-most stripe, although these values do not contribute any knowledge as to the processes of change that may be occurring across the hillfort. Although there are indicators of change occurring in the regions that have been discussed in previous epochs, i.e. the landslip and ramparts, the underlying hillshaded DSM suggests that the terrain extraction process in SocetGXP has failed to recreate the ramparts. The eastern-most ramparts look flat and do not consist of a slope and bank. The DoD for the 1997 data, shown in Figure 7.9f, suggests that there has been material accretion of up to 3.73m and loss of -4.583m in this area alone. Therefore this data is unusable for discussing monument change in this area of the hillfort.

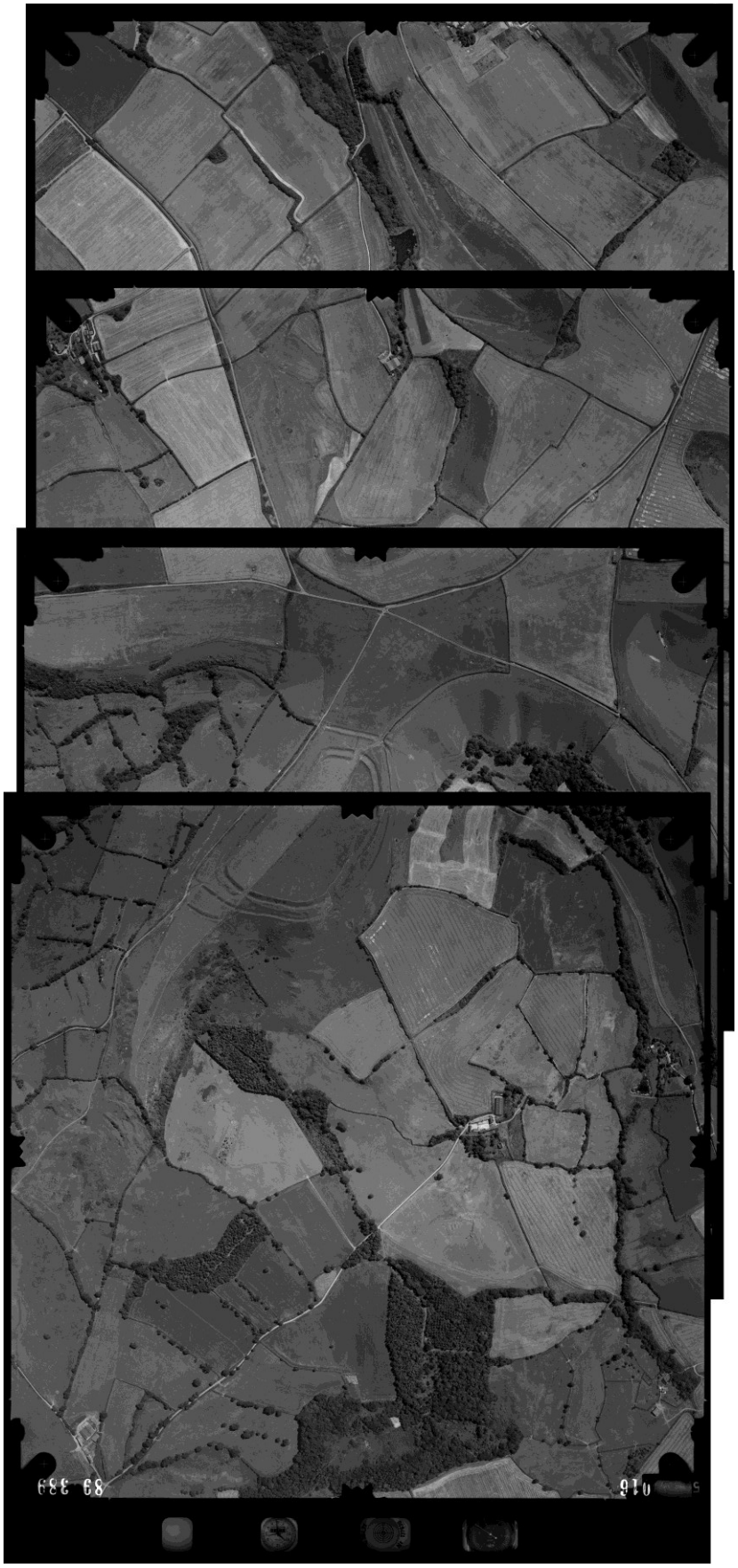

Figure 7.29: 1989 Photographic Strip.

Figure 7.30: 1997 Photographic Strip.

However, the landslip is contained within a region that falls between the two spurious stripes and the southern half of the hillfort in which it sits contains many non-significant values. The landslip is predominantly covered by statistically significant high values, which indicates that the 2013 TLS data is higher than the 1997 DSM and thus accretion is likely to have occurred across most of this feature. The orange patches that appear on the landslip in the DoD (Figure 7.9f) represent up to ~2m of accretion, whereas the lighter green colours indicate accumulation of material between 0m and 0.8m. The SD value of the 1997 residuals is 0.505m, which throws into doubt the regions of change that are within this measure. Based upon the noisy appearance of the DSM, as shown by the underlying hillshade in both of the henge and hillfort Moran's I diagrams, it is unlikely that the 1997 SAP dataset can provide meaningful data as regards the processes of change occurring across the landscape for this epoch.

As the 1997 SAPs were processed using the same GCPs as the other SAP datasets, the poor results obtained from this data are due to a number of factors: the lack of lens distortion data, the reduced amount of information contained within a print rather than a negative, the further influence of the distortions introduced during the scanning process, and potentially the way in which the prints have been archived which is not known.

The Moran's I results for the 2010 DSM, shown in Figure 7.22g, suggest that there is an offset in the terrain, which has been caused by information stripes in the imagery for both the 1972 and 1997 SAP DSMs. Information stripes do not occur in the 2010 photographs as they have been produced by a digital camera system. However, the edge of one of the photographs from the SAP dataset, as shown in Figure 7.31, passes through the hillfort at the same location as the change from red to blue values in the Moran's I diagram. There is also a subtle colour change in the DoD for the 2010 data, shown in Figure 7.9g, indicating where this image overlap occurs. Based upon this observation, SocetGXP seems to have difficulty in generating terrain values when more than one stereo-pair of images overlap. There is an option in the software to produce a terrain model by considering more than one stereo-pair of images, which is particularly appropriate where a block of images, rather than just a single strip, is being processed. The results of generating a DSM from the 2010 photography by using this method has evidently caused the issue. The offset between the TLS and the 2010 DSM in the eastern half of the hillfort, where the DoD is a turquoise colour, is ~0.17m, whilst in the western half the light green colour represents a difference of ~0.45m. It is therefore more likely that the results in the east of the hillfort are the most representative, as it is unlikely that significant change has occurred to either half of the hillfort in a three year period. As the SD of the hillfort residuals is 0.155m, it appears that the TLS elevations should be similar to that of the 2010 DSM.

The issue with the elevation offset in the 2010 DSM makes the interpretation of the Moran's I diagram a challenge. The statistically significant high values suggest that the TLS data is much higher than the 2010 elevations, although this appears to be an effect caused by Socet GXP processing more than one stereo-pair to obtain an elevation value. However, there are a larger number of non-significant values in the western-half of the hillfort, which coincides with a noisy DSM surface, as illustrated by the underlying hillshaded DSM.

Figure 7.31: 2010 Photographic Strip.

The east of the hillfort does not contain such noise, which further suggests that this is the area in which elevation measures are more representative of the 2010 terrain. In comparison with the other SAP epochs, accretion is still occurring along the rampart slope at the western end of the hillfort, although in contrast to the other epochs accretion is also occurring along the top of the bank. The DoD indicates that the depth of material here has increased between 2010 and 2013 by ~0.669m, which seems unlikely. However, the SD for the 2010 DSM is 0.122m, the value of which is exceeded by the values in the DoD and thus the indication of change in this region is not a false positive result.

The landslip feature displays a similar pattern of change in the Moran's I diagram for both the 1989 and 2010 DSMs, indicating accretion along the top of the feature and in places at the base of it, whilst the majority of the landslip appears to be losing material. The yellow areas are indicative of between ~0.6m and 0.7m of accretion, whilst the lighter and darker blues represent 0m to ~0.7m of erosion. Another feature which has also consistently shown changes occurring in each epoch are the ramparts to the east of the hillfort. However, the Moran's I suggests that western face of this slope is losing material whereas the east-facing slope is gaining it, which is contrary to observations made of the other epochs. The DoD reveals that the material loss is generally subtle, with the turquoise regions representing a ~0.17m loss and the darker blue regions resembling a ~0.5m loss. In addition to this region, there are other sites where material appears to be eroding. There is a feature that is perpendicular to the ramparts that has lost ~0.5m between 2010 and 2013, whilst ~0.77m is eroding from the bank across which the access path to the hillfort runs.

In the areas where material has built up over three years, the yellow colours in the DoD represent between ~0.5m and ~0.9m of accrual, whilst the red areas are as large as 1.949m. It is unlikely that this change is due to vegetation height, although the 2010 orthophotograph, as shown in Figure 7.32, depicts healthy grass coverage at the base of the ditch whilst the slopes of the ramparts appear to be quite dry and lacking in vigour.

7.4.3.2 Henge

The errors contained within the 1948 DSMs of the henge do not appear to have structure, which is unsurprising based upon the appearance of the underlying hillshade of the 1948 data. Whilst a vague outline of the henge and the barrow to the north of it are discernible, the DSM appears to contain a great deal of noise. This is due to two factors: the point density that was created in Socet GXP, as shown in Figure 7.33a, and the interpolation procedure. There are regions of the triangulated 1948 SAPs that SocetGXP has not been able to create a post for, which subsequently requires the natural neighbour interpolation algorithm to fill the large gaps. These gaps can give rise to errors, especially in regions with sparse point data, although the Moran's I map (Figure 7.23a) contains a large number of non-significant values, which is surprising given

Figure 7.32: 2010 orthophotograph of Eggardon Hillfort.

the appearance of the DSM. The statistically significant high and low values tend to conform to regions where the interpolator has had to fill in large gaps.

The Moran's I results from the 1969 SAPs, shown in Figure 7.23b, is impressive. The underlying hillshaded DSM look detailed and the majority of the Moran's I values are grey, meaning that there is no significant difference between the TLS and the 1969 DSM. There is a large covering of blue values within the henge monument, indicating that the TLS data is significantly lower than the DSM elevations, although this can be explained by examining the 1969 orthophotograph (Figure 7.21). In 1969 the henge was covered in gorse, which had been removed by the 2013 TLS survey, and hence the reduction in height of the elevation values over this 44 year period. Areas marked in red appear to be regions of accrual that occur on north and north-east facing slopes within the henge area, which itself slopes from the south-west to the north-east. Any positive changes are small, with the maximum difference between the TLS and 1969 DSM being 0.376m. The standard deviation of residual values in this dataset is 0.111m, and thus the changes detected here are actually occurring and not just the result of outliers.

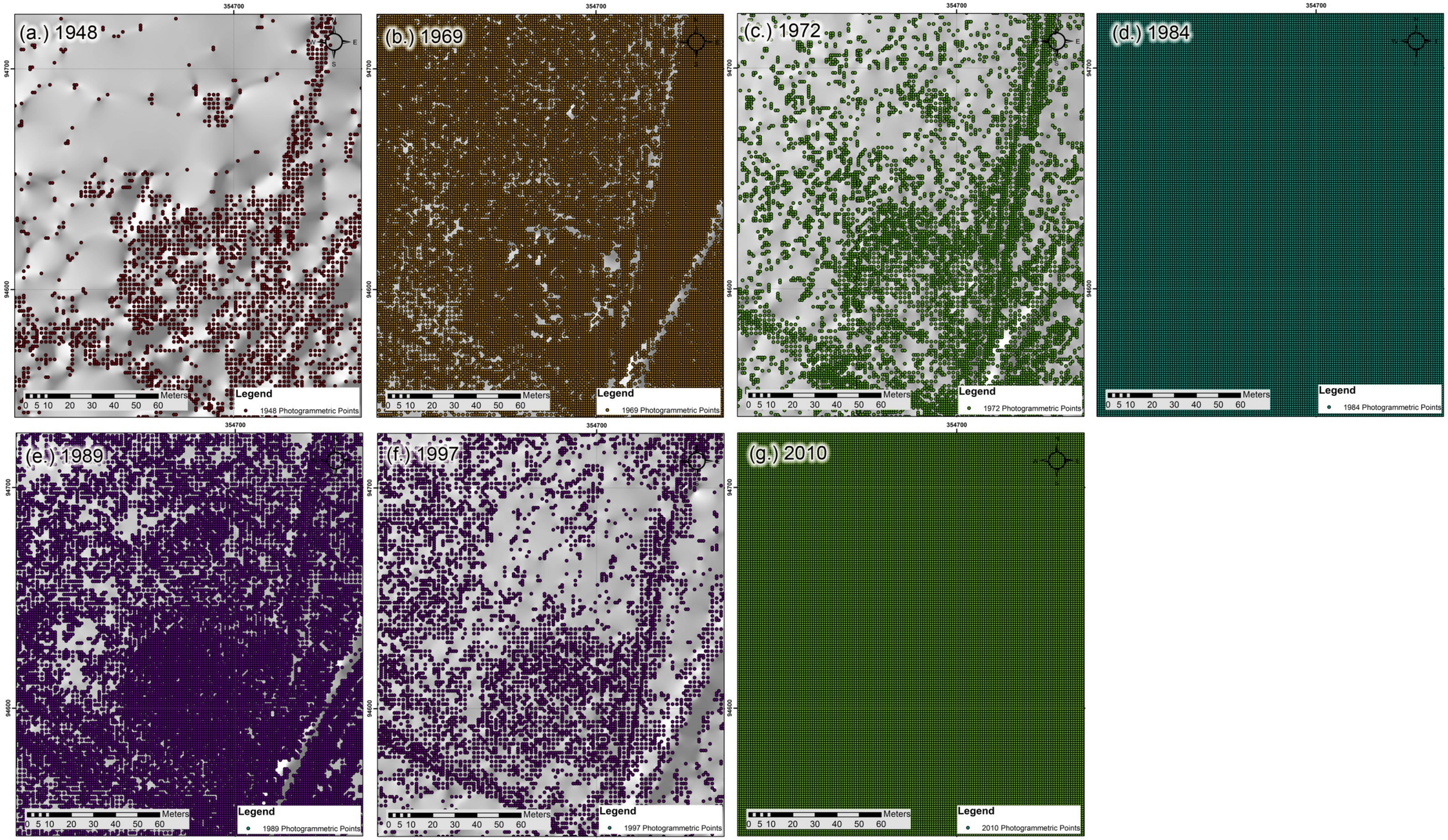

Figure 7.33: SAP DSM point densities, prior to interpolation, for Eggardon henge monument.

The Moran's I diagram for the 1972 SAP representation of the henge monument (see Figure 7.23c) also suggests that the area within the henge at this time was higher than in 2013. The 1972 orthophotograph (see Figure 7.34) shows that gorse vegetation had still not been removed, explaining the offset between the TLS data and the 1972 DSM. However, there are a significant number of low values that run along the east border of the Moran's I diagram and it is difficult to identify the reason for this. By examining the DoD (Figure 7.17c) there appears to be a seam running along the edge of the low values, although this does not appear to be visible in the hillshaded DSM underlying the DoD. The majority of the Moran's I values across the henge are not significantly different between the TLS and the 1972 data, although there are patches of statistically significant high values, especially to the west of the monument. The field within which the henge sits looks recently ploughed in the 1972 orthophotograph, whilst in 2013 the area was used for pasture and was covered in grass. This explains why there is a positive offset between the 1972 and TLS data, the latter of which would have scanned the grass and contains higher elevation values.

Figure 7.34: 1972 orthophotography of the henge monument.

The 1984 Moran's I diagram, shown in Figure 7.23d, indicates that a slight tilt still remains in the elevation data, despite attempting to remove it by using a trend surface. This observation is also visible in the DoD (see Figure 7.17d) as both diagrams indicate that all of the high, positive residuals are located north of the henge, and all the low, negative residuals are to the south. Unlike the other Moran's I or DoD datasets, there is no random appearance to the residual distribution in the 1984 data, and thus any meaningful discussion relating to residuals surrounding the henge is not possible. However, the tilt appears to have been removed from the area of the DSM in which the hillfort resides and also exhibits some spatial structure relating to the distribution of residual values.

Figure 7.23e shows the Moran's I diagram for the 1989 SAP henge region. The significant low residuals are located within and around the henge itself, indicating that material has been lost here over 24 years between the 1989 survey and the 2013 TLS scans. The henge has a rough appearance in the 1989 orthophotograph, shown in Figure 7.35, which could indicate the presence of vegetation in the 1989 dataset, explaining the elevation offset between the 1989 DSM and the TLS. The 1989 DOD (see Figure 7.17e) shows that the maximum loss of material is only 0.489m, which may be even smaller when considering the σ of the residuals for this dataset is 0.141m. Whilst the majority of the field surrounding the henge consists of non-significant residual values, there are patches of highly significant positive values that occur, particularly to the north of the Moran's I diagram, close to the barrow monument. In previous SAP datasets, this area looked to be under the plough, but in the 1989 imagery the appearance of the field is quite uniform. This area may have been turned over to pasture by the time the 1989 SAPs were created. Whether it is a difference between vegetation heights in the 1989 and TLS DSMs that is causing a maximum difference of 0.688m is difficult to say. However, the vast majority of values across this area are much lower; between 0m and 0.3m. As the σ of residuals is 0.141m the variation in elevation between the TLS and 1989 DSM may be caused by random fluctuations in the data as well as variations in vegetation height.

Based upon the noisy appearance of the underlying hillshaded DSM, the Moran's I result for the henge monument in the 1997 DSM looks quite random. In the 1997 orthophotograph, shown in Figure 7.36, there are clumps of gorse growing on the henge monument, whilst the barrow to the north of the henge appears to be covered by unhealthy or no vegetation. The Moran's I diagram for this region, shown in Figure 7.23f, suggests that the TLS barrow elevations are lower than those in the 1997 DSM, based upon the cluster of significant low values. However, the positioning of the other low values within the henge locale, and high values for that matter, do not appear to coincide with any notable details in the orthophotograph and nor do they appear to be influenced by the point density of the SocetGXP output.

Figure 7.35: 1989 orthophotograph of Eggardon henge monument.

Figure 7.36: 1997 orthophotograph of Eggardon henge monument.

As the most up-to-date set of SAPs obtained for this research, the 2010 data should be the most superior SAP dataset. The Moran's I result for the henge region, as shown in Figure 7.23g, is predominantly covered by non-significant differences between the 2010 and TLS DSMs. The regions of statistically significant high values are concentrated around the henge itself, on the banks of the outer ring and the flat interior of the monument. This suggests that there has been accretion of some description over the three years between these datasets. However, upon examination of the DoD, shown in Figure 7.17g, the maximum positive difference between the TLS and 2010 DSM is 0.611m. The SD of residuals between these datasets is 0.122m, and therefore along the top of the henge banks up to ~0.5m of material has accrued. This is likely to be related to vegetation growth as, in some places along the top of the banks, as shown in Figure 7.37, there appear to be patches without vegetation coverage. This area is grazed by cattle and thus patches of bare earth may be a sign of over-grazing.

The barrow monument is between 0.15 and 0.35m higher in the TLS data than in the 2010 DSM. Whilst these values are both larger than the SD of residuals, there may also be discrepancies in the elevation values of the TLS. These discrepancies are related to the control method used to provide OSGB coordinates for the TLS locations, namely a GNSS, and thus ~±0.1m further error may be influencing these results. However, even if the standard deviation

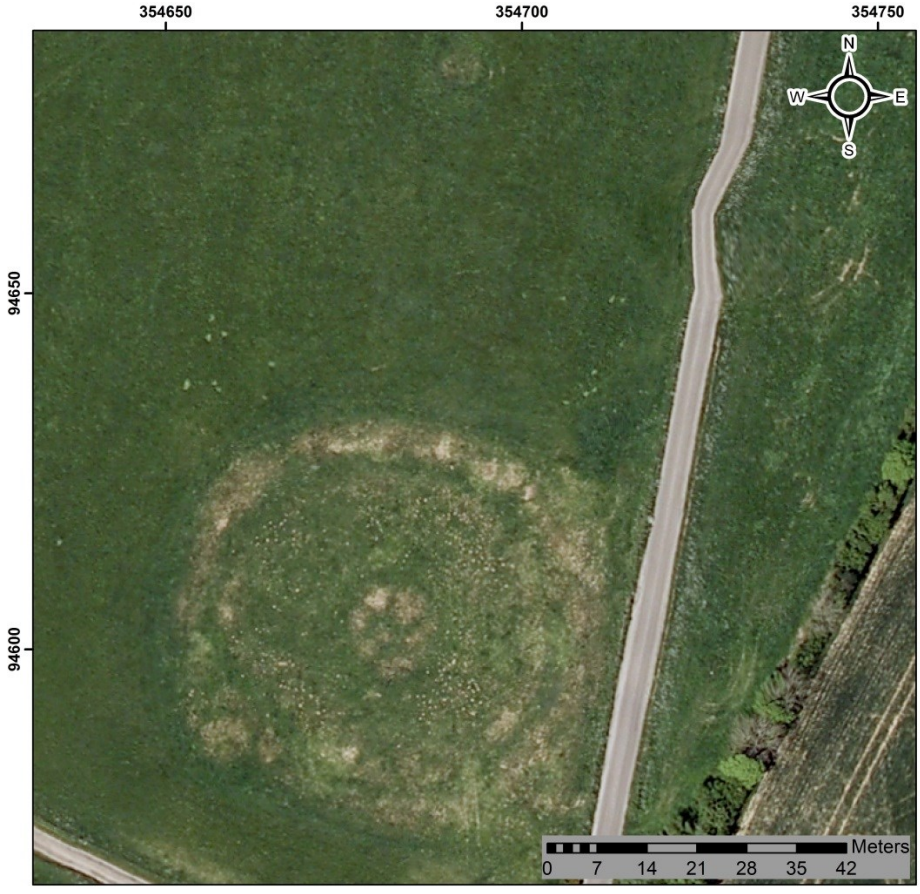

Figure 7.37: Henge monument as shown in the 2010 SAP orthophotograph.

of residual values between the TLS and 2010 DSM and the approximate elevation error of a GNSS system were considered, the TLS data would still be more likely to contain higher elevation values over the barrow, albeit by a small margin, which could be related to vegetation height.

7.5 Slope Assessment

In the previous section examining elevation differences between the TLS and SAP DSMs, the 1948, 1972 and 1997 datasets produced the least desirable results. Bimodal distributions were displayed by the 1948 and 1972 histograms, and the 2010 dataset, which suggested that either noise in the data or the presence of stripes across the DSM was having a detrimental influence on the terrain. As the presence of imperfections in a DSM is enhanced when converting it to a derivative product, the residual values between the slope data from TLS data and each SAP epoch were examined and the results are presented here.

7.5.1 Eggardon Hillfort

There are distinct visual differences between the slope derivatives from each SAP epoch as compared to the TLS, which are shown in Figure 7.38. As with the elevation results in Section 7.4.1, it is the 1948, 1972 and 1997 SAP slope models that have the most noisy appearance. The summary statistics for the residual values between each SAP slope model and the TLS, as shown in Table 7.6, also confirm this pattern. The distributions of residuals for each dataset is predominantly normal, as shown in Figure 7.39, and thus the ME is a reasonable indicator of the hierarchy of data quality across the epochs. The ‘range’ measure is a good indicator of how far slope values deviate from those of the benchmark, namely the TLS, and can indicate the severity of outliers in the dataset. Although ‘variance’ is the measure of dispersion around the mean, its units are the square of whatever the measure happens to be, which in this case is degrees. Therefore a more appropriate indication of variance is the SD, which also confirms that the worst performing datasets are the 1948, 1972 and 1997 SAPs, in that order.

		TLS Minus 1948	TLS Minus 1969	TLS Minus 1972	TLS Minus 1984	TLS Minus 1989	TLS Minus 1997	TLS Minus 2010
N	Valid	89021	89021	89021	89021	89021	89021	89021
	Missing	0	0	0	0	0	0	0
Mean (degrees)		-14.410	-1.171	-3.540	-0.666	0.191	-3.166	0.481
Std. Error of Mean (degrees)		0.041	0.014	0.021	0.011	0.010	0.020	0.008
Median (degrees)		-11.926	-0.922	-2.991	-0.617	-0.020	-3.163	0.169
Mode (degrees)		-6.236	-0.516	-1.808[a]	-0.091	-0.221	-3.121	0.091
Std. Deviation (degrees)		12.253	4.249	6.385	3.300	3.021	5.959	2.278
Variance (degrees^2)		150.145	18.054	40.767	10.887	9.125	35.510	5.189
Skewness		-0.842	-0.100	-0.219	0.681	1.777	0.800	2.033
Std. Error of Skewness		0.008	0.008	0.008	0.008	0.008	0.008	0.008
Kurtosis		0.864	8.547	4.123	8.603	14.469	5.751	14.496
Std. Error of Kurtosis		0.016	0.016	0.016	0.016	0.016	0.016	0.016
Range (degrees)		109.844	67.373	87.775	66.607	66.817	95.649	54.990
Minimum (degrees)		-68.786	-35.952	-43.657	-29.809	-30.019	-45.755	-26.028
Maximum (degrees)		41.058	31.421	44.118	36.798	36.798	49.894	28.962
RMSE (degrees)		18.915	4.408	7.301	3.366	3.027	6.748	2.328

Table 7.6: Summary statistics for Eggardon Hillfort Slope residuals.

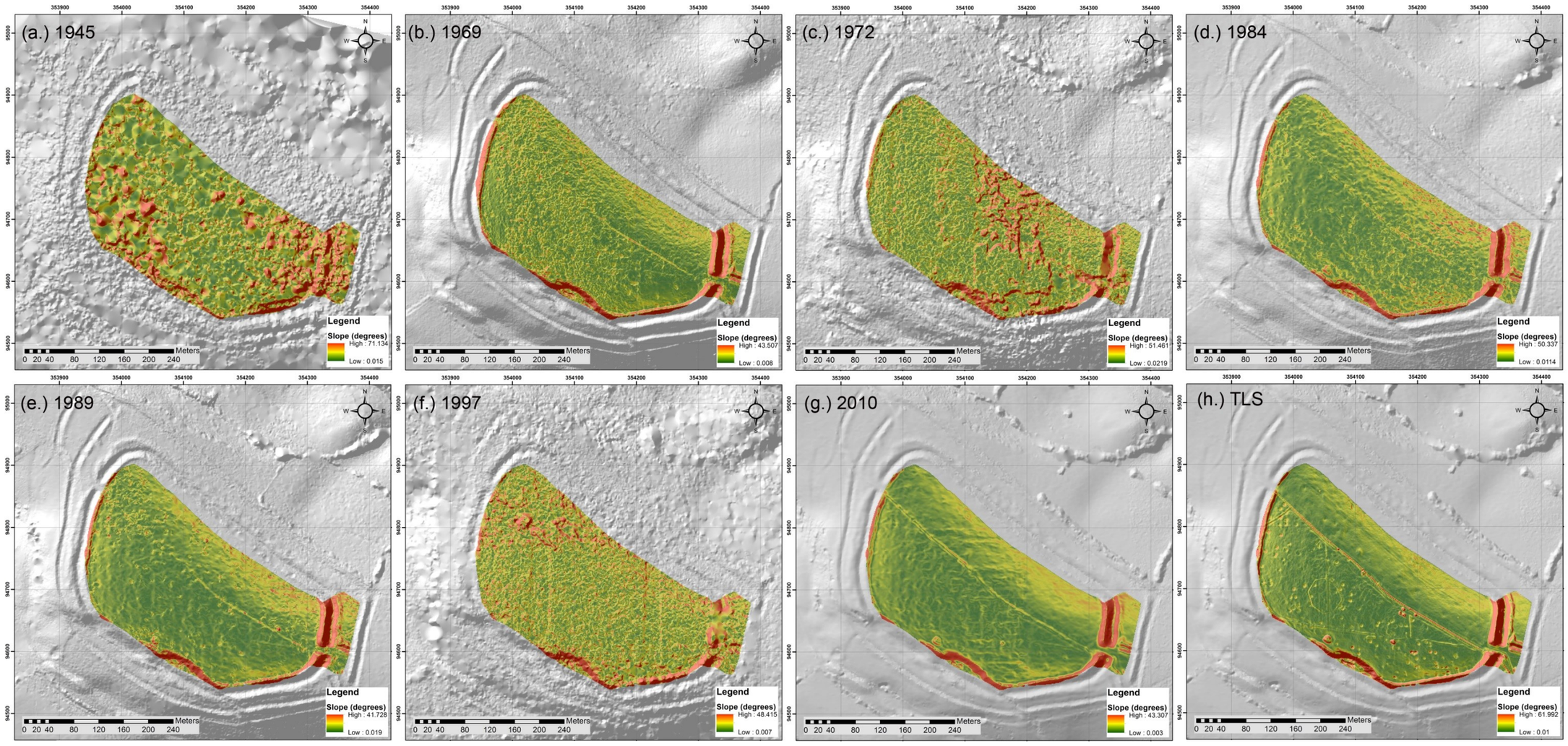

Figure 7.38: Slope derivatives for the Eggardon Hillfort SAP epochs and TLS data.

The histograms representing the 1948, 1972 and 1997 SAP slope residuals, as shown in Figure 7.39a, c and f, exhibit a wider spread of residual values and a shorter peak for those values that are closer to 0, unlike the remaining SAP datasets that all have much higher kurtosis values. The extent of dissimilarities between the three worst performing epochs is enhanced in the linear scatterplots, shown in Figure 7.40. This is especially so for the 1948 epoch (see Figure 7.40a), in which the slope values ranging from 0º to 10º in the TLS dataset, that incidentally form the majority of slope measurements, are represented by values of up to 70º in the 1948 data. There is an extremely poor correlation between the 1948 and TLS datasets, as evidenced by an r value of 0.3.

The 1972 and 1997 scatterplots contain fewer extreme differences between themselves and the TLS, although the correlation still remains poor: 0.419 and 0.423 respectively. Table 7.7 contains the results of the paired t-test conducted on each of the SAP epochs, which have been paired with the TLS for comparison. The 2010 photography has performed well, as shown by the high r value of 0.917, which constitutes a near perfect score. Whilst not as impressive, the 1984 and 1989 SAPs also show strong correlations, namely 0.832 and 0.851 respectively, as does the 1969 datasets with a score of 0.725. These results are indicated by the relationships illustrated in the scatterplots for the 1969, 1984, 1989 and 2010 SAPs (Figure 7.40b, d, e and g). Whilst they display positive linear correlation, especially in the case of the 2010 SAP slope values, the correlation deteriorates as the SAP epochs get older and the slope values deviate more readily from those of the TLS.

	Paired Samples Correlations		**Paired Samples Test**			
	Correlation	**Sig.**	**95% Confidence Interval of the Difference**		**t**	**Sig. (2-tailed)**
			Lower	**Upper**		
TLS Slope vs 1948 Slope	0.300	0.000	-14.490	-14.329	-350.869	0.000
TLS Slope vs 1969 Slope	0.725	0.000	-1.199	-1.144	-82.255	0.000
TLS Slope vs 1972 Slope	0.419	0.000	-3.582	-3.498	-165.433	0.000
TLS Slope vs 1984 Slope	0.832	0.000	-0.687	-0.644	-60.204	0.000
TLS Slope vs 1989 Slope	0.851	0.000	0.172	0.211	18.908	0.000
TLS Slope vs 1997 Slope	0.423	0.000	-3.206	-3.127	-158.537	0.000
TLS Slope vs 2010 Slope	0.917	0.000	0.466	0.496	62.948	0.000

Table 7.7: Results of the paired t-test for the hillfort slope values.

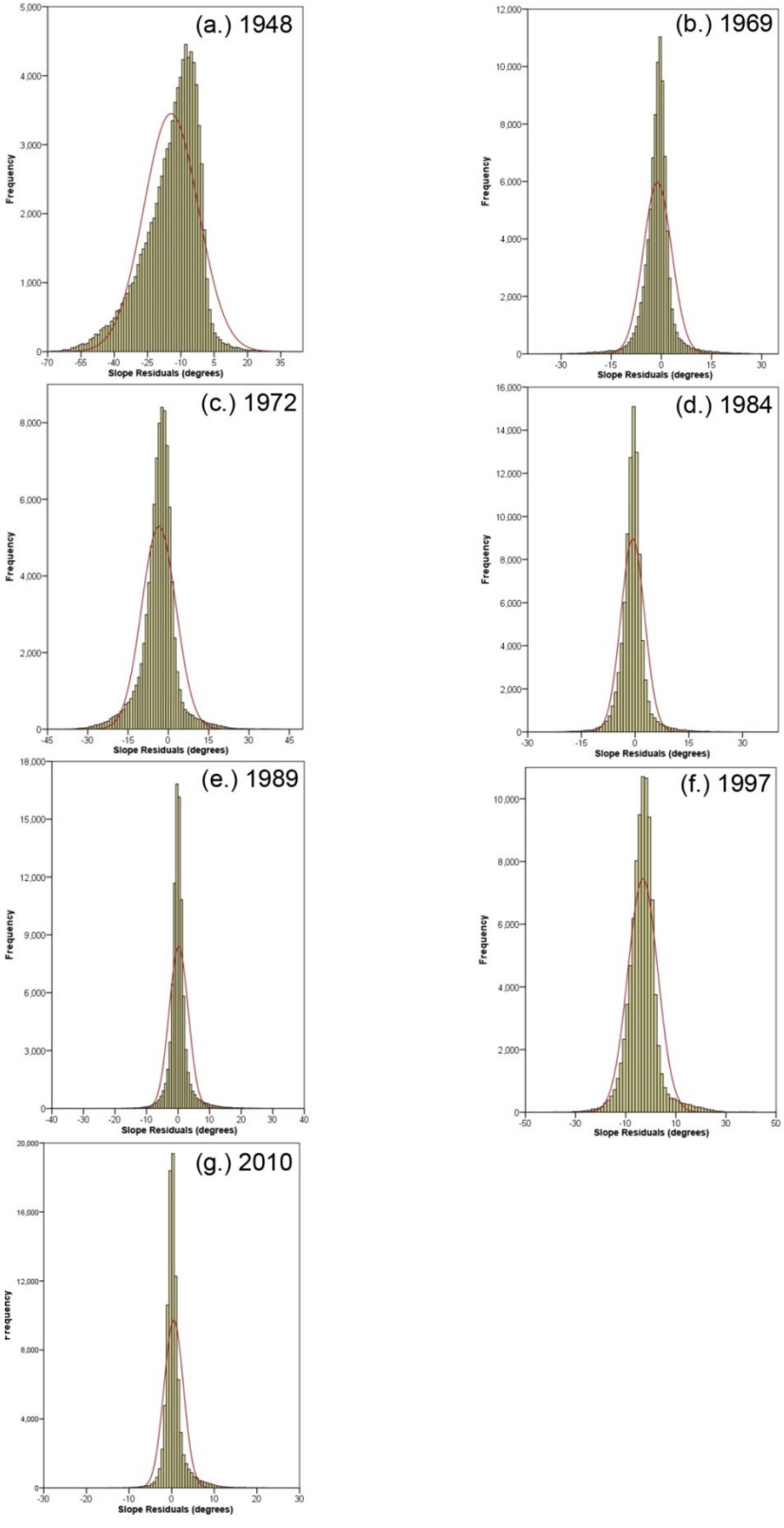

Figure 7.39: Frequency Histograms showing the residual distribution of slope values across Eggardon Hillfort.

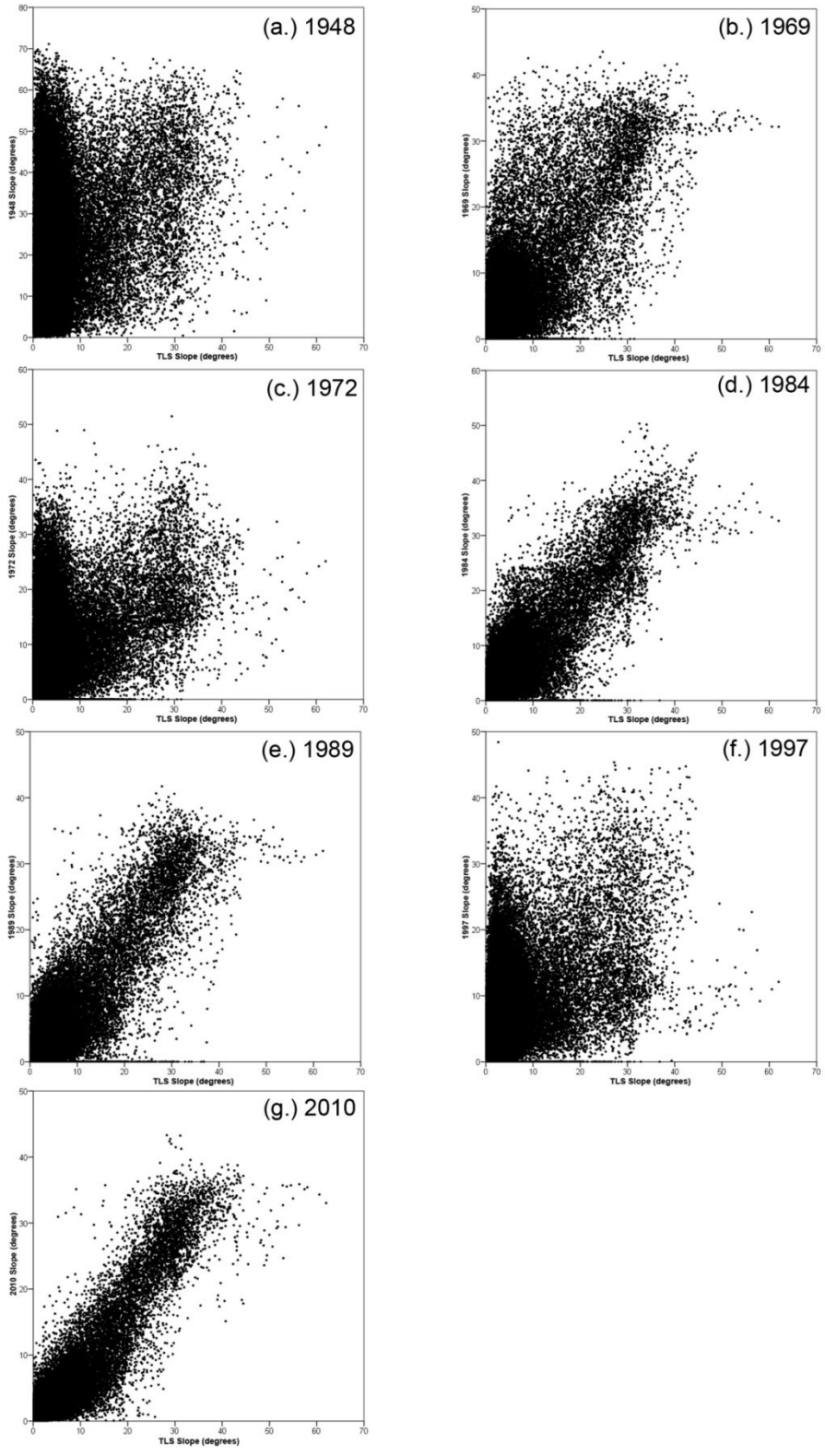

Figure 7.40: Linear scatterplots showing the correlation between the TLS slope values and those of the SAP datasets across Eggardon Hillfort.

7.5.2 Eggardon Henge Monument

As with the hillfort area, there are also distinct visual differences between the representation of slope across the henge monument and barrow in each SAP epoch as compared to those of the TLS, which are shown in Figure 7.41. The 1948, 1972 and 1997 SAP epochs fail to generate slope values that are representative of the archaeological earthworks, which is also inferred by the summary statistics contained in Table 7.8. Variance values are much higher for the three worst performing datasets, with the 1948 SAPs in last place with a measure of 173.932, followed by the 1972 SAPs at 15.05 and subsequently the 1997 SAPs with a value of 13.767. The next highest variance value is appended to the 2010 dataset, namely 5.636, which is a large difference when compared to the 1997 result, whilst the best performing SAP epoch is 1984, with a variance of 3.689. The 1984 SAPs exhibit the smallest SD value of 1.921, although if considering the ME then it is the 2010 SAPs who perform best, with a value of -0.234. Yet again, there is no one statistical value that can really convey the overall picture of DSM and derivative accuracy.

		TLS Minus 1948	TLS Minus 1969	TLS Minus 1972	TLS Minus 1984	TLS Minus 1989	TLS Minus 1997	TLS Minus 2010
N	Valid	11544	11544	11544	11544	11544	11544	11544
	Missing	0	0	0	0	0	0	0
Mean (degrees)		-15.153	-0.260	-2.233	-0.770	-0.299	-1.925	-0.234
Std. Error of Mean (degrees)		0.123	0.020	0.036	0.018	0.021	0.035	0.022
Median (degrees)		-11.756	-0.236	-2.102	-0.678	-0.257	-1.710	-0.216
Mode (degrees)		-9.622	-0.346	-4.007[a]	-1.316	-0.752[a]	-0.648	-0.565[a]
Std. Deviation (degrees)		13.188	2.138	3.879	1.921	2.262	3.710	2.374
Variance (degrees^2)		173.932	4.572	15.050	3.689	5.116	13.767	5.636
Skewness		-0.850	0.087	0.059	-0.185	0.282	-0.034	0.103
Std. Error of Skewness		0.023	0.023	0.023	0.023	0.023	0.023	0.023
Kurtosis		0.037	5.295	1.574	1.561	2.861	1.335	3.142
Std. Error of Kurtosis		0.046	0.046	0.046	0.046	0.046	0.046	0.046
Range (degrees)		77.214	31.046	40.051	22.328	27.838	33.337	28.290
Minimum (degrees)		-64.950	-17.276	-21.976	-12.385	-13.435	-18.502	-17.199
Maximum (degrees)		12.264	13.770	18.075	9.943	14.403	14.835	11.091
RMSE (degrees)		20.088	2.154	4.476	2.069	2.281	4.180	2.385

Table 7.8: Summary statistics for slope residuals across the henge monument.

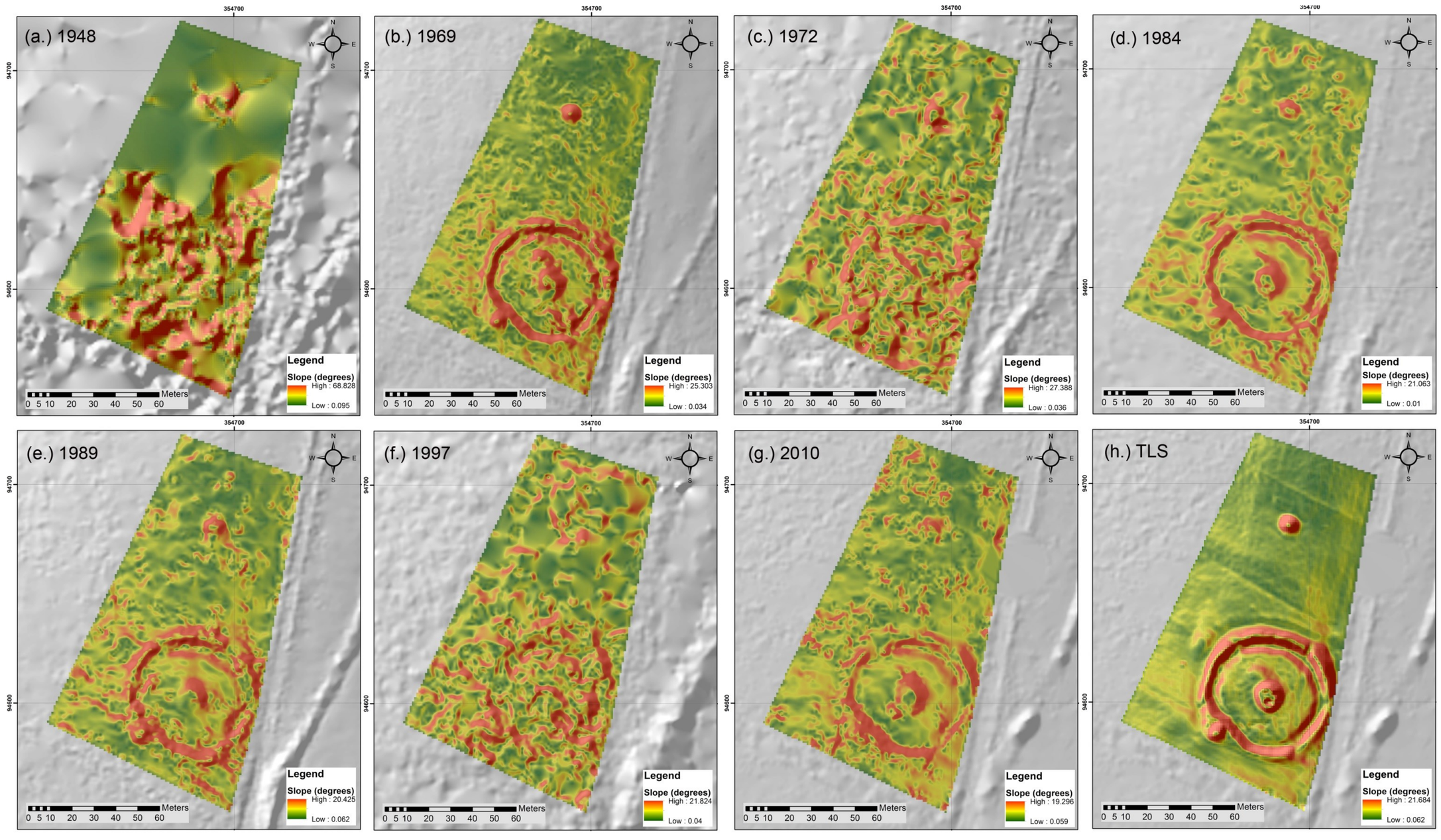

Figure 7.41: Slope derivatives for the Eggardon henge monument SAP epochs and TLS data.

	Paired Samples Correlations		Paired Samples Test				
	Correlation	Sig.	95% Confidence Interval of the Difference		t	df	Sig. (2-tailed)
			Lower	Upper			
TLS Slope vs 1948 Slope	0.334	0.000	-15.393	-14.912	-123.447	11543	0.000
TLS Slope vs 1969 Slope	0.741	0.000	-0.299	-0.221	-13.081	11543	0.000
TLS Slope vs 1972 Slope	0.324	0.000	-2.304	-2.162	-61.850	11543	0.000
TLS Slope vs 1984 Slope	0.795	0.000	-0.805	-0.735	-43.098	11543	0.000
TLS Slope vs 1989 Slope	0.690	0.000	-0.340	-0.257	-14.192	11543	0.000
TLS Slope vs 1997 Slope	0.330	0.000	-1.993	-1.857	-55.746	11543	0.000
TLS Slope vs 2010 Slope	0.639	0.000	-0.277	-0.190	-10.575	11543	0.000

Table 7.9: Paired t-test comparing the similarities between the TLS and SAP slope values for the henge region.

The slope histograms for the henge area are shown in Figure 7.42. Aside from the 1948 slope residuals that display a negative skew, the remaining SAP datasets have the appearance of a normal distribution. What differentiates the least accurate datasets, namely the 1948, 1972 and 1997 epochs, are ME values that deviate further from 0 towards increasingly negative values and a wider range of residuals, fewer of which are found close to 0 as suggested by the σ appended to each dataset. As regards the relationship between the TLS and each SAP epoch, the same pattern is visible in the scatterplots, depicted in Figure 7.43, as for the hillfort data. The 1948, 1972 and 1997 scatterplots do not show positive linear correlation and thus their r values are extremely weak, as shown in Table 7.9. In fact, the 1972 SAPs have the lowest correlation (r=0.324), followed by the 1997 data (r=0.33) and then the 1948 SAPs (r=0.334). It is surprising that the 2010 SAPs do not have the highest r value, as would be expected from a dataset that was both recent and provided with camera calibration information. It is the 1984 SAPs that perform the most favourably across the henge region, followed by the 1969 dataset, then the 1989 and finally 2010 SAPs. It is encouraging to note that the 1969 data has performed so well.

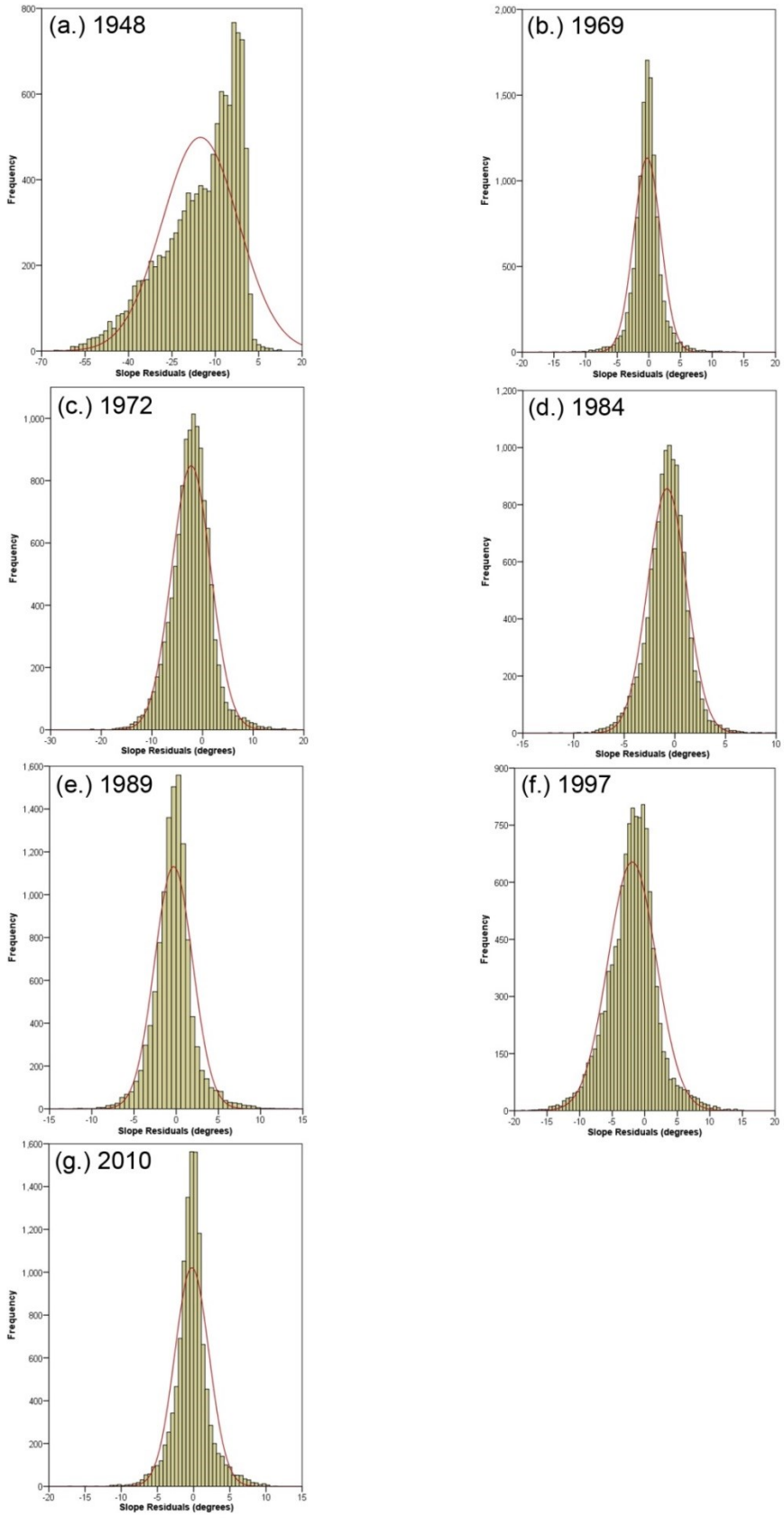

Figure 7.42: Frequency histograms of slope residuals for the henge region.

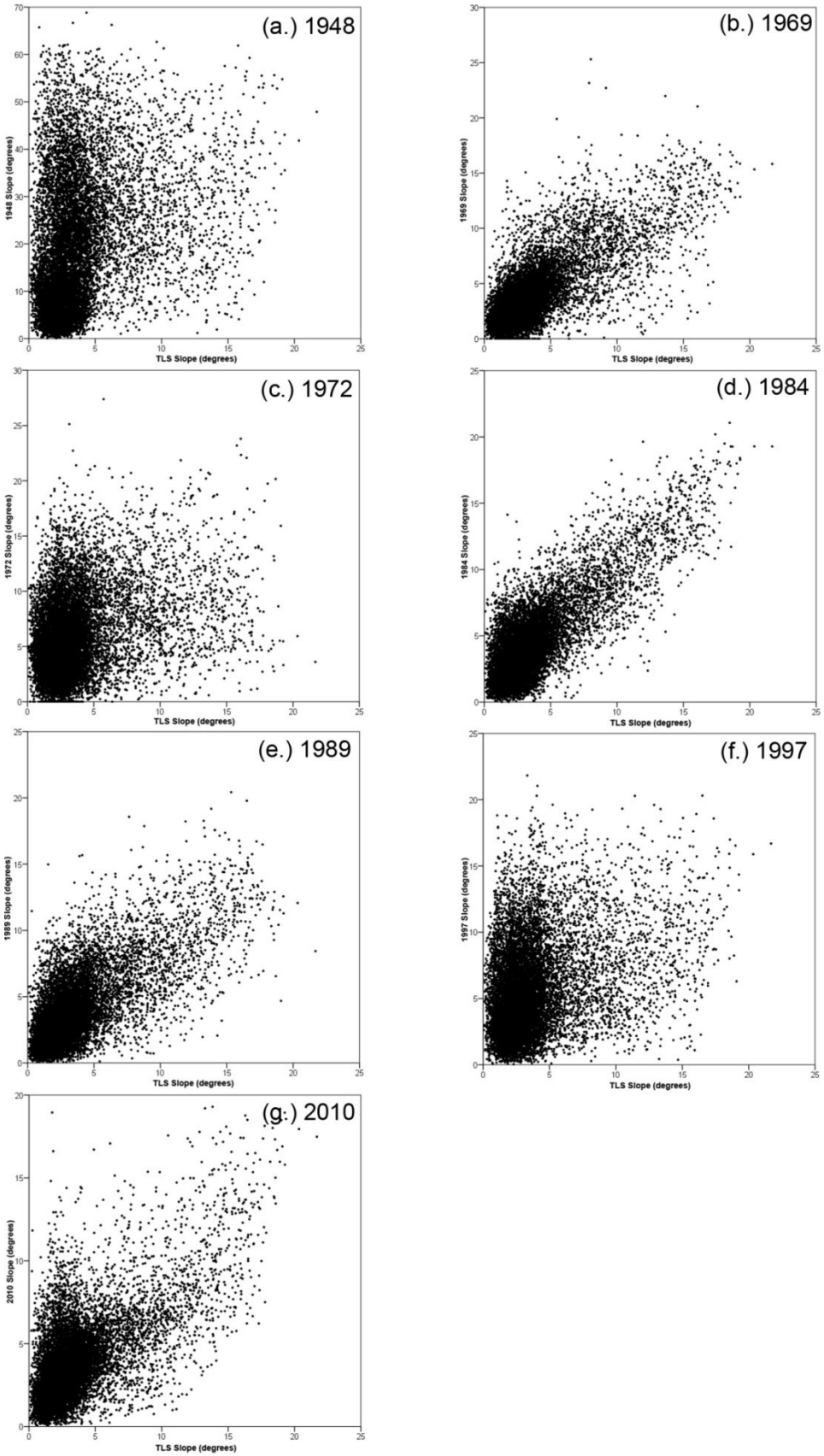

Figure 7.43: Scatterplots showing the linear correlation between TLS and SAP slope values across the henge region.

Although an r value of 0.741 is considered to be strong, rather than very strong, it is a good indication that obtaining favourable results from older SAP data is possible. This subsequently gives rise to the hope of being able to reconstruct archaeological features that may have disappeared after this date.

7.5.3 Local Moran's I Analysis

7.5.3.1 Hillfort

The Moran's I result for the 1948 SAP slope residual values within the hillfort, as shown in Figure 7.44a, contains many statistically significant high and low values and very few non-significant results. It is also interesting to note that there are locations across the hillfort where high values are bordered by low values, indicating that there are a number of 'troughs' in the data. Based upon the appearance of the underlying hillshade in the DoD (see Figure 7.45a), these troughs can clearly be seen in the south-west and east of the hillfort, as indicated by the areas of blue. There is very little in the way of a pattern to the distribution of the significant residual values, although there is a noticeable line of high values that runs the length of the fence line. This feature is marginally visible in the DOD too, which suggests that there is spatial structure in the 1948 slope model, as a subtle slope separates the southern and northern half of the hillfort. Based upon the yellow and orange colours appended to this feature in the DOD, it appears that the TLS slope is between 3º and 9º steeper than the 1948 results. This result is not unexpected as the severity of the slope should have increased over the years due to ploughing activity on the northern half of the hillfort.

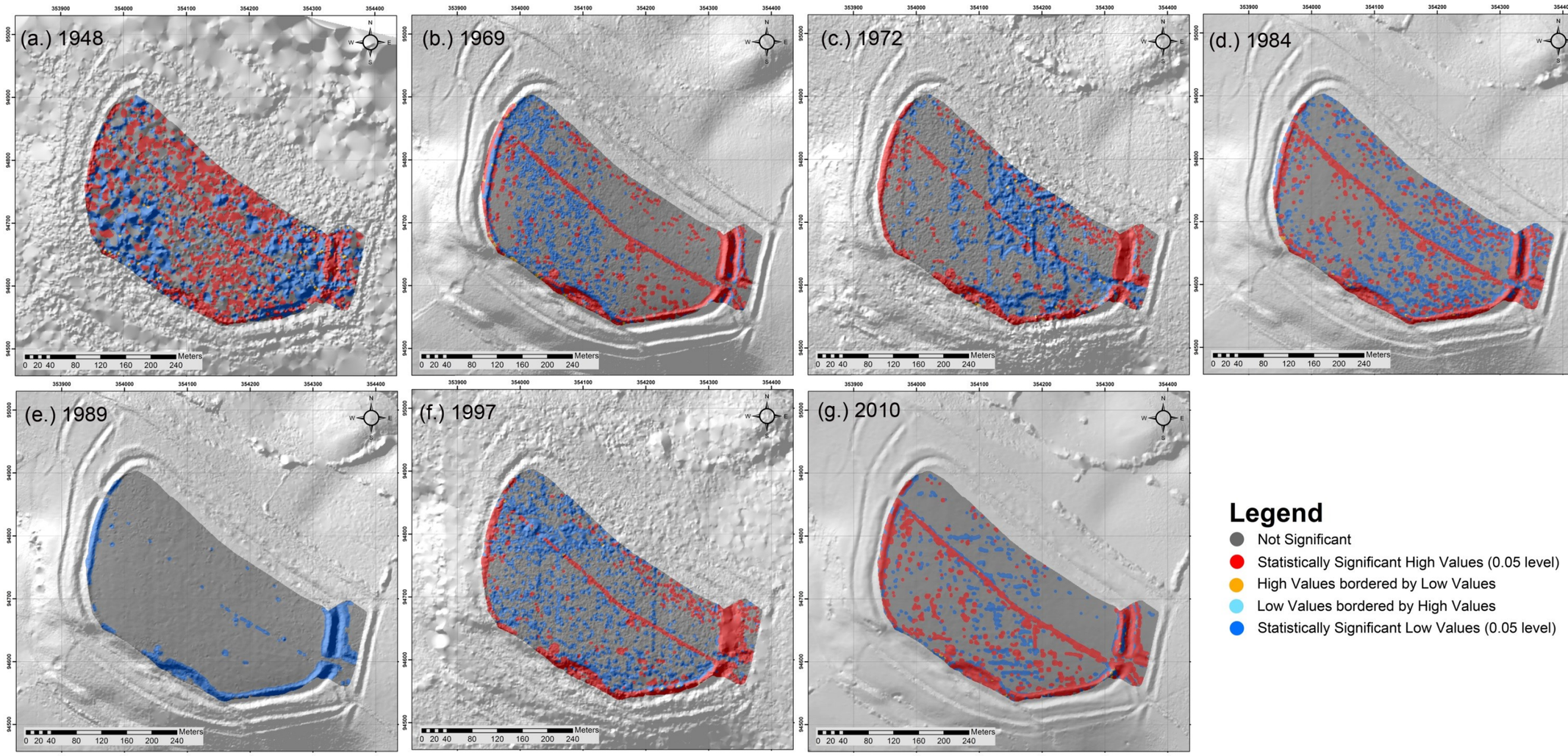

Figure 7.44: Moran's I diagrams of Eggardon Hillfort showing the distribution of residual values of difference between the TLS slope and SAP slope derivative values.

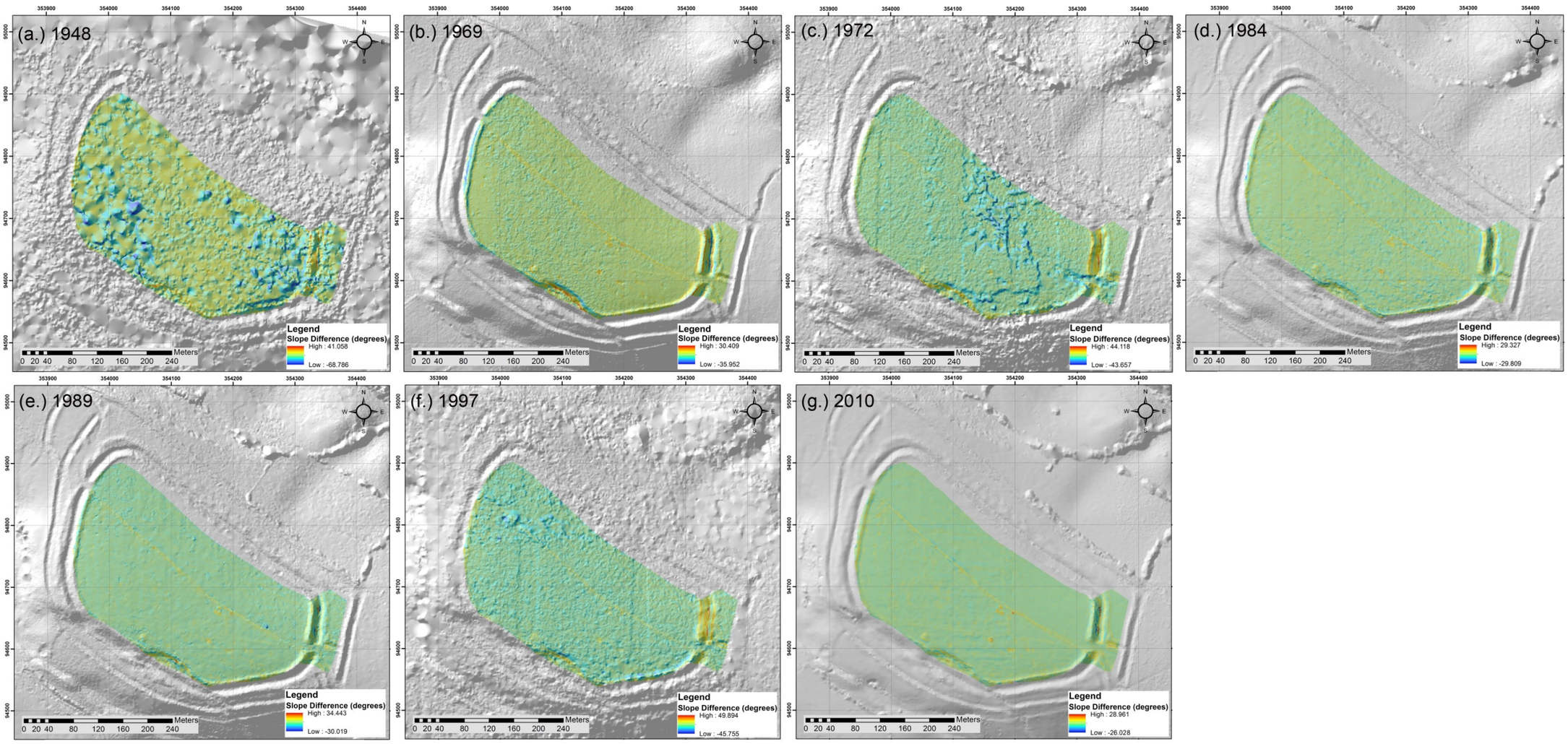

Figure 7.45: DSMs of Difference between the Eggardon hillfort TLS and the SAP slope derivatives.

Slope Dataset (Hillfort)	Moran's Index	z-score	p-value	Residual Distribution	Likelihood of random chance result (%)
1948	0.848	357.156	0.000	Clustered	1.000
1969	0.715	300.878	0.000	Clustered	1.000
1972	0.787	331.109	0.000	Clustered	1.000
1984	0.678	285.566	0.000	Clustered	1.000
1989	0.953	401.049	0.000	Clustered	1.000
1997	0.758	319.064	0.000	Clustered	1.000
2010	0.699	294.373	0.000	Clustered	1.000

Table 7.10: Moran's I statistics for the slope residuals across Eggardon Hillfort.

There are other areas within the 1948 slope model that suggests change has been detected in the DoD, and these are located on the ramparts to the east and on the landslip. There are coherent regions of yellow and red strips close to the base of the ramparts and along the landslip breakline. As these areas are also regions of change that have been detected in the other SAP datasets, as shown in Figure 7.45b to g, a greater confidence can be appended to the 1948 results. The Moran's I value for the 1948 SAP slope dataset are clustered, as shown in Table 7.10. This is suggestive of a systematic error in the data, which is expected as any lens distortion errors could not be accounted for in the 1948 data. Although a large number of GCPs were utilised to try and minimise the impact of these errors on the 1948 DSM, it is likely that they still remain. A random distribution of residuals would have been preferable, as this would suggest that any systematic errors had been removed. However, without camera calibration data it is unlikely that this would be achievable. Error clustering may also indicate the severity of the slopes within a DSM (Weng 2002, p410), of which there are many severe slopes created by the ramparts. Large errors have been stated by Gonga-Saholiariliva et al (2011) to occur along slopes and valley bottoms, which in this case are also represented by the rampart ditches, whilst minimal errors are to be found in flatter regions. The authors also state that any deviations from the expected elevation values of a feature will propagate through to first and second order derivatives, such as slope.

The Moran's I result for the 1969 SAP residuals is shown in Figure 7.44b. The statistically significant high values appear to have spatial structure, as indicated by the fence line running through the middle of the hillfort, and a concentration of highly significant values on the ramparts and landslip slopes. They are also present in concentration around a barrow that is situated to the north-east of the landslip feature. Conversely, the statistically significant low values appear to be more scattered, especially throughout the southern half of the hillfort interior. Whilst there are many pits to be found to the south of the fence line, these features do not necessarily correlate with the results of the Moran's I test. The scattered high and low statistically significant values are more representative of the region of apparent noise that afflicts the western half of the hillfort interior in the 1969 SAPs, as shown in Figure 7.44b. The 1969 orthophotograph (see Figure 7.25) contains a range of contrast values in this region, and thus image matching should

have worked well here. However, in one of the images in the strip, this area of the hillfort is situated next to the information strip and thus very close to the extreme edges of the imagery. Therefore the result of this 'noise' may be due to the presence of lens distortion, which is a type of systematic error that subsequently exhibits in the Moran's I clustered results.

Within the DoD (Figure 7.45b) there is spatial structure to the differences between the 1969 and TLS slope values. The fence line and south barrow indicate that the TLS displays higher slope values along the outline of these features. This could be for two reasons: firstly the TLS records slopes in a direction perpendicular to their face, and thus is able to capture variations that may be occluded from a vertical perspective. Secondly, the TLS was set to perform the hillfort survey with a point spacing of 10cm, which was subsequently decimated to 1m for comparative purposes with the SAP DSMs. However, this initially higher point spacing may influence the value of each grid square when interpolated to a lower resolution value as the greater the number of values the interpolator has to consider, the more representative the calculated result. Despite digitising the SAPs so that the ground sample distance (GSD) is between 10cm and 15cm, the detail contained within the photography depends on the image contrast and the image scale.

An apparent increase in slope values is identifiable at the base of the landslip, along the fence line, the crest of the eastern ramparts and on the slope faces, as shown by the yellow and red patches in the DoD (see Figure 7.45b). This may indicate either a change in slope between the 1969 and 2013 TLS survey, or it may highlight regions where the photogrammetric process has underestimated slope at certain points, such as on the rampart. Along the vertical face of the landslip there is a slope difference of up to 20º. By using the 'identify' tool in ArcMap and selecting a particular point within the landslip for comparison, the 1969 slope value is 23.423º whilst the TLS slope value is 43.306º. The difference between these datasets is also apparent on the rampart slopes, where the TLS values are higher than those generated by the 1969 SAPs. As slope underestimation has been identified as a side-effect of the photogrammetric process (Adams and Chandler 2002; Hodgson et al. 2005), there is a strong possibility that this is the observed effect here. However, there are large swaths of the 1969 data that are not significantly different from the TLS, as shown by the large number of non-significant values in the Moran's I diagram (see Figure 7.44b). Whilst these values are mostly found on the flatter interior of the hillfort, they also provide confidence that there is a significant level of agreement between the two datasets, as confirmed by the r value returned by the paired t-test of 0.725.

Whilst the distribution of significant high values appear to have some form of spatial structure in the 1972 Moran's I diagram of the hillfort, as shown in Figure 7.44c, the significant low values enhance the region in which triangulation or image matching has failed. The significant low values, shown in blue, outline the spurious terrain results that have been generated by SocetGXP, thus highlighting the effects of elevation offset on the slope derivative. In these areas the 1972 SAP data contains steeper slope values than recorded by the TLS. The significant high values, as denoted by the red patches, are found along the rampart slopes, on the landslip and along the fence line. In these areas, the TLS exhibits steeper slope values than

the 1972 data. As there has evidently been a failure in the terrain extracting process to create representative elevation values from the 1972 SAPs, the slope values derived from this data are likely to have been underestimated. There is no evidence of the fence line in the 1972 slope map (See Figure 7.38c) and thus the change in slope that is identifiable in the DoD (see Figure 7.45c) and the Moran's I diagram (Figure 7.44c) is based solely on the TLS results rather than its detection by the 1972 SAPs. The eastern ramparts have not been reconstructed by SocetGXP, as evidenced by the flat, texture-less appearance of the slopes in the underlying hillshaded elevation model that appears in the 1972 Moran's I and DoD Figures. Therefore the changes that have been identified by the DoD and that exhibit statistically significant high and low values in this area are not representative of any changes that have occurred here.

Although there are large regions in the Moran's I diagram (Figure 7.44c) that are grey, signifying the presence of non-significant values, there is little confidence that any meaning can be derived from areas of change. This is especially so as there is a poor correlation between the TLS and 1972 slope values (r=0.419). The failure of SocetGXP to perform triangulation and/or image matching and, subsequently, terrain extraction to suitably recreate the hillfort from the 1972 SAPs is due to the SAP dataset itself. The 1972 photographs were scanned from prints in an uncharacterised desktop scanner which further introduces error into the digital images (see Section 2.2.6.3 for details). As there is also no existing camera calibration data appended to this dataset and no metadata relating to the care of the prints over their lifetime, there are a large number of unaccountable error sources that cannot be removed during the photogrammetric workflow. These types of systematic error are indicated by the Moran's I, which has returned a score of 0.787 that identified a clustered residual distribution. Therefore the 1972 DSM is unlikely to provide a means by which to detect change and reconstruct the earthworks here.

The Moran's I result for the 1984 SAP hillfort slope values, as shown in Figure 7.44d, display both spatial structure and randomness. As with the previous SAP datasets, highly significant values are to be found along the fence line, rampart slopes and across the landslip. However, unlike the 1948 and 1972 SAP datasets, the fence line is visible, albeit subtly, in the 1984 slope map (see Figure 7.38d). Certain features in the south of the hillfort, such as the round barrow close to the landslip and the linear feature situated in the north-west corner, are also apparent, as is the north-eastern edge of the coppice hexagon. Each of these features is also present in the Moran's I diagram, although the hexagon and the linear feature do not form a coherent set of lines. They are denoted by significant high values however, indicating that the TLS slopes in these areas is steeper than those recorded by the 1984 SAPs. This is unsurprising as the TLS is more likely to detect subtle earthworks in a landscape than aerial photography, the scale of which is 1:8000.

In the DoD for the 1984 and TLS datasets, shown in Figure 7.45d and h, the slopes of the east ramparts show a difference in slope between ~3º to ~10º in the yellow regions, and up to ~17º in the orange. These subtle colour differences also occur on the landslip face and along the fence line. As previously explained, this indicates areas where the TLS slope is steeper than the 1984 slope. It is unlikely that material has accumulated over a ~30 year period, as there is no

concurrent change on the ridge of the bank, which is the only place extra material may have travelled from. Both the TLS and 1984 surveys were conducted before or during mid-April, when the grass is ~10cm high (measured in the field), and thus the change in slope is not due to grass length. Therefore the most likely explanation for slope difference here is due to the underestimation of elevation values during terrain extraction in SocetGXP.

There are some regions along the southern ramparts, the east-facing slope of the east ramparts and the west-facing slope of the western ramparts that suggest the 1984 slope is steeper than the TLS. These areas are denoted by the blue regions in the Moran's I diagram (Figure 7.44d), although many of these are obscured by the red areas, and the DoD (Figure 7.45d). By examining these areas in the 1984 and TLS slope maps (Figure 7.38d and h respectively) this observation is confirmed, although stating why this pattern has emerged is difficult. Initially, the reduction in slope over time may be due to erosion caused by walkers along the top of the southern ramparts. However, upon inspection of the 1984 slope map, there is also some degree of 'noise' as indicated by the wavy appearance of the slope values, which will influence the slope difference between the TLS and the 1984 data. Within the 1984 orthophotograph, shown in Figure 7.46, there is little to suggest any further influence the SAPs may have on the production of these slope values. The southern ramparts are not in shadow, which can influence the accuracy of photogrammetric terrain extraction, and nor does there appear to be artifacts in the imagery that may also cause noise.

On the eastern facing slopes of the east ramparts there are linear features that run along the rampart slopes, as shown in the orthophotograph (Figure 7.46). These features may be caused by soil slumping or creep and it is also likely that the presence of shadow across them may influence the accuracy of the terrain extraction process in SocetGXP (Figure 7.47). Whilst each slope map, as shown in Figure 7.38d and h, exhibits some variation in slope structure here, as is apparent in the variation in red and yellow values across the ramparts, the magnitude of difference between the TLS and 1984 slope values is largely small: the majority differ by ~3º across most of this region, although in some areas the difference can be as great as ~30º. The DoD (see Figure 7.45d) identifies the largest variation as occurring at the base of the slope. The decrease in slope, shown in blue, occurs just above the increase in slope, which is situated close to or in the ditch. This indicates that material from the slope has moved in this area over the 30 years between surveys. In 1984, the majority of the rampart slope had an angle of ~30º. However, by the 2013 TLS survey, sections of this rampart had altered, with the blue region indicating a slope value of 8º and the red region a slope value of 50º.

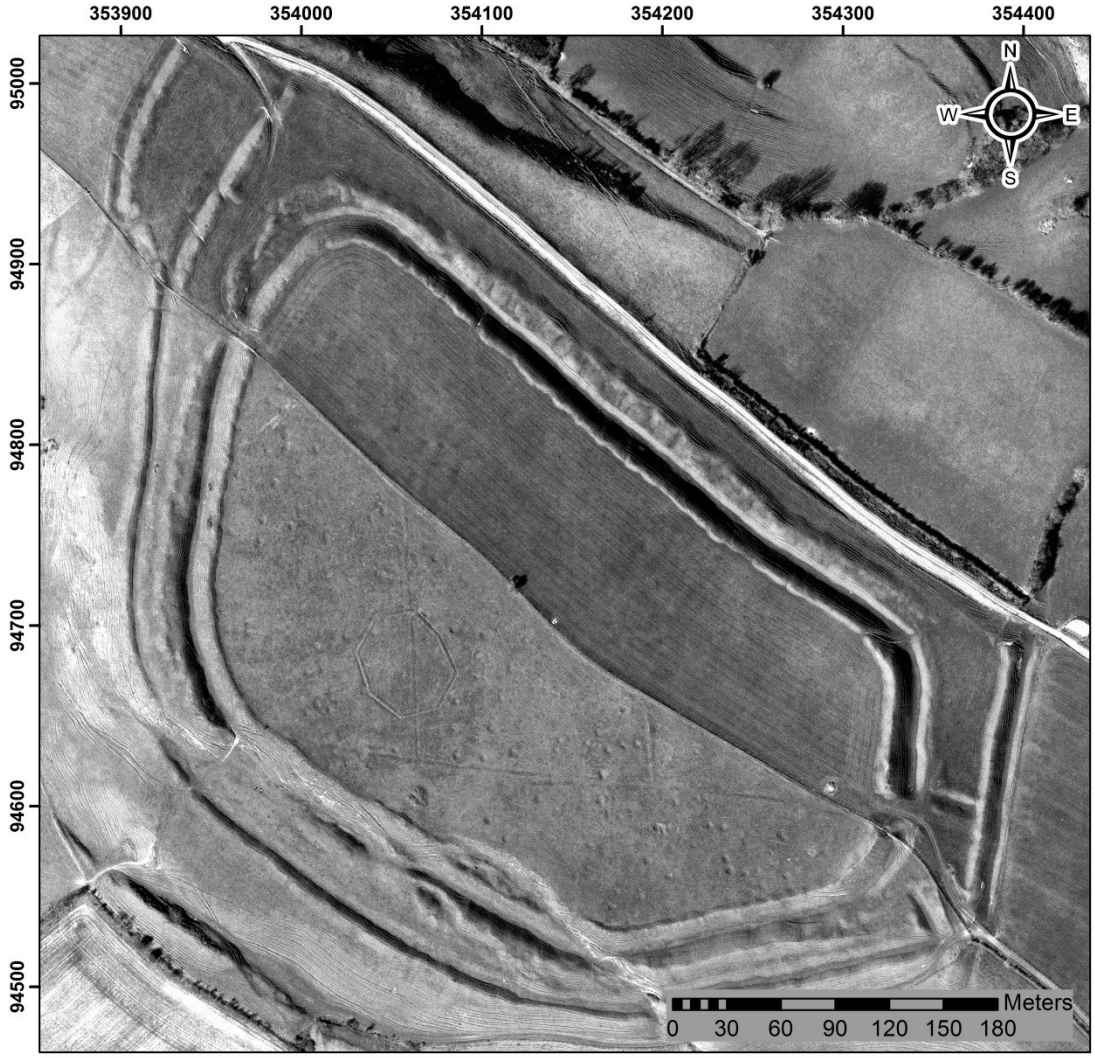

Figure 7.46: 1984 orthophotograph of Eggardon hillfort.

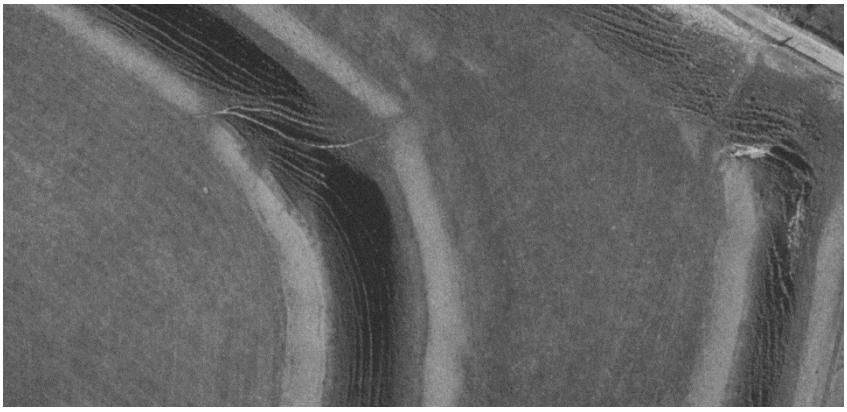

Figure 7.47: Slumping features on the eastern ramparts of the hillfort.

To further establish the processes at work here, elevation values were re-examined in both datasets within this area. In the elevation DoD, shown in Figure 7.45d, for the 1984 and TLS datasets, the TLS is 0.86m higher than the 1984 DSM in the area that is marked as blue in the slope DoD (Figure 7.45d). Whilst there is an elevation offset between the datasets here, the relative elevation values within the TLS DSM does not change rapidly i.e. from 244.479 to 244.428, which is consistent with a slope angle of 8º. There is a more notable change in elevation across this region in the 1984 data as the elevation changes from 244.854m to 244.189m in a short distance, which will create a steeper slope value of 30º. However, in the red region of the slope DoD (Figure 7.45d) it is the 1984 DSM elevations that show minimal change i.e. 242.896m to 242.277m, and hence exhibit a slope value of 30º here. The TLS elevations, however, change more abruptly over this region, from 244.425m to 241.657m, which is commensurate with the recorded slope angle of ~50º in the TLS data. As the 1984 slope values are so consistent, this suggests that there is little noise in this dataset, and thus the detection of change between the 1984 SAPs and TLS data is not due to spurious results. Figure 7.47 is an example of the type of damage occurring on the ramparts slopes at Eggardon, which is commensurate to the changes detected between 1984 and 2013.

In contrast to all of the other datasets, the Moran's I result for the 1989 hillfort slope residuals, as shown in Figure 7.44e, contains only highly significant low values, with the vast majority of residuals registering as non-significant. There are a small number of these values situated along the fence line, but this feature is predominantly covered by non-significant residuals. However, the landslip and the ramparts to the west, south and east of the hillfort are covered by significant low values, indicating that the 1989 DSM has steeper slope values than that of the TLS. As with the 1984 dataset, the majority of the 1989 slope values on the east-facing ramparts slopes to the east of the hillfort are ~30º to ~37º, whilst the TLS is shallower by between 2º to 7º. The same patterns of change are observed in this dataset as they were in the 1984 slope data, which is unsurprising as there is only a 5 year difference between datasets, and it is unlikely that much will have changed. Based upon the results shown in the 1989 DoD, shown in Figure 7.45e, the slope difference between the 1989 and TLS data is the same, with the blue region showing a slope difference of -28.021º and the red region showing a difference of 16.987º. These values very by up to ~2º in comparison with the same regions in the 1984 DoD (see Figure 7.45d).

It would appear that the 1989 slope values display greater similarities with the TLS than those in the 1984 dataset, given the larger number of non-significant values displayed in the Moran's I map (Figure 7.44e). The lack of significant high values suggests that the TLS does not contain steeper slope values than the 1989 data, although the large number of significant low values along the rampart slopes indicates that the 1989 slope values are steeper here. On comparison of the 1984 and 1989 slope maps (see Figure 7.38d and e respectively), there is remarkably less noise in the hillfort interior in the 1989 dataset, which explains the lack of significant high or low values in the 1989 Moran's I result. However, the concentration of significant low values along the rampart slopes is more difficult to explain.

The ‘identify’ tool in ArcMap was used to measure a number of locations along the southern ramparts to compare slope values in the TLS, 1984 and 1989 slope maps to ascertain why the 1989 data performed differently here than the 1984 SAPs. As an example, at one location the TLS slope was 21.119º, the 1984 slope was 6.440º and the 1989 slope was 20.607º, and thus the 1989 data is much similar to the TLS. However, there are other examples whereby the 1984 data exhibits greater similarity to the TLS, which further complicates the issue. The statistical results of the Moran’s I test, shown in Table 7.10, indicate that the errors in the 1989 slope data are more clustered than those in the 1984 SAPs, as the Moran’s I value for 1989 is 0.953 whilst the value for 1984 is 0.678. This may help to explain why the 1989 clusters are so polarised towards the rampart slopes. The 1989 slope values also have a slightly higher correlation with the TLS data, namely 0.851, as compared to the 1984 data (r=0.832), although there is very little difference between these values. What does help to explain the difference in residual distribution between the 1984 and 1989 data is the 95% confidence intervals, also shown in Table 7.7. Whilst neither of these intervals cross 0, therefore removing any confidence that there is no difference between the 1984 and 1989 data and the TLS, the 1984 data deviates further from 0 as compared to the 1989 dataset.

As with the majority of the SAP datasets, the 1997 Moran’s I map, shown in Figure 7.44f, exhibits statistically significant high values along the fence line, landslip and the ramparts. There are fewer statistically significant low values, although two lines run vertically through the east and west of the hillfort interior. These represent the area at which triangulation has been sub-optimal or image matching has failed to provide an accurate match, which can be seen in the 1997 slope map in Figure 7.41f. The slope map also highlights where photogrammetry has failed to reconstruct the east and west ramparts, the latter of which have a patchy appearance, whilst the former appear to have a large gap running through the centre of them. The majority of the interior is afflicted with noise, which is characterised by the wavy appearance of the slope values. This is especially evident in the north-west of the interior, where there are a significant number of steeper slope values where there should be few.

The ramparts to the east of the hillfort demonstrate that the TLS slope values are much higher here, particularly in the 1997 DoD (Figure 7.45f), which is expected due to the lack of slope values here in the 1997 data. The increase in slope values at the base of the ramparts, depicted in red, are features that have been detected in the TLS slope map, shown in Figure 7.41h. The slope values across the landslip and the ramparts in the 1997 data are also patchy and inconsistent with the structure of the features here. It is therefore expected that the Moran’s I results here show that the TLS slope values are steeper, as indicated by the presence of significant high values. The correlation between the TLS and 1997 slope values is poor (r=0.423) and the Moran’s I score of 0.758 indicates that the residuals between these datasets are highly clustered. Whilst the Moran’s I result may show signs of spatial structure in the residual values, these regions highlight where the 1997 SAPs fail to match the TLS data, which is concentrated along the ramparts, landslip and fence line. These areas are not a crisply defined as with the other SAP datasets, excepting the 1948 and 1972 results.

Within the 2010 Moran's I result for the hillfort slope values, as shown in Figure 7.44g, there is spatial structure to both the statistically significant high and low values. Yet again the fence line is defined by significant high values, although towards the west of the hillfort these are lined by significant low values on the northern side. High values also occur along the inner slopes of the west and south ramparts along the face of the landslip, around the base of the south barrow, the ridge on the east ramparts, and along the west-facing slope of the outer bank here. Along each of these areas the TLS exhibits steeper slope values than the 2010 SAPs, to the magnitude of between ~4º and ~11º. As photogrammetry tends to underestimate slopes and make them appear 'softer', this is not unexpected.

At the base of the landslip there are regions of both high and low significant values, for which the subtlety of change between these values can be best seen in the 2010 DoD (see Figure 7.45g). The ridge and slope of the landslip exhibits positive values between ~6º and ~9º, indicating that the slope here was steeper in 2013 than in the 2010 SAP survey. Negative values occur along the base of the slope and tend to vary between ~-4º and ~-9º, indicating that these areas were detected as steeper in the 2010 SAP DSM. In comparison with the result of the elevation difference here, as discussed in Section 7.4, many of the significant low values in the elevation dataset have become significant high values in the slope dataset. This suggests that, where the TLS elevations were lower than those in the 2010 DSM, in some areas this has equated to an increase in the TLS slope steepness, which at first appears to be counter-intuitive: why would lower elevation values produce high slope values? Ultimately, slope is the measure of rate of change and it is likely that the slope of the TLS may produce a greater change from one pixel to another in comparison with the 2010 DSM, explaining this phenomena. It is also likely that the TLS, despite having been decimated to a 1m resolution to match that of the 2010 DSM, contains a greater range of more accurate elevation values that display greater variation in the terrain surface than the 2010 DSM, which also transfers into the slope derivative.

Within the east ramparts, changes in the east-facing slope are apparent, as they have been in many of the previous SAP datasets. The range of slope differences, as shown in the DoD legend (Figure 7.45g) are smaller, which represents the smaller timeframe between the SAP and TLS surveys. However, in comparison with the 1989 DoD for slope (see Figure 7.45e), the extent of slope change has increased. In the dark blue regions that are situated halfway down the rampart slope, there has been a slope decrease between the 2010 and 2013 surveys of 23.758º, which is slightly less than the 25.993º detected in the same place using the 1989 slope values. In real terms, this means that either the 2010 DSM was slightly more accurate in comparison with the TLS data, or the difference between the SAP DSMs and the TLS DSM is much greater than the difference between the SAP DSMs in relation to each other. In the red regions at the base of the rampart slope, there has been an increase in slope of up to 28.25º between the 2010 and 2013 surveys, whilst this was recorded as being 21.858º between the 1989 and TLS surveys. As there appears to be a much greater difference between the TLS and the SAP surveys, than there does between the SAPs themselves, it may be that the change

Slope Dataset (Henge)	Moran's Index	z-score	p-value	Residual Distribution	Likelihood of random chance result (%)
1948	0.877	132.386	0.000	Clustered	1.000
1969	0.590	89.188	0.000	Clustered	1.000
1972	0.718	108.479	0.000	Clustered	1.000
1984	0.682	102.971	0.000	Clustered	1.000
1989	0.670	101.203	0.000	Clustered	1.000
1997	0.764	115.367	0.000	Clustered	1.000
2010	0.720	108.797	0.000	Clustered	1.000

Table 7.11: Moran's I statistics for the slope residuals across Eggardon Henge region.

being detected along the east ramparts has occurred more recently, and after the 2010 photography was produced.

The residual differences between the TLS and 2010 slope datasets are clustered, and thus there would appear to be a systematic error remaining in the SAP dataset, despite the use of camera calibration data. There is, however, a very strong correlation between the TLS and 2010 slope values (r=0.917) and a SD of 2.278º, which is small. As the significant high values are all greater than the SD, it is likely that there has been a change in slope caused by a change in elevation between the 2010 SAP and 2013 TLS survey. However, as the monument is thought to be in a stable condition (English Heritage 2012) this change could either be due to vegetation growth or minor degradation due to trampling by cattle.

7.5.3.2 Henge Monument

The Moran's I result for the 1948 residual slope values, shown in Figure 7.48a, depicts clusters of statistically significant high and low values, with the latter tending to form around the henge monument itself. Whilst there are many non-significant values, unlike the hillfort dataset, there is no spatial structure to the distribution of residual values. The residual clustering present in the henge dataset has a value of 0.877 for the 1948 slope residuals, as shown in Table 7.11. As this is the SAP dataset with a value closest to 1, which denotes a perfectly clustered dataset, it is also the dataset with the least random distribution of residual values, which further indicates the presence of some form of systematic error in the data. In comparison with the 1948 slope DoD (Figure 7.49), there is no detectable spatial structure in either diagram, and thus the 1948 SAPs do not appear to contain any useable information within the henge region.

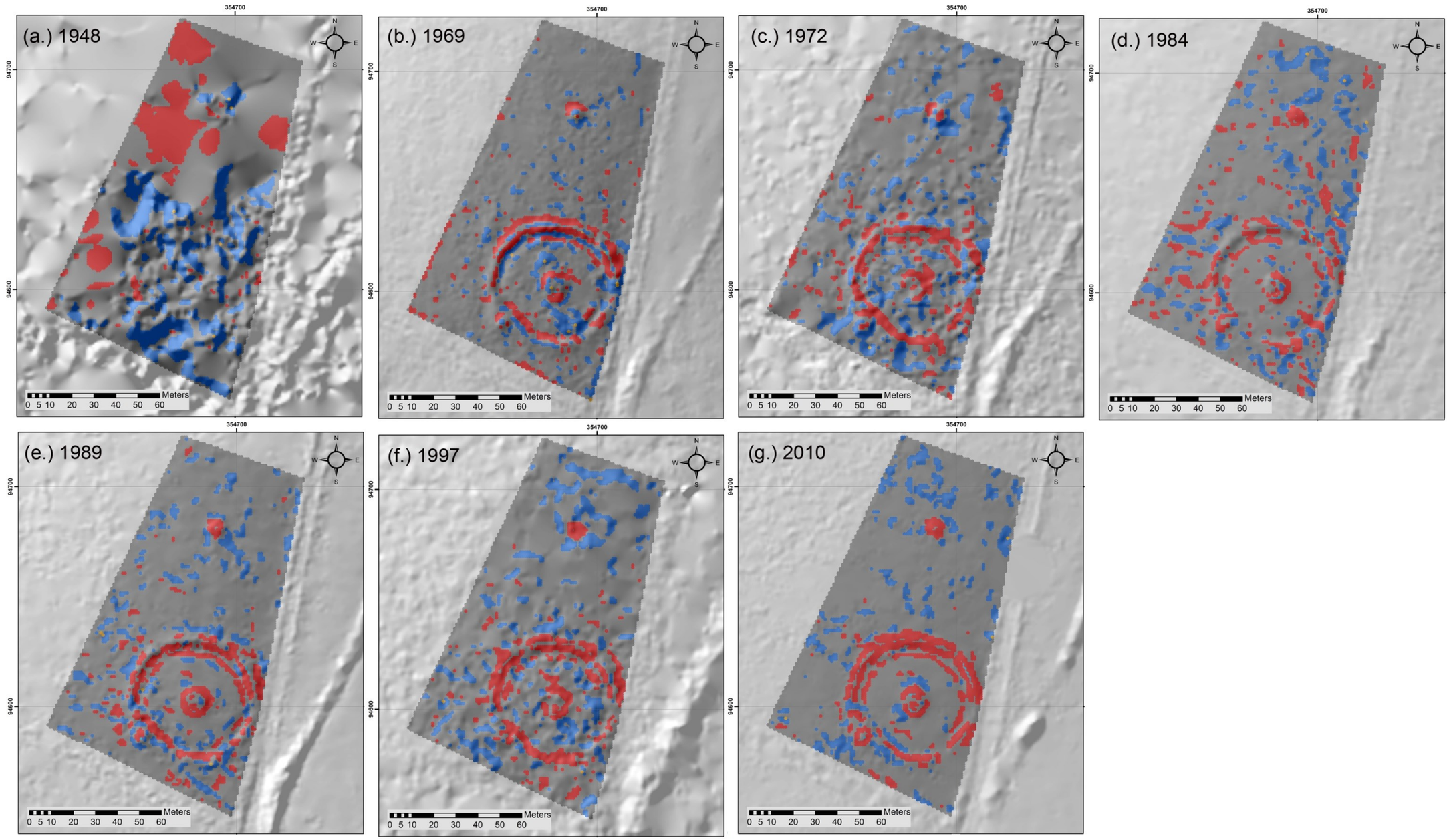

Figure 7.48: Moran's I diagrams of Eggardon henge monument and barrow showing the distribution of residual values of difference between the TLS slope and SAP slope derivative values.

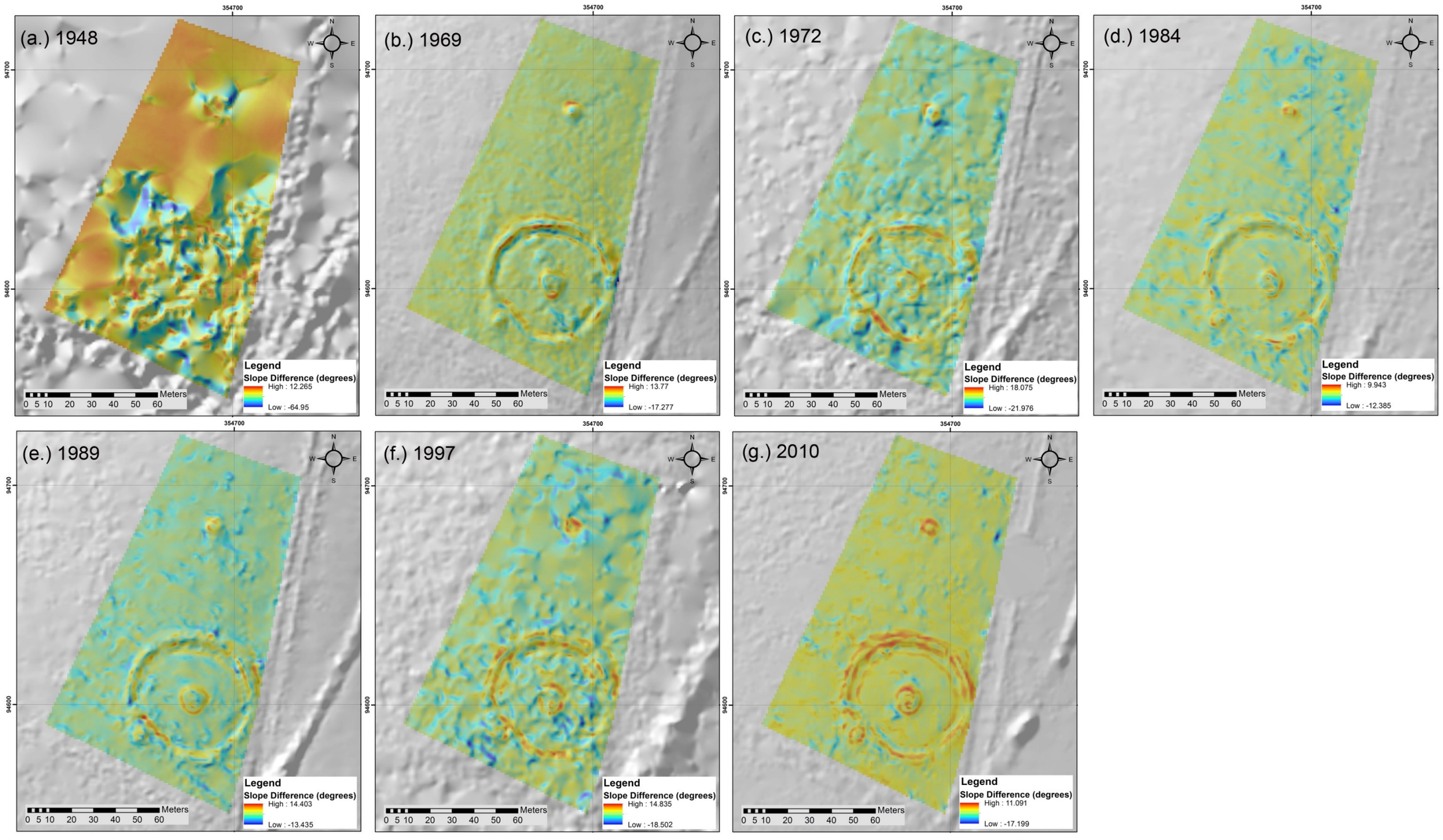

Figure 7.49: DSMs of Difference between the TLS and the SAP slope derivatives across Eggardon henge monument.

The Moran's I results for the 1969 SAPs exhibits spatial structure as many of the highly significant positive and negative values follow the contours of the henge and barrow slopes, as shown in Figure 7.48b. The remainder of the area is covered by non-significant values, which highlights the similarity between the TLS and 1969 data in this region. The DoD, as shown in Figure 7.49b, illustrates how the large positive differences in slope tend to occur along the slopes, whilst the large negative differences are situated along the ridge and ditch. The maximum positive slope difference between the TLS and 1969 data is 13.77º, although the maximum negative slope difference is a misleading -17.277. This value is to be found to the east of the henge monument, by the border of the image and cannot be reliably used. The maximum negative slope values across the monument are -12.578º. The areas of negative difference indicate regions where the 1969 data has a higher slope value than the TLS i.e. where SocetGXP has overestimated the slope. The alternative suggestion is that these regions have seen an increase in material over the 44 years between surveys. Along the slopes of the banks, the positive differences highlight areas that the 1969 data may have underestimated, such that the TLS has a higher slope value. This may also indicate areas of material loss over the years because the TLS slope is more severe than that recorded by the 1969 SAPs.

Based upon the use of this area for pasture and, at one time, ploughing (see Section 7.2.6), there has been little damage inflicted on the henge monument, save for the evidence of cattle rubbing and the periods during which it spent in an overgrown state. Therefore very little change should have occurred here, although the monument is thought to be at medium risk of degradation. As the correlation between the TLS and 1969 slope values is strong (r=0.741) and large differences between the datasets have been detected in specific areas, there can be confidence that change has actually occurred here. However, based upon the appearance of subtle noise in the 1969 slope map (see Figure 7.41b), there is also likely to be an element of uncertainty in these values.

Within the 1972 Moran's I result for the slope residuals, statistically significant high values display spatial structure and are located on the slopes of the banks and the barrows, as shown in Figure 7.48c. The TLS slope values are thus steeper in these regions than in the 1972 dataset, which is evident by comparison of the 1972 and TLS slope maps (see Figure 7.41c and h). Conversely, the statistically significant low values do not have a spatial structure and are more randomly distributed. Despite containing a large number of non-significant values, the correlation between these two datasets is also poor, with an r value of 0.324. Overall, the residuals exhibit a clustered distribution, which suggests that there is a systematic error within this region of the 1972 data.

The 1984 results of the Moran's I test within the henge region, as shown in Figure 7.48d, do not appear to adhere to a pattern, with the exception of the barrow to the north of the henge and the base of the barrow within the henge itself. There are statistically significant high values in these areas, which suggests that the TLS contains steeper slope values here than in the 1984 data. The DoD, as shown in Figure 7.49d, confirms this, although the difference in slope is not a large one and varies in these areas between ~2º to ~7º around the henge barrow, to ~3º to ~8º

around the north barrow. Based upon the appearance of the 1984 and TLS slope maps for this area (see Figure 7.41d and h respectively) this result is not unexpected as the 1984 data looks noisy and, although the slopes of the barrow and henge are defined, their outline is not sharp. This gives rise to differences between the two datasets, although the correlation value of 0.795 indicates that there is a strong relationship, and thus these differences are minimal. However, the residual distribution is still clustered, which suggests that systematic error also afflicts this dataset too.

The 1989 slope data surrounding the henge monument appears to exhibit spatial structure in the Moran's I map, shown in Figure 7.48e. The significant high values are concentrated along the slopes and ditches of the henge monument and the barrows, whilst there is little spatial structure to the significant low values. The significant high values indicate that the TLS has recorded steeper slope values for the henge and barrow slopes than the 1989 SAPs, which can differ by a value of ~15º, although in the vast majority of cases it is usually less than ~10º. It is also in these areas that the elevations of the TLS were between ~10cm and ~45cm higher than the 1989 SAPs, whilst the flatter area in the middle of the henge was higher in the 1989 data than in the TLS. This reduced elevation difference could explain the shallower slopes generated by the 1989 SAPs. It is difficult, therefore, to identify whether the subtle differences between the 1989 and TLS data are indicative of change over this 24 year period. However, the mean error between these datasets is -0.299º, and the difference between them exceeds this value, which may therefore indicate change. However, as it is the TLS which exhibits the steeper slope values and there is little negative change occurring above the slopes and ditches where the increase in slope has been detected, it is more likely that the photogrammetric process has underestimated the henge and barrow slopes.

There appears to be spatial structure in the 1997 Moran's I map of the henge monument region, as shown in Figure 7.48f. The significant high values are concentrated around the slopes of the henge and barrows, although the significant low values appear to be distributed randomly. Within the 1997 DoD, shown in Figure 7.49f, the significant high values are comparable to those found in the 1989 DoD. The maximum slope difference between the 1997 and TLS slope values is ~15º, however these differences cover a larger area than in the 1989 DOD and appear to be less coherent in their shape. By examining the 1997 henge slope map (see Figure 7.41f) the slope values for the henge and barrow monuments are noisy and do not describe the outline of the monument, unlike in the 1989 dataset. Therefore it is doubtful that meaningful data about the change in slope between 1997 and the 2013 TLS survey can be detected.

As with the previous henge datasets, the Moran's I result for the 2010 slope data, as shown in Figure 7.48g, displays no pattern for the significant low values, but does exhibit spatial structure for the significant high values. The high values are situated on the slopes of the barrows and the banks of the henge. The differences in slope between the TLS and 2010 datasets are not as large as the other SAP slope values, as shown in the DoD legend in Figure 7.49g. Whilst many of the significant high values in the 2010 slope Moran's I diagram appear on slope of the barrows and henge monument in the 2010 elevation Moran's I map (see Figure 7.48g), they do

not extend into the flat centre of the henge itself. This suggests that the 2010 DSM data contains minimal noise in this region as the rate of change of slope across the 2010 dataset does not greatly differ from that of the TLS, despite the disparity in elevation that was detected between the two datasets. This is also supported by the large number of non-significant values that cover the henge region.

The Moran's I score for the 2010 slope dataset across the henge is 0.72, which identifies a clustered distribution to the residual values. Despite the quantity of non-significant differences between the TLS data and the 2010 slope values, the correlation between these datasets is surprisingly low (r=0.639). There may subsequently be more outliers in this particular region of the 2010 DSM, as illustrated by the linear scatterplot shown for this area in Figure 7.43g, which exhibits a noisier appearance than the 1969, 1984 and 1989 datasets. The SD between the TLS and 2010 slope values is still low, namely 2.374, and thus any values greater than this are likely to be caused either by outliers or by actual change to the monuments themselves. Based upon the results from comparing the TLS to the remaining SAP datasets, the variation in slope values are more likely to be caused by change occurring in the landscape as the presence of spatial structure in the same areas across each of the datasets is consistent.

7.6 Aspect Assessment

In the previous section examining slope differences between the TLS and SAP DSMs, it was found that the 1948, 1972 and 1997 datasets yet again produced results that were noisy and unreliable. Although no bimodal distributions were displayed by any of the SAP slope histograms, the 1948 slope residuals contained a significant negative skew and proved to be the worst performing dataset. The 1972 and 1997 also exhibited excess noise due to the stripes that had appeared in the elevation datasets, which had also progressed to the slope derivatives. Despite the 2010 SAP terrain also containing stripe artifacts, the effect was not so obvious in the slope derivative, suggesting that the influence of this feature in the 2010 data is not extreme enough to be considered as noise. To further investigate the influence of noise and outliers in the SAP elevations, the aspect derivative was utilised to enhance imperfections in the data. Based upon the results of this Section, it will be possible to comment on which of the SAP datasets can reproduce terrain information describing the hillfort and henge features and whether it is possible to use this data to detect degradation of the monuments themselves.

The aspect assessment of both the hillfort and henge datasets is more complicated than that of the elevation and slope derivatives, for the reasons described at the beginning of Section 6.6. Initial analysis of the differences between the TLS and SAP aspect datasets will begin with an examination of the histogram from each dataset as well as the linear scatterplots showing the correlation between the TLS and each of the SAP aspect values. This approach facilitates the identification of discrepancies between these data more so than examining the aspect maps (Figure 7.50 and Figure 7.51), which can appear confusing due the wide variations in aspect

values. Subsequently, an analysis of the normalised aspect values will then be conducted to examine the residual differences between the TLS and SAP aspect datasets. This is more straightforward when the aspect data has been normalised, due to the otherwise circuitous nature of aspect representation.

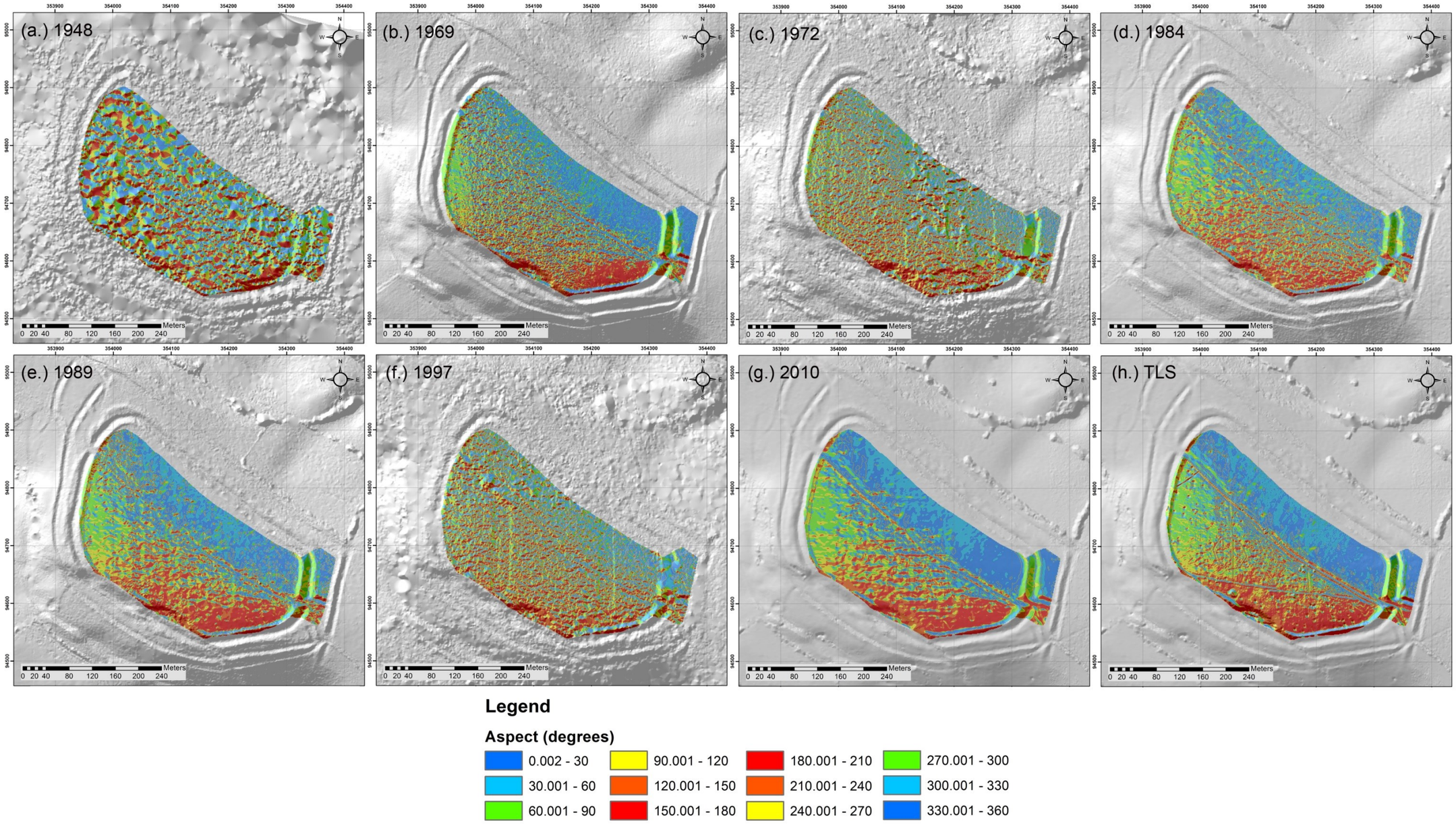

Figure 7.50: Aspect derivatives for the Eggardon Hillfort SAP epochs and TLS data.

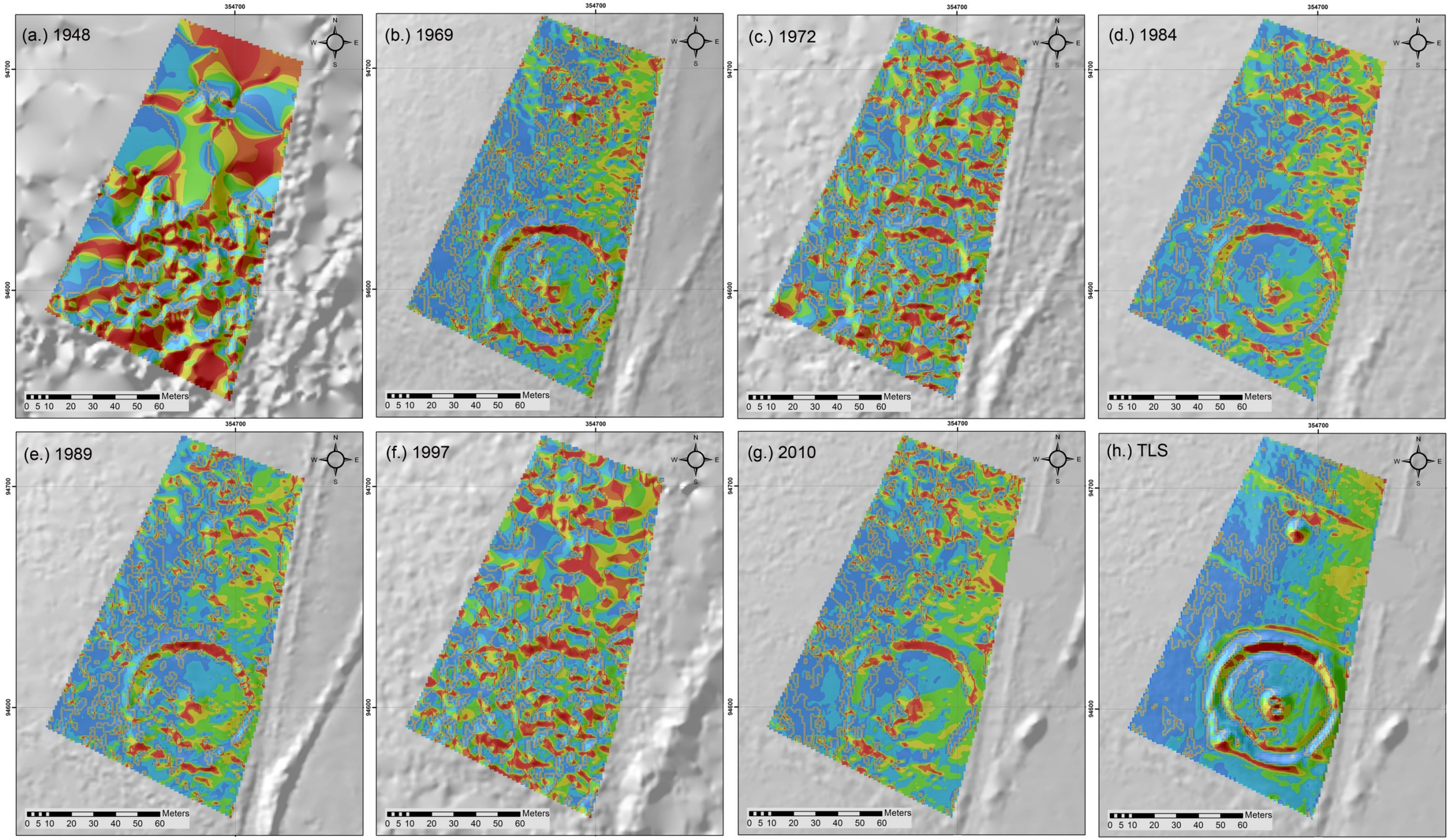

Figure 7.51: Aspect derivatives for the Eggardon henge monument SAP epochs and TLS data.

7.6.1 Eggardon Hillfort

Upon visual inspection of the aspect maps of all of the SAP and TLS datasets, as shown in Figure 7.50, it is the 1948, 1972 and 1997 epochs that appear to contain little useful information. Unlike the remaining data, these three epochs exhibit minimal, if any, spatial structure in the distribution of their aspect values. Both the 1972 and 1997 aspect values do outline the landslip and the east ramparts of the hillfort, although the latter feature is not as detailed as in the remaining SAP datasets, and both features are not apparent in the 1948 aspect map (Figure 7.50a). The disparities between the TLS and SAP aspect values are distinctly represented in the histograms shown in Figure 7.52, which illustrate how the various aspect values are distributed over the entire dataset. The 2010 data (Figure 7.52g) displays a remarkable similarity with the TLS data, whilst the1989 SAPs also appear to perform well (Figure 7.52e), although there is a reduced number of aspect values within the 0º to 45º range than in the TLS. Both the 1969 and 1984 SAP aspect values display peaks and troughs in the same locations as the TLS, although they are not as pronounced, which results in the aspect values between 90º and 225º occurring more frequently than in the TLS. Neither the 1972 and 1997 aspect datasets, shown in Figure 7.52c and f, contain the level of detail exhibited by the TLS, although there is a subtle peak between 0º to 90º that approximates the much larger peak within the TLS. However, their lack of distinct peaks and troughs elsewhere in the histogram indicates that these SAP have failed to recreate terrain aspect to the same degree as their photogrammetrically scanned and TLS counterparts. Further, the 1948 aspect results exhibit no correlation with the TLS.

The linear scatterplots showing the correlation between the TLS and SAP aspect values are shown in Figure 7.53. Whilst noise afflicts all of the results, there are identifiable linear correlations within the 1969, 1984, 1989 and 2010 SAP datasets, as indicated by the red line running diagonally across these graphs. There is also a hint of linearity in the 1972 scatterplot (Figure 7.53c), although this is by no means strong. What confuses the interpretation of these graphs is the fact that both 0º and 360º represent the same compass direction i.e. ‘north’, which explains the occurrence of a thick cluster of values close to 0º and 360º on both the x and y axis. Therefore, the analysis of TLS and SAP aspect value similarities is best conducted once the data has been normalised, the results of which are presented and discussed below.

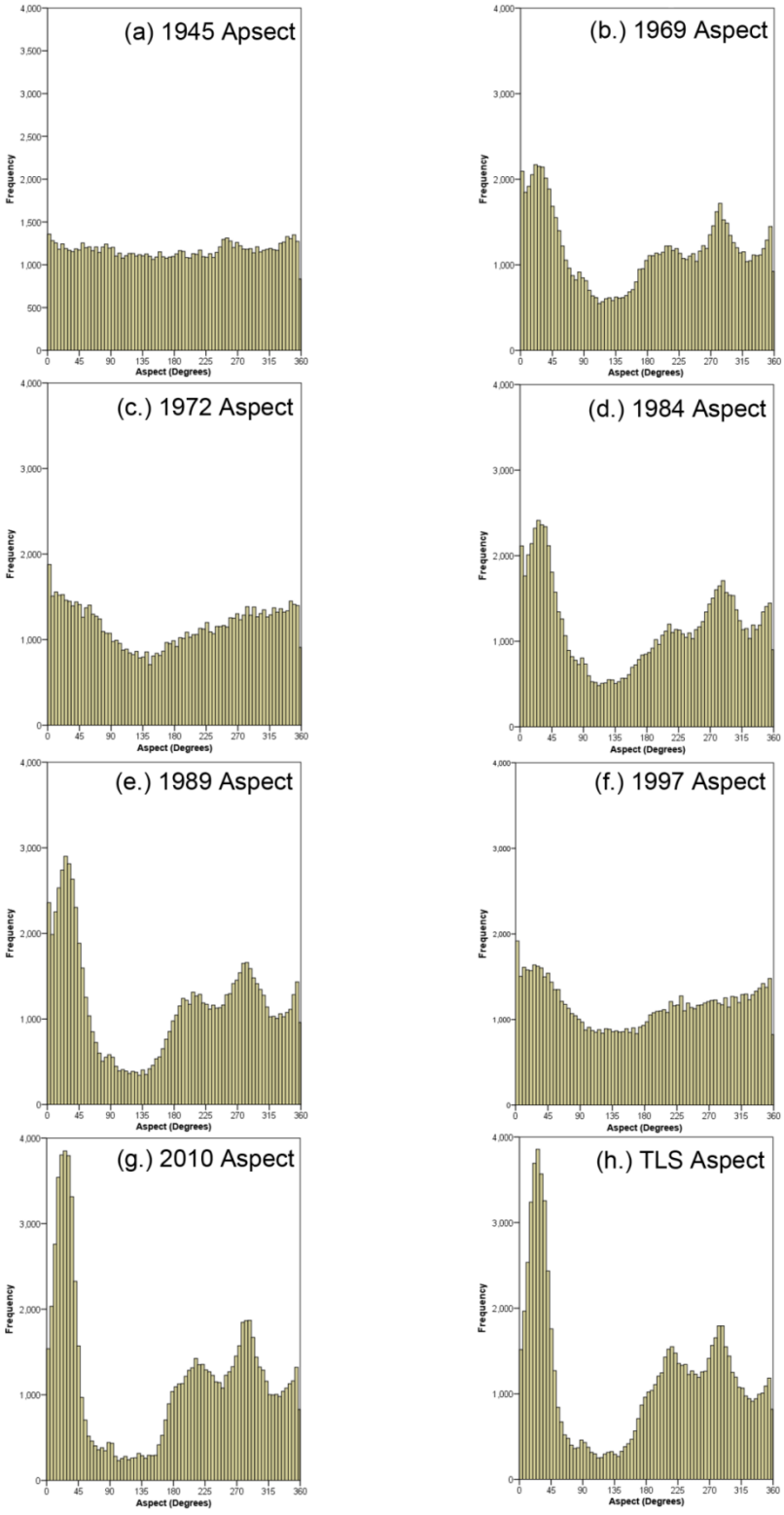

Figure 7.52: Histograms showing the aspect values contained within each of the SAP and TLS datasets.

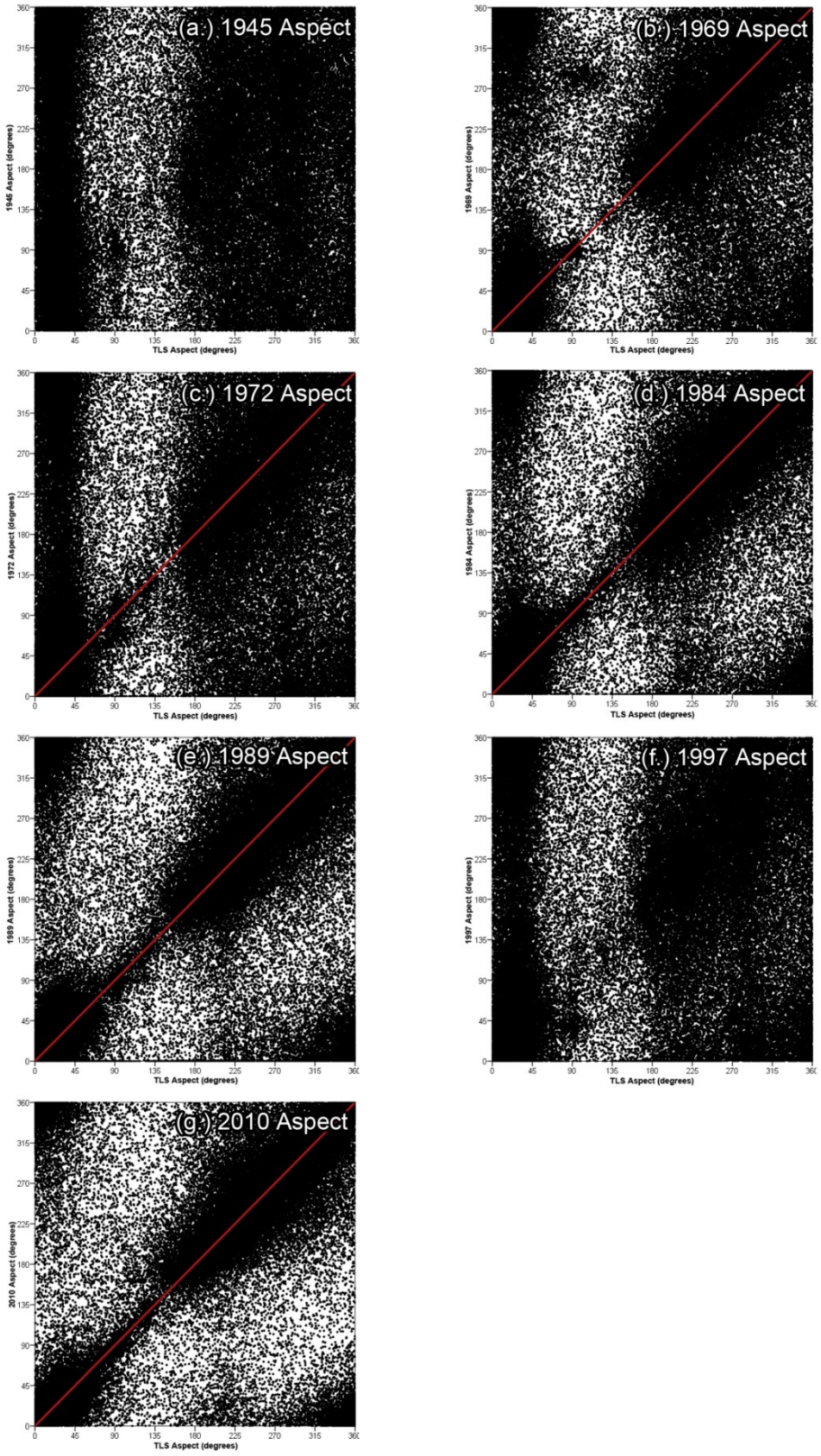

Figure 7.53: Scatterplots showing the linear correlation between the TLS and SAP aspect values.

7.6.1.1 Normalised Residuals

Table 7.12 contains summary statistics relating to the normalised residual values between the SAP aspect derivatives and the TLS aspect data. The ME for each of the datasets is at its highest for the 1948, 1972 and 1997 epochs, which is not unexpected, and at its lowest for the 1984, 1989 and 2010 datasets. As each of the residual histograms, as shown in Figure 7.54, broadly exhibit normal distributions, then the ME is a good indicator of central tendency in the data. As discussed in Section 3.4.2, the SD is a good measure of variation between datasets and it highlights that the 1948, 1972 and 1997 datasets deviate from the TLS aspect values to a far greater degree than the remaining SAP datasets: 68.852º, 61.173º and 62.097º respectively, in comparison with the 1969 SD of 52.521º and the lowest value of 39.191º for the 2010 dataset.

Kurtosis values are significantly lower for the 1948, 1972 and 1997 datasets, which is evidenced by the lack of a distinctive peak in their histograms (Figure 7.54 a, c and f), whilst the frequency values for the largest residual differences in each of these datasets remains high. The degree of noise within these three epochs is apparent in the linear scatter plots shown in Figure 7.55.

		TLS Minus 1948	TLS Minus 1969	TLS Minus 1972	TLS Minus 1984	TLS Minus 1989	TLS Minus 1997	TLS Minus 2010
N	Valid	89021	89021	89021	89021	89021	89021	89021
	Missing	0	0	0	0	0	0	0
Mean (degrees)		-13.663	-4.581	-7.232	-1.202	-0.681	-7.487	1.569
Std. Error of Mean (degrees)		0.231	0.176	0.205	0.163	0.148	0.208	0.131
Median (degrees)		-12.348	-2.821	-5.262	-1.135	-0.626	-5.628	0.753
Mode (degrees)		-41.221	-105.680	-53.727	-114.388	-41.129	-55.274	-22.010
Std. Deviation (degrees)		68.852	52.521	61.173	48.557	44.069	62.097	39.191
Variance		4740.644	2758.499	3742.163	2357.795	1942.088	3856.046	1535.967
Skewness		0.090	-0.008	0.028	0.092	0.115	0.058	0.156
Std. Error of Skewness		0.008	0.008	0.008	0.008	0.008	0.008	0.008
Kurtosis		-0.347	0.943	0.185	1.738	2.509	0.146	3.655
Std. Error of Kurtosis		0.016	0.016	0.016	0.016	0.016	0.016	0.016
Range (degrees)		357.778	359.145	358.881	358.801	356.641	359.072	357.475
Minimum (degrees)		-179.171	-179.425	-179.161	-178.815	-176.712	-179.087	-178.821
Maximum (degrees)		178.607	179.720	179.720	179.986	179.929	179.986	178.654
RMSE (degrees)		70.195	52.721	61.599	48.572	44.074	62.546	39.223

Table 7.12: Summary statistics showing the normalised aspect residuals for the hillfort region.

	Paired Samples Correlations		Paired Samples Test				
	Correlation	Sig.	95% Confidence Interval of the Difference		t	df	Sig. (2-tailed)
			Lower	Upper			
TLS Aspect vs 1948 Aspect	0.144	0.000	-14.115	-13.211	-59.207	89020	0.000
TLS Aspect vs 1969 Aspect	0.510	0.000	-4.926	-4.236	-26.024	89020	0.000
TLS Aspect vs 1972 Aspect	0.323	0.000	-7.634	-6.830	-35.272	89020	0.000
TLS Aspect vs 1984 Aspect	0.572	0.000	-1.521	-0.883	-7.387	89020	0.000
TLS Aspect vs 1989 Aspect	0.656	0.000	-0.970	-0.391	-4.610	89020	0.000
TLS Aspect vs 1997 Aspect	0.308	0.000	-7.895	-7.079	-35.975	89020	0.000
TLS Aspect vs 2010 Aspect	0.729	0.000	1.311	1.826	11.944	89020	0.000

Table 7.13: Paired t-test results comparing the normalised TLS and SAP aspect values for the hillfort region.

Although the majority of the SAP epochs appear noisy, a positive linear correlation can be identified in the 1984, 1989 and 2010 SAP epochs, but less so in the 1969 dataset. However, there is minimal evidence for a linear correlation in the 1948, 1972 and 1997 aspect values, which is supported by their correlation coefficient with the TLS data, as shown in Table 7.13. The 1948 dataset is the worst performing, with an 'r' value of 0.144, demonstrating poor correlation with the TLS dataset. Both the 1972 and 1997 epochs return 'r' values of 0.323 and 0.308 respectively, which is considered to be weak. The remaining SAP epochs all have 'r' values above 0.5, showing moderate correlation. The 2010 data displays the greatest correlation of the group, namely 0.729, which is considered to be strong.

Due the sample size of residuals being tested, namely the entire dataset or census, then the 'p' value or significance of the correlation coefficient is meaningless because there are a large number of values from which to calculate the correlation. This issue could be addressed by conducting a population analysis using the GNSS random points, as explained in Section 6.4. However, based upon the 95% confidence interval for each SAP epoch, as shown in Table 7.13, none of differences between the TLS and each SAP dataset are likely to be 0, as none of the intervals cross this threshold.

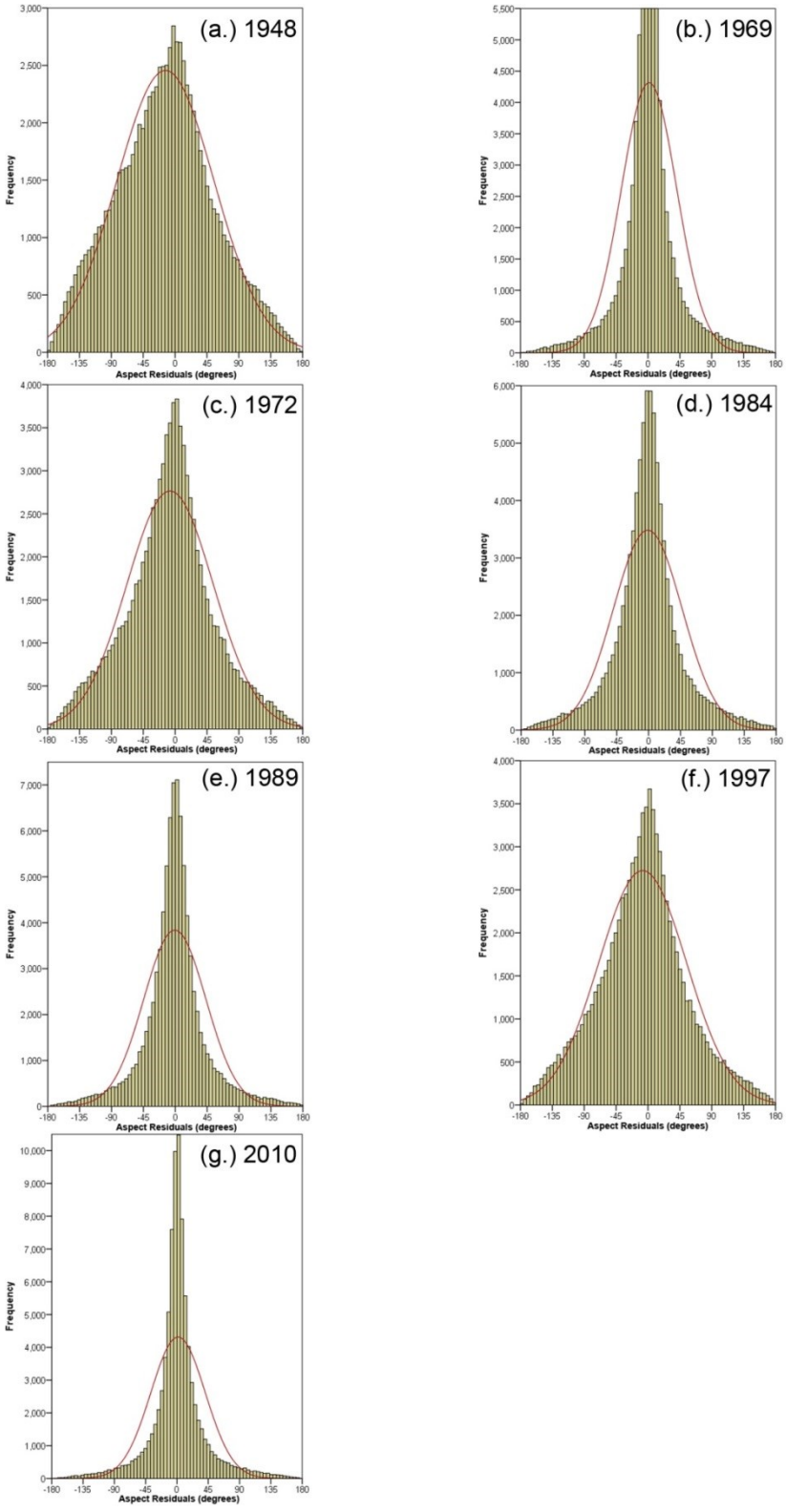

Figure 7.54: Frequency histogram showing normalised aspect residuals between the TLS and each SAP epoch for the hillfort region.

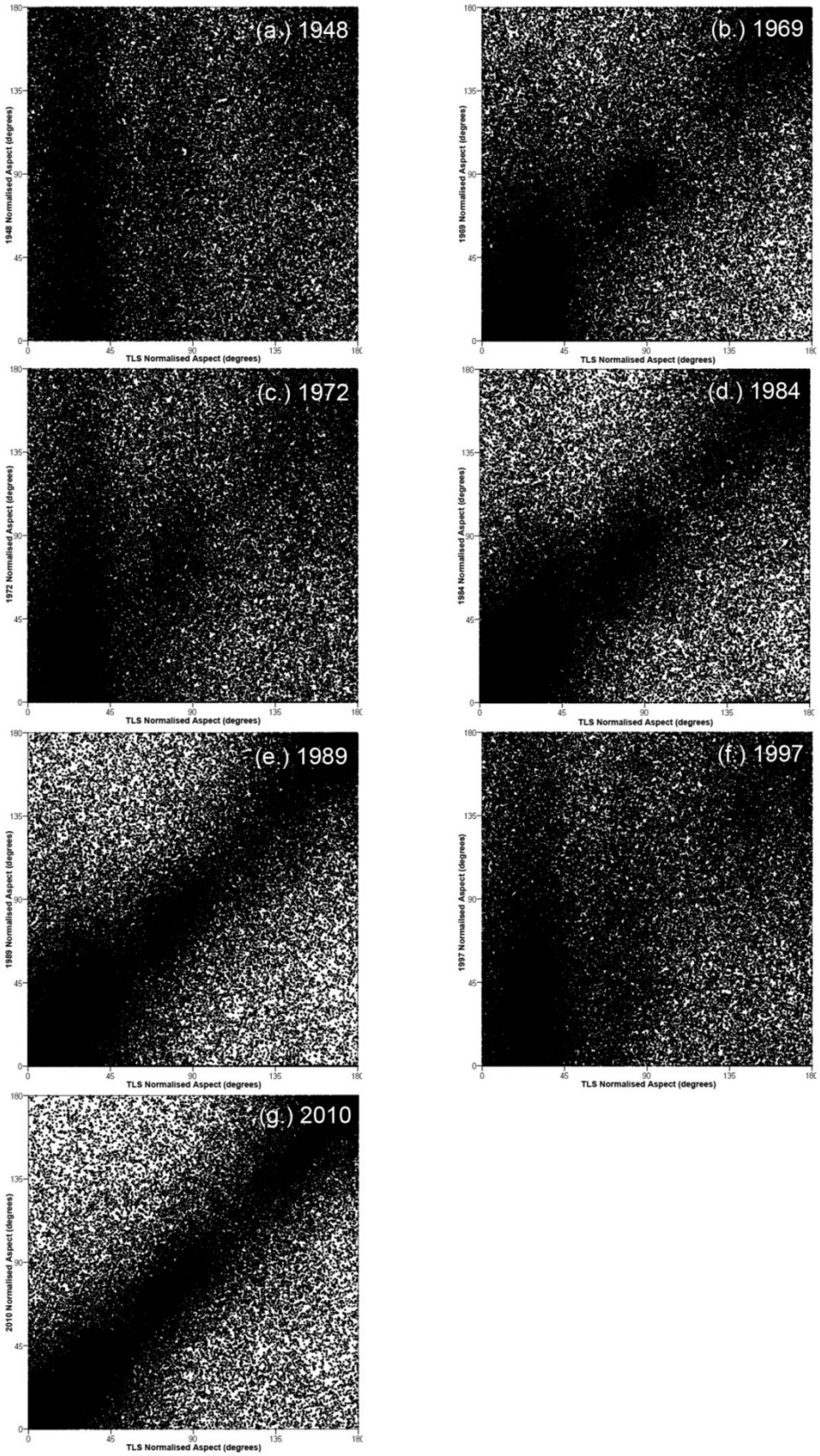

Figure 7.55: Scatterplot showing linear correlations between the TLS and SAP normalised aspect values for the hillfort region.

7.6.2 Eggardon Henge Monument

Histograms for the henge monument, as shown in Figure 7.56, also confirm that the 1948 SAP data is unrepresentative of the aspect values as captured by the TLS. The 1972 and 1997 SAP histograms (Figure 7.56c and f) display both of the peaks and the trough in the right location, as compared to the TLS aspect distribution (Figure 7.56h), although neither are as pronounced. The height of each peak is reduced, resulting in a shallower trough, which indicates that in the 1972 and 1997 SAP aspect datasets some of the north-facing slopes are represented as east, south or west facing slopes instead. These unrepresentative aspect values are exhibited in the aspect maps for both the 1972 and 1997 datasets, shown in Figure 7.51c and f, as noise. Whilst the 1969, 1984 and 1989 SAP aspect values are comparable to the TLS data, it is the 2010 dataset that is the most analogous. There are still minor differences between the two datasets, in particular the smaller number of values surrounding ~45º and the slightly larger number between 135º and 270º in the 2010 histogram (Figure 7.56g). As there is unlikely to have been significant change to the hillfort between the 2010 SAP capture and the 2013 TLS survey, the difference between these two datasets is more likely to be related to errors in the SAP DSM.

The correlation between the TLS and each of the SAP aspect values is shown in a series of scatterplots in Figure 7.57. As with the hillfort data, the 1948, 1972 and 1997 aspect values are unrepresentative of the TLS data, whilst a linear correlation can be identified in the 1969, 1984, 1989 and 2010 graphs. The trajectory of positive correlation is identified by the red line running diagonally across the scatterplots. However, the same situation exists here as with the hillfort scatterplots, namely that the aspect values are more straightforward to interpret once they have been normalised. The results of normalising the henge aspect datasets are discussed below.

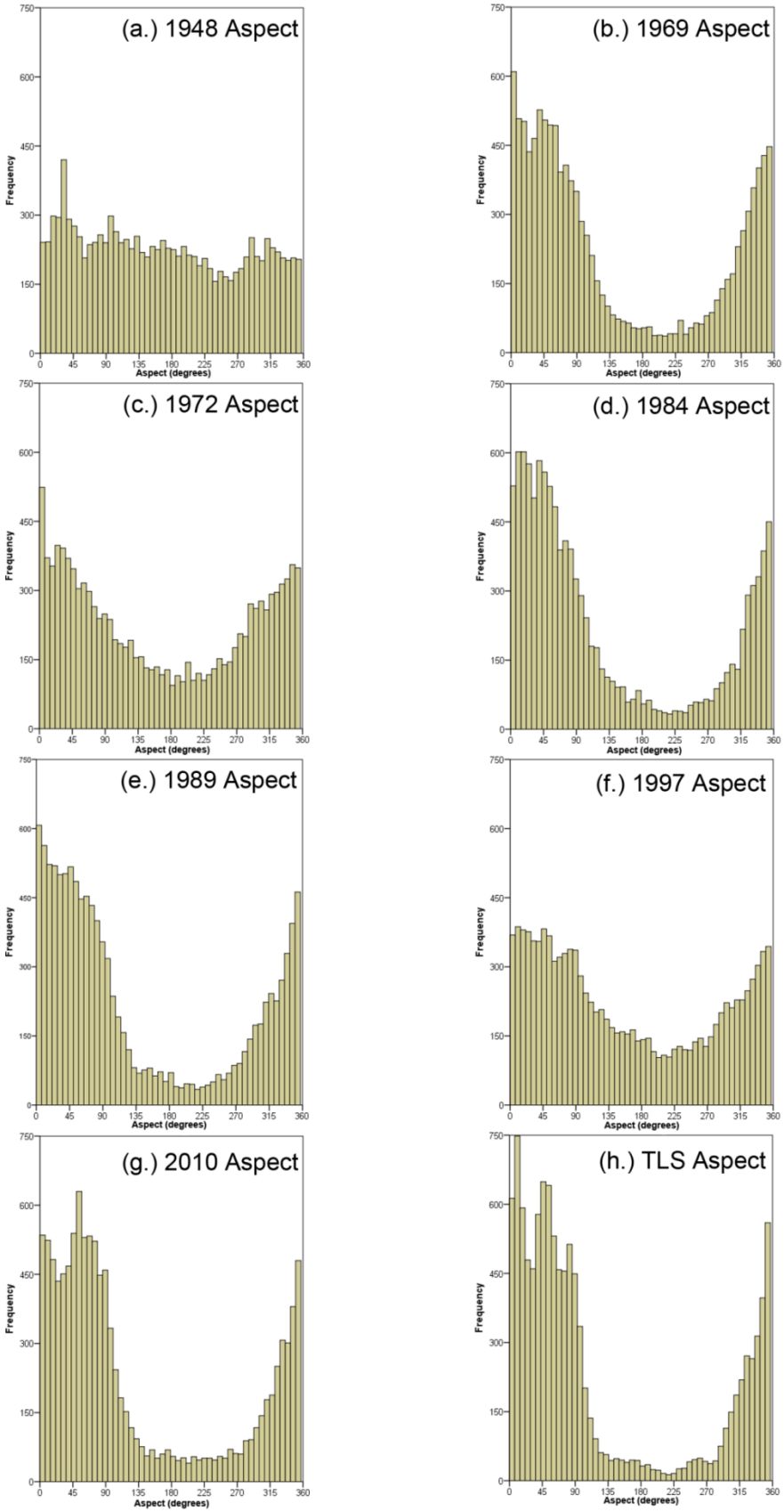

Figure 7.56: Histograms showing the frequency of aspect values across the henge region for the TLS and SAP datasets.

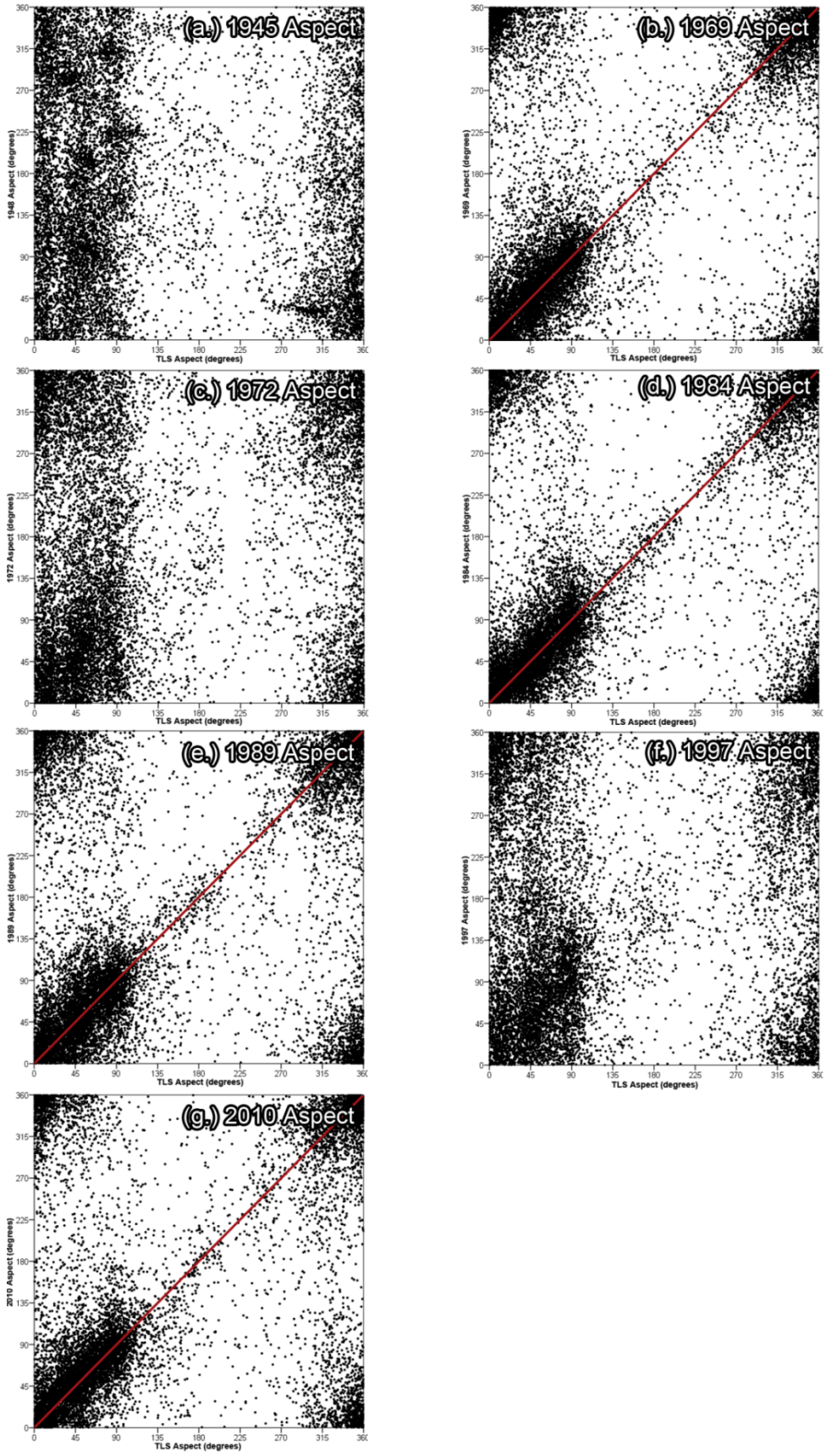

Figure 7.57: Scatterplots showing the linear correlations between the TLS and SAP aspect values in the henge region.

7.6.2.1 Normalised Residuals

As with the normalised aspect values that were analysed across the hillfort, there is little spatial structure to the 1948, 1972 and 1997 aspect datasets, as shown in Figure 7.51 a, c and f respectively. Within the remaining epochs, namely 1969, 1984. 1989, 2010 and the TLS (see Figure 7.51 b, d, e, g and h), the banks of the henge monument can be identified, although the barrow to the north of this earthwork can only be visually detected in the 1969 aspect map. The residual distribution in the aspect histograms for the henge region, as shown in Figure 7.58, is similar to those of the hillfort aspect histograms. Kurtosis values are at their lowest for the 1948, 1972 and 1997 datasets, whilst the SD values are at their highest: 61.618º, 54.873º and 54.619º respectively. Table 7.14 shows the 1984 SAP aspect dataset as having the lowest SD of 35.392º, which is in contrast to the hillfort dataset whereby the 2010 data had the lowest SD value.

The linear scatterplots, shown in Figure 7.59, yet again illustrate the lack of correlation between the TLS and the 1948, 1972 and 1997 SAPs, especially in the case of the 1948 data. Table 7.15 lists the correlation coefficients between each of the SAP epochs and the TLS, which identifies the 1984 aspect data as the most comparable to the TLS with an 'r' value of 0.629.

		TLS Minus 1948	TLS Minus 1969	TLS Minus 1972	TLS Minus 1984	TLS Minus 1989	TLS Minus 1997	TLS Minus 2010
N	Valid	11544	11544	11544	11544	11544	11544	11544
	Missing	0	0	0	0	0	0	0
Mean (degrees)		-37.243	-5.376	-18.587	-5.565	-5.672	-22.623	-6.919
Std. Error of Mean (degrees)		0.573	0.355	0.511	0.329	0.367	0.508	0.357
Median		-36.166	-3.446	-14.264	-2.197	-2.530	-17.477	-3.090
Mode (degrees)		-177.305	-177.293	-178.785	-172.175	-172.481	-178.385	-179.154
Std. Deviation (degrees)		61.618	38.114	54.873	35.392	39.446	54.619	38.353
Variance		3796.816	1452.697	3011.046	1252.565	1555.979	2983.240	1470.924
Skewness		0.125	-0.229	-0.096	-0.515	-0.412	-0.153	-0.517
Std. Error of Skewness		0.023	0.023	0.023	0.023	0.023	0.023	0.023
Kurtosis		-0.300	2.568	0.220	2.587	2.230	0.147	2.614
Std. Error of Kurtosis		0.046	0.046	0.046	0.046	0.046	0.046	0.046
Range (degrees)		346.275	355.812	352.438	328.090	332.469	353.380	355.353
Minimum (degrees)		-177.305	-177.293	-178.785	-172.175	-172.481	-178.385	-179.154
Maximum (degrees)		168.969	178.519	173.653	155.915	159.988	174.994	176.199
RMSE (degrees)		71.997	38.490	57.933	35.825	39.850	59.117	38.970

Table 7.14: Summary statistics for the normalised aspect values in the henge region.

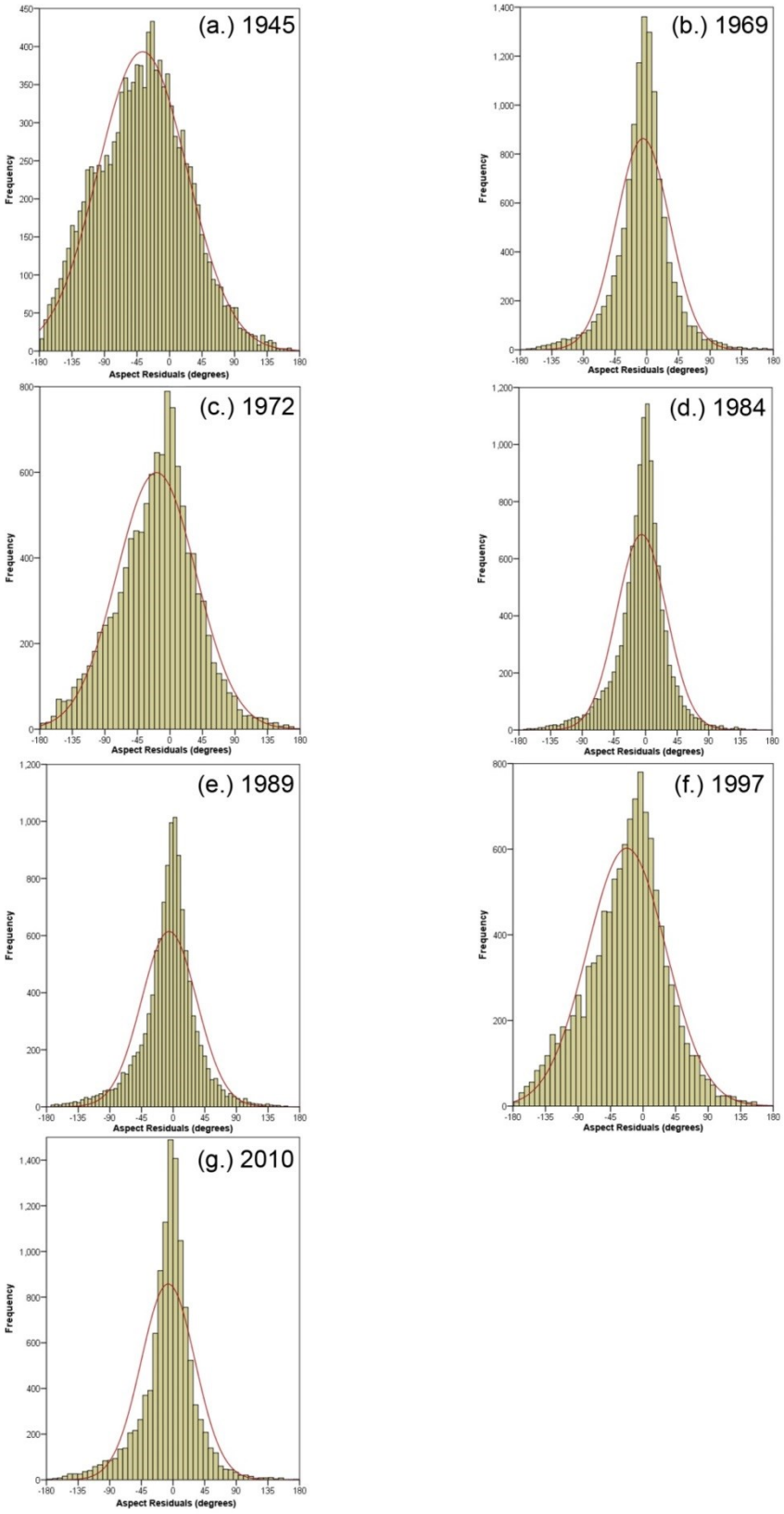

Figure 7.58: Frequency histograms showing the residual distribution of normalised aspect values across the henge region.

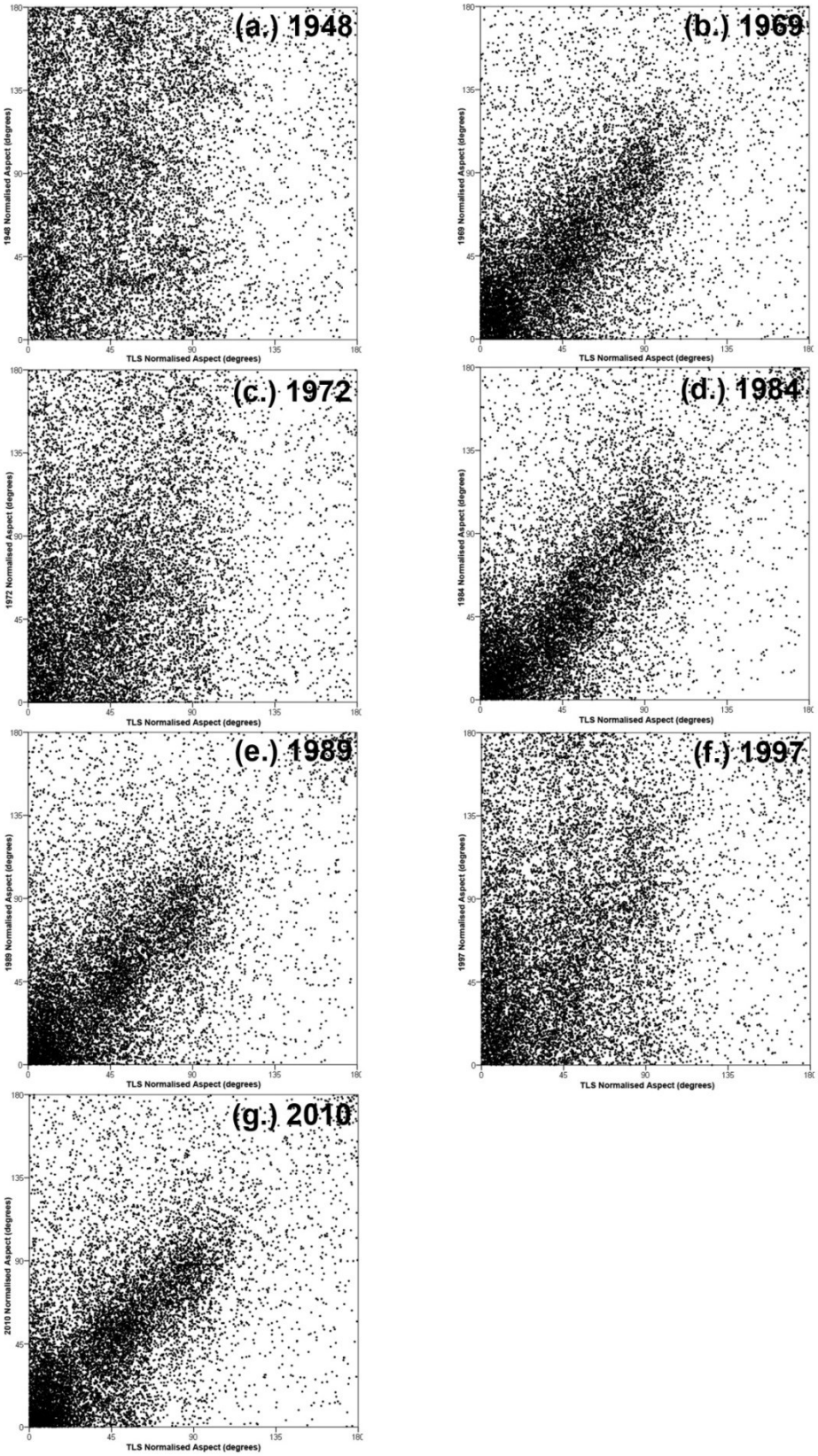

Figure 7.59: Scatterplots showing the linear correlation between the normalised TLS and SAP aspect values across the henge region.

	Paired Samples Correlations		Paired Samples Test				
	Correlation	Sig.	95% Confidence Interval of the Difference		t	df	Sig. (2-tailed)
			Lower	Upper			
TLS Aspect vs 1948 Aspect	0.102	0.000	-38.367	-36.118	-64.939	11543	0.000
TLS Aspect vs 1969 Aspect	0.554	0.000	-6.072	-4.681	-15.156	11543	0.000
TLS Aspect vs 1972 Aspect	0.231	0.000	-19.589	-17.586	-36.395	11543	0.000
TLS Aspect vs 1984 Aspect	0.629	0.000	-6.210	-4.919	-16.894	11543	0.000
TLS Aspect vs 1989 Aspect	0.525	0.000	-6.391	-4.952	-15.449	11543	0.000
TLS Aspect vs 1997 Aspect	0.256	0.000	-23.619	-21.626	-44.502	11543	0.000
TLS Aspect vs 2010 Aspect	0.547	0.000	-7.619	-6.219	-19.383	11543	0.000

Table 7.15: Paired t-test results for the TLS and SAP normalised aspect values across the henge region.

The 'r' value for the 2010 aspect data is 0.547, which is not as high as it was across the hillfort. Whilst each of the linear scatterplots exhibit a great deal of noise, the 1989 and 2010 plots, shown in Figure 7.59e and g, have a weaker linear appearance than the 1984 and 1969 datasets, which is unexpected as the general pattern thus far has suggested that it is the older SAPs and those scanned on a desktop printer from prints are the most likely to display poor correlation. However, the 2010 data has, in this example, a lower correlation with the TLS than the 1969 and 1984 datasets.

As with the hillfort aspect results, none of the SAP aspect residuals within the henge region have a 95% confidence interval of difference that crosses the 0 boundary, as shown in Table 7.15. Therefore there is a difference between the TLS and all of the SAP datasets. Each of the confidence intervals are also negative, which is expected as the ME for each of the datasets is a negative value (see Table 7.15).

7.6.3 Local Moran's I Analysis

The similarities between the TLS aspect values and those of the SAPs have been discussed, based upon the appearance of their histograms, the scatterplot correlations and their statistical differences. However, the spatial distribution of the differences between the TLS and each SAP epoch has not been identified using these techniques. Subsequently, Moran's I analysis and the patterns shown in DoDs will further identify where the largest differences lie and whether these are the result of noise in the data or actual changes to the material across the hillfort and henge

monument. As the Moran's I and DoDs are based upon the residual differences between the TLS and SAP datasets, this analysis has been performed on the normalised data.

7.6.3.1 Eggardon Hillfort

The Moran's I diagram for the 1948 aspect data across the hillfort, as shown in Figure 7.60a, exhibits a distinct separation between the southern and northern half of the hillfort interior. The majority of statistically significant high values are found to the south of the fence line, whilst the majority of statistically significant low values are found to the north of this boundary. Had this result been returned by the elevation dataset, this would have been a clear indication that significant change had occurred between 1948 and 2013, as the residuals on the northern side of the hillfort indicate that the TLS values here are lower than those of the 1948 SAPs. This is the expected result as the northern half has been degraded due to ploughing. However, in this instance, the difference between the TLS and 1948 aspect values indicate the areas whereby there is a difference in slope direction between the two datasets.

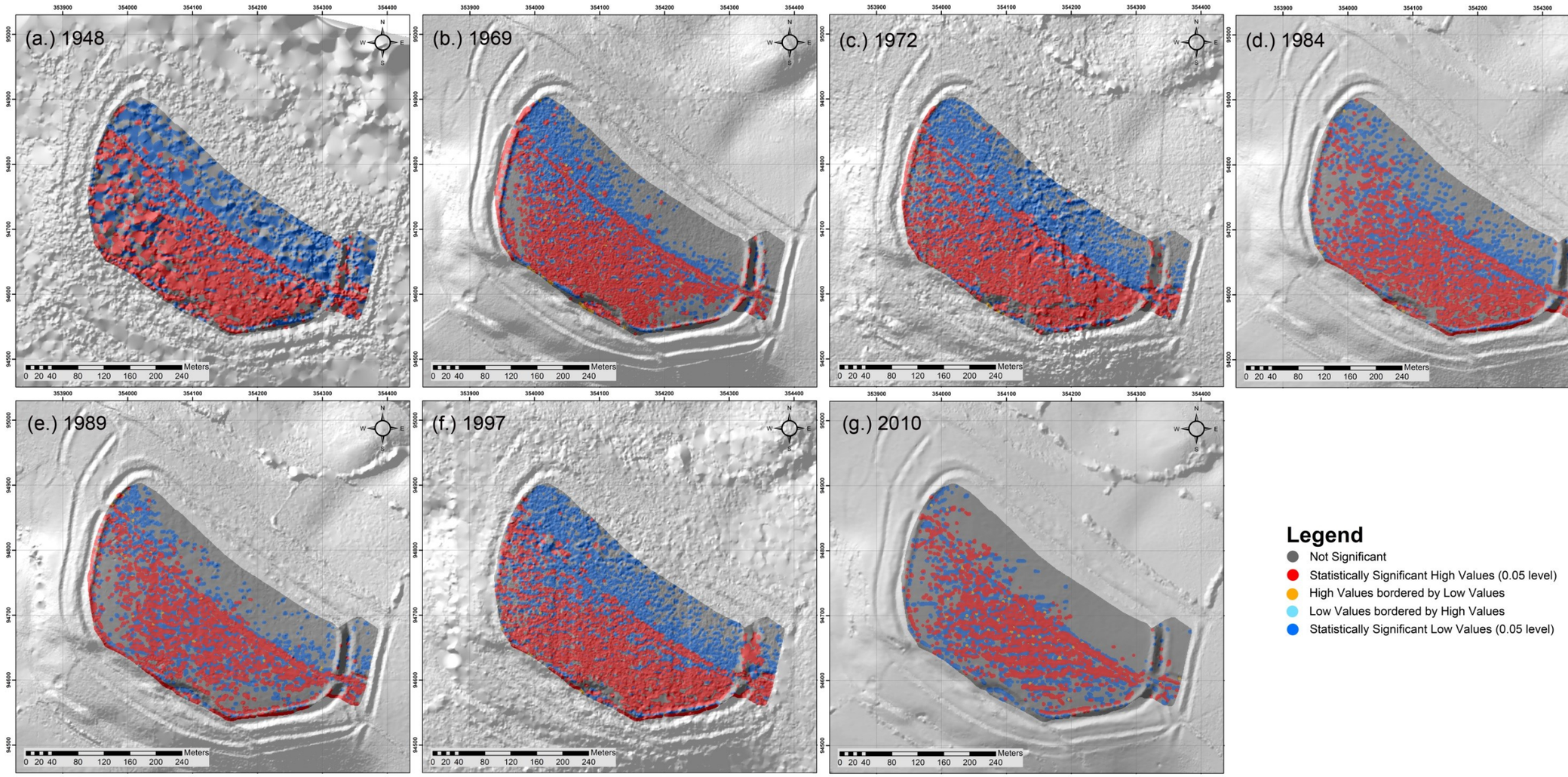

Figure 7.60: Moran's I diagrams of Eggardon Hillfort showing the distribution of residual values of difference between the TLS slope and SAP aspect derivative values.

In comparison with the TLS aspect map, shown in Figure 7.50h, the majority of the northern half of the hillfort contains north-facing slopes, whilst the southern half of the hillfort is characterised by east, south and west-facing slopes. The appearance of the 1948 aspect map (Figure 7.50a) bears no resemblance to this distribution. By utilising the 'identify' tool in ArcMap, the difference in values between the normalised TLS and 1948 aspect values can be deduced. Within the Moran's I map of Figure 7.60a the large blue patches in the northern half of the hillfort represent areas whereby the TLS has a smaller angle than the 1948 SAP data i.e. 19.704º versus 158.014º, or 27.681º versus 174.130º for example. The large red patches in the southern hillfort represent areas whereby the TLS has a larger angle than the 1948 SAP data i.e. 152.094º versus 12.098º, or 73.343º versus 6.442º for example. Whilst these differences do not suggest that many of the 1948 slopes face in the opposite direction to those recorded by the TLS, it does identify the areas by which there is a significant change in aspect of slope. The majority of the 1948 SAP aspect data is characterised by significant differences between it and the baseline dataset (the TLS), suggesting that the 1948 DSM contains myriad errors and is unlikely to facilitate subsequent analysis of the hillfort terrain. The DoD shown in Figure 7.61a exhibits the noisy appearance between the normalised 1948 and TLS data, so called because there appears to be no spatial pattern to the residual distribution other than a north-south divide between the significant high and low values.

The distribution of residuals across the 1969 Moran's I map, shown in Figure 7.60b, does not display such large clusters of significantly difference aspect values. However, it still exhibits a north-south divide between the statistically significant high and low values, with the former predominantly found in the southern half of the hillfort. The low values are distributed along the fence line, within the north-west corner of the northern half of the hillfort, and across the majority of the southern half, with fewer values located to the extreme east and west of this area. The south west, south east and north east sectors of the hillfort are characterised by non-significant residual values and in the DoD (see Figure 7.61b) these area appear to contain very little noise, as illustrated by the more subtle green and yellow bands.

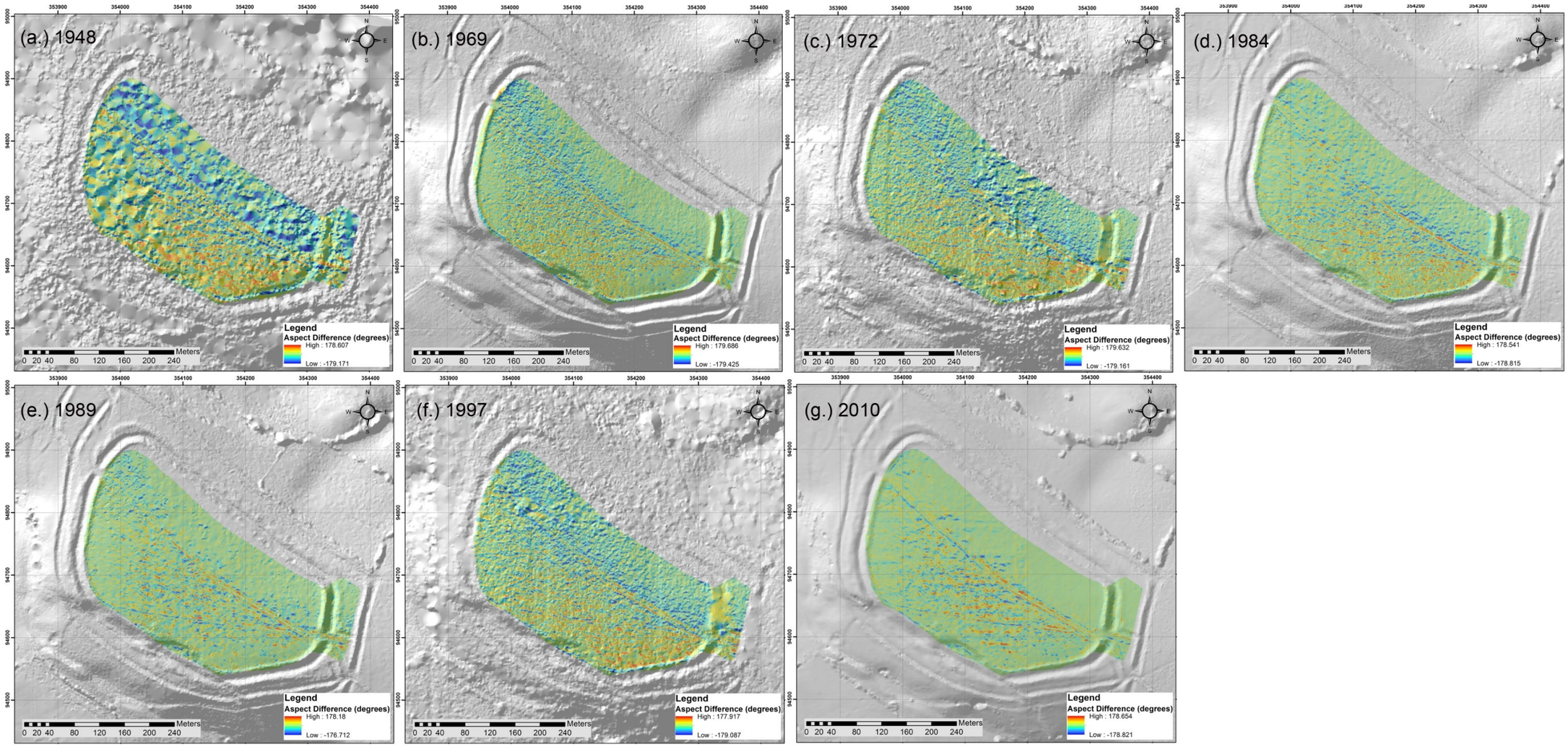

Figure 7.61: DSMs of Difference between the Eggardon hillfort TLS and the SAP aspect derivatives.

The large high and low residual differences, as characterised by the red and blue patches across the 1969 DoD (Figure 7.61b), indicate that there is an aspect difference greater than 100º between the TLS and the 1969 DSM in these areas. In some instances, such as the fence line and the two linear features present within the southern half, there appears to be structure to the residuals. All of these features are visible in the 1969 aspect map (see Figure 7.50b), albeit their expression is subtle, whilst they are clearly identified in the TLS aspect map (see Figure 7.50h). Thus the 1969 SAPs have had some success in detecting some of the subtle interior earthworks within the hillfort, although their aspect values are significantly different to the TLS. Generally, this difference is at least ±90º, and in many cases more so. However, by examining the 1969 and TLS aspect maps (Figure 7.50b and h respectively), the linear features all display the same aspect values i.e. the fence line and the north-west linear feature exhibit aspect values between 150º to 210º.

Some of the larger pits within the south-east of the hillfort have also been detected in the 1969 aspect map. This is one of the areas that is not afflicted with noise, which is represented in the DoD as a rippled pattern of red and blue values across the majority of the southern hillfort interior. This pattern, which is also visible in the DoD (Figure 7.61b), enhances the stippled effect that is identifiable in the 1969 elevation data. It is uncertain as to why SocetGXP has calculated elevation values within this region that have given rise to this rippled effect. By examining the 1969 imagery, it can be seen that this area of the hillfort is well covered by the lower strip of images. However, the noise occurs where the edge of the photograph to the far right of this strip overlaps with the other two photographs. As SocetGXP was set to utilise up to two image pairs to create elevation values, it may well be that the result ATE has calculated using both the first and second, and second and third images to generate an elevation has subsequently produced an unrepresentative average value of the two results. The calculation may also be compromised by the lack of camera calibration data and the position of the hillfort at the extreme edge of the third image, which is where the largest lens distortions will reside.

There are very few non-significant values displayed upon the Moran's I map for the 1972 aspect residuals (see Figure 7.60c). The pattern of significant high and low values is similar to the other SAP aspect Moran's I maps (see Figure 7.60), with the northern half of the hillfort containing statistically significant low values and the southern half containing a large number of statistically significant high and low values. There is little spatial structure to their distribution, although a line of high residual values runs along the fence line. Within the DoD, as shown in Figure 7.61c, there are also large differences that occur along the paths of the linear features in the southern half of the hillfort, and along the ramparts to the south-east. Whilst there may be some similarity between the 1972 and TLS aspect values along these southern ramparts, as shown by their respective aspect maps in Figure 7.50c and h, the two linear features in the south section cannot be determined in the 1972 aspect map. This highlights the disparity between the detail in the TLS and the lack of it as extracted from the 1972 SAP dataset.

What is evident by examining the DoD map for the 1972 aspect residuals is the ripple effect that appears across the entire hillfort, as seen in the 1969 data. This is enhanced in the northern section of the hillfort where there has been a failure in the ATE process to match the images pairs, thus producing a stripe effect in the 1972 DSM. The error in the elevation values here has caused ArcMap to calculate an aspect value that is unrepresentative of the north-facing ground here. Instead, there are areas of aspect in the 1972 data that face south. One area that does not exhibit this effect is the eastern ramparts, which contain very few significant residual differences between the TLS and 1972 data. By examining the underlying hillshaded DSM of the 1972 dataset, which is visible in the DoD (Figure 7.61c), it appears that the rampart slopes have not been properly reconstructed here and have taken on a flat, featureless appearance. Whilst the slope aspect in the 1972 data may be representative in this area, the difference in slope that was identified in Section 7.5.3.1 and Figure 7.45c, is not, which illustrates why analysis should not be undertaken on only one terrain derivative.

Although aspect errors in the 1972 DSM are explainable where triangulation is poor or the image matching process has failed, there are no obvious features in the 1972 orthophotograph, shown in Figure 7.62, that may otherwise cause an error in aspect values between the 1972 data and the TLS. There are a larger number of gorse bushes situated along the fence line to the east, some of which still exist today. However, these do not explain the aspect errors across the rest of the hillfort. Therefore it must be concluded that these errors are caused of a number of reasons. Firstly, the lack of camera calibration data, in the form of lens distortion values and, secondly, the digitisation of prints rather than the original negatives. The use of an uncharacterised DTS to digitise the print will have introduced a second source of lens distortion to the data. Thus there are a number of systematic errors that have been introduced into the DSM from a number of sources that will have propagated through to each of the terrain derivatives, and these will have influenced the results obtained here.

The statistically significant values shown in the 1984 Moran's I aspect map of the hillfort (see Figure 7.60d) do not appear to be as densely clustered as those in the 1969 dataset. Whilst there are a slightly higher number of statistically significant low values within the northern half of the hillfort, those within the north-west of this region have a scattered appearance. This is also true of the statistically significant high values in the southern section of the hillfort, which appear to be less clustered, although they are spread across the entire region and interspersed with some statistically significant low residuals. There is spatial structure to the fence line, the linear earthworks in the southern hillfort, the ridge of the southern ramparts and the base of these same slopes. The fence line and the short linear feature to the north-west appear in the 1984 aspect map, shown in Figure 7.50d, although they are not very pronounced, whilst the longer linear earthwork that runs from the south-west to the east of the hillfort cannot be discerned at all.

There are a large number of non-significant residuals within the 1984 aspect Moran's I map, and most notably on the rampart and landslip slopes. The DoD between the TLS and 1984 aspect values, shown in Figure 7.61d, more clearly identifies the regions of minimal difference,

Figure 7.62: 1972 orthophotograph of Eggardon Hillfort.

particularly in the southern half of the hillfort which also exhibits a rippled pattern of noise. However, it is worthy of note that the aspect values in the TLS aspect map (see Figure 7.50h) have a rippled effect throughout this area, as do the aspect values in the 1984 aspect map (Figure 7.50d). Thus it may only take a very subtle change in the elevation data in this region of the hillfort to produce differing results across a number of terrain models. This is particularly so as the TLS will be capable of detecting more subtle variations in the vegetation present across the hillfort which will still be present in the TLS dataset despite creating a DSM that has attempted to remove the influence of vegetation. This was achieved by specifying that the minimum elevation value should be allocated to each square metre during the rasterisation process. Therefore the rippling effect in the DoD and aspect maps may not only represent errors in the elevation data caused by systematic errors, but by the increased detail within the TLS data.

The Moran's I map of the 1989 aspect values, shown in Figure 7.60e, contains slightly fewer statistically significant residual values than in the 1984 dataset. There is still a north-south divide between the significant high and low values, with the former predominantly limited to the

southern half of the hillfort, whilst the northern half contains mostly statistically significant low values. The majority of residual values are non-significant, as indicated by the grey coverage across the Moran's I map, whilst the usual earthwork features have produced spatially distinct patterns, namely the fence line and two linear features within the southern section of the hillfort. Although partial segments of the fence line can be determined in the 1989 Aspect Map, as shown in Figure 7.50e, there are very few indicators that the subtle linear features have been detected, as their signature in the aspect values is barely visible. Despite the lack of distinctive aspect values for the smaller features, the 1989 aspect map is similar in its appearance to that of the TLS (see Figure 7.50h), with the south-east of the hillfort characterised by red hues, the west by green colours and the north predominantly in blue.

The rippled effect that has been present in the central south of the hillfort within the other SAP datasets can also be seen in the 1989 data. As has previously been discussed, this is the result of a similar pattern appearing in the TLS aspect data as well as in the SAP aspect datasets, which have contributed to the rippled appearance in the Moran's I datasets (see Figure 7.60) and the DoD maps (see Figure 7.61). Therefore these ripples are not necessarily noise artifacts, but a complicated interaction between the subtle aspect values produced by the TLS survey and those generated from the SAP DSMs. As the southern half of the hillfort is characterised by dense patches of grass, whilst in the northern half they are more sparsely distributed, as demonstrated in Figure 7.27, this further explains why there is a much greater variation in aspect values within the southern half of the hillfort in each of the SAP datasets.

Yet again there are slight but noticeable artefacts that run vertically through the 1989 aspect values of the hillfort, which are situated just to the east and west of the landslide. These are characterised by a strip of green values that run through the red and blue clusters in the DoD (see Figure 7.61e). They are not well defined in the Moran's I map, however (Figure 7.60e). In the underlying hillshaded DSM, which is visible in the elevation dataset shown in Figure 7.9, these stripes are also extremely subtle, but they have evidently been detected by the aspect algorithm. Based upon the overlap between the 1989 SAPs, as illustrated in Figure 7.29, these artifacts could be due to a poor triangulation result or an error caused by image matching between the two image pairs that are formed by the first and second photographs, and the second and third frames. There are no other defects visible in the imagery to suggest that the error could be due to image imperfections. However, as the western half of the hillfort is situated close to the edge of the frame in the first photograph, the lens distortion here may also influence the production of erroneous elevation values in this region.

The same distribution pattern of high and low statistically significant residuals is visible in the 1997 Moran's I map, as shown in Figure 7.60f, whereby the northern half of the hillfort is characterised by low significant values, whilst the southern half contains both. However, there are fewer non-significant values within this dataset than there are in some of the previous examples. Whilst it is still the 1948 aspect data that is the worst performing set of SAPs, the 1997 data is akin to the 1972 results, which were found to exhibit poor correlation with the TLS dataset.

The appearance of the 1997 hillshaded DSM that lies beneath the 1997 Moran's I map (see Figure 7.60f) indicates why the 1997 aspect values contain a large number of significant residual differences between the TLS and 1997 SAPs. The terrain has a rough appearance, unlike that of the 1969, 1984 and 1989 DSMs. Flat, triangular patches occur along the eastern ramparts and in the surrounding fields, which suggests that the interpolation algorithm has had to cover large gaps between elevation posts, as shown in Figure 7.26f. As with previous datasets, there are stripes running vertically through the DSM, although they do not appear to have produced a significant difference to the aspect values. Within both the Moran's I map (Figure 7.60f) and the DoD (Figure 7.61f), there is no indication of these features.

One region of the 1997 aspect data that differs from the similar results produced by the 1972 SAP dataset is the large number of statistically significant high values that cover a large proportion of the east ramparts. Within this region there is a ~60º to ~90º difference between the TLS and the 1997 aspect values, which occur over one of the flat, triangular patches whereby triangulation was sub-optimal or the image matching process has failed to produce suitable elevation data from the 1997 SAPs.

Whilst the fence line and both of the linear features appear in the DoD (Figure 7.61f), only the fence line is visible in the Moran's I map (Figure 7.60f). The fence line is observable in the 1997 aspect map, as shown in f, but neither of the linear features in the southern half of the hillfort can be identified. Therefore the expression of each of these earthworks in the DoD and Moran's I map is due to their presence in the TLS data and the large difference in aspect values between it and the 1997 SAP data. However, the entirety of the 1997 aspect map (Figure 7.50f) exhibits a noisy appearance, and not just in the region whereby all of the SAP datasets have displayed this ripple effect, although the north-east of the hillfort does not contain many extreme residual values. As there is minimal spatial structure observable in the DOD, and even less in the Moran's I map, then it can be concluded that the 1997 SAP aspect data does not convey any useful information about the archaeological earthworks here.

The 2010 Moran's I result, as shown in Figure 7.60g, is the most visually impressive, with the largest number of non-significant residual values and a highly structured appearance to the statistically significant high and low residuals. This data also differs from the previous SAP Moran's I results as there is no north-south divide between the residuals. There is also a clearly identifiable spatial structure to the 2010 Moran's I data, which clearly shows the fence line and the two linear features in the southern section of the hillfort. Along the base of the southern ramparts inner bank there is a line of significant high values and at the base of the landslip there is a collection of significant low values. As none of these significant distances are comprised of a thick band of residual values, this difference is caused by the much tighter definition of feature edges in the TLS aspect data (see Figure 7.50h) and the less well defined features in the 2010 (see Figure 7.50g). However, there is only a subtle hint of the two linear earthworks in the southern section in the 2010 aspect map (Figure 7.50g), neither of which are expressed as clearly as in the TLS data, which is not unexpected.

Whilst these results are meaningful in terms of the hillfort structure, there is also evidence of error in the 2010 DSM. To the west of the hillfort there are horizontal stripes of significant low values that cross the fence boundary from the southern to the northern half of the hillfort. These artifacts are more clearly seen in the DoD, shown in Figure 7.61g, as thick blue lines. These features have appeared in the 2010 elevation DoD, discussed in Section 7.4.1 and shown in Figure 7.9g, and they are just visible in the 2010 aspect map (see Figure 7.50g). Unlike the previous SAP datasets, these features cannot be attributed to the overlap between the 2010 photographs or to the hillfort's position towards the edges of each image strip. None of the frame edges run through the hillfort itself, and the 2010 SAPs were provided with camera calibration data to enable the removal of the already minimal distortion present in the imagery. The cause of this particular striping effect is therefore unknown.

Across the remainder of the hillfort, the aspect values in the 2010 aspect map (see Figure 7.50g) are broadly representative of those in the TLS aspect map (see Figure 7.50h). It is evident that the hillfort sits atop the ridge, known as Eggardon Hill, in the landscape as the north-eastern half faces northwards, whilst the southern half faces south and west. These aspect values follow the contours of the ridge and explain why this hillfort has been referred to as a ridge fort (Harding 2012). Unlike the random appearance of aspect values in the middle of the hillfort within the TLS dataset, the ripples across this same region of the hillfort in the 2010 data look more structured and are forming horizontal stripes, as discussed above. Subsequently there is some unaddressed issue in the 2010 data that is causing this pattern and that is obscuring the expression of any of the more subtle features here. However, the fact that the northern half of the hillfort in both the TLS and 2010 aspect data is similar suggests that very little change has taken place here over the 3 year period in between these surveys, thus confirming that ploughing has been halted here. This also indicates that the effect of using this land for pasture is not inflicting extensive damage.

7.6.3.2 Eggardon Henge Monument

Based upon the appearance of the 1948 aspect map of the henge monument (see Figure 7.51a), the Moran's I map, shown in Figure 7.63a, contains a surprising number of non-significant differences. These residuals tend to occur in the flat regions of the 1948 DSM, which can be seen in the hillshaded layer underlying the Moran's I and 1948 aspect maps. These are regions whereby no elevation data has been created in SocetGXP and the natural neighbour interpolator has had to fill these holes. Subsequently, in the regions where SocetGXP has returned elevation values, these have created a noisy appearance across both the henge and barrow monument that have, in turn, created unrepresentative aspect values. These are highlighted in the Moran's I map as statistically significant high values that predominantly occur across the slopes of the henge and barrow, and statistically significant low values that do not appear to have any spatial pattern to their distribution.

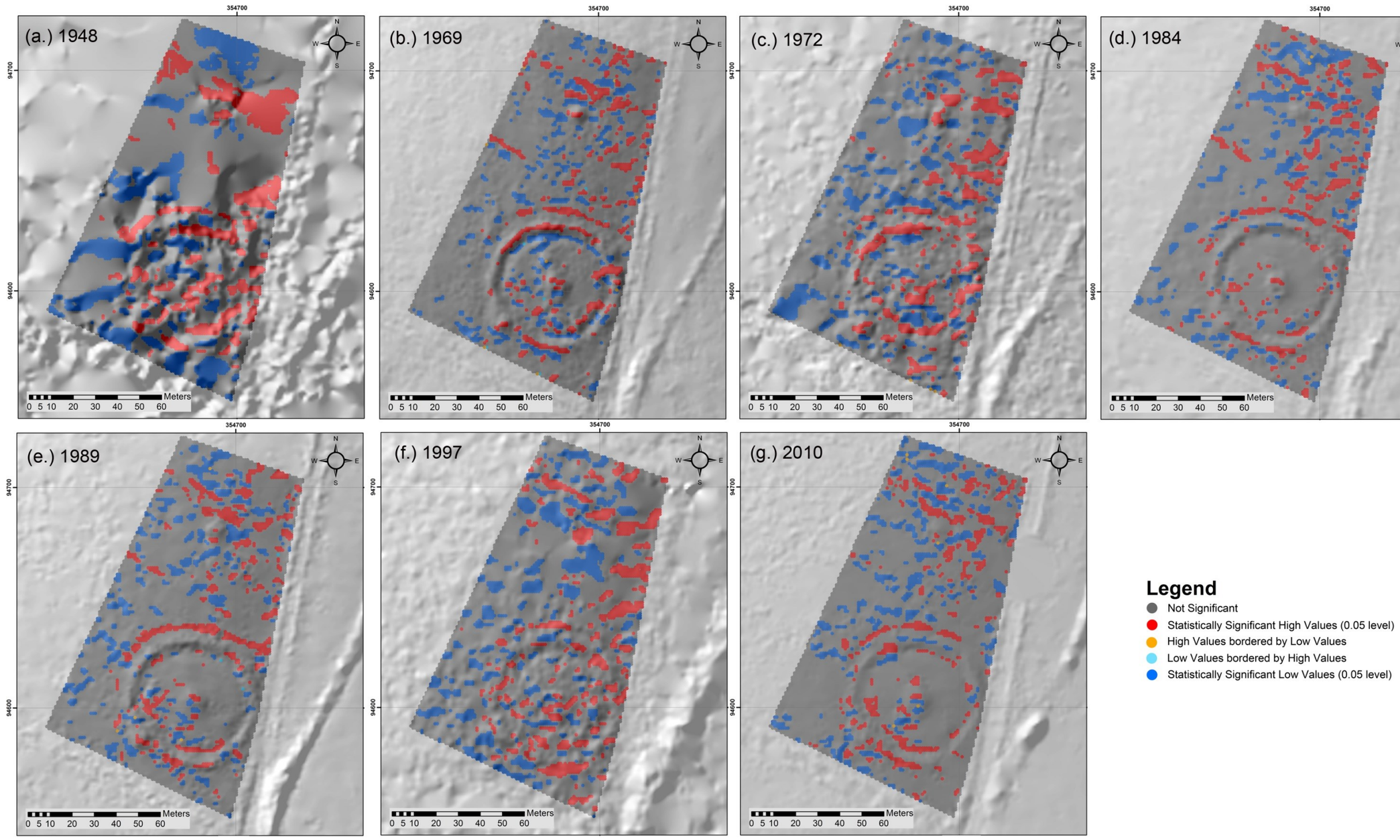

Figure 7.63: Moran's I diagrams of Eggardon henge monument showing the distribution of residual values of difference between the TLS slope and SAP aspect derivative values.

By examining the DoD between the normalised TLS and 1948 aspect values within the henge area, shown in Figure 7.64a, the northern-most slopes of the henge can just be identified, although they have a wavy appearance to them. Trying to delineate the shape of the henge features from this dataset would not produce an accurate record of this monument, and thus the 1948 SAPs have failed to provide any useful data for documenting archaeological earthworks.

The Moran's I result for the 1969 henge aspect map, as shown in Figure 7.63b, exhibits spatial structure of the residuals. The statistically significant high values are situated along the top of the henge bank, whilst the statistically significant low values are found along the bottom of the ditches. There is little significant difference to the barrow between the 1969 SAP aspect data and the 2013 TLS aspect dataset. There is a small patch of high values on the top of this feature that indicate a maximum difference of ~154º between the two datasets, which suggests that the slope direction has altered to face the opposite direction in the 44 years between surveys. This is also true of the maximum high and low values along the ridges and ditches of the henge banks. Whilst the residuals that exhibit spatial structure may indicate the occurrence of change, by examining the 1969 orthophotograph (see Figure 7.21) it is evident that the henge was, at this time, covered by gorse, which has since been cleared. This helps to explain why a difference between the 1969 and TLS datasets has been detected here. However, what it does not explain is the presence of other significantly high and low residuals within the flat regions surrounding the henge and barrow. The 1969 orthophotograph (see Figure 7.21) indicates that this area has seen vehicle movement across it, as evidenced by the subtle stripes that run in a north-south direction. As this area has been ploughed previously it is likely that this is the cause of the change in aspect values due to the loosening and turning of the soil here.

The 1972 Moran's I result for the henge monument, as shown in Figure 7.63c, displays spatial structure across the slopes of the henge banks and in the ditches in a similar pattern to the 1969 Moran's I map (Figure 7.63b), although this result is not as clear-cut. In the 1972 orthophotograph, shown in Figure 7.34, the henge is still covered in gorse, which has since been cleared. Therefore it is expected that a difference between the TLS and 1972 data would be identified here. The barrow also exhibits a large patch of statistically significant high values, although it is larger than that displayed in the 1969 aspect Moran's I (Figure 7.63b). The patches of statistically significant high and low values in this dataset that are scattered across the remainder of the area are also larger than in the 1969 dataset and do not exhibit any spatial structure. Although there are some similarities between the 1969 and 1972 aspect Moran's I and DoD maps, on closer inspection of the imagery from which they have been derived, the 1972 data is not as sharp and comprises a lower contrast ratio than the 1969 imagery. This will affect the image matching process from which the elevation data is created and subsequently the derivatives produced from it.

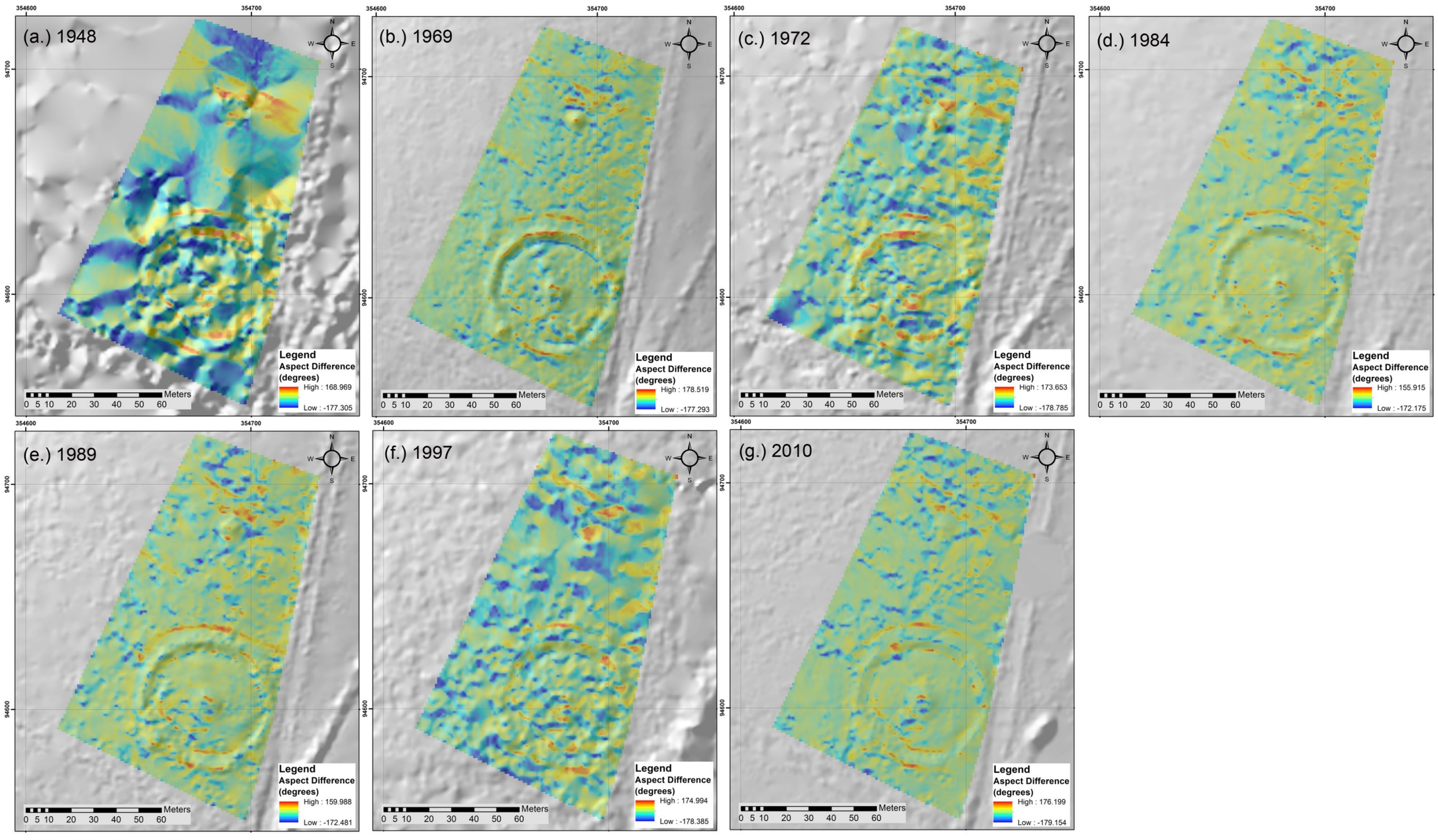

Figure 7.64: DSMs of Difference between the Eggardonhnge monument TLS and the SAP aspect derivatives.

Within the henge region of the 1984 SAP dataset, the Moran's I map of aspect residuals, as shown in Figure 7.63d, exhibits minimal spatial structure. There are a large number of non-significant values, which illustrates the high parity between the TLS and 1984 DSM data here. There is little difference in aspect values across the henge monument, unlike the results from previous SAP aspect datasets. By examining the 1984 orthophotograph of the henge monument the density of gorse bushes has decreased dramatically and thus the difference between the 1984 and TLS datasets are likely to be smaller across this earthwork. There is also no detectable difference in aspect values across the barrow to the north of the henge either. However, there are a greater number of significant residual differences surrounding the barrow, which are still comparable in size to those detected in the 1969 dataset. The 1984 photography (Figure 7.18) also exhibits stripes that run from north to south in the area surrounding the henge and barrow, which are again synonymous with ploughing. The tracks made by a tractor turning in the field can also be seen, although they are not in close proximity to the henge or barrow. Therefore these residuals could be the result of alterations in the soil texture which will not be present in the TLS data as ploughing here had long since stopped.

The appearance of the Moran's I for the 1989 henge region is similar to that of the 1984 dataset, as shown in Figure 7.63e and d respectively. As illustrated by the 1984 and 1989 summary statistics, provided in Table 7.14, these datasets are comparable, with the 1989 aspect values performing marginally worse. The most notable difference between the 1984 and 1989 Moran's I maps are located within the southern region of the henge monument, with a slightly higher number of statistically significant high and low values present within the henge interior. A comparison of the orthophotographs of this area from 1984 (Figure 7.18) and 1989 (Figure 7.35) indicate why this may be the case. The gorse has been all but cleared by 1989, whilst the surrounding field looks to have been left to turn to pasture, as there are no stripes of vehicle tracks that suggest the region has been ploughed recently. However, this has reduced the amount of contrast within the 1989 photograph of this region, and thus image matching here will struggle to perform as well as the 1984 SAPs, which contain greater contrast. This observation is supported by the point densities returned by SocetGXP, which are shown in Figure 7.33, with the 1984 and 1989 datasets shown in Figure 7.33d and e respectively. It can be seen that there are no holes in the 1984 dataset whilst there are a number of small holes situated to the south of the henge and in the surrounding field. It is the lack of point data in these gaps, rather than the interpolator, that has given rise to a slightly larger number of residual differences between the 1984 and 1989 datasets, which are remarkably similar.

There is no spatial structure to the distribution of high and low statistically significant values across the 1997 Moran's I map of the henge, as shown in Figure 7.63f. As the appearance of the 1997 aspect map differs so greatly from that of the TLS, as shown in Figure 7.63f and h respectively, this is unsurprising. The barrow to the north of the henge has not been reproduced by the 1997 SAPs, and thus there is a large patch of statistically significant high values covering this area in the Moran's I and DoD maps (Figure 7.63f and Figure 7.64f respectively). Based upon the appearance of the hillshaded DSM beneath each of these figures, there is little topographic expression of the henge and the surrounding terrain has a lumpy texture. Therefore

any hint of spatial structure within the Moran's I and DoD maps are due to the large difference between the 1997 and TLS aspect values rather than an expression of actual physical change in this area.

The 2010 Moran's I result for the henge area is shown in Figure 7.63g. Although there are a large number of non-significant residual values situated across the region, including over the barrow, there is spatial structure to the statistically significant high values surrounding the henge itself. These are situated at the base of the slopes, along the breaklines, whilst there are a small number of the statistically significant low values running along the ridge of the banks. These are related to the irregular outlines of the 2010 aspect values versus the sharp outlines defined by the TLS data, which are each clearly visible in the aspect maps, shown in Figure 7.51g and h respectively. These differences appear to be relatively minor, although they do give confidence that the 2010 data has recreated many aspect values to a standard comparable with the TLS. However, as was noted in the slope DoD for the 2010 data (see Section 7.5.3.2, Figure 7.49g), there was some disparity between the TLS and 2010 slope values. This further supports the observation that utilising only one derivative to assess data quality will not reveal the full extent of the differences and errors with a dataset.

7.7 Archaeological Assessment

Although the DSMs and their first-order derivatives have facilitated the identification of regions across the hillfort and henge monument that have changed over the decades, they only give a very abstract notion of how well these datasets have recreated the profiles of various earthwork features. To understand the full extent to which each SAP epoch has successfully reconstructed the lateral and vertical expression of earthworks, two approaches have been taken. Firstly, profiles are used to establish the ability of archive SAPs to reconstruct the vertical expression of earthworks (see Section 7.7.1). To achieve this goal GNSS profiles were measured across a selection of these features in the Eggardon Hill landscape. These points were used to extract elevation values at the same locations in each of the SAP DSMs for comparison in Microsoft Excel. Secondly, breaklines are examined using a classification algorithm, which has been discussed in Section 4.5.4. By comparing breaklines extracted from archive SAPs against those from the 1950 hachure plan from the RCHME, it will be possible to assess whether archive SAPs are capable of recreating this data.

7.7.1 Profile Assessment

As there are a number of archaeological earthworks within the Eggardon landscape, a number of profiles were created to visually examine the reconstruction of these features by the SAP datasets in comparison with the RCHME and GNSS data. The features chosen to examine

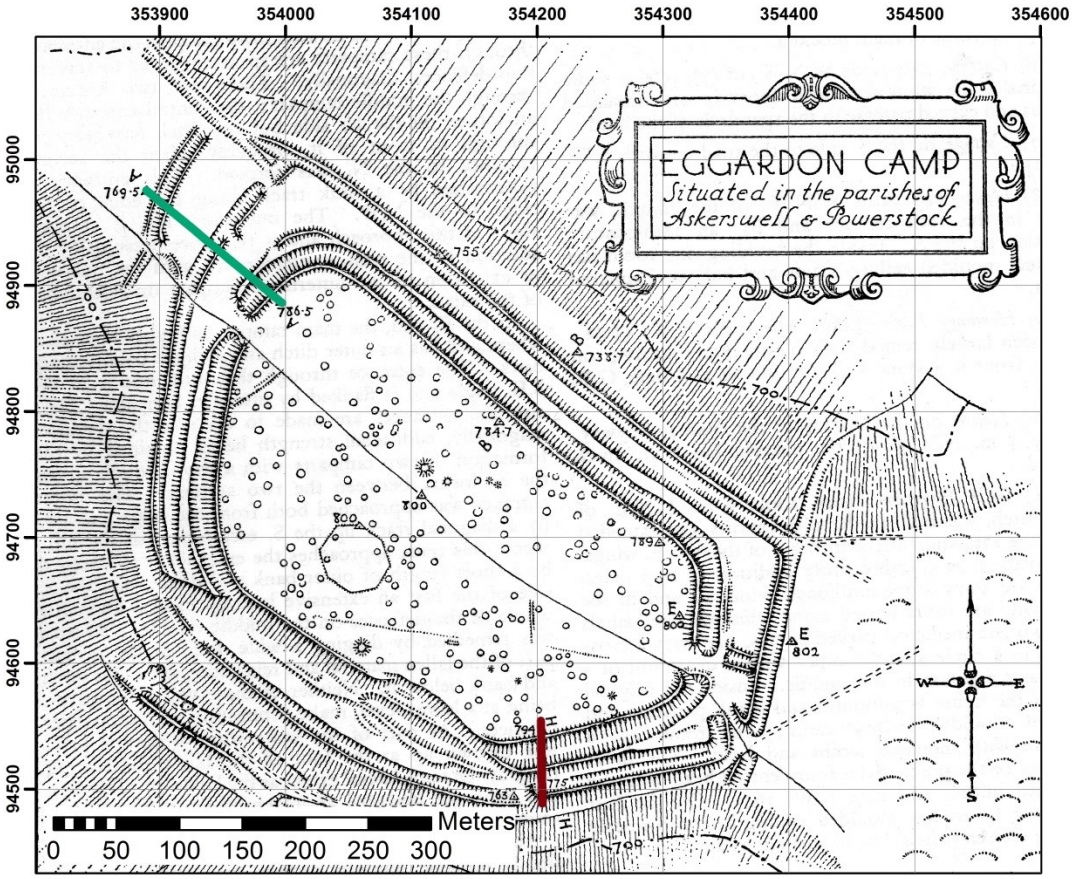

Figure 7.65: Location of rampart Profiles 'A' (in green) and 'H' (in red) across Eggardon Hillfort.

reconstruction potential were the hillfort ramparts (Section 7.7.1.1), henge monument (Section 7.7.1.2), the barrow to the north of the henge (Section 7.7.1.3), and the change in elevation across the hillfort interior (Section 7.7.1.4).

7.7.1.1 Ramparts

Two profiles were recreated based upon those recorded in the 1950s RCHME hachure plan, namely profiles A and H. Profile A is the longest and runs across the north-west ramparts, whilst profile H is situated to the south-east of the hillfort, as illustrated in Figure 7.65. The results from both Profiles 'A' and 'H' were separated into two categories: SAPs that performed well, based upon their RMSE results and general observations from the statistical analysis, and those that performed badly.

Profile A

The results amongst the best-performing SAPs from profile ‘A’, shown in Figure 7.66, are broadly similar in terms of their shape. However, there is a vertical offset between the RCHME and GNSS profiles that appears towards the peak of the second bank (second peak from left in Figure 7.66) and ends as it nears the fourth bank approximately 100m along the profile. As the remainder of these two profiles are concurrent with one another, this suggests that either there is a disparity in the data recorded during the 1950s survey, or that there has been material deposition in this area over the last 60 years. If this were true it would be expected that the 1969 SAPs display an offset that was somewhere between the GNSS and RCHME data, but this is not the case. The 1969 profile contains elevation values closer to that of the GNSS, although it appears to contain a horizontal offset and a degree of noise. Despite correcting the 1984 DSM for horizontal and vertical offsets prior to conducting any analysis on the dataset, the profile line would suggest that there is still a disparity in the vertical plane. This could be due to the over-estimation of the degree to which the elevation was altered, which was calculated by examining the mean difference between the DSM elevations and the GNSS random points. However, there is a near perfect match between the GNSS and the 1989 SAP profile.

The results obtained by extracting profiles using the poorest performing SAP DSMs are evident, as shown in Figure 7.67. There is very little resemblance between the RCHME, GNSS and 1948 SAP profiles. The 1997 SAP data also performs badly, particularly between 100m and 140m along the profile, where the two more subtle banks and the ditch are situated. There is no coherent record of these features in the 1997 profile, although the 1972 dataset appears to have reconstructed these earthworks reasonably well.

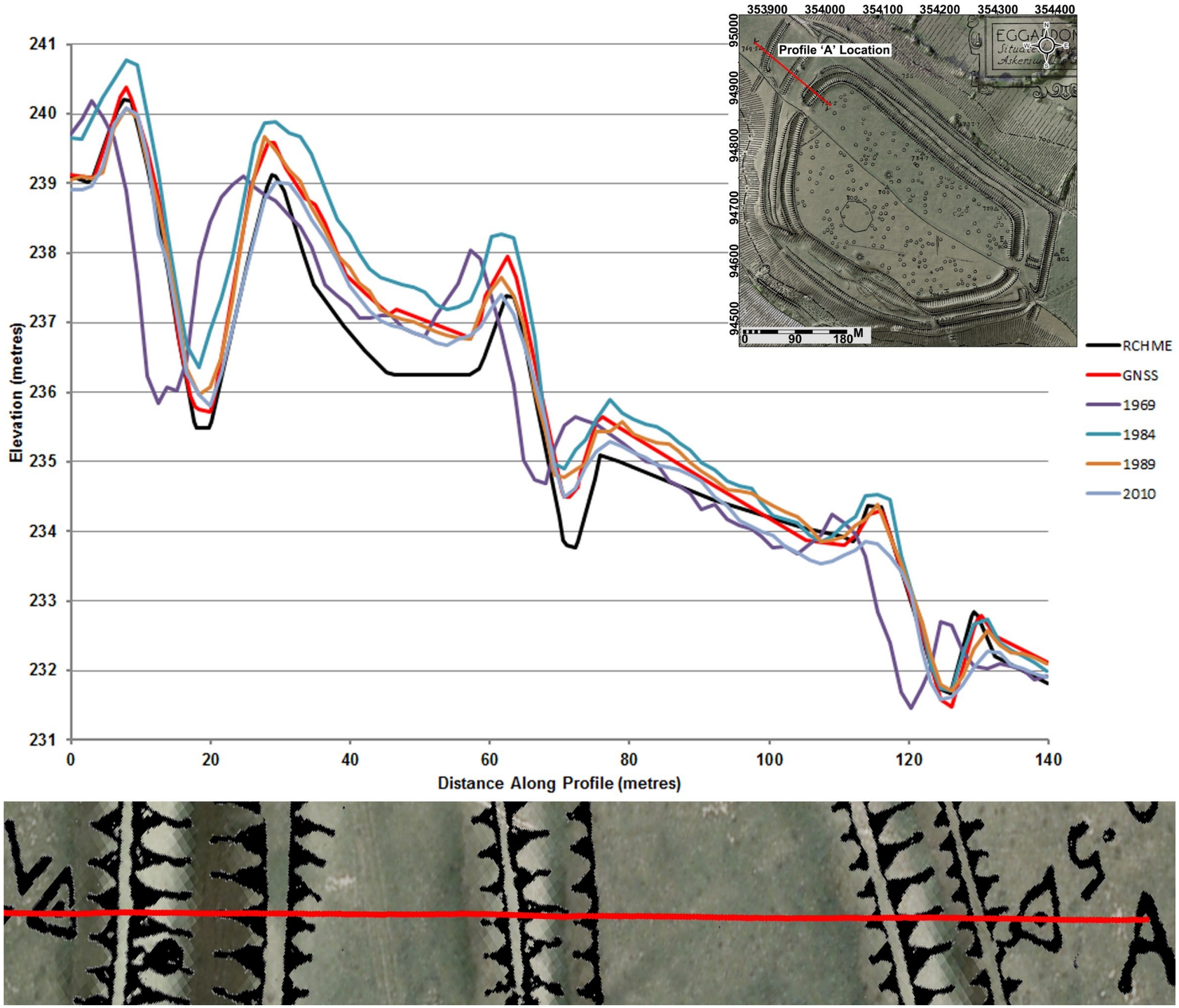

Figure 7.66: Graph of Profile 'A' extracted from the best-performing SAP epochs.

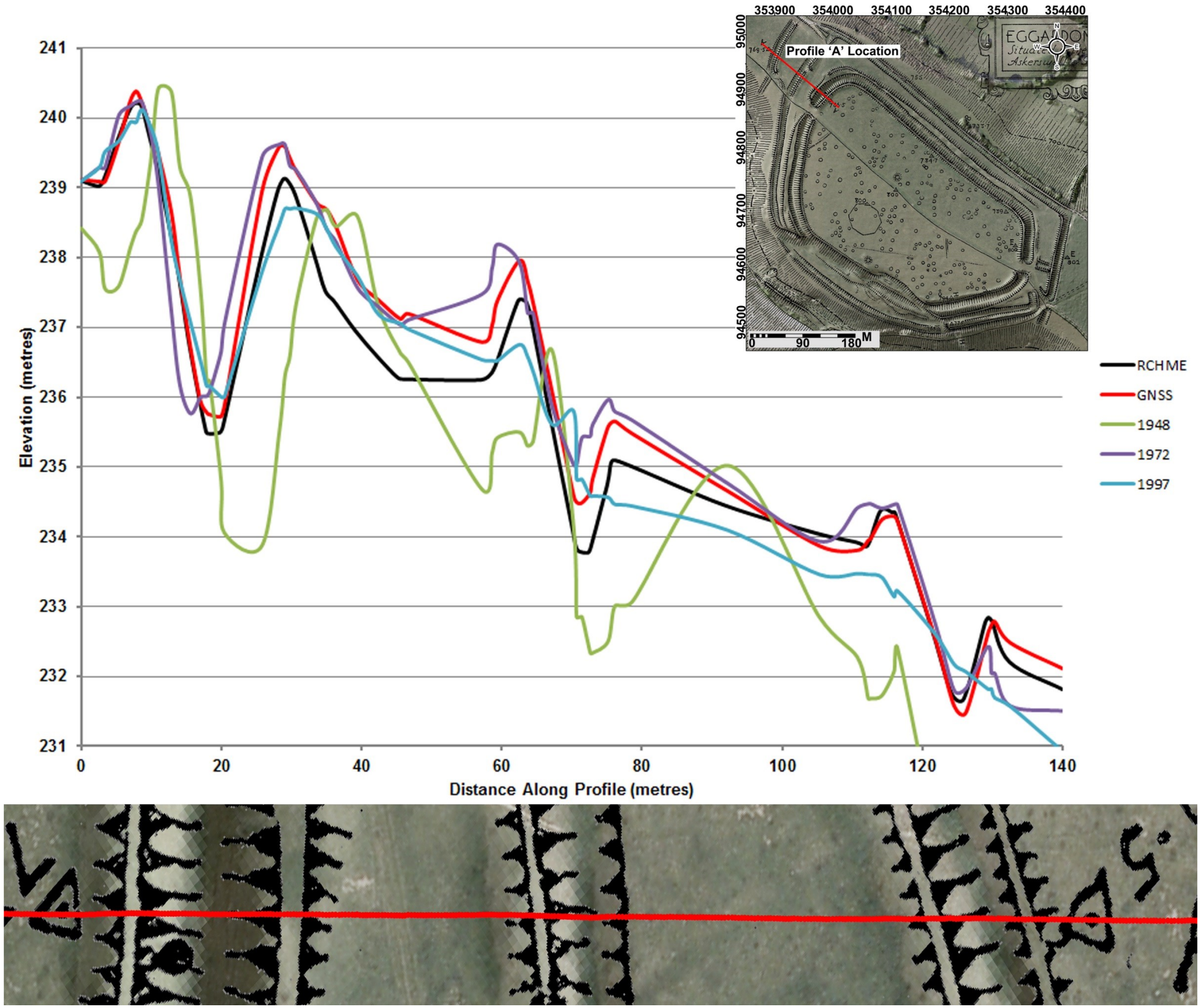

Figure 7.67: Graph of Profile 'A' extracted from the worst-performing SAP epochs.

Profile H

The reconstruction of profile H by many of the SAP datasets, which contains more extreme elevation variations, is impressive, particularly from the best-performing epochs as shown in Figure 7.68. The shape of the profile looks visually identical across all of the epochs in comparison with the RCHME and GNSS data. There is also no evidence for either horizontal or vertical offsets in any of the SAP DSMs. Within the poorly-performing SAP datasets, as shown in Figure 7.69, the first 25m of profile H have not been faithfully reproduced. However, there are encouraging results from 30m onwards to the end of the profile from the 1972 and 1997 SAP datasets as the both follow the shape of the GNSS curve. The result from the 1948 SAP DSM also shows promise, especially along the slopes, although its overall appearance is noisy.

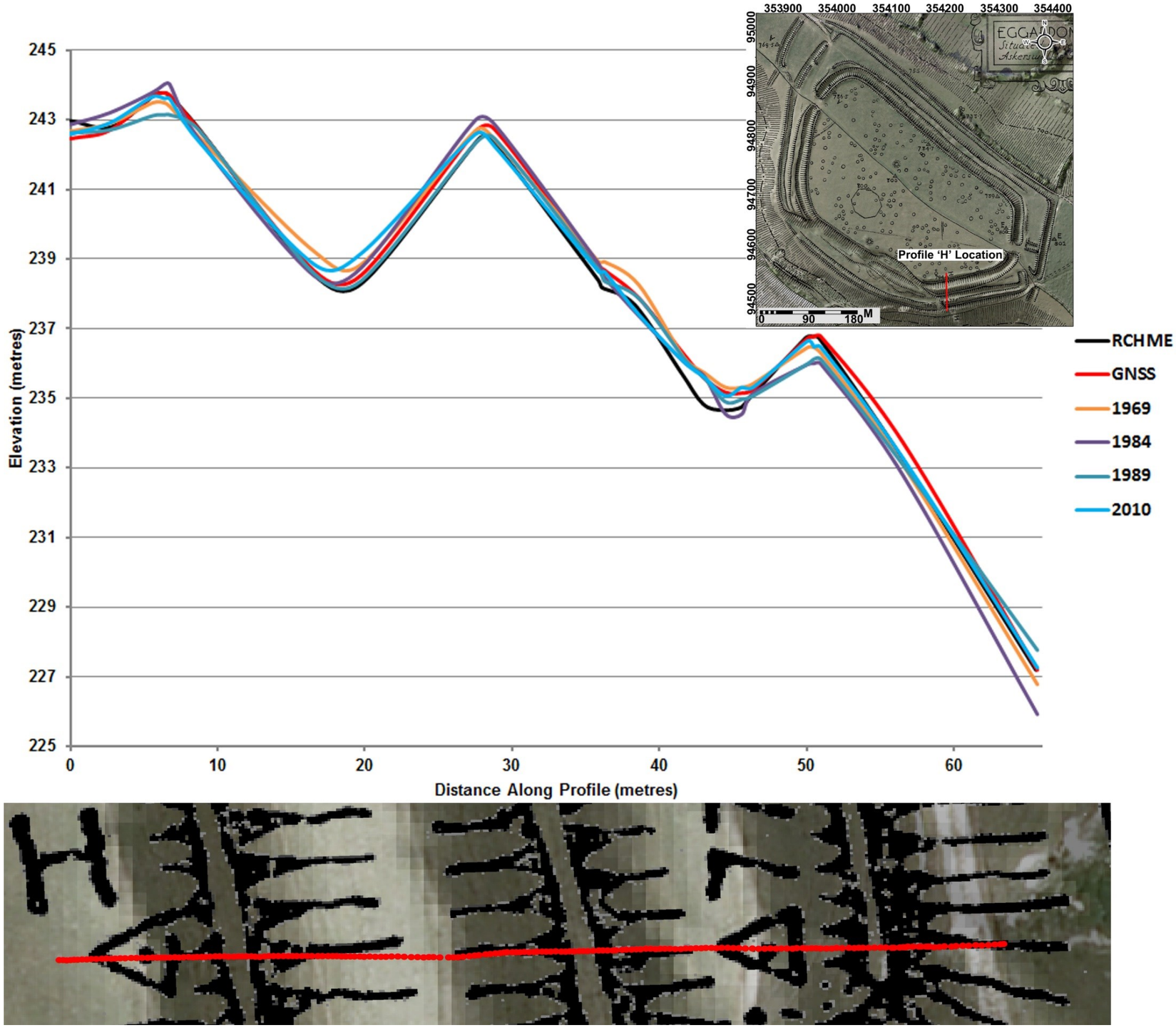

Figure 7.68: Graph of Profile 'H' extracted from the best-performing SAP epochs.

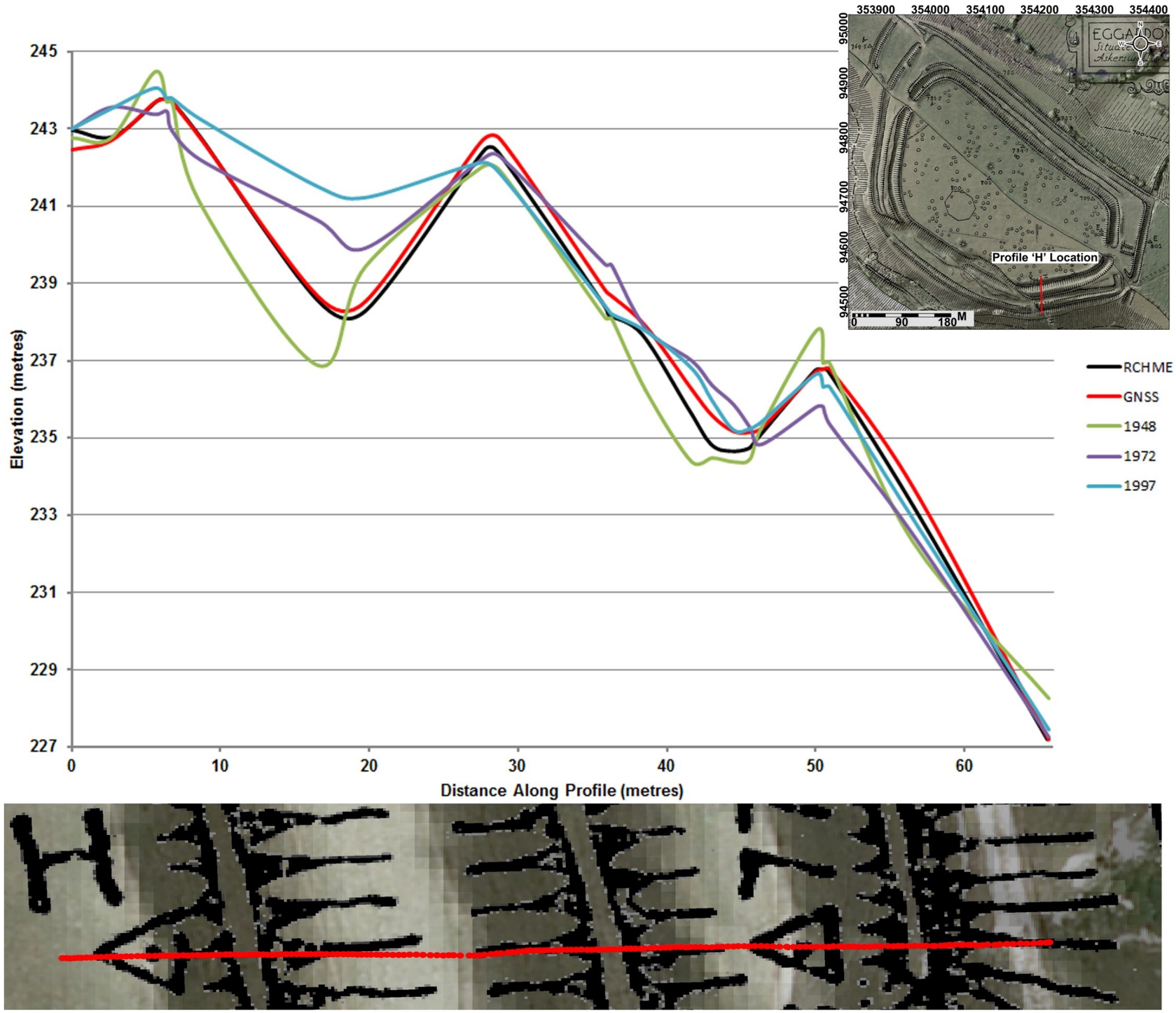

Figure 7.69: Graph of Profile 'H' extracted from the worst-performing SAP epochs.

7.7.1.2 Henge Monument

A profile was collected across the henge monument, as shown in Figure 7.70, to test the ability of SAPs to reconstruct more subtle earthwork features. As is apparent from the profile graph, shown in Figure 7.71, the best-performing SAP DSMs have reconstructed the banks and the inner barrow within the henge. There appears to be a slight vertical offset towards the end of the profile at c.45m, particularly in the 1984 DSM, although this does not appear to be significant at the start of the profile. This is suggestive of a tilt in the 1984 DSM, which was thought to have been removed by adding a trend surface and warping the DSM.

The 1948 profile, as shown in Figure 7.72, bears no relation to the henge profile and it indicates that there is a significant height difference in the DSM as compared to the GNSS data. This result is not unexpected based upon the previous analysis of the elevation, slope and aspect derivatives of the 1948 DSM. Whilst the 1972 and 1997 profiles both look convincing, this is due to the exaggerated vertical scale of the graph caused by the large elevation disparity of the 1948 data. The banks and the barrow are almost indistinct in comparison with the GNSS profile, although the 1972 dataset appears to be more pronounced across the banks at the farthest end of the curve at c.64m. Irrespective of the elevation offsets between the GNSS and SAP datasets, the results from DTS prints do not suggest that they can be used for reconstructing more subtle earthworks.

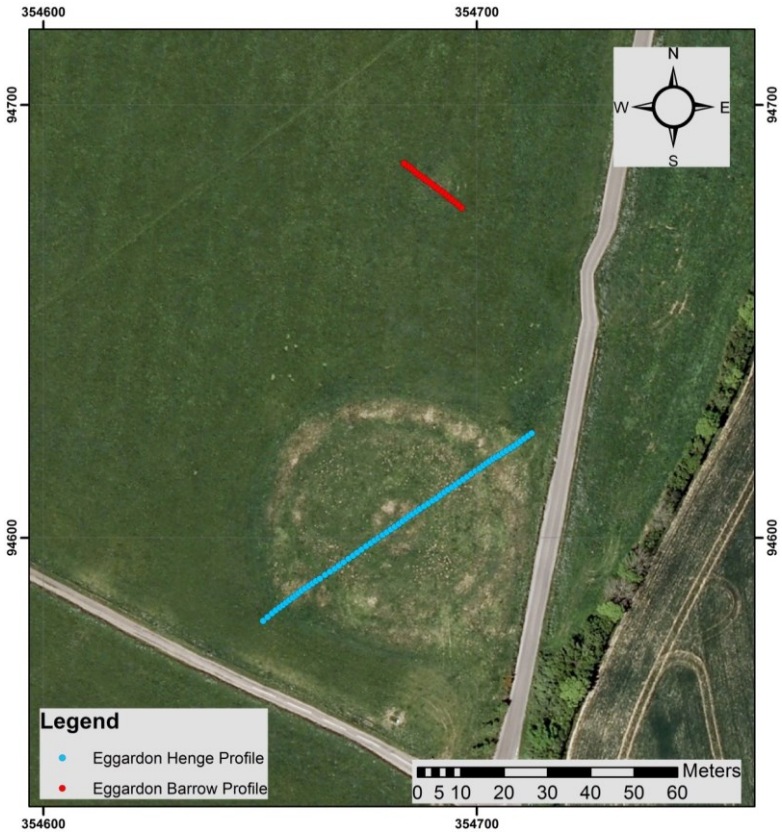

Figure 7.70: Map showing the locations of the GNSS profiles taken across the henge monument (bottom) and the barrow (top).

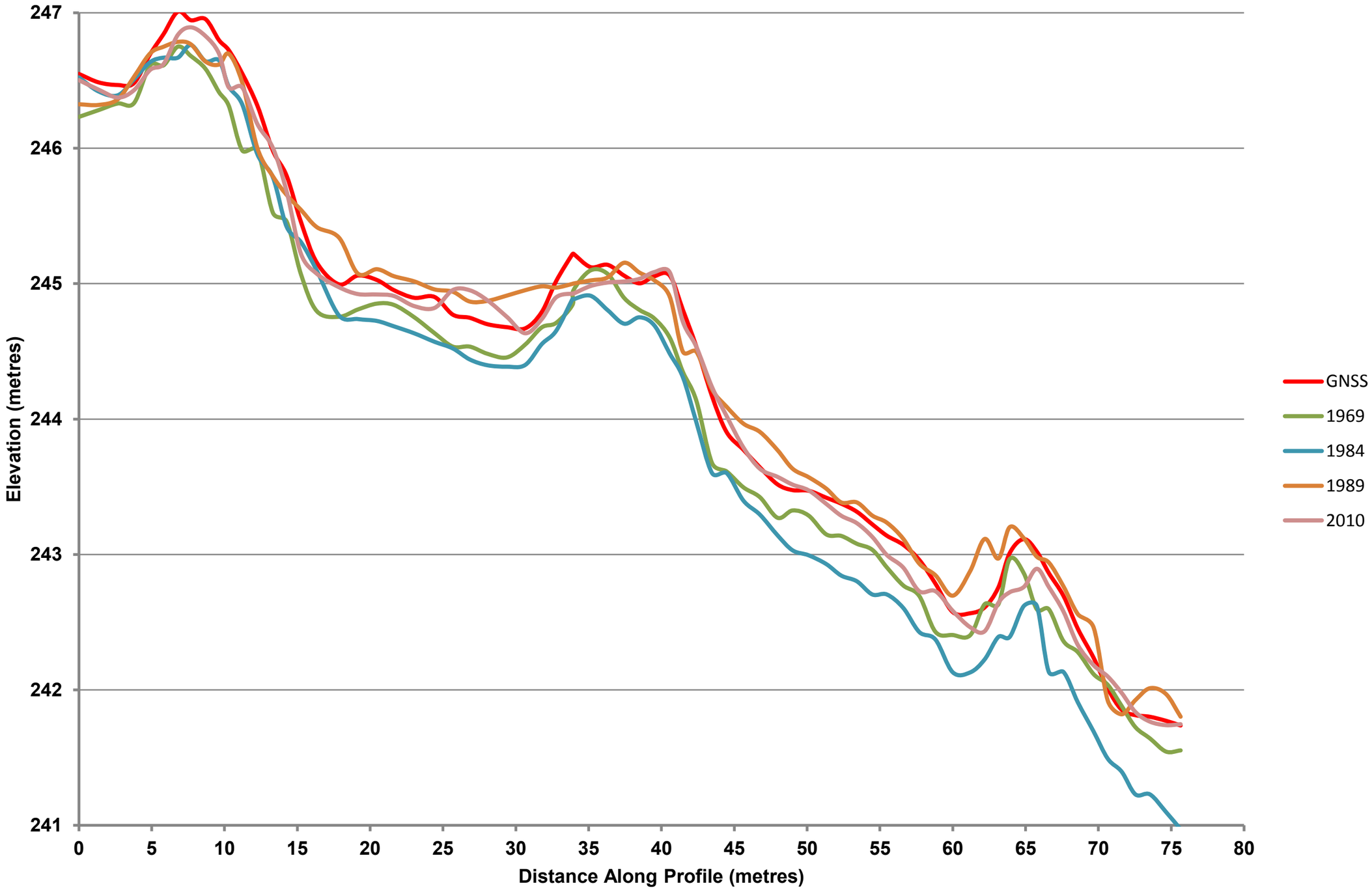

Figure 7.71: Graph showing the profile across Eggardon henge monument collected with the GNSS and extracted from the best-performing SAPs.

Figure 7.72: Graph showing the profile across Eggardon henge monument collected with the GNSS and extracted from the worst-performing SAPs.

7.7.1.3 Barrow

The barrow to the north of the henge monument is just under 1m high and offers one of the more difficult challenges for SAP DSMs. However, as shown in Figure 7.73, the results from the best-performing SAPs are encouraging. Irrespective of any apparent elevation offsets in the data, the majority of the DSMs have recreated the basic shape of the barrow. Elevation values from both the 1969 and 2010 SAPs show the poorest coherence in comparison with the GNSS dataset. The 1969 curve looks to be lacking in horizontal resolution, as indicated by the 'stepped' appearance, which is more exaggerated than in the other profiles. Beyond this observation, the basic shape of the barrow can be seen. It is therefore surprising that the newest SAP data from 2010 has underestimated the height of the barrow. As there is only a gap of 3 years between the 2010 SAPs and the collection of the barrow profile with the GNSS in 2013, there should be minimal difference in elevation. It is unlikely that, over this period, material would have accrued on the top of the barrow. Vegetation cannot be cited as the cause because the GNSS will still record its measurements at the ground surface.

As with the henge monument discussed in Section 7.7.1.2, the worst performing SAP datasets have failed to reproduce the shape of the barrow, as illustrated in Figure 7.74. The 1948 SAPs are unrepresentative, with the profile elevations differing by over 2m from the lowest point to the highest and thus it is double the actual height of the barrow itself. Based upon the shape of the barrow in the 1948 data, it is unlikely that there has been over 1m of material lost from the monument to explain the difference in relative elevation between the 1948 DSM and the GNSS. There is also a significant elevation offset within the 1948 DSM that has not been removed by utilising a trend surface, as explained in Section 5.1, or by adding a constant value to the DSM that is representative of the mean difference between it and the random GNSS points. Whilst this does not appear to be an issue with the 1972 and 1997 SAP DSMs, the latter of the two exhibits a curve that is unrepresentative of the barrow, which also contains a dip where the peak of the feature should be. The 1972 SAP DSM is more akin to the barrow profile, but there is still a significant visual difference so as to preclude this dataset from being considered as useful for reconstructing this feature.

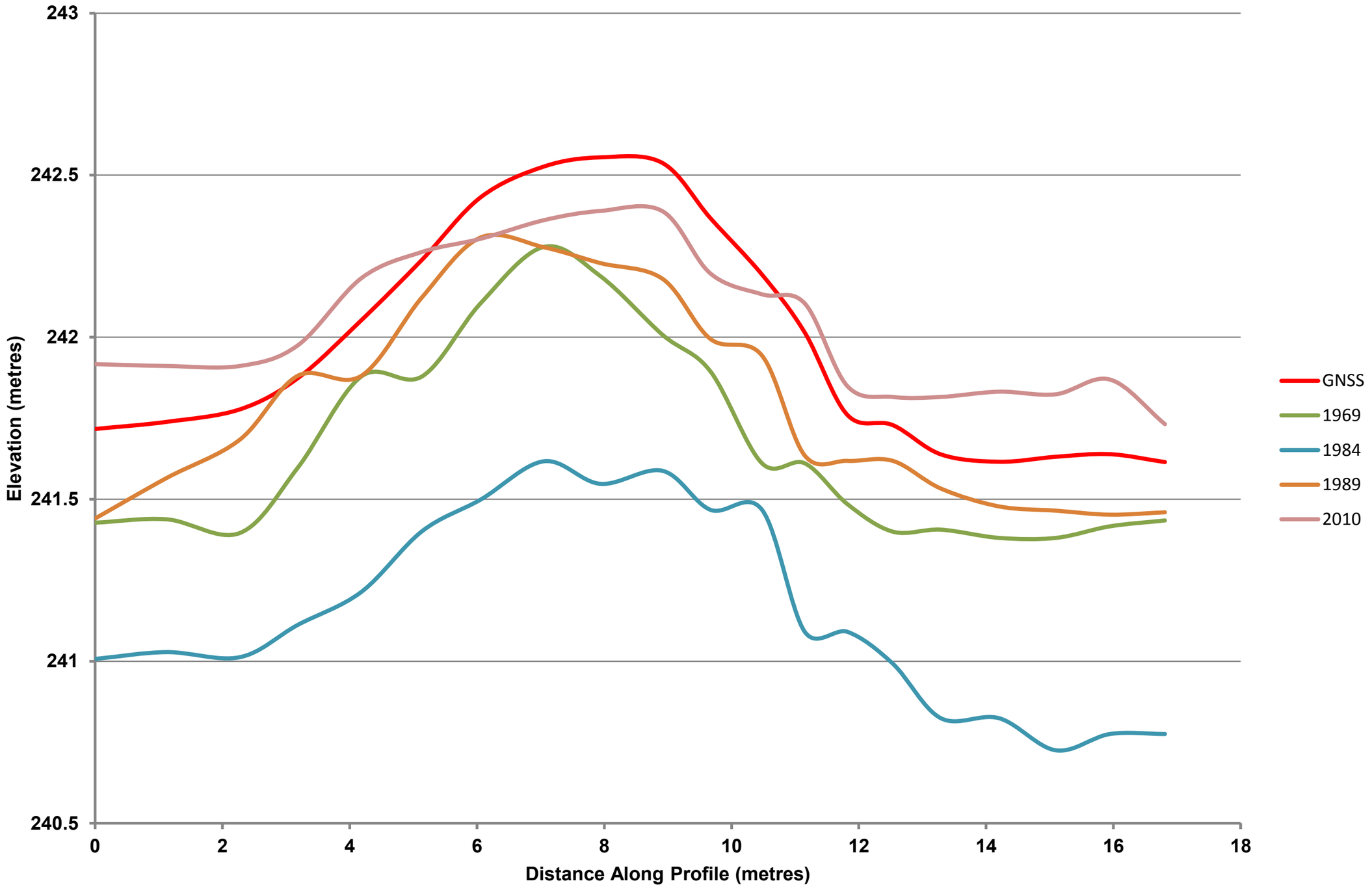

Figure 7.73: Graph showing the profile across Eggardon barrow collected with the GNSS and extracted from the best-performing SAPs.

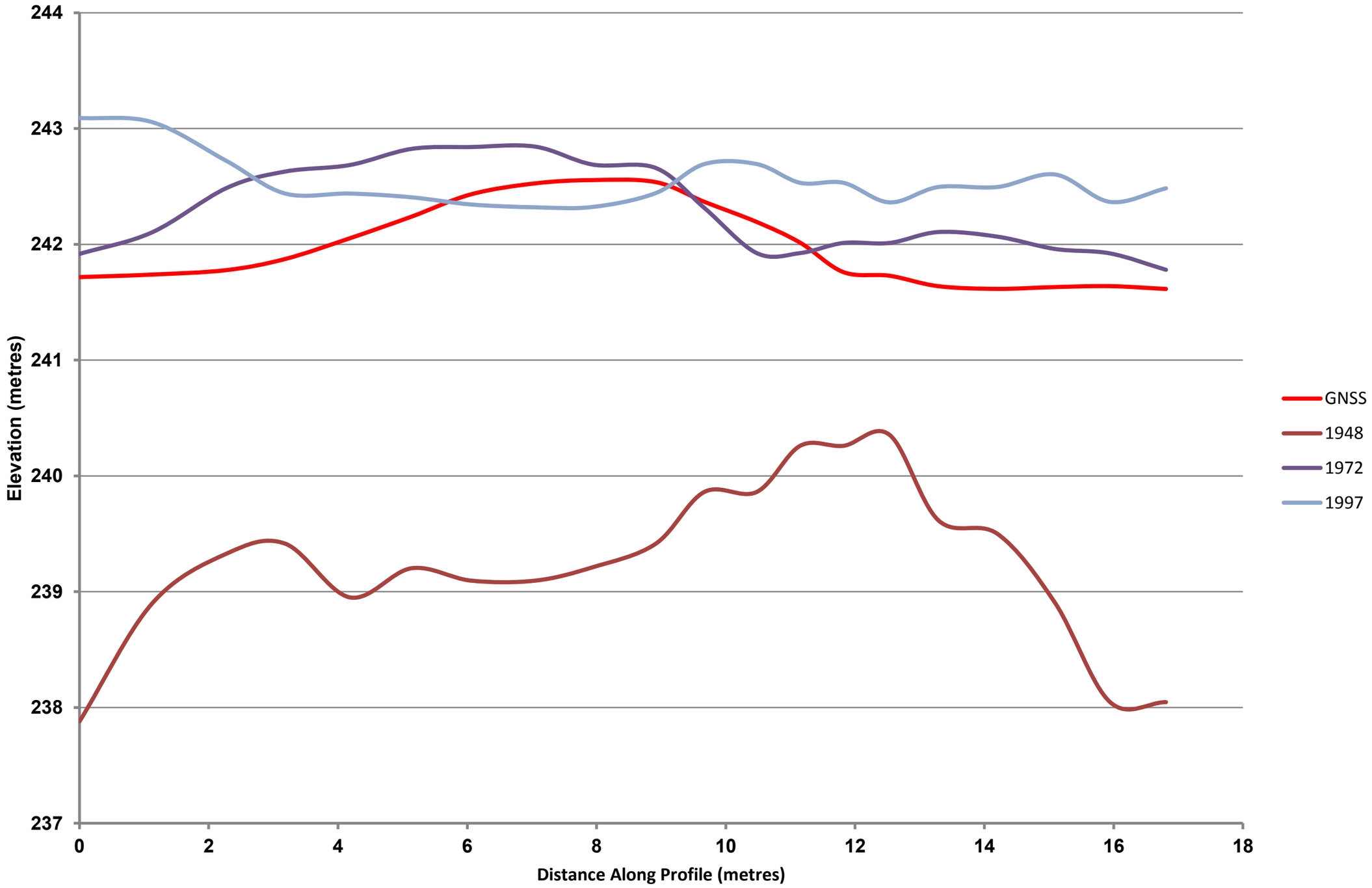

Figure 7.74: Graph showing the profile across Eggardon barrow collected with the GNSS and extracted from the worst-performing SAPs.

7.7.1.4 Change Detection: Preserved versus Intensive Agriculture

It was postulated that the effects of ploughing may be visible in the SAP DSMs on comparison of elevation values within the north half of the hillfort, which has suffered plough damage in the past, with those in the preserved southern half. A transect across the hillfort was surveyed using the GNSS, which defined the location of elevation measures to extract from the SAP DSMs and the TLS dataset. These profiles produced from these values were then examined to try and identify the difference in elevation between the north and south of the hillfort.

The results from the best-performing SAPs, as shown in Figure 7.75, are not as clear as those for the rampart, henge and barrow. It can be seen that the fence has not been removed from the TLS DSM, shown approximately 15m along the profile, which will have influenced the results observed in the local Moran's I analysis of the SAP DSM datasets, as discussed in Sections 7.4.3, 7.5.3 and 7.6.3. This is reflective of the lack of access to PC and software facilities to undertake the requisite registration and cleaning of the TLS point cloud. However, it is interesting to observe that the 1969 SAP DSMs have recreated this feature, which is clearly present in the profile curve, although the remainder of the profile is noisy. There are indications of the fence appearing in the other SAP DSMs, although it is not as pronounced. Although the 1989 SAPs have performed well throughout the elevation, slope and aspect assessments, they do not concur with the TLS and GNSS results in the region surrounding the fence. The most convincing result can be seen in the 1984 profile, whereby the elevation values towards the right-hand side of the graph are much flatter. This is the region that represents the northern half of the hillfort, and thus the area that has been ploughed. However, this is not replicated by the other DSMs, including the TLS, and thus it cannot be stated with confidence that there is an obvious difference between the southern and northern halves of the hillfort. Fortuitously, it can be seen that the 1984 and 2010 DSMs show a drop in elevation values just after the fence at c.20m, which is in the northern half, much like the TLS and GNSS, which is encourage as this suggests these DSM have produced a result similar to the most accurate survey techniques.

The poorly-performing SAP DSMS, as shown in Figure 7.76, are again unrepresentative of the terrain across the hillfort, although the 1997 DSM adheres to the GNSS and TLS elevations in the southern half, or the first 15m of the profile. It increasingly diverges from these curves within the northern half of the hillfort, however. The 1972 DSM has not provided any useful information, and the 1948 SAPs have again failed to replicate the form of the hillfort surface.

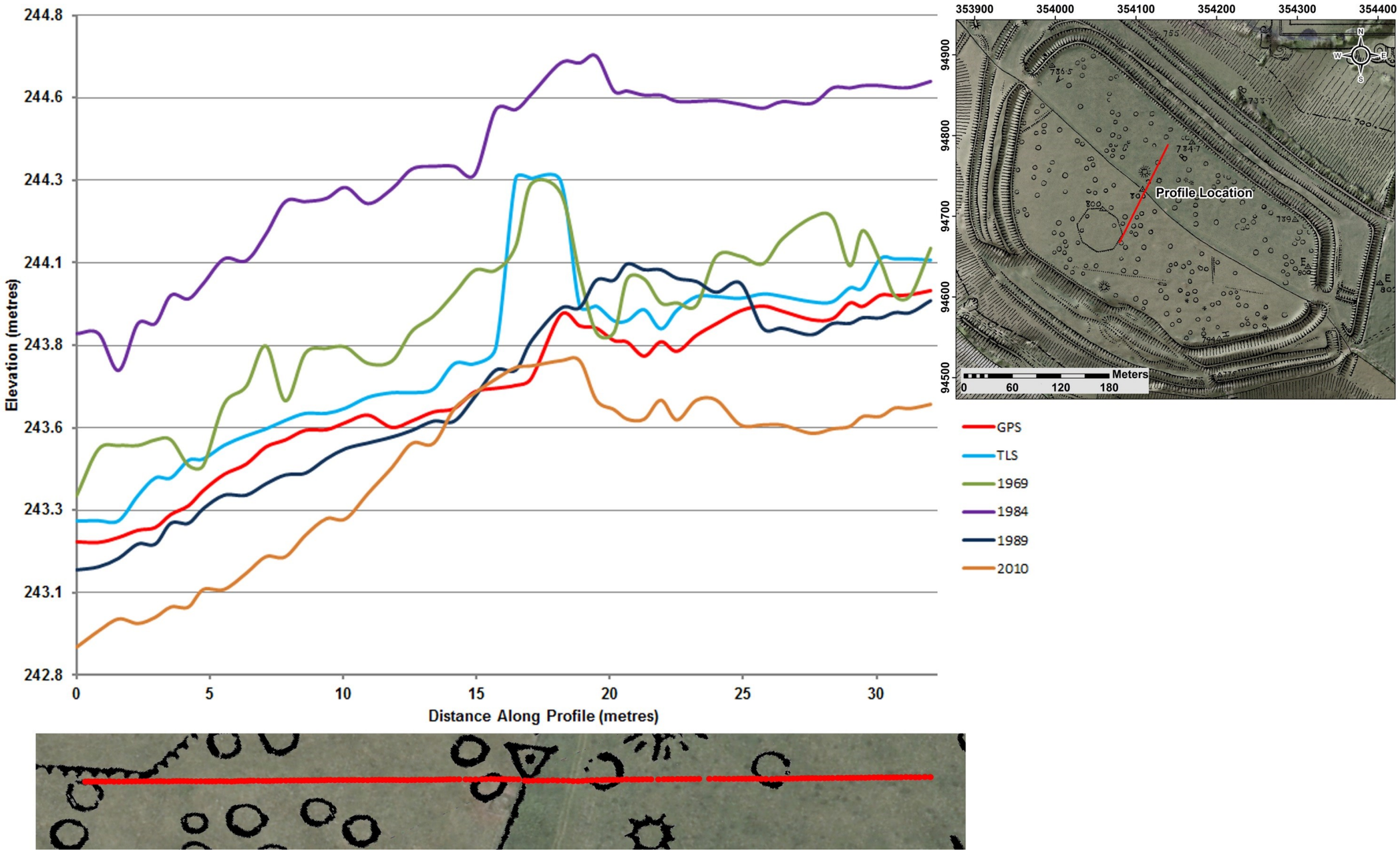

Figure 7.75: Graph showing the transect profile across Eggardon hillfort extracted from the best-performing SAPs using GNSS data.

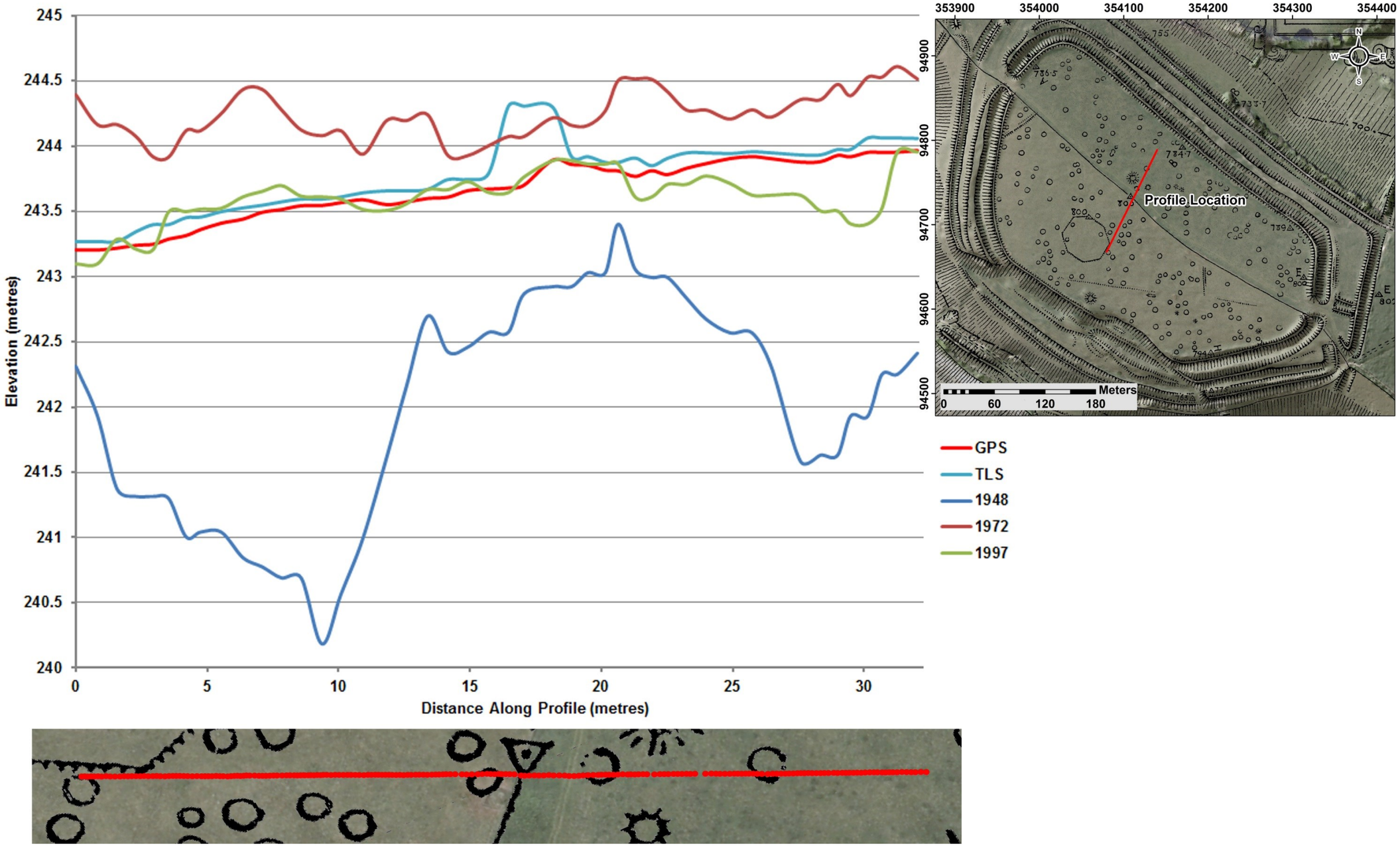

Figure 7.76: Graph showing the transect profile across Eggardon hillfort extracted from the worst-performing SAPs using GNSS data.

7.7.2 Breakline Assessment

The *Geomorphons* classification routine was applied to the Eggardon SAP DSMs to establish how well each of these datasets recreated breaklines across the hillfort. As with the Flowers Barrow study, presented in Section 6.7.2, the hillfort breaklines were digitised from the RCHME hachure plan (see Figure 7.77) and used to extract pixel values from the best performing DSM of Eggardon, namely the 2010 SAPs. An error matrix was constructed to assess the degree of agreement between these two datasets, from which the overall accuracy value was calculated to be 15.08%. Thus the subsequent comparisons between the 2010 SAP DSMs and the remaining DSMs were required to equal or better this score. This would indicate that they were capable of recreating breaklines to a greater degree of agreement between them and the 2010 DSMs than the RCHME breaklines.

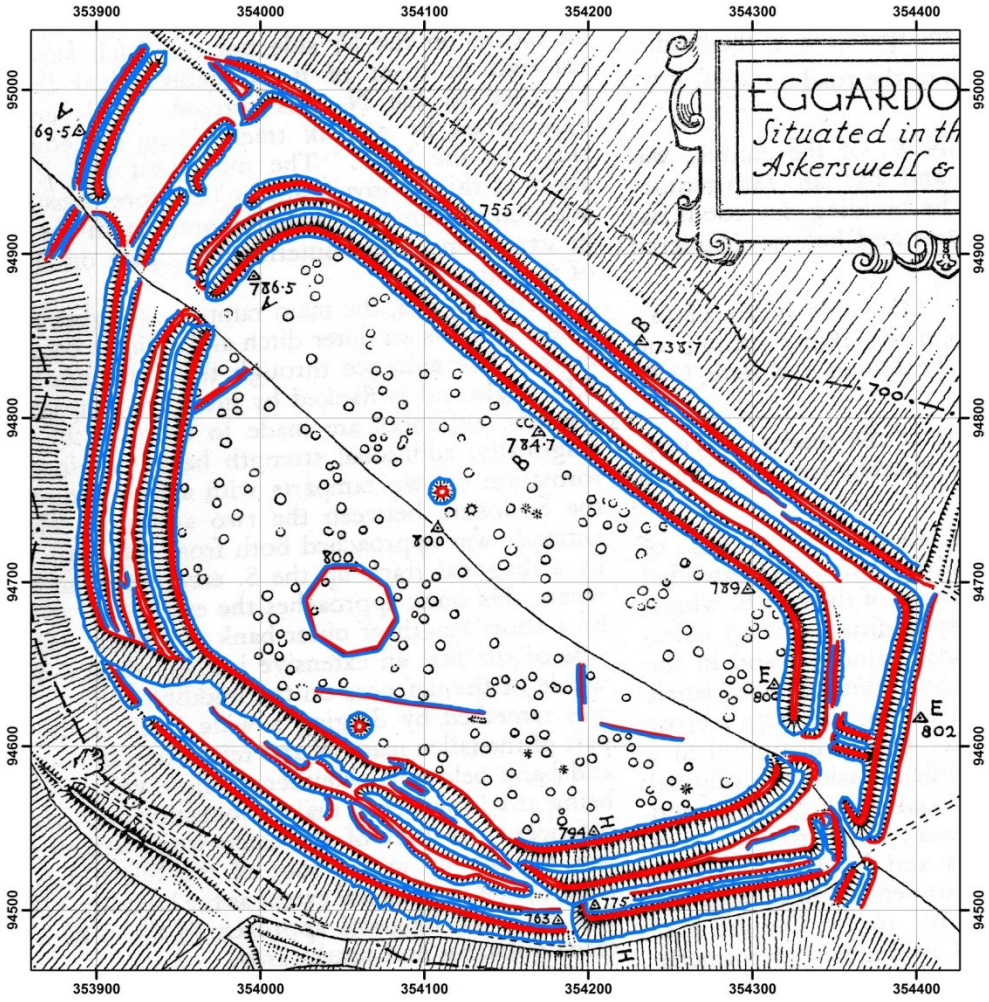

Figure 7.77: Breaklines digitised from the 1950s RCHME hachure plan of Eggardon Hillfort. Top-of-Slope breaklines are in red, whilst Bottom-of-Slope is shown in blue.

SAP Year	Overall Accuracy (%)
1948	28.0
1969	53.0
1972	48.6
1984	65.9
1989	67.7
1997	44.2

Table 7.16: Results of comparing the Geomorphons breakline classification of SAP DSMs with the 2010 SAP DSM.

The results from comparing the SAP DSMs to the 2010 data are provided in Table 7.16. There is a large degree of similarity between the 2010 and 1989 DSMs, with an accuracy score of 67.7%, indicating that over two-thirds of the pixels were in agreement. The 1984 SAP DSM also scored highly, with 65.9% accuracy. By looking at the *Geomorphons* models, as shown in Figure 7.78d, e and g, the 1984, 1989 and 2010 look similar. However, the 1984 and 1989 datasets have a noisier appearance than the 2010 data, which is likely to reduce the degree of similarities between these DSMs. Conversely, the 1948 results, shown in Figure 7.78a, have returned an accuracy of 28% between them and the 2010 data, which is a much better performance than the RCHME breaklines in comparison with the 2010 classification. This result is misleading as the appearance of the 1948 data signifies that extracting breakline data from it would be difficult, if not impossible. Therefore the benefits of visual examination cannot be understated.

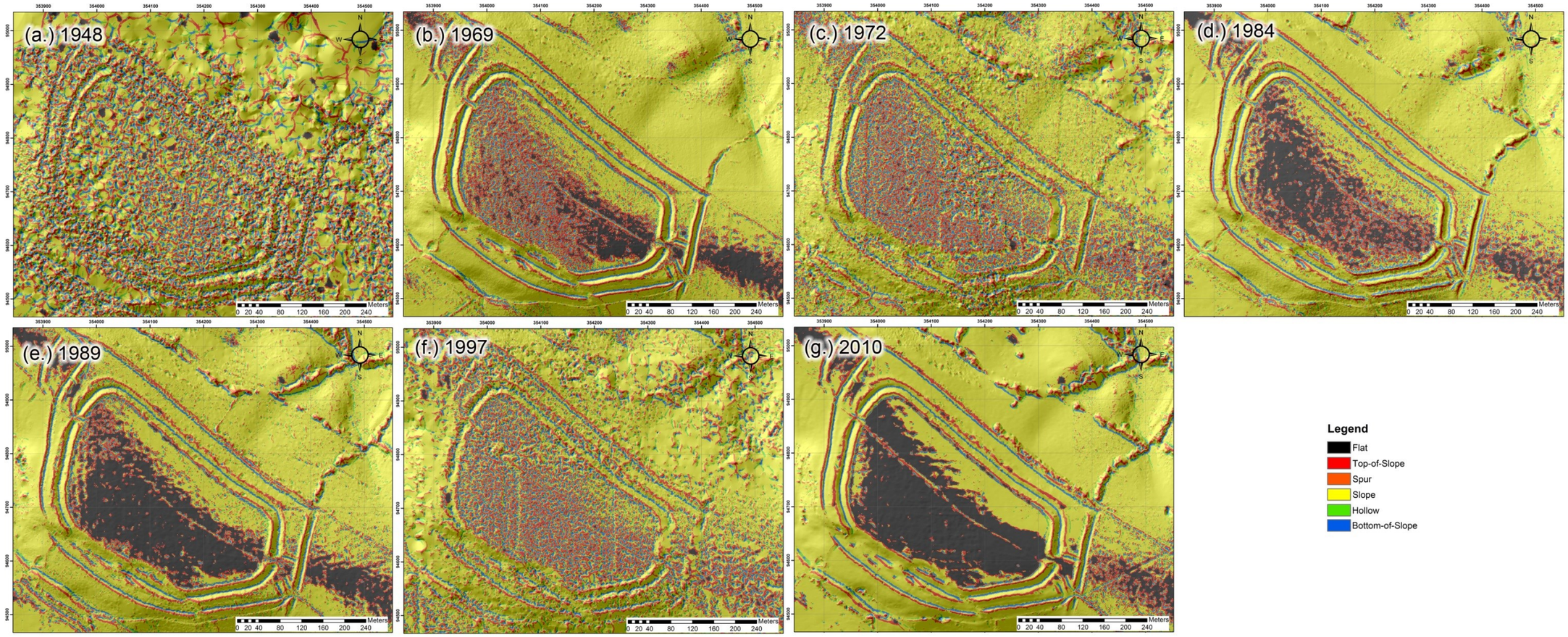

Figure 7.78: Geomorphons classification of the SAP and TLS elevation DSMs across Eggardon Hillfort.

Identifying the cause behind the poor overall accuracy result between the RCHME breaklines and those from the 2010 SAPs relates to the way in which the original survey was created and the subsequent efforts made to georeference the survey drawing to match the modern-day DSM data. Although it is unclear what methods were used to produce the hachure plan, data collection by older techniques will contain larger distortions in them than the new technologies, providing the latter are operated correctly. This could be due to the additive errors that may accrue in measurements as the surveyor moves their instrument around the site, particularly if minimal control is used during the survey. If the control has not been adjusted to remove measurement errors between the control points than any human errors in noting down the measurements will go unchecked and will propagate throughout the remainder of the survey. Modern technologies, however, are often have data quality measures in-built, as is the case for GNSS, or software packages that can account for errors in the data, much like Leica Cyclone and its TLS processing workflows. Whilst any distortions in the RCHME hachure plan could have been removed using warping techniques in software packages such as AutoCAD, it was felt that the inherent distortions should remain. This was to ensure that the performance of the hachure plan and the DSM classifications were based upon the limitations of the survey techniques used to create them. However, the breaklines in the hachure plan are much clearer and, as is the case for the smaller features in the southern interior of the hillfort, contains greater detail that many of the SAP DSMs.

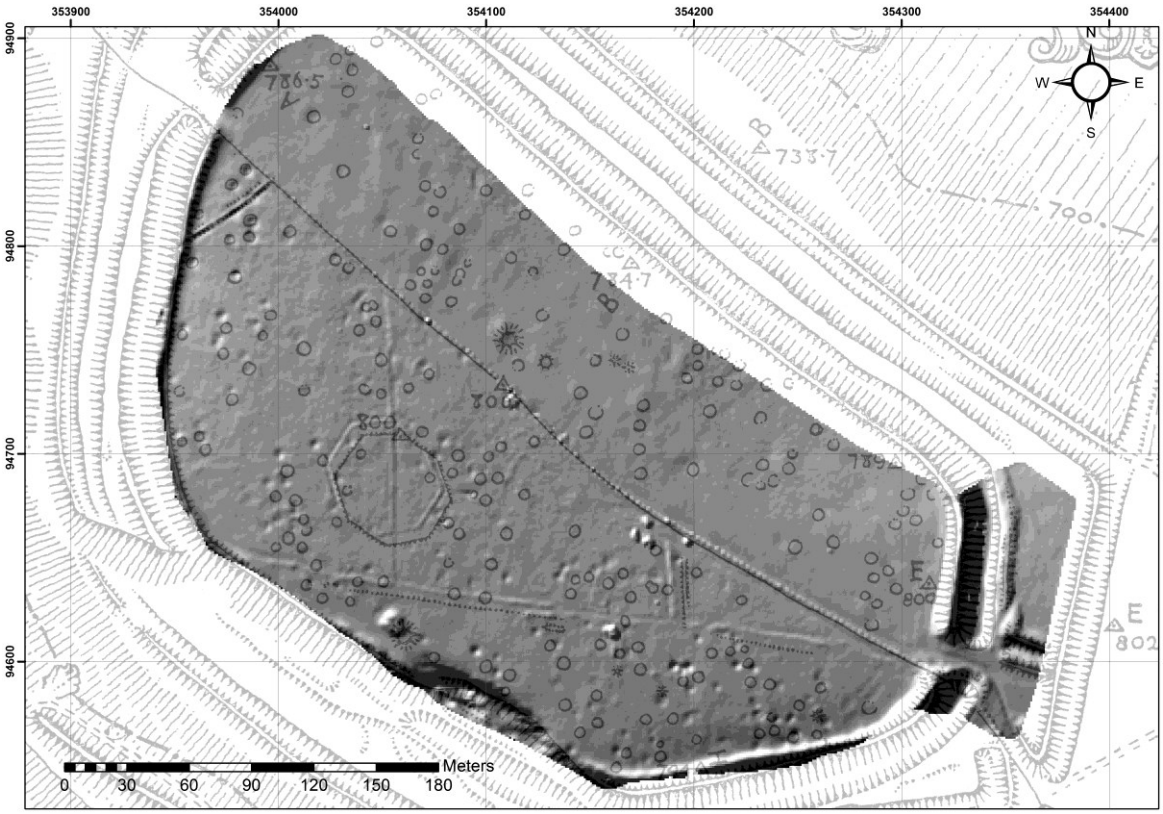

Figure 7.79: Map showing the TLS DSM overlain by the 1950s Hachure plan, highlighting the small details that the TLS data can detect.

On this latter point regarding the subtle earthworks within the southern half of the hillfort, the TLS survey has detected the linear features, barrow and pits with remarkable clarity. This is in spite of the data resolution of the TLS survey being reduced from 10cm to 1m, which was thought necessary to ensure compatibility with the 1m datasets from the SAP DSMs and, in the case of Flowers Barrow, the ALS data. In Figure 7.79 it can be seen that the comparison between these two datasets illustrates the degree to which the TLS generates a record of the subtle earthworks. Whilst the SAP DSMs have detected the larger earthwork features at Eggardon, they have not reconstructed the small pits and linear features.

7.7.3 Information Content Assessment

As with the Flowers Barrow information content assessment in Section 6.7.3, examining the survey data from TLS and SAP DSMs provides an indication of earthwork scale that can be detected by these technologies. Based upon the observations in Section 6.7.3 it is unsurprising that the hillfort ramparts, depicted in Figure 7.80 are clearly seen across each dataset, with the exception of the 1948 SAP DSM. However, to the eastern edge of each image in the top row, the more subtle set of earthen banks and ditch loose clarity in the SAP DSMs whilst it is remarkably clear in the TLS dataset.

The TLS DSM also replicates the subtle earthworks, in the form of linear banks, pits, a misshapen barrow and the coppice hexagon, as depicted in the RCHME 1950 hachure plan. Whilst the barrow is also visible in the 2009, 1989, 1984 and 1969 SAP DSMs, it gets progressively less clear as the age of the SAPs increases. In the 1989 SAP DSM there is a subtle hint of the linear bank that runs in the north-south direction through the hexagonal earthwork, although this cannot be distinguished in the DSM. The hexagon is however just observable in the 1984 SAP DSM.

Within the ploughed region of the hillfort, very little can be seen in the 1989, 1984, and 1969 SAP DSMs. The 1948 SAP DSM was not included as its quality was not conducive to identifying any subtle earthworks. A barrow situated close to the fence line in the bottom right-hand corner of the RCHME survey can also be identified in the TLS and 2010 SAP DSM. This earthwork was suspected to have been destroyed through ploughing and is not easily identifiable in the field. A number of pits can also be seen in the TLS data, which are not depicted in any of the other surveys, save for the RCHME plan. Yet again, this result suggests that employing TLS data is more likely to reveal previously unobserved subtle features. What is also interesting is that the TLS data was interpolated to create a 1m spatial resolution raster to conform to the SAP DSMs. However, despite identical resolutions, the TLS contains archaeological information beyond that of the SAPs.

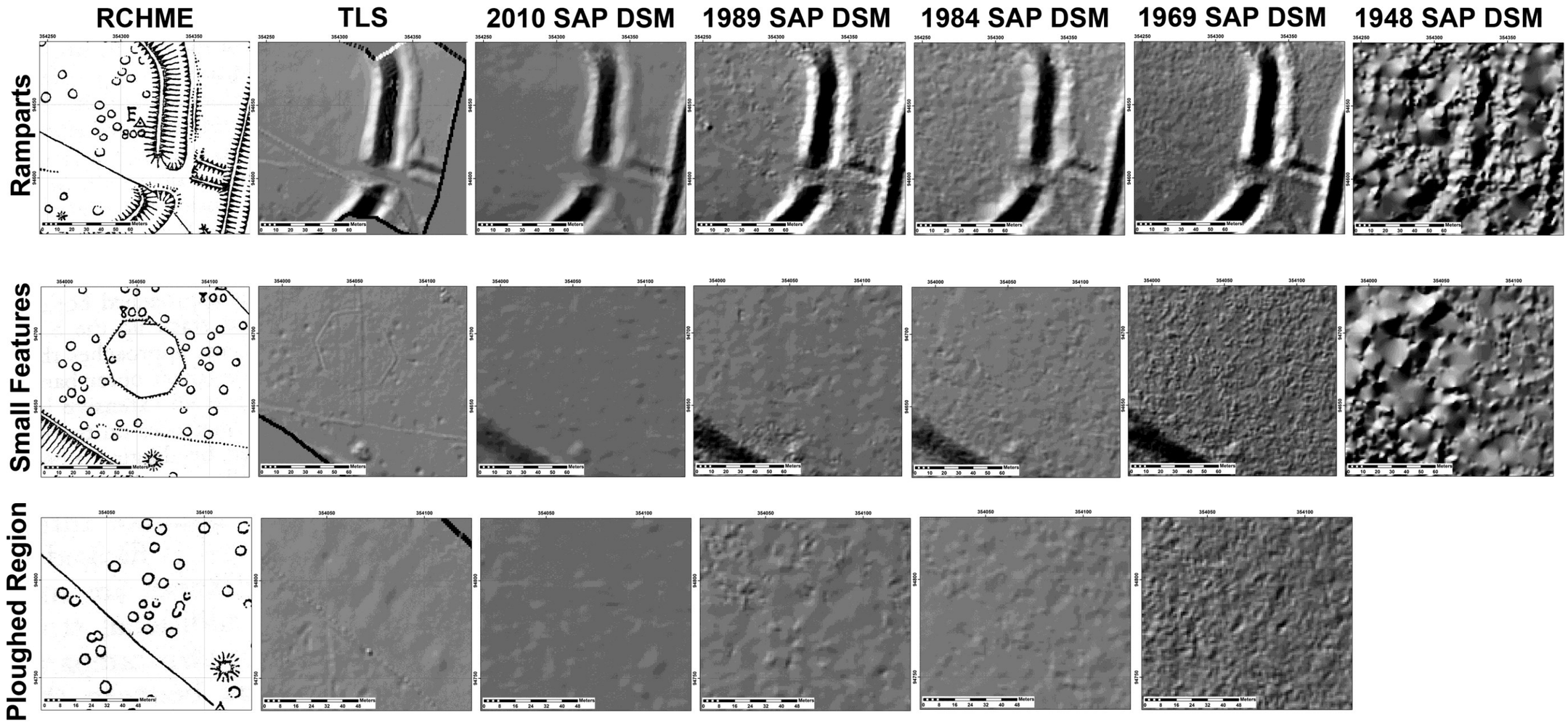

Figure 7.80: Diagram illustrating the information content of the RCHME hachure plan in comparison with data from TLS, ALS and SAP DSMs depicting Eggardon Hillfort. Top: comparison of results across the large earthwork ramparts; Middle: comparison of results showing the most subtle earthworks at Eggardon, namely the linear banks, pits, misshapen barrow and the hexagonal ditch; Bottom: results from the ploughed northern section of the hillfort.

7.8 Discussion

As with the Flowers Barrow case study, it was shown that DSM quality increased as the age of the photography decreased. The best performing SAPs at Eggardon were those from the NMR, which were scanned from negatives using the photogrammetric scanner and the digital photographs from GetMapping Ltd. Archive SAPs digitised with a DTS generated poor results within SocetGXP, resulting in the output of lower point densities from the terrain extraction process. Again, the NN interpolator was required to fill these gaps which in turn produced unrepresentative terrain values. Image-matching issues were also identified in the 2010 GetMapping dataset and the DSMs extracted from the DTS prints. These were exhibited as stripes in the data, although it was suggested that further manipulation of the terrain extraction options would resolve this issue.

Correlation between the TLS data and the SAP DSMs was strong for all of the elevation datasets, although this decreased for slope and further still for aspect. The Moran's I distribution for residual elevation, slope and aspect values were all clustered, indicating that systematic error was still present in the SAP DSMs that had propagated through to their derivatives. Residual values for the Moran's I aspect analysis contain a north/south divide within the significance values, with the majority of statistically significant low values occurring in the northern half, whilst the southern half is characterised by significant high values. It was suggested that vegetation could be the cause, due to the much flatter appearance of the northern section of the hillfort in comparison with the larger tufts of grass in the south. Vegetation was also identified as an influence across the henge monument, particularly as this earthwork had spent a long time covered by gorse.

SD values from the best-performing SAP DSMs indicated that, whilst change may not be as large as suggested by the DoDs, change is occurring within the hillfort and henge regions. Whether this is due to vegetation difference, footfall or damage caused by grazing animals is indeterminate. Profiles extracted from these same SAP DSMs were similar to those generated by the GNSS and the RCHME survey. This is particularly so across earthworks with a more extreme vertical exaggeration, such as the ramparts. However, the results of the breakline assessment indicated that DSMs produced by the archive SAPs were not representative of the RCHME hachure plan, although this was attributed to the difference in survey techniques used to produce the hachure plan as well as the way in which it was georeferenced to match the location of the modern-day DSMs.

7.9 Summary

The results from this chapter confirm that the metric quality of SAP DSMs improves as the age of the imagery decreases, although this is dependent on image quality, scanner properties (i.e.

whether the scanner is photogrammetric or desktop) and the result of the block bundle adjustment in the photogrammetric software.

8 DISCUSSION

8.1 Introduction

This Chapter discusses the major findings from the three results Chapters, which have examined the implications of workflow and a number of variables on photogrammetric DSMs obtained from SAPs (Chapter 7), as well as the effects they have on the archaeological earthworks identified in two case studies (Chapters 8 and 9). Subsequently, the implication of these results for reconstructing archaeological earthwork metrics from SAPs and the impact this could have on the archaeological discipline is discussed.

The aim of this research was to determine whether archive SAPs could be utilised to reconstruct extant, damaged or destroyed archaeology and provide data that can be used to manage and mitigate the loss of this finite resource. It was noted that, in some cases, the only records that exist of archaeological earthworks are hachure plans, which are valuable interpretational tools but they do not provide full metric documentation of these features. Consequently there was potential for the loss of vital information should earthworks have been destroyed with only a subjective record to attest to their existence, or lost without any record at all. Therein lay the question as to whether such data could be regained by utilising archive SAPs.

8.2 Archaeological Implications

This section summarises the archaeological findings from this research and highlights the significant impact that it has upon the archaeological community. A discussion of the considerations necessary for using archive SAPs for archaeological reconstruction is then provided in Section 8.3.

Overall it has been demonstrated that archive SAPs can be used to generate a number of datasets that are utilised by archaeologists to create a 3D record of earthwork form. These data range from DSMs that can be compared to other, modern DSMs to identify regions of change across a monument, as well as breaklines and profiles that describe the form of an earthwork. Breaklines and profiles have been successfully extracted from a number of archive SAPs for each field site, with the former assessed using an empirical approach and the latter visually critiqued.

The recovery of breakline and profile information was identified as being one of the most important requirements of an archaeological survey of earthworks (see Section 1.1.4). As the RCHME hachure surveys are the only records of both Flowers Barrow and Eggardon hillforts, it was important to establish whether SAP, ALS and TLS DSMs could recreate this information or

even improve upon it. This analysis would subsequently be indicative of whether archive SAPs and laser scan datasets would be capable of reconstructing earthworks. As the RCHME plans are the only archaeological surveys that are known to exist of these sites, if both had since been destroyed, these hachure plans would be the only remaining topographic survey from which to generate a reconstruction of these features.

The results of the analysis showed that there was little agreement between the planimetric locations of the RCHME breaklines and the Flowers Barrow TLS DSM (28.823%) or the 2010 SAP DSM of Eggardon Hillfort (15.08%). There are a number of reasons for this that relate to the disparity in the survey methods used to produce each survey. The RCHME county-by-county surveys, conducted between 1920 and 1970 (Payne 2006), are likely to have employed plane tables, alidades and tapes, whilst this research has utilised mass-capture techniques. As discussed in Sections 1.1.3 and 1.1.4, mass-capture techniques can create dense and detailed surveys across smaller areas, whilst this is not possible with manual, analogue methods. As technology has improved, so has the accuracy and precision of measuring instruments (assuming they are used appropriately), which includes the methods with which to geo-reference a survey. Subsequently, there are likely to be disparities between the produces created by using older direct techniques in comparison with newer, mass-capture methods.

A further issue relates to the way in which the RCMHE plans were georeferenced to match the location of the TLS DSM. Each plan was scanned from the originals held at the NMR, which were then scaled and rotated in AutoCAD by the author to fit the extents of the TLS DSMs as best as possible. No steps were taken to warp the RCHME plans to improve upon the position of the RCHME data as the intention was to preserve the integrity of these surveys. The plans were imported into ArcMap for comparison, from which the measures of overall accuracy, as stated above, were obtained. These were employed to signify the value that must be achieved between the best DSM and the remaining SAP and ALS DSMs to indicate that a particular dataset is capable of recreating the same level of breakline detail. By taking this approach, each of the SAPs recreated a greater volume of breakline data in comparison with the best DSM of the area in contrast to the measure of agreement between the best DSM and the RCHME plan.

A visual comparison of the breakline datasets from both Flowers Barrow and Eggardon Hillfort predominantly displayed a convincing representation of such information, with the exception of a small number of SAP DSMs. However, there were discrepancies between each field site and the information content of some of the oldest photography. The 1945 SAPs from Flowers Barrow exhibits convincing breakline structures across the majority of the site, whilst the 1948 data from Eggardon does not display intelligible information in this regard. The reason for this disparity is less likely to be the variation in flying height, which is 2133.6m for Flowers Barrow versus 5080m at Eggardon. This is due to the differing focal lengths used, which were 203.2mm and 508mm respectively, which provided photo-scales of 1:10,500 and 1:10,000. Whilst the photo-scales remain the same, the base to height ratio will differ, which affects the degree of parallax in the imagery. A suitable base-to-height ratio is suggested by Walstra et al. (2004) to be 1:6, and thus it is recommended that archaeologists ascertain this value. This can be

achieved by identifying the approximate position of each photograph's principle point, and locating this position on an OS map. As the flying height can be ascertained by the information strip on the image, or by the information supplied by the NMR, an approximate base-to-height ratio can be calculated.

It was noted that the 1948 Eggardon imagery had been captured whilst the camera was tilted due to the aircraft rolling. The hillfort itself was also situated at the extreme edges of the photographs where lens distortion is at its greatest. Whilst this latter point may also be true of the 1945 photographic strip across Flowers Barrow hillfort, subsequently causing the DSM to lack the extreme western edge of this earthwork, the imagery appears to be vertical and contains greater contrast. Upon examination of Table 4.1 it was also noted that the focal length of the lens was much longer for the 1948 photography, which compensated for the increased height of the aircraft. Therefore any alteration to the orientation of the aircraft would have resulted in a much greater tip and tilt effect in the imagery. Overall, the Flowers Barrow imagery has a much less noisy appearance, which indicates that archaeologists must assess archive SAP DSM data on a site-by-site basis, as the quality of results varies from region to region.

The importance of earthwork and survey scale was identified as a significant consideration in Section 1.1.5 of Chapter 1 because the likelihood of detecting the smallest earthwork within an archaeological site or landscape is dependent on the information content in the survey data. A comparison of the RCHME hachure plans, TLS, SAP DSMs and ALS data, as obtained for the Flowers Barrow case study, was conducted in Section 6.7.3 and Section 7.7.3 for Flowers Barrow and Eggardon Hill respectively. The results conclusively illustrated that the TLS data depicted the information captured in the RCHME surveys and also contained data relating to earthworks that had not been recorded in the hachure plan. As the RCHME plans are the only known surveys of both Flowers Barrow and Eggardon Hillfort, it was suggested that consideration should be given to resurveying earthworks in sites at risk of damage and destruction. This is particularly important for discovering previously unknown features.

Profiles from the ramparts of both Flowers Barrow and Eggardon Hillfort, as well as the henge and barrow earthworks from the latter, were indicative of the performance of SAPs in recreating the variations of elevation across these features. The profiles of the ramparts from both Flowers Barrow and Eggardon Hillfort recreated from the SAP DSMs extracted from photogrammetrically scanned negatives were in excellent agreement with the GNSS profile and that recorded by the RCHME survey. The only exception to this was the 1940s photography, which is further discussed in Section 8.3. Whilst the profiles extracted from the desktop scanned SAP prints did not perform as well on the shallower slopes, particularly at Eggardon Hillfort, they did recreate the steeper slopes. Across the more subtle features, namely the barrow and henge monument at Eggardon Hillfort, the profiles from photogrammetrically scanned SAP negatives were exceptional, illustrating the variation in elevation across both of these features and displaying a high-parity result with the GNSS data.

That the DSMs extracted from archive SAPs can provide data of archaeological utility, albeit accompanied by a number of considerations as outlined in Section 8.3, has huge implications

for the archaeological community and managers of archaeological sites. However there are two different approaches to surveying, as discussed in Section 1.1.4, depending on whether interpretation or a metric record is required. This research has focused on the creation of metric data in the form of DSMs, albeit utilising interpretive hachure plans to validate their archaeological content. As metric information can be obtained from archive SAPs, particularly those obtained from photogrammetrically scanned negatives, as shown in Chapters 6 and 7, it could be argued that interpretive surveys should form the greater fraction of such activity on earthworks. What negates this argument are the issues surrounding the detection of changes to a monument and the identification of smaller features within DSMs obtained from archive SAPs. Change detection has proven to be challenging, particularly with the older photography, whilst smaller features are rarely seen in SAP DSMs. These facets are more easily identified when employing modern technologies that generate dense amounts of data, such as a TLS, which are not thought to facilitate interpretive mapping (Bowden and McOmish 2011; Bowden 1999).

However, as stated in Section 1.1.4 (Chapter 1), hachure plans may provide a planimetric map of a site, but they do not objectively describe the variation in elevation across it. Whilst the RCHME profiles show excellent parity with the DSM data used by this research, these records have only been taken at discreet locations across the site. Subsequently, elevation data is not retrievable from the hachures, including measures of slope as these are purely subjective indicators of slope severity. Further, it has been shown that the breaklines of an RCHME hachure plan do not coincide well with DSMs from SAPs, ALS or TLS. Whilst this information is retrievable from archive SAPs, they cannot be thought of as anti-disaster records because they were not produced with this goal in mind.

Although many of the photogrammetrically scanned SAP DSMs have compared favourably with the GNSS and TLS datasets, showing high correlation between their elevation values but less so between their derivatives, quantification of change has been less productive. Areas that have consistently indicated the occurrence of material accretion or loss have been identifiable in the SAP DSMs but quantifying the amount of loss for management purposes can only be as accurate as the SD of values from the mean which, in some SAP datasets can be large. For example, the 1945 Flowers Barrow SAP DSM has a SD of 1.204m, whilst the SD for the 1948 Eggardon SAP DSM is 2.572m. As the conservation charters and principles advocate regular recording for management, monitoring and understanding (ICOMOS General Assembly 1996, Bassegoda-Nonell et al. 1964), then the collection of metric survey results across areas of risk is to be encouraged and undertaken regularly, as is the generation of interpretive survey, if this is felt necessary.

However, there are a number of important issues that archaeologists must consider prior to working with archive SAPs, which are identified in Section 8.3 below. But the results from both the breakline and profile studies confirm that archaeologists must continue to conduct visual assessments of the data obtained from DSM and not simply rely on empirical analysis. This is not a new concept to the archaeological community as other authors have advocated the same approach (Doneus et al. 2008; Corns and Shaw 2009), albeit with reference to ALS DSMs.

8.3 Archive SAPs: Considerations for Use

Throughout the course of this research, a number of important variables were identified that archaeologists, heritage managers and practitioners must consider prior to working with archive SAPs for archaeological purposes. The influence of many of these variables can be identified prior to undertaking a project with them by visiting the NMR, County Council or any other official body who retain archives of SAPs. By visually examining the photographs and considering the points contained within the following Sections, a high-quality, effective dataset can be obtained.

8.3.1 Age of the Photography

In general it is to be expected that the newer the archival film photography, the more accurate the DSM created from it. The DSMs produced from both the 1945 (Flowers Barrow) and 1948 (Eggardon Hillfort) SAPs were the worst-performing datasets. These photographs were taken with non-metric and smaller-format (i.e. 5x5") cameras that, aside from not having any camera calibration information associated with them, did not include components that had been manufactured to mitigate for distortions. It was also noted that in the 1948 SAPs there was some distortion caused by the aircraft tilting during exposure. As the 1940s imagery was captured by the RAF in the immediate post-WWII era, it is more likely such sorties were flown irrespective of the adverse wind conditions for aerial survey work e.g. cross-winds and/or turbulence. In turn they are less likely to have quality control in place which considered the influence of these conditions on photogrammetry such as the effects of crabbing, tip and tilt on stereo coverage, perspective and parallax. Therefore careful examination of RAF photography from this era should be conducted to note any tip, tilt or crabbing that may be visible, as described in Section 2.2.7.2. In contrast, professional survey companies of the 1950s onwards, flying contract work on behalf of the OS and others, would have been more likely to wait for more favourable wind conditions. Any photography acquired would have been subject to quality control either internally and/or from the respective government agency/Department with photogrammetry in mind. Should the photography have been deemed unsuitable then it would have been disposed of and the sortie re-flown until such time it met the required standards. It is this photography that will have been archived.

The SAPs produced from the late 1960s onwards generated good-quality DSMs, although this observation is dependent upon the photographic material it was scanned from and the type of scanner used to scan it, both of which are discussed in Section 2.2.6.3, whilst experimental results from this research are presented in Section 5.4. As photography from the 1950s was not available no inferences can be made about the SAP data performance from this decade. However, by carefully considering the issues raised within this Section, it will be possible for users of archive SAPs to make an educated decision as to whether an SAP dataset will provide them with usable results.

It is also worth noting that the most recent digital SAP datasets may not always provide the most accurate DSMs. Modern digital imagery used for the Flowers Barrow case study did not out-perform the 1982 SAPs or the 2009 ALS data in terms of its correlation with the TLS DSM. However, the 1982 SAP DSM was manipulated to remove horizontal and vertical offsets by using the TLS data as a template, and thus this process is one of the reasons that has allowed the 1982 SAP DSM to provide the most accurate dataset. The 2010 SAPs used in the Eggardon Hillfort case study performed equally with the 1989 SAPs, each of which returned the same correlation value on comparison with the TLS DSM. This raises the question as to why the 1989 OS imagery, which required digitisation prior to its use, created a superior DSM to that of the latest imagery, namely the 2010 digital photography from GetMapping Ltd.

The suggestion from these findings is that stereo-photography from metric, analogue cameras is still superior to newer, digital cameras, such as the Ultracam that was used to collect the 2009 and 2010 photographs. One of the major differences between these two camera systems is the multiple lens configuration of the panchromatic and “multi-spectral” cameras in the Ultracam system, which utilises 9 CCDs that are subsequently stitched together to create one large image (Wiechert and Gruber 2009). This process is said to create the parallax-free 9 sub-images, along with a system designed to ensure that the linearly arrange CCDs are exposed when their perspective centres are at the same position in the ground control system, otherwise known as ‘synoptic exposure’ (Kraus, 2000 p.145). The image size produced using the panchromatic system equates to 17,310x 11,310 pixels (Microsoft Corp. 2008). However, the images used by this research were created using the colour, or “multi-spectral”, capability and are smaller, namely 5770x3770 pixels. Whilst the pixels size is said to be the same as the panchromatic imagery, namely 6µm (Microsoft Corp. 2008), the value given on the calibration certificate is 18 µm (Vexcel Imaging GmbH 2010). Therefore, the older, analogue imagery contains a greater amount of information per pixel, as indicated by the GSD values given in Table 4.1.

However, it should also be noted that the 2010 imagery was provided in JPEG format, which is a lossy compression file format that had to be converted to a TIFF format for use in SocetGXP. Whether the original images were converted from a TIFF to a JPEG file for easier delivery from the image vendor is unknown. As noted by Axford (2000, p.445), decompressing a JPEG image can introduce artefacts into the imagery, which may have occurred when the images were saved as a TIFF format. This process may have further degraded the 2010 image quality, and thus archaeologists looking to purchase modern aerial photography should investigate whether the suppliers initially captured the aerial photographs in TIFF formats. If so, these are the data to purchase, otherwise any imagery supplied as a JPEG may require conversion to TIFF format using image processing software such as Adobe Photoshop, particularly if using SocetGXP to process the SAPs. Modern APs are also collected primarily for the purpose of orthophoto production, rather than generating topography (i.e. parallel-pair stereo airphotos for the production of contours and DSMs). The production of a DSM via digital photogrammetry is a secondary activity at best. Subsequently, the collection of imagery suitable for orthophotographs dictates the flying height of the aircraft, image overlap and conditions required for optimal survey (i.e. time of day and associated shadow, haze etc.).

8.3.2 Photographic Materials and Scanners

The lifecycle of archive SAPs is often ambiguous, which is problematic given that poor care can damage the photographs, as described in Section 2.2.9. If possible, it is worth asking the archive from which the SAPs come if they can provide any information on their background. It may not be possible to view the original negatives, but it should be possible to see prints. However, the latter may be no indication of the negative quality, as prints are also likely to suffer from similar degradations themselves.

Whilst the age of an SAP dataset has the greatest influence on the quality of the output DSM, the second greatest issue is the combination of photographic material the photograph is scanned from and the type of scanner used to digitise the imagery. Whilst it has not been possible to separate the effects of these two factors, the results from Section 5.4 found that the SAPs scanned from negatives using a photogrammetric scanner will produce the best DSMs. SAPs scanned from prints using a widely available desktop scanner will generate poor-quality DSMs. This result is not unexpected as the photogrammetric scanner is manufactured to reduce geometric distortions in the photographic material by flattening it. However, what it cannot do is remove distortions that are the result of poor care and archival practices. Suggestions as to how this facet of research could be advanced are given in Section 9.1.

Archaeologists should therefore avoid the combination of prints and desktop scanners unless the scanner itself has been characterised to provide a measure of the distortion it introduces into the image. This activity is discussed in Section 9.1 on further work.

8.3.3 Control and Orientation Information

In Section 4.3.1 it was acknowledged that archive SAPs are usually devoid of their associated camera calibration information, whilst collecting GCPs can be challenging. These include the limited site access and changes to identifiable markers in the landscape, which were also discussed in Section 4.3.1

It can be seen from the results presented in Section 5.5 of Chapter 5 and in Chapter 6 that the quality of GCPs influenced both the planimetric and vertical accuracy of the SAP DSMs used for the Flowers Barrow case study. This was illustrated by the need to ‘warp’ a number of SAP DSMs to obtain horizontal congruence with those from the ALS and TLS, as well as address vertical offsets in this data. Utilising GNSS control to perform triangulation is preferable to employing GCPs that have been extracted from other mapping sources, such as the OS 1:1000 MasterMap data and Landmap’s photogrammetric DSM (see Section 4.3.1 in Chapter 4). These mapping sources are not accompanied by accuracy measurements, unlike those from GNSS, and thus it is difficult to identify how far GCPs derived from these sources deviate from their true locations. This research has shown that there is a larger degree of latitude for the SocetGXP

software to alter the location of these GCPs within the accuracy boundaries provided to resolve the bundle adjustment, based upon the horizontal and vertical disparities identified in the SAP DSMs (see Sections 5.5, 6.3 and 7.3). If the accuracy parameters for each image are also large, then the horizontal and elevation offsets found with the DSMs will be significant enough to affect any comparative analysis conducted on them i.e. creating DODs or comparing SAP DSMs to GNSS values.

Planimetric and vertical offsets within the SAP DSMs were addressed by performing a number of steps, including the construction of trend surfaces, as outlined in Section 5.1 in Chapter 5 (see Figure 5.1 and Figure 5.2). Vertical offsets were established by using GNSS data against which to compare the SAP DSM elevations and generating a mean elevation error using the residual differences between each dataset. This mean value was subsequently added to the SAP DSM using the 'Raster Calculator' tool in ArcMap. Planimetric errors that could not be resolved by using SocetGXP were imported into ENVI and warped to fit the dimensions of another DSM, namely the TLS data. This approach raises concerns over the relative accuracy of the DSMs output from archive SAPs using SocetGXP. Whilst the warping procedure addressed this issue, GCP quality is the most likely source of error causing the problem because of the large uncertainties associated with the values taken from other mapping sources. Both of the approaches employed to address horizontal and vertical offsets advocate the use of at least one modern DSM product against which to assess the DSMs obtained from archive SAPs.

It should also be noted that it is very important to select, wherever possible, the appropriate geoid/ellipsoid/spheroid and associated vertical datum in the photogrammetric software. SocetGXP permitted the use of the Ordnance Survey British National Grid (1936) horizontal projection, but does not currently have the ability to use the Ordnance Survey's Mean Sea Level (MSL, at Newlyn, Cornwall) vertical datum and associated Airy spheroid. Instead a geoid model, the Earth Gravitational Model 1996 (EGM96) was used as the next-best option. This introduced errors in the orthometric height of the SAP DSMs. The lack of UK or other European geoids/ellipsoids/spheroids and their associated vertical datums is expected to be addressed in future releases of SocetGXP (BAE Systems 2013, p331).

This research has found that a deficit of exterior orientation information does not always have an influence on the resultant DSMs, as shown in Section 5.3. Archive SAPs that were created by using a non-metric camera, such as the 1940s photographs, produced statistically and visually poor DSMs, as the cameras themselves were not manufactured to be distortion-free, unlike their metric counterparts. The storage conditions of these images, prior to their deposition in the NMR, is unknown, and thus the likelihood of extracting useable archaeological data from such old imagery is unlikely, irrespective of GCP quality. However, many of the photogrammetrically scanned negatives dating from the late 1960s onwards, all of which were devoid of camera calibration data, have produced useable DSMs that, in some cases, have been akin to data expected from ALS, such as the 1989 SAPs from Eggardon Hillfort. It was also possible to extend the examination of orientation data by utilising the latest 2009 SAP

digital imagery taken over Flowers Barrow, which was provided with both camera calibration data and IMU files. The result of performing triangulation with various combinations of IMU orientation data and GCPs resulted in the use of purely the GCPs producing optimal triangulation solutions (see Section 5.3).

For archaeological applications, therefore, the lack of IMU data should not overly concern archaeologists, who should focus on creating the most accurate set of GCPs possible.

8.3.4 Vegetation

The results of the initial investigation into the influence of vegetation on archive SAPs DSM accuracy, given in Section 5.6.3, were inconclusive. The most likely reason for this outcome was human error when visually classifying random points into gorse and grass categories using orthophotographs produced from each SAP epoch. The cause is most likely to be low contrast in some of the orthophotographs. However, the effect of vegetation on DSM elevation values in SAPs was prominent in the discussion relating to the henge monument in the Eggardon Hillfort case study (see Chapter 7). Gorse covered the Eggardon henge monument until the mid-1980s when there was a visually significant reduction in its coverage within the SAPs, which can be easily identified due to the improved image contrast in the SAPs here. The comparison of the SAP DSMs and the TLS data covering this area showed that the photogrammetric process was detecting the offset between these data due to the presence of gorse.

Archaeologists working with archive SAPs should take note of any extensive vegetation covering the area in which they wish to work. Photogrammetry, unlike ALS and TLS, cannot recover any measurement of terrain covered by vegetation and thus it will be included in the resultant DSM. Within these areas breaklines and profiles cannot be reliably extracted. Alternatively, ALS data has been found to penetrate certain types of vegetation. This research examined the performance of ALS across Flowers Barrow in grass and gorse-dominated regions, as discussed in Section 5.6. As expected, the statistical summary provided in Table 5.15 demonstrated that ALS returned favourable ME and SD values within both grass and gorse categories in comparison to the SAP DSMs, with the exception of the 1982 data.

It was also possible to remove the majority of gorse coverage in the TLS scans of Flowers Barrow. Filtering the TLS was not a rapid process and required a methodical approach to removing gorse and other outliers from the data. Subsequently, the TLS data was rasterised and the DSM was interpolated in the same way as the SAP and ALS DSMs, although the software was set to utilise the minimum elevation values rather than the mean to produce the terrain model. This further assisted in the removal of outliers and gorse.

8.3.5 Earthwork Scale

This research examined whether DSMs constructed from archive SAPs could recreate smaller earthworks within each field site. An indication of the survey tools suitable for recording objects of differing size was given in Figure 1.3 and discussed in Section 1.1.3, whilst considerations based upon earthwork size and image scale were provided in Section 1.1.5. Within both Flowers Barrow and Eggardon Hillfort there are a number of smaller earthworks relating to occupation platforms, storage pits and linear features. There are further examples of more subtle features at Eggardon, in the form of a barrow and henge monument. The challenge of detecting these earthworks by using SAP photogrammetry, whose photo scale may not be ideal for detecting them, was a matter for investigation.

As demonstrated in Section 7.7.1 of Chapter 7, the profile results across both the barrow and henge monuments was very encouraging, and illustrated high parity between the TLS and GNSS and the archive SAP datasets digitised with a photogrammetric scanner. Very little evidence of the occupation platforms at Flowers Barrow, or the pits and linear features at Eggardon hillfort were present, however, in any dataset other than the TLS DSM. Subsequently, it is recommended that TLS should be utilised for recording sites where these subtle features are to be found, especially if the site is at risk of damage or loss.

8.3.6 Photogrammetry versus Laser Scanning

Prior to conducting this research it was assumed that TLS and ALS would produce more accurate data than the photogrammetric DSMs from modern and archival SAPs. However, this research has shown that, in some cases, archive SAPs have produced a superior result to ALS data when compared to the TLS. This was particularly the case with the SAP DSMs from the Flowers Barrow case study (see Chapter 6), which demonstrated that the 1982 SAP DSM was the most accurate, closely followed by the 2009 ALS based upon their RMSE scores, as shown in Table 8.1. Based upon the alterations made to the 1982 DSM, these are a contributory factor to their success.

It is interesting to note that a large elevation offset was still found to be present between the Flowers Barrow ALS and TLS data of 0.561m, whereby the ALS was lower than the TLS by this amount. It was postulated that the cause of this offset was the presence of gorse, in which the largest amount of noise was located at the eastern end of the hillfort and along the north-facing rampart slopes. This result is despite attempting to remove gorse from the TLS data using the minimum elevation values during interpolation, with the last return values utilised for creating the ALS DSM. The most likely cause of this offset is the density of the gorse preventing many of the laser pulses from the ALS and possibly the TLS reaching the ground surface. As noted in

Section 8.3.4, careful consideration has to be given to both photogrammetric and laser scanning datasets when working in areas covered by dense vegetation.

In the Eggardon case study, presented in Chapter 7, the 2010 digital SAPs were the most comparable to the TLS data, whilst both the 1984 and 1989 SAP DSMs performed favourably. Whilst the elevation values were identical, differences between the SAP DSMs were found within the first order derivatives, as shown in Table 8.1. However, as the TLS data was utilised as the baseline against which to compare the SAP DSMs, the clearest comparison between the SAP DSMs and the TLS data is based upon the transect profile study provided in Section 7.7.1.4 and shown in Figure 7.75. As discussed in Section 7.7.1.4, there is some disparity between the TLS and SAP DSM datasets, although the 2010 SAP DSM is similar irrespective of the elevation offset. Many of the other SAP DSMs are not as smooth as the TLS profile, although variation in vegetation could cause this disparity, particularly as there are stands of grass across the southern half of the hillfort where the majority of these differences occur (see Figure 7.27). None of the desktop scanned prints produced satisfactory results.

Based upon the results presented by this research, photogrammetry has produced exceptional results from archive SAPs in comparison with ALS and TLS data. Based upon this discovery and the continual advancement of digital photogrammetry towards a more automated workflow, it is likely that archaeologists will enthusiastically adopt photogrammetry once more. As discussed in Section 2.2.3, SfM is gaining popularity in archaeology and other disciplines, which is founded upon the less expensive means by which to create a DSM in comparison with laser scanning technologies, particularly TLS. Although SfM and low-cost alternatives provide somewhat of a push-button, immediate ‘product’ solution in comparison with higher-cost, specialist photogrammetric software, these more accessible programmes have not been produced to principally work with standard, parallel-pair stereo-photography. They are designed to work with lower-resolution, converging, multiple overlapping images although this does not preclude their application to assessing the outputs they generate for archive SAPs.

However, dedicated digital photogrammetry software, such as SocetGXP, are designed for use with SAPs, albeit the modern product, which are accompanied by the requisite metadata such as camera calibration certificates and either exterior orientation information, ground control, or both. Woking with archive SAPs requires careful consideration as they are often lacking camera calibration data, although this can be calculated to some degree by SfM and other digital photogrammetry software. Exterior orientation information is also rarely available, whilst the collection of ground control can be hindered by changes in the landscape across the 70 year period for which SAPs are available in the UK.

Flowers Barrow Hillfort							
Date Flown	**Scale**	**Ground Sample Distance (m)**	**Original Media**	**Elevation RMSE (m)**	**Slope RMSE (m)**	**Aspect RMSE (m)**	**Ranking**
27/03/1945	1:10500	0.110	Negative	1.205	9.184	48.057	**5th**
26/08/1968	1:10000	0.118	Negative	0.759	8.410	45.046	**4th**
16/04/1982	1:8000	0.081	Negative	0.248	3.538	20.453	**1st**
27/09/2009		0.150	Digital	0.626	7.852	31.629	**3rd**
Nov 2009 (ALS)		1 point/m^2	Raw Points	0.561	6.087	28.097	**2nd**

Eggardon Hillfort							
Date Flown	**Scale**	**Ground Sample Distance (m)**	**Original Media**	**Elevation RMSE (m)**	**Slope RMSE (m)**	**Aspect RMSE (m)**	**Ranking**
22/01/1948	1:10000	0.104	Negative	2.577	18.915	70.195	**7th**
09/03/1948	1:10000	0.114	Negative	2.577	18.915	70.195	**7th**
02/04/1969	1:7500	0.072	Negative	0.392	4.408	52.721	**4th**
18/04/1969	1:7500	0.072	Negative	0.392	4.408	52.721	**4th**
19/10/1972	1:12000	0.122	PRINT	0.680	7.301	61.599	**6th**
13/04/1984	1:8000	0.078	Negative	0.459	3.366	48.572	**3rd**
20/07/1989	1:8200	0.084	Negative	0.168	3.027	44.074	**2nd**
21/9/1997	1:10000	0.104	PRINT	0.533	6.748	62.546	**5th**
23/05/2010		0.150	Digital	0.321	2.328	39.223	**1st**

Eggardon Henge Monument							
Date Flown	**Scale**	**Ground Sample Distance (m)**	**Original Media**	**Elevation RMSE (m)**	**Slope RMSE (m)**	**Aspect RMSE (m)**	**Ranking**
22/01/1948	1:10000	0.104	Negative	5.002	20.088	71.997	**7th**
09/03/1948	1:10000	0.114	Negative	5.002	20.088	71.997	**7th**
02/04/1969	1:7500	0.072	Negative	0.334	2.154	38.490	**3rd**
18/04/1969	1:7500	0.072	Negative	0.334	2.154	38.490	**3rd**
19/10/1972	1:12000	0.122	PRINT	0.640	4.476	57.933	**6th**
13/04/1984	1:8000	0.078	Negative	0.698	2.069	35.825	**2nd**
20/07/1989	1:8200	0.084	Negative	0.249	2.281	39.850	**4th**
21/9/1997	1:10000	0.104	PRINT	0.353	4.180	59.117	**5th**
23/052010		0.150	Digital	0.131	2.385	38.970	**1st**

Table 8.1: Rankings of the SAP and ALS DSMs from Flowers Barrow and Eggardon Hillfort and henge monument in comparison with the TLS DSM.The best result is highlighted in green, the second-best result is showin orange and the third-best result is highlighted in red.

Dedicated photogrammetric software, such as SocetGXP offered the flexibility to alter many of the accuracy parameters within the photogrammetric workflow to generate the best possible outcome: something that cannot be achieved with SfM. One of the outputs from this research was therefore a workflow diagram that informs the archaeological community of the steps taken in SocetGXP to obtain the best results from using archive SAPs in the software.

For laser scanning technologies to retain their popularity with archaeologists, they will have to provide a significant cost-benefit in comparison with SfM, which has demonstrated its flexibility in providing airborne and terrestrial datasets. UAVs and the lighter payload of compact digital cameras offer aerial views of a site at higher resolutions than those available from off-the-shelf EA ALS data, as well as the opportunity for archaeologists to produce their own datasets with low-cost equipment. What is questionable, though, is the performance of SfM software in comparison with high-end products, such as SocetGXP. This issue will be further considered in Section 9.1.

8.4 Summary

This chapter has discussed the archaeological implications of the results obtained from utilising archive SAPs for creating earthwork metrics. Based upon these results and the practical issues encountered during the research, a list has been created that highlights the considerations archaeologists should acknowledge when utilising archive SAPs for reconstructing earthworks.

9 CONCLUSIONS

This research has confirmed the ability of archive SAPs to provide metric data for reconstructing archaeological earthworks that have been damaged or destroyed. Based upon the results presented in Chapters 6 and 7 it has been demonstrated that it is possible to obtain DSMs from which interpretive information, in the form of breaklines and profiles, can also be extracted. However, a number of recommendations were identified from the experiments conducted on a number of variables that affect the analysis of archive SAPs using digital photogrammetric techniques (see Chapter 5). Along with the results presented in the case studies from Chapters 6 and 7, and discussed in Chapter 8, these recommendations are:

Age of archive SAPs

- Larger format metric cameras produce better results than those from smaller-format, non-metric cameras. As older imagery is taken with smaller-format cameras, it generates the poorest results (Section 2.2.2.5, Chapters 6 and 7);
- SAPs from metric, analogue cameras are still superior to those from newer, digital cameras (Chapter 6);
- Ensure the base-to-distance ratio is close to or exactly 1:6 to ensure sufficient parallax (Section 8.2);
- Avoid using SAPs that contain excessive tip, tilt or crabbing (Section 2.2.7.2, Section 8.2);
- Modern, digital SAPs should be provided by panchromatic, not multi-spectral, cameras (Section 8.3.1).

Photographic Materials and Scanners

- Photogrammetric scans from negatives provide the best results, whilst scans from desktop scanners and print materials produce poor results (Section 5.4, Chapter 5);
- Avoid the combination of prints and desktop scanners, unless the scanner has been characterised (Section 5.4.4, Chapter 5);
- Ensure digitised and digital photography is provided in a lossless format i.e. TIFF, EWC etc. (Section 8.3.1).

Control and Orientation Information

- Lack of camera calibration and exterior orientation information is not an issue (Section 5.3);

- Obtain the most accurate GCPs as possible (Section 5.5);
- It is imperative to ensure that there is sufficient SAP coverage of the area of interest to guarantee a suitable number of retrospective GCPs can be created.

Vegetation

- Areas covered by significant amounts of vegetation should be avoided (Section 5.6, Chapters 6 and 7).

Earthwork Scale

- Reconstruction of archaeological earthworks is scale-dependent (Section 7.7.1);
- Small earthworks will not be reconstructed (Section 7.7.1.3).

Photogrammetry versus Laser Scanning

- The terrain extraction strategy will influence the accuracy of a DSM (Section 5.2);
- Whilst a repository of EA ALS exists and can be superior to SAPs, coverage is not as extensive as SAPs nor is the same temporal resolution available as SAPs (Section 2.3.3.1).

Further to these recommendations, there is a suggestion relating to the general analysis of archive SAP DSMs that have been noted throughout this research. Analysis must include more than one method of assessment. Simply relying on the results from only the summary statistics or from the examination of one first-order derivative will not reveal the full picture as regards the spatial distribution of outliers or whether there is one outlier skewing a whole set of results. Nor should the importance of visual examination of the DSMs and their derivatives be understated (Sections 2.2.4, 3.4.3.1 and 3.4.4 and Chapters 5, 6 and 7).

9.1 Future Work

The discussion of current archaeological practices using SAPs (see Section 2.2.3 in Chapter 2), including SfM, and the identification of variables that are known to influence the quality of a DSM extracted from archive SAPs (see Section 8.3) have revealed a number of areas that require further investigation. This is particularly the case as regards the SAP prints that were digitised using a desktop scanner. As stated in Section 5.4.4 of Chapter 5, the influence of photographic print materials on DSM quality and the scanner used to digitise them could not be separated. Two experiments could be performed to clarify this issue, with the first designed to

characterise the desktop scanner using a glass plate. This would provide a measure of the distortion characteristics of the scanner optics and facilitate the removal of their influence from the digitised image. Secondly, to determine the influence that photographic materials have on the DSM, it would be of utility to scan one epoch of SAPs in both negative and print form with the photogrammetric and desktop scanner. As the latter option was declined by the NMR, further consultations with other EH have been initiated to discuss the possibilities of conducting a combined research project to address this problem.

This research has been conducted over areas that are still extant yet have been recorded using only interpretive survey techniques. To extend testing of the reconstruction abilities of archive SAPs it would be useful to select an area that has been surveyed using metric techniques, designed as a preservation-by-record exercise, which has subsequently been destroyed. It would also be of utility to repeat this research but with the focus not on creating DSMs but extracting vector data within the photogrammetric software. This process has been applied to historic buildings that have been recorded using stereo-photography with photogrammetry in mind, particularly for disaster-recovery applications (Dallas et al. 1995). However, this has not been undertaken for earthworks using archive SAPs for extracting breaklines and profiles.

As alluded to in Section 5.2, there are a number of settings within SocetGXP that may influence the quality of DSM output by the software. Whilst LPS has been examined by researchers to establish the influence of a number of variables within the software have on DSM quality (Gooch 1999; Gooch et al. 1999), this process could be repeated with the settings in SocetGXP.

As regards the issue of SfM, a small number of archaeologists have begun to investigate the quality of DSM outputs from SfM with those of other survey methods, such as TSTs and ALS, although further work is necessary to fully determine SfM performance against higher-end software packages, such as SocetGXP. Whilst the processing algorithms employed by SocetGXP are not completely transparent, there are many more options for controlling the variables involved in the photogrammetric process than there are with the more opaque workflows employed by SfM manufacturers. Whether the outputs from SfM can provide DSMs akin to those produced using archive SAPs in SocetGXP and by a TLS system is a matter for further consideration and investigation.

By discussing the history of aerial photography, it is evident that there are a number of archives worldwide that preserve this important resource. The opportunity therefore exists to investigate the ability of international archive SAPs for reconstructing archaeological monuments and sites, and discovering what variables affect the quality of the DSMs they can generate. Whilst authors such as Aguilar et al. (2013) and Doneus et al. (2014) have examined archive SAPs in Spain and Norway respectively, there are other archives beyond these countries that can be utilised for this research. It is important to investigate these repositories, as each will have its own issues, both in terms of access and the quality of the data held within them, which includes the archives of declassified satellite imagery, such as CORNOA. As this research has discovered by using two field sites based within the UK county of Dorset, different results can be obtained from archive SAPs that are not far away from one another, let alone in another country.

10 REFERENCES

Abramov, O. and McEwen, A. 2004. An evaluation of interpolation methods for Mars Orbiter Laser Altimeter (MOLA) data. *International Journal of Remote Sensing*, 25(3), 669-676.

Adams, J. and Chandler, J., 2002. Evaluation of Lidar and Medium Scale Photogrammetry for Detecting Soft-Cliff Coastal Change. *The Photogrammetric Record*, 17 (99), 405-418.

Aguilar, F. J., Aguilar, M. A. and Agüera, F., 2007. Accuracy assessment of digital elevation models using a non-parametric approach. *International Journal of Geographical Information Science*, 21 (6), 667-686.

Aguilar, M., Aguilar, F. and Negreiros, J., 2009. Self-Calibration Methods for Using Historical Aerial Photographs with Photogrammetric Purposes. *In: Ingegraf XXI* Lugo.

Aguilar, M. A., Aguilar, F. J., Fernández, I. and Mills, J. P., 2013. Accuracy Assessment of Commercial Self-Calibrating Bundle Adjustment Routines Applied to Archival Aerial Photography. *The Photogrammetric Record*, 28 (141), 96-114.

Ainsworth, S., Bowden, M., McOmish, D. and Pearson, T., 2007. *Understanding the Archaeology of Landscapes: A guide to good recording practice*. Swindon: English Heritage.

Al-kheder, S., Al-shawabkeh, Y. and Haala, N., 2009. Developing a documentation system for desert palaces in Jordan using 3D laser scanning and digital photogrammetry. *Journal of Archaeological Science*, 36 (2), 537-546.

Albertz, J., 2001, 18th - 21st September. *ALBRECHT MEYDENBAUER – PIONEER OF PHOTOGRAMMETRIC DOCUMENTATION OF THE CULTURAL HERITAGE.* Paper presented at the 18th International Symposium CIPA, Potsdam, Germany.

Altmaier, Angela and Kany, Christoph. 2002. Digital surface model generation from CORONA satellite images. *ISPRS Journal of Photogrammetry and Remote Sensing*, 56, 221–235.

Anders, N. S., Seijmonsbergen, A. C. and Bouten, W., 2011. Segmentation optimization and stratified object-based analysis for semi-automated geomorphological mapping. *Remote Sensing of Environment*, 115 (12), 2976-2985.

Anderton, M. and Went, D., 2002. Turning the Plough: Loss of a landscape legacy, *Conservation Bulletin* (pp. 52-55). Swindon: English Heritage.

ASC Scientific, No Date. *Stereoscopes and Stereo Photographs* [online]. ASC Scientific. Available from: http://www.ascscientific.com/stereos.html [Accessed 3rd July 2014]

Aslib, 1993. *NAPLIB (National Association of Aerial Photographic Libraries) Directory of Aerial Photographic Collections in the United Kingdom*

Association of Local Government Archaeological Officers, No Date. *Planning Advice* [online]. ALGO. Available From: http://www.algao.org.uk/localgov/planning [Accessed 23rd November 2013]

Aston, M. and Rowley, T., 1974. *Landscape Archaeology: An Introduction to Fieldwork Techniques on Post-Roman Landscapes*. Newton Abbot: David and Charles.

Austin, T. and Mitcham, J., 2007. Preservation and Management Strategies for Exceptionally Large Data Formats: 'Big Data'. 2010 (12/01/2010).

Australia ICOMOS, 1999. Burra Charter. 2009 (08/12/09).

Axford, N., 2000. Theory of image formation. *In:* Jacobson, R. E., Ray, S. F., Attridge, G. G. and Axford, N., eds. *The Manual of Photography*. Ninth Edition. Focal Press.

BAE Systems, 2007. *Next-Generation Automatic Terrain Extraction (NGATE): Innovation in the cost-effective derivation of elevation data from imagery* [online]. BAE Systems. Available from: http://www.geospatialexploitationproducts.com/docs/education/white_papers/wp_ngate.pdf [Accessed 29th January 2014].

BAE Systems, 2009. *SOCET SET User's Manual Version 5.5*. BAE Systems.

BAE Systems, 2013. *SOCET GXP® User's Manual Version 4.1*. BAE Systems.

BAE Systems. 2014. *Resources – Case Studies* [online]. BAE Systems. Available from: http://www.geospatialexploitationproducts.com/content/resources/case-studies [Accessed 27th May 2014]

Baily, B., Collier, P., Farres, P., Inkpen, R. and Pearson, A., 2003. Comparative assessment of analytical and digital photogrammetric methods in the construction of DEMs of geomorphological forms. *Earth Surface Processes and Landforms*, 28 (3), 307-320.

Baltsavias, E. P. and Waegli, B., 1996. Quality analysis and calibration of DTP Scanners.

Banning, E. B., 2002. *Archaeological Survey*. New York: Kluwer Academic/Plenum Publishers.

Barazzetti, L., Binda, L., Scaioni, M. and Taranto, P., 2011. Photogrammetric survey of complex geometries with low-cost software: Application to the `G1' temple in Myson, Vietnam. *Journal of Cultural Heritage*, In Press, Corrected Proof.

Barber, D., Bryan, P., Austin, T., Blake, B., Bohler, W., Carty, A., Cooper, M., Cromwell, T., Dowman, I., Horne, P., Hunter, G., Leith, A., May, K., Ravi, F. and Stonehoue, P., 2007. 3D Laser Scanning for Heritage. In Heritage, E. (Ed.). Swindon: English Heritage.

Barber, M., 2011. *A History of Aerial Photography and Archaeology: Mata Hari's glass eye and other stories*. Swindon: English Heritage.

Barnes, I., 2003. Aerial Remote-sensing Techniques Used in the Management of Archaeological Monuments on the British Army's Salisbury Plain Training Area, Wiltshire, UK. *Archaeological Prospection*, 13 (10), 83-90.

Barrand, N.E., Murray, T., Hames, T.D., Barr, S.L. and Mills, J.P. 2009. Optimizing photogrammetric DEMs for glacier volume change assessment using laser-scanning derived ground-control points. *Journal of Glaciology*, 55(189), 106-116.

Bassegoda-Nonell, J., Benavente, L., Boskovic, D., Daifuku, H., Flores, C., Gazzola, P., Langberg, H., Lemaire, R., Matteucci, M., Merlet, J., Pane, R., Pavel, S. C. J., Philippot, P., Pimentel, V., Plenderleith, H., Redig de Campos, D., Sonnier, J., Sorlin, F., Stikas, E., Tripp, G., de Vrieze, P. L., Zachwatovicz, J. and Zbiss, M. S., 1964. The Venice Charter. In ICOMOS (Ed.). Venice.

Bater, C. W. and Coops, N. C., 2009. Evaluating error associated with lidar-derived DEM interpolation. *Computers and Geosciences*, 35 (2), 289-300.

Beck, Anthony, Philip, Graham, Abdulkarim, Maamoun and Donoghue, Danial. 2007. Evaluation of Corona and Ikonos high resolution satellite imagery for archaeological prospection in western Syria. *Antiquity*, 81, 161-175.

Beck, A., 2011. Archaeological applications of multi/hyper-spectral data - challenges and potential. *In:* Cowley, D. C., ed. *Remote Sensing for Archaeological Heritage Management.* EAC Occasional Paper No.5. Brussels: Europae Archaeologia Consilium and Association Internationale sane But Lucratif, 87-98.

Bedford, J. and Papworth, H. (Eds.), 2009. *Measured and Drawn: Techniques and practice for the metric survey of historic buildings (second edition)*. Swindon: English Heritage.

Bedford, J., Pearson, T. and Thomason, B., 2011. *Traversing the Past*. Swindon: English Heritage.

Bennett, R., Welham, K., Hill, R. A. and Ford, A., 2012. A Comparison of Visualization Techniques for Models Created from Airborne Laser Scanned Data. *Archaeological Prospection*, 19 (1), 41-48.

Beraldin, J.A., Blais, F., abd Lohr, U. 2010. Laser Scanning Technology. *In:Vosselman, G, and Mass, H.G. (eds.) Airborne and Terrestrial Laser Scanning*. Caithness, Scotland: Whittles Publishing, 1-44.

Bernardini, F., Sgambati, A., Montagnari Kokelj, M., Zaccaria, C., Micheli, R., Fragiacomo, A., Tiussi, C., Dreossi, D., Tuniz, C. and De Min, A., 2013. Airborne LiDAR application to karstic areas: the example of Trieste province (north-eastern Italy) from prehistoric sites to Roman forts. *Journal of Archaeological Science*, 40 (4), 2152-2160.

Bettess, F., 1998. *Surveying for Archaeologists*. Cleadon, Sunderland: Penshaw Press.

Bevan, A. and Conolly, J., 2011. Terraced fields and Mediterranean landscape structure: An analytical case study from Antikythera, Greece. *Ecological Modelling*, 222 (7), 1303-1314.

Bewley, R. and Raczkowski, W., 2002. *Aerial Archaeology. Developing Future Practice*. NATO.

Bewley, R. H., 2003. Aerial survey for archaeology. *Photogrammetric Record*, 18 (104), 273-292.

Bewley, R. H., Crutchley, S. P. and Shell, C. A., 2005. New light on an ancient landscape: lidar survey in the Stonehenge World Heritage Site. *Antiquity*, 79 (305), 636-647.

Biswas, A. and Si, B.C. 2013. Model Averaging for Semivariogram Model Parameters. *In: Grundas, S. and Stepniewski, A. (eds). Advances in Agrophysical Research*. Available from: http://www.intechopen.com/books/advances-in-agrophysical-research/model-averaging-for-semivariogram-model-parameters [Accessed 28th May 2014]

Blachut, T. J., 1995. Uuno Vilho Helava at the National Research Council of Canada from December 1953 to September 1965. *ISPRS Journal of Photogrammetry and Remote Sensing*, 50 (6), 7-13.

Blak, T. A., 2007. DEM Quality Assessment. *In:* Maune, D. F., ed. *Digital Elevation Model Technologies and Applications: The DEM Users Manual.* 2nd Edition. Bethesda: American Society for Photogrammetry and Remote Sensing, 425-448.

Blake, B., 2010. Bill Blake Heritage Documentation Kite Aerial Photography. 2011 (24th February).

Blake, B., 2014. The slippery slope: CAD hachures. *billboyheritagesurvey*. 13th March. Available from: http://wp.me/pYvo7-1ZR [Accessed 14th March 2014]

Blom ASA, 2012. *Aerial Survey* [online]. Blom ASA. Available from: http://www.blomasa.com/main-menu/products-services/aerial-survey.html [Accessed 10th June 2014].

Bogacki, M., Giersz, M., Przadka-Giersz, P., Malkowski, W. and Misiewicz, K., 2010. *GPS RTK Mapping, Kite Aerial Photogrammetry, Geophysical Survey and GIS Based Analysis of Surface Artifact Distribution at the Pre-Hispanic Site of the Castillo de Huarmey, North Coast of Peru.* Paper presented at the 30th EARSeL Symposium: Remote Sensing for Science, Education and Natural and Cultural Heritage, Paris, France.

Bohler, W. and Marbs, A., 2002. *3D Scanning Instruments.* Paper presented at the Proceedings of CIPA WG6 Scanning for Cultural Heritage Recording, Corfu, Greece.

Bollandsås, O. M., Risbøl, O., Ene, L. T., Nesbakken, A., Gobakken, T. and Næsset, E., 2012. Using airborne small-footprint laser scanner data for detection of cultural remains in forests: an experimental study of the effects of pulse density and DTM smoothing. *Journal of Archaeological Science*, 39 (8), 2733-2743.

Bowden, M., 1999. *Unravelling The Landscape: An Inquisitive Approach to Archaeology*. Stroud: Tempus.

Bowden, M., 2002. *With Alidade and Tape: Graphical and plane table survey of archaeological earthworks*. Swindon: English Heritage.

Bowden, M. and McOmish, D., 2012. A British Tradition? Mapping the Archaeological Landscape. *Landscapes*, 12 (2), 20-40.

Britain From Above, No Date. *About the project* [online]. English Heritage, RCAHMS, RCAHMW, HLF,. Available from: http://www.britainfromabove.org.uk/about-project [Accessed 11th April 2013].

Brookes, A. J., 1975. *Photo Reconnaissance*. Shepperton, Surrey: Ian Allan Ltd.

Brooks, G., 1992. The Burra Charter: Australia's Methodology for Conserving Cultural Heritage. *Places*, 8 (1), 84-88.

Bruno, F., Bruno, S., De Sensi, G., Luchi, M.-L., Mancuso, S. and Muzzupappa, M., 2009. From 3D reconstruction to virtual reality: A complete methodology for digital archaeological exhibition. *Journal of Cultural Heritage*, In Press, Corrected Proof.

Brunsden, D., 1996. *Landslides of the Dorset Coast: some unresolved questions.* Paper presented at the Proceedings of the Ussher Society.

Brunsden, D. (Ed.). 2003. *The Official Guide to the Jurassic Coast: Dorset and East Devon's World Heritage Coast (A Walk Through Time)*. Wareham: Coastal Publishing.

Bryan, P., Blake, B., Bedford, J., Barber, D. and Mills, J., 2009. *Metric Survey Specifications for Cultural Heritage*. Second. English Heritage.

Bryan, P. G. and Chandler, J. H., 2008. *Cost-Effective Rock-Art Recording withing a Non-Specialist Environment.* Paper presented at the Silk Road for Information from Imagery. Proceedings of ISPRS 2008, Beijing, China.

Buchanan, M., Christison, D. and Anderson, J. 1905. Report on the Society's excavation of Ruogh Castle on the Antonine vallum. *Proceedings of the Society of Antiquities of Scotland*, 39.

Bulmer, M. G., 2003. *Principles of Statistics*. Dover Publications Ltd.

Burrough, P. A. and McDonnell, R. A., 1998. *Principles of Geographic Information Systems*. 2nd Edition. Oxford: OUP Oxford.

Calkin, J. B., 1948. *The Isle of Purbeck in the Iron Age.* Paper presented at the Proceedings of the Dorset Natual History and Archaeological Society.

Camarda, M., Guarnieri, A., Milan, N. and Vettore, A., 2010. *Health monitoring of complex structure using TLS and photogrammetry.* Paper presented at the The International Archives of the Photogrammetry, Remote Sensing and Spatial Information Sciences, Newcastle-upon-Tyne.

Canciani, M., Gambogi, P., Romano, F. G., Cannata, G. and Drap, P., 2003. *Low Cost Digital Photogrammetry for Underwater Archaeological Site Survey and Artifact Insertion. The Case Study of the Dolia Wreck in Secche Della Meloria, Livorno, Italia.* Paper presented at the Vision Techniques for Architectural and Archaeological Archives. International Workshop WG/V4 & INTCOM III/V, Ancona, Italy.

Canham, R. and Chippindale, C., 1988. Managing for Effective Archaeological Conservation: The Example of Salisbury Plain Military Training Area, England. *Journal of Field Archaeology*, 15 (1), 53-65.

Carey, C. J., Brown, T. G., Challis, K. C., Howard, A. J. and Cooper, L., 2006. Predictive modelling of multiperiod geoarchaeological resources at a river confluence: a case study from the Trent-Soar, UK. *Journal of Archaeological Prospection*, 13 (4), 241-250.

Casana, J., Cothren, J. and Kalayci, T., 2012. Swords into Ploughshares: Archaeological Applications of CORONA Satellite Imagery in the Near East. *Internet Archaeology*, 32. Available from: http://intarch.ac.uk/journal/issue32/2/1.html [Accessed 23rd Februaru 2014]

Casana, J. and Cothren, J., 2008. Stereo analysis, DEM extraction and orthorectification of CORONA satellite imagery: archaeological applications from the Near East. *Antiquity*, 82 (317), 732-749

Cavers, G., 2007. Towards an Integrated 3D Archaeological database - Keiss Foreshore, Caithness. 2011 (29th March).

Celikoyan, T. M., Altan, M. O., Kemper, G. and Toz, G., 2003. *Evaluation of a Theatre by Using Low-Altitude Aerial and Terrestrial Photogrammetry.* Paper presented at the New Perspectives to Save Cultural Heritage, Antalya, Turkey.

Centre for Photogrammetric Training, No Date. *History of Photogrammetry* [online]. Ferris State University, Michigan. Available from: http://spatial.curtin.edu.au/local/docs/HistoryOfPhotogrammetry.pdf [Accessed 11th June 2014].

Challis, K., Priestnall, G., Gardner, A., Henderson, J. and O'Hara, S. 2004. Corona Remotely-Sensed Imagery in Dryland Archaeology: The Islamic City of al-Raqqa, Syria. *Journal of Field Archaeology*, 29 (1-2), 139-153

Challis, K., 2006. Airborne laser altimetry in alluviated landscapes. *Journal of Archaeological Prospection*, 13 (2), 103-127.

Challis, K. and Howard, A. J., 2006. A review of trends within archaeological remote sensing in alluvial environments. *Journal of Archaeological Prospection*, 13 (4), 231-240.

Challis, K., Carey, C. J., Kincey, M. and Howard, A. J., 2008a. *Analysis of the Effectiveness of Airborne Lidar Intensity for Predicting Organic Preservation Potential of Waterlogged Deposits: Stage 2 Report*. University of , Birmingham Archaeology.

Challis, K., Howard, A. J., Kincey, M., Carey, C., Moscrop, D. and Hill, T., 2008b. *Analysis of the Efectiveness of Airborne Lidar Intensity for Predicting Organic Preservation Potential of Waterlogged Deposits: Stage 1 Report*. University of Birmingham, Birmingham Archaeology.

Challis, K., Kokalj, Z., Kincey, M., Moscrop, D. and Howard, A. J., 2008c. Airborne lidar and historic environment records. *Antiquity*, 82 (318), 1055-1064.

Challis, K., Kincey, M., and Howard, A. J. 2009. Airborne Remote Sensing of Valley Floor Geoarchaeology using Daedalus ATM and CASI. *Archaeological Prospection*. 16, 17-33.

Challis, K., Forlin, P. and Kincey, M., 2011. A generic toolkit for the visualization of archaeological features on airborne LiDAR elevation data. *Archaeological Prospection*, 18 (4), 279-289.

Chandler, J., 1989. *The Acquisition of Spatial Data from Archival Photographs and Their Application to Geomorphology.* (PhD). City University, London.

Chandler, J. 1999. Effective Application of Automated Digital Photogrammetry for Geomorphological Research. *Earth Surface Processes and Landforms*, 24, 51-63.

Chandler, J. H., Bryan, P. and Fryer, J. G., 2007. The Development And Application Of A Simple Methodology For Recording Rock Art Using Consumer-Grade Digital Cameras. *The Photogrammetric Record*, 22 (117), 10-21.

Chang, K. T. and Tsai, B. W., 1991. The effect of DEM resolution on slope and aspect mapping. *Cartography and Geographical Information Systems*, 18, 69-77.

Chapman, H., 2006. *Landscape Archaeology and GIS*. Stroud, Gloucestershire: The History Press Ltd.

Chapman, H., Adcock, J. and Gater, J., 2009. An approach to mapping buried prehistoric palaeosols of the Atlantic seaboard in Northwest Europe using GPR, geoarchaeology and GIS and the implications for heritage management. *Journal of Archaeological Science*, 36 (10), 2308-2313.

Chiabrando, F., Costamanga, E., Rinaudo, F. and Spano, A., 2010. *Very Close Nadiral Images: A Proposal for Quick Digging Survey.* Paper presented at the Close Range Image Measurement Techniques, Newcastle upon Tyne, UK.

Chiabrando, F. and Spanò, A., 2009. Digital wide scale orthoprojections and mapping from low-height aerial images. *Journal of Cultural Heritage*, 10 (Supplement 1), e49-e58.

Clark, J., Darlington, J. and Fairclough, G. (Eds.), 2003. *Chapter 5 - Reading and Understanding: Landscape as Information*. Heide, Germany: EPCL.

Clark, K., 2003. *Informed Conservation: Understanding Historic Buildings and Their Landscapes for Conservation*. English Heritage.

Clarke, T. A. and Fryer, J. G., 1998. The development of camera calibration methods and models. *Photogrammetric Record*, 16 (91).

Colley March, H. and Solly, H. S., 1901. *A Critical and Material Examination of the Hill Fortress called Eggardun.* Paper presented at the Proceedings of the Dorset Natural History and Antiquarian Field Club.

Colosi, F., Fangi, G., Gabrielli, R., Orazi, R., Angelini, A. and Bozzi, C. A., 2009. Planning the Archaeological Park of Chan Chan (Peru) by means of satellite images, GIS and photogrammetry. *Journal of Cultural Heritage*, 10 (Supplement 1), e27-e34.

Cooper, M. I., La Pensee, A. and Parsons, J. B., 2006. *The Use of Laser Scanning and Rapid Manufacturing Techniques for Museum Exhibitions.* Paper presented at the The e-volution of Information Communication Technology in Cultural heritage. Where Hi-Tech Touches the Past: Risks and Challenges for the 21st Century., Nicosia, Cyprus.

Corns, A. and Shaw, R., 2009. High resolution 3-dimensional documentation of archaeological monuments & landscapes using airborne LiDAR. *Journal of Cultural Heritage*, 10 (Supplement 1), e72-e77.

Costantino, D., Angelini, M. G. and Caprino, G., 2010. *Laser Scanner Survey of an Archaeological Site - Scala di Furno (Lecce, Italy).* Paper presented at the Close Range Image Measurement Techniques., Newcastle upon Tyne, UK.

Council of Europe, 1992. *European Convention on the Protection of the Archaeological Heritage.* Council of Europe.

Cowell, Ben, 2009. The evolution of conservation principles, *Conservation Bulletin*, 60, 5-6. Swindon: English Heritage

Cowley, D. C. and Gilmore, S. M. D., 2005. Some Observations on the Nature of Aerial Survey. *In:* Brophy, K., and Cowley, D., eds. *From The Air: Understanding Aerial Archaeology.* Stroud, Gloucestershire: Tempus.

Crawford, O. G. S., 1928. *Air Survey and Archaeology*. HMSO.

Crow, P., 2004. Trees and Forestry on Archaeological sites in the UK: A review document.

Crutchley, S., 2006. Light detection and ranging (lidar) in the Witham Valley, Lincolnshire: an assessment of new remote sensing techniques. *Archaeological Prospection*, 13 (4), 251-257.

Crutchley, S., 2009. Ancient and modern: Combining different remote sensing techniques to interpret historic landscapes. *Journal of Cultural Heritage*, 10 (Supplement 1), e65-e71.

Crutchley, S. and Crow, P., 2010. The Light Fantastic: Using airborne laser scanning in archaeological survey. Swindon: English Heritage.

Crutchley, S. 2013. Using lidar data – drawing on 10 year's experience at English Heritage. *In: Opitz, R.S. and Cowley, D.C. (eds) Interpreting Archaeological Topography: 3D Data, Visualisation and Observation*. Occasional Publication of the Aerial Archaeology Research Group No.5. Oxford: Oxbow Books

Dallas, R. W. A., Kerr, J. B., Lunnon, S. and Bryan, P. G., 1995. Windsor Castle: Photogrammetric and Archaeological Recording After The Fire. *The Photogrammetric Record*, 15 (86), 225-240.

Darvill, T. and Fulton, A., 1998. *Monuments at Risk Survey 1995*. Bournemouth and London: Bournemouth University and English Heritage.

Davies, B. 2013. *Precision and accuracy in glacial geology* [online]. AntarcticGlaciers.org. Available from: http://www.antarcticglaciers.org/glacial-geology/dating-glacial-sediments-2/precision-and-accuracy-glacial-geology/ [Accessed 29th May 2014].

Dawson, P. C. and Levy, R. M., 2005. A Three-Dimensional Model of a Thule Inuit Whale Bone House. *Journal of Field Archaeology*, 30 (4), 443-455.

Dawson, P. C., Levy, R. M., Arnold, C., Oetelaar, G. and Lacroix, D., 2008. Documenting Mackenzie Inuit Architecture using 3D Laser Scanning. *In: Computer Applications in Archaeology*: BAR International Series.

De Reu, J., De Smedt, P., Herremans, D., Van Meirvenne, M., Laloo, P. and De Clercq, W., 2014. On introducing an image-based 3D reconstruction method in archaeological excavation practice. *Journal of Archaeological Science*, 41 (0), 251-262.

De Reu, J., Plets, G., Verhoeven, G., De Smedt, P., Bats, M., Cherretté, B., De Maeyer, W., Deconynck, J., Herremans, D., Laloo, P., Van Meirvenne, M. and De Clercq, W., 2013. Towards a three-dimensional cost-effective registration of the archaeological heritage. *Journal of Archaeological Science*, 40 (2), 1108-1121.

Deegan, A. 1999. *A short guide to aerial photography, interpretation and mapping* [online]. Alison Deegan. Available from: http://freespace.virgin.net/paul.alice/guide/fguide.html [Accessed 10th June 2014].

DEFRA, 2002. *The Futurecoast Project*.

Dellepiane, M., Dell'Unto, N., Callieri, M., Lindgren, S. and Scopigno, R., 2013. Archeological excavation monitoring using dense stereo matching techniques. *Journal of Cultural Heritage*, 14 (3), 201-210.

Devereux, B. J., Amable, G. S. and Crow, P., 2008. Visualisation of LiDAR terrain models for archaeological feature detection. *Antiquity*, 82 (316), 470-479.

Devereux, B. J., Amable, G. S., Crow, P. and Cliff, A. D., 2005. The potential of airborne lidar for detection of archaeological features under woodland canopies. *Antiquity*, 79 (305), 648-660.

DiBiase, D. and Dutton, J.A. 2014. *Systematic vs. Random Errors* [online]. Pennsylvania State University. Available from: https://www.e-education.psu.edu/natureofgeoinfo/c5_p5.html [Accessed 28th May 2014]

Díez, A., Arozarena, A., Ormeño, S., Aguirre, J., Rodríguez, R. and Sáenz, A., 2008. *Fusion and Optimization of LiDAR and Photogrammetric Technologies and Methodologies for Cartographic Production.* Paper presented at the Silk Road for Information from Imagery. ISPRS Congress 2008. Proceedings of Commission I, Beijing, China.

Doneus, M., 2013. Openness as Visualization Technique for Interpretative Mapping of Airborne Lidar Derived Digital Terrain Models. *Remote Sensing*, 5 (12), 6427-6442.

Doneus, M., Briese, C., Fera, M. and Janner, M., 2008. Archaeological prospection of forested areas using full-waveform airborne laser scanning. *Journal of Archaeological Science*, 35 (4), 882-893.

Doneus, M. and Neubauer, W., 2003. *Digital Recording of Stratigraphic Excavations.* Paper presented at the [Enter the Past] CAA, Vienna.

Dormor, I., 1999. Current Planning Policies and Legislation for Historical Rural Landscapes. *In:* Grenville, J., ed. *Managing the Historic Rural Landscape.* London: Routledge, 43-56.

Dowman, I.J. 1996. Fundamentals of Digital Photogrammetry. *In: Atkinson, K.B. ed. Close Range Photogrammetry and Machine Vision*. Scotland: Whittles Publishing, 52-77.

Downman, I.J. and Muller, J.P. 2011. *Evaluation of Spaceborne DEMs: A Guide to Methodology*. Committee on Earth Observation Satellites, Terrain Mapping Subgroup.

Drap, P., Seinturier, J., Scaradozzi, D., Gambogi, P., Long, L. and Gauch, F., 2007. *Photogrammetry for Virtual Exploration of Underwater Archaeological Sites.* Paper presented at the AntiCIPAting the Future of the Cultural Past, Athens, Greece.

Ducke, B., Score, D. and Reeves, J., 2011. Multiview 3D reconstruction of the archaeological site at Weymouth from image series. *Computers & Graphics*, 35 (2), 375-382.

Eisenbeiss, H. and Sauerbier, M., 2011. Investigation of UAV systems and flight modes for photogrammetric applications. *The Photogrammetric Record*, 26 (136), 400-421.

English Heritage, 2008. *Conservation Principles: Policies and Guidance for the Sustainable Management of the Historic Environment* [online]. Swindon: English Heritage. Available from: http://www.english-heritage.org.uk/publications/conservation-principles-sustainable-management-historic-environment/conservationprinciplespoliciesguidanceapr08web.pdf [Accessed 3rd July 2013]

English Heritage, 2012a. *Long Internal Report: Eggardon Hill Camp*. English Heritage,.

English Heritage, 2012b. *Long Internal Report: Lynchets W of Eggardon Hill Farm*. English Heritage.

English Heritage, No Date. *Monument Class Descriptions* [online]. English Heritage. Available from: http://www.eng-h.gov.uk/mpp/mcd/index.htm [Accessed 27th October 2014].

English Heritage, No Date-a. *Aerofilms* [online]. English Heritage. Available from: http://www.english-heritage.org.uk/professional/archives-and-collections/nmr/archives/photographs/aerofilms/ [Accessed 23rd March 2013].

English Heritage, No Date-b. *Our Photographic Collections* [online]. English Heritage. Available from: http://www.english-heritage.org.uk/professional/archives-and-collections/nmr/archives/photographs/ [Accessed 23rd March 2013].

Entec UK Ltd, Quarry Products Association, British Marine Aggregate Producers Association and British Geological Survey, 2006. *Planning4Minerals: A Guide on Aggregates*. Shrewsbury: British Geological Survey and Natural Environment Research Council.

Entwistle, J. A., McCaffrey, K. J. W. and Abrahams, P. W., 2009. Three-dimensional (3D) visualisation: the application of terrestrial laser scanning in the investigation of historical Scottish farming townships. *Journal of Archaeological Science*, 36 (3), 860-866.

Environment Agency. 2014. *About us* [online]. Geomatics Group. Available from: https://www.geomatics-group.co.uk/GeoCMS/AboutUs.aspx [Accessed 3rd January 2014].

Eppich, R. and Chabbi, A., 2006. How Does Hi-tech Touch the Past? *In:* Ioannides, M., Arnold, D., Niccolucci, F., and Mania, K., eds. *The e-volution of Information Communication Technology in Cultural Heritage. Where Hi-Tech Touches the Past: Risks and Challenges for the 21st Century.* Nicosia, Cyprus: Archaeolingua. 94-99.

ESRI, 2008. ArcGIS 9.3 Desktop Help. Spatial Analyst: Neighbourhood Filters.

ESRI, 2012. ArcGIS 10.1 Desktop Help. How IDW works.

Field, A., 2005. *Effect Sizes: Null Hypothesis Significance Testing (NHST)* [online]. Available from: http://www.statisticshell.com/docs/effectsizes.pdf [Accessed 21st November02013].

Fisher, P. F. and Tate, N. J., 2006. Causes and consequences of error in digital elevation models. *Progress in Physical Geography*, 30 (4), 467-489.

Florinsky, I. V., 1998. Accuracy of local topographic variables derived from digital elevation models. *International Journal of Geographical Information Science*, 12 (1), 47-61.

Forde-Johnston, J., 1976. *Hillforts of the Iron Age in England and Wales. A survey of the surface evidence*. Liverpool University Press.

Fryer, J. G., 1996. Camera Calibration. *In:* Atkinson, K. B., ed. *Close Range Photogrammetry and Machine Vision.* Scotland: Whittles Publishing,, 156-180.

Fryer, J. G., Chandler, J. H. and El-Hakim, S. F., 2005. *Recording and modelling an aboriginal cave painting: with or without laser scanning?* Paper presented at the Proceedings of the ISPRS Working Group V/4 Workshop. 3D-ARCH 2005: Virtual Reconstruction and Visualization of Complex Architectures, Mestre-Venice, Italy.

Fugro, 2014. *Aerial Mapping* [online]. Fugro. Available from: http://www.fugro.com/services/survey/geospatial-services/aerial-mapping [Accessed 21st May 2014]

Fujii, Y., Fodde, E., Watanabe, K. and Murakami, K., 2009. Digital photogrammetry for the documentation of structural damage in earthen archaeological sites: The case of Ajina Tepa, Tajikistan. *Engineering Geology*, 105 (1–2), 124-133.

Gale, J., 2010. *Prehistoric Dorset*. Stroud: The History Press, Tempus Publishing Ltd.

Galiatsatos, N., Donoghue, D.N.M, and Philip, G. 2005. *An evaluation of the stereoscopic capabilities of CORONA declassified spy satellite image data*. Paper presented at the 25th EARSeL Symposium: Workshop on 3D Remote Sensing, Porto, Portugal.

Gallagher, J. M. and Josephs, R. L., 2008. Using LiDAR to Detect Cultural Resources in a Forested Environment: an Example from Isle Royale National Park, Michigan, USA. *Archaeological Prospection*, 15 (3), 187-206.

Gallant, J. C. and Wilson, J. P., 2000. Primary Topographic Attributes. *In:* Wilson, J. P., and Gallant, J. C., eds. *Terrain Analysis. Principles and Practice.*: John Wiley & Sons Inc.

Gallay, M., Lloyd, C. D., McKinley, J. and Barry, L., 2013. Assessing modern ground survey methods and airborne laser scanning for digital terrain modelling: A case study from the Lake District, England. *Computers & Geosciences*, 51 (0), 216-227.

Gao, J. A. Y., 1997. Resolution and accuracy of terrain representation by grid DEMs at a micro-scale. *International Journal of Geographical Information Science*, 11 (2), 199-212.

Garcia-Lázaro, F. J., Sala-Ballester, P. and Farjas-Abadía, M., 2012. Morphometric analysis of engravings from photogrammetric point cloud data. *Archeologia e Calcolatori*, 23, 135-150.

Gascoyne, A., 2006. *Conservation Management of the Rural Historic Environment in Essex. Action 3C: Archaeological Strategies for Towns and Rural Settlements.* Essex County Council Historic Environment Branch.

Geomatics Group, 2010. *LiDAR Quality Control Report, Project: PM_0204 Coastal Monitoring Programme. Survey Area: P_6695 Ringstead Bay to Durlston Head*. Channel Coast Observatory: Environment Agency.

Gomez-Lahoz, J. and Gonzalez-Aguilera, D., 2009. Recovering traditions in the digital era: the use of blimps for modelling the archaeological cultural heritage. *Journal of Archaeological Science*, 36 (1), 100-109.

Gonga-Saholiariliva, N., Gunnell, Y., Petit, C. and Mering, C. 2011. Techniques for quantifying the accuracy of gridded elevation models and form mapping uncertainty in digital terrain analysis. *Progress in Physical Geography*, 35(6), 739-764.

Gonzalez, R. C. and Woods, R. E., 1992. *Digital Image Processing*. 3rd Edition. Prentice Hall.

Gooch, M. 1999. *Accuracy optimisation and error detection in automatically generated elevation models derived using digital photogrammetry.* (PhD). Loughborough University.

Gooch, M.J., Chandler, J.H. and Stojic, M. 1999. Accuracy assessment of digital elevation models generated using the Erdas Imagine Orthomax Digital Photogrammetric System. *Photogrammetric Record*, 16(93), 519-531.

Goossens, R., De Wulf, A., Bourgeois, J. Wouter, G. and Willems, T. 2006. Satellite imagery and archaeology: the example of CORONA in the Altai Mountains. *Journal of Archaeological Science*, 33 (6), 745-755.

Goudie, A. and Brunsden, D., 1997. *Classic Landforms of the East Dorset Coast*. Sheffield: Geographical Association.

Green, Kevin. 2002. Archaeology: An Introduction. Fourth Edition. Abingdon: Routledge.

Green, S., Bevan, A. and Shapland, M., 2014. A comparative assessment of structure from motion methods for archaeological research. *Journal of Archaeological Science*, 46 (0), 173-181.

Grinsell, L. V., 1959. *Dorset Barrows*. Dorchester: Dorset Natural History and Archaeological Society.

Guarnieri, A., Vettore, A., Pirotti, F., Menenti, M. and Marani, M., 2009. Retrieval of small-relief marsh morphology from Terrestrial Laser Scanner, optimal spatial filtering, and laser return intensity. *Geomorphology*, 113 (1-2), 12-20.

Guidi, G.C. and Salvagno, G.L. 2010. Reference intervals as a tool for total quality management. *Biochemia Medica*, 20(2), 165-172.

Gulyaev, S. A. and Buckeridge, J. S., 2004. Terrestrial Methods for Monitoring Cliff Erosion in an Urban Environment. *Journal of Coastal Research*, 20 (3), 871-878.

Hall, G., Groves, K., Ogle, R., Spiers, D. and Runciman, C., 2003. *NMR Archives: An Overview of the Aerial Photograph Collections of the NMR*. Swindon: National Monuments Record.

Hanks, N., 2012. Internal Long Report for Monument Legacy number 21942. Record of Scheduled Monuments. Field Monument Warden's Site Synopsis: English Heritage.

Harding, D. 2012. *Iron Age Hillforts in Britain and Beyond*. Oxford: OUP.

Harmon, J. M., Leone, M. P., Prince, S. D. and Snyder, M., 2006. Lidar for Archaeological Landscape Analysis: A Case Study of Two Eighteenth-Century Maryland Plantation Sites. *American Antiquity*, 71 (4), 649-670.

Hart, M., 2009. *Dorset and East Devon: Landscape and Geology*. Marlborough, Wiltshire: The Crowood Press Ltd.

Hassani, M. and Carswell, J. 1992. Transition from Analogue to Digital Photogrammetry. *EARSeL Advances in Remote Sensing*, 1(3) VII.

Hatna, E. and Benenson, I. 2012. The Schelling Model of Ethnic Residual Dynamics: Beyond the Integrated – Segregated Dichotomy of Patterns. *Journal of Artificial Societies and Social Simulation*, 15(1), 6.

Hauser, K., 2008. *Bloody Old Britain*. London: Granta Books.

Heipke, C. 1997. Automation of interior, relative and absolute orientation. *ISPRS Journal of Photogrammetry & Remote Sensing*, 52, 1-19.

Hesse, R., 2010. LiDAR-derived local relief models-a new tool for archaeological prospection. *Archaeological Prospection*, 17 (2), 67-72.

Hetherington, D., German, S., Cannon, D., Chisholm, N. and Tegzes, T., 2007. Accurately representing a complex estuarine environment using terrestrial lidar. *In: Challenges for Earth Observation: Remote Sensing and Photogrammetry Society Annual Conference* Newcastle Upon Tyne: Remote Sensing and Photogrammetry Society.

Hodgson, M. E., Jensen, J., Raber, G., Tullis, J., Davis, B. A., Thompson, G. and Schuckman, K., 2005. An Evaluation of Lidar-derived Elevation and Terrain Slope in Leaf-off Conditions. *Photogrammetric Engineering & Remote Sensing,*, 71 (7), 817-823.

Höhle, J. and Höhle, M., 2009. Accuracy assessment of digital elevation models by means of robust statistical methods. *ISPRS Journal of Photogrammetry & Remote Sensing*, 64 (4), 398-406.

Horn, B. K. P., 1981. *Hill shading and the reflectance map.* Paper presented at the Proceedings of the IEEE.

Horne, P. D., 2009. *A Strategy for the National Mapping Programme*. York: English Heritage.

Howard, A. J., Brown, A. G., Carey, C. J., Challis, K., Cooper, L. P., Kincey, M. and Toms, P., 2008. Archaeological resource modelling in temperate river valleys: a case study from the Trent Valley, UK. *Antiquity*, 82 (318), 1040-1054.

Howard, P., 2007. *Archaeological Surveying and Mapping: Recording and Depicting the Landscape*. Oxford: Routledge.

Huggett, Richard John., 2007. *Fundamentals of Geomorphology*. Second Edition. Abingdon: Routledge.

Hullo, F., Grussenmeyer, P. and Fares, S., 2009. Photogrammetry and dense stereo matching approach applied to the documentation of the cultural heritage site of Kilwa (Saudi Arabia). *International Archives of Photogrammetry, Remote Sensing and Spatial Information Sciences*, XXXVIII-3.

Hunter, G., Cox, C. and Kremer, J., 2006. *Development of a Commerical Laser Scanning Mobile Mapping System - Streetmapper.* Paper presented at the The Future of Remote Sensing, Antwerp, Belgium.

Hutchins, J., 1861. *The History and Antiquities of The County of Dorset. Volume 1*. 3rd.

ICOMOS General Assembly, 1996. *Principles for the Recording of Monuments, Groups of Buildings and Sites*, Sofia, Bulgaria 5-9 October.

Iwahashi, J. and Pike, R. J., 2007. Automated classifications of topography from DEMs by an unsupervised nested-means algorithm and a three-part geometric signature. *Geomorphology*, 86 (3–4), 409-440.

Jacobson, R. E., Ray, S. F., Attridge, G. G. and Axford, N., 2000. *The Manual of Photography*. Ninth Edition. Focal Press.

James, M.R., and Robson, S., 2014. Mitigating systematic error in topographic models derived from UAV and ground-based image networks. *Earth Surface Processes and Landforms*, doi: 10.1002/esp.3609.

Januchowski, S. R., Pressey, R. L., VanDerWal, J. and Edwards, A., 2010. Characterizing errors in digital elevation models and estimating the financial costs of accuracy. *International Journal of Geographical Information Science*, 24 (9), 1327-1347.

Jasiewicz, J. and Stepinski, T. F., 2013. *Geomorphons* — a pattern recognition approach to classification and mapping of landforms. *Geomorphology*, 182 (0), 147-156.

Jenness, J. 2012. *Repeating Shapes for ArcGIS* [online]. Jenness Enterprises. Available from: http://www.jennessent.com/arcgis/repeat_shapes.htm [Accessed 11th June 2014].

Johnson, K. M. and Ouimet, W. B., 2014. Rediscovering the lost archaeological landscape of southern New England using airborne light detection and ranging (LiDAR). *Journal of Archaeological Science*, 43 (0), 9-20.

Jones, B., 1985. Introduction. *In: Macready, S. and Thompson, F.H. (eds) Archaeological Field Survey in Britain and Abroad*. Vol. Occasional Paper (New Series) VI. London: The Society of Antiquaries of London, 1-7.

Jones, K. H., 1998. A comparison of algorithms used to compute hill slope as a property of the DEM. *Computers and Geosciences*, 24, 315-323.

Keevill, G. D. and Linford, N., 1998. Landscape with Gardens: Aerial, Topographical and Geophysical Survey at Hamstead Marshall, Berkshire. *In: Pattison, P., ed. There by Design: Field Archaeology in Parks and Gardens : Papers Presented at a Conference Organised by the Royal Commission on the Historical Monuments of England and the Garden History Society.* Archaeopress.

Kennie, T. J. M. and McKay, W. M., 1987. Monitoring of geotechnical processes by close range photogrammetry. *In:* Culshaw, M. G., Bell, F. G., Cripps, J. C., and O'hara, M., eds. *Planning and Engineering Geology.* Geological Society Engineering Geology Special Publication, 163-170.

Kienzle, S., 2004. The Effect of DEM Raster Resolution on First Order, Second Order and Compound Terrain Derivatives. *Transactions in GIS*, 8 (1), 83-111.

Kincey, M. and Challis, K., 2010. Monitoring fragile upland landscapes: The application of airborne lidar. *Journal for Nature Conservation*, 18 (2), 126-134.

Konecny, G., 1985. The International Society for Photogrammetry and Remote Sensing - 75 Years Old, or 75 Years Young. *Photogrammetric Engineering & Remote Sensing,*, 51 (7), 919-933.

Koutsoudis, A., Vidmar, B. and Arnaoutoglou, F., 2013. Performance evaluation of a multi-image 3D reconstruction software on a low-feature artefact. *Journal of Archaeological Science*, 40 (12), 4450-4456.

Kuna, M. and Adelsbergerova, D., 1995. Prehistoric location preferances: an application of GIS to the Vinorsky potok project, Bohemia, the Czech Republic. *In:* Lock, G., and Stancic, Z., eds. *Archaeology and geographical information systems: a European perspective.* London: Taylor and Francis, 117-131.

Kvamme, K. L., Ernenwein, E. G. and Markussen, C. J., 2006. Robotic total station for microtopographic mapping: an example from the Northern Great Plains. *Archaeological Prospection*, 13 (2), 91-102.

Lambers, K., Eisenbeiss, H., Sauerbier, M., Kupferschmidt, D., Gaisecker, T., Sotoodeh, S. and Hanusch, T., 2007. Combining photogrammetry and laser scanning for the recording and modelling of the Late Intermediate Period site of Pinchango Alto, Palpa, Peru. *Journal of Archaeological Science*, 34 (10), 1702-1712.

Leica Geosystems AG, 2011. *Leica ScanStation C10* [online]. Heerbrugg, Switzerland. Available from: http://hds.leica-geosystems.com/downloads123/hds/hds/ScanStation%20C10/brochures/Leica_ScanStation_C10_Brochure_en.pdf [Accessed 11th June 2014]

Leica Geosystems AG, 2012. *Leica Viva GNSS GS15 receiver Datasheet* [online]. Heerbrugg, Switzerland. Available from: http://www.leica-geosystems.co.uk/downloads123/zz/gpsgis/Viva%20GNSS/brochures-datasheet/Leica_Viva_GNSS_GS15_receiver_DS_en.pdf [Accessed 1st June 2014]

Leica Geosystems AG, 2014. *Targets* [online]. Heerbrugg, Switzerland. Available from: http://hds.leica-geosystems.com/en/Targets_19143.htm [Accessed 11th June 2014]

Le Pard, G., 2011. *Dorset Then and Now From the Air*. Dorset Books.

Lemmens, M., 1999. *Quality Description Problems of Blindly Sampled DEMs.* Paper presented at the Proceeding of the International Symposium on Spatial Data Quality.

Lerma, J. L., Navarro, S., Cabrelles, M. and Villaverde, V., 2010. Terrestrial laser scanning and close range photogrammetry for 3D archaeological documentation: the Upper

Palaeolithic Cave of Parpallo as a case study. *Journal of Archaeological Science*, 37 (3), 499-507.

Lerones, P. M., Fernández, J. L., Gil, Á. M., Gómez-García-Bermejo, J. and Casanova, E. Z., 2009. A practical approach to making accurate 3D layouts of interesting cultural heritage sites through digital models. *Journal of Cultural Heritage*, In Press, Corrected Proof.

Letellier, R., 2007. *Recording, Documentation, and Information Management for the Conservation of Heritage Places: Guiding Principles*. Los Angeles: The Getty Conservation Institute.

Li, Z., Zhu, Q. and Gold, C., 2005. *Digital terrain Modeling: Principles and Methodology*. Boca raton, Florida: CRC Press.

Lichti, D. and Skaloud, J., 2010. Registration and Calibration. *In:* Vosselman, G., and Maas, H.-G., eds. *Airborne and Terrestrial Laser Scanning.* Caithness, Scotland: Whittles Publishing.

Lillesand, T., Kiefer, R. W. and Chipman, J., 2008. Basic Principles of Photogrammetry. *In: Remote Sensing and Image Interpretation.* Sixth Edition. John Wiley & Sons, 123-188.

Lim, M., Petley, D. N., Rosser, N. J., Allison, R. J., Long, A. J. and Pybus, D., 2005. Combined Digital Photogrammetry and Time-of-Flight Laser Scanning for Monitoring Cliff Evolution. *The Photogrammetric Record*, 20 (110), 109-129.

Lim, M., Rosser, N. J., Allison, R. J. and Petley, D. N., 2010. Erosional processes in the hard rock coastal cliffs at Staithes, North Yorkshire. *Geomorphology*, 114 (1-2), 12-21.

Linder, W., 2009. *Digital Photogrammetry: A practical Course*. Berlin: Springer.

Llobera, M., 1996. Exploring the topography of mind: GIS, social space and archaeology. *Antiquity*, 70 (269), 612-622.

Lloyd, C. D., 2007. *Local Models for Spatial Analysis*. Boca Raton: CRC Press.

Lloyd, C. D. and Atkinson, P. M., 2002. Deriving DSMs from LiDAR data with kriging. *International Journal of Remote Sensing*, 23 (12), 2519-2524.

Lobb, M., Krawiec, K., Howard, A. J., Gearey, B. R. and Chapman, H. P., 2010. A new approach to recording and monitoring wet-preserved archaeological wood using three-dimensional laser scanning. *Journal of Archaeological Science*, 37 (12), 2995-2999.

Lock, G., 2003. *Using Computers in Archaeology: Towards Virtual Pasts*. Routledge.

Macdonald, A. 1996. *Mapping the World: History of the Directorate of Overseas Surveys, 1946-85*. Stationary Office Books.

Maune, D. F., Kopp, S. M., Crawford, C. A. and Zervas, C. E., 2007. Introduction. *In:* Maune, D. F., ed. *Digital Elevation Model Technologies and Applications: The DEM Users Manual, 2nd Edition.* Bethesda, Maryland: The American Society for Photogrammetry and Remote Sensing.

May, V. J. 2003. The Dorset Coast: Peveril Point to Furzy Cliff. *In:* May, V. J., and Hansom, J. D. eds. *Coastal Geomorphology of Great Britain* Vol. Geological Review Series No. 28. Peterborough: Joint Nature Conservation Committee, 640.

McCarthy, J., 2014. Multi-image photogrammetry as a practical tool for cultural heritage survey and community engagement. *Journal of Archaeological Science*, 43 (0), 175-185.

Millard, K., Burke, C., Stiff, D. and Redden, A., 2009. Detection of a Low-Relief 18th-Century British Siege Trench Using LiDAR Vegetation Penetration Capabilities at Fort Beausejour-Fort Cumberland National Historic Site, Canada. *Geoarchaeology-an International Journal*, 24 (5), 576-587.

Miller, P., 2007. *A robust surface matching technique for coastal geohazard monitoring.* (PhD). Newcastle University.

Miller, P., Mills, J. and Bryan, P., 2008a. Scanning for change: assessing coastal erosion at Whitby Abbey Headland. *Research News*, (Number 9), 4-7.

Miller, P., Mills, J., Edwards, S., Bryan, P., Marsh, S., Mitchell, H. and Hobbs, P., 2008b. A robust surface matching technique for coastal geohazard assessment and management. *ISPRS Journal of Photogrammetry and Remote Sensing*, 63 (5), 529-542.

Mills, J. and Barber, D., 2007. Rapid mapping techniques in coastal environments: monitoring the coastline. In Surveyors, R. I. O. C. (Ed.). London: RICS.

Minár, J. and Evans, I. S., 2008. Elementary forms for land surface segmentation: The theoretical basis of terrain analysis and geomorphological mapping. *Geomorphology*, 95 (3–4), 236-259.

Mitchell, H., 2007. Fundamentals of photogrammetry. *In:* Fryer, J., Mitchell, H., and Chandler, J., eds. *Applications of 3D Measurement from Images.* Caithness, Scotland: Whittles Publishing.

Monuments Men Foundation, 2013. *The Heroes* [online]. Available from: http://www.monumentsmenfoundation.org/the-heroes?id=285 [Accessed 22nd April02013].

Mozas-Calvache, A. T., Perez-Garcia, J. L., Cardenal-Escarcena, F. J., Mata-Castro, E. and Delgado-Garcia, J., 2012. Method for photogrammetric surveying of archaeological sites with light aerial platforms. *Journal of Archaeological Science*, 39, 521-530.

Murphy, P., Thackray, D. and Wilson, E., 2009. Coastal Heritage and Climate Change in England: Assessing Threats and Priorities. *Conservation and Management of Archaeological Sites*, 11 (1), 9-15.

National Parks Service, 2010. HABS Guidelines. 2011 (30th March).

National Trust, No Date. *Conservation Principles* [online]. National Trust. Available from: http://tinyurl.com/nmeljzd [Accessed 3rd July 2013]

National Trust, 2004. *The Cerne Giant & Dorset Hill-Forts: Their Past Revealed*. Charmouth, Dorset: National Trust.

Natural England, 2009. *Farming for the Historic Environment* [online]. Natural England. Available from: http://www.helm.org.uk/upload/pdf/Stewardship.pdf?1265813638 [Accessed 24th March 2012].

NCAP. 2008. *A future for TARA – The Aerial Reconnaissance Archives* [online]. NCAP. Available from: http://www.rcahms.gov.uk/a-future-for-tara-the-aerial-reconnaissance-archives.html [Accessed 4th May 2014]

NCAP, 2012. *NCAP Digitisation Policy* [online]. NCAP. Available from: http://ncap.org.uk/sites/default/files/NCAP%20DIGITISATION%20POLICY_20120601.pdf [Accessed 26th May 2013]

NCAP, No Date-a. *History of the Collection* [online]. NCAP. Available from: http://ncap.org.uk/about-ncap/history-of-the-collection [Accessed 26th May 2013]

NCAP, No Date-b. *Preservation and Conservation* [online]. NCAP. Available from: http://ncap.org.uk/about-ncap/our-work/preservation-and-conservation [Accessed 26th May 2013]

Nesbit, R. C., 2003. *Eyes of the RAF: A History of Photo-Reconnaissance*. Stroud: Sutton Publishing Limited.

Neubauer, W., 2004. GIS in archaeology—the interface between prospection and excavation. *Archaeological Prospection*, 11 (3), 159-166.

Neubauer, W., Doneus, M., Studnicka, N. and Riegl, J., 2005. *Combined high resolution laser scanning and photogrammetrical documentation of the Pyramids at Giza.* Paper presented at the CIPA XX International Symposium, Torino, Italy.

Nex, F. and Rinaudo, F., 2010. *Photogrammetric and Lidar Integration for the Cultural Heritage Metric Surveys.* Paper presented at the Close Range Image Measurement Techniques, Newcastle upon Tyne, UK.

Norfolk County Council. 2012. *1946 Aerial Photography: Aerial photographs of Norfolk taken between 1945-1946* [online]. Norfolk County Council. Available from: http://www.historic-maps.norfolk.gov.uk/1946-aerial-photography.aspx [Accessed 27th June 2013]

Núñez Andrés, M. A. and Buill Pozuelo, F., 2009. Evolution of the architectural and heritage representation. *Landscape and Urban Planning*, 91 (2), 105-112.

Oksanen, J. and Sarjakoski, T. 2006. Uncovering the statistical and spatial characteristics of fine toposcale DEM error. *International Journal of Geographical Information Science*, 20(4), 345-369.

OldAerialPhotos, 2010. *Bluesky's OldAerialPhotos Website Signs Up Fugro-BKS* [online]. OldAerialPhotos. Available from: http://oldaerialphotos.wordpress.com/tag/fugro-bks/ [Accessed 10th June 2014].

Olson, B. R., Placchetti, R. A., Quartermaine, J. and Killebrew, A. E., 2013. The Tel Akko Total Archaeology Project (Akko, Israel): Assessing the suitability of multi-scale 3D field recording in archaeology. *Journal of Field Archaeology*, 38 (3), 244-262.

Ordnance Survey, 2006. *OS Net™ Ordnance Survey's RTK GPS Network* [online]. Ordnance Survey. Available from: http://www.**gps**.gov/cgsic/international/2006/manchester/greaves.ppt [Accessed 14th June 2014].

Ordnance Survey, 2010. *A bird's-eye view* [online]. Ordnance Survey. Available from: http://www.ordnancesurvey.co.uk/blog/2010/09/a-birds-eye-view/ [Accessed 21st May 2014]

Orengo, H. A., 2013. Combining terrestrial stereophotogrammetry, DGPS and GIS-based 3D voxel modelling in the volumetric recording of archaeological features. *ISPRS Journal of Photogrammetry and Remote Sensing*, 76 (0), 49-55.

Östman, A., 1987. Accuracy estimation of digital elevation data banks. *Photogrammetric Engineering & Remote Sensing,* 54 (4), 425-430.

Owen, T. and Pilbeam, E., 1992. *Ordnance Survey: map makers to Britain since 1791*. HMSO: London.

Oxford Archaeology, 2002. *Management of Archaeological Sites in Arable Landscapes*. London: DEFRA.

Page, M., Driver, T., Barker, L., Murphy, K. and Crane, P., 2009. *Prehistoric Defended Enclosures: Remote Sensing 2008-2009*. Llandeilo, Wales: Dyfed Archaeological trust and Royal Commission on Ancient and Historical Monuments Wales for CADW. 2009/12.

Palmer, R. and Cowley, D., 2010. *Interpreting aerial images – developing best practice.* Paper presented at the Space, Time, Place: Third International Conference on Remote Sensing in Archaeology, Tiruchirappalli, Tamil Nadu, India.

Papasaika, H., Poli, D. and Baltsavias, E., 2008. A Framework for the Fusion of Digital Elevation Models. *In: XXI ISPRS Conference "Silk Road for Information From Imagery"* Beijing, China.

Payne, A. 2006. Hillfort Studies and the Wessex Project. *In: Payne, A., Corney, M. and Cunliffe, B. (eds) The Wessex Hillforts Project: Extensive survey of hillfort interiors in central southern England*. English Heritage: London.

Pennie, J. F., 1827. *Tale of a Modern Genius, or, The Miseries of Parnassus: in a series of letters*. London: J. Andrews.

Pérez Álvarez, J. A., Herrera, V. M., Martínez del Pozo, J. Á. and de Tena, M. T., 2013. Multi-temporal archaeological analyses of alluvial landscapes using the photogrammetric restitution of historical flights: a case study of Medellin (Badajoz, Spain). *Journal of Archaeological Science*, 40 (1), 349-364.

Perko, R. and Gruber, M. 2002. Copmarison of Quality and Information Content of Digital and Film-based Images. Paper Presented at ISPRS Commission III Symposium, Graz, Austria.

Petrie, G., 2009. *Current Developments in Airborne Laser Scanning Technology.* Paper presented at the IX International Scientific & Technical Conference: "From Imagery to Map: Digital Photogrammetric Technologies", Attica, Greece.

Petrie, G. and Toth, C. K., 2009. Introduction to Laser Ranging, Profiling, and Scanning. *In:* Shan, J., and Toth, C. K., eds. *Topographic Laser Ranging and Scanning: Principles and Processing.* Boca Raton: CRC Press, 1-27.

Plets, G., Verhoeven, G., Cheremisin, D., Plets, R., Bourgeois, J., Stichelbaut, B., Gheyle, W. and De Reu, J., 2012. The Deteriorating Preservation of the Altai Rock Art: Assessing Three-Dimensional Image-Based Modelling in Rock Art Research and Management. *Rock Art Research*, 29 (2), 139-156.

Pollefeys, M., Koch, R., Vergauwen, M. and Van Gool, L., 2000. Automated reconstruction of 3D scenes from sequences of images. *ISPRS Journal of Photogrammetry and Remote Sensing*, 55 (4), 251-267.

Pope, A. 2011. *Digimap® Blog: OS MasterMap background maps* [online]. Edina. Available from: http://digimap.blogs.edina.ac.uk/2011/04/05/os-mastermap-background-maps/ [Accessed 14th June 2014].

Portland Bill to Durlston Head Coastline Group, 1998. Portland Bill to Durlston Head Shoreline Management Plan: Non-technical Summary.

Poulter, A. G. and Kerslake, I., 1997. Vertical Photographic Site Recording: "The Holmes Boom". *Journal of Field Archaeology*, 24, 221-232.

Prima, O. D. A., Echigo, A., Yokoyama, R. and Yoshida, T., 2006. Supervised landform classification of Northeast Honshu from DEM-derived thematic maps. *Geomorphology*, 78 (3–4), 373-386.

Ravibabu, M. V. and Jain, K., 2008. Digital elevation model accuracy aspects. *Journal of Applied Sciences*, 8 (1), 134-139.

Ray, S. F., 1999. *Scientific Photography and Applied Imaging*. Oxford: Focal Press.

Ray, S.F. 2000. Optical Filters. In: Jacobson, R. E., Ray, S. F., Attridge, G. G. and Axford, N. *The Manual of Photography*. Ninth Edition. Focal Press.

RCAHMW, 2007-a. *National Monuments Record of Wales* [online]. RCAHMW. Available from: http://www.cbhc.gov.uk/HI/ENG/Search+Records/National+Monuments+Record+of+Wales/ [Accessed 28th February 2012]

RCAHMW, 2007-b. *History and Collections* [online]. RCAHMW. Available from: http://www.cbhc.gov.uk/HI/ENG/Search+Records/National+Monuments+Record+of+Wales/History+and+Collections/ [Accessed 28th February 2012]

RCAHMW, 2010. *The Aerofilms Collection* [online]. RCAHMW. Available from: http://www.cbhc.gov.uk/HI/ENG/Heritage+of+Wales/Gallery/Aerofilms+Collection/ [Accessed 15th March 2013]

RCAHMW, 2013. *Aerial Survey* [online]. RCAHMW. Available from: http://www.cbhc.gov.uk/HI/ENG/Search+Records/National+Monuments+Record+of+Wales/History+and+Collections/ [Accessed 15th March 2013]

Remondino, F., Gruen, A., von Schwerin, J., Eisenbeiss, H., Rizzi, A., Girardi, S., Sauerbier, M. and Richards-Rissetto, H., 2009. *Multi-Sensor 3D Documentation of the Maya Site of Copan.* Paper presented at the 22nd CIPA Symposium, Kyoto, Japan.

Remondino, F. and Menna, F., 2008. Image-based surface measurement for close-range heritage documentation. *In: International Archives of Photogrammetry, Remote Sensing and Spatial Information Sciences,* Beijing, China. 199-206.

Reuter, H. I., Hengl, T., Gessler, P. and Soille, P., 2009. Preparation of DEMs for geomorphometric analysis. *In:* Hengl, T., and Reuter, H. I., eds. *Geomorphometry: Concepts, Software and Applications.* Amsterdam: Elsevier, 87-120.

Riegl, J., Studnicka, N. and Ullrich, A., 2003. *Merging and processing of laser scan data and high-resolution digital images aquired with a hybrid 3D laser sensor.* Paper presented at the XIX CIPA Symposium, Antalya, Turkey.

Risbøl, O., Briese, C., Doneus, M. and Nesbakken, A., 2014. Monitoring cultural heritage by comparing DEMs derived from historical aerial photographs and airborne laser scanning. *Journal of Cultural Heritage*, (0).

Robson, S., Bucklow, S., Woodhouse, N.G., Papadaki, H., 2004. *Periodic photogrammetric monitoring and surface reconstruction of a historical wood panel painting for restoration purposes*. In: Proceedings of the International Archives of Photogrammetry and Remote Sensing. (pp. 395 - 401). Istanbul, Turkey.

Rowlands, A. and Sarris, A., 2007. Detection of exposed and subsurface archaeological remains using miilti-sensor remote sensing. *Journal of Archaeological Science*, 34 (5), 795-803.

Rowley, T. and Wood, J., 2008. *Deserted Villages*. Shire Publications Ltd.

Royal Commission on Historic Monuments, 1970. *An Inventory of the Historical Monuments of the County of Dorset: Volume II, South-East Part 3*.

Royal Commission on Historical Monuments, 1952. *An Inventory of the Historical Monuments in Dorset: Volume I, West Part 1*.

Royall, C., 2011. *South Dorset Ridgeway Mapping Project*. Truro: Dorset County Council and English Heritage,. 2011R031.

Ruffner, K.C., 1995. Preface. *In:* Ruffner, K.C., ed. *CORONA: America's First Satellite Program.* CIA Cold War Records. Washington D.C. Available from: https://www.cia.gov/library/center-for-the-study-of-intelligence/csi-publications/books-and-monographs/corona.pdf [Accessed 27th October 2014].

Rusk, R., 2007. *Move Over LiDAR - Precision Photogrammetry Raises The Bar.* Paper presented at the Spatial Information Day, Spatial Sciences Institute, Adelaide, Australia.

Saadat, H., Bonnell, R., Sharifi, F., Mehuys, G., Namdar, M. and Ale-Ebrahim, S., 2008. Landform classification from a digital elevation model and satellite imagery. *Geomorphology*, 100 (3–4), 453-464.

Salonia, P., Scolastico, S., Pozzi, A., Marcolongo, A. and Messina, T. L., 2009. Multi-scale cultural heritage survey: Quick digital photogrammetric systems. *Journal of Cultural Heritage*, 10 (Supplement 1), e59-e64.

Sands, R., 2010. Terrestrial Scanning in the Intertidal Zone. In Papworth, H. (Ed.) (Electronic Mail.).

Sanz, J. O., Docampo, M. d. l. L. G., Rodríguez, S. M., Sanmartín, M. T. R. and Cameselle, G. M., 2010. A simple methodology for recording petroglyphs using low-cost digital image correlation photogrammetry and consumer-grade digital cameras. *Journal of Archaeological Science*, 37 (12), 3158-3169.

Seinturier, J., Drap, P., Durand, A., Cibecchini, F., Vincent, N., Papini, O. and Grussenmeyer, P., 2004. *Orthophoto Imaging and GIS for Seabed Visualization and Underwater*

Archaeology. Paper presented at the Beyond the artefact - Digital Interpretation of the Past - Proceedings of CAA 2004, Prato, Budapest.

Shaw, R. and Devlin, G., 2010. *Laser Scanning Fishweirs: Boarland Rock, Fergus Estuary*.

Shell, C. and Roughley, C., 2004. Exploring the Loughcrew landscape: a new airborne approach. *Archaeology Ireland*, 18 (2), 22-25.

Small, Fiona. 2002. *The Lambourn Downs Report on the Aerial Photographic Transcription and Analysis* [online]. English Heritage. Available from: http://www.english-heritage.org.uk/professional/research/landscapes-and-areas/national-mapping-programme/lambourn-downs-nmp/ [Accessed 12th February 2012].

Stal, C., Van Liefferinge, K., De Reu, J., Docter, R., Dierkens, G., De Maeyer, P., Mortier, S., Nuttens, T., Pieters, T., van den Eijnde, F., van de Put, W. and De Wulf, A., 2014. Integrating geomatics in archaeological research at the site of Thorikos (Greece). *Journal of Archaeological Science*, 45 (0), 112-125.

Steer, K., 1947. Archaeology and the National Air-Photograph Survey. *Antiquity*, 21 (81), 50-53.

Stone, J. L. and Clowes, M., 2004. Photogrammetric recording of the Roman earthworks "Cawthorn Camps", North Yorkshire. *Photogrammetric Record*, 19 (106), 94-110.

Štular, B., Kokalj, Ž., Oštir, K. and Nuninger, L., 2012. Visualization of lidar-derived relief models for detection of archaeological features. *Journal of Archaeological Science*, 39 (11), 3354-3360.

Sutherland, T. L., 1994. *A comparative archaeological and geophysical survey of the ploughed and unploughed interoir of an Iron Age hillfort.* (Masters). Bradford University.

Taylor, C., 1974. *Fieldwork in Medieval Archaeology*. Batsford.

Taylor, C., 1998. *Parks and Gardens of Britain: A Landscape from the Air*. Edinburgh: Edinburgh University Press.

Thompson, E.H. 1962. Non-topographic Photogrammetry. *Photogrammetric Record*, 5(27), 147-149.

Thompson, M. M. and Gruner, H., 1980. Foundations of Photogrammetry. *In:* Slama, C., ed. *Manual of Photogrammetry.* 4th Edition. Falls Church, Virginia: American Society of Photogrammetry, 1-36.

Trier, Ø. D., Larsen, S. Ø. and Solberg, R., 2009. Automatic detection of circular structures in high-resolution satellite images of agricultural land. *Archaeological Prospection*, 16 (1), 1-15.

Ullrich, A., Hollaus, M., Briese, C., Wagner, W. and Doneus, M., 2007. Utilization of full-waveform data in airborne laser scanning applications - art. no. 65500S. *Laser Radar Technology and Applications XII*, 6550, S5500-S5500.

University of Cambridge, 2014. *CUCAP – Cambridge University Collection of Aerial Photography. About the collection* [online]. University of Cambridge Department of Geography. Available from: http://www.geog.cam.ac.uk/cucap/about/ [Accessed 21st May 2014]

U.S. National Archives and Records Administration, No Date. *How should I store my photographic prints?* [online]. Available from: http://www.archives.gov/preservation/family-archives/storing-photos.html [Accessed 24th April 2014]

Verhoeven, G., 2011. Taking computer vision aloft – archaeological three-dimensional reconstructions from aerial photographs with photoscan. *Archaeological Prospection*, 18 (1), 67-73.

Verhoeven, G., Doneus, M., Briese, C. and Vermeulen, F., 2012a. Mapping by matching: a computer vision-based approach to fast and accurate georeferencing of archaeological aerial photographs. *Journal of Archaeological Science*, 39 (7), 2060-2070.

Verhoeven, G., Taelman, D. and Vermeulen, F., 2012b. COMPUTER VISION-BASED ORTHOPHOTO MAPPING OF COMPLEX ARCHAEOLOGICAL SITES: THE ANCIENT QUARRY OF PITARANHA (PORTUGAL–SPAIN). *Archaeometry*, 54 (6), 1114-1129.

Verhoeven, G. J. J., Loenders, J., Vermeulen, F. and Docter, R., 2009. Helikite aerial photography – a versatile means of unmanned, radio controlled, low-altitude aerial archaeology. *Archaeological Prospection*, 16 (2), 125-138.

Vozikis, G., Haring, A., Vozikis, E. and Kraus, K., 2004. Laser Scanning: A New Method for Recording and Documentation in Archaeology. *In: FIG Working Week* Athens, Greece, 22-27 May.

Walker, S. and Alspaugh, D., 2013. A Brief History of Photogrammetry. *In:* Mcglone, J. C., ed. *Manual of Photogrammetry.* Sixth Edition. Bethesda, Maryland: American Society for Photogrammetry and Remote Sensing.

Walstra, J., 2006. *Historical Aerial Photographs and Digital Photogrammetry for Landslide Assessment.* (PhD). Loughborough University.

Walstra, J., Chandler, J. H., Dixon, N. and Dijkstra, T. A., 2004. *Time for change - quantifying landslide evolution using historical aerial photographs and modern photogrammetric methods*.

Walstra, J., Chandler, J. H., Dixon, N. and Dijkstra, T. A., 2007. Aerial photography and digital photogrammetry for landslide monitoring (Vol. 283, pp. 53-63).

Walstra, J., Chandler, J. H., Dixon, N. and Wackrow, R., 2011. Evaluation of the controls affecting the quality of spatial data derived from historical aerial photographs. *Earth Surface Processes and Landforms*, 36 (7), 853-863.

Wehr, A. and Lohr, U., 1999. Airborne laser scanning--an introduction and overview. *ISPRS Journal of Photogrammetry and Remote Sensing*, 54 (2-3), 68-82.

Wells, C., 1978. *Excavations by the late George Rybot, FSA, on Eggardon Hillfort 1963-66.* Paper presented at the Proceedings of the Dorset Natural History and Archaeological Society.

Weng, Q. 2002. Quantifying Uncertainty of Digital Elevation Models Derived from Topographic Maps. *In: Richardson, D., and van Oosterom, P., eds. Advances in Spatial Data Handling: 10th International Symposium on Spatial Data Handling.* Springer, p403-418.

Wessex Archaeology, 2001. Lulworth Ranges, South Dorset. Archaeological Intergrated Land Management Plan (ILMP) Baseline Study. Desk-Based Archaeological Assessment and Monument Condition Survey.

West, I., 2013. *Worbarrow Bay, Dorset; Geology of the Wessex Coast of England (World Heritage Site, Jurassic Coast)* [online]. Available from: http://www.southampton.ac.uk/~imw/worbar.htm. [Accessed 29th December 2013].

Wheatley, D. and Gillings, M., 2002. *Spatial Technology and Archaeology*. Bury St Edmunds: Taylor & Francis.

Wiechert A., Gruber, M., 2009. Vexcel Imaging GmbH - Innovating in Photogrammetry UltraCamXp, UltraCamLp and UltraMap. *Proceedings of the Photogrammetric Week 2009*, Stuttgart, Germany.

Wilson, D. R., 2000. *Air Photo Interpretation for Archaeologists*. Stroud: Tempus Publishing Ltd.

Wilson, D. R., 2005. Bias in aerial reconnaissance. *In:* Cowley, D., and Brophy, K., eds. *From The Air: Understanding Aerial Archaeology.* Stroud: Tempus Publishing Limited, 64-72.

Wilson, J. P., 2012. Digital terrain modeling. *Geomorphology*, 137 (1), 107-121.

Wise, S., 2000. Assessing the quality for hydrological applications of digital elevation models derived from contours. *Hydrological Processes*, 14 (11-12), 1909-1929.

Wise, S., 2011. Cross-validation as a means of investigating DEM interpolation error. *Computers & Geosciences*, 37 (8), 978-991.

Wolf, P. R. and Dewitt, B. A., 2000. *Elements of Photogrammetry: with Applications in GIS*. 3rd. Boston, USA and London, UK: McGraw-Hill.

Yastikli, N., 2007. Documentation of cultural heritage using digital photogrammetry and laser scanning. *Journal of Cultural Heritage*, 8 (4), 423-427.

Zhang, B., Miller, S., Walker, S. and Devenecia, K. 2007. *Next Generation Automatic Terrain Extraction Using Microsoft Ultracam Imagery.* Paper presented at the ASPRS 2007 Annual Conference, Tampa, Florida.

11 APPENDIX ONE

11.1 Total Station Theodolite (TST)

The TST is a combination of an electronic theodolite, used for measuring horizontal and vertical angles, and an electronic distance measurement unit (EDM) (Bettess 1998), both of which used to be separate instruments until relatively recently. A brief history of TST development is provided by Bedford et al. (2011). The instrument produces measurements of angle and distance to an object that are relative to the instrument position at the time of measurement, thus producing a polar vector. TSTs are equipped with on-board computers and data-loggers that facilitate the automatic recording of this data and its subsequent transformation into 3D Cartesian coordinates using trigonometric functions. The process by which a TST operates is described below.

When a measurement is to be taken with a TST from an arbitrary or known location, the surveyor uses the telescope of the TST to identify the target for measurement from this position. The centre of the telescope is aligned with the centres of vertical and horizontal measurement and the centre of distance measurement (Bedford et al., *ibid.*), such that all of the values recorded by the instrument are relative to this one point. Cross-hairs are visible through the telescope to facilitate accurate centring on the target, which in turn can be finely tuned using horizontal and vertical drives on the body of the instrument. When a measurement is taken, an infrared pulse of light is emitted, returning to the instrument after being reflected from the target. The instrument subsequently records the slope distance to the target, the horizontal and vertical angles to the target (the angles of rotation and inclination respectively), as well as other information entered into the TST instrument's software, such as instrument height, target height, point number or code, for example (Bedford et al., *ibid.*).

There are two types of target that a TST can measure to: a retro-reflective prism or any surface that will reflect infrared laser radiation. The former is often utilised for control work i.e. during the construction of a traverse, and for topographic survey, during which it is mounted on a metallic pole of known height that is manoeuvred by another surveyor to sit directly over the point on the ground that is to be measured. In instances where it is not possible to position a prism prior to measurement, due to lack of access for example, then the instrument can be used in 'reflectorless' mode. The reflective quality of the material at which the instrument is aimed will dictate the strength of the return signal from the object to the TST. Operating in this mode is useful when surveying objects such as buildings whereby the use of a prism to record details across a façade, for example, is impossible.

Whilst many instruments operate over a range of 0.2 – 1000m in reflectorless mode, the quality of distance measurement is affected by a number of factors when using a TST (Bedford et al. *ibid.*). Range is an important consideration, as the strength of the return signal decreases as the distance increases between instrument and object. It also causes the infrared laser beam to diverge, resulting in the inaccurate measurement of detail, especially if the beam spreads across a target. Target reflectance and surface texture can also affect the accuracy of a measurement, with matt black materials being the worst (Bedford et al. *ibid.*). If the target to be measured is at an oblique angle to the instrument, it is likely that beam-spreading and scattering may occur, and the measured distance to the target will be wrong. To a lesser extent, atmospheric conditions can affect the precision of measurements, such as airborne particles, rain and fog, which can be quoted as parts per million (ppm) in the instrument manuals. As an example, precision of a single measurement is often quoted as being ±2mm at 2ppm at 1800m, with 1ppm equal to 1mm in 1000m (Bedford et al. *ibid.*). Overall, measurement precision is generally within ±2mm to ±10mm, if care is taken when setting up the instrument and taking measurements, which includes accounting for the weather conditions.

As the TST can record all of the measurements made using an on-board data logger, the speed at which a surveyor can make measurements is increased as they do not have to take the time to write a series of numbers down. This also assists in reducing any mistakes made in manually noting the measurements. As previously stated, the recorded values are converted into 3D coordinates that are already in a digital format, and are easily exported to software packages that will allow a surveyor to create a map, plan or another product for which the data are intended.

12 APPENDIX TWO

12.1 Global Navigation Satellite Systems

Global Navigation Satellite Systems (GNSS) describe the various satellite constellations, either in operation or under construction, that allow surveyors and other users to calculate a location somewhere on the earth's surface to within approximately 10m (Ainsworth and Thomason 2003). The most familiar of these is the Global Positioning System (GPS) operated by the United States Department of Defence, which is also indicative of the origins of this technology. The constellation of satellites that comprise the GPS is known as Navigation Satellite Timing and Range (NAVSTAR), and consists of 24 satellites that orbit the earth at an altitude of 20,200km (c.12,552 miles).

Whilst a full description of the operating principles of GNSS are provided by (CITE - Ainsworth and Thomason *.ibid*, WHO ELSE?) only a brief summary will be provided here. The instruments used by surveyors in the field allow them to detect the radio signals emitted by a satellite using an antenna and a receiver. The location of a receiver is usually established based upon distance measurements made between it and a minimum number of satellites, often quoted as at least 4 (CITE), that are required to calculate a more accurate position. Trilateration is the fundamental principle behind this distance calculation, although triangulation is often the favoured term when referring to GPS as it is a more widely known concept. Whilst triangulation utilises angles and distances between the vertices of a triangle through which to establish any unknown distances or angles, trilateration, on the other hand, tends to utilise only distance measurements.

Errors introduced to the radio signals as they travel through the Ionosphere and Troposphere, delay the signal as it travels through the atmosphere. The effects of these errors are difficult to model although, with the advent of differential GPS (DGPS), the accuracy of a receiver can be increased from c.10m to approximately 2-3m. DGPS is dependent on two receivers, one of which remains stationary and is known as the base station or reference receiver. The other receiver is known as the rover, and it is this receiver that collects individual location measurements over the area to be surveyed. As long as the rover does not travel too great a distance from the reference, each receiver will collect data from the same satellites. Consequently, the same timing errors will be afflicting both receivers allowing the reference station to monitor how these errors affect its static position, and to subsequently provide a correction factor to the rover to apply to each of its measurements, eliminating any errors in the survey data. The correction factor is relayed to the rover via a radio link with the reference receiver.

Depending on whether the reference station is setup over a known or arbitrary position will dictate whether the survey will need post-processing. If the reference station has not be situated over a known point prior to undertaking the survey, its own position will only be accurate to approximately 2-3m, which also impacts upon the measurements produced using the rover. Post-processing is thus necessary to establish a more accurate position for the reference and the survey as a whole. This is achieved by calculating the position of the reference receiver by using a series of permanent reference stations monitored and maintained by the Ordnance Survey, which have known, accurately surveyed locations. This data is available from the OS website from the RINEX data server, which contains information about the location of each of the OS reference stations. By selecting the OS stations closest to the area where the survey was conducted, these permanent stations can be used to triangulate the reference station location to give it a more accurate location. There are various commercial software packages available that process this data to provide the finished result.

Post-processing can also be avoided by using equipment, such as the Leica SmartNet, consisting of a rover that is able to receive corrections via a mobile connection to the internet that allow it to download data from permanently maintained reference stations. These permanent stations are maintained by the Ordnance Survey and Leica. Subsequently, a correction factor can be generated for the rover using the permanent stations that are closest to the rover, allowing it to triangulate a more accurate location in real time, to a planimetric accuracy of approximately 1-1.5cm and elevation accuracy of 2-3cm (CITE). However, issues can arise when the SmartNet rover is used in regions where intermittent mobile phone signal is available, such as in steep-sided valleys. A reference station system is available to accompany the SmartNet rover should network coverage be problematic.

13 APPENDIX THREE

This Appendix presents the contents of e-mails from BAE Systems relating to the suggested processing stages for working with archive SAPs (Section 13.1) and the potential causes of the stripes in the Eggardon DSMs (Section 13.2).

13.1 Email Content (29th November 2012)

Hi Heather,

I have now looked at your data and have been able to progress slightly, but you still need to tweak the data, as it still contains some errors. Any limitations you will find will have to do with the quality of the input data and there is nothing we can do about it. I have attached my *.gpf file, the *.sup files and the *.ipf files. I suggest that you start a new *.atf file and tweak the data further to get a better output result. Here is what I did, using the *.sup files you have sent me:

1. I first added 13 tie points manually equally over the images and measured them in IPM.

2. We loosened the image accuracies for all images to 100m for X and Y and Z and ran a solve, using the default.solve strategy.

3. We then ran APM, using the default apm.apm_strat with a 3x3.tpp and then added two more tie points manually on the right hand side, as APM did not find any points in this area.

4.We then tightened the image accuracies again to 30m for X, Y and Z and then ran a solve with the auto_blunder_detect.solve strategy.

5. We then saved the *.atf file (at which point the *.sup files are overwritten) and made a backup of the *.sup and the *.ipf files as the relative orientation of the data was OK at this point.

6. We then specified three GCPs evenly over the whole area (using your GCP accuracies) and measured them in IPM.

7. We then ran a solve and received an overall RMS of around 2.22.

The data I sent you is at this stage of the process. You will see that the relative fit is good, but the absolute fit is not so good yet. You will notice that the whole model slants from left to right. I you load your data in stereo and check your cursor on the ground on the beach at the right hand side it will be around -25m. If you move the cursor to the left hand side of the beach and move it

to the ground, you will receive a height of around -40m. So there is a tilt in height of about 15m. So here is what you can do to further improve your data:

- Place maybe four height GCPs (only Z) all along the beach area and specify a similar height for all of them (something between 1m and 5m).

- Add more GCPs to the model.

- Use the default.solve strategy for solving and not the auto_blunder_detect.sove strategy as the auto_blunder_detect strategy will keep deleting 10% of the worst points every time you run it and as you do not have many points, you do not want to lose them all.

- If the RMS error goes up too high after solving, you might have to loosening up your image accuracies again.

- Make a backup of your *.sup, *.ipf and the *.gpf files every time you feel you have received a good result.

As I said above, we cannot guarantee that you will get a perfect result with your data, but the reason would be the limitations of the input data and not the software and there is not much more we can do about this.

Best regards,

Ms. Rut Gallmeier

Technical Manager EMEA

GXP Customer Support Facility

BAE Systems

http://www.baesystems.com/gxp

13.2 Email Content (11th April 2014)

Hi Heather

I don't have access to the MyGXP portal right now (some technical snafu at our end) so I'm emailing you directly regarding your current support case involving the odd offset elevation difference stripes you see in the 1997 data.

I can't offer a definitive answer on why these two vertical stripes appear in the 1997 elevation difference image, but I'll hazard a guess and give a few suggestions based on the screenshots you sent through.

The eastern stripe appears to be in the same location as the right edge of the photo 31-97-449.sup.It may be coincidence, but I would remove that photo from the strip being triangulated (and used in the terrain generation).I would give consideration to just running the triangulation (and subsequent ATG) on the two photos which have complete coverage of the hill fort (448 and 447). I assume you have looked at each of the tie points and GCPs in turn in the IPM Multiport to ensure that they correctly located in all the images.

Whilst I'd say the RMS values are OK, they could be improved by a further iteration, by identifying the points with largest image residuals (sort by clicking on the column headings in the IPM details window) and unticking the 'use' checkbox on those before running another solve. You have a high value of redundancy in the solve so you have enough leeway to be able to remove some of the highest residual points from your solution. You may wish to experiment with other Solve strategies too. The auto_blunder_detect solve strategy for example would automatically remove 10% of points with the highest residuals.

You should look at the DSM that GXP created and see if there are any obvious flaws in that. Sometimes displaying it as a TSR (Terrain Shaded Relief) can quickly identify anomalies, and using the 3D multiport to display the terrain in a perspective view can highlight errors that are not obvious from a vertical nadir viewpoint. The ATE setup looks OK, with no obvious mistake, but as noted above, if I thought there was an issue with the generated DSM, then I would remove some of the 'none-default' settings, such as resetting:

Maximum no. of image pairs = 1

Turn off back-matching

Just use 1 core ('number of processes')

And see if this made any difference.

I'd also run NGATE rather than the older ATE algorithm to see what difference that would make. With the release of the March 2014 patch of GXP 4.1 we also have a further algorithm, called ASM (Automatic Spatial Modeler), which should further enhance accuracy and speed of creation of DTMs.

These are just a few thoughts about the issue you are seeing with this dataset. It's perhaps a little academic now, but if you wish to incorporate any of these thoughts into your thesis, please do so.

Good luck with the write-up!

best regards

Steve

Stephen Foster
Technical Support and Training Manager - EMEA
GXP Customer Support Facility